

INTERACTIONS OF LIGHT WITH ORGANIC CHROMOPHORES:  
A PHOTOCHEMICAL AND PHOTOPHYSICAL INVESTIGATION

A Dissertation  
Submitted to the Graduate Faculty  
of the  
North Dakota State University  
of Agriculture and Applied Science

By

Anthony Marcel Clay

In Partial Fulfillment of the Requirements  
for the Degree of  
DOCTOR OF PHILOSOPHY

Major Department:  
Chemistry and Biochemistry

November 2017

Fargo, North Dakota

North Dakota State University  
Graduate School

---

**Title**

INTERACTIONS OF LIGHT WITH ORGANIC CHROMOPHORES: A  
PHOTOCHEMICAL AND PHOTOPHYSICAL INVESTIGATION

---

**By**

Anthony Marcel Clay

---

The Supervisory Committee certifies that this *disquisition* complies with North Dakota  
State University's regulations and meets the accepted standards for the degree of

**DOCTOR OF PHILOSOPHY**

SUPERVISORY COMMITTEE:

Dr. Jayaraman Sivaguru

---

Chair

Dr. Gregory Cook

---

Dr. Wenfang Sun

---

Dr. Achintya Bezbaruah

---

Approved:

20 November 2017

---

Date

Dr. Gregory Cook

---

Department Chair

## ABSTRACT

Over the past century, light has emerged as a useful tool finding utility in various fields such as device fabrication, the medical field, as well as utility as an energy source. Chemists have adopted this abundant energy source to do work in material applications and to mediate simple chemical transformations. In regards to the latter, light utilized as a traceless benign reagent for organic transformations has proven fruitful and therefore unequalled in its ability to afford structural complexity from simple starting material(s). Photon absorption of the correct energy elevates organic molecules to a high energy excited state of “short” finite lifetime. In order to afford photoproducts of high selectivity or merely dictate the outcome of a desired photoreaction, control must exist during this short-lived excited state.

This dissertation describes a complementary approach to already established photochemical methodologies by which excited state control can be employed in efforts to afford photoproducts of enhanced selectivity. By employing the NEER principle (Non-Equilibrating Excited State Rotamers) and exploiting axial chiral substrates and thereby implementing rotamer control in the excited state, photoproducts of high chemoselectivity, diastereoselectivity and enantioselectivity can be accessed.

Additionally, by judicious choice of chromophore control over the excited state process can be gained affording materials of desired physical properties. It was determined that altering the functionality of bio-based feedstocks afforded photoresponsive molecules with altered photoreactivity. Photoacids and photoinitiators were synthesized and their photophysical properties were investigated. Photoinitiators were evaluated for their efficacy towards photochemical polymerization.

This dissertation details synthesis, characterization and photophysical investigations of various organic chromophores in efforts to provide mechanistic rationale regarding atropisomeric photoreactions and utility of biobased photoresponsive molecules.

## ACKNOWLEDGEMENTS

It is impossible to name everyone who has aided me in my development and growth. I thank everyone named and unnamed who has assisted me or aided in my growth in some way shape or form. Specifically, I would like to thank and acknowledge Prof. Jayaraman Sivaguru, my advisor, for his support encouragement and guidance during my career as a graduate student. His excitement and passion for scientific investigations and photochemistry served as a source of motivation over the past few years. I would like to extend a special thank you to my committee members, Prof. Gregory Cook, Prof. Wenfang Sun and Prof. Achintya Bezbaruah for their input and direction along my journey. I also extend a special thanks to Prof. Cook who initially piqued my interest in chemistry research by serving as my mentor during a research experience for undergraduates (REU) program, exposing me to the stimulating world of research.

I thank all of my collaborators whose aid and influence have increased my knowledge and lead to some intriguing investigations. A special thanks to Prof. John A. Porco Jr., Dr. Steffen Jockusch, Prof. Dean Webster, Prof. Mukund P. Sibi who have made various investigations possible teaching me along the way.

I thank Prof. Yasuharu Yoshimi and his research group who extended their hospitality during my visit to the University of Fukui. They opened my eyes to another culture and increased my horizon. I am forever grateful for their warmth and kindness.

I thank my lab mates in no particular order Dr. Barry C. Pemberton, Dr. Anoklase Jean-Luc Ayitou, Dr. Elango Kumarasamy, Dr. Nandini Vallavoju, Dr. Ramya Raghunathan, Dr. Akila Iyer, Sunil Kandappa, Ravichandranath Singathi, Sapna Ahuja as well as post-doc fellows Dr. Saravana Kumar Rajendran and Dr. Retheesh Krishnan, for their efforts, encouragement and

aid over my PhD. career. I thank Dr. Rethesh Krishnan for numerous scientific and intellectual conversations as well as his patience, devotion and instruction in regards to photophysics.

I thank the entire chemistry and biochemistry department and the administration for their assistance and support over the years as well as all my friends at NDSU. In particular I thank the following research groups Sibi group, Sun group, Zhao group and the Liu group for their assistance and various scientific discussions over the years. I thank Mr. Kirk Shoger, my high school physics teacher who encouraged my academic growth. Additionally, I thank my english and reading teacher Ms. Monika Pahl who aided me in various ways including academic growth and character growth. Additionally, I thank the numerous teachers and professors who challenged me intellectually and encouraged me throughout the years.

I thank my family especially my immediate family namely LaTanya Flynn (mother), Maurice Hicks (brother), LaTanya Stewart (sister), and Latisha Jackson (sister), as well as my extended family namely Kiesha Clay (aunt) Kevin Clay (uncle) and Steven Clay (uncle) whose love and support aided me throughout this lengthy journey. I thank my friends Charles Brown and Sam Brown (unrelated) who engaged in numerous scientific discussions, whose love and support aided me over the years. A special thanks to Charles Brown with whom I began my post-secondary education. I thank him for always having a listening ear, a shoulder to lean on and for being a pillar of support. Last but not least, I thank my life partner, my wife Christina Renee Clay for her love and patience over my graduate student career. She stood by me through every moment, the good the bad and the ugly times accepting me for who I am and growing through this journey with me.

Above all I thank my Lord and savior Jesus Christ for perseverance without whom I could have done nothing but with whom all things are possible.

It is the combination of the paths I've crossed and those of whom I have connected with that has aided me along in this journey. In the words of Booker T. Washington "Success is to be measured not so much by the position that one has reached in life but by the obstacles which he has overcome." It is my assertion that this dissertation is an attainment of some measure of success. Everyone mentioned above holds a special place in my heart and played a key role in my success. Thank you

## **DEDICATION**

This dissertation is dedicated to my mother who is always there for me extending her love, support and prayers. Whose hard work served as an example as well as a source of motivation.

Thank you mother with love.



## TABLE OF CONTENTS

ABSTRACT.....	iii
ACKNOWLEDGEMENTS.....	v
DEDICATION.....	viii
LIST OF TABLES.....	xvi
LIST OF FIGURES.....	xvii
LIST OF SCHEMES.....	xxvi
LIST OF CHARTS.....	xxix
LIST OF ABBREVIATIONS.....	xxx
1. FOUNDATIONAL KNOWLEDGE OF PHOTOCHEMISTRY AND PHOTOPHYSICS.....	1
1.1. Introduction.....	1
1.2. Light as an energy source.....	2
1.3. Practical considerations for photochemical reactions.....	4
1.4. Light and organic chromophores.....	5
1.4.1. Direct excitation.....	7
1.4.2. Trivial energy transfer.....	9
1.4.3. Resonance energy transfer (RET)/Förster energy transfer.....	9
1.4.4. Dexter energy transfer.....	10
1.4.5. Photoinduced electron transfer (PET).....	10
1.5. Organic photochemistry.....	11
1.6. Asymmetric photoreactions.....	13
1.6.1. Asymmetric photochemistry: Circularly polarized light (CPL).....	15
1.6.2. Asymmetric photochemistry: Chiral auxillary.....	16

1.6.3. Asymmetric photochemistry: Chiral sensitizers .....	18
1.6.4. Asymmetric photochemistry: Templates, solid state and supramolecular scaffolds.....	22
1.7. Axial to point chiral: A methodology for asymmetric photochemistry in solution.....	25
1.7.1. Atropisomers in thermal chemistry.....	25
1.7.2. Atropisomers in photochemistry: Atropselective photoreactions.....	26
1.8. Smart materials .....	27
1.9. Photoacids .....	28
1.9.1. Reversible photoacids .....	28
1.9.2. Metastable photoacids.....	29
1.9.3. Photoacid generators (PAGs).....	30
1.10. Photoinitiators .....	31
1.11. Summary and outlook .....	33
1.12. References.....	34
<b>2. METAL FREE VISIBLE LIGHT MEDIATED PHOTOCATALYSIS: CONTROLLING INTRAMOLECULAR [2+2] PHOTOCYCLOADDITION OF ENONES THROUGH AXIAL CHIRALITY.....</b>	<b>40</b>
2.1. Introduction to [2+2] photocycloaddition: Rule of five.....	40
2.2. Thermal cyclobutane formation.....	42
2.3. Photochemical cyclobutane formation.....	44
2.4. Photocycloaddition of enones .....	46
2.5. Racemization kinetics of atropisomeric enones.....	48
2.6. [2+2] Photocycloaddition of atropisomeric enones. ....	52
2.6.1. Optimization of reaction conditions.....	52
2.6.2. Atropselective photoreactions of atropisomeric enones. ....	57

2.7. Evaluating relationship <i>cis,cis</i> -94f major and <i>cis,cis</i> -94f minor photoproducts.....	58
2.7.1. Evaluating racemization in <i>cis,cis</i> -94f photoproduct.....	58
2.7.2. Physical separation of atropisomeric enone imides <i>cis,cis</i> -94 major and minor ....	60
2.7.3. UV-Vis spectra of atropisomeric enones 92a, 92c-g. ....	61
2.7.4. Thioxanthone quenching experiments with 92f.....	61
2.8. Mechanistic rationale of atropisomeric enones.....	63
2.9. Summary and outlook .....	65
2.10. Experimental section.....	65
2.10.1. General methods .....	65
2.10.2. General methods for photophysical investigations .....	67
2.10.3. General methods for X-ray crystal structure determination .....	67
2.11. General procedure for the synthesis of atropisomeric enones 92 .....	68
2.11.1. Synthetic protocol for 4-amino-3-tert-butylphenol 100.....	68
2.11.2. Synthetic protocol of 4-amino-3-tert-butylanisole 101.....	71
2.11.3. Synthetic protocol for 2,4-diketo-6methylhept-5-enoate 102.....	74
2.11.4. Synthetic protocol of 3,4-dihydro-2-,2-dimethyl-4-oxo-2H-pyran-6-carboxylic acid 103.....	77
2.11.5. Synthetic protocol for <i>N</i> -substituted anilines 96a-d.....	79
2.11.6. Synthetic protocol for secondary amide derivatives 99a-c .....	88
2.11.7. Synthetic protocol for substituted atropisomeric amides 92a-d.....	95
2.11.8. Synthetic protocol for substituted atropisomeric-enone imides 92e-g .....	108
2.12. General procedure for irradiation of atropisomeric-enones.....	118
2.12.1. Procedure for direct irradiation of atropisomeric-enones. ....	118

2.12.2. Procedure for sensitized irradiation of atropisomeric-enones in the presence of TX-95 .....	118
2.12.3. <sup>1</sup> H and <sup>13</sup> C NMR of atropisomeric-enones.....	119
2.12.4. X-Ray crystal structure data for atropisomeric enone photoproducts .....	147
2.13. References.....	153
<b>3. INVESTIGATING 6π-PHOTOCYCLIZATION OF ATROPISOMERIC ACRYLANILIDES.....</b>	<b>162</b>
3.1. Introduction: 6π-photocyclization of acrylanilides.....	162
3.2. Asymmetric photochemistry of acrylanilides in solution .....	163
3.3. Photochemical investigations of α,β-unsaturated atropisomeric acrylanilides .....	164
3.4. Photochemical investigations of α-substituted atropisomeric acrylanilides.....	165
3.5. Role of alkali metal ions during photochemical investigations of α-substituted atropisomeric acrylanilides .....	166
3.5.1. Photochemical investigation of α-substituted atropisomeric acrylanilides in the presence of alkali metals .....	168
3.5.2. Photophysical investigations of α-substituted atropisomeric acrylanilides 114a and 114d .....	172
3.5.3. UV/Vis spectra of 114a and 114d.....	172
3.5.4. Emission spectra of 114a and 114d .....	173
3.5.5. Mechanistic rationale 6π-photocyclization α-substituted atropisomeric acrylanilides.....	176
3.5.6. Summary and outlook of 6π-photocyclization α-substituted atropisomeric acrylanilides.....	178
3.6. 6π-photocyclization of various acyl <i>ortho</i> -substituted acrylanilides.....	179
3.6.1. Background of acyl substituted acrylanilides .....	179
3.7. Photochemistry of atropisomeric acrylanilides.....	182
3.8. Summary and outlook of acyl substituted acrylanilides .....	186

3.9. Experimental section.....	186
3.9.1. General methods .....	186
3.9.2. General methods for photophysical investigations .....	188
3.9.3. UV/Vis spectra of acyl substituted acrylanilides .....	188
3.10. General procedure for the synthesis of $\alpha$ -substituted atropisomeric acrylanilides....	188
3.10.1. Synthetic protocol for acid chloride 116.....	189
3.10.2. Synthetic protocol for $\alpha$ -substituted atropisomeric acrylanilides 114d.....	189
3.11. General procedure for the synthesis and characterization of acyl substituted acrylanilides 129a-d and their precursors.....	194
3.11.1. Synthetic protocol for primary amine 133 .....	194
3.11.2. Synthetic protocol for primary amide 132 .....	197
3.11.3. Synthetic protocol for primary ester substituted amine 133a .....	200
3.11.4. Synthetic protocol for acyl substituted acrylanilide 129a and secondary amides 132a-c .....	202
3.11.5. Synthetic protocol for <i>ortho</i> -acyl substituted acrylanilides 129b,c .....	209
3.12. General procedure for irradiation of $\alpha$ -substituted atropisomeric acrylanilides 114a-c .....	213
3.13. General procedure for irradiation of acyl <i>ortho</i> -substituted acrylanilides 129a-c.....	213
3.13.1. Procedure for direct irradiation of acrylanilides 129a-c .....	213
3.13.2. Procedure for sensitized irradiation of acyl <i>ortho</i> -substituted acrylanilides 129a-c.....	214
3.14. Charecterization of cyclized photoproduct(s) 130a-c .....	214
3.14.1. X-ray crystal structure data for acyl migration product 130b.....	221
3.15. HPLC separation and analysis conditions for $\alpha$ -substituted atropisomeric acrylanilides 114a-c and photoproducts 114a-c .....	222
3.16. References.....	225

4. EVALUATING EXCITED STATE ACIDITY OF BIOBASED PHOTOACIDS .....	230
4.1. Introduction.....	230
4.2. Biobased vanillin derived photoacids .....	232
4.3. Photoacidity of vanillin derivatives .....	234
4.4. Summary and outlook.....	242
4.5. Experimental Section.....	243
4.5.1. General methods .....	243
4.5.2. Photophysical methods .....	244
4.6. General procedure for synthesis of vanillin derived photoacids 137a-e.....	244
4.6.1. Synthetic procedure for the synthesis of vanillin derived photoacids 137a-e .....	244
4.7. References.....	261
5. VANILLIN DERIVED PHOTOINITIATORS .....	264
5.1. Introduction.....	264
5.2. Biobased vanillin derived photoacids .....	266
5.3. Vanillin derived photoinitiators .....	268
5.4. Photophysical investigation of PIs 138a-d.....	275
5.5. Summary and outlook.....	281
5.6. Experimental section.....	282
5.6.1. General methods .....	282
5.6.2. Photophysical methods .....	283
5.7. General procedure for synthesis of vanillin derived photoinitiators.....	284
5.7.1. Synthetic protocol for secondary alcohol 137a-e.....	284
5.7.2. Synthetic protocol for vanillin derived photoinitiators.....	289

5.8. Procedures for photochemical investigations. ....	299
5.8.1. Synthetic protocol for photopolymerization of MA, MMA and styrene monomers.....	299
5.9. References.....	300

## LIST OF TABLES

<u>Table</u>	<u>Page</u>
1.1: Common light sources used for photochemical reactions .....	2
2.1. Racemization of atropisomeric enones <sup>a</sup> .....	52
2.2: [2+2] Photocycloaddition of Enone-Imide 92f under Direct and Sensitized Irradiation Conditions. <sup>a</sup> .....	53
2.3: Solvent Effects on [2+2] Photocycloaddition Involving Enone-Amide 92c and 94f with Thioxanthone as the Sensitizer (10 mol%).....	54
2.4: Intramolecular [2+2] Photocycloaddition of Atropisomeric Enones.....	56
2.5: X-ray crystal data for atropisomeric enones. ....	147
2.6: X-ray crystal data for atropisomeric enones continued. ....	150
3.1: Enantioselective 6 $\pi$ -photocyclization of atropisomeric acrylanilides in the presence of alkali metal ions. <sup>a,b</sup> .....	170
3.2: Enantioselective 6 $\pi$ -photocyclization of 114b in the presence of varying CsF mol%. <sup>a-d</sup> ..	172
3.3: 6 $\pi$ -photocyclization of acyl substituted acrylanilide 129a under direct and sensitized irradiation conditions.....	183
3.4 Optimization of solvent during visible light irradiation of acrylanilide 129a. ....	184
3.5: Visible light mediated acyl migration of acyl <i>ortho</i> -substituted acrylanilides.....	185
3.6: Crystal structure data for acyl migration product 130b .....	221
4.1: Ground and excited state acidity of vanillin derivatives 137a-e <sup>a</sup> .....	241
5.1: Optimization of photopolymerization of PI 138a: Co-initiator trials. <sup>a,b</sup> .....	271
5.2: Photopolymerization of MA and thiophenol as coinitiator with various PIs.....	272
5.3: Photopolymerization of MMA with various PIs. ....	274
5.4: Photopolymerization of styrene with various PIs. ....	275
5.5: Photophysical parameters of 138a-d and BP. ....	279



## LIST OF FIGURES

<u>Figure</u>	<u>Page</u>
1.1: Wavelength (nm) and energy (kcal/mol) of electromagnetic spectrum. ....	2
1.2: Various light sources for photochemical transformations .....	3
1.3: a) Absorption of a photon and depiction of singlet excited state $R_s^*$ . b) State diagram and timescale of photophysical processes. ....	6
1.4: Depiction of orbitals of common chromophores in organic molecules. ....	8
1.5 a) depiction of asymmetric synthesis affording selectivity b) asymmetric synthesis reaction coordinate diagram. ....	14
1.6: Reversible photoacids a) process of excited state proton transfer (photoacidity) b) common photoacids .....	29
1.7: Chemical structure of known Photoacid Generators. ....	31
2.1: Natural products containing cyclobutane .....	42
2.2: Racemization kinetics of atropisomeric enone-amide 92c. ....	50
2.3: Racemization kinetics of atropisomeric enone-imides 92f and 92g. ....	51
2.4: Atropselective photoreaction of enone-carboxamide 92c .....	57
2.5: Diastereomerization kinetics of atropisomeric cyclized product <i>cis,cis</i> -94f minor. Left: $^1\text{H}$ NMR spectrum of <i>cis,cis</i> -94f minor in $\text{DMSO-}d_6$ at various times. Right: plot depicting kinetics of $N\text{-C}_{\text{aryl}}$ bond rotation. ....	59
2.6: Physical separation of <i>cis,cis</i> -94f minor and <i>cis,cis</i> -94f major over time at room temperature by crystallization. ....	60
2.7: Physical separation of <i>cis,cis</i> -94f minor and <i>cis,cis</i> -94f major via crystallization over time. $^1\text{H}$ NMR spectrum trace recorded in $\text{CDCl}_3$ . ....	60
2.8: UV-Vis spectra of atropisomeric-enones 92a, 92c-g. ....	61
2.9: Quenching of thioxanthone [0.04 mM] in the presence of 92f (1 equiv.) Lifetimes recorded 21.7 $\mu\text{s}$ (TX-95, red) and 3.4 $\mu\text{s}$ (TX-95 and 92f, blue). ....	62

2.10: Quenching studies of thioxanthone (TX-95) in the presence of 92f. Laser flash photolysis performed using ND:YAG laser (355 nm, 5 mj/pulse, 7 ns pulse width). The Transient absorption spectra were plotted 4 ms after laser flash. (Inset) Stern-Volmer quenching plot of TX-95 in the presence of 92f. ....	63
2.11: <sup>1</sup> H NMR (400 MHz, CDCl <sub>3</sub> , δ ppm) spectrum of 4-amino-3- <i>tert</i> -butylphenol 100. ....	70
2.12: <sup>1</sup> H NMR (400 MHz, CDCl <sub>3</sub> , δ ppm) spectrum of 4-amino-3- <i>tert</i> -butylanisole 101. ....	72
2.13: <sup>13</sup> C NMR (100 MHz, CDCl <sub>3</sub> , δ ppm) spectrum of 4-amino-3- <i>tert</i> -butylanisole 101. ....	73
2.14: <sup>1</sup> H NMR (400 MHz, CDCl <sub>3</sub> , δ ppm) spectrum of 2,4-diketo-6methylhept-5-enoate 102..	75
2.15 <sup>13</sup> C NMR (100 MHz, CDCl <sub>3</sub> , δ ppm) spectrum of 2,4-diketo-6methylhept-5-enoate 102..	76
2.16: <sup>1</sup> H NMR (400 MHz, CDCl <sub>3</sub> , δ ppm) spectrum of carboxylic acid 103. ....	78
2.17: <sup>1</sup> H NMR (400 MHz, CDCl <sub>3</sub> , δ ppm) spectrum of amine derivative 96a. ....	80
2.18: <sup>13</sup> C NMR (100 MHz, CDCl <sub>3</sub> , δ ppm) spectrum of amine derivative 96a. ....	81
2.19: <sup>1</sup> H NMR (400 MHz, CDCl <sub>3</sub> , δ ppm) spectrum of <i>N</i> -butenyl aniline 96b.....	82
2.20: <sup>13</sup> C NMR (100 MHz, CDCl <sub>3</sub> , δ ppm) spectrum of <i>N</i> -butenyl aniline 96b. ....	83
2.21: <sup>1</sup> H NMR (400 MHz, CDCl <sub>3</sub> , δ ppm) spectrum of <i>N</i> -pentenyl aniline 96c. ....	84
2.22: <sup>13</sup> C NMR (100 MHz, CDCl <sub>3</sub> , δ ppm) spectrum of <i>N</i> -pentenyl aniline 96c.....	85
2.23: <sup>1</sup> H NMR (400 MHz, CDCl <sub>3</sub> , δ ppm) spectrum of <i>N</i> -pentenyl- <i>ortho</i> -methoxy aniline derivative 96d. ....	86
2.24: <sup>13</sup> C NMR (100 MHz, δ ppm, CDCl <sub>3</sub> ) spectrum of <i>N</i> -pentenyl- <i>ortho</i> -methoxy aniline derivative 96d.....	87
2.25: <sup>1</sup> H NMR (500 MHz, CDCl <sub>3</sub> , δ ppm) spectrum of secondary amide derivative 99a. ....	89
2.26: <sup>13</sup> C NMR (125 MHz, CDCl <sub>3</sub> , δ ppm) spectrum of secondary amide derivative 99a. ....	90
2.27: <sup>1</sup> H NMR (400 MHz, CDCl <sub>3</sub> , δ ppm) spectrum of secondary amide derivative 99b. ....	91
2.28: <sup>13</sup> C NMR (100 MHz, CDCl <sub>3</sub> , δ ppm) spectrum of secondary amide derivative 99b. ....	92
2.29: <sup>1</sup> H NMR (400 MHz, CDCl <sub>3</sub> , δ ppm) spectrum of secondary amide derivative 99c.....	93
2.30: <sup>13</sup> C NMR (100 MHz, CDCl <sub>3</sub> , δ ppm) spectrum of secondary amide derivative 99c.....	94

2.31:	<sup>1</sup> H NMR (400 MHz, CDCl <sub>3</sub> , δ ppm) spectrum of atropisomeric amide derivative 92a.....	96
2.32:	<sup>13</sup> C NMR (100 MHz, CDCl <sub>3</sub> , δ ppm) spectrum of atropisomeric amide derivative 92a....	97
2.33:	(400 MHz, CDCl <sub>3</sub> , δ ppm) spectrum of atropisomeric amide derivative 92b.....	98
2.34:	<sup>13</sup> C NMR (100 MHz, CDCl <sub>3</sub> , δ ppm) spectrum of atropisomeric amide derivative 92b.....	99
2.35:	HRMS of atropisomeric amide derivative 92b.....	100
2.36:	<sup>1</sup> H NMR (400 MHz, CDCl <sub>3</sub> , δ ppm) spectrum of atropisomeric amide derivative 92c..	101
2.37:	<sup>13</sup> C NMR (100 MHz, CDCl <sub>3</sub> , δ ppm) spectrum of atropisomeric-enone amide derivative 92c.....	102
2.38:	HRMS of atropisomeric-enone amide derivative 92c.....	103
2.39:	<sup>1</sup> H NMR (400 MHz, CDCl <sub>3</sub> , δ ppm) spectrum of atropisomeric-enone amide derivative 92d.....	105
2.40:	<sup>13</sup> C NMR (100 MHz, CDCl <sub>3</sub> , δ ppm) spectrum of atropisomeric-enone amide derivative 92d.....	106
2.41:	HRMS of atropisomeric-enone amide derivative 92d.....	107
2.42:	<sup>1</sup> H NMR (400 MHz, CDCl <sub>3</sub> , δ ppm) spectrum of atropisomeric-enone imide derivative 92e.....	109
2.43:	<sup>1</sup> H NMR (400 MHz, CDCl <sub>3</sub> , δ ppm) spectrum of atropisomeric-enone imide derivative 92f.....	110
2.44:	<sup>13</sup> C NMR (100 MHz, CDCl <sub>3</sub> , δ ppm) spectrum of atropisomeric-enone imide derivative 92f.....	111
2.45:	HRMS of atropisomeric-enone imide derivative 92f.....	112
2.46:	<sup>1</sup> H NMR (400 MHz, CDCl <sub>3</sub> , δ ppm) of atropisomeric-enone imide derivative 92g.....	114
2.47:	<sup>13</sup> C NMR (100 MHz, CDCl <sub>3</sub> , δ ppm) of atropisomeric-enone imide derivative 92g.....	115
2.48:	HRMS of atropisomeric-enone imide derivative 92g.....	116
2.49:	<sup>1</sup> H NMR (400 MHz, CDCl <sub>3</sub> , δ ppm) spectrum of <i>cis,cis</i> -94a minor.....	120
2.50:	<sup>13</sup> C NMR (100 MHz, CDCl <sub>3</sub> , δ ppm) spectrum of <i>cis,cis</i> -94a minor.....	121

2.51:	$^1\text{H}$ NMR (400 MHz, $\text{CDCl}_3$ , $\delta$ ppm) spectrum of <i>cis,cis</i> -94a mixture of isomers. ....	122
2.52:	$^{13}\text{C}$ NMR (100 MHz, $\text{CDCl}_3$ , $\delta$ ppm) spectrum of <i>cis,cis</i> -94a mixture of isomers. ....	123
2.53:	$^1\text{H}$ NMR (400 MHz, $\text{CDCl}_3$ , $\delta$ ppm) spectrum of <i>cis,cis</i> -94b. ....	124
2.54:	$^{13}\text{C}$ NMR (100 MHz, $\text{CDCl}_3$ , $\delta$ ppm) spectrum of <i>cis,cis</i> -94b mixture of isomers. ....	125
2.55:	$^1\text{H}$ NMR (400 MHz, $\text{CDCl}_3$ , $\delta$ ppm) spectrum of <i>cis,trans</i> -94b. ....	126
2.56:	$^{13}\text{C}$ NMR (100 MHz, $\text{CDCl}_3$ , $\delta$ ppm) spectrum of <i>cis,trans</i> -94b. ....	127
2.57:	$^1\text{H}$ NMR (400 MHz, $\text{CDCl}_3$ , $\delta$ ppm) spectrum of <i>cis,cis</i> -94c. ....	128
2.58:	$^{13}\text{C}$ NMR (100 MHz, $\text{CDCl}_3$ , $\delta$ ppm) spectrum of <i>cis,cis</i> -94c. ....	129
2.59:	$^1\text{H}$ NMR (400 MHz, $\text{CDCl}_3$ , $\delta$ ppm) spectrum of <i>cis,trans</i> -94c. ....	131
2.60:	$^{13}\text{C}$ NMR (100 MHz, $\text{CDCl}_3$ , $\delta$ ppm) spectrum of <i>cis,trans</i> -94c. ....	132
2.61:	$^1\text{H}$ NMR (400 MHz, $\text{CDCl}_3$ , $\delta$ ppm) spectrum of <i>cis,cis</i> -94d. ....	133
2.62:	$^{13}\text{C}$ NMR (100 MHz, $\text{CDCl}_3$ , $\delta$ ppm) spectrum of <i>cis,cis</i> -94d. ....	134
2.63:	$^1\text{H}$ NMR (400 MHz, $\text{CDCl}_3$ , $\delta$ ppm) spectrum of <i>cis,trans</i> -94d. ....	136
2.64:	$^{13}\text{C}$ NMR (100 MHz, $\text{CDCl}_3$ , $\delta$ ppm) spectrum of <i>cis,trans</i> -94d. ....	137
2.65:	$^1\text{H}$ NMR (400 MHz, $\text{CDCl}_3$ , $\delta$ ppm) <i>cis,cis</i> -94f (mixture of <i>N</i> - $\text{C}_{\text{Aryl}}$ rotamers).....	139
2.66:	$^{13}\text{C}$ NMR (100 MHz, $\text{CDCl}_3$ , $\delta$ ppm) <i>cis,cis</i> -94f (mixture of <i>N</i> - $\text{C}_{\text{Aryl}}$ rotamers).....	140
2.67:	$^1\text{H}$ NMR (400 MHz, $\text{CDCl}_3$ , $\delta$ ppm) <i>cis,cis</i> -94f (minor <i>N</i> - $\text{C}_{\text{Aryl}}$ rotamer).....	141
2.68:	$^{13}\text{C}$ NMR (100 MHz, $\text{CDCl}_3$ , $\delta$ ppm) <i>cis,cis</i> -94f (minor <i>N</i> - $\text{C}_{\text{Aryl}}$ rotamer).....	142
2.69:	$^1\text{H}$ NMR (400 MHz, $\text{CDCl}_3$ , $\delta$ ppm) <i>cis,cis</i> -94g (major <i>N</i> - $\text{C}_{\text{Aryl}}$ rotamers). ....	143
2.70:	$^{13}\text{C}$ NMR (100 MHz, $\text{CDCl}_3$ , $\delta$ ppm) <i>cis,cis</i> -94g (major <i>N</i> - $\text{C}_{\text{Aryl}}$ rotamers).....	144
2.71:	$^1\text{H}$ NMR (400 MHz, $\text{CDCl}_3$ , $\delta$ ppm) (minor <i>N</i> - $\text{C}_{\text{Aryl}}$ rotamer). ....	145
2.72:	$^{13}\text{C}$ NMR (100 MHz, $\text{CDCl}_3$ , $\delta$ ppm) spectrum of minor <i>N</i> - $\text{C}_{\text{Aryl}}$ rotamer. ....	146

2.73: Photoproduct <i>cis,cis</i> -94b (crystallized from: hexanes/chloroform).....	148
2.74: Photoproduct <i>cis,trans</i> -94b (crystallized from: hexanes/chloroform).....	148
2.75: Photoproduct ( <i>1S, 6R, 12R, aP</i> )- <i>cis,cis</i> -94c (crystallized from: hexanes/chloroform).....	148
2.76: Photoproduct <i>cis,cis</i> -94d (crystallized from: hexanes/chloroform).....	149
2.77: Photoproduct <i>cis,trans</i> -94d (crystallized from: hexanes/chloroform).....	149
2.78: Photoproduct <i>cis,cis</i> -94f (major rotamer) (crystallized from: hexanes/chloroform). ....	151
2.79: Photoproduct <i>cis,cis</i> -94f (minor rotamer) (crystallized from: hexanes/chloroform).....	151
2.80: Photoproduct <i>cis,cis</i> -94g (major rotamer) (crystallized from: hexanes/chloroform). ....	152
3.1: Atropselectivity in $6\pi$ -photocyclization of $\alpha$ -substituted acrylanilide 114b in the presence of various additives .....	169
3.2: UV-Vis spectra of 3a (left) and 3d (right) in ethanol and acetonitrile respectively. ....	172
3.3: Fluorescence spectra of 114a in ethanol at 77K (— green), at rt (— blue) and in presence of CsF at 77 K (—red). [114a] = 2mM. ....	173
3.4: Left: Luminescence of 114d in ethanol glass (—red) and 114d in presence of CsF in ethanol (— green) at 77K. Right: Fluorescence of 3d in ethanol at 77K (—red) and at RT (— blue). [114d] = 0.5 mM). ....	174
3.5: Fluorescence spectra of 114d in ethanol, at rt (— blue) and in presence of CsF at rt (—red). [114d] =0.5m.....	174
3.6: Left: Fluorescence lifetime of 3d in ethanol (—red), 3d in presence of CsF in ethanol (— blue) at 77K. Right: Standard deviation of fit for 3d in ethanol (—red, top) and 3d in presence of CsF in ethanol (— blue, bottom) ([114d] = 0.5 mM). ....	175
3.7: Absorbance spectra of acrylanilides 129a-c recorded in MeCN. [129a-c] = 0.1mM and 4 mM respectively. ....	188
3.8: $^1\text{H}$ -NMR (400 MHz, $\text{CDCl}_3$ $\delta$ ppm) spectrum of atropisomeric acrylanilide 114d.....	191
3.9: $^{13}\text{C}$ -NMR (100 MHz, $\text{CDCl}_3$ , $\delta$ ppm) spectrum of atropisomeric acrylanilide 114d.....	192
3.10: HRMS of atropisomeric acrylanilide 114d. ....	193
3.11: $^1\text{H}$ NMR (400 MHz, $\text{CDCl}_3$ , $\delta$ ppm) spectrum of primary amine 131. ....	195

3.12: $^{13}\text{C}$ NMR (100 MHz, $\text{CDCl}_3$ , $\delta$ ppm) spectrum of primary amine 131. ....	196
3.13: $^1\text{H}$ NMR (400 MHz, $\text{CDCl}_3$ , $\delta$ ppm) spectrum of amine 132. ....	198
3.14: $^{13}\text{C}$ NMR (100 MHz, $\text{CDCl}_3$ , $\delta$ ppm) spectrum of amine 132. ....	199
3.15: $^1\text{H}$ NMR (400 MHz, $\text{CDCl}_3$ , $\delta$ ppm) spectrum of ester substituted amine 133. ....	201
3.16: $^1\text{H}$ NMR (400 MHz, $\text{CDCl}_3$ , $\delta$ ppm) Mixture of rotamers of acrylanilide 129a. ....	203
3.17: $^{13}\text{C}$ NMR (100 MHz, $\text{CDCl}_3$ , $\delta$ ppm) Mixture of rotamers- spectrum of acrylanilide 129a. ....	204
3.18: $^1\text{H}$ NMR (400 MHz, $\text{CDCl}_3$ , $\delta$ ppm) spectrum of secondary amide 134a. ....	205
3.19: $^{13}\text{C}$ NMR (100 MHz, $\text{CDCl}_3$ , $\delta$ ppm) spectrum of secondary amide 134a. ....	206
3.20: $^1\text{H}$ NMR (400 MHz, $\text{CDCl}_3$ , $\delta$ ppm) spectrum of secondary amide 134b. ....	207
3.21: $^{13}\text{C}$ NMR spectrum of secondary amide 134b. ....	208
3.22: $^1\text{H}$ NMR (400 MHz, $\text{CDCl}_3$ , $\delta$ ppm) spectrum of acrylanilide 129b. ....	210
3.23: $^{13}\text{C}$ NMR (100 MHz, $\text{CDCl}_3$ , $\delta$ ppm) spectrum of acrylanilide 129b. ....	211
3.24: $^1\text{H}$ NMR (400 MHz, $\text{CDCl}_3$ , $\delta$ ppm) spectrum of acrylanilide 129c. ....	212
3.25: $^1\text{H}$ NMR (400 MHz, $\text{CDCl}_3$ , $\delta$ ppm) spectrum of acyl migration photoproduct 130a. ....	215
3.26: $^{13}\text{C}$ NMR (100 MHz, $\text{CDCl}_3$ , $\delta$ ppm) spectrum of acyl migration photoproduct 130a. ....	216
3.27: $^1\text{H}$ NMR (400 MHz, $\text{CDCl}_3$ , $\delta$ ppm) spectrum of acyl migration photoproduct 130b. ....	217
3.28: $^{13}\text{C}$ NMR (100 MHz, $\text{CDCl}_3$ , $\delta$ ppm) spectrum of 130b. ....	218
3.29: $^1\text{H}$ NMR (400 MHz, $\text{CDCl}_3$ , $\delta$ ppm) spectrum of acyl migration photoproduct 130c. ....	219
3.30 $^{13}\text{C}$ NMR (100 MHz, $\text{CDCl}_3$ , $\delta$ ppm) spectrum of 130c. ....	220
3.31: Photoproduct 130b (crystallized from: hexanes/chloroform) ....	222
4.1: Depiction of thermodynamic cycle (Föster Cycle) for proton transfer and decay processes in reversible photoacids. ....	231

4.2: Left: Absorbance of 137a at various pH in aqueous solution. [137a] = 0.05 mM. Right: $\alpha$ - plot of 137a in acidic (HCl) and basic (NaOH) aqueous solution. [137a] = 0.05 mM;.....	235
4.3: Left: pH dependence of conjugate acid vs conjugate base in aqueous solution and Right: $\alpha$ -plot of 137b; [137b] = 0.05 mM.....	236
4.4: Left: pH dependence of conjugate acid vs conjugate base in aqueous solution and Right: $\alpha$ -plot of 137c. [137c] = 0.05 mM; .....	236
4.5: Left: pH dependence of conjugate acid vs conjugate base in aqueous solution and Right: $\alpha$ -plot of 137d. [137d] = 0.05 mM; .....	237
4.6: Left: pH dependence of conjugate acid vs conjugate base in aqueous solution and Right: $\alpha$ -plot of 137e. [137e] = 0.05 mM; .....	237
4.7: Top left - pH dependent fluorescence spectra of 137a $\lambda_{exc} = 265$ nm; OD @ $\lambda_{exc} \approx 0.2$ ; Top right: excitation spectra recorded in acidic aqueous solution. $\lambda_{em} = 309$ nm, $\lambda_{exc} = 240 - 304$ nm; Bottom right: excitation spectra recorded in basic aqueous solution. $\lambda_{em} = 335$ nm, $\lambda_{exc} = 240 - 330$ nm; HCl and NaOH used to adjust pH in acidic and basic aqueous solutions respectively.....	238
4.8: Molar extinction coefficient of 137a (red) and conjugate base (blue) recorded in aqueous solution. [137a] = 0.05 mM; HCl and NaOH used respectively to adjust pH.....	239
4.9: Molar extinction coefficient of 137b (red) and conjugate base (blue) recorded in aqueous solution. [137b] = 0.05 mM; HCl and NaOH used respectively to adjust pH. Right: Fluorescence of 137b at pH = 2.9 and decreased fluorescence at pH = 10.7 in aqueous solution. OD@ $\lambda_{exc} \approx 0.2$ . HCl and NaOH used respectively to balance pH. $\lambda_{exc} = 269$ nm. No fluorescence was observed upon adding more NaOH. ....	239
4.10: Left: Molar extinction coefficient of 137c (red) and conjugate base (blue) recorded in aqueous solution. [137c] = 0.05 mM HCl and NaOH used respectively to adjust pH. Right: Fluorescence of 137c at pH = 2.7 and decreasing fluorescence at pH = 10.4 . HCl and NaOH used respectively to adjust pH. $\lambda_{exc} = 268$ nm. No fluorescence was observed upon adding more NaOH. ....	240
4.11: Molar extinction coefficient of conjugate acid (red) and conjugate base (blue) of 137d recorded in aqueous solution. [137d] = 0.05 mM. HCl and NaOH used respectively to adjust pH. No observable emission from either the conjugate acid nor conjugate base under similarly employed conditions as derivatives 137a-c. ....	240
4.12: Absorbance spectrum of conjugate acid (red) and conjugate base (blue) of 137e recorded in aqueous solution. [137e] = 0.05 mM. HCl and NaOH used respectively to adjust pH. No observable emission from either the conjugate acid nor conjugate base under similarly employed conditions as derivatives 137a-d. ....	241

4.13: $^1\text{H}$ NMR (500 MHz, $\text{CDCl}_3$ , $\delta$ ppm) spectrum of vanillin derivative 137a.....	246
4.14: $^{13}\text{C}$ NMR (125 MHz, $\text{CDCl}_3$ , $\delta$ ppm) spectrum of vanillin derivative 137a.....	247
4.15: HRMS of vanillin derivative 137a.....	248
4.16: $^1\text{H}$ NMR (400 MHz, $\text{CDCl}_3$ , $\delta$ ppm) spectrum of vanillin derivative 137b.....	249
4.17: $^{13}\text{C}$ NMR (125 MHz, $\text{CDCl}_3$ , $\delta$ ppm) spectrum of vanillin derivative 137b.....	250
4.18: HRMS of vanillin derivative 137b.....	251
4.19: $^1\text{H}$ NMR (500 MHz, $\text{CDCl}_3$ , $\delta$ ppm) spectrum of vanillin derivative 137c.....	252
4.20: $^{13}\text{C}$ NMR (125 MHz, $\text{CDCl}_3$ , $\delta$ ppm) spectrum of vanillin derivative 137c.....	253
4.21: HRMS of vanillin derivative 137c.....	254
4.22: $^1\text{H}$ NMR (500 MHz, $\text{CDCl}_3$ , $\delta$ ppm) spectrum of vanillin derivative 137d.....	255
4.23: $^{13}\text{C}$ NMR (125 MHz, $\text{CDCl}_3$ , $\delta$ ppm) spectrum of vanillin derivative 137d.....	256
4.24: HRMS of vanillin derivative 137d.....	257
4.25: $^1\text{H}$ NMR (400 MHz, $\text{CDCl}_3$ , $\delta$ ppm) spectrum of vanillin derivative 137e.....	258
4.26: $^{13}\text{C}$ NMR (100 MHz, $\text{CDCl}_3$ , $\delta$ ppm) spectrum of vanillin derivative 137e.....	259
4.27: HRMS of vanillin derivative 137e.....	260
5.1: Absorbance spectra of vanillin derived photoinitiators. [138a-d] = 0.15mM.....	269
5.2: a) Absorbance spectra of 138a recorded in various solvents [138a] = 0.15 mM; b) absorbance (blue) and phosphorescence (red) at 77 K in EtOH. $\lambda_{\text{exc}}$ 385 nm, OD. @ $\lambda_{\text{exc}}$ = 0.35, $\lambda_{\text{em}}$ 400 nm to 750 nm.....	276
5.3: Phosphorescence of PIs 138a-d recorded at 77 K in EtOH glass, $\lambda_{\text{exc}}$ 385 nm, $\lambda_{\text{em}}$ 400 nm to 750 nm. ....	277
5.4: Low temperature luminescence (solid lines) and phosphorescence (dotted lines) recorded at 77 K in EtOH glass, $\lambda_{\text{exc}}$ 385 nm, $\lambda_{\text{em}}$ 400 nm to 750 nm of PIs 138b-d respectively.....	278
5.5: $^1\text{H}$ NMR (500 MHz, $\text{CDCl}_3$ , $\delta$ ppm) spectrum of secondary alcohol 137f.....	285
5.6: $^{13}\text{C}$ NMR (125 MHz, $\text{CDCl}_3$ , $\delta$ ppm) spectrum of secondary alcohol 137f. ....	286



5.7: $^1\text{H}$ NMR (500 MHz, $\text{CDCl}_3$ , $\delta$ ppm) spectrum of secondary alcohol 137g. ....	287
5.8: $^{13}\text{C}$ NMR (125 MHz, $\text{CDCl}_3$ , $\delta$ ppm) spectrum of secondary alcohol 137g. ....	288
5.9: $^1\text{H}$ NMR (400 MHz, $\text{CDCl}_3$ , $\delta$ ppm) spectrum of photoinitiator 138a. ....	290
5.10: $^{13}\text{C}$ NMR (100 MHz, $\text{CDCl}_3$ , $\delta$ ppm) spectrum of photoinitiator 138a. ....	291
5.11: $^1\text{H}$ NMR (400 MHz, $\text{CDCl}_3$ , $\delta$ ppm) spectrum of photoinitiator 138b. ....	292
5.12: $^{13}\text{C}$ NMR (100 MHz, $\text{CDCl}_3$ , $\delta$ ppm) spectrum of photoinitiator 138b. ....	293
5.13: $^1\text{H}$ NMR (400 MHz, $\text{CDCl}_3$ , $\delta$ ppm) spectrum of photoinitiator 138c. ....	294
5.14: $^{13}\text{C}$ NMR (100 MHz, $\text{CDCl}_3$ , $\delta$ ppm) spectrum of photoinitiator 138c. ....	295
5.15: $^1\text{H}$ NMR (400 MHz, $\text{CDCl}_3$ , $\delta$ ppm) spectrum of photoinitiator 138d. ....	296
5.16: $^{13}\text{C}$ NMR (100 MHz, $\text{CDCl}_3$ , $\delta$ ppm) spectrum of photoinitiator 138d. ....	297
5.17: $^{13}\text{C}$ NMR (375 MHz, $\text{CDCl}_3$ , $\delta$ ppm) spectrum of photoinitiator 138d. ....	298

## LIST OF SCHEMES

<u>Scheme</u>	<u>Page</u>
1.1: Global paradigm for organic photochemistry .....	5
1.2: Photochemical sensitized processes of some acceptor A. ....	9
1.3: Non-radiative bimolecular processes.....	11
1.4: Photochemistry of $\alpha$ -santonin (1). Adapted from references 11, and 15-20. ....	13
1.5: Asymmetric synthesis utilizing CPL a) cyclization forming hexhelicene b) cyclization forming dihydroindole c) ring closure of tropolone. Adapted from references 33, 46 and 47. ....	15
1.6: Asymmetric synthesis of hexahelicene employing chiral auxillary. Adapted from reference 42. ....	17
1.7: Asymmetric photochemistry use of chiral auxilliary. a) optimizing selectivity by use of solvent; b) optimizing selectivity by change in temperature. Adapted from references 50 and 51. ....	18
1.8: Asymmetric photochemistry use of chiral sensitizer 23. Adapted from references 52-54....	19
1.9: Asymmetric photochemical synthesis a) enantiodiffrentiation by use of chiral sensitizer; b) [4+2] photocycloaddition employing chiral sensitizer. Adapted from references 42 and 55-56. ....	20
1.10: Asymmetric photochemical synthesis exploiting H-Bonding reagents. a) PET catalyst for cycloaddition; b) thiourea organocatalyst for [2+2] photocycloaddition; c) light initiated photoredox chemistry. Adapted from references 57 - 60. ....	21
1.11: Asymmetric photochemistry use of chiral template. a) photocyclization of enamide 41. b) [4+2] photocycloaddition of pyridine 45 and cyclopentadiene 46. Adapted from references 42 and 61. ....	23
1.12: Asymmetric photochemistry in the solidstate. Adapted from reference 63. ....	24
1.13: Asymmetric photochemistry in the solid state. a) barrier to rotation (enatiomerization); b) solid state oxetane formation with high selectivity. Adapted from reference 64. ....	25
1.14: Atropisomers in thermal chemistry. a) selective radical addition followed by equilibration of atropisomers; b) radical addition achieving high selectivity and stability of atropisomers. Adapted from references 65-67. ....	26

1.15: Atropselective photochemical reactions. a) Axial chiral to point chiral transformation. b) $6\pi$ -photocyclization of acrylanilides c) $4\pi$ -ring closure of pyridones d) [2+2] photocycloaddition of acrylimides. Adapted from references 68-70. ....	27
1.16: Design and operation of metastable photoacids. Adapted from reference 75. ....	30
1.17: Photoreactivity of PAGs 64. Adapted from reference 74. ....	31
1.18: a) Type I and Type II photoinitiators b) polymerization. ....	32
2.1: [2+2] intramolecular photocycloaddition; Irradiation of carvone forming carvone camphor; b) triplet enone addition to singlet olefin tether forming cyclobutane product via five-membered ring intermediate. Adapted from reference 6 and 7. ....	41
2.2: Heterocyclic [2+2] photocycloaddition; a) optimizing <i>N</i> substitution b) optimizing alkenyl tether. ....	42
2.3: Thermal synthesis of cyclobutane derivatives. a) double alkylation reaction with epichlorohydrin to afford cyclobutane 82. b) Use of catalyst assisted in situ ketenamine cycloaddition to afford cyclobutane 85. Adapted from references 20 and 21 respectively. .	43
2.4: Intramolecular photocycloaddition of atropisomeric enones 92a-g. ....	46
2.5: Photochemical cyclobutane formation. a) Photocyclization of enone-amides exclusively straight addition and b) Photocyclization of enone-amides cross vs straight addition. Adapted from references 61 and 62. ....	47
2.6: Synthesis of atropisomeric enone-amides.....	48
2.7: Racemization kinetics of atropisomeric enones.....	49
2.8: <i>N</i> -C <sub>Ar</sub> yl bond rotation in <i>cis,cis</i> -94f (minor <i>N</i> -C <sub>Ar</sub> yl rotamer).....	58
2.9: Mechanistic rationale of [2+2] photocycloaddition of atropisomeric enones. ....	64
2.10: Synthesis of carboxylic acid derivative 103. ....	77
2.11: Synthesis of protocol for <i>N</i> -substituted anilines 96a-d.....	79
2.12: Synthetic protocol for secondary derivatives 99a-c.....	88
2.13: Synthesis of atropisomeric-enone imides 92e-g. ....	108
3.1: $6\pi$ -photocyclization of acrylanilides. ....	163

3.2: Asymmetric synthesis of acrylanilide using chiral template 49. ....	164
3.3: Regioselectivity in $6\pi$ -photocyclization of $\alpha,\beta$ -substituted atropisomeric acrylanilide.....	165
3.4: Acetone sensitized photochemical reaction of $\alpha$ -substituted atropisomeric acrylanilides. .	166
3.5: $6\pi$ -Photocyclization of $\alpha$ -substituted acrylanilides 114a-c in the presence metal ions.....	168
3.6: Mechanistic rationale for atropselective $6\pi$ -photocyclization of $\alpha$ -substituted acrylanilides 114a-c in the presence of alkali metal ions.....	178
3.7: Photocyclization of <i>ortho</i> -acyl substituted acrylanilides.....	180
3.8: Differing photoreactivity of acyl substituted acrylanilides.....	180
3.9: Differing reactivity of enone-carboxamides axial chiral vs. achiral reactivity.....	181
3.10: Synthesis of acyl substituted acrylanilides. ....	182
3.11: Visible light mediated acyl migration of acyl <i>ortho</i> -substituted acrylanilides.....	185
3.12: Synthesis of atropisomeric acrylanilide 114d.....	189
3.13: Synthesis of primary amine 131. ....	194
3.14: Synthesis of primary amide 132. ....	197
3.15: Synthesis of <i>ortho</i> -ester substituted primary amine 133. ....	200
4.1: Brönsted acid base equilibrium of photoacid. ....	230
4.2: Photoacidity of phenols .....	233
4.3: Synthesis of biobased photoacids .....	234
5.1: Biobased Type II photoinitiators. ....	268
5.2: synthesis of vanillin derived photoinitiators.....	268
5.3: Synthesis for secondary alcohol 137a-e.....	284
5.4: Synthesis of vanillin derived photoinitiator.....	289
5.5: Synthesis for photopolymerization of MA, MMA and styrene monomers. ....	299

## LIST OF CHARTS

<u>Chart</u>	<u>Page</u>
2.1. Structures of atropisomeric enones 92a-g, and their corresponding photoproducts.....	48
2.2: Structures of precursors to atropisomeric enones 92a-g.....	68
3.1: Structures of $\alpha$ -substituted atropisomeric acrylanilides, their corresponding photoproducts and the precursors/reactants employed.....	165
3.2: Structures of acyl substituted acrylanilides, their corresponding photoproducts and precursors/reactants employed in the study.....	182
4.1: Vanillin analogs and derivatives.....	233
5.1: Vanillin photoinitiators, precursors and reagents utilized to investigate photoinitiators. ...	266

## LIST OF ABBREVIATIONS

Å.....	Angstrom
MeCN .....	Acetonitrile
Ac .....	Acetyl
<i>anhyd</i> .....	Anhydrous
BeT.....	Back electron transfer
$k_B$ .....	Boltzmann's constant
CHCl <sub>3</sub> .....	Chloroform
Cp.....	Cyclopentyl
CRIP.....	Contact radical ion pair
CDCl <sub>3</sub> .....	Deuterated chloroform
<i>de</i> .....	Diastereomeric excess
<i>dr</i> .....	Diastereomeric ratio
DCM .....	Dichloromethane
eT .....	Electron transfer
<i>ee</i> .....	Enantiomeric excess
Et.....	Ethyl
EtOH .....	Ethanol
EtOAc .....	Ethyl acetate
equiv.....	Equivalent(s)
S <sub>1</sub> or S <sub>n</sub> .....	First or n <sup>th</sup> singlet excited state
T <sub>1</sub> or T <sub>n</sub> .....	First or n <sup>th</sup> triplet excited state
GPC.....	Gel permeation chromatography
S <sub>0</sub> .....	Ground state (singlet)
Hex .....	Hexanes

HPLC .....	High Performance Liquid Chromatography
HOMO .....	Highest Occupied Molecular Orbital
HRMS .....	High Resolution Mass Spectrometry
h.....	Hours
ISC .....	Intersystem crossing
<sup>t</sup> PR.....	Isopropyl
IPA .....	Isopropyl alcohol (2-propanol)
LASER.....	Light Amplification by Stimulated Emission of Radiation
LED.....	Light-Emitting Diode(s)
LUMO.....	Lowest Unoccupied Molecular Orbital
<i>m</i> .....	Meta
MeOH .....	Methanol
Me .....	Methyl
MCH .....	Methylcyclohexane
mM.....	Millimolar
min .....	Minute(s)
M.....	Molarity
$\epsilon$ .....	Molar absorptivity
DMF .....	<i>N,N</i> -Dimethylformamide
OD.....	Optical density
<i>op</i> .....	Optical purity
<i>o</i> .....	Ortho
<i>p</i> .....	Para
ppm .....	Parts per million
PET .....	Photoinduced electron transfer

<i>h</i> .....	Planck's constant
PDI.....	Polydispersity index
<i>rac</i> .....	Racemic
Redox.....	Reduction-oxidation
rt.....	Room temperature
satd.....	Saturated
SBR.....	Singlet biradical
SET.....	Single Electron Transfer
SRIP.....	Solvent Radical Ion Pair
<i>R/S</i> .....	Stereodescriptors for asymmetric atom
<i>P/M</i> .....	Stereodescriptors for axial chirality
<i>T</i> .....	Temperature
<sup>t</sup> Bu.....	<i>Tert</i> -butyl
TX.....	Thioxanthone
NEt <sub>3</sub> .....	Triethylamine
TFE.....	2,2,2-trifluoroethanol
E <sub>T</sub> .....	Triplet energy
TBR.....	Triplet biradical
UV-VIS.....	Ultra-Violet/Visible Light
XRD.....	X-ray diffraction
ZW.....	Zwitterionic intermediate



# 1. FOUNDATIONAL KNOWLEDGE OF PHOTOCHEMISTRY AND PHOTOPHYSICS

## 1.1. Introduction

Paraphrasing the Italian chemist Giacomo Ciamician, photochemistry studies the conversion of light into chemical energy and chemical phenomena related to such processes.<sup>1</sup> Beginning in the late 1900's, Ciamician was one of the first chemists to conduct a systematic study of photochemical reactions. It was then he realized the great potential of light to perform chemical work. Ciamician was quoted saying "...there is another agent that has a profound effect on the processes of organisms and that deserves to be deeply investigated: that is light".<sup>2, 3</sup> As the years' pass, increasing amounts of photochemical and photophysical investigations, including industrial processes, have surfaced. Light has permeated the medical fields by way of natural product synthesis, photodynamic therapy as well as simple sanitation. Interactions of light with the cones and rods in the human eye allow for vision. Thus light is responsible for what we see and how we see it. Carbon dioxide and water is consumed to produce glucose and oxygen via photosynthesis by various plants due to the presence of light. Thus light aids in the formation of the air we breathe. Light is vital for everyday life.

Photochemistry is a multidisciplinary field involving various scientists which include synthetic chemists, who both develop and utilize photochemical methodology, physical chemists and photophysicists, who probe systems to deepen understanding of light initiated processes. Photochemistry encompass photochemical methodology development with the aim of divulging a mechanistic understanding, aiding in the wielding of photochemistry for synthetic, medicinal and industrial means.

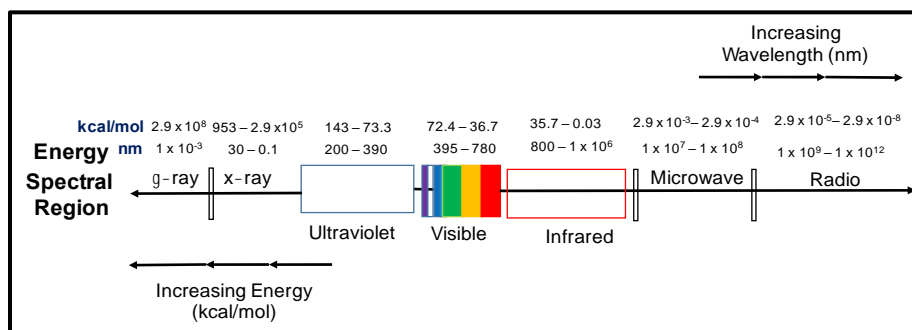


**Figure 1.1:** Wavelength (nm) and energy (kcal/mol) of electromagnetic spectrum.

**Table 1.1:** Common light sources used for photochemical reactions.

Entry	Light Source	Wavelength
1	Medium Pressure Mercury Lamp	200 – 800 nm
2	Rayonet Reactor	$300 \pm 50$ nm
		$350 \pm 50$ nm
		$419 \pm 38$ nm
3	Compact Fluorescent Lamp (CFL)	395-800 nm
4	Purple LED	$400 \pm 5$ nm

## 1.2. Light as an energy source

Energy either applied or stored in the reactants or products is required in order for a chemical transformation to occur. The first law of photochemistry states that light must be absorbed in order for a photochemical transformation to occur.<sup>4</sup> Absorption of light energy necessitates spectral overlap of the emission distribution of the light source and the absorbance spectra of the absorbing compound. Quite generally photochemistry is restricted to the process and transformations that occur upon absorption of ultra violet (200 – 400 nm) and visible light

(~400 - 800 nm) energy of the electromagnetic spectrum (Figure 1). However, due to the advent of two-photon absorption (TPA), infra-red irradiation can also be used to mimic UV/Vis reactivity. TPA allows for excitation of molecules to their electronic excited states as opposed to mere vibronic excitation.

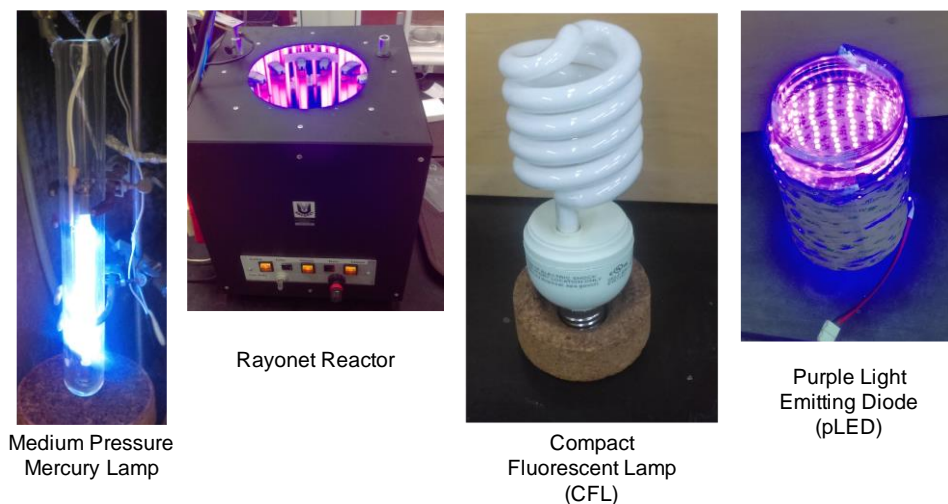


**Figure 1.2:** Various light sources for photochemical transformations

There exists a number of light sources available for photochemical reactions, ranging from commercially available light sources to specialized laboratory and/or industrially employed light sources. Table 1.1 and Figure 1.2 display common light sources and the wavelength of light transmitted from these sources. Common UV/Vis broadband light sources include low, medium and high pressure mercury lamps often placed in a cooling jacket to dissipate heat. Mercury lamps (low, medium or high pressure) emit light between the wavelengths of 200 – 800 nm. Depending on the specific type of mercury lamp (low, medium or high pressure mercury lamp) the wavelength of maximum emission ( $\lambda_{\text{max}}$  emission) slightly shifts along with the specific emission intensity at each individual wavelength. Commercially available compact fluorescent lamps have been utilized for visible light transformations as well as various light emitting diodes (LEDs). LEDs offer near monochromatic light ( $\pm 5$  nm) with low heat emanation. Due to the low

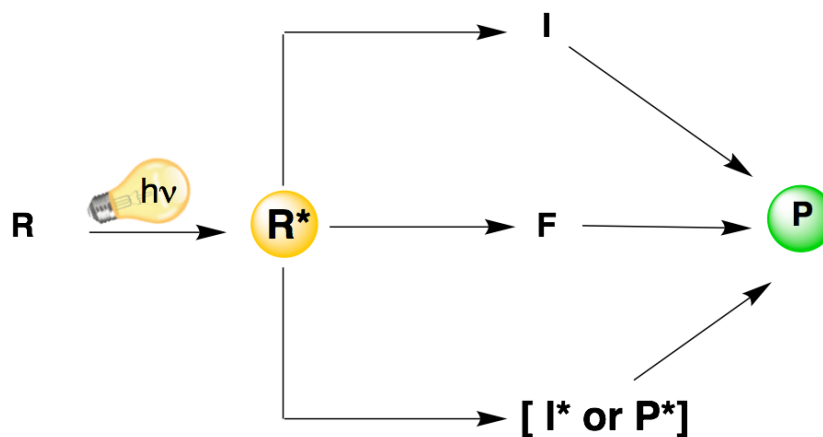
dissipation of heat less energy is wasted thus LEDs are more efficient by way of energy usage. LEDs can be found of various wavelengths ranging from UV to Visible light of respectable energy output varying in shape and size. The sun is the best energy source available surpassing that of LED by way of availability, efficiency and sustainability whose emission spans the entire electromagnetic spectrum.

### **1.3. Practical considerations for photochemical reactions**

Depending on the composition of the reaction mixture i.e. phase, chromophores present and wavelength of light utilized, differing photophysical phenomena can occur. Lack of solvation of molecules can result in colloidal suspension. Colloidal suspensions often cause light to scatter making the incident radiation difficult to absorb thus hindering the photochemical reaction. Not only can highly concentrated reaction mixtures cause light scattering, concentrated solutions can also cause inner-filter effect. Inner-filter effect occurs when the flux of incident light through a medium is reduced due to the absorbance of molecules closer to the irradiation source. When inner-filter effect occurs photons are unequally available to chromophores at distances further from irradiation source. Additionally, it is important to keep in mind that solvent and reaction vessels can absorb light at differing wavelengths therefore hindering the absorbance of the intended chromophores. Various lists of solvent and common glassware and their absorbance wavelength cutoff exist and can be found elsewhere.<sup>5</sup> Lastly, solvent can play multiple roles in photochemical reactions (ie. sensitizer, reactant(s) and/or reagent(s) etc.). Curious readers are directed elsewhere for further information regarding the role of solvent in photochemical reactions.<sup>6</sup> It is important to mention, in regards to photochemical reactions a photon is absorbed (consumed) making light a reagent. Thus the photon flux plays a significant role in any photochemical process.

## 1.4. Light and organic chromophores

As mentioned above, the first law of photochemistry, often coined the Law of Grotthus-Draper, states that only light that is absorbed is effective in photochemical transformations. In 1905 Einstein detailed the dual particle and wave nature of light giving birth to quantum theory. Thus the second law of photochemistry was outlined, the absorption of light occurs with discrete energy and is therefore a quantum process.<sup>4</sup>



**Scheme 1.1:** Global paradigm for organic photochemistry<sup>7</sup>

A photon having energy equal to the energy difference between two electronic states of a chemical species is absorbed. Absorption of light of the appropriate energy excites an available valence electron from the highest occupied molecular orbital (HOMO) to the lowest unoccupied molecular orbital (LUMO) (Figure 1.3). The absorption of a photon results in an electron being excited to a different potential energy surface which has vibrational levels and its own corresponding zero-point energy. The energy transferred to a molecule due to absorption of a photon can be calculated using equation 1.1.<sup>4,7</sup>

$$\Delta E = hc/\lambda \quad (\text{Eq. 1.1})$$

Where,

$$h = 6.626 \times 10^{-34} \text{ js (Planck's constant)}$$

$$c = 2.998 \times 10^8 \text{ m/s (speed of light)}$$

$\lambda$  = wavelength used for irradiation in m

In its simplest form (Eq 1.2), Beer-Lambert law can be used to determine the molar absorptivity ( $\epsilon$ ) of a compound assuming no concentration dependent aggregation occurs.<sup>4, 8</sup>

$$A(\lambda) = \epsilon(\lambda)c \quad (\text{Eq. 1.2})$$

Where,

$\epsilon(\lambda)$  = wavelength dependent molar absorptivity in  $\text{M}^{-1}\text{cm}^{-1}$

$c$  = concentration of the molecule of interest in M (molarity)

Scheme 1.1 depicts the working paradigm of organic photochemical reactions thereby establishing our frame of reference. The reactant is designated R,  $R^*$  is the excited state of R, I is some intermediate and P is product. The electronic configuration of P and energies associated with it may differ greatly from R as P is a new and independent species.

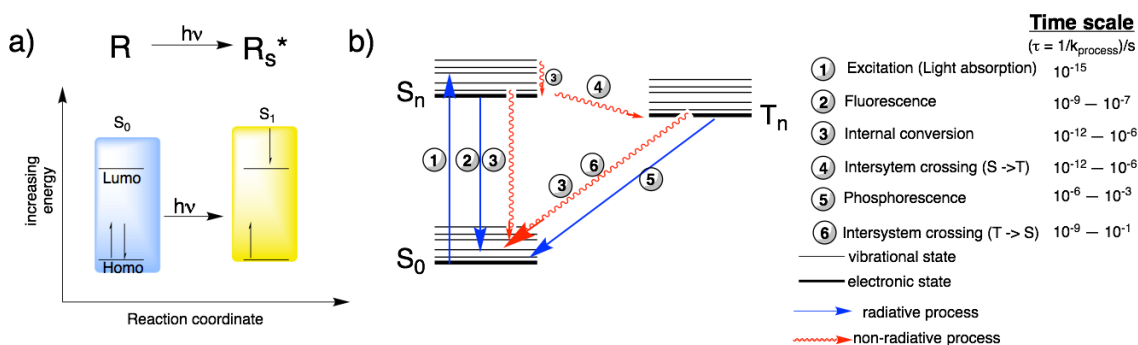


**Figure 1.3:** a) Absorption of a photon and depiction of singlet excited state  $R_s^*$ . b) State diagram and timescale of photophysical processes.

Kasha's rule states "the emitting level of a given multiplicity is the lowest excited state of that multiplicity".<sup>9</sup> This same lowest level of any given multiplicity is generally responsible for any noticed photochemical reactivity. Due to the relatively fast internal conversion (commonly occurring on the picosecond time scale) this is most commonly the case. Thus only the ground

state ( $S_0$ ) and the first and/or second low-energy excited state configurations ( $R^* = S_1, S_2, T_1, \text{ or } T_2$ ) need to be considered for the great majority of organic photochemical reactions.<sup>7</sup> Figure 1.3b displays a state diagram depicting available molecular process upon excitation of a photon and their associated timescales. Limiting factors regarding a process includes lifetimes of the attainable processes and quantum efficiency of said process. The quantum efficiency defines the efficiency of a photochemical process in the terms of a ratio of the number of molecules that undergoes the desired process by the number of photons absorbed (Equation 1.3).

$$\text{Quantum efficiency } (\Phi) = \frac{\text{Number of molecules undergoing desired process}}{\text{Number of photons absorbed}} \quad (\text{Eq. 1.3})$$

#### 1.4.1. Direct excitation

The chromophore, light absorbing unit, has great bearing on the electronic transition and electronic configuration of an excited species. Analogous to thermal chemistry, it is the functional groups that bear electrons which play a significant role in electronic excitation. Figure 1.4 displays molecular orbitals for common functional groups of organic chromophores. Knowledge of the type of frontier orbitals accessed in the excited state of the molecule gives insight into plausible electronic and molecular changes upon excitation. With this in mind, one can easily envisage how the bond order changes upon excitation of a  $\pi$  orbital causing the transition  $\pi \rightarrow \pi^*$  (Figure 1.4-inset). Lack of functionality or lack of heteroatoms leaves only covalent single bonds available for excitation which absorb in the deep UV region. For example, excitation of C-C single bond would cause a  $\sigma \rightarrow \sigma^*$  transition. Since the C-C single bond (the most common bond found in organic compounds) absorb energy greater than 110 kcal/mol, light of wavelengths shorter than 254 nm is often destructive causing homolytic cleavage of C-C bonds and thus decomposition of the irradiated compound in most cases.<sup>10</sup>

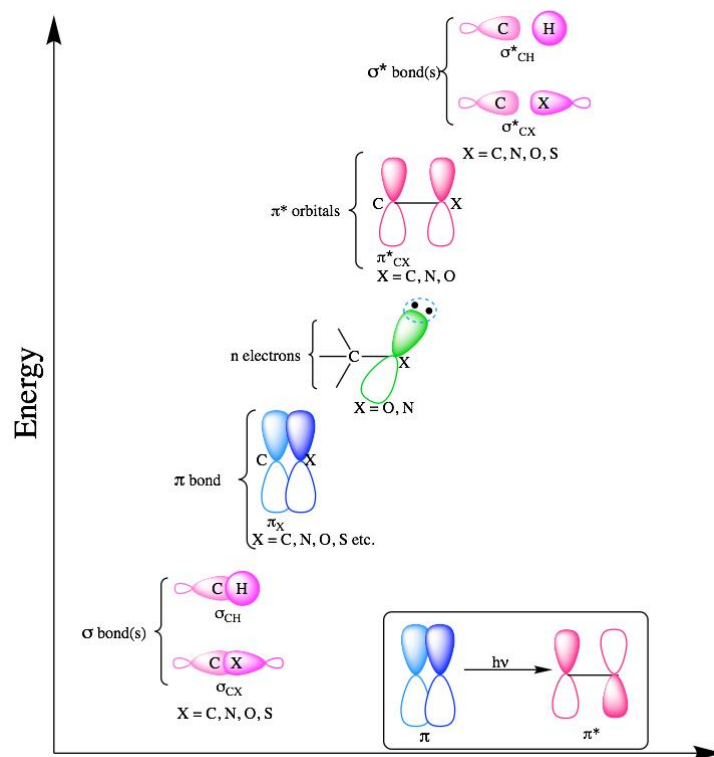
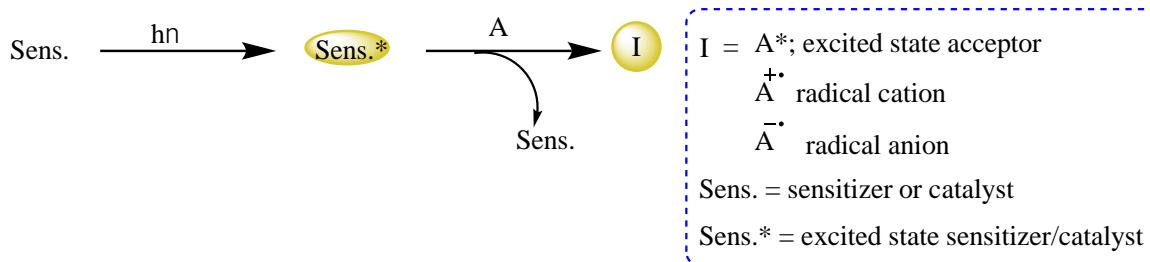


**Figure 1.4:** Depiction of orbitals of common chromophores in organic molecules.

Promotion of a molecule to an excited state can occur via direct excitation (as mentioned above) or sensitization. If the molecule of interest (“A”) does not bear a chromophore capable of absorbing the incident light of irradiation, a molecule that contains the necessary chromophore can be utilized to aid the molecule of interest to its excited state. A sensitizer is used in order to activate “A” to some reactive intermediate I where I is some electronic excited state and/or radical ion thereof (Scheme 1.2). There exist two distinct mechanistic pathways of sensitization 1) energy transfer (trivial, Foster or Dexter) and 2) photoinduced electron transfer (PET). Below short descriptions of each are provided. However, for more comprehensive and detailed descriptions interested readers are directed to other sources.<sup>4, 6, 11</sup>





**Scheme 1.2:** Photochemical sensitized processes of some acceptor A.

### 1.4.2. Trivial energy transfer

In order for energy transfer to occur it is necessary that the energy transfer is a downhill process. Thus the energy of the excited state of the acceptor “A” is lower than that of the donor “D”. For simplicity we will invoke this requirement for all common energy transfer processes. Trivial energy transfer is also called radiative energy transfer. Quite simply put, trivial energy transfer occurs when “D\*” emits a photon and the emitted photon is reabsorbed by “A”.

Radiative energy transfer occurs with the highest efficiency at wavelengths where the donor “D” has the greatest quantum efficiency of emission and the acceptor “A” has the greatest efficiency of absorbance (high molar extinction coefficient) (Scheme 1.3).<sup>11</sup>

### 1.4.3. Resonance energy transfer (RET)/Förster energy transfer

There exist two mechanisms of non-radiative energy transfer, resonance energy transfer and Dexter energy transfer. The first of which, resonance energy transfer (RET) is often referred to as a coulombic mechanism or dipole-induced mechanism. Significant spectral overlap between the excited donor D\* and the absorption of “A” is necessary for a favorable resonance energy transfer. Additionally, the extent of energy transfer is distant dependent. RET does not depend on the relaxation and reabsorption of a photon (e.g. Trivial energy transfer) instead the donor and acceptor are coupled by a dipole-dipole interaction. It is worth mentioning that RET occurs only from the singlet excited state.<sup>11, 12</sup>

#### 1.4.4. Dexter energy transfer

Dexter energy transfer is often called an electron exchange interaction or collisional transfer mechanism. Orbital overlap between “D” and “A” is necessary for electron exchange mechanism to occur. In order to achieve the orbital overlap, collision is necessary resulting in an encounter complex. Higher concentrations are generally needed for Dexter energy transfer. Shorter D-A distances also favor Dexter energy transfer. Though spectral overlap between “D” and “A” play a role in Dexter energy transfer, it is often the case that Dexter energy transfer is correlated with quenching of “D\*” resulting in no net observable emission.<sup>11, 12</sup> Dexter energy transfer can occur from either singlet or triplet excited state of “D” resulting in the corresponding excited state of “A”.

#### 1.4.5. Photoinduced electron transfer (PET)

Similar to Dexter energy transfer, photoinduced electron transfer (PET) can be a collisional process by which electrons are exchanged. Conversely, electron hopping can occur from an excited species giving rise to a solvated electron and radical cation species. All in all, PET involves electron and excited state and ground state species. In the case of the former, after excitation, collision of excited state and ground state molecules can occur forming a charge transfer complex. The resulting charge transfer complex has a net energy that is lower than the sum of the donor and acceptor energies. A significant difference between Dexter energy transfer and PET is that in the PET process only one electron is exchanged from one species to another. While for energy transfer electron exchange occurs in pairs. The excited state molecule can be either an electron donor or an electron acceptor. Transfer of an electron from one species to another forms a radical ion pair. The donor species is electron deficient and thus a radical cation ( $D^{\cdot+}$ ) while the acceptor species becomes a radical anion. Excitation delivers the necessary

energy to drive charge separation. The energy change of PET is given by the Rehm Weller equation (Eq 1.4) and thus Eq 1.4 can be utilized to determine the feasibility of PET.<sup>11, 12</sup> However, whether or not PET occurs is a separate case from feasibility and further investigation is necessary.

$$\Delta G = E^{ox} - E^{red} - E_{00}^* - C \quad (\text{Eq. 1.4})$$

Where,

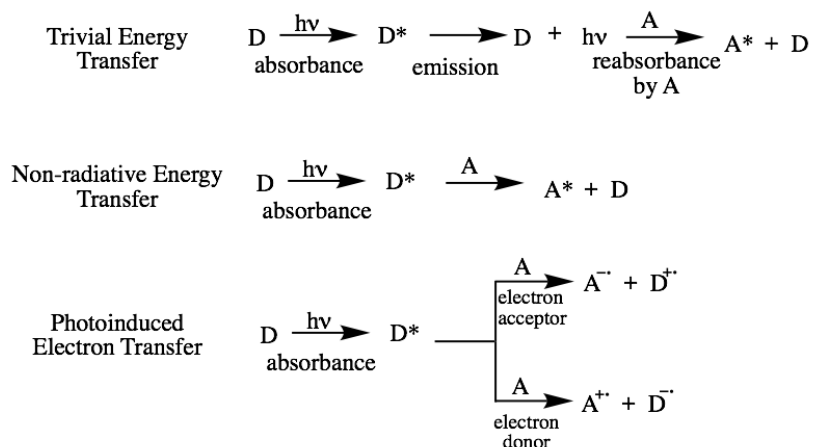
$\Delta G$  = Gibbs Free energy

$E^{ox}$  = oxidation potential of electron donor ( $D \rightarrow D^+ + e^-$ )

$E^{red}$  = reduction potential of electron acceptor A ( $A + e^- \rightarrow A^-$ )

$E_{00}^*$  = the energy of the excited molecule

$C$  = the Coulombic term



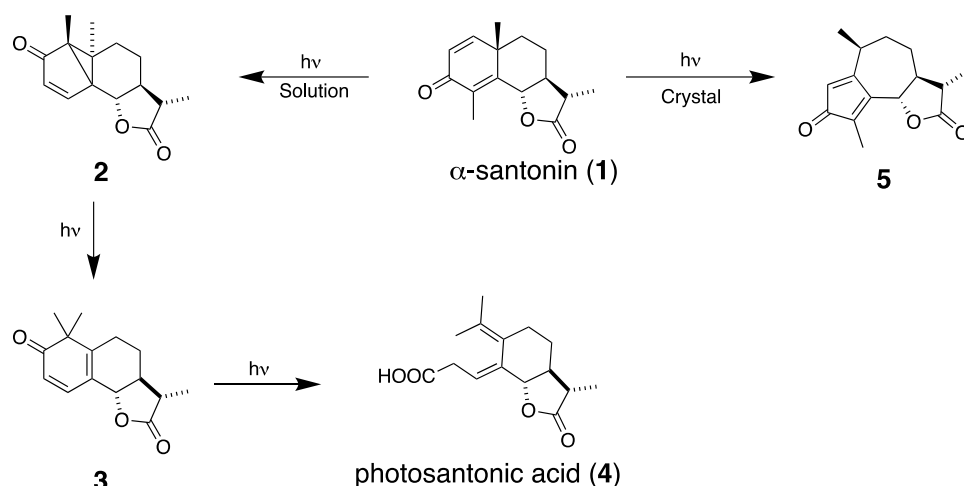
**Scheme 1.3:** Non-radiative bimolecular processes.

## 1.5. Organic photochemistry

The argument can be made that sunlight induced photochemistry commenced with the beginning of organic matter itself.<sup>2, 7</sup> The origin of documented scientific investigations in regards to organic photochemistry is rooted in the investigations of santonin. Cannizzaro is celebrated for his in depth, extensive investigation of santonin.<sup>1, 2</sup> Santonin was first isolated in

1830 by Kahler. However, the photochemistry of santonin wasn't observed until 1834 and again in 1847 by H. Trommsdorf and W.Heldt respectively.<sup>2, 13 14, 15</sup> Thus the first documented photochemical reaction was documented by Trommsdorf. It was Trommsdorf who observed the rupture of santonin crystals when exposed to ideal solar conditions. The mechanistic consideration of solid state irradiation of  $\alpha$ -santonin remained essentially unprobed for nearly the next two centuries. Eventually, in 2007 Garcia-Garibay and co-workers determined the bursting of  $\alpha$ -santonin crystals when irradiated was due to the single crystal-to-single crystal transformation of  $\alpha$ -santonin **1** to **5** (Scheme 1.4).<sup>16</sup> The expansion of the central ring (from six to seven carbons) and the displacement of the axial methyl group caused the molecular displacement and the physical rupturing of the crystal.<sup>16</sup>

Although the mechanism of solid state irradiation of  $\alpha$ -santonin eluded chemists for over 150 years, mechanistic investigation and product determination of  $\alpha$ -santonin commenced with Sestini and eventually was transferred to Cannizzaro in 1865 and 1872 respectively. Sestini and Cannizzaro collaborated and published their findings on santonin photochemistry.<sup>2, 3, 17-20</sup> Eventually they pursued separate photochemical investigations of santonin.<sup>3, 17-22</sup> Due to his influence on prominent photochemists, such as Ciamician and Silber, his advocacy for light as an energy source and his work in photochemistry, Cannizzaro is highly regarded in the field of photochemistry.<sup>1, 23</sup>



**Scheme 1.4:** Photochemistry of  $\alpha$ -santonin (1). Adapted from references 11, and 15-20.

Organic photochemistry, as a field of study, has advanced since the times of Sestini and Cannizzaro. Organic photochemistry is concerned with observing, understanding and utilizing photochemical reactions where reactant (R) gives rise to product (P) (Scheme 1.1). Various photochemical reactions have since been discovered and exploited, ranging from pericyclic cycloadditions [2+2], [4+2], and [4+4]-photocycloaddition to classical named reactions such as Paterno-Büchi, and De Mayo to simply list a few.<sup>24-28</sup> As displayed with  $\alpha$ -santonin investigations have not only been limited to solution phase but solid phase photochemistry has also been investigated with varying degrees of success. The prophetic views of Ciamician has somewhat been noticed as publications involving light mediated reactions continues to steadily rise.

## 1.6. Asymmetric photoreactions

IUPAC defines chirality as the geometric property of a rigid object, or spatial arrangement of points or atoms that are non-superimposable on its mirror image. In 1815 Jean Baptiste Biot coined the identifiable characteristic of chirality, as the ability to rotate the plane of polarized light, a property which he deemed optical activity. Biot noticed that solutions of

specific organic compounds were optically active.<sup>29-31</sup> Advancing the field of chirality, Louis Pasteur was the first chemist to link molecular structure and chirality. Pasteur investigated tartaric acid and various salt derivatives separating conglomerate crystals and measuring their optical activity.<sup>31, 32</sup>

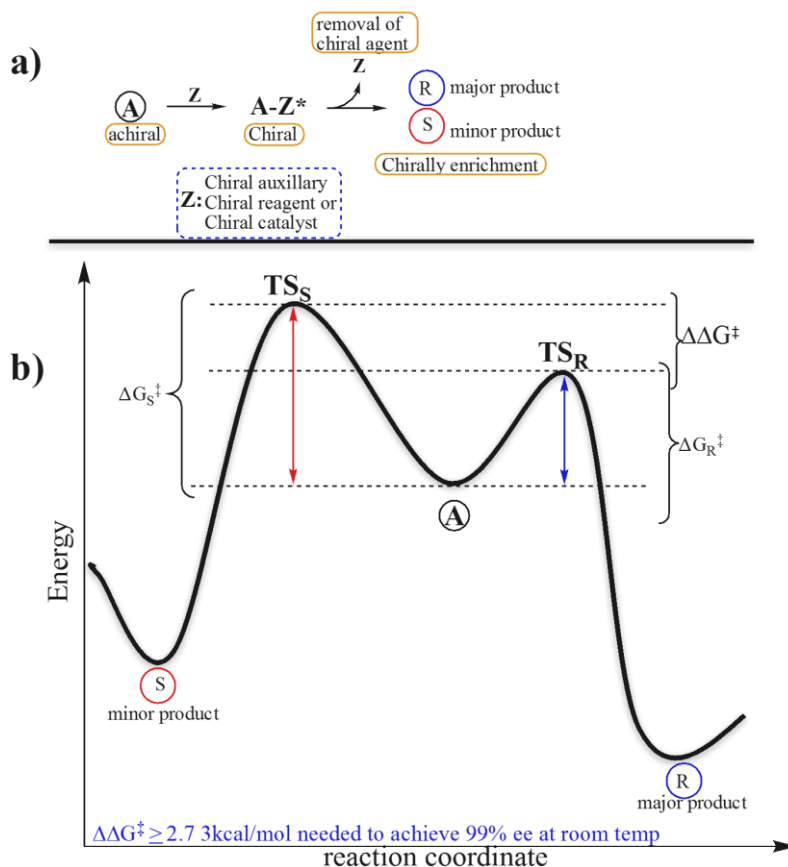
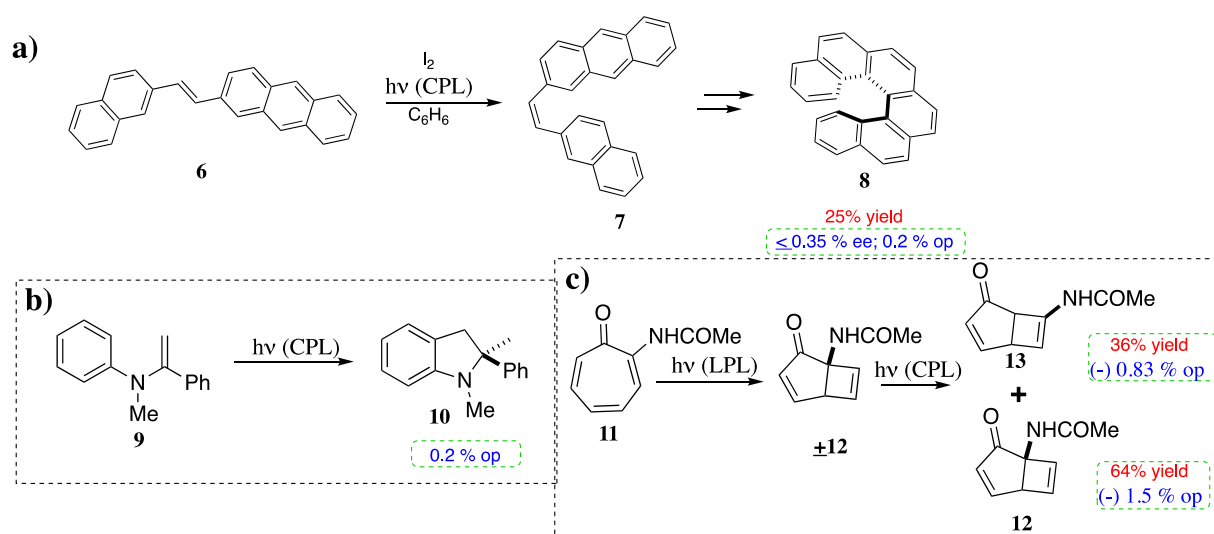


**Figure 1.5:** a) depiction of asymmetric synthesis affording selectivity b) asymmetric synthesis reaction coordinate diagram.

In 1860 Pasteur recognized that many natural products were optically active in contrast to those synthesized in lab which lacked optical activity. Pasteur once said “one needs to use dissymmetric forces to have recourse to solenoids, to dissymmetric movements of light, to the action of substances themselves dissymmetric...” Pasteur recognized the need for chirality in preparative chemistry to induce chirality in product formation.

In 1904 Marckwald defined asymmetric synthesis as “those reactions which produce optically active substances from symmetrically constituted compounds with the intermediate use of optically active materials but with the exclusion of all analytical processes”.<sup>33, 34, 35</sup> Thus asymmetric synthesis necessitates the use of a chiral agent(s) which will be introduced as part of the substrate, as a reagent or catalyst in order to afford chiral product in enriched selectivity (enantiomeric excess (*ee*) or diastereomeric excess (*de*)).<sup>33</sup> Figure 1.5a displays the process for affording enantioenriched compounds. In order to afford desired selectivity thermally ( $\geq 99\%$  *ee*) the difference between activation energies necessitates a minute difference of  $\sim 3$  kcal/mol (Figure 1.5b).<sup>36-38</sup>



**Scheme 1.5:** Asymmetric synthesis utilizing CPL a) cyclization forming hexahelicene b) cyclization forming dihydroindole c) ring closure of tropolone. Adapted from references 33, 46 and 47.

### 1.6.1. Asymmetric photochemistry: Circularly polarized light (CPL)

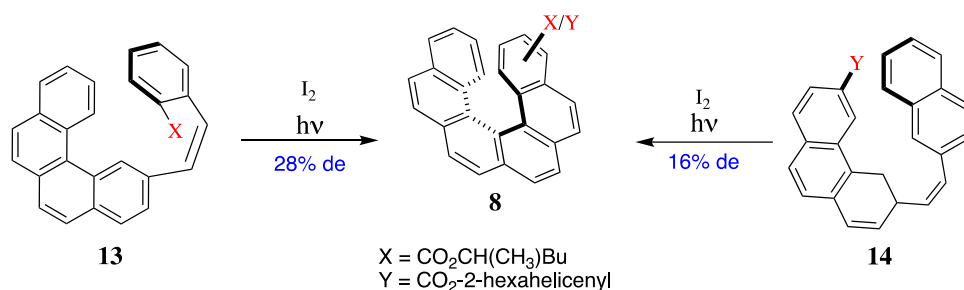
As early as 1874 the use of circularly polarized light was hypothesized to be able to afford chirality in product formation independently by both Le Bel and van't Hoff.<sup>33, 39, 40</sup> Significant progress in asymmetric photochemistry was not made until the late 1900's where new optically active products were formed. Reproducible results with measurable optical purity

employing circularly polarized light did not arise until nearly a century after the hypothesis of Le Bel and van't Hoff. In 1971 Kaiser and Lee demonstrated that both left and right CPL could afford hexahelicene albeit with low optical purity ( $\leq 0.35\%$  ee) (Scheme 1.5a).<sup>33, 41-45</sup> Other cyclization reactions utilizing CPL were also investigated. Cavazza and coworkers employed CPL for the ring closure of tropolone derivatives while Nicoud and coworkers displayed photocyclization followed by hydrogen shift of *N*-aryl-*N*-methylenamine to dihydroindoles (Scheme 1.5b-c).<sup>42, 46, 47</sup> All of the aforementioned examples of asymmetric photochemical reactions employing CPL suffered low optical purity. Enantioselectivity utilizing CPL is limited by *g*-factor ( $g = \Delta\epsilon/\epsilon$  where  $\Delta\epsilon$  is the difference in molar absorptivity for right- and left- CPL of a single enantiomer. Thus utility of CPL is limited due to an enantiomer's inherent ability to differentially absorb right vs left CPL thus, limiting the utility of CPL.<sup>48, 49</sup>

### 1.6.2. Asymmetric photochemistry: Chiral auxiliary

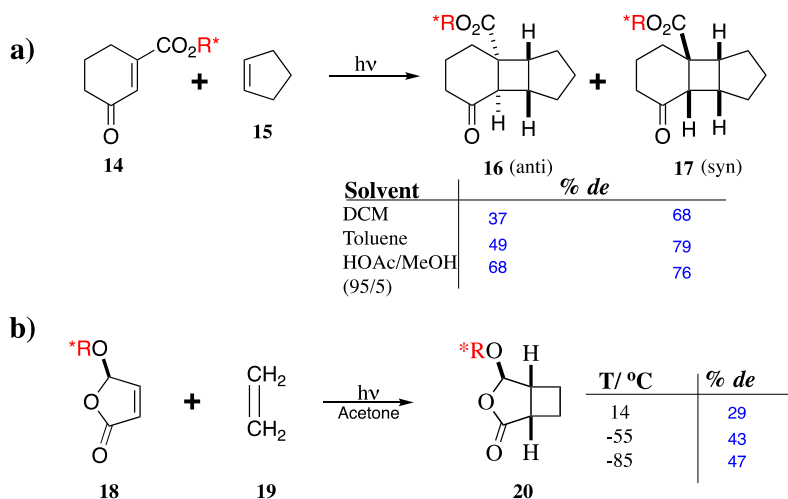
More successful methods of inducing chirality upon product formation in photochemical asymmetric synthesis were realized upon the implementation of chiral auxiliaries. Utilizing chiral auxiliary appended to prochiral substrate adds complexity. Investigations utilizing chiral auxiliary in photochemistry did not arise until the mid-1970's. The ability of an auxiliary to induce chirality upon product formation is dictated by a number of factors such as steric interactions, electronics, hydrogen-bonding as well as other foreseeable non-bonding interactions in the excited and/or groundstate.<sup>42</sup> Since the built in chirality of the substrate is needed for chiral induction upon product formation, photoreactions involving chiral auxiliaries are processes where selectivity arises due to preferential reactivity of one diastereomer over the other. Thus high values of diastereomeric excess are desired.





**Scheme 1.6:** Asymmetric synthesis of hexahelicene employing chiral auxiliary. Adapted from reference 42.

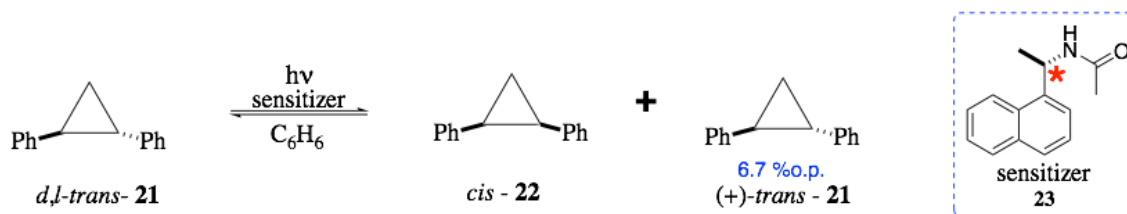
Martin and coworkers were able to achieve greater extent of optical purity in the asymmetric synthesis of hexahelicene implementing chiral auxiliary.<sup>42</sup> Greater induction was afforded with the chiral substituent in the 1-position as opposed to the 2-position (X vs Y respectively) as seen in Scheme 1.6. The utility of chiral auxiliaries has been displayed in a number of different types of reactions such as photocycloadditions, hydrogen abstractions and di- $\pi$ -methane rearrangement to simply list a few. Schemes 1.6 and 1.7 displays examples of usage of chiral auxiliaries in photochemistry. Temperature, solvent, and the number of chiral centers the substrate contains all effect the diastereomeric excess (*de*).<sup>42, 50</sup> Optimizing all aforementioned conditions chemists were able to afford moderate selectivity with respect to *de* (Scheme 1.7). Lange and coworkers optimized the selectivity (*de*) by changing the solvent employed in the [2+2] photocycloaddition of chiral cyclohexanone to cyclopentene. They afforded the cyclized *anti* product **16** in 68% *de* in a mixture of HOAc:MeOH (95:5).<sup>50</sup> Scharf and coworkers were able to increase the *de* in the [2+2] photocycloaddition of substituted furanone derivative **18** to ethylene **19** by reducing the temperature to -85 °C (Scheme 1.7b).<sup>51</sup>



**Scheme 1.7:** Asymmetric photochemistry use of chiral auxiliary. a) optimizing selectivity by use of solvent; b) optimizing selectivity by change in temperature. Adapted from references 50 and 51.

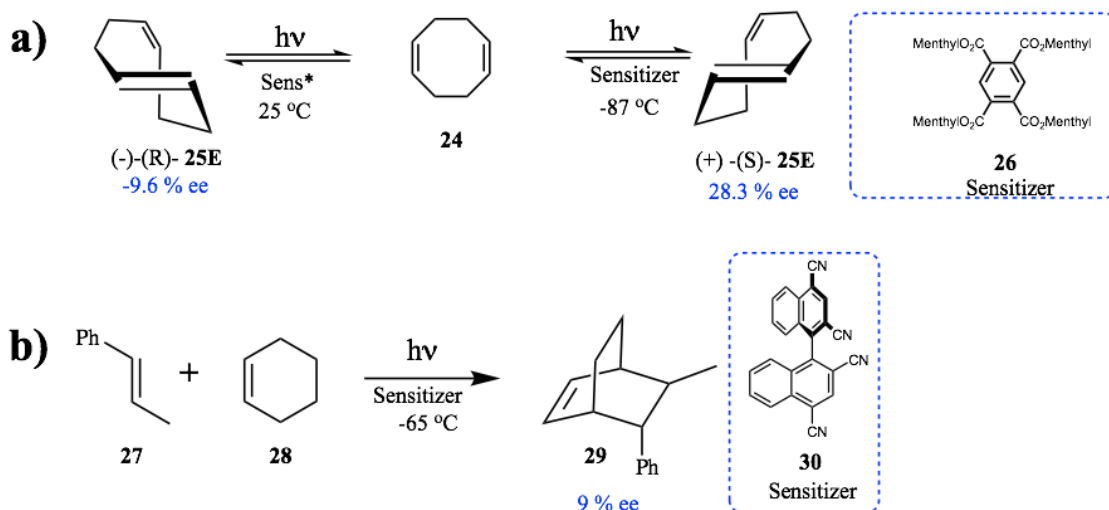
### 1.6.3. Asymmetric photochemistry: Chiral sensitizers

The use of chiral auxiliary enables the induction of chirality for the newly formed chiral elements. However, utilizing chiral auxiliary causes the reaction mixture to be composed of a mixture of diastereomers. This mixture of diastereomers often increases complexity of the methodology and increases the difficulty of separation. Hammond and coworkers were the first to display that a chiral sensitizer could be employed to afford optical activity in the desired product. Hammond and coworkers displayed that naphthalene derivative **23** could be employed as a sensitizer to initiate isomerization of *trans*-1,2-diphenylcyclopropane **21** to afford optically active *cis*-1,2-cyclopropanone **22** albeit low optical purity. More noticeable selectivity was that of the *trans*-isomer from enantiodifferentiation yielding ~7% optical purity (Scheme 1.8).<sup>52-54</sup>



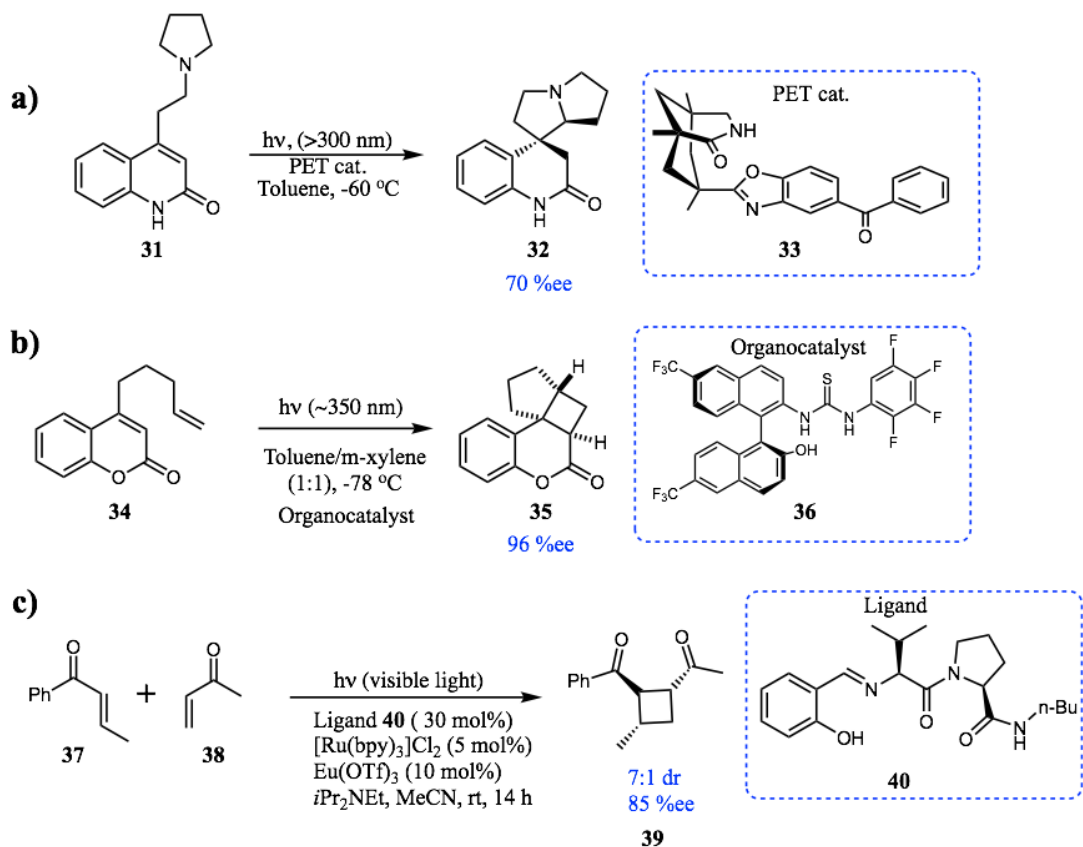
**Scheme 1.8:** Use of chiral sensitizer **23** for asymmetric photochemistry. Adapted from references 52-54.

After 72 hours of irradiation, the photostationary state was reached which afforded the 1:1 mixture of *cis* (**21**) and *trans* (**22**) 1,2-diphenylcyclopropane with **21** of greater optical purity (~7%). Since the pioneering work of Hammond and coworkers numerous investigations have been centered around the use of chiral sensitizers. Inoue and coworkers displayed enantiodifferentiation of enantiomers of *trans*-cyclooctene upon irradiation of a solution of *cis*-cyclooctene in the presence of various chiral benzoate sensitizers, the first of its kind.<sup>42, 55</sup> By merely altering the temperature Inoue and coworkers were able to afford either optical antipode of *trans*-cyclooctene **24E** (Scheme 1.9a). By way of intermolecular photochemical reactions Kim and Schuster reported the first asymmetric photochemical [4+2] photocycloaddition. Kim and Schuster employed (-)-1,1'-bis(2,4-dicyanonaphthalene) **30** as the sensitizer in order to obtain the cyclized product of 1,3-cyclohexadiene and *trans*- $\beta$ -methylstyrene, **27** and **28** respectively. In nonpolar solvents (e.g. toluene) Kim and Schuster were able to afford **29** in 9% *ee* at -65 °C.<sup>42, 56</sup>



**Scheme 1.9:** Asymmetric photochemical synthesis a) enantiodifferentiation by use of chiral sensitizer; b) [4+2] photocycloaddition employing chiral sensitizer. Adapted from references 42 and 55-56.

In the cases listed above, upon irradiation the sensitizer contains the chromophore and thus becomes excited. The excited sensitizer is responsible for transferring its chiral information to the substrate during the sensitization process. In order for chiral induction from the sensitizer to the substrate, sensitizer-substrate interaction must be of sufficient strength and duration (lifetime- $\tau$ ). This often manifests itself by way of excited complex formation (ie. exciplex) between the excited sensitizer and the ground-state substrate. The nature of the exciplex and thus reaction mechanism depends on the energies of the substrate and sensitizer. The sensitization may occur via singlet, triplet or even electron-transfer and thus affording the corresponding exciplex.<sup>42</sup>



**Scheme 1.10:** Asymmetric photochemical synthesis exploiting H-Bonding reagents. a) PET catalyst for cycloaddition; b) thiourea organocatalyst for [2+2] photocycloaddition; c) light initiated photoredox chemistry. Adapted from references 57 - 60.

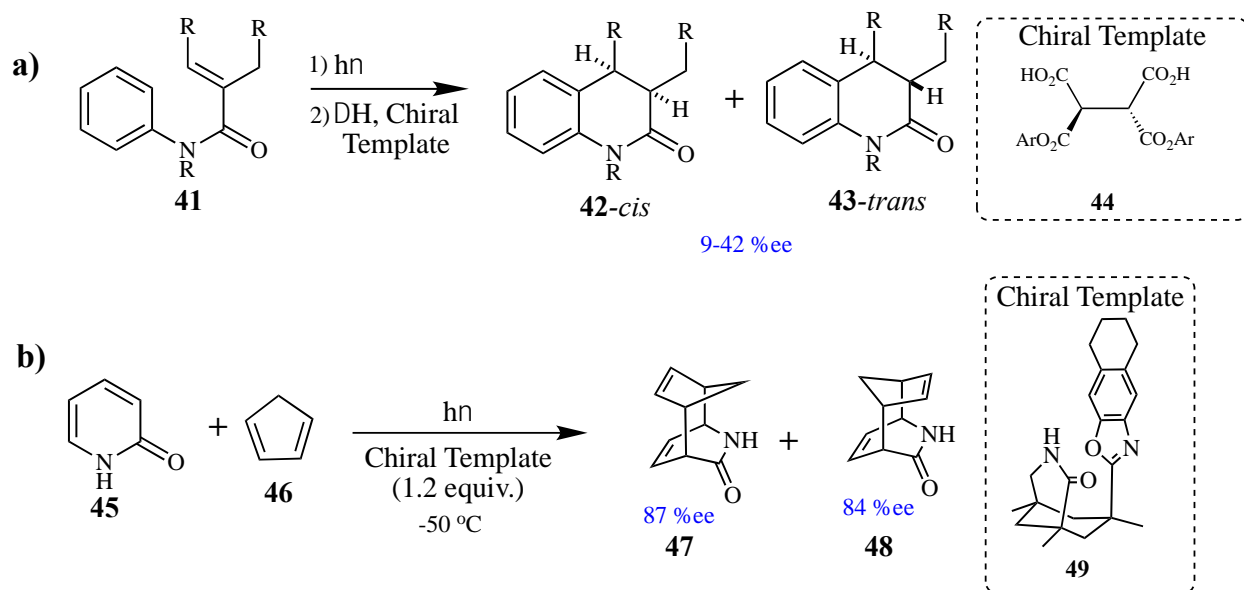
Since the investigations of Inoue, Kim and Schuster significant advances in asymmetric photochemical reactions involving sensitizer and/or catalyst have surfaced. The difference between catalyst and sensitizer depends on, which species is in the excited state (substrate vs catalyst/sensitizer), the amount of catalyst/sensitizer utilized and if the employed catalyst/sensitizer can be hypothetically recovered and reused. Quite often these two terms are used interchangeably. The groups of Bach and Sivaguru have independently displayed the capability of organic photocatalysts to afford high selectivity. Scheme 1.10 displays PET induced intramolecular photocyclization of tethered quinolinone derivatives and photocycloaddition of tethered coumarin derivatives respectively (Scheme 1.10a-b).<sup>57, 58</sup> It is noteworthy to mention

Sivaguru and coworkers' advancements in intermolecular cyclization of coumarin and tetramethylethylene where selectivity was afforded with respect to dimerization of coumarin vs cycloaddition with tetramethylethylene.<sup>59</sup> Yoon and coworkers were able to employ chiral Ruthenium catalyst, an inorganic photoredox variant, for the photochemical cycloadditions of enones achieving high selectivity but only moderate diastereoselectivity (Scheme 1.10c)<sup>60</sup>. Thus employing chiral catalysts has currently been able to achieve selectivity >90%. However, methods employing chiral catalysts quite often necessitate low temperature irradiation, with the exception of Yoon and coworkers as displayed above. Low temperature allows for a greater extent of organization.

#### **1.6.4. Asymmetric photochemistry: Templates, solid state and supramolecular scaffolds**

In the presence or absence of solution, e.g. solid state irradiation, molecular restriction has been displayed to afford chirality in the desired photoproduct. Chiral templates are often utilized in superstoichiometric amounts. Intermolecular interactions govern host-guest interactions thus solvent choice and temperature must be regulated in order to optimize the host-guest interaction.

Ninomiya and coworkers employed chiral template in the photocyclization of enamides **41**. The chiral ditoluoyltartaric acid template **44** attained respectable selectivity up to 42% *ee*. (Scheme 1.11a).<sup>42</sup> Bach and coworkers achieved high enantioselectivity (84-87% *ee*) by employing chiral template **49** in the [4+4]-photocycloaddition of prochiral 2-pyridones **45** and cyclopentadiene **46** (Scheme 1.11b).<sup>61</sup> Both chiral templates mentioned above mainly exploit H-bonding as the major intermolecular interaction to orient the molecule in a favorable conformation to achieve the observed selectivity.

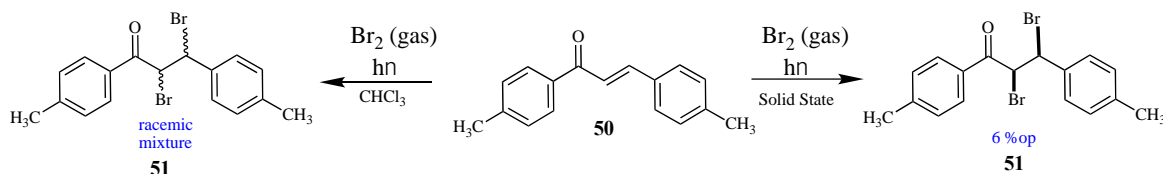


**Scheme 1.11:** Asymmetric photochemistry use of chiral template. a) photocyclization of enamide **41**. b) [4+2] photocycloaddition of pyridine **45** and cyclopentadiene **46**. Adapted from references 42 and 61.

There exists a number of supramolecular scaffolds that have been utilized to afford chirality in solution eg. cucurbital, cyclodextrins, and zeolites to simply list a few.<sup>62, 63</sup> Much like chiral templates the host-guest interactions of these supramolecular scaffolds are governed by intermolecular interactions. There have been plenty advancements in the field of supramolecular photochemistry and remains a successful method of asymmetric photochemical induction. Greater knowledge with respect to supramolecular photochemistry can be found in a recent chemical review and references therein.<sup>63</sup>

Solid state irradiation has also displayed promise with respect to asymmetric photochemistry. The crystal matrix itself, by way of chiral space group, can be utilized for chiral induction or a molecule containing chirality can be crystalized with the substrate in order to induce chirality upon the substrate. The rigidity of the crystal matrix aids in chiral induction due to the close proximity of the chiral information and the substrate. Schmidt and coworkers recognized the first absolute asymmetric synthesis in the solid state with measurable optical

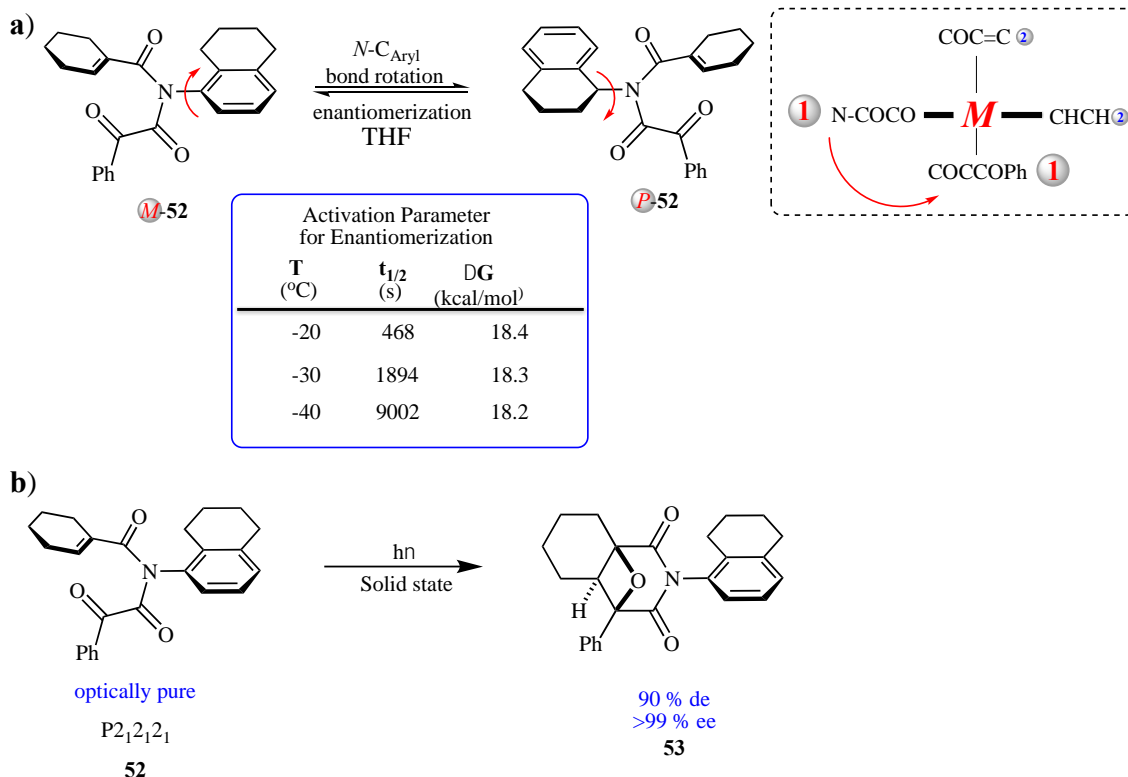
yields.<sup>64</sup> Irradiation of the  $\alpha,\beta$ -unsaturated ketone **50** in the presence of bromine gas afforded the addition product **51** in high chemical yields (>90%) albeit low optical yield 6% (Scheme 1.12) pioneering the first measurable solid state absolute asymmetric synthesis.<sup>64</sup>



**Scheme 1.12:** Asymmetric photochemistry in the solid state. Adapted from reference 63.

Since the seminal work of Schmidt and Penzien various methodologies displayed greater selectivity such as co-crystallization, ionic auxiliaries and the use of atropisomers in the solid state. In regards to the former, Sakamoto and coworkers utilized the chiral amide **52** to afford the oxetane **53** product in high diastereoselectivity (90% *de*) and enantioselectivity (>99% *ee*)(Scheme 1.13).<sup>65</sup> The torsional strain caused by steric interactions hinders rotation about the  $N\text{-C}_{\text{Aryl}}$  bond affording atropisomers in the amide **52**. Thus **52** existed in two forms *M*-**52** and *P*-**52** which are enantiomers. However, in solution the barrier to rotation is rather low for **52** thus free rotation occurs (Scheme 1.13a). Though the  $N\text{-C}$  bond rotates freely in solution achieving no selectivity in solution phase reactions the inherent chirality allowed for spontaneous crystallization of a chiral crystal. The chiral crystal of **52** was exploited by Sakamoto and coworkers to afford the aforementioned selectivity. Spontaneous crystallization of a chiral crystal is rare and limited due to inherent packing properties of the particular substrate. Their methodology lacked the ability to yield any predictive power over the photochemical transformation. Thus the use of chiral crystalline matrix is limited especially with regard to synthetic chemistry.





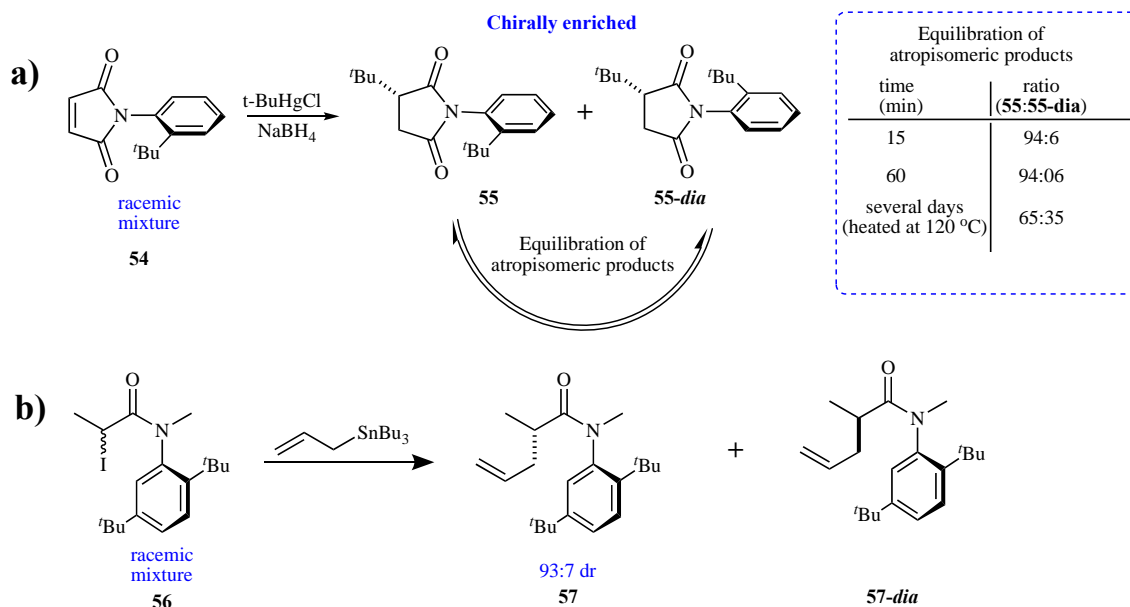
**Scheme 1.13:** Asymmetric photochemistry in the solid state. a) barrier to rotation (enantiomerization); b) solid state oxetane formation with high selectivity. Adapted from reference 64.

## 1.7. Axial to point chiral: A methodology for asymmetric photochemistry in solution

### 1.7.1. Atropisomers in thermal chemistry

Before the turn of the century Curran and coworkers demonstrated the advantageous of utilizing axial chirality for asymmetric thermal transformations. In efforts to attenuate unfavorable steric interactions with the *ortho* hydrogens of the phenyl ring the imides **54** and amides **56** exist in a twisted conformation in the ground state. Similar to the amide **52** imide **54** and amide **56** existed as stable atropisomers under specific temperature and pressures depending on the barrier to rotation of the *N*-C<sub>Aryl</sub> bond. Curran et al embarked on an investigation to relate *ortho*-aryl substitution, to *N*-Aryl torsion angle, *N*-C<sub>Aryl</sub> bond rotation and the ease of equilibrating the atropisomers.<sup>66-68</sup> They displayed the feasibility and efficacy of non-biaryl

atropisomers in asymmetric synthesis geared towards thermal transformations. Curran et al achieved success in the radical addition of both cyclic and acyclic atropisomers **54** and **56** respectively in solution (Scheme 1.14).

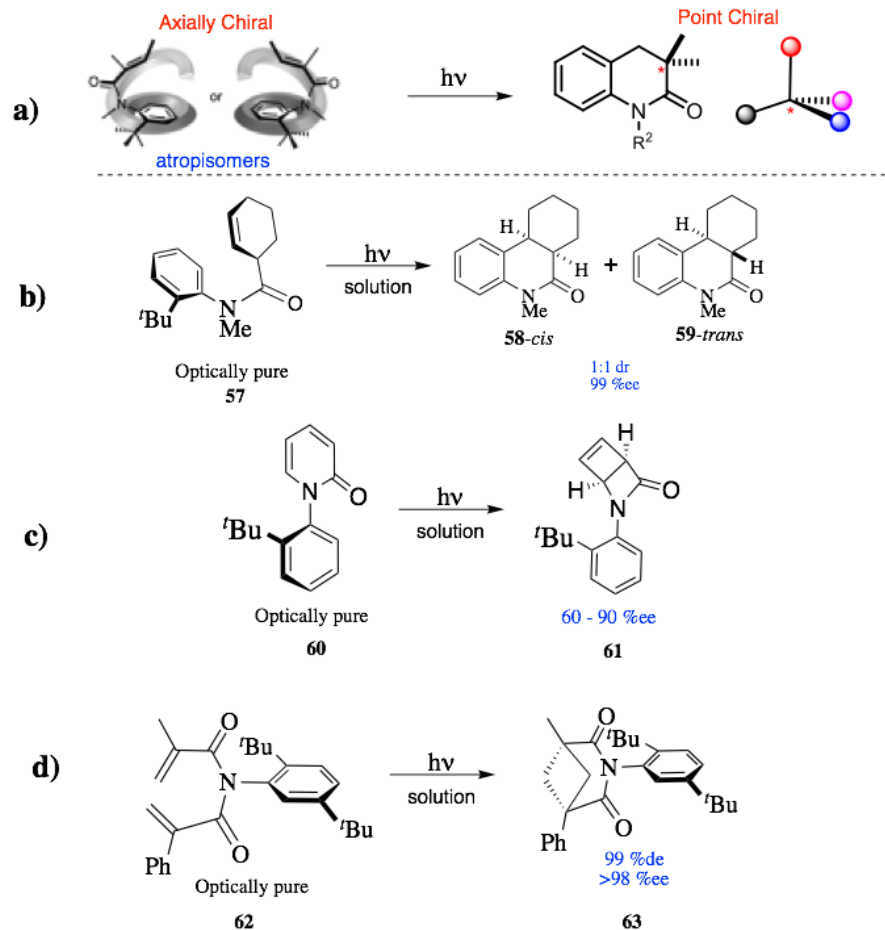


**Scheme 1.14:** Atropisomers in thermal chemistry. a) selective radical addition followed by equilibration of atropisomers; b) radical addition achieving high selectivity and stability of atropisomers. Adapted from references 65-67.

### 1.7.2. Atropisomers in photochemistry: Atropselective photoreactions

Shifting to photochemistry and focusing exclusively on the photoreactivity of the substrate Sivaguru and coworkers have devised a methodology to afford high selectivity in the photoproduct beginning from axially chiral starting material in an axial to point chiral transformation. This is a true example of axially chiral excited state chemistry. Rotamer control, is well established in the literature. Employing axially chiral rotamers, where reactant conformations dictate the mechanistic route and thus the product distribution draws inspiration from Havinga's NEER principle (Non-Equilibrating Excited Rotamers). Sivaguru and coworkers achieved success in various chemical systems such as  $6\pi$ -cyclization, [2+2]-cycloaddition, and

4 $\pi$ -cyclization highlighting their ability to transfer axial chirality to point chirality with high selectivity (Scheme 1.15).<sup>69-71</sup>



**Scheme 1.15:** Atropselective photochemical reactions. a) Axial chiral to point chiral transformation. b) 6 $\pi$ -photocyclization of acrylanilides c) 4 $\pi$ -ring closure of pyridones d) [2+2] photocycloaddition of acrylimides. Adapted from references 68-70.

## 1.8. Smart materials

Throughout the decades, light mediated processes have gained much attention due to the spatial and temporal control that light affords as an external stimulus. Light has proven useful in materials fabrication by way of photolithography and smart materials e.g. photochromic lenses. The 21<sup>st</sup> century has seen the rise of smart materials and molecular machines. In order for a smart

material to operate utilizing light there needs to be an appropriate chromophore which upon excitation affords some observable change i.e. color, pH or transparency etc. Various scaffolds have proven useful to aid in the operation of smart materials such as photoacids and photoinitiators.

## 1.9. Photoacids

As mentioned above light has been utilized for various industrial processes namely photolithography. In order to exploit the benefits of light, temporal and spatial control, an appropriate light harvesting reagent is necessary. This change in acidity can be exploited for device fabrication, kinetic investigations, small molecule systems and to manipulate chemical systems (e.g. smart materials). In a broad sense, photoacids are molecules that increase in acidity upon irradiation of light. Photoacids have been exploited for their ability to alter a chemical system by use of light as an external stimulus. There exists three type of photoacids 1) reversible photoacids 2) meta-stable photoacids and 3) photoacid generators (PAGs).

### 1.9.1. Reversible photoacids

Reversible photoacids are aromatic molecules that have an excited-state  $pK_a$  lower than the ground state  $pK_a$ . As the name implies, reversible photoacids are reversible in that the increased acidity, due to irradiation, dissipates as irradiation ceases. By way of structure, reversible photoacids are hydroxyl substituted aromatics. Excitation of an appropriate hydroxy arene accessing  $\pi-\pi^*$  singlet excited state often results in proton dissociation in the excited state.<sup>72-74</sup> If the dissociation of the resultant conjugate base and proton ( $k_{diss}$ ) is of sufficient lifetime permitting solvent separation an increase in acidity (Bronstead acidity) can result. Hence the synonymous term with photoacid is excited state proton transfer. Photoacids have been displayed to exhibit excited state acidities ( $pK_a^*$ ) with pH as low as -8 when compared to the

corresponding ground state acid. Photoacids can transport protons faster than the picosecond time scale.<sup>72-74</sup> Emission properties of photoacids are mainly dominated by excited state conjugate base. Characteristic of their excited state increase in acidity is a redshift in the emission spectra. The magnitude of the Stokes shift is proportionate to the shift in acidity.<sup>19</sup>

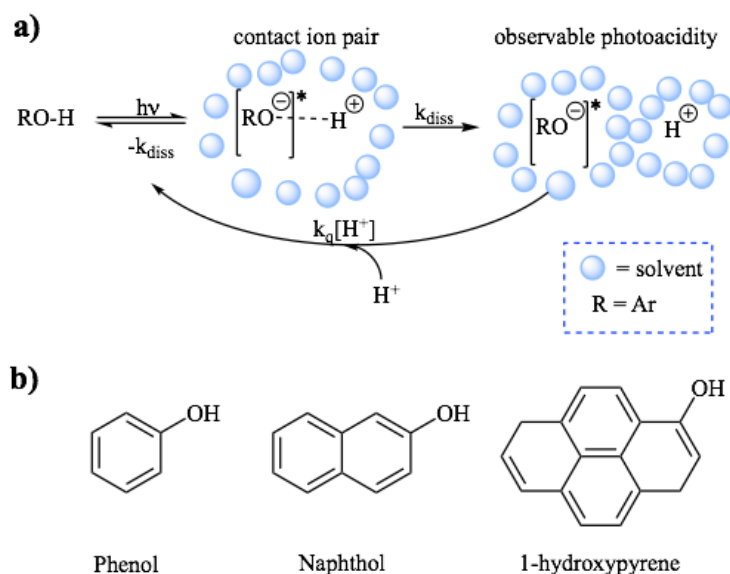
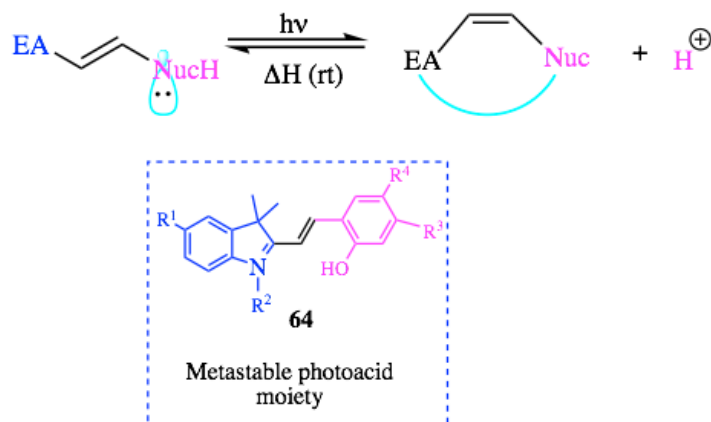


**Figure 1.6:** Reversible photoacids a) process of excited state proton transfer (photoacidity) b) common photoacids

### 1.9.2. Metastable photoacids

Metastable photoacids are another class of reversible photoacids. The difference between metastable photoacids and simple reversible photoacids lies in the length of time that the increased acidity persists. As mentioned above removal of light source causes simple reversible photoacids to return to its ground state thus decreasing the overall acidity. Metastable photoacids upon irradiation undergo some secondary reaction which gives rise to an intermediate species of relatively long lived life time. In absence of the light source re-protonation of the intermediate species occurs slowly allowing the acidity to persist for some finite time while in the dark. The design of a metastable photoacid features and electron-accepting unit and a nucleophilic moiety

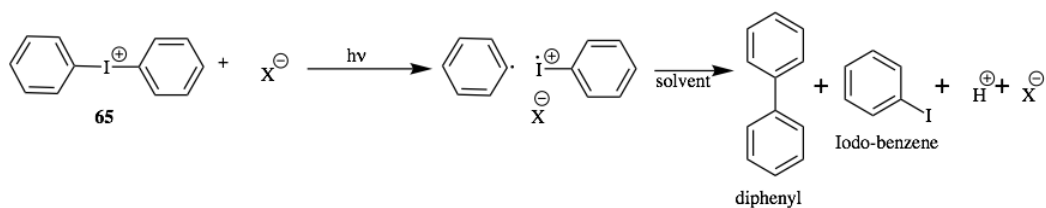
often resembling familiar photochromic molecules (Scheme 1.16). Metastable photoacids find utility in operating molecular machines and smart materials. The high acidity of activated metastable photoacids and the ability to modulate the rate of re-protonation by way of synthetic modification are just a few benefits of metastable photoacids.



**Scheme 1.16:** Design and operation of metastable photoacids. Adapted from reference 75.

### 1.9.3. Photoacid generators (PAGs)

Photoacid generators differ fundamentally from both metastable photoacids and reversible photoacids. PAGs are commonly called irreversible photoacids. PAGs generally undergo a series of decomposition processes in order to afford either a mineral acid or some strong organic acid (Scheme 1.17). Irradiation causes rapid decomposition of the PAGs liberating a high concentration of the resultant small molecule acid. It is this rapid shift in proton concentration that is responsible for the photoacidity of PAGs. PAGs find great utility in photolithography.<sup>75</sup> Simple functional group manipulation allows for the PAG unit to be incorporated within a polymer.<sup>75-77</sup> Irradiation of the resulting polymer activates the PAG to accomplish the desired patterning. Activation of the PAG achieves two objectives, activation increases the acidity followed by removal (in this case decomposition) of the PAG. Figure 1.7 displays some known PAGs.



**Scheme 1.17:** Photoreactivity of PAGs **64**. Adapted from reference 74.

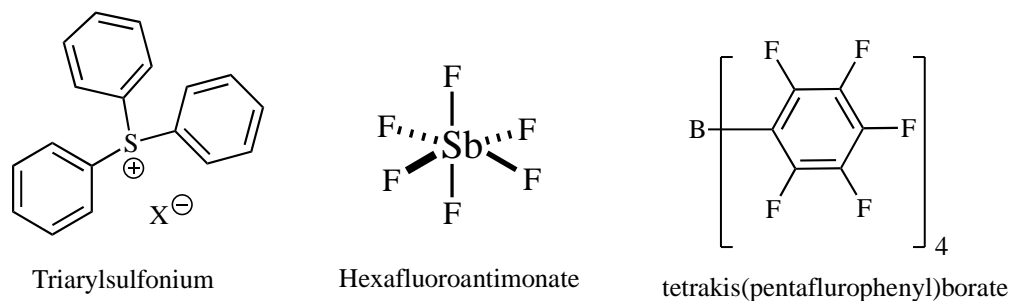
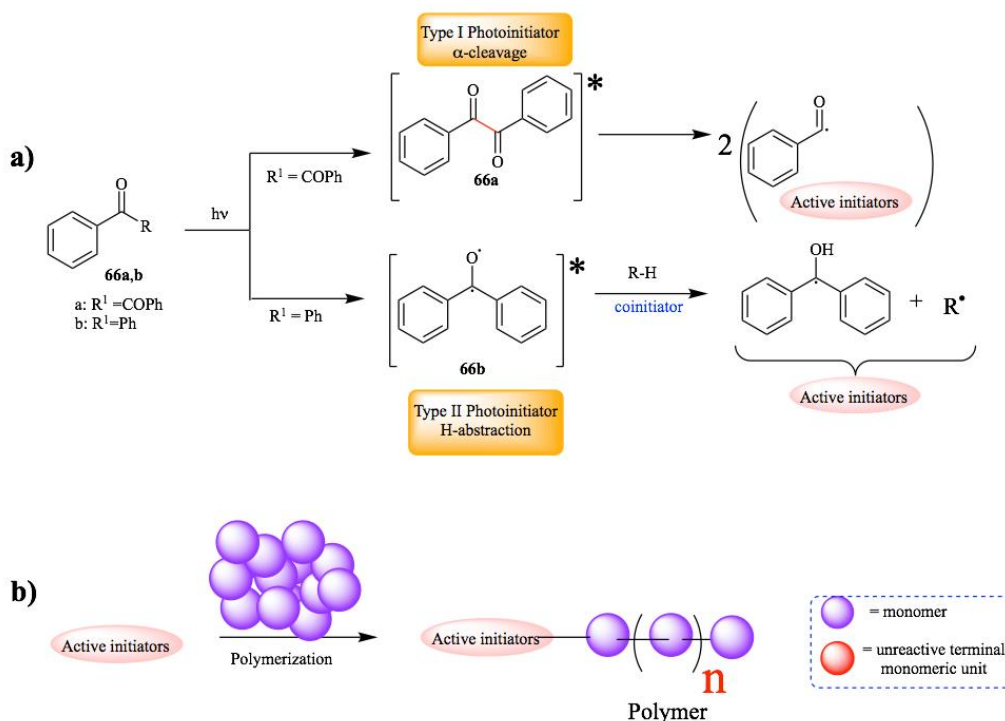


**Figure 1.7:** Chemical structure of known Photoacid Generators.

### 1.10. Photoinitiators

Since the turn of the century innovations involving polymeric materials has reshaped and redefining the world. Today, photochemical methods of fabrication lead the charge towards sustainable methods and materials. In this regard photoinitiators have been used for various applications such as polymerization, photocuring and device fabrication, to simply list a few. There exist two main classes of photoinitiators Type I ( $\alpha$ -cleavage) and Type II (H-abstraction). Type I is an unimolecular processes. Type II photoinitiators necessitate the use of a co-initiator with an hydrogen available for abstraction. It is quite generally the co-initiator that initiates the polymerization process. However, it is possible for the geminate photoinitiator radical to initiate polymerization. Thus creating the active initiator for polymerization utilizing Type II photoinitiators is a bimolecular process and therefore limited by diffusion. Optimal polymerization necessitates synergy between the initiator and co-initiator. Though they differ

with respect to mechanistic pathway, both Type I and Type II photoinitiators form active initiator species that proceed to polymerization by reaction with a monomer (Scheme 1.16). Upon irradiation excitation to the singlet excited state occurs followed by intersystem crossing to the triplet excited state. In the triplet excited state Type I photoinitiators undergo homolytic cleavage while Type II photoinitiators abstract an available neighboring hydrogen. Both of which eventually form reactive radical intermediates (active initiators) that go on to initiate the polymerization process (Scheme 1.16). Spatial and temporal control, the ability to make high energy intermediates at room temperature and the simplicity of photoinitiators are just a few inherent advantages of photoinitiators over commonly employed thermal reagents.<sup>78, 79</sup>



**Scheme 1.18:** a) Type I and Type II photoinitiators b) polymerization.



### **1.11. Summary and outlook**

As mentioned above the use of light has permeated all aspects of life from sustaining life to various industrial fields. Fundamental investigations aimed at exploiting the abundance of light has seen great advancement in the past century. Asymmetric photochemical methodologies as well as material fabrications have also seen respectable advances. Chapters 2-3 will outline photochemical investigations affording high selectivity in the photoproduct taking advantage of the chiral bias of atropisomers.<sup>80,81</sup> Chapters 4 and 5 will highlight applications of light utilizing its ability to do work and afford spatial and temporal control by way of photoacids and photoinitiators respectively.<sup>82</sup>

## 1.12. References

1. Albini, A.; Dichiarante, V., *Photochemical & Photobiological Sciences* **2009**, 8 (2), 248-254.
2. Roth, H. D., *Angewandte Chemie International Edition in English* **1989**, 28 (9), 1193 - 1207.
3. Roth, H. D. Y., *Photochemical & Photobiological Sciences* **2011**, 10 (12), 1849 - 1853.
4. Klán, P.; Wirz, J., *Photochemistry of Organic Compounds: From Concepts to Practice*. John Wiley and Sons Ltd: United Kingdom, 2009.
5. Raghunathan, R. *Photons in Action: Asymmetric Synthesis and Polymer Degradation*. North Dakota State University, Fargo, North Dakota, 2016.
6. Turro, N. J.; Ramamurthy, V.; Scaiano, J. C., *Modern Molecular Photochemistry of Organic Molecules*. University Science Books: Sausalito, CA, 2010; p 1084.
7. Turro, N. J.; Ramamurthy, V.; Scaiano, J. C., *Modern Molecular Photochemistry of Organic Molecules*. 2010; p 1084.
8. Swinehart, D. F., *Journal of Chemical Education* **1962**, 39 (7), 333 - 335.
9. Kasha, M., *Discussions of the Faraday Society* **1950**, (9), 14-19.
10. *CRC Handbook of Chemistry and Physics*. 84 ed.; CRC Publisher: 2003-2004.
11. Klessinger, M.; Michl, J., *Excited States and Photochemistry of Organic Molecules*. VCH Publishers, Inc.: 1995.
12. Lakowicz, J. R., *Principles of Fluorescence Spectroscopy*. 3 ed.; Springer US: 2006.
13. Kahler, *Arch. Pharm.* **1830**, 34, 318.
14. Trommsdorff, H., *Ann. Chem. Pharm.* **1834**, 11, 190-208.
15. Heldt, W., *Ann. Chem. Pharm.* **1847**, 63, 10-47.

16. Natarajan, A.; Tsai, C. K.; Khan, S. I.; McCarren, P.; Houk, K. N.; Garcia-Garibay, M. A., *Journal of the American Chemical Society* **2007**, *129* (32), 9846 - 9847.
17. Cannizzaro, S.; Sestini, F., *Gazz. Chim. Ital.* **1873**, *6*, 241 - 251
18. Sestini, F., *Gazz. Chim. Ital.* **1876**, *6*, 367-369.
19. Sestini, F., *Gazz. Chim. Ital.* **1879**, *9*, 298-304.
20. Sestini, F.; Danesi, L., *Gazz. Chim. Ital.* **1882**, *12*, 82 - 83.
21. Cannizzaro, S., *Gazz. Chim. Ital.* **1876**, *6*, 341 - 348.
22. Cannizzaro, S., *Gazz. Chim. Ital.* **1876**, *6*, 355 - 356.
23. Ciamician, *Science* **1912**, *36*, 384 - 294.
24. Schuster, D. a. I.; Lem, G.; Kaprinidis, N. A., *Chemical Reviews* **1993**, *93* (1), 3 - 22.
25. Becker, H. D., *Chemical Reviews* **1993**, *93* (1), 145 - 172.
26. Poplata, S.; Tr ö ster, A.; Zou, Y.-Q.; Bach, T., *Chemical Reviews* **2016**, *117* (17), 9748 - 9815.
27. Hoffmann, N., *Chemical Reviews* **2008**, *108* (3), 1052 - 1103.
28. Paterno, E.; Chieffi, G., *Gass. Chim. Ital.* **1909**, *39*, 341.
29. Suh, I.-H.; Park, K. H.; Jensen, W. P.; Lewis, D. E., *Journal of Chemical Education* **1997**, *74* (7), 800 - 805.
30. Biot, J. B., *Mem. Acad. Sci. inst.* **1819**, *2*, 41.
31. Barron, L. D., An Introduction to Chirality at the Nanoscale. In *Chirality at the Nanoscale: Nanoparticles, Surfaces, Materials and more*, Amabilino, D. B., Ed. Wiley-VCH Verlag GmbH & Co.: Weinheim, Germany, 2009; pp 1 - 27.
32. Pasteur, L., *Ann. Chim. Phys.* **1848**, *24* (3), 442.
33. Kagan, H. B.; Gopalaiah, K. Y., *New Journal of Chemistry* **2011**, *35* (10), 1933 - 1937.

34. Marckwald, M., *Ber. Dtsch. Chem. Ges.* **1904**, 37 (2), 1368.
35. Kenyon, J.; Ross, W. A. Y., *Journal of the Chemical Society (Resumed)* **1952**, 0 (0), 2307 - 2310.
36. Hartwig, J. F., *Organotransition metal chemistry : from bonding to catalysis*. 2010; 1,127 pages.
37. Walsh, P. J.; Kozlowski, M. C., *Fundamentals of asymmetric catalysis*. University Science Books: United States of America, 2009; p 674 pages.
38. Anslyn, E. V.; Dougherty, D. A., *Modern Physical Organic Chemistry*. University Science: Sausalito, CA, 2006.
39. Van't Hoff, J. H., Die Lagerung der Atom and Raume. 2nd edn ed.; 1894; p 30.
40. Le Bel, J. A., *Bull. Soc. Chim. Fr.* **1874**, 22.
41. Rau, H., *Chemical Reviews* **1983**, 83 (5), 535 - 547.
42. Inoue, Y., *Chemical Reviews* **1992**, 92 (5), 741 - 770.
43. Avalos; n, M. í.; Babiano, R.; Cintas, P.; Jiménez , J. L.; Palacios, J. C.; Barron, L. D., *Chemical Reviews* **1998**, 98 (7), 2391 - 2404.
44. Buchardt, O., *Angewandte Chemie International Edition in English* **1974**, 13 (3), 179 - 185.
45. Kagan, H.; Moradpour, A.; Nicoud, J. F.; Balavoine, G.; Tsoucaris, G., *Journal of the American Chemical Society* **1971**, 93 (9), 2353 - 2354.
46. Cavazza, M.; Morganti, G.; Zandomenighi, M. Y., *Journal of the Chemical Society, Perkin Transactions 2* **1984**, 0 (5), 891 - 895.
47. Nicoud, J. F.; Kagan, H. B., *Israel Journal of Chemistry* **1976**, 15 (1-2), 78 - 81.

48. Richardson, R. D.; Baud, M. G. J.; Weston, C. E.; Rzepa, H. S.; Kuimova, M. K.; Fuchter, M. J. Y., *Chemical Science* **2015**, *6* (7), 3853 - 3862.
49. Kuhn, W. Y., *Transactions of the Faraday Society* **1930**, *26* (0), 293 - 308.
50. Lange, G. L.; Decicco, C.; Lee, M., *Tetrahedron Letters* **1987**, *28* (25), 2833 - 2836.
51. Hoffman, N.; Scharf, H.-D.; Runsink, J., *Tetrahedron Letters* **1989**, *30* (20), 2637 - 2638.
52. Hammond, G. S.; Cole, R. S., *Journal of the American Chemical Society* **1965**, *87* (14), 3256 - 3257.
53. Inoue, Y.; Yamasaki, N.; Shimoyama, H.; Tai, A., *The Journal of Organic Chemistry* **1993**, *58* (7), 1785 - 1793.
54. Aratani, T.; Nakanisi, Y.; Nozaki, H., *Tetrahedron* **1970**, *26* (7), 1675 - 1684.
55. Inoue, Y.; Yamasaki, N.; Yokoyama, T.; Tai, A., *The Journal of Organic Chemistry* **1992**, *57* (5), 1332 - 1345.
56. Kim, J. I.; Schuster, G. B., *Journal of the American Chemical Society* **1990**, *112* (26), 9635 - 9637.
57. Bauer, A.; Westkämper, F.; Grimme, S.; Bach, T., *Nature* **2005**, *436* (7054), 1139 - 1140.
58. Vallavoju, N.; Selvakumar, S.; Jockusch, S.; Sibi, M. P.; Sivaguru, J., *Angew. Chem. Int. Ed.* **2014**, *53* (22), 5604-5608.
59. Vallavoju, N.; Selvakumar, S.; Pemberton, B. C.; Jockusch, S.; Sibi, M. P.; Sivaguru, J., *Angewandte Chemie International Edition* **2016**, *55* (18), 5446 - 5451.
60. Meggers, E. Y., *Chemical Communications* **2015**, *51* (16), 3290 - 3301.
61. Bach, T.; Bergmann, H.; Harms, K., *Organic Letters* **2001**, *3* (4), 601 - 603.
62. Vallavoju, N.; Sivaguru, J., *Chemical Society Reviews* **2014**, *43* (12), 4084-4101.
63. Ramamurthy, V.; Sivaguru, J., *Chemical Reviews* **2016**, *116* (17), 9914 - 9993.

64. Penzien, K.; Schmidt, G. M. J., *Angewandte Chemie International Edition in English* **1969**, 8 (8), 608 - 609.
65. Sakamoto, M.; Iwamoto, T.; Nono, N.; Ando, M.; Arai, W.; Mino, T.; Fujita, T., *The Journal of Organic Chemistry* **2003**, 68 (3), 942 - 946.
66. Curran, D. P.; DeMello, N. C., *Journal of the Chemical Society, Chemical Communications* **1993**, (17), 1314-1317.
67. Curran, D. P.; Qi, H.; Geib, S. J.; DeMello, N. C., *Journal of the American Chemical Society* **1994**, 116 (7), 3131-3132.
68. Curran, D. P.; Geib, S.; DeMello, N., *Tetrahedron* **1999**, 55 (18), 5681-5704.
69. Clay, A.; Kumarasamy, E.; Ayitou, A. J. L.; Sivaguru, J., *Chemistry Letters* **2014**, 43 (12), 1816-1825.
70. Kumarasamy, E.; Jesuraj, J. L.; Omlid, J. N.; Ugrinov, A.; Sivaguru, J., *J. Am. Chem. Soc.* **2011**, 133, 17106-17109.
71. Kumarasamy, E.; Ayitou, A. J. L.; Vallavoju, N.; Raghunathan, R.; Iyer, A.; Clay, A.; Kandappa, S. K.; Sivaguru, J., *Accounts of Chemical Research* **2016**, 49 (12), 2713-2724.
72. Pines, E., UV-Visible spectra and photoacidity of Phenols, Naphthols and Pyrenols. . In *The chemistry of phenols*, Rappoport, Z., Ed. Wiley: Chichester, England ; Hoboken, NJ, 2003.
73. Pines, E., The Kinetic Isotope Effect in The Photo-Dissociation Reaction of Excited-State Acids in Aqueous Solution. In *Isotope effects in chemistry and biology*, Kohen, A.; Limbach, H.-H., Eds. Taylor & Francis: Boca Raton, 2006; pp 451-464.

74. Pines, D.; Pines, D., Solvent Assisted Photoacidity. In *Hydrogen-Transfer Reactions*, Hynes, T.; Klinman, J. P.; Limbach, H.-H.; Schowen, R. L., Eds. Wiley Imprint: Weinheim, Germany, 2007.
75. Liao, Y., *Accounts of Chemical Research* **2017**, 50 (8), 1956-1964.
76. Gupta, M. G. Photoacid Generators for Catalytic Decomposition of Polycarbonate. Georgia Institute of Technology Georgia, USA, 2006.
77. Klikovits, N.; Knaack, P.; Bomze, D.; Krossing, I.; Liska, R. Y., *Polymer Chemistry* **2017**, 8 (30), 4414 - 4421.
78. Chatani, S.; Kloxin, C. J.; Bowman, C. N. Y., *Polym. Chem.* **2014**, 5 (7), 2187-2201.
79. Fouassier, J. P.; Lalevée, J., *Polymers* **2014**, 6, 2588-2610.
80. Clay, A.; Vallavoju, N.; Krishnan, R.; Ugrinov, A.; Sivaguru, J., *Journal of Organic Chemistry*, **2016**, 81 (16), 7191-7200.
81. Ayitou, A. J.L-; Clay, A.; Elango, K.; Jockusch, S.; Sivaguru, J., *Photochemical & Photobiological Sciences*, **2013**, 13, 141-144.
82. Clay, A.; Krishnan, R.; Sibi, M.P.; Webster, D.; Jockusch, S.; Sivaguru, J., *Journal of Photochemistry and Photobiology A*, **2017**, DOI: 10.1016/j.jphotochem.2017.11.039

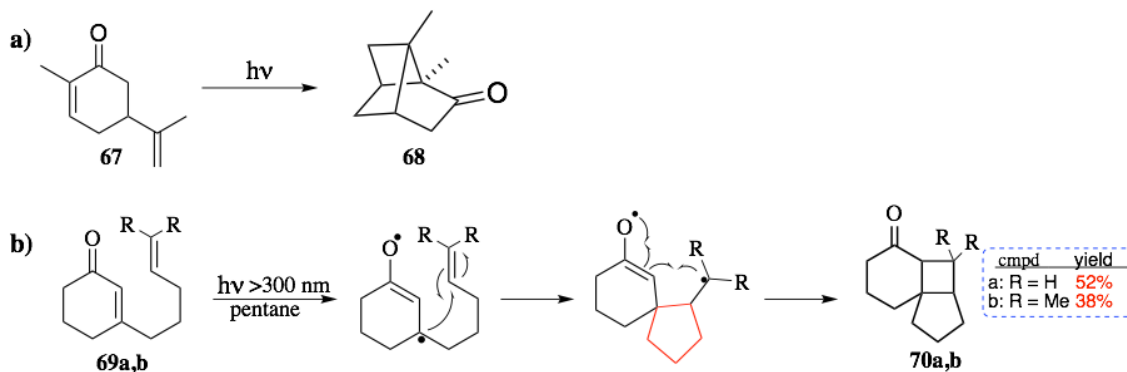
## 2. METAL FREE VISIBLE LIGHT MEDIATED PHOTOCATALYSIS: CONTROLLING INTRAMOLECULAR [2+2] PHOTOCYCLOADDITION OF ENONES THROUGH AXIAL CHIRALITY

### 2.1. Introduction to [2+2] photocycloaddition: Rule of five

The first reported intramolecular enone-olefin photocycloaddition is dated back to 1908. In 1908 Ciamician, the Italian chemist, exposed carvone **67** to “Italian sunlight” for a prolonged period of time forming carvone camphor **68** (Scheme 2.1a).<sup>1-3</sup> In 1957 Büchi and Goldman revisited photocycloaddition of carvone to camphor unequivocally determining the structure of **68**.<sup>4,5</sup> Since the photochemical investigations of Ciamician on carvone, various chemists investigated enone-olefin cycloadditions, such as Corey, Turro, Schuster, Eaton and de Mayo to simply list a few.

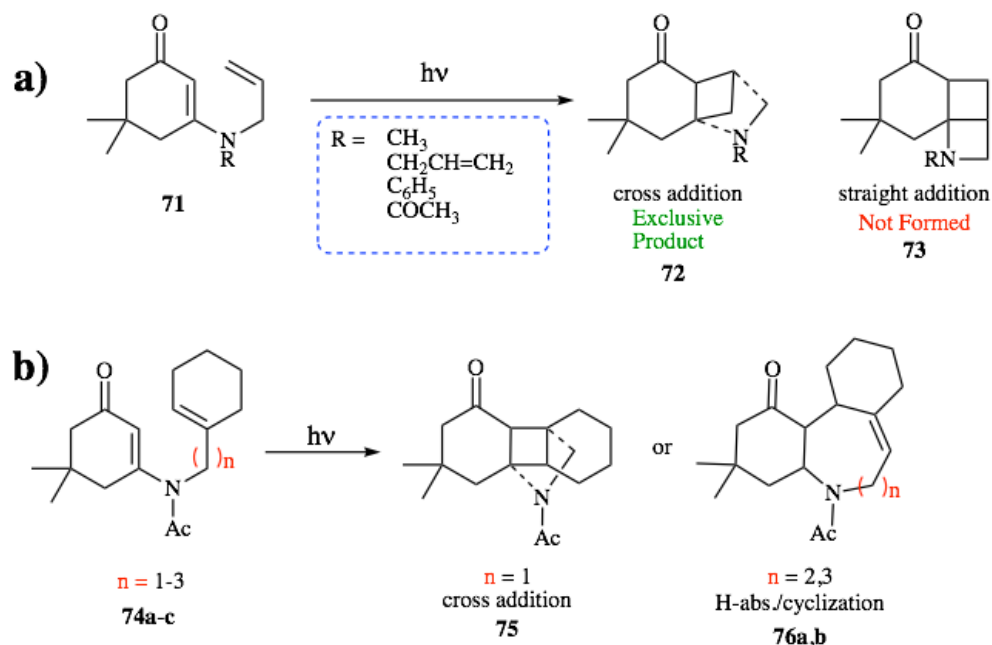
Focusing on intramolecular [2+2] photocycloadditions which allows for greater control and thus greater selectivity, over the years much work has been focused on tethered enone-olefin systems (e.g. Scheme 2.1b). Tethering the olefin and enone allows greater control with a respectable level of predictability in photocycloadditions.<sup>6</sup> It is commonly accepted that cycloadditions between a triplet and singlet reactive partner (e.g. enone and olefin respectively) afford a biradical intermediate. Often the biradical intermediate contains a five-membered ring when possible in route to form the desired product. This five-membered ring also sets the regiochemistry of the product as seen in **70a,b**.





**Scheme 2.1:** [2+2] intramolecular photocycloaddition; Irradiation of carvone forming carvone camphor; b) triplet enone addition to singlet olefin tether forming cyclobutane product via five-membered ring intermediate. Adapted from reference 6 and 7.

Tamura and coworkers investigated the bearing of heteroatoms in tethered enone-olefin [2+2] photocycloadditions. In agreement with the rule of five only cross addition product **72** was formed. Additionally, Tamura and coworkers noticed that the free nitrogen electrons, when the nitrogen was unsubstituted or merely bear an alkyl substitution, the reaction was sluggish and suffered from diminished yields. This indicated that the nitrogen electron hindered the photochemical reaction.<sup>7</sup> In a similar investigation Schell and coworkers utilized differing alkenyl tethers which altered the reactivity. A tether longer than three carbons total resulted in a different product formation entirely. Increasing the chain length precludes the formation of a five membered ring intermediate thus the rule of five no longer applies. It is hypothesized that **76** is formed due to H-abstraction that occurs from a plausible ring closed 6-7-6 tricyclic ring intermediate. Overall tethering the alkene addition partner allows for greater predictability and reduced formation of side products. Utilizing alkenyl tether of three carbon length allows for formation of fused ring cyclobutane product(s).



**Scheme 2.2:** Heterocyclic [2+2] photocycloaddition; a) optimizing *N* substitution b) optimizing alkenyl tether.

## 2.2. Thermal cyclobutane formation

The cyclobutane moiety exists in numerous natural products often with inherent biological activity ranging from antivirals to antibiotics. Its relevance alone makes the development of new methods for the synthesis of cyclobutanes of great interest to pharmaceutical, biological, medicinal and natural product scientists alike.<sup>8-15</sup> Figure 2.1 displays natural products containing cyclobutane motif.<sup>16-18</sup> Additionally, cyclobutane analogues have proven as useful scaffolds for various functional group manipulations in synthetic organic and materials chemistry.<sup>10,19</sup>

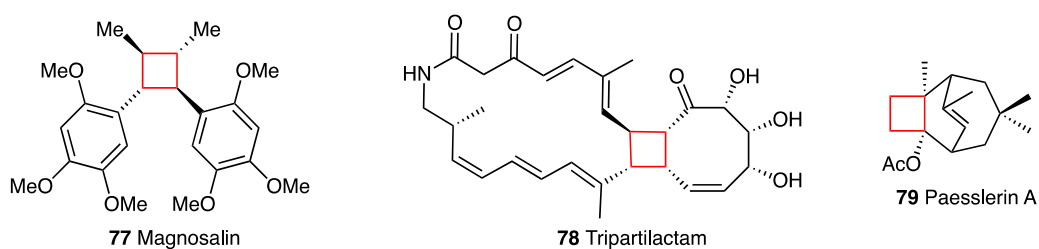
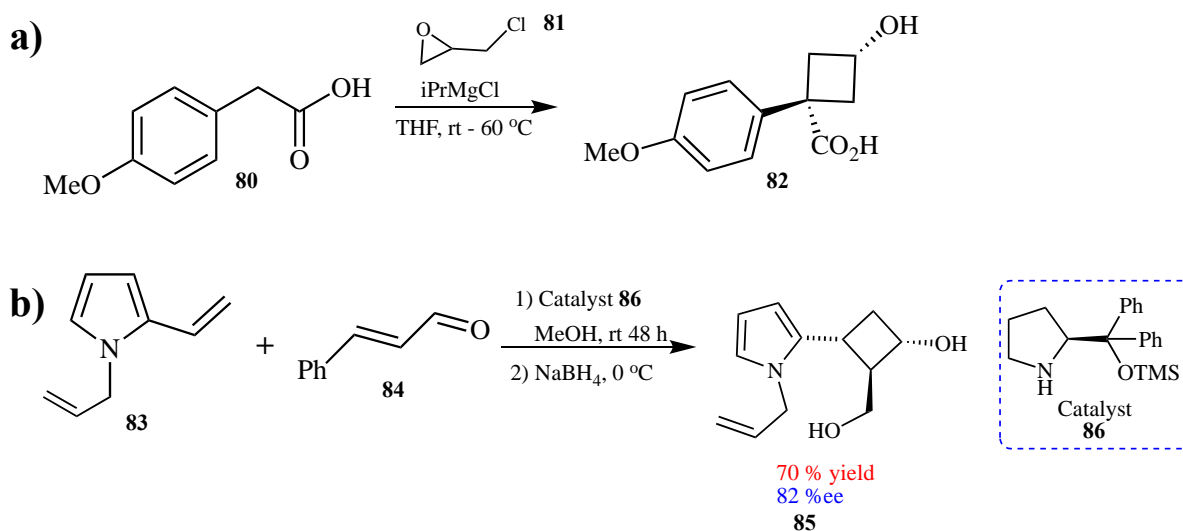


**Figure 2.1:** Natural products containing cyclobutane

Not only has cyclobutane analogues proven useful as intermediates for various functional group manipulations cyclobutane moiety is also a formidable challenge to access in natural product synthesis.<sup>8,10,11,14</sup> Surveying the literature, it can be seen that organic chemists have transitioned from sole dependency on early transition metal techniques<sup>20</sup> to organocatalytic methodologies. Over the past few decades, a plethora of thermal methods have been displayed including [2+2] cycloadditions involving reactive reagents such as ketenes, ketenamines<sup>21</sup> and enamines as well as enantioselective methods involving chiral allenes and organocatalysts.<sup>16,20,22-</sup>

25



**Scheme 2.3:** Thermal synthesis of cyclobutane derivatives. a) double alkylation reaction with epichlorohydrin to afford cyclobutane **82**. b) Use of catalyst assisted in situ ketenamine cycloaddition to afford cyclobutane **85**. Adapted from references 20 and 21 respectively.

Success in achieving the desired cyclobutane adduct in high specificity, in the latter mentioned thermal method generally hinges upon the reactivity of the employed organic catalyst. Access and overall utility of these small molecule organic catalysts are obvious drawbacks to the organocatalytic techniques.<sup>16,22-25</sup>

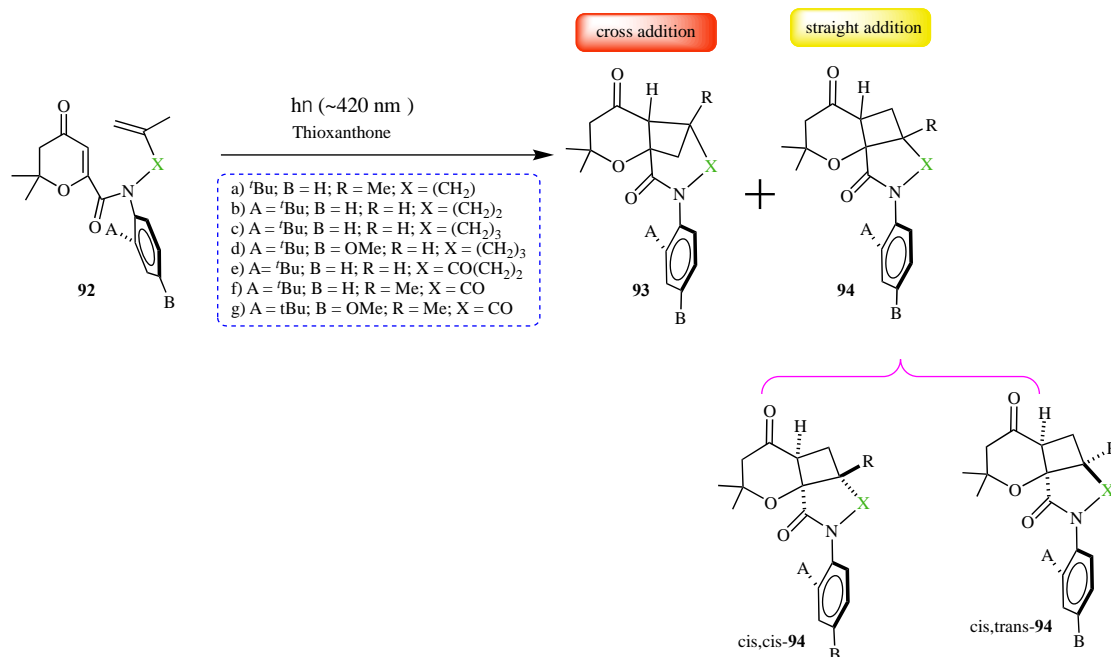
### 2.3. Photochemical cyclobutane formation

In contrast to thermal methods photochemical methods too have been employed in order to afford cyclobutane adducts. Photochemistry is unmatched in its ability to yield complex structures from simple and easily accessible reactants. Additionally, compounds with multiple stereocenters can be easily accessible by utilizing photochemistry. The short lifetimes involved in photochemical reactions lead to multiple photoproducts with stereocenters reducing its appeal. Efforts to address the complex reactivity and selectivity involved in photochemical transformations have met with differing success. Organized media yield amongst the highest of selectivity due to the lack of degrees of freedom during the photochemical transformation. Supramolecular scaffolds such as crystals, zeolites, assorted molecular cages and hydrogen bonding templates have been utilized to control excited state reactivity.<sup>26-28</sup>

Progress has been made throughout the past decade, wherein photochemical transformations in the absence of organized media with the advent of novel photocatalytic methods. Recently, photoredox chemistry received particular attention,<sup>22,23,29-34</sup> wherein one electron oxidation or reduction of the reactant by a light-absorbing sensitizer generates a ground state radical anion/cation. The ground state radical anion/cation undergoes an increase in potential thus electron transfer enhances its reactivity thereby making it react effectively from the ground state to form products. Following the ecofriendly trend of green chemistry, many chemists such as MacMillan, Stephenson, Yoon, Nicewicz and Akita to simply list a few, have employed ruthenium and iridium catalysts for various visible light mediated SET (single electron transfer) processes including [2+2] cycloadditions forming various cyclobutane derivatives (Scheme 1.10c).<sup>2,3</sup>

Other noteworthy photochemical methodologies is the use of chiral templates and organic photocatalyst for the formation of cyclobutane rings. Scheme 1.10b and Scheme 1.11b highlight the contributions from the groups of Sivaguru and coworkers and Bach and co-workers of photochemical investigations affording high selectivity in the desired photoproduct(s). Though the aforementioned methodologies have garnered success, the question is still left to answer, how does one control the excited state of the substrate in solution and afford selectivity of the product without the use of some external reagent?

Efforts to address this question necessitates evaluation of new approaches to control reactivity and achieve selectivity from the excited state of the reactant due to its short lifetimes. In this regard, atropisomeric chromophores were employed<sup>35-43</sup> to control excited state reactivity.<sup>44</sup> It has been displayed that excited state rotamer control<sup>45-55</sup> can be employed to achieve high enantio- and diastereo- selectivity in the photoproduct in solution at ambient conditions. The utility of this methodology has been highlighted in various systems with differing photochemical transformations *viz.*,  $6\pi$ -photocyclization,<sup>45-48</sup> Norrish-Yang cyclization,<sup>49,50</sup>  $4\pi$ -ring closure,<sup>51</sup> Paternò-Büchi reaction<sup>52</sup> and various photocycloadditions (Scheme 1.15).<sup>53-55</sup> In efforts to further increase the scope, display the breadth and highlight the excited state control of the methodology employed, focusing attention on [2+2] photocycloaddition of enones **92** leading to cyclobutanes photoproducts **93** and **94** (Scheme 2.4).



**Scheme 2.4:** Intramolecular photocycloaddition of atropisomeric enones **92a-g**.

## 2.4. Photocycloaddition of enones

Enones have been utilized extensively to synthesize various natural products employing photochemical methodologies.<sup>4,56</sup> Enones often feature a mixture of  $n\pi^*$  and  $\pi\pi^*$  excited states.<sup>57</sup>

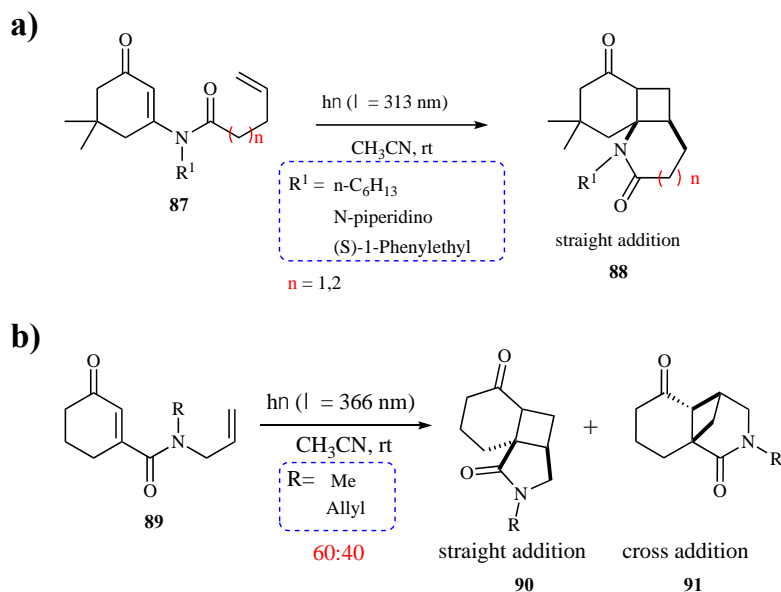
Thus the reactivity of enones can differ by simply manipulating the reaction conditions.

Additionally, the implementation of atropisomers can further alter the reactivity of enones.

Numerous groups previously investigated the complexities involved in photochemical

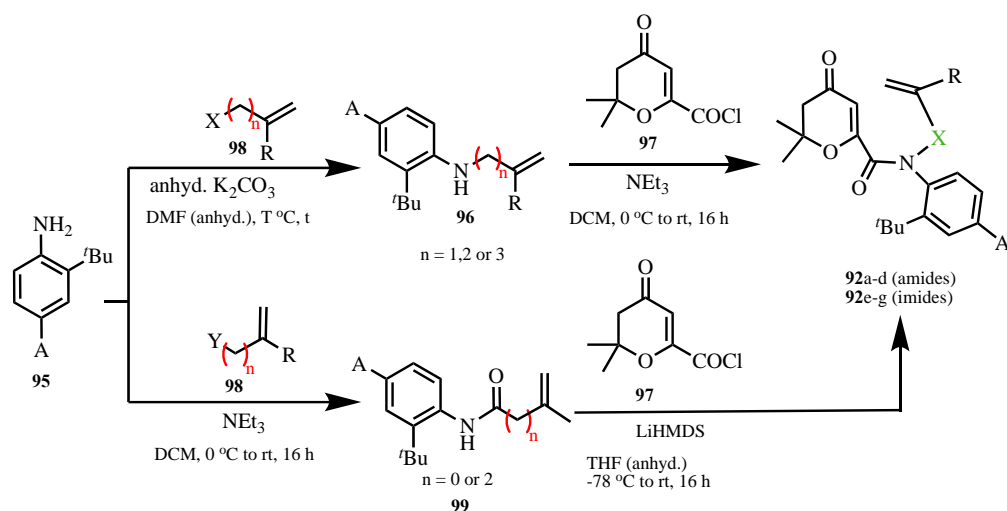
cycloadditions of enones.<sup>8,9,58-60</sup> Piva and co-workers evaluated the [2 + 2] photocycloaddition of enone-amides with *N*-allyl substitution. Piva and coworkers observed that product formation slightly favored straight addition with a straight-to-cross addition ratio of 60:40.<sup>61,62</sup>

Investigations unveiled that both reactivity and selectivity were impacted by *N*-substitution (Scheme 2.4).



**Scheme 2.5:** Photochemical cyclobutane formation. a) Photocyclization of enone-amides exclusively straight addition and b) Photocyclization of enone-amides cross vs straight addition. Adapted from references 61 and 62.

Thus a platform has arisen to highlight our methodology involving atropisomers to control the reactivity of enones. In this regard, the two sets of enones, enone-amides **92a–d** and enone-imides **92e–g**, were synthesized and their photo-chemical properties evaluated for atropselective [2 + 2] photocycloaddition. Atropisomeric enone-amides **92a–d** and enone-imides **92e–g** with varying substitutions were synthesized from the corresponding aniline derivative (Scheme 2.5) and evaluated for [2 + 2] photocycloaddition. Chart 2.1 displays the atropisomeric enones, various intermediates needed for synthesis of the atropisomeric enones and the corresponding cyclobutane products. Atropisomeric enones were characterized by  $^1\text{H}$  and  $^{13}\text{C}$  NMR spectroscopy, high- resolution mass spectrometry, and single-crystal XRD.



**Scheme 2.6:** Synthesis of atropisomeric enone-amides

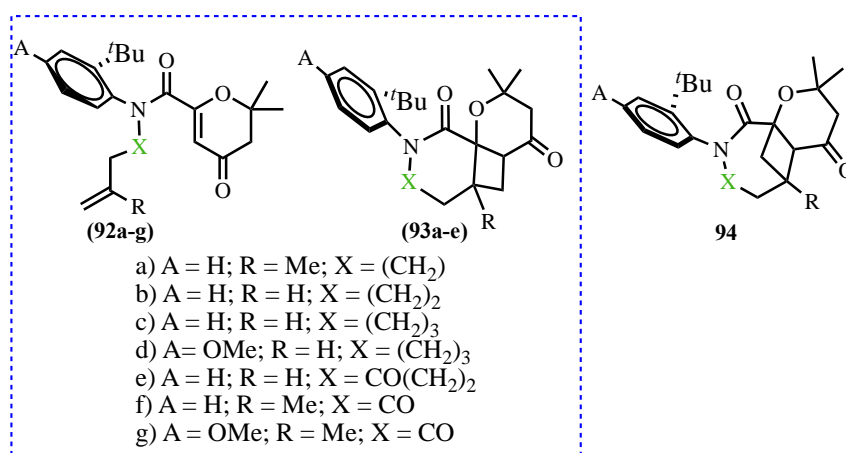


**Chart 2.1.** Structures of atropisomeric enones **92a-g**, and their corresponding photoproducts.

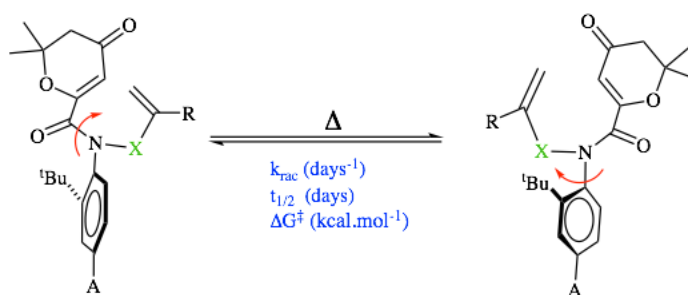
## 2.5. Racemization kinetics of atropisomeric enones

In order to employ atropisomeric enones for controlling photoreactions, the activation barrier for racemization (*N*-C<sub>Aryl</sub> bond rotation) of enones were evaluated. The individual atropisomers of enones were separated on a chiral stationary phase using preparative HPLC. As the atropisomers were stable at room temperature, the racemization barrier at 45 °C in toluene and acetonitrile were ascertained. Inspection of Table 2.1 reveals a high barrier for *N*-C<sub>Aryl</sub> bond rotation that was reflected in the high values for *t*<sub>1/2-rac</sub> in both toluene and acetonitrile.

Depending on the substitution of the nitrogen (amide vs imide), and the length of the alkenyl



tether (propenyl or pentenyl) the racemization barrier ranged from ~25 kcal/mol to ~29 kcal/mol. Inspection of Table 2.1 it can be seen that the atropisomeric enone amides (**92a,c**) have greater barrier to rotation than atropisomeric enone imides (**92e-g**). Both the alkenyl chain has bearing on the barrier to rotation seen in the difference between barriers of **92a** vs **92c** (atropisomeric enone amides) and **92e** vs **92f** (atropisomeric enone imides). It can be seen that the longer chain lengths (e.g. pentenyl **92c,f**) has greater influence and affords more stable atropisomer that is less susceptible to racemization. The longer chain length increases the barrier to rotation ~1 kcal/mol. Further inspection of Table 2.1 brings to light the influence that substitution has on *N*-C<sub>aryl</sub> bond rotation. The *N*-substitution (amide vs imide) apparently has greater bearing on the *N*-C<sub>aryl</sub> bond rotation as **92a** vs **92f** and **92c** vs **92e** highlights the greater stability of the sp<sup>3</sup> amide carbons imparts on the atropisomeric amides. The greater steric hindrance of the sp<sup>3</sup> amide carbons increased the barrier to rotation ~2kcal/mol. Overall, Table 2.1 reveals a high barrier for *N*-C<sub>Aryl</sub> bond rotation that was reflected in the high values for *t*<sub>1/2-rac</sub> in both toluene and acetonitrile.



**Scheme 2.7:** Racemization kinetics of atropisomeric enones.

$$k_{rac} = \kappa \left( \frac{k_B T}{h} \right) e^{-\Delta G^\ddagger_{rac}/RT} \quad (\text{Eq. 2.1})$$

$$\Delta G^\ddagger_{rac} = -RT \ln \left( \frac{h k_{rac}}{\kappa T \kappa_B} \right) \quad (\text{Eq. 2.2})$$

The half-life of racemization,  $\tau_{1/2rac}$ , can be calculated using the rate constant of racemization  $k_{rac}$  (assuming  $\mathbf{1-P}_0 = 0$  at  $t = 0$ ).

$$\ln\left(\frac{x_{eq}}{x_{eq}-x}\right) = \ln\left(\frac{R_0}{2R-R_0}\right) = \ln\left(\frac{R+S}{R-S}\right) = 2k_{enant}t \quad (\text{Eq.2. 3})$$

$$\ln\left(\frac{R_0}{R-x}\right) = k_{rac}t \quad (\text{Eq. 2.4})$$

Where,

$$k_{rac} = 2.k_{enant}$$

$R_0$  is the initial concentration of the (*R*)-enantiomer;

$x = R_0 - R$ ,  $S$  (concentration of the racemate at time  $t$ );

$k_{rac}$  is the rate constant for racemization

Note:  $R_0 = R + S$

At 50% *ee*, the equation becomes:

$$\tau_{1/2(rac)} = \frac{\ln 2}{k_{rac}} \quad (\text{Eq.2.5})$$

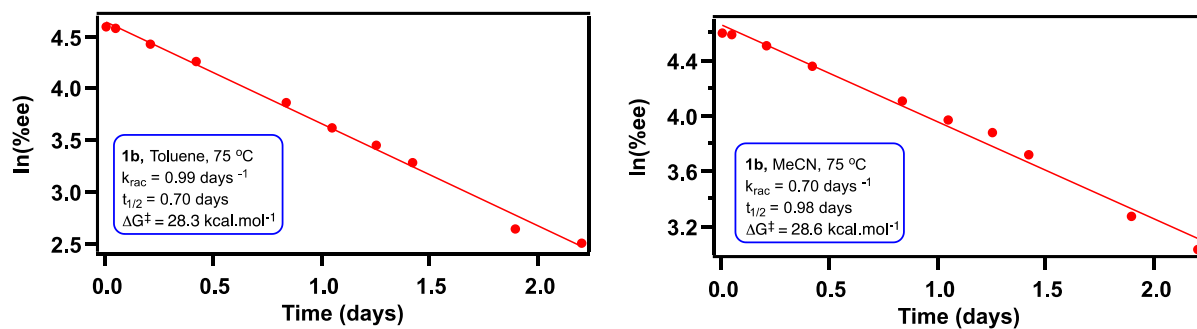


**Figure 2.2:** Racemization kinetics of atropisomeric enone-amide **92c**.

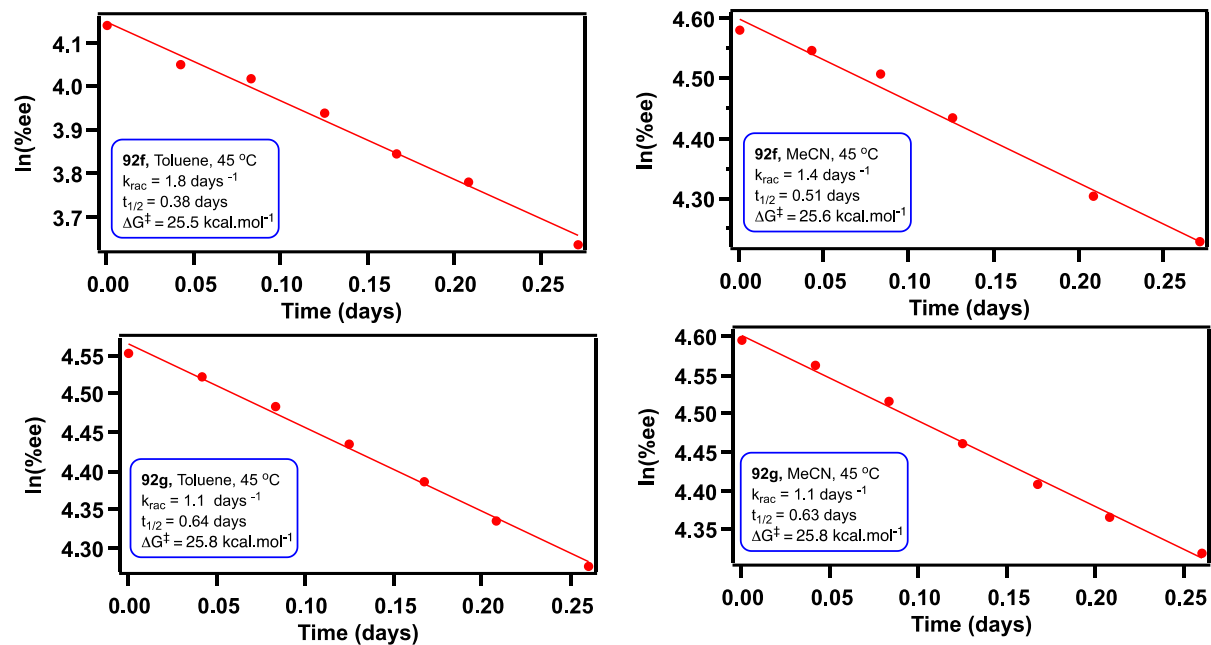


**Figure 2.3:** Racemization kinetics of atropisomeric enone-imides **92f** and **92g**.

**Table 2.1.** Racemization of atropisomeric enones<sup>a</sup>

entry	cmpd	solvent	T (°C)	racemization parameters		
				<b>k<sub>rac</sub></b> (days <sup>-1</sup> )	<b>t<sub>1/2-rac</sub></b> (days)	<b>ΔG<sup>‡</sup><sub>rac</sub></b> (kcal/mol)
1	<b>92a</b>	toluene	45	0.094	7.4	27.3
2		MeCN	45	0.12	5.5	27.2
1	<b>92c</b>	toluene	75	1.0	0.7	28.3
2		MeCN	75	0.70	1.0	28.6
1	<b>92e</b>	toluene	45	0.29	4.7	26.6
2		MeCN	45	0.30	2.3	26.6
3	<b>92f</b>	toluene	45	1.8	0.4	25.5
4		MeCN	45	1.4	0.5	25.6
5	<b>92g</b>	toluene	45	1.1	0.6	25.8
6		MeCN	45	1.1	0.6	25.8

<sup>a</sup> Optically pure isomers were employed for racemization kinetic measurements in a given solvent at a set temperature. Racemization was monitored by HPLC analysis on a chiral stationary phase (error = ± 3%).

## 2.6. [2+2] Photocycloaddition of atropisomeric enones

### 2.6.1. Optimization of reaction conditions

In efforts to optimize the reaction conditions (Tables 2.2 and 2.3) irradiation of enones was carried out under both direct and sensitized irradiations. Thioxanthone under visible light irradiation was used as the triplet sensitizer / catalyst. After the photoreaction, the reaction mixture was concentrated and the photoproduct(s) purified by column chromatography and characterized by NMR spectroscopy, HRMS and single crystal XRD (Table 2.4).

**Table 2.2:** [2+2] Photocycloaddition of Enone-Imide **92f** under Direct and Sensitized Irradiation Conditions.<sup>a</sup>

entry	irradiation conditions	<b>94f</b> (% yield)
1	bb/Pyrex cutoff, 1 h	>98
2	~350 nm, 3 h	>98
3	~420 nm, 9 h	>98
4	~420 nm, thioxanthone, 1 h <sup>b</sup>	84

<sup>a</sup>Irradiation of **92f** (c ≈ 2.7 mM) in MeCN at room temperature under a N<sub>2</sub> atmosphere unless otherwise noted. Values are based on <sup>1</sup>H NMR spectroscopy (error = ± 5%). bb/Pyrex cutoff = broadband irradiation performed using a medium pressure 450 W mercury lamp with a Pyrex cutoff (<295 nm cutoff); ~350 nm and ~420 nm irradiations were carried out in a Rayonet reactor. <sup>b</sup>Utilized 10 mol % of thioxanthone.

The conversion, yield, and mass balance were calculated by <sup>1</sup>H NMR spectroscopy using triphenylmethane as an internal standard. Inspection of the crystal structure of the photoproducts shows that, in the case of both enone-amides **92a–d** and enone-imides **92e–g**, the straight addition product **94** was exclusively obtained. More importantly, in the case of amides, two stereoisomers were observed, *cis,cis-94* and *cis,trans-94* in approximately 1:1 ratio in the solvents investigated except for EtOAc where the ratio was 3:2 respectively ( Table 2.2 and Table 2.3). In the *cis,cis-94*, there was *cis*-fusion of both ring systems (e.g., *cis,cis-94d* features *cis*-fusion of four-six and four-five ring systems). On the other hand, in *cis,trans-94*, there was *cis*-fusion of the six-four ring and *trans*-fusion of the second bicyclic-ring system (e.g., *cis,trans-94f* features *cis*-fusion of four-six ring system and *trans*-fusion of four-five ring system). To our surprise, in the case of enone- imides **94f–g**, exclusive formation of *cis,cis-94* as the product was observed.

**Table 2.3:** Solvent Effects on [2+2] Photocycloaddition Involving Enone-Amide **92c** and **94f** with Thioxanthone as the Sensitizer (10 mol%).

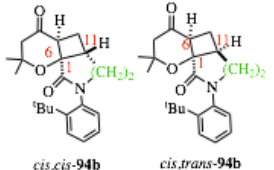
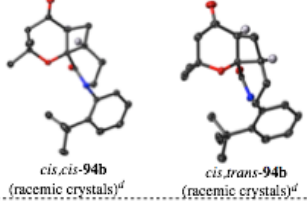
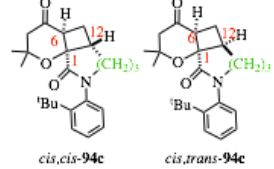
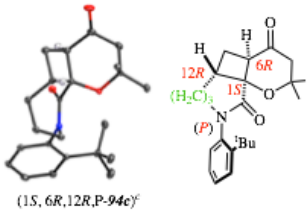
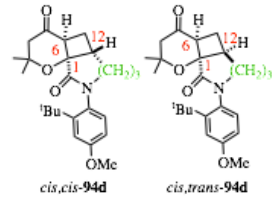
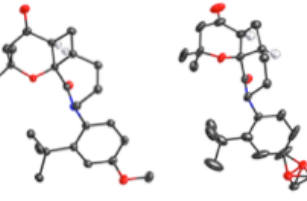
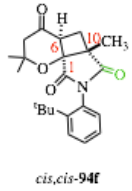
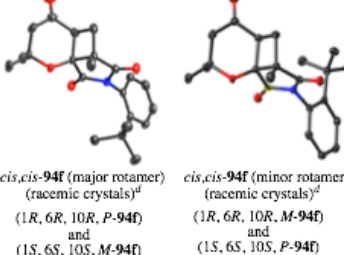
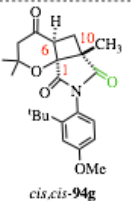
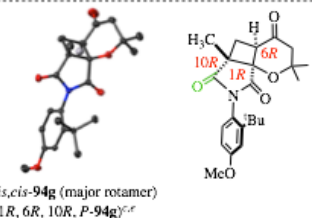
entry	solvent	<b>94c</b> (% yield)	<b>94f</b> (% yield)(dr)
1	MCH	-	>98 (4:1)
2	Toluene	15	>98 (3:1)
3	DCM	24	>98 (2:1)
4	Chloroform	12	>98 (3:1)
5	EtOAc	18	>98 (2:1)
6	MeOH	-	>98 (3:1)
7	MeCN	34	84 (4:1)
8	DMSO- <i>d</i> <sub>6</sub>	-	>98 (4:1)

<sup>a</sup>All reactions were performed in a Rayonet Reactor at  $\lambda \approx 420$  nm using thioxanthone (10 mol %) as a sensitizer; **92c** with 6 h of irradiation, and **92f** with 1 h of irradiation). Values are an average of three runs. <sup>b</sup>The % yield and ratios were determined by <sup>1</sup>H NMR spectroscopy using triphenylmethane as an internal standard (error =  $\pm 5\%$ ). <sup>c</sup>The ratio of *cis,cis*-**94c** : *cis,trans*-**94c** was found to be  $\sim 1:1$  in all the solvents except EtOAc, where it was 3:2. <sup>d</sup>The **94f** diastereomeric ratio from *N*-C<sub>Aryl</sub> bond rotation.

Inspection of Table 2.2 shows that the reaction of **92f** in acetonitrile was efficient both under direct irradiation (Pyrex cutoff) and visible light irradiation with 10 mol % loading of thioxanthone (acting as a catalyst/sensitizer). Inspection of Table 2.3 shows that the [2 + 2] photocycloaddition of enone-imide **92f** was clean and efficient when compared to the enone-amide **92c**. Enone-imide **92f** gave excellent yield and mass balance in all of the investigated solvent systems. The irradiation time was kept constant at 6 h of enone-amide **92c** in order to compare the efficiency of the reaction in different solvents. The conversion of **92c** varied from 12 to 34% (Table 2.3). Longer irradiation time gave higher conversions. In contrast, excellent yield was observed with enone-amides **92c** and **92d** upon direct irradiation at  $\sim 350$  nm (Table

2.4 entries 2 and 5). It can be inferred from examination of Table 2.3 and 2.4 that the type of functionality and the length of the *N*-alkenyl chain of atropisomeric enones played a crucial role in determining the product distribution. In the case of enone-imides **92f** and **92g**, exclusive formation of the corresponding *cis,cis*-**94** as the product was observed. Two diastereomeric rotamers of *cis,cis*-**92f** were observed, which arise due to hindered rotation of the *N*-C<sub>Aryl</sub> bond, as a racemic mixture of atropisomeric reactant **92f** and **92g** were employed, (Table 2.4, entries 8 and 9). More importantly, the diastereomeric rotamers were separated by chromatography and confirmed their relationship by <sup>1</sup>H NMR spectroscopy and by single crystal XRD analysis. Both the major and minor diastereomeric rotamers of *cis,cis*-**94f** crystallized as racemic crystals (containing a mixture of enantiomers; Table 2.4, entry 8). From single crystal XRD analysis, the configuration of the minor diastereomeric rotamer of *cis,cis*-**94f** was established as (1*R*,6*R*,10*R*,*M*)-**94f** and (1*S*,6*S*,10*S*,*P*)-**92f**. Similarly, from single crystal XRD analysis, the configuration of the major diastereomeric rotamer of *cis,cis*-**94f** was established as (1*R*,6*R*,10*R*,*P*)-**94f** and (1*S*,6*S*,10*S*,*M*)-**94f**. Surprisingly, the chiral crystal of the major diastereomeric rotamer of *cis,cis*-**94g** (as it was a mixture of conglomerate crystals of individual enantiomers) were isolated and its absolute configuration was determined to be (1*R*,6*R*,10*R*,*P*)-**94g** (Table 2.4, entry 9).

**Table 2.4:** Intramolecular [2+2] Photocycloaddition of Atropisomeric Enones

Entry	Substrate	t (h)	Photoproduct	% yield / selectivity	Single crystal XRD
1	<b>92b</b>	12	 <i>cis,cis-94b</i> <i>cis,trans-94b</i>	Yield = 88% <b>94b</b> : <b>93b</b> = >49 : 1 <i>cis,cis-94b</i> : <i>cis,trans-94b</i> = 3 : 1	 <i>cis,cis-94b</i> (racemic crystals) <sup>d</sup> <i>cis,trans-94b</i> (racemic crystals) <sup>d</sup>
2	<b>92c</b>	7	 <i>cis,cis-94c</i> <i>cis,trans-94c</i>	Yield = 73% (isolated yield) <sup>b</sup> <b>94c</b> : <b>93c</b> = >49 : 1 <i>cis,cis-94c</i> : <i>cis,trans-94c</i> = 1 : 1	 <i>cis,cis-94c</i> <i>cis,trans-94c</i> (1 <i>S</i> , 6 <i>R</i> , 12 <i>R</i> , <i>P</i> - <b>94c</b> ) <sup>c</sup>
3	pkA- <b>92c</b>			<i>cis,cis-94c</i> : 91% ee	
4	pkB- <b>92c</b>			<i>ent-cis,cis-94c</i> : 86% ee	
5	<b>92d</b>	6	 <i>cis,cis-94d</i> <i>cis,trans-94d</i>	Yield = 66% (isolated yield) <sup>b</sup> <b>94d</b> : <b>93d</b> = >49 : 1 <i>cis,cis-94d</i> : <i>cis,trans-94d</i> = 1 : 1	 <i>cis,cis-94d</i> <i>cis,trans-94d</i> (racemic crystals) <sup>d</sup> (racemic crystals) <sup>d</sup>
6	pkA- <b>92d</b>			<i>cis,cis-94d</i> : <5% ee	
7	pkB- <b>92d</b>			<i>ent-cis,cis-94d</i> : <5% ee	
8	<b>92f</b>	1	 <i>cis,cis-94f</i>	<b>94f</b> : <b>93f</b> = >49 : 1 Yield = 84% <i>cis,cis-94f</i> : <i>cis,trans-94f</i> = >49 : 1 <i>N</i> -C <sub>Aryl</sub> rotamer ratio <i>cis,cis-94f</i> = 4 : 1	 <i>cis,cis-94f</i> (major rotamer) (racemic crystals) <sup>d</sup> (1 <i>R</i> , 6 <i>R</i> , 10 <i>R</i> , <i>P</i> - <b>94f</b> ) and (1 <i>S</i> , 6 <i>S</i> , 10 <i>S</i> , <i>M</i> - <b>94f</b> ) <i>cis,cis-94f</i> (minor rotamer) (racemic crystals) <sup>d</sup> (1 <i>R</i> , 6 <i>R</i> , 10 <i>R</i> , <i>M</i> - <b>94f</b> ) and (1 <i>S</i> , 6 <i>S</i> , 10 <i>S</i> , <i>P</i> - <b>94f</b> )
9	<b>92g</b>	1	 <i>cis,cis-94g</i>	<b>94e</b> : <b>93e</b> = >49 : 1 Yield = 99% (70% isolated) <i>cis,cis-94g</i> : <i>cis,trans-94g</i> = >49 : 1 <i>N</i> -C <sub>Aryl</sub> rotamer ratio <i>cis,cis-94g</i> = 4 : 1	 <i>cis,cis-94g</i> (major rotamer) (1 <i>R</i> , 6 <i>R</i> , 10 <i>R</i> , <i>P</i> - <b>94g</b> ) <sup>c,e</sup>

<sup>a</sup> Irradiations were carried out with 10 mol % of thioxanthone in a Rayonet reactor equipped with ~420 nm (16 bulbs ×14 W) unless otherwise noted. Reaction carried out with the 1:1 mixture of atropisomers. For atropselective reaction in entries 3, 4, 6, and 7, optically pure atropisomers that were separated from HPLC were employed. pkA and pkB refer to the first and second peak that elutes out of the HPLC on a chiral stationary phase. Reported values carry an error of ±5%. <sup>b</sup>Isolated yields for **92c** and **92d** were determined from direct irradiation conditions in a Rayonet reactor at ~350 nm (16 bulbs ×14 W). Visible light irradiation was also effective and gave similar selectivity. <sup>c</sup>Stereochemistry was deduced from single crystal XRD analysis using Flack parameters. <sup>d</sup>Racemic crystals of **94f** (major and minor rotamers of *cis,cis-94f*) had both of the



enantiomeric forms within the same unit cell. <sup>e</sup>Optically pure crystals from **94g** were picked from a mixture of conglomerate crystals.

### 2.6.2. Atropselective photoreactions of atropisomeric enones

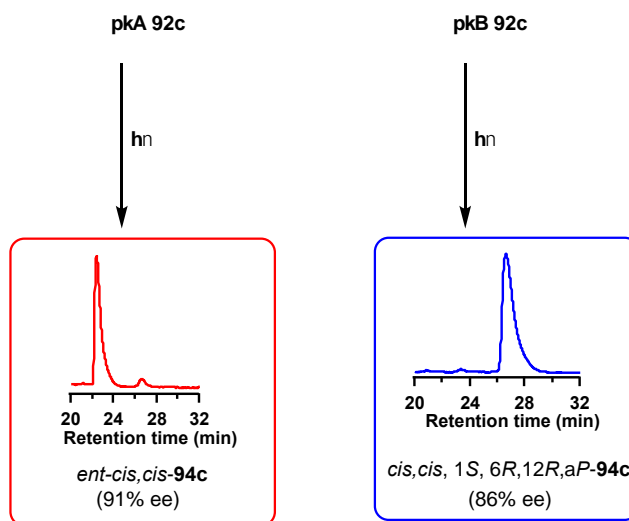


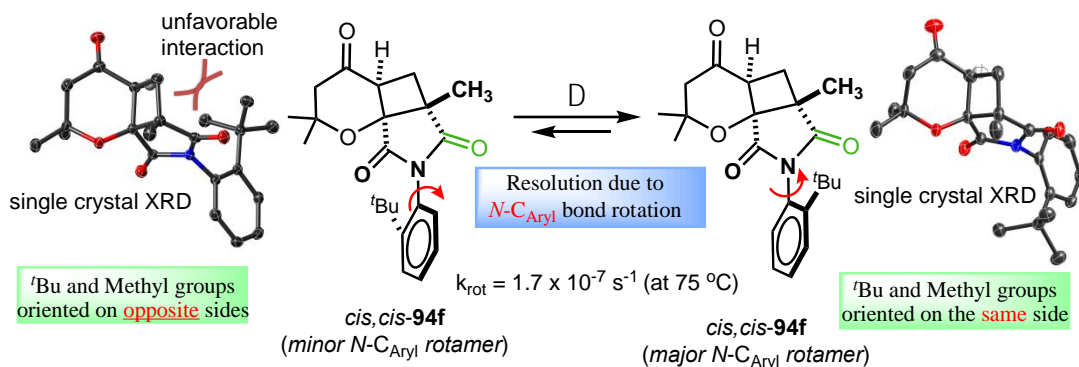
**Figure 2.4:** Atropselective photoreaction of enone-carboxamide **92c**

The photochemical reaction of optically pure atropisomers of amides **92c** and **92d** in order to evaluate how axial chirality dictates the stereochemistry of the product. Optically pure atropisomeric enone-amides were obtained from preparative HPLC separation on a chiral stationary phase. The optically pure enone was dissolved in MeCN followed by the addition of 10 mol % of thioxanthone. The reaction mixture was degassed with N<sub>2</sub> for 10 min. and then sealed for photoreaction. The solution was irradiated in a Rayonet reactor (~420 nm) for 6 h. After the reaction, was completed, the solvent was removed, and the product was purified by preparative HPLC. The product was then analyzed by analytical HPLC and the enantiomeric excess was determined. High enantioselectivity was observed in the photoproduct during the photochemical transformation of optically pure atropisomers of enone-amide **92c**. Unfortunately, only *cis,cis-92c* was investigated for enantioselectivity due to limitations in separating enantiomers of *cis,trans-92c*. To our surprise, para- methoxy derivative **92d** afforded near

racemic photoproducts *cis,cis*-**94d** and *cis,trans*-**94d**. This necessitated a mechanistic understanding to rationalize the behavior of enones (vide infra).

## 2.7. Evaluating relationship *cis,cis*-**94f** major and *cis,cis*-**94f** minor photoproducts

### 2.7.1. Evaluating racemization in *cis,cis*-**94f** photoproduct



#### Scheme 2.8: *N*-C<sub>Aryl</sub> bond rotation in *cis,cis*-**94f** (minor *N*-C<sub>Aryl</sub> rotamer)

The kinetics of *N*-C<sub>Aryl</sub> bond rotation in optically pure atropisomeric *cis,cis*-**94f** was performed at various temperatures. The rotation of the *N*-C<sub>Aryl</sub> bond of *cis,cis*-**94f** minor transforming into *cis,cis*-**94f** major was followed by <sup>1</sup>H NMR spectroscopy with triphenylmethane as the internal standard in DMSO-*d*<sub>6</sub> as the solvent at different time intervals.

The activation energy for *N*-C<sub>Aryl</sub> bond was computed from equations 2.8 and 2.9.

$$k_{rot} = \kappa \left( \frac{k_B T}{h} \right) e^{-\Delta G^\ddagger_{rot}/RT} \quad (\text{Eq. 2.6})$$

$$\Delta G^\ddagger_{rot} = -RT \ln \left( \frac{h k_{rot}}{\kappa T \kappa_B} \right) \quad (\text{Eq. 2.7})$$

The half-life of diastereomerization,  $\tau_{1/2rot}$ , can be calculated using the rate constant of diastereomerization  $k_{rot}$  (assuming  $1-P_0 = 0$  at  $t = 0$ ).

$$\ln \left( \frac{x_{eq}}{x_{eq} - x} \right) = \ln \left( \frac{P_0}{2P - P_0} \right) = \ln \left( \frac{P+M}{P-M} \right) = 2k_{rot}t \quad (\text{Eq. 2.8})$$

$$\ln \left( \frac{P_0}{P - x} \right) = k_{rot}t \quad (\text{Eq. 2.9})$$

Where,

$$k_{\text{rac}} = 2 \cdot k_{\text{epim}}$$

$P_0$  is the initial concentration of the diastereomer with (*P*)-axial chirality;

$x = P_0 - M$ ,  $P$  (concentration of the atropisomer at time  $t$ ); and

$k_{\text{rot}}$  is the rate constant for  $N\text{-C}_{\text{Aryl}}$  bond rotation

Note:  $P_0 = P + M$

At 50% *de*, the equation becomes:

$$\tau_{1/2(\text{rot})} = \frac{\ln 2}{k_{\text{rot}}}$$

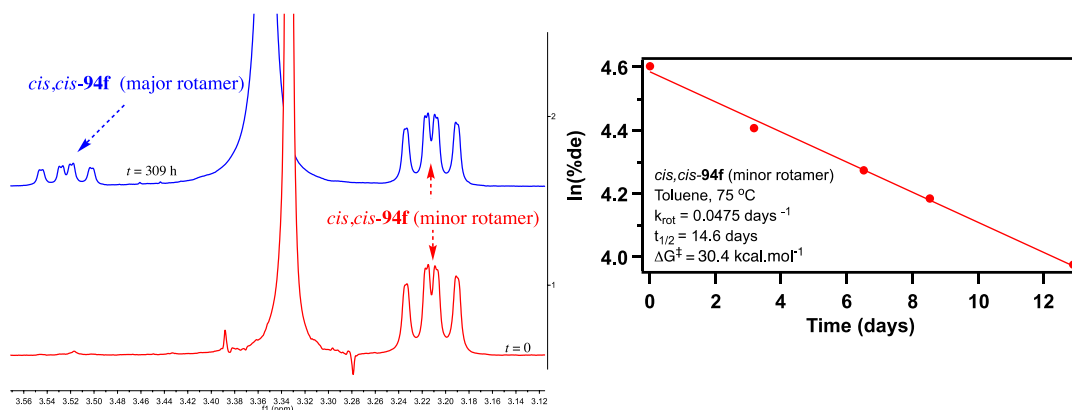


**Figure 2.5:** Diastereomerization kinetics of atropisomeric cyclized product *cis,cis-94f* minor. Left: <sup>1</sup>H NMR spectrum of *cis,cis-94f* minor in DMSO-*d*<sub>6</sub> at various times. Right: plot depicting kinetics of  $N\text{-C}_{\text{Aryl}}$  bond rotation.

Thus, the major and minor rotamers in *cis,cis-94f* differed only by rotation about the  $N\text{-C}_{\text{Aryl}}$  bond (the same is true for *cis,cis-94g*).<sup>40,42,63-66</sup> Heating of the minor diastereomeric rotamer of *cis,cis-94f* in DMSO-*d*<sub>6</sub> resulted in the major diastereomeric rotamer *cis,cis-94f* (Scheme 2.8). The rate constant (monitored by <sup>1</sup>H NMR spectroscopy) for  $N\text{-C}_{\text{Aryl}}$  bond rotation was found to be  $1.7 \times 10^{-7} \text{ s}^{-1}$  at 75 °C in DMSO-*d*<sub>6</sub>.

## 2.7.2. Physical separation of atropisomeric enone imides *cis,cis-94* major and minor

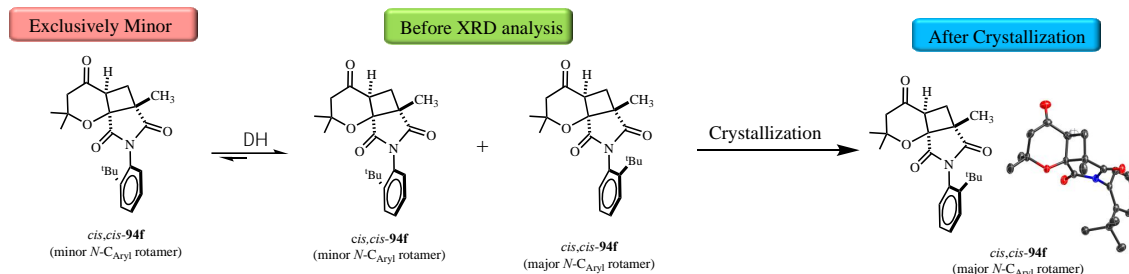


**Figure 2.6:** Physical separation of *cis,cis-94f* minor and *cis,cis-94f* major over time at room temperature by crystallization.

Over time, the *cis,cis-94f* minor was allowed to slowly crystallize. It was noticed that the resultant crystal was that of the *cis,cis-94f* major. Figure 2.6 displays the  $^1\text{H}$  NMR spectrum (in  $\text{CDCl}_3$ ) throughout the crystallization process.

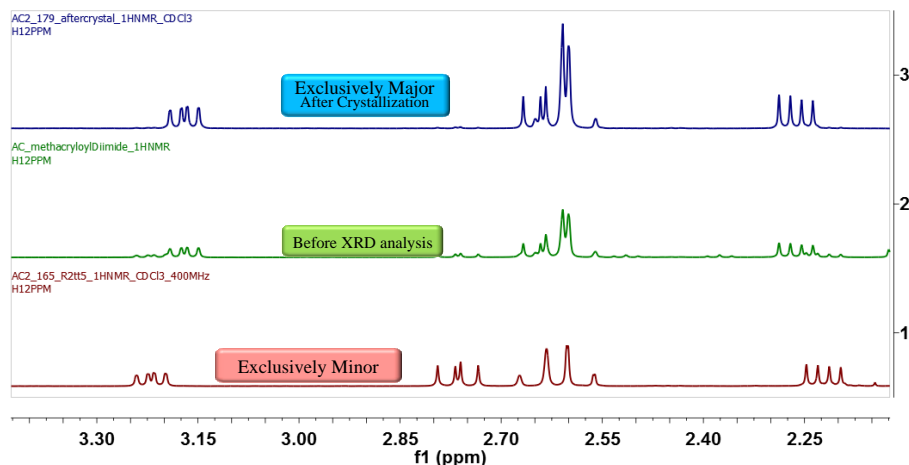


**Figure 2.7:** Physical separation of *cis,cis-94f* minor and *cis,cis-94f* major via crystallization over time.  $^1\text{H}$  NMR spectrum trace recorded in  $\text{CDCl}_3$ .

### 2.7.3. UV-Vis spectra of atropisomeric enones 92a, 92c-g

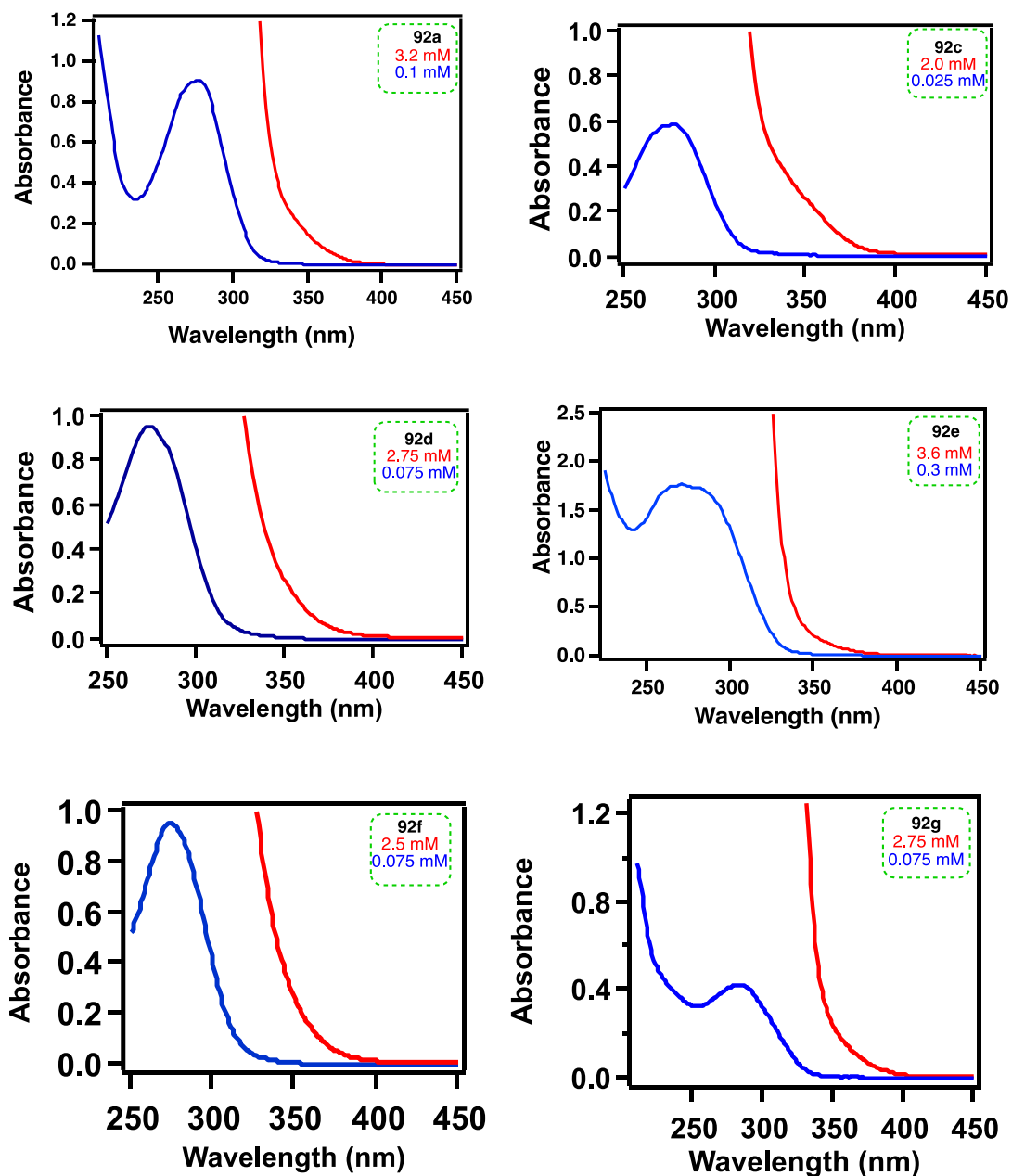


**Figure 2.8:** UV-Vis spectra of atropisomeric-enones 92a, 92c-g.

### 2.7.4. Thioxanthone quenching experiments with 92f

In an effort to understand the mechanistic details, photophysical measurements were obtained for **92f**. At 77 K, there was no observable phosphorescence, showing that there is efficient deactivation of the excited state by another pathway. As the reaction was efficient with

thioxanthone (TX) acting as a visible light photocatalyst/sensitizer, its role in promoting the reaction was investigated using transient absorption studies. Laser excitation ( $\lambda_{\text{ex}} = 355 \text{ nm}$ ; 7 ns pulse width; 5 mJ/pulse) of TX in the presence of varying concentrations of **92f** in  $\text{N}_2$ -degassed acetonitrile solution showed that the triplet of thioxanthone was efficiently quenched (Figures 2.8 and 2.9) with a bimolecular quenching rate constant ( $k_{\text{Q}}$ )  $8.2 \times 10^9 \text{ M}^{-1} \text{ s}^{-1}$ .<sup>55,67</sup> No new transient species were observed, and the bleach at 380 nm showed very fast recovery in the presence of **92f**. The photophysical data implicates an energy transfer pathway rather than electron transfer from the excited thioxanthone to the enone.

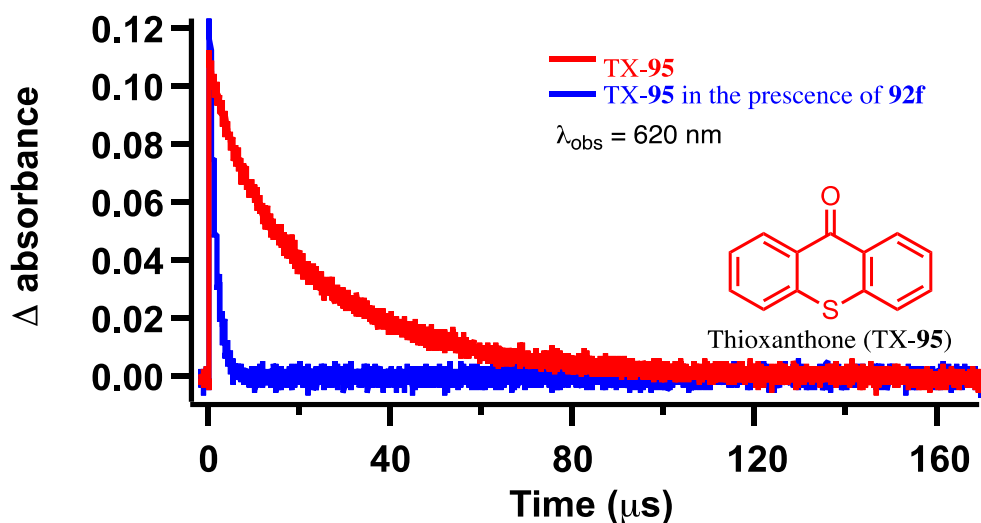


**Figure 2.9:** Quenching of thioxanthone [0.04 mM] in the presence of **92f** (1 equiv.) Lifetimes recorded 21.7  $\mu\text{s}$  (TX-**95**, red) and 3.4  $\mu\text{s}$  (TX-**95** and **92f**, blue).

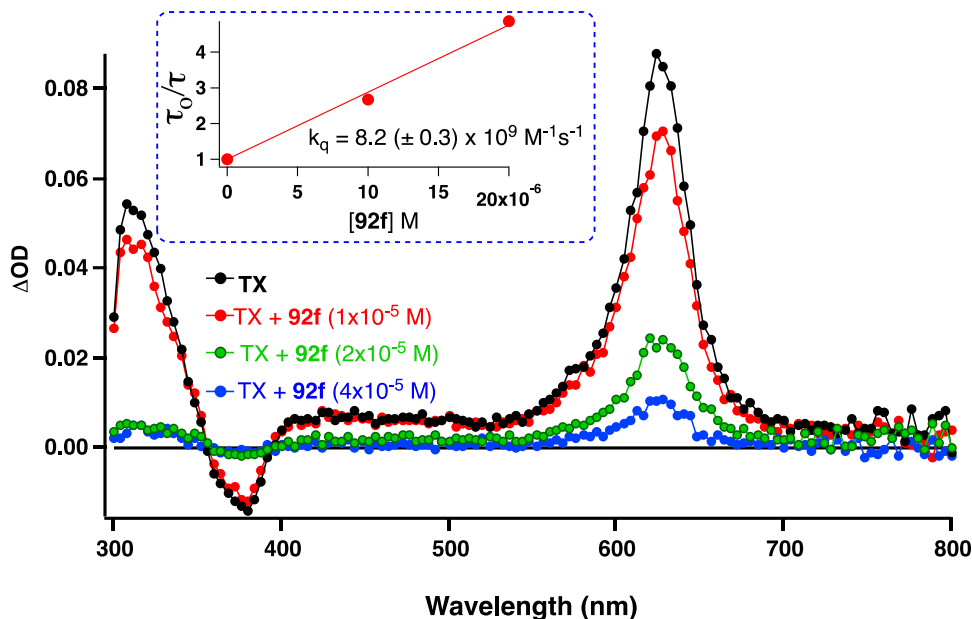
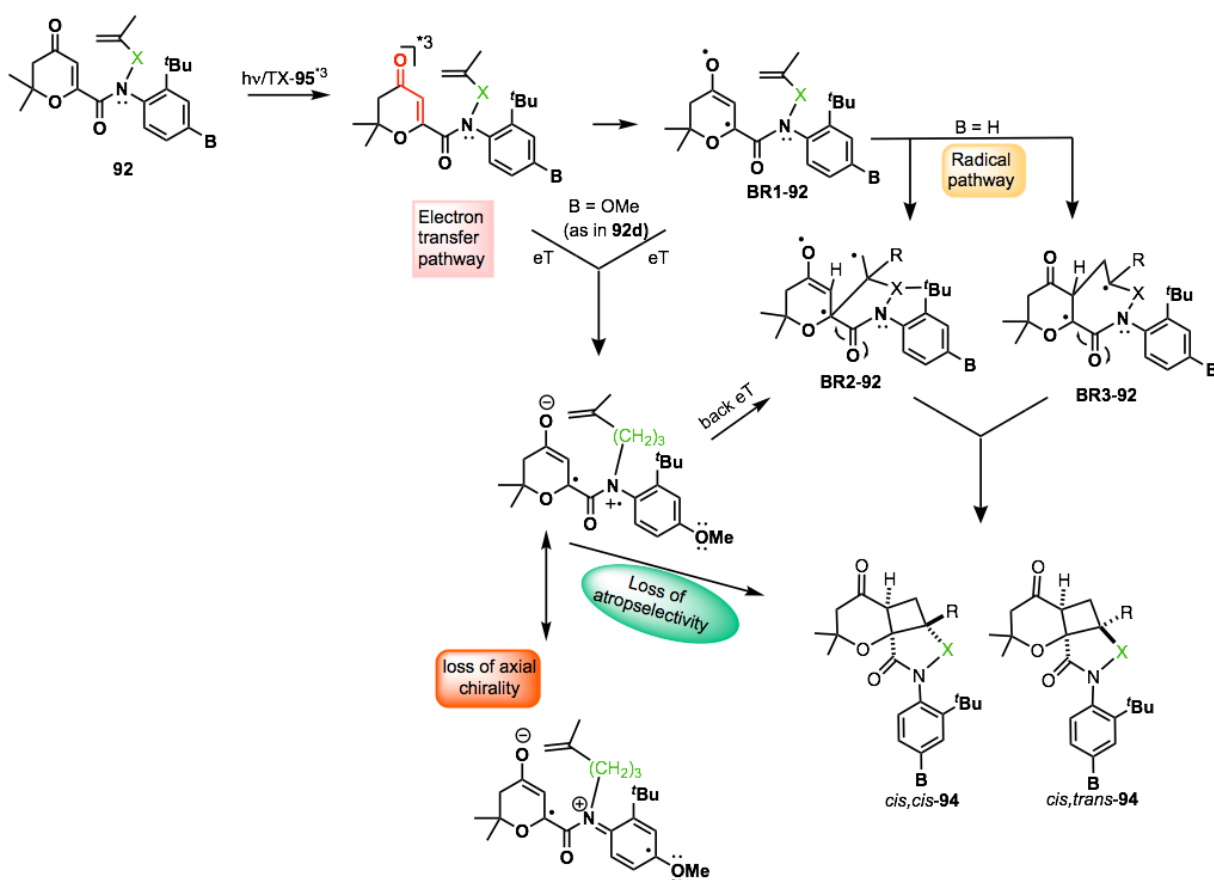


**Figure 2.10:** Quenching studies of thioxanthone (TX-95) in the presence of **92f**. Laser flash photolysis performed using ND:YAG laser (355 nm, 5 mj/pulse, 7 ns pulse width). The Transient absorption spectra were plotted 4 ms after laser flash. (Inset) Stern-Volmer quenching plot of TX-95 in the presence of **92f**.

## 2.8. Mechanistic rationale of atropisomeric enones

On the basis of the results above, it can be hypothesized that upon excitation the enone reaches the triplet excited state upon energy transfer from excited thioxanthone. Due to the triplet state reactivity of enone with electron-deficient alkene (e.g. imides **92f** and **92g**), the reaction is likely triggered by a  $\pi^* \rightarrow \pi^*$  interaction<sup>9</sup> between the excited enone and the electron deficient alkene leading to biradical BR2 that cyclizes to form *cis,cis*-**94** products. Upon increasing the chain length of the *N*-alkenyl substituent (as in amide **92b** or **92c**), the longer flexible alkenyl chain likely orients itself by exposing one of the two faces of the alkene double-bond to the excited enone leading to BR2-**92**, which cyclizes to *cis,cis*-**94** and *cis,trans*-**94** products.<sup>55</sup> In a parallel scenario, our present mechanism cannot rule out the formation of BR3-**92** in the reaction pathway as it can lead to *cis,cis*-**94** and *cis,trans*-**94** products. However, considering that the reaction is likely originating from the  $\pi^*$  of excited enone, this intermediate is less likely. The

last aspect addressed was the loss of atropselectivity with enone-amide **92d** that features a para-methoxy substituent. The electron transfer pathway has previously been implicated for hydrogen abstraction involving amido-cycloalkenones.<sup>61</sup> On the basis of this precedence, it is possible that the electron-rich nature of the *p*-OMe substituent likely triggers an electron transfer pathway leading to loss of axial chirality. This results in the loss of atropselectivity (Scheme 2.9), which is reflected in the near racemic product despite employing optically pure atropisomers in **92d** (Table 2.4, entries 6 and 7).



**Scheme 2.9:** Mechanistic rationale of [2+2] photocycloaddition of atropisomeric enones.



## 2.9. Summary and outlook

Our investigation has displayed that intramolecular [2+2] photocycloaddition of excited enone could be effectively controlled by incorporating axial chirality into the system. The selectivity is dependent on the type of substituent on the nitrogen. For short chain imide substituents, exclusive formation of straight addition was observed. Our results showcase that one may achieve excellent control of excited state reactivity by employing restricted bond rotation(s) leading to stereo-enriched product(s). Controlling such transformations under visible light-mediated photocatalytic conditions will open avenues to devise strategies to perform light-initiated reactions in a stereocontrolled fashion.<sup>68-70</sup>

## 2.10. Experimental section

### 2.10.1. General methods

All commercially obtained reagents/solvents were used as received; chemicals were purchased from Alfa Aesar<sup>®</sup>, Sigma-Aldrich<sup>®</sup>, Acros organics<sup>®</sup>, TCI America<sup>®</sup>, Mallinckrodt<sup>®</sup>, and Oakwood<sup>®</sup> Products, and were used as received without further purification. Spectrophotometric grade solvents (ethanol and methylcyclohexane) were purchased from Sigma-Aldrich<sup>®</sup> and used without further purification for emission measurements. Unless stated otherwise, reactions were conducted in oven-dried glassware under nitrogen atmosphere. <sup>1</sup>H NMR and <sup>13</sup>C NMR spectra were recorded on Varian 400 MHz (100 MHz for <sup>13</sup>C) and on 500 MHz (125 MHz for <sup>13</sup>C) spectrometers. Data from the <sup>1</sup>H NMR spectroscopy are reported as chemical shift ( $\delta$  ppm) with the corresponding integration values. Coupling constants ( $J$ ) are reported in hertz (Hz). Standard abbreviations indicating multiplicity were used as follows: s (singlet), b (broad), d (doublet), t (triplet), q (quartet), m (multiplet) and virt (virtual). Data for <sup>13</sup>C NMR spectra are reported in terms of chemical shift ( $\delta$  ppm). In many instances it was not

possible to obtain the signal for the carbonyl carbon where ever possible it was have reported all the signals. High-resolution mass spectrum data in Electrospray Ionization mode were recorded on a Bruker – Daltronics<sup>®</sup> BioTof mass spectrometer in positive (ESI+) ion mode. HPLC analyses were performed on Waters<sup>®</sup> HPLC equipped with 2525 pump or on Dionex<sup>®</sup> Ultimate 3000 HPLC. Waters<sup>®</sup> 2767 sample manager was used for automated sample injection on Waters<sup>®</sup> HPLC or Ultimate 3000 sample injector was used for injection on Dionex<sup>®</sup> HPLC. All HPLC injections on Waters<sup>®</sup> HPLC were monitored using a Waters<sup>®</sup> 2487 dual wavelength absorbance detector at 254 and 270 nm or on Dionex<sup>®</sup>. HPLC were monitored using a diode array detector (DAD3000125). Analytical and semi-preparative injections were performed on chiral stationary phase using various columns as indicated below.

Regis<sup>®</sup> PIRKLE COVALENT (*R,R*) WHELK-01

- a) 25 cm x 4.6 mm column for analytical injections.
- b) 25 cm x 10 mm column for semi-preparative injections.

CHIRAPAK<sup>®</sup> AD-H

- a) 0.46 cm x 25 cm column for analytical injections.
- b) 10 mm x 25 cm column for semi-preparative injections.

Masslynx software version 4.1 was used to monitor/analyze the HPLC injections on Waters<sup>®</sup> and to process HPLC traces. Chromeleon 7 software was used to monitor and process HPLC injections on Dionex<sup>®</sup> HPLC. Igor Pro<sup>®</sup> Software version 6.0 was used to process the HPLC graphics. UV-Vis spectra were recorded on Cary 300 series UV-Vis spectrometer using UV quality fluorimeter cells (with range until 190 nm) purchased from Luzchem. When necessary, the compounds were purified by combiflash equipped with dual wavelength UV-Vis absorbance detector (Teledyne ISCO) using hexanes: ethyl acetate as the mobile phase and Redisep<sup>®</sup> cartridge filled with silica (Teledyne ISCO) as stationary phase. In some cases,

compounds were purified by column chromatography on silica gel (Sorbent Technologies®, silica gel standard grade: porosity 60 Å, particle size: 230 x 400 mesh, surface area: 500 – 600 m<sup>2</sup>/g, bulk density: 0.4 g/mL, pH range: 6.5 – 7.5). Unless indicated, the Retardation Factor ( $R_f$ ) values were recorded using a 5-50% hexanes:ethyl acetate as mobile phase and on Sorbent Technologies®, silica Gel TLC plates (200 mm thickness w/UV254).

### **2.10.2. General methods for photophysical investigations**

Spectrophotometric solvents (Sigma-Aldrich®) were used whenever necessary unless or otherwise mentioned. UV quality fluorimeter cells (with range until 190 nm) were purchased from Luzchem®. Absorbance measurements were performed using a Cary 300 UV-Vis spectrophotometer., Emission spectra were recorded on a Horiba Scientific® Fluorolog 3 spectrometer (FL3-22) equipped with double-grating monochromators, dual lamp housing containing a 450-watt CW xenon lamp and a xenon flash lamp (FL-1040), Fluorohub/MCA/MCS electronics and R928 PMT detector.

The nanosecond transient absorption experiments were done with a laser flash photolysis kinetic spectrometer obtained from Edinburg Instruments (LP-980 K) equipped with a 300mm focal length monochromator in Czerny Turner configuration, and an analyzing photomultiplier in standard LP980 housing, featuring Hamamatsu R928 side window photomultiplier detector. The pulses for the experiment were from third harmonic of Newport INDI-40-10 ultra compact flash lamp pumped Nd-YAG laser (355 nm, 5 mj/pulse, 5 ns pulse width).

### **2.10.3. General methods for X-ray crystal structure determination**

Single crystal X-ray diffraction data of the compounds **92a-e** were collected on a Bruker Apex Duo diffractometer with an Apex 2 CCD area detector at  $T = 100$  K. Cu radiation was used. All structures were process with Apex 2 v2010.9-1 software package (SAINT v. 7.68A,

XSHELL v. 6.3.1). Direct method was used to solve the structures after multi-scan absorption corrections. Details of data collection and refinement are given in the table below.

## 2.11. General procedure for the synthesis of atropisomeric enones **92**

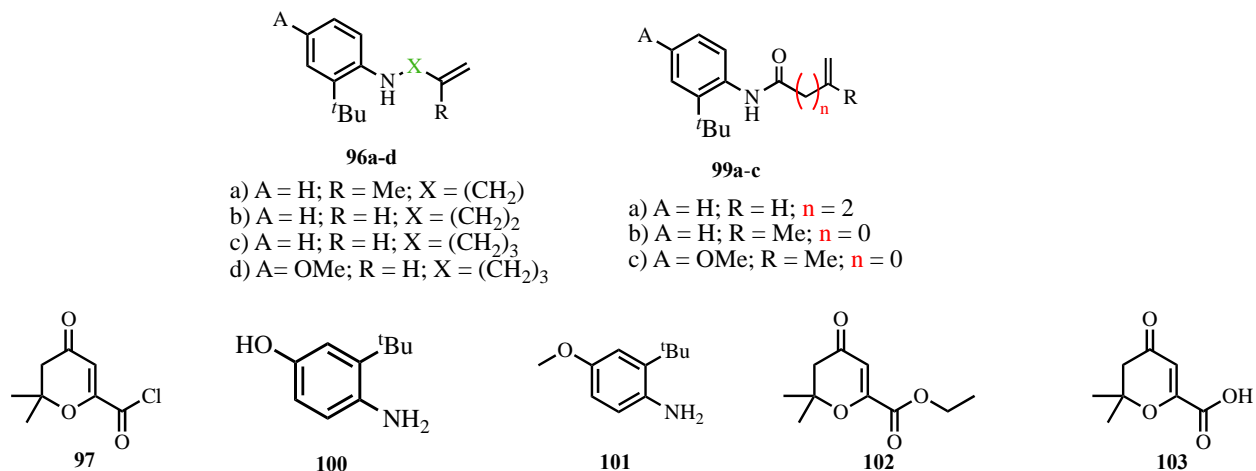


**Chart 2.2:** Structures of precursors to atropisomeric enones **92a-g**.

### 2.11.1. Synthetic protocol for 4-amino-3-tert-butylphenol **100**

Following a reported procedure<sup>71</sup> a solution of sulfanilic acid (55.9 mmol, 1.2 equiv.), Na<sub>2</sub>CO<sub>3</sub> (28 mmol, 0.6 equiv.) was prepared in 60 mL of deionized H<sub>2</sub>O. The solution was then set to reflux for 30 minutes. Initially the solution was colorless, yet turbid. Upon refluxing the solution turned pale yellow and became turbid then clear. After reflux the clear pale yellow solution was cooled to 0 °C. Next NaNO<sub>2</sub> (55.9 mmol, 1.2 equiv.) was dissolved in 25 mL and added dropwise. Upon addition of NaNO<sub>2</sub> the reaction mixture became dark yellow. The yellow solution was added to a mixture of 9 mL of concentrated HCl and 56 g of ice. The resulting yellow solution was added to another solution containing 3-*tert*-butanol (46.6 mmol, 1 equiv.) prepared in 20% NaOH (Note, both solutions were cooled to 0 °C.). Mixing of the two solutions at 0 °C resulted in a blood red solution. The blood red solution was allowed to stir at room temperature overnight. Approximately 16 hours later the red mixture was heated to 60 °C and

$\text{Na}_2\text{S}_2\text{O}_4$  (140 mmol, 3 equiv.) was added portion wise. Upon addition of  $\text{Na}_2\text{S}_2\text{O}_4$  the solution became brownish yellow in color. After 30 minutes the reaction mixture was cooled to room temperature and filtered. The filter cake was added to a separation funnel and extracted with  $\text{CHCl}_3$  (3 x 30 mL). After every extraction the colloidal solution was refiltered. The organic portions were combined then washed with 5%  $\text{Na}_2\text{CO}_3$  solution then brine, dried and concentrated. The dark purple solid was confirmed to be the product by  $^1\text{H}$  NMR spectroscopy. The dark purple solid **100** was used without further purification in the subsequent step.

$^1\text{H}$  NMR (400 MHz,  $\text{CDCl}_3$ ,  $\delta$  ppm) 6.75 (t,  $J = 1.6$  Hz, 1H), 6.52 (d,  $J = 1.6$  Hz, 2H), 4.27 (bs, 1H), 3.54 (bs, 2H), 1.38 (s, 9H).

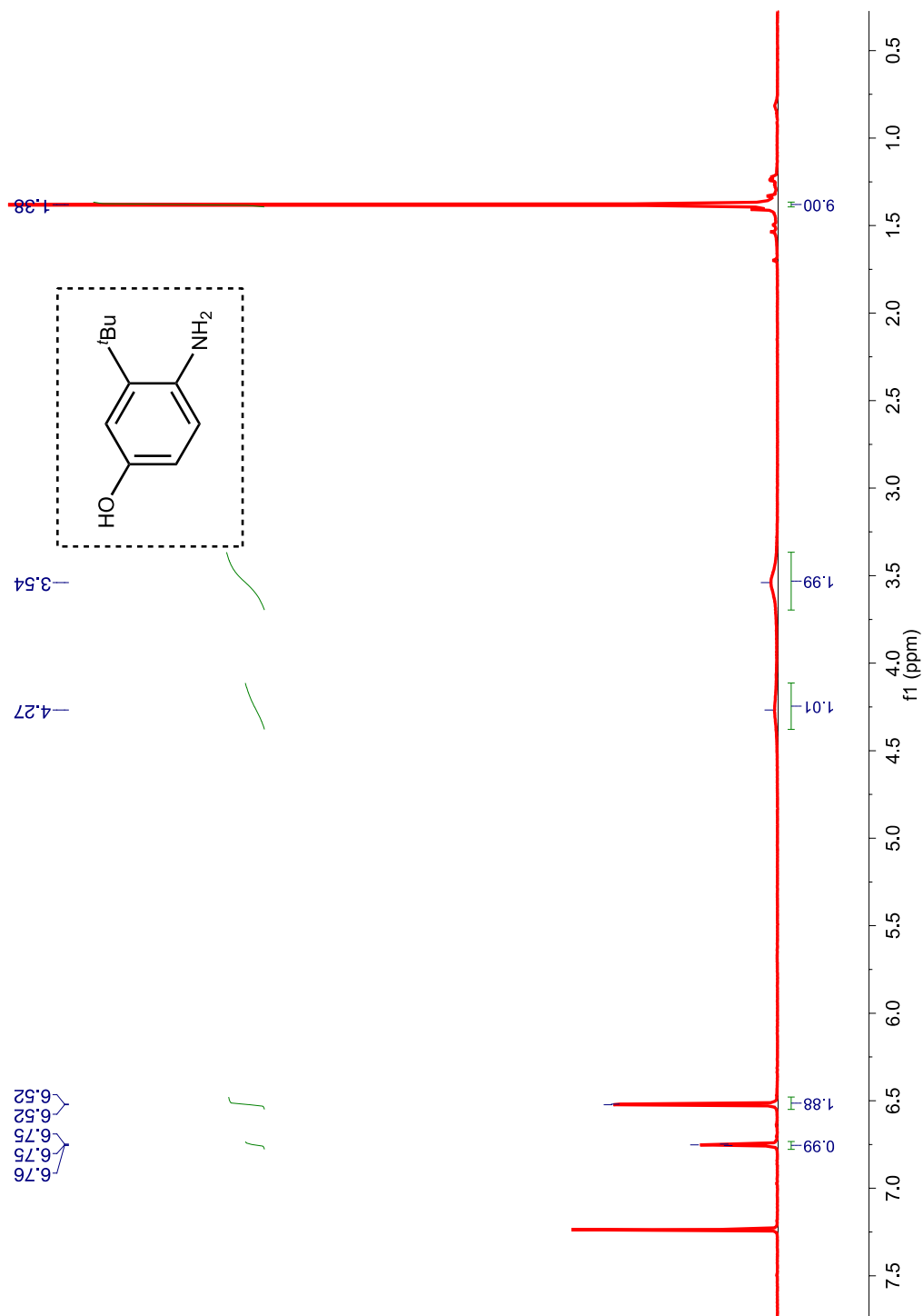


**Figure 2.11:**  $^1\text{H}$  NMR (400 MHz,  $\text{CDCl}_3$ ,  $\delta$  ppm) spectrum of 4-amino-3-*tert*-butylphenol **100**.

### 2.11.2. Synthetic protocol of 4-amino-3-tert-butylanisole **101**

Primary amine **100** (18.6 mmol, 1 equiv.) and KO<sup>t</sup>Bu (19 mmol, 1.02 equiv.) was evacuated and purged with N<sub>2</sub> then dissolved in DMSO (10 mL). The reaction mixture was allowed to stir for 1 h before the addition of Me<sub>2</sub>SO<sub>4</sub> (19.7 mmol, 1.06 equiv.). After ~15 min water was used to quench the reaction in order to hinder further methylation. The mixture was extracted with Et<sub>2</sub>O, washed with brine, dried over Na<sub>2</sub>SO<sub>4</sub>, filtered, and concentrated in vacuo.. The crude reaction mixture was purified via Combiflash using 80:20 hexanes : EtOAc as the mobile phase. A brown oil (**101**, 40% yield) was obtained and confirmed by <sup>1</sup>H NMR spectroscopy.

$^1\text{H}$  NMR (400 MHz,  $\text{CDCl}_3$ ,  $\delta$  ppm) 6.85 (m, 1H), 6.60 (m, 2H), 3.73 (s, 3H), 3.55 (bs, 2H), 1.40 (s, 9H).

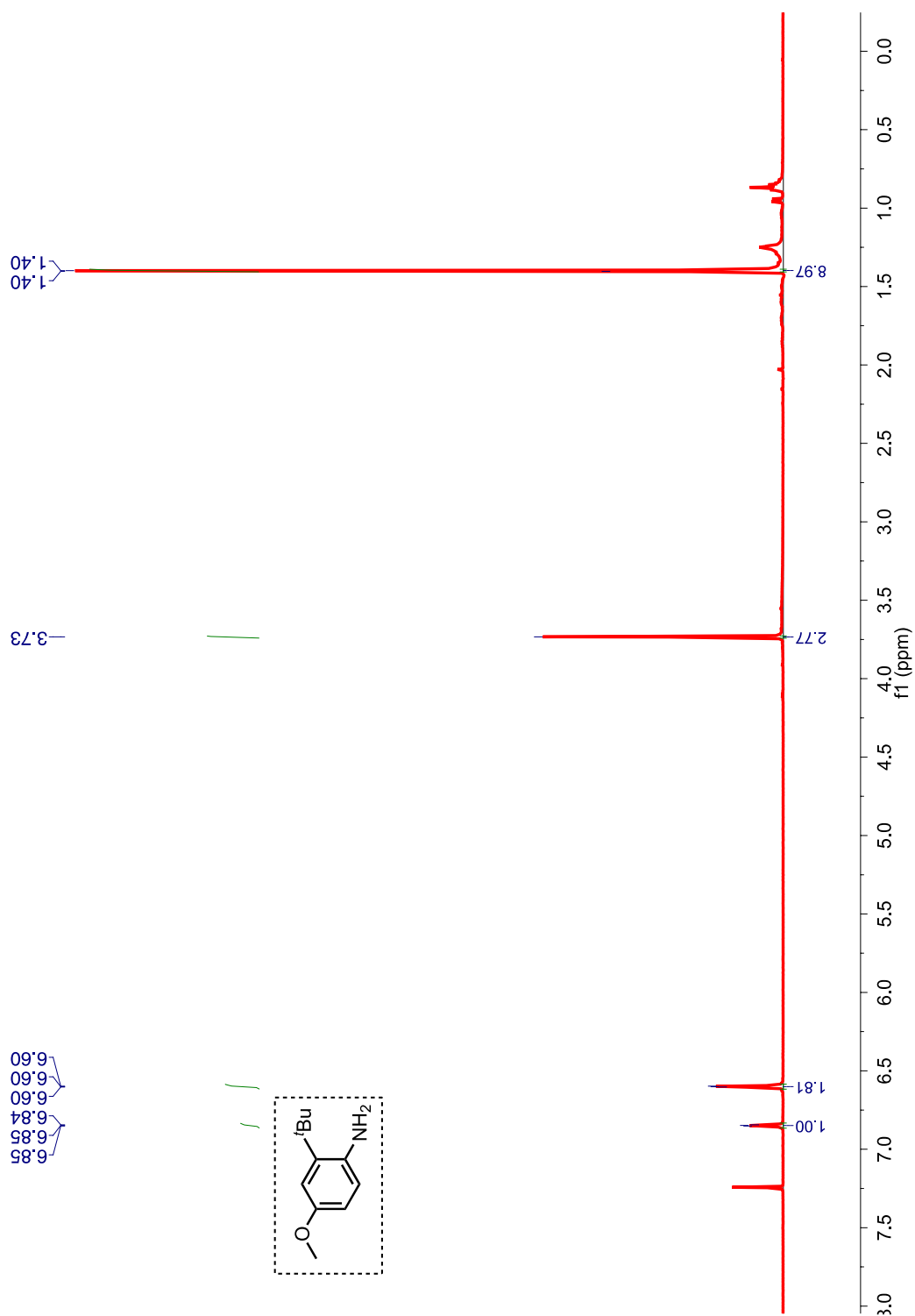


**Figure 2.12:**  $^1\text{H}$  NMR (400 MHz,  $\text{CDCl}_3$ ,  $\delta$  ppm) spectrum of 4-amino-3-*tert*-butylanisole **101**.



$^{13}\text{C}$  NMR (100 MHz,  $\text{CDCl}_3$ ,  $\delta$  ppm) 152.9, 138.5, 136.1 119.0, 111.3, 55.8, 34.7, 29.8.

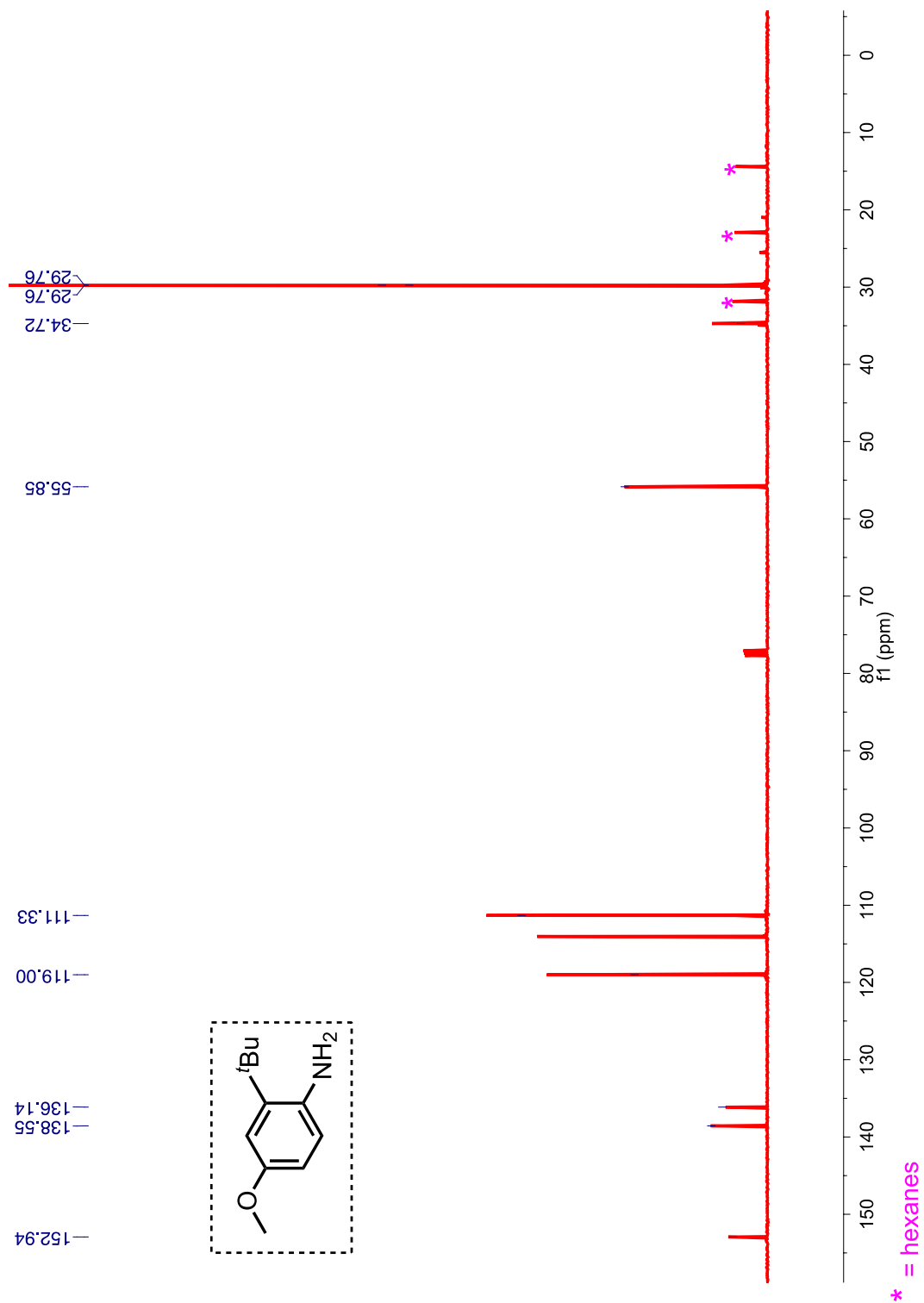


**Figure 2.13:**  $^{13}\text{C}$  NMR (100 MHz,  $\text{CDCl}_3$ ,  $\delta$  ppm) spectrum of 4-amino-3-*tert*-butylanisole **101**.

### 2.11.3. Synthetic protocol for 2,4-diketo-6methylhept-5-enoate **102**

Enone **102** derivative was synthesized according to a procedure reported in the literature.<sup>72</sup> A flask was evacuated and purged with N<sub>2</sub>. Absolute ethanol (EtOH) was added to the empty round bottom under nitrogen. Then mixtures of mesityl oxide (10.2 mmol, 1 equiv.), and diethyl oxalate (10.2 mmol, 1 equiv.) in EtOH were added to the round bottom at 0 °C. After the reaction mixture was allowed to stir for 5 minutes then sodium ethoxide in ethanol (21 wt%, a yellow solution) (11.2 mmol, 1.1 equiv.) was added dropwise over 20 min. The resulting reaction mixture was dark yellow in color. The reaction mixture was allowed to stir at 0 °C for an additional 10 min before slowly rising to room temperature. The reaction mixture was allowed to stir overnight. After approximately 20 hours the reaction was diluted with diethyl ether, then poured into a flask containing 2 N H<sub>2</sub>SO<sub>4</sub> (~5 mL *conc.* acid into 76 mL H<sub>2</sub>O). The organic layer was separated and the aqueous layer was extracted with ethyl acetate. The crude product was purified by Combiflash yielding a light yellow oil in 30% yield.

$^1\text{H}$  NMR (400 MHz,  $\text{CDCl}_3$ ,  $\delta$  ppm) 6.18 (s, 1H), 4.30 (q,  $J = 7.1$  Hz, 2H), 2.52 (s, 2H), 1.47 (s, 6H), 1.33 (t,  $J = 7.1$  Hz, 3H).

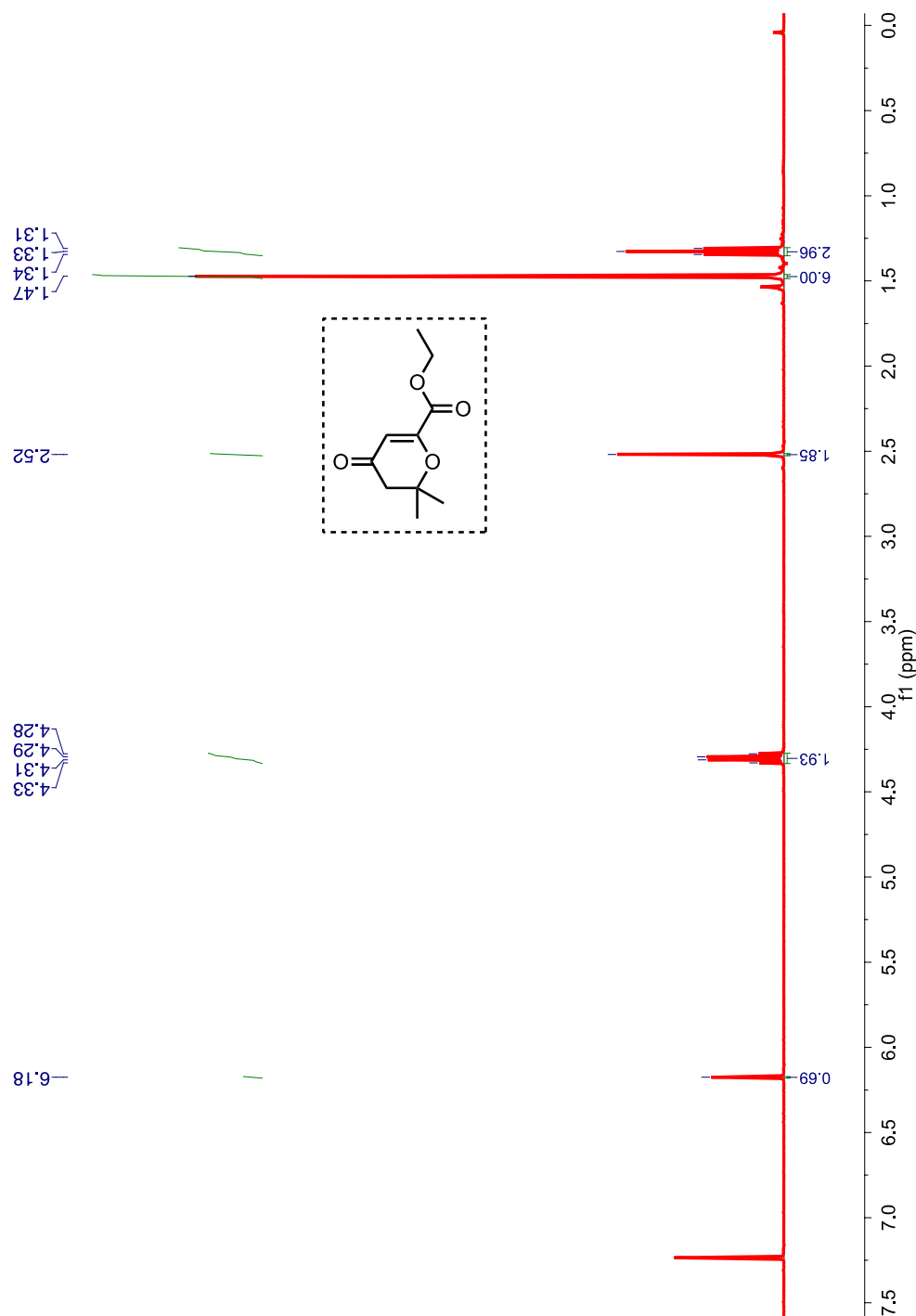


**Figure 2.14:**  $^1\text{H}$  NMR (400 MHz,  $\text{CDCl}_3$ ,  $\delta$  ppm) spectrum of 2,4-diketo-6-methylhept-5-enoate 102.

$^{13}\text{C}$  NMR (100 MHz,  $\text{CDCl}_3$ ,  $\delta$  ppm) 193.8, 162.3, 157.4, 107.5, 82.7, 62.6, 47.8, 26.0, 14.2.

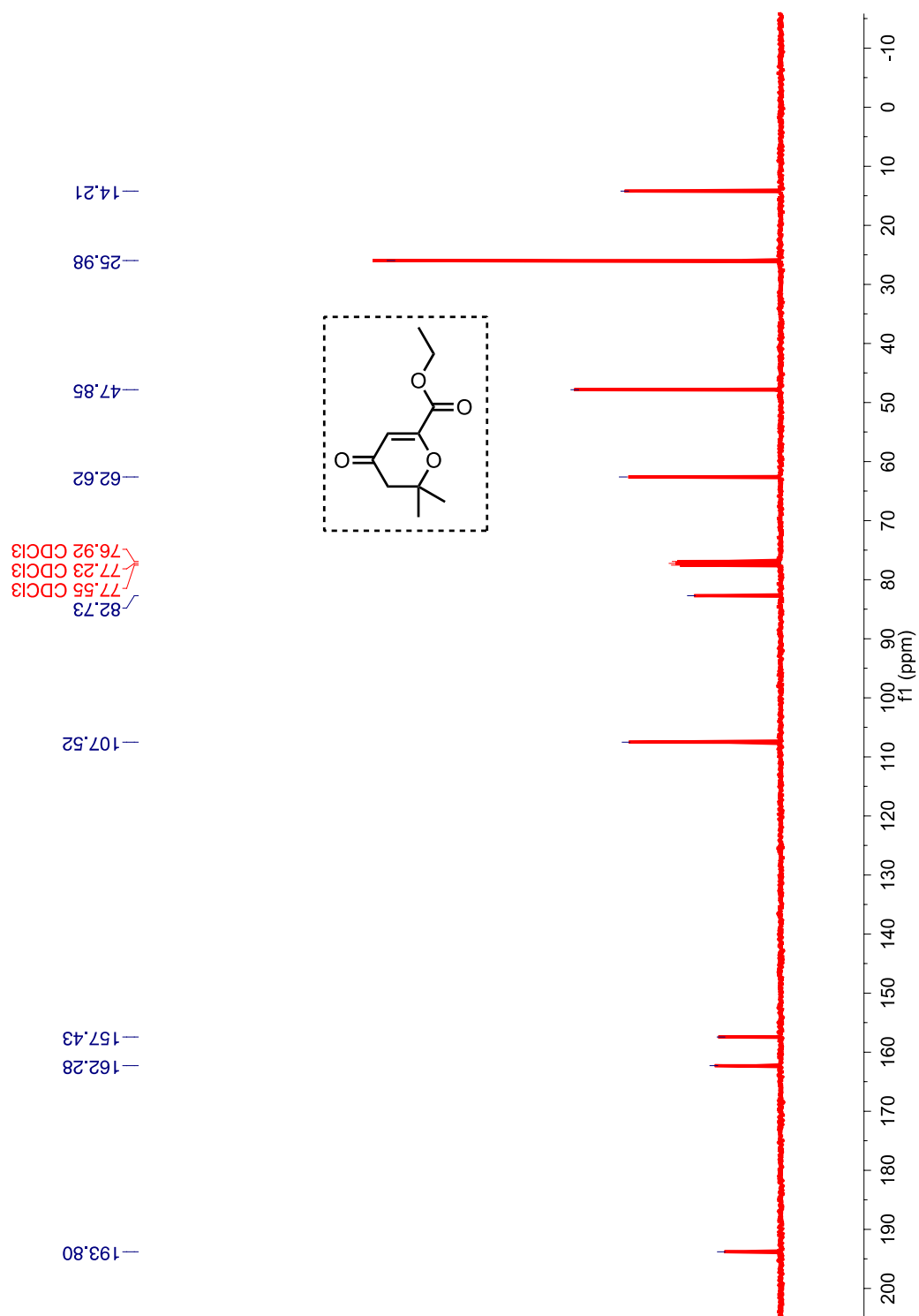
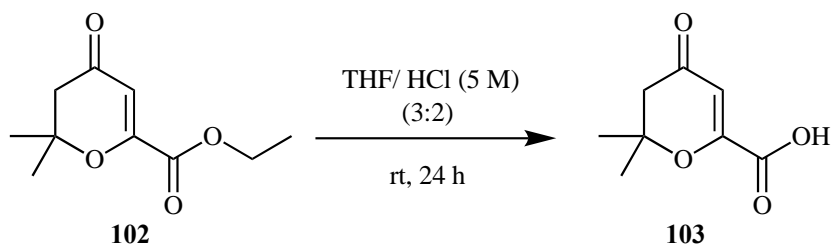


**Figure 2.15**  $^{13}\text{C}$  NMR (100 MHz,  $\text{CDCl}_3$ ,  $\delta$  ppm) spectrum of 2,4-diketo-6-methylhept-5-enoate **102**.

#### 2.11.4. Synthetic protocol of 3,4-dihydro-2,2-dimethyl-4-oxo-2H-pyran-6-carboxylic acid

103



#### **Scheme 2.10:** Synthesis of carboxylic acid derivative **103**.

To a solution of **102** (2 g) in THF (45 mL), 5 M HCl (30 mL) was added and stirred for 24 h or until precipitation occurred. After starting material was consumed, the solvent was removed under vacuum. Followed by washing with water and removing under vacuum. The crude product was purified by recrystallization in THF: hexanes mixture to yield an off white solid (80 % yield).

$^1\text{H}$  NMR (400 MHz,  $\text{CDCl}_3$ ,  $\delta$  ppm) 6.30, (s, 1H), 2.57 (s, 2H), 1.50 (s, 6H).

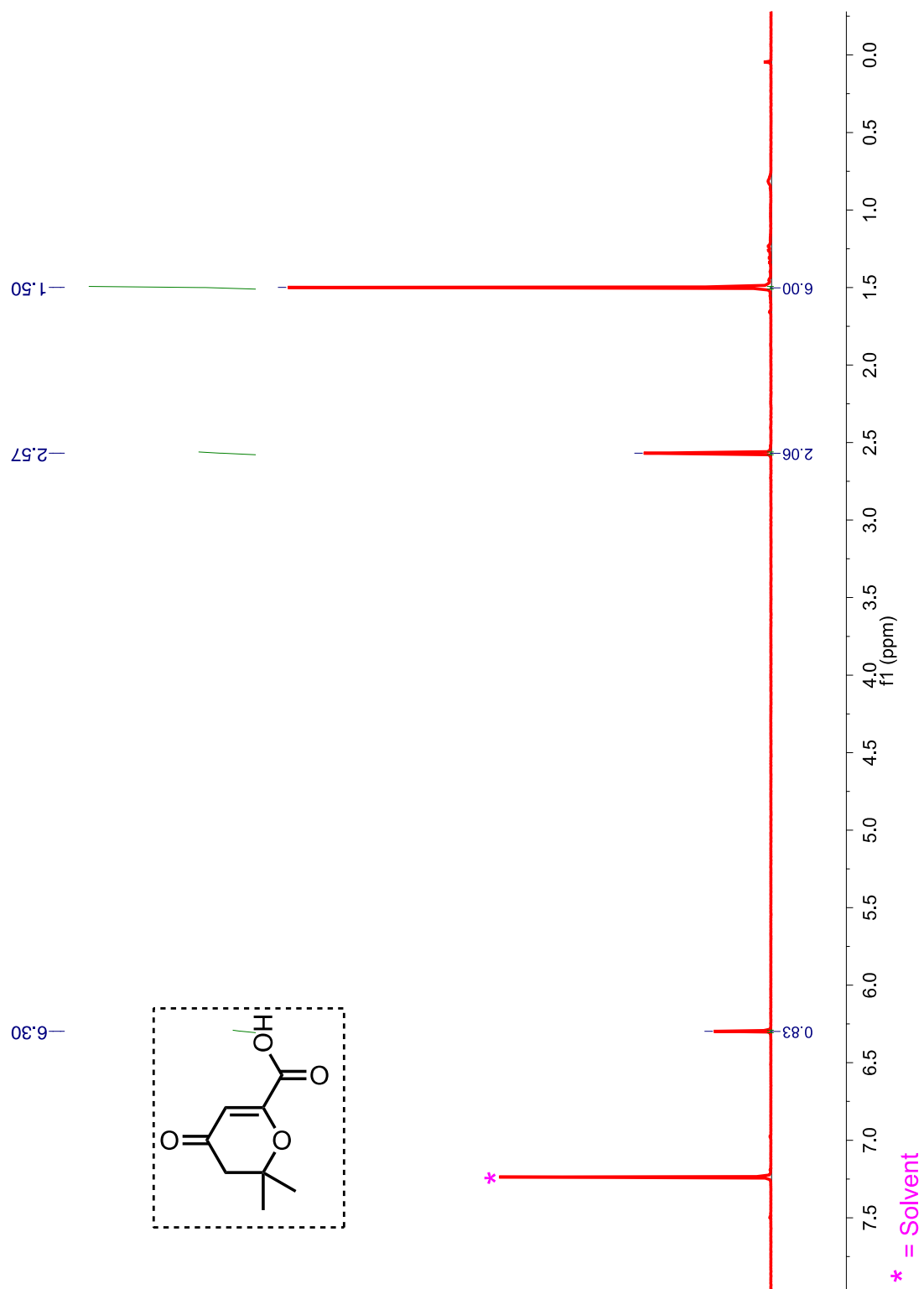
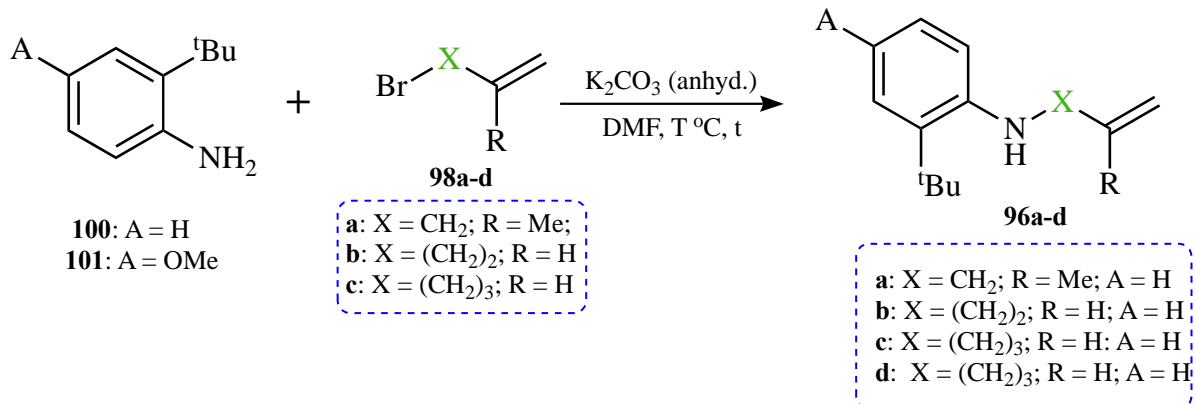


**Figure 2.16:**  $^1\text{H}$  NMR (400 MHz,  $\text{CDCl}_3$ ,  $\delta$  ppm) spectrum of carboxylic acid **103**.

### 2.11.5. Synthetic protocol for *N*-substituted anilines **96a-d**



#### Scheme 2.11: Synthesis of protocol for *N*-substituted anilines **96a-d**

Following a reported procedure<sup>55,73</sup> the aniline derivative (*2-tert*-butyl aniline **101a** or **101b**) (6.7 mmol, 1.5 eq.) was added to an oven dried, N<sub>2</sub> purged round bottom, followed by activated K<sub>2</sub>CO<sub>3</sub> (11.2 mmol, 2.5 eq.). The resulting mixture was dissolved in DMF (22 mL) followed by the addition of appropriate alkene **98a-d** (4.5 mmol, 1 eq.). The reaction mixture was set to 90 °C and allowed to stir overnight. The reaction mixture was removed from heat, quenched with H<sub>2</sub>O then extracted with EtOAc followed by washing with brine solution after approximately 16 h. The organic layers were combined, dried over Na<sub>2</sub>SO<sub>4</sub> (*anhyd.*), filtered concentrated and purified by combiflash hexanes : EtOAc (95:5) as the mobile phase. Products were afforded as **96a** pale yellow liquid (44 % yield); **96b** a yellow liquid in (44 % yield); **96c** amber liquid (76 % yield); **96d** amber liquid (66 % yield).

$^1\text{H}$  NMR (400 MHz, Chloroform- $\delta$ ) 7.25-7.22 (m, 1H), 7.12 - 7.07 (m, 1H), 6.72 - 6.63 (m, 2H), 5.00 - 4.99 (m, 1H), 4.91 (m, 1H), 3.74 (s, 2H), 1.81 (d,  $J = 1.1$  Hz, 3H), 1.42 (d,  $J = 1.1$  Hz, 9H).

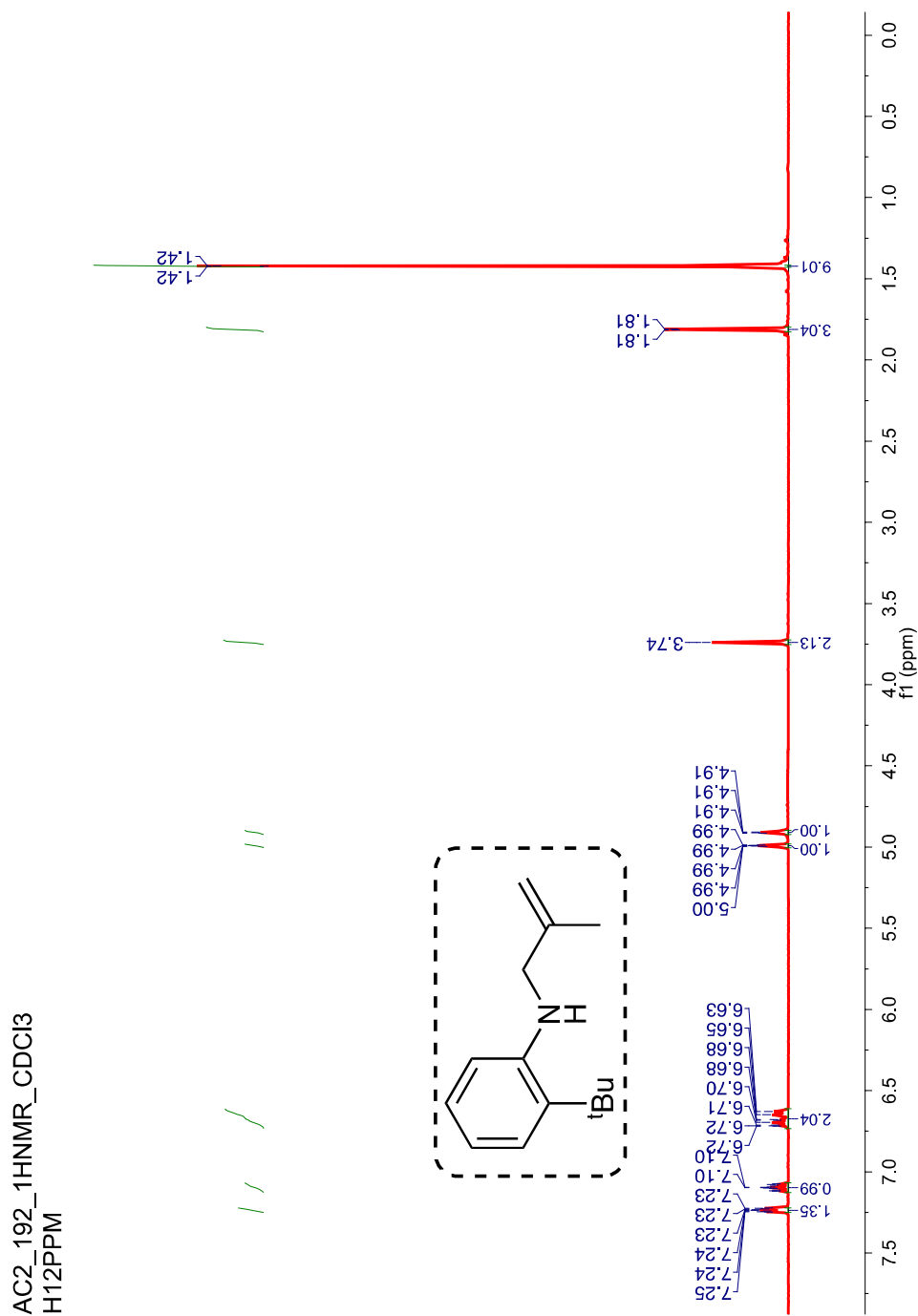


**Figure 2.17:**  $^1\text{H}$  NMR (400 MHz, Chloroform- $\delta$ ) spectrum of amine derivative **96a**



$^{13}\text{C}$  NMR (100 MHz, Chloroform- $\delta$ ) 146.4, 143.1, 133.3, 127.4, 126.4, 117.4, 112.2, 111.3, 50.7, 34.45, 30.3, 21.1.

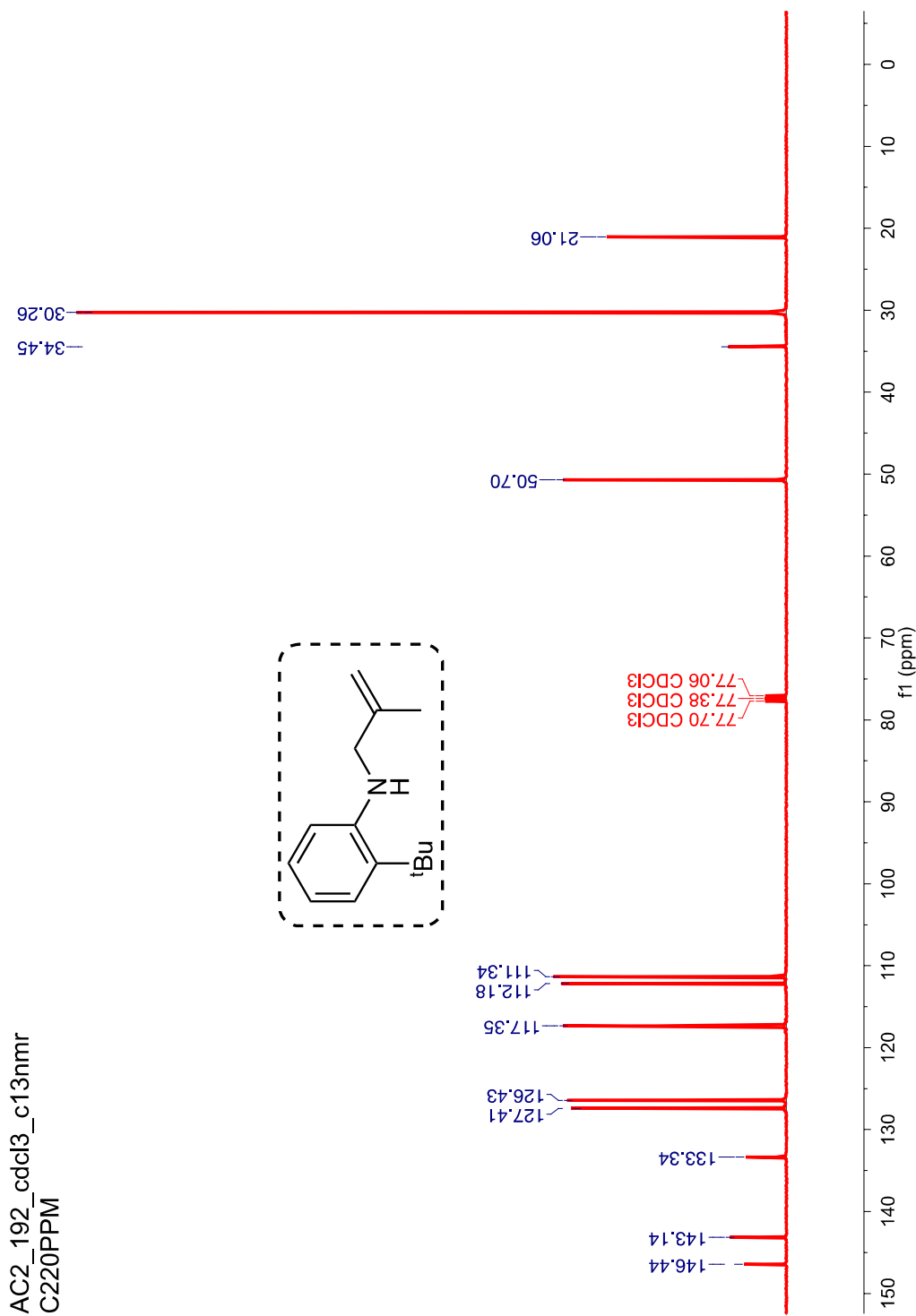


**Figure 2.18:**  $^{13}\text{C}$  NMR (100 MHz, Chloroform- $\delta$ ) spectrum of amine derivative **96a**.

$^1\text{H}$  NMR (400 MHz,  $\text{CDCl}_3$ ,  $\delta$  ppm) 7.23 – 7.20 (m, 1H), 7.12 – 7.08 (m, 1H), 6.68 – 6.64(m, 2H), 5.89 - 5.79 (m, 1H), 5.21 – 5.12 (m, 3H), 3.96 (bs, 1H), 3.22 (t,  $J = 6.4$  Hz, 3H), 2.48 – 2.43 (m,  $J = 3$ H), 1.37 (s, 9H).

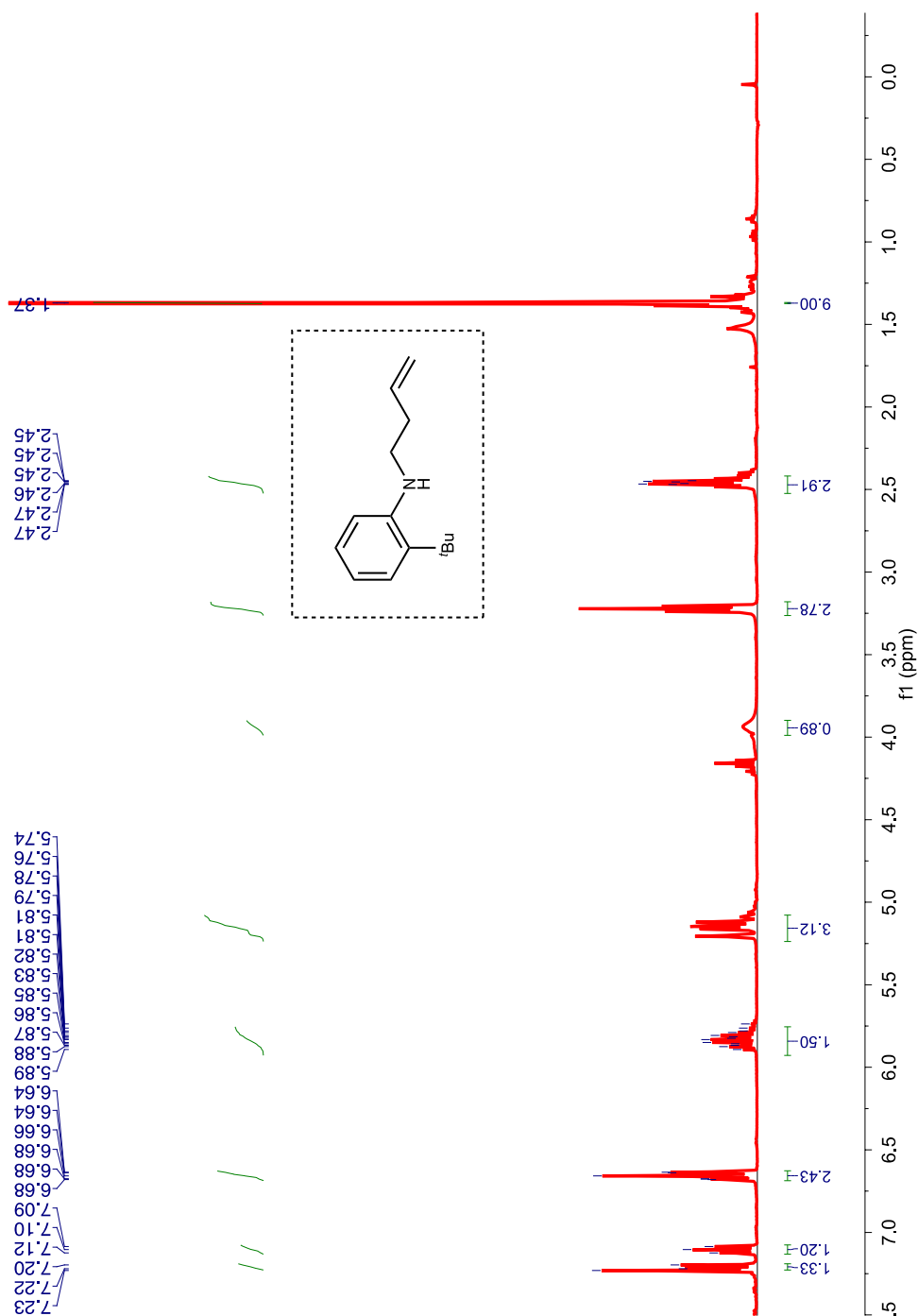


**Figure 2.19:**  $^1\text{H}$  NMR (400 MHz,  $\text{CDCl}_3$ ,  $\delta$  ppm) spectrum of *N*-butenyl aniline **96b**

$^{13}\text{C}$  NMR (100 MHz,  $\text{CDCl}_3$ ,  $\delta$  ppm) 146.6, 136.6, 133.3, 127.3, 126.4, 117.6, 117.0, 111.7, 43.4, 34.0, 30.1.

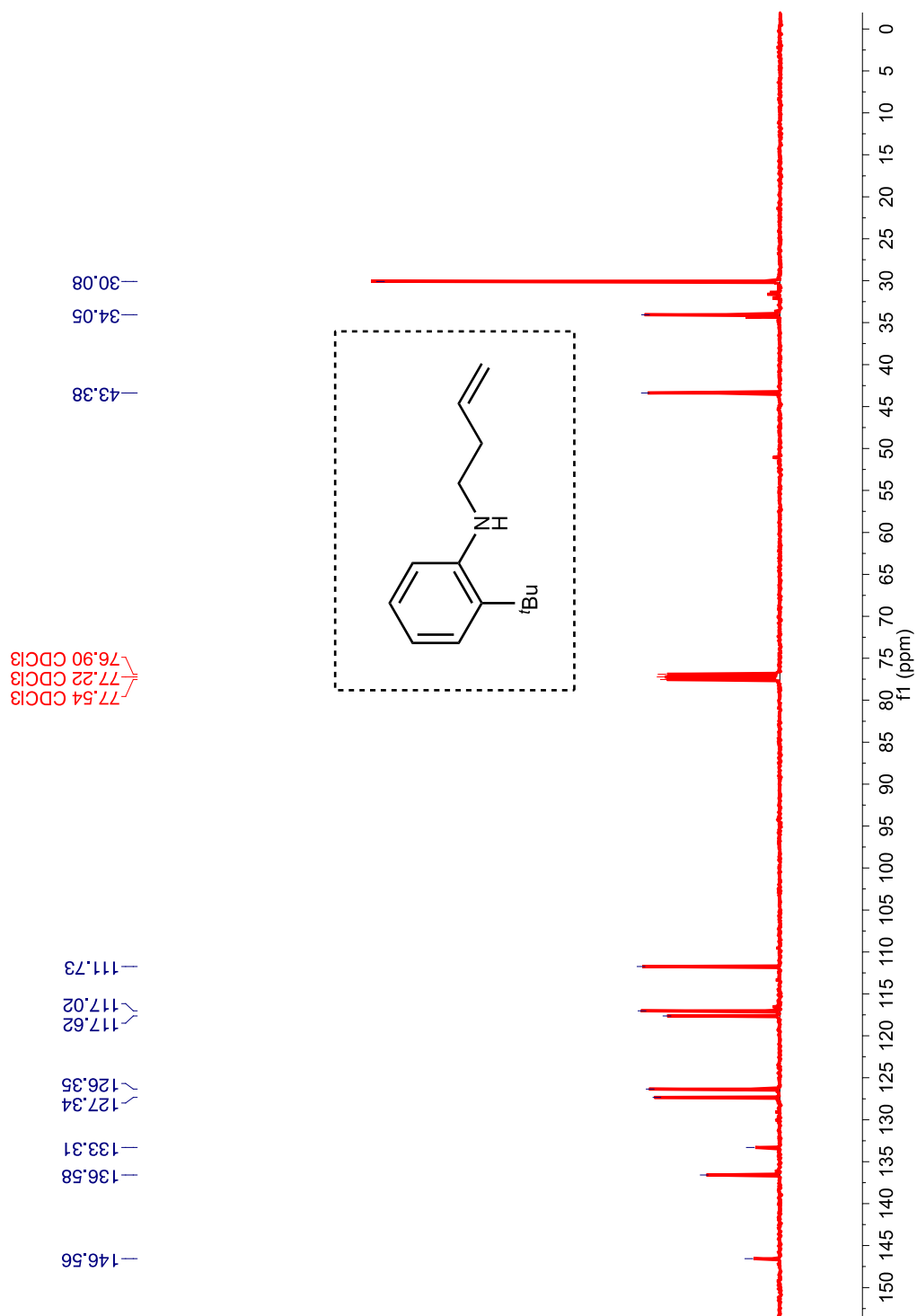


**Figure 2.20:**  $^{13}\text{C}$  NMR (100 MHz,  $\text{CDCl}_3$ ,  $\delta$  ppm) spectrum of *N*-butenyl aniline **96b**.

$^1\text{H}$  NMR (400 MHz,  $\text{CDCl}_3$ ,  $\delta$  ppm) 7.26 - 7.24 (m, 1H), 7.16 - 7.12 (m, 1H), 6.69 (t,  $J = 7.4$  Hz, 2H), 5.94 - 5.82 (m, 1H), 5.13 - 4.99 (m, 2H), 3.86 (s, 1H), 3.21 (t,  $J = 7.0$  Hz, 2H), 2.27 - 2.19 (m, 2H), 1.85 - 1.77 (m, 2H), 1.43 (s, 9H).

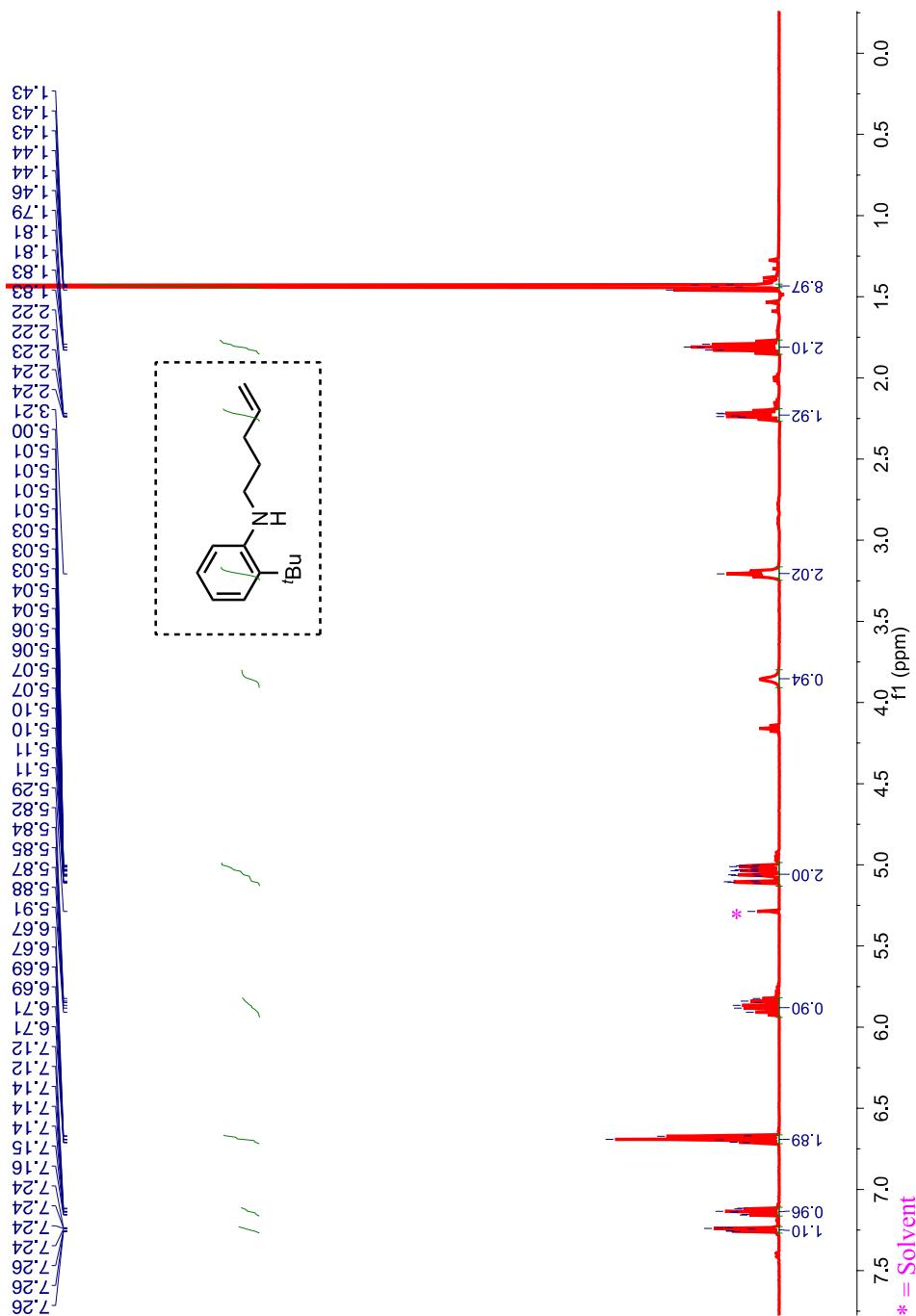


**Figure 2.21:**  $^1\text{H}$  NMR (400 MHz,  $\text{CDCl}_3$ ,  $\delta$  ppm) spectrum of *N*-pentenyl aniline **96c**.

$^{13}\text{C}$  NMR (100 MHz,  $\text{CDCl}_3$ ,  $\delta$  ppm) 146.7, 138.2, 133.2, 127.4, 126.4, 117.0, 115.4, 111.8, 44.0, 34.4, 31.8, 30.2, 29.1.

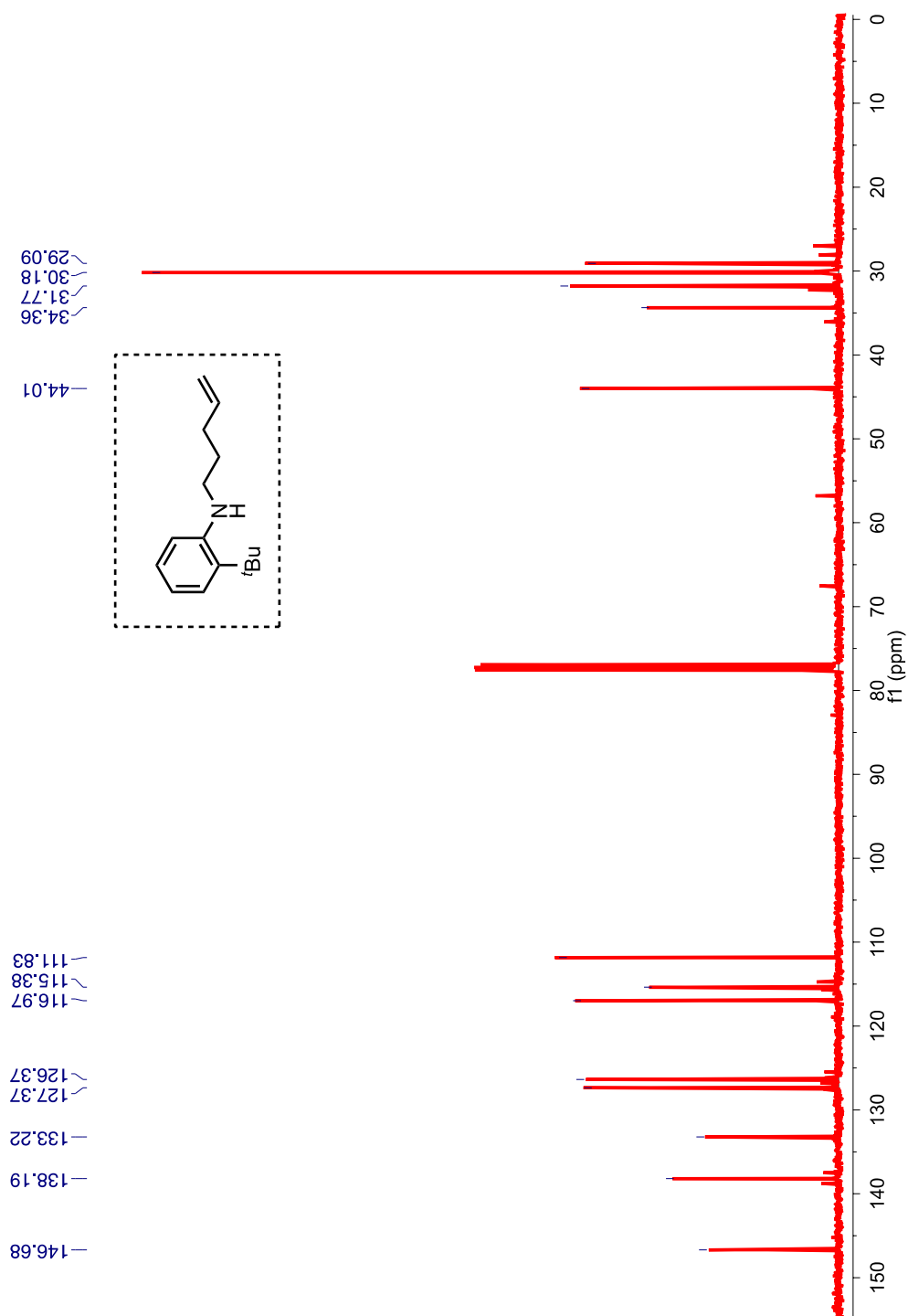


**Figure 2.22:**  $^{13}\text{C}$  NMR (100 MHz,  $\text{CDCl}_3$ ,  $\delta$  ppm) spectrum of *N*-pentenyl aniline **96c**.

$^1\text{H}$  NMR (400 MHz,  $\text{CDCl}_3$ ,  $\delta$  ppm) 6.89 – 6.88 (m, 1H), 6.71 - 6.68 (m, 1H), 6.63 – 6.61 (m, 1H), 5.91 - 5.80 (m, 1H), 5.09 - 4.97 (m, 2H), 3.74 (s, 3H), 3.56 (bs, 1H), 3.13 (t,  $J = 7.0$  Hz, 2H), 2.24 - 2.16 (m, 2H), 1.82 - 1.73 (m, 2H), 1.40 (s, 9H).

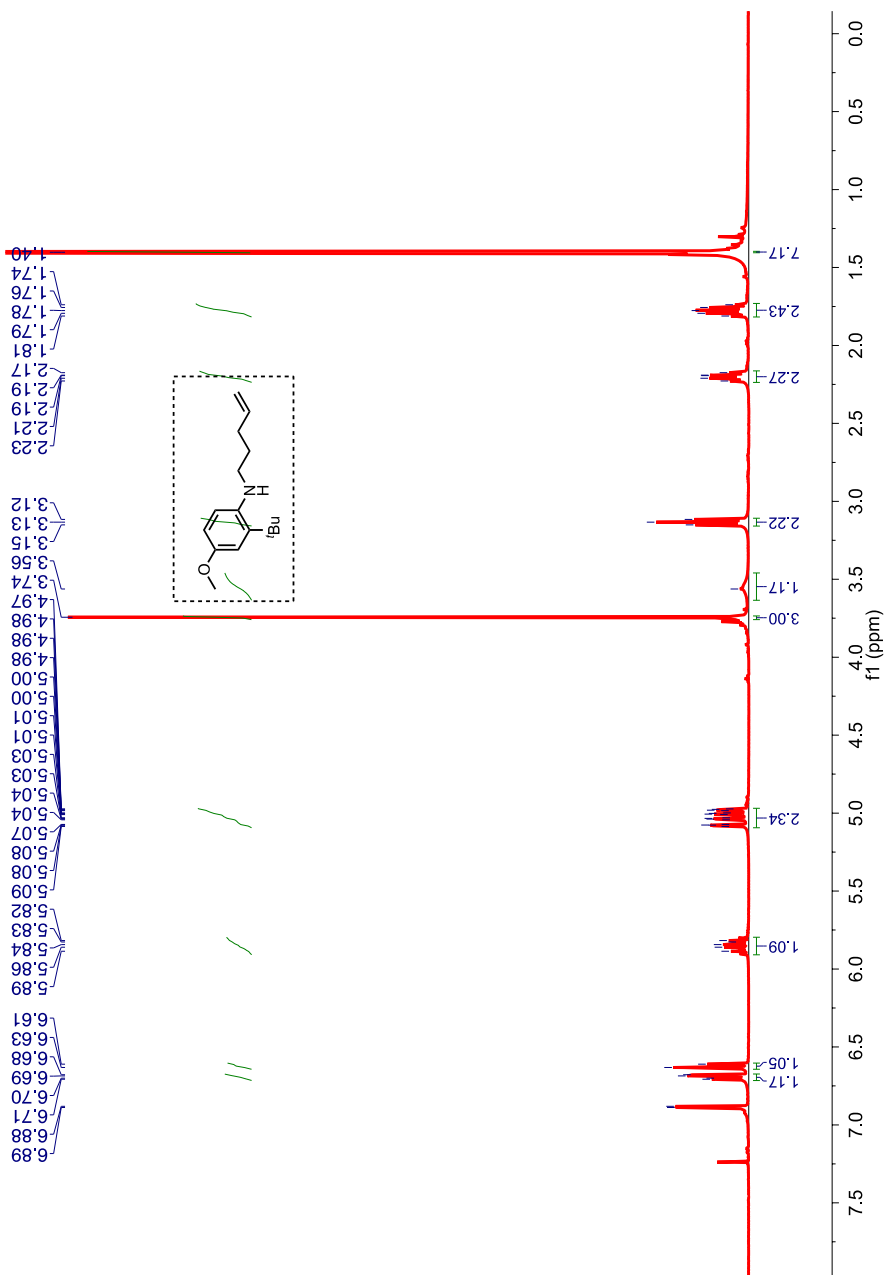


**Figure 2.23:**  $^1\text{H}$  NMR (400 MHz,  $\text{CDCl}_3$ ,  $\delta$  ppm) spectrum of *N*-pentenyl-*ortho*-methoxy aniline derivative **96d**.

$^{13}\text{C}$  NMR (100 MHz,  $\text{CDCl}_3$ ,  $\delta$  ppm) 151.8, 141.1, 138.3, 135.8, 115.3, 114.5, 113.2, 110.8, 55.9, 45.0, 34.6, 31.8, 30.1, 29.2.

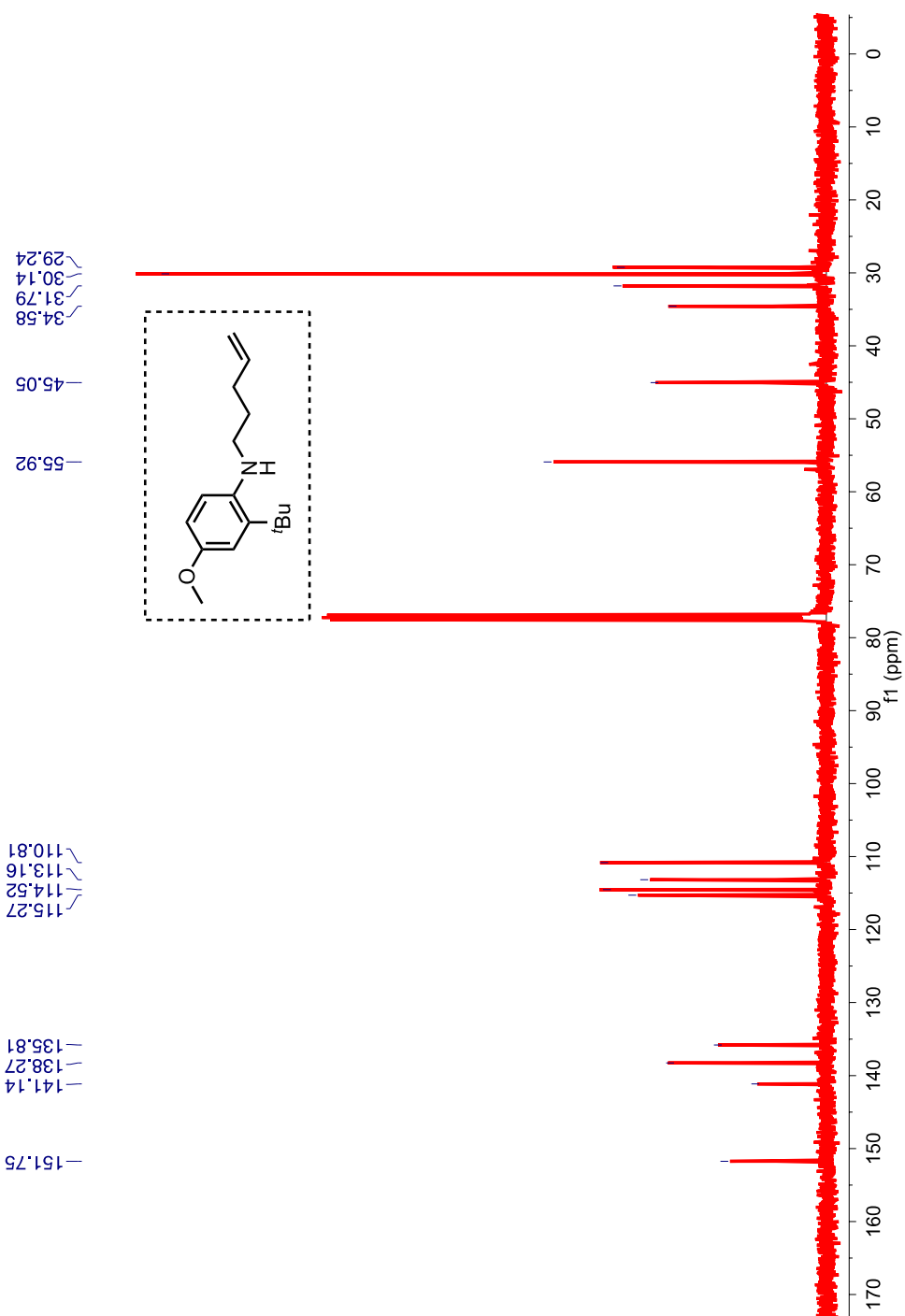
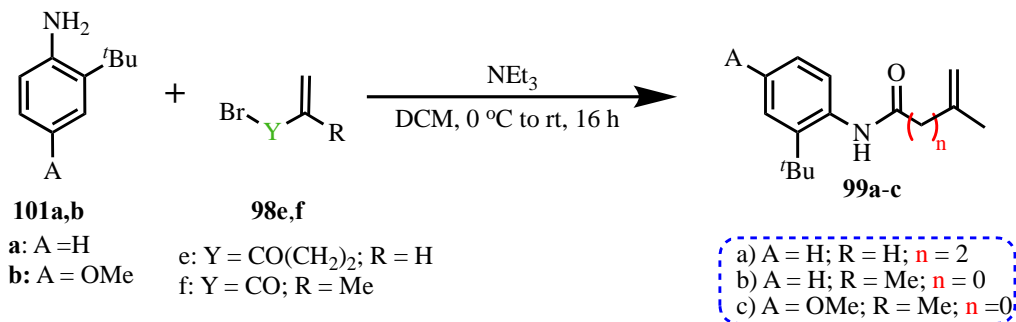


**Figure 2.24:**  $^{13}\text{C}$  NMR (100 MHz,  $\delta$  ppm,  $\text{CDCl}_3$ ) spectrum of *N*-pentenyl-*ortho*-methoxy aniline derivative **96d**.

### 2.11.6. Synthetic protocol for secondary amide derivatives **99a-c**



#### Scheme 2.12: Synthetic protocol for secondary derivatives **99a-c**.

Literature reported procedure<sup>54,74</sup> was employed as reported for the synthesis of amides **99a-c**. To a solution of the aniline derivative (2-*tert*-butyl-aniline or **101**) (1.0 g, 1.0 equiv), triethylamine (2.0 equiv) in dry DCM (15 mL) at 0 °C under N<sub>2</sub> atmosphere the corresponding acyl chloride **98** e-g (1.1 equiv) was added. The resulting solution was slowly allowed to warm to room temperature over 6 h. After the reaction, water was added, stirred and the layers were separated. The organic layer was washed with DI water (2 × 15 mL), dried over *anhyd.* Na<sub>2</sub>SO<sub>4</sub>, filtered and the solvent was removed under reduced pressure to yield crude product. The crude product was purified by combiflash using hexanes ethyl acetate as the mobile phase. Products were obtained as white solids in 80% = **99b** and 50% = **99c**.



$^1\text{H}$  NMR (500 MHz,  $\text{CDCl}_3$ ,  $\delta$  ppm) 7.60 (d,  $J = 7.9$  Hz, 1H), 7.41 (d,  $J = 7.9$  Hz, 1H), 7.25 - 7.24 (m, 1H), 7.20 - 7.16 (m, 1H), 5.97 - 5.92 (m, 1H), 5.19 - 5.16 (m, 1H), 5.10 - 5.08 (m, 1H), 2.56 - 2.53 (m, 4H), 1.43 (s, 9H), 1.41 (s, 2H).

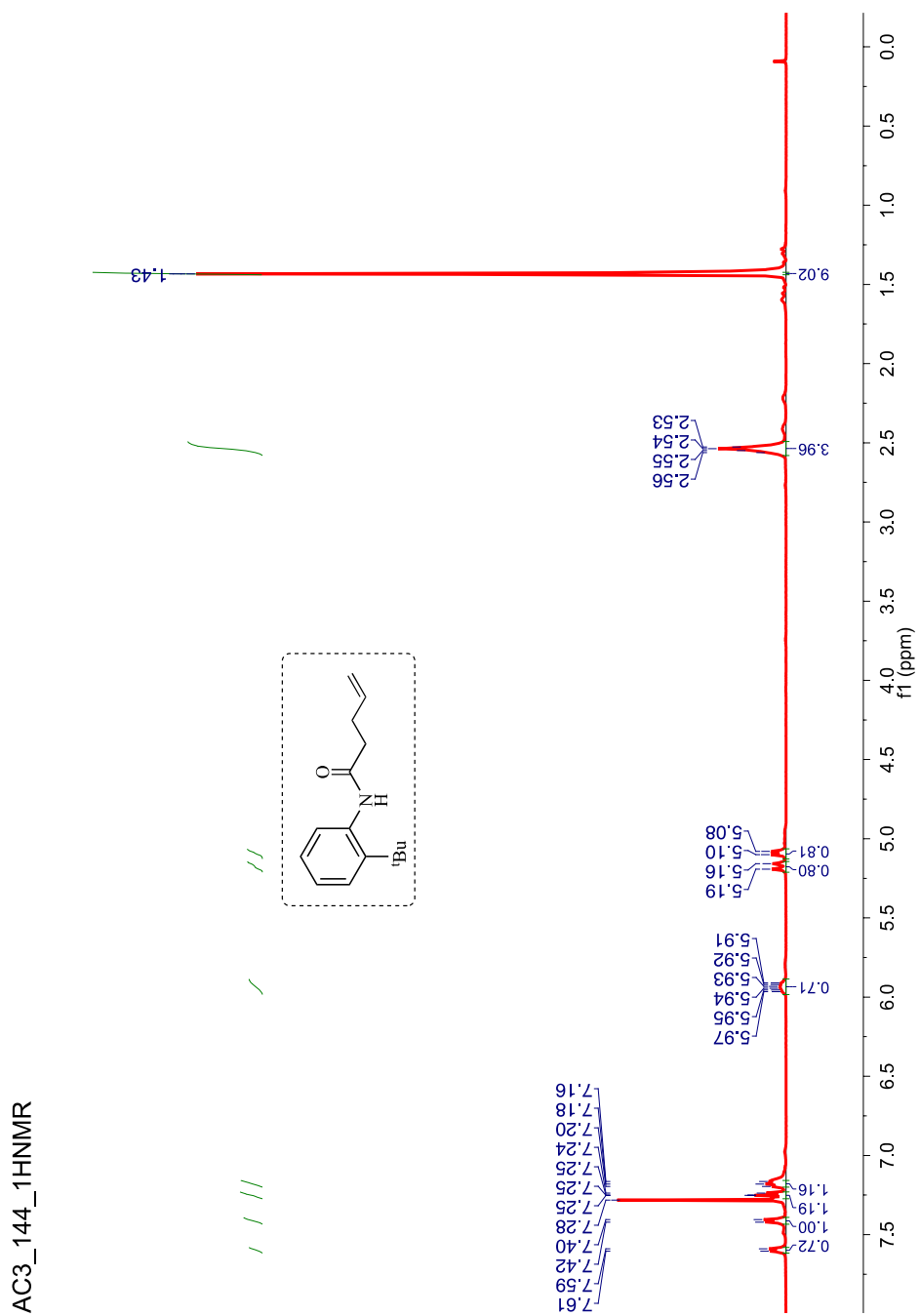


**Figure 2.25:**  $^1\text{H}$  NMR (500 MHz,  $\text{CDCl}_3$ ,  $\delta$  ppm) spectrum of secondary amide derivative **99a**.

$^{13}\text{C}$  NMR (125 MHz,  $\text{CDCl}_3$ ,  $\delta$  ppm) 171.7, 144.5, 137.4, 135.5, 129.9, 115.8, 36.5, 35.0, 31.0, 30.0 .

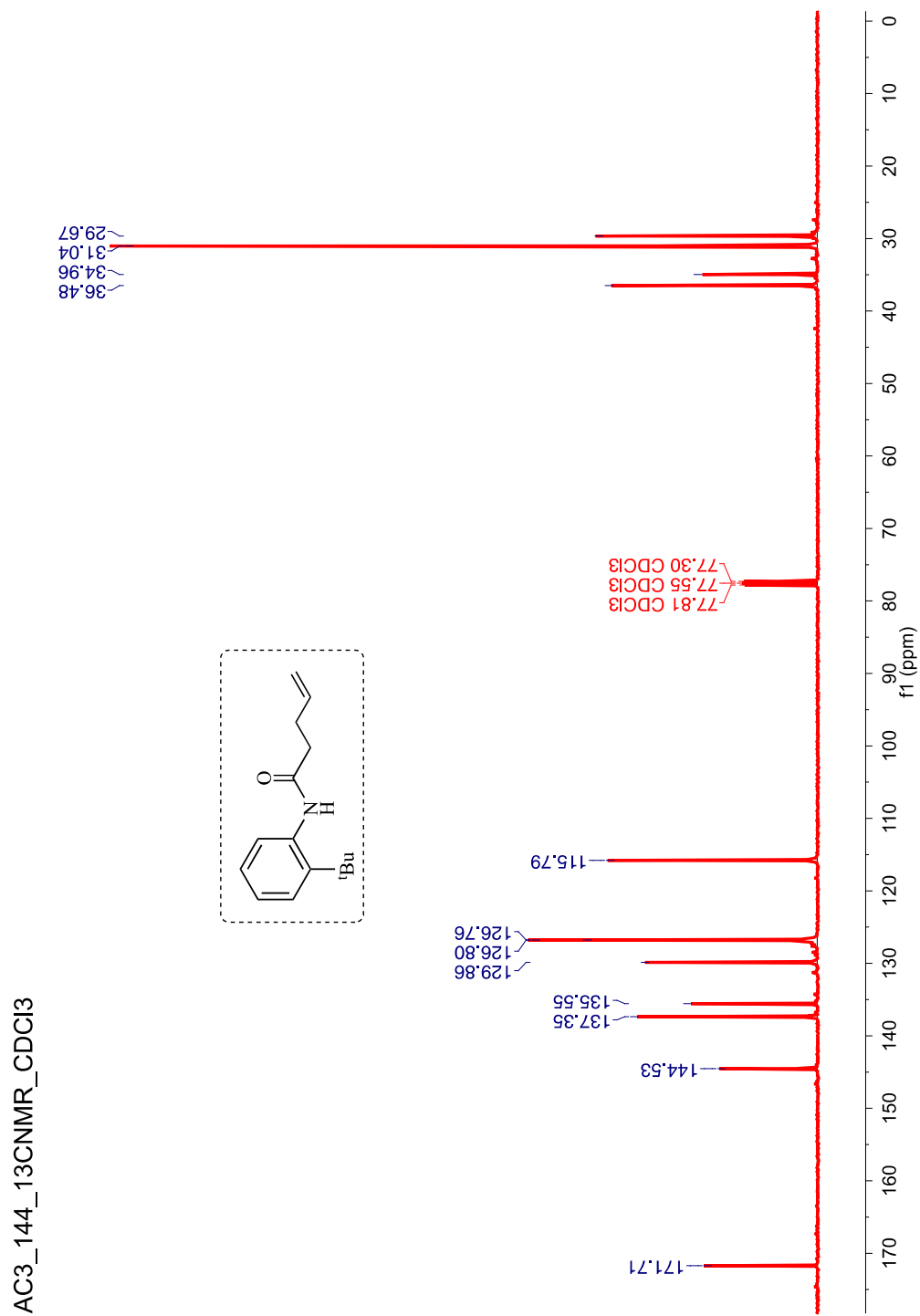


**Figure 2.26:**  $^{13}\text{C}$  NMR (125 MHz,  $\text{CDCl}_3$ ,  $\delta$  ppm) spectrum of secondary amide derivative **99a**.

$^1\text{H}$  NMR (400 MHz,  $\text{CDCl}_3$ ,  $\delta$  ppm) 7.66- 7.64 (m, 1H), 7.59 (bs, 1H), 7.39 – 7.37 (m, 1H), 7.23 – 7.19 (m, 1H), 7.16 – 7.13 (m, 1H), 5.82 (s, 1H), 5.45 (d,  $J = 0.6$  Hz, 1H), 2.07 (s, 3H), 1.40 (s, 9H,  $\delta$  ppm).

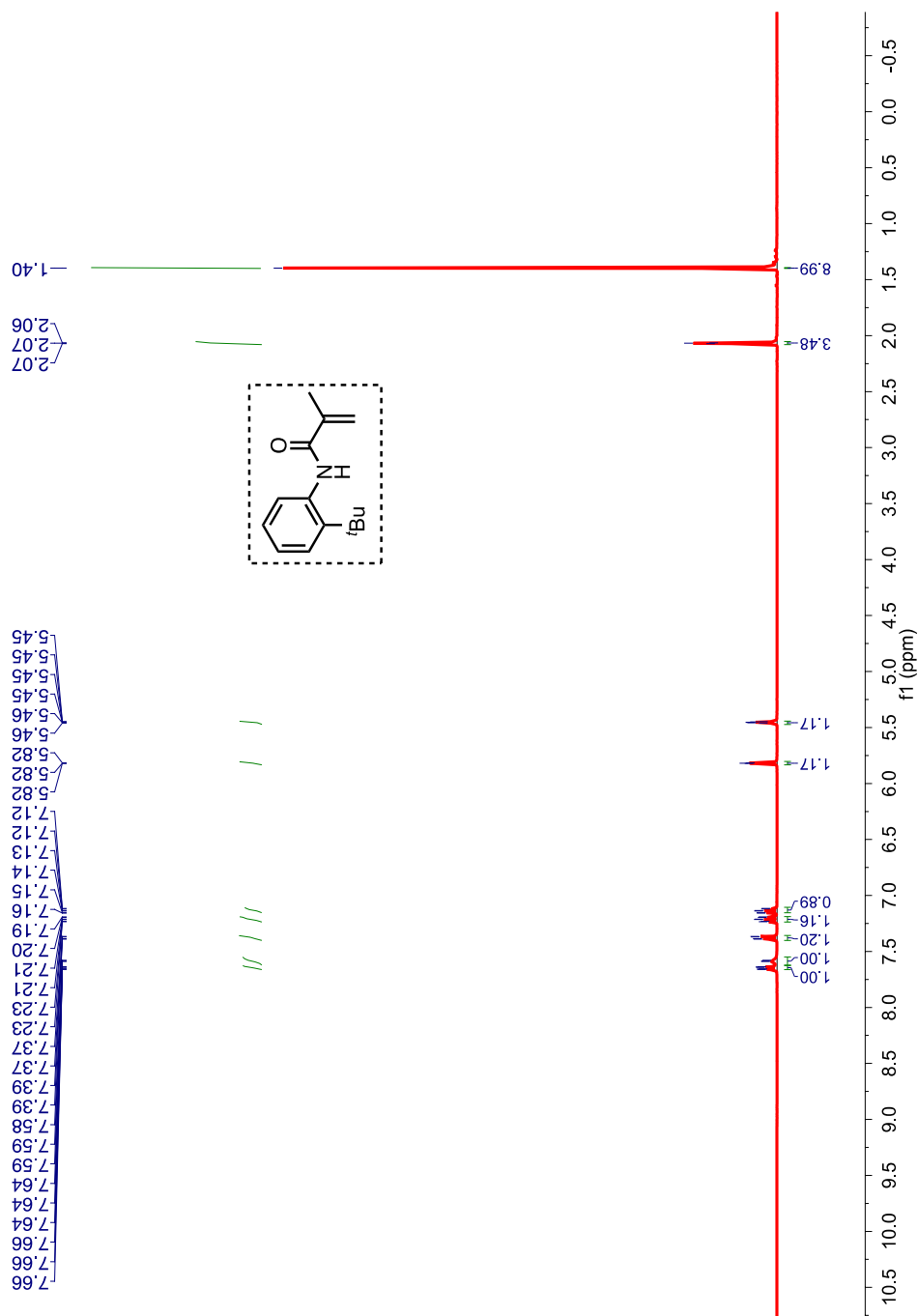


**Figure 2.27:**  $^1\text{H}$  NMR (400 MHz,  $\text{CDCl}_3$ ,  $\delta$  ppm) spectrum of secondary amide derivative **99b**.

$^{13}\text{C}$  NMR (100 MHz,  $\text{CDCl}_3$   $\delta$  ppm) 166.6, 142.4, 141.2, 135.4, 127.7, 127.0, 126.7, 126.2, 120.0, 34.7, 30.9, 19.1.

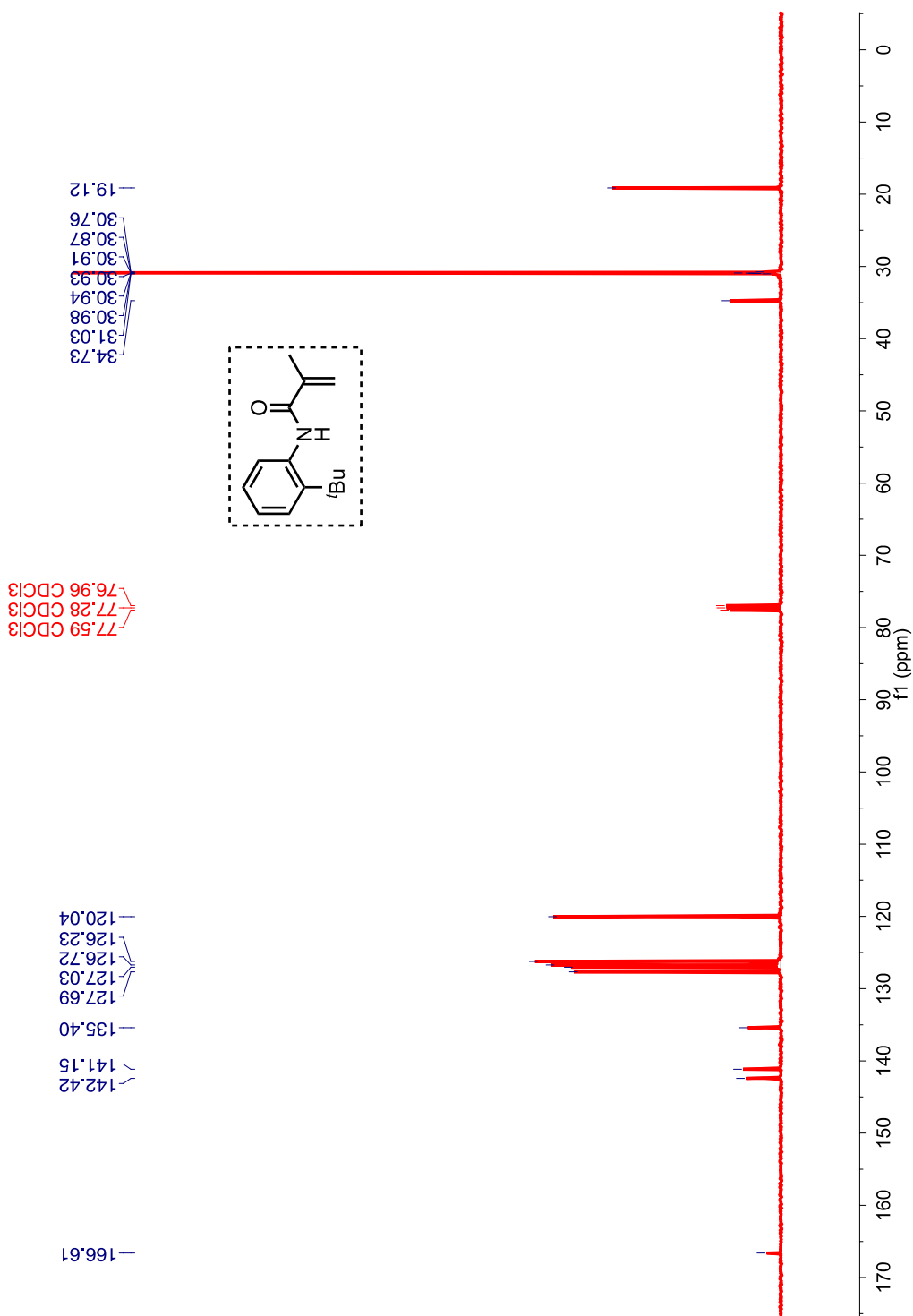


**Figure 2.28:**  $^{13}\text{C}$  NMR (100 MHz,  $\text{CDCl}_3$ ,  $\delta$  ppm) spectrum of secondary amide derivative **99b**.

$^1\text{H}$  NMR (400 MHz,  $\text{CDCl}_3$ ,  $\delta$  ppm) 7.43 – 7.36 (m, 1H), 6.94 – 6.93 (m, 1H), 6.76 – 6.73 (m, 1H), 5.81 (s, 1H), 5.43 (s, 1H), 3.78 (s, 3H), 2.05 (s, 3H), 1.37 (d,  $J = 2.2$  Hz, 9H).

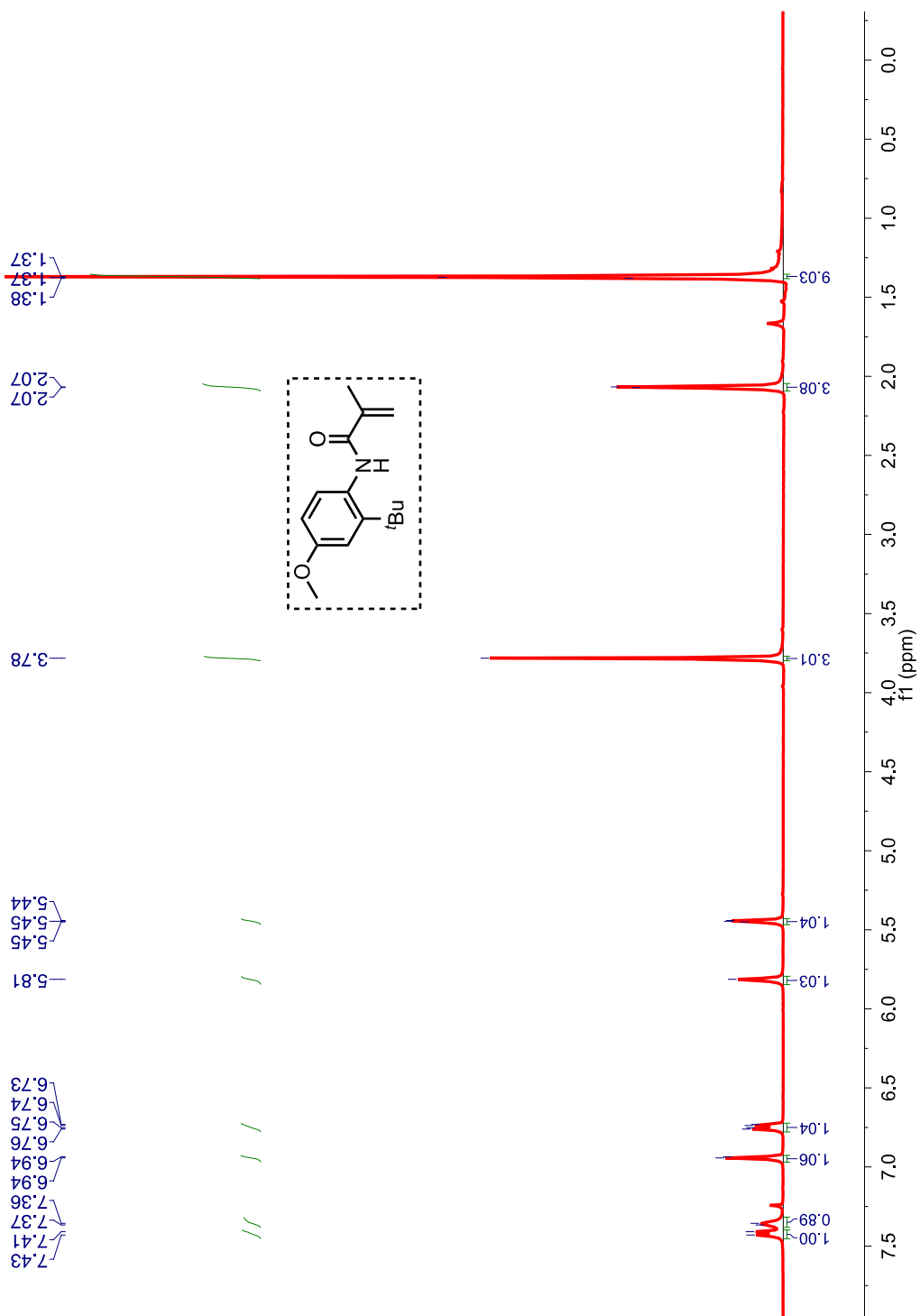


**Figure 2.29:**  $^1\text{H}$  NMR (400 MHz,  $\text{CDCl}_3$ ,  $\delta$  ppm) spectrum of secondary amide derivative **99c**.

$^{13}\text{C}$  NMR (100 MHz,  $\text{CDCl}_3$ ,  $\delta$  ppm) 167.0, 157.9, 145.5, 141.0, 130.0, 128.1, 119.9, 113.9, 110.7, 55.6, 35.0, 30.7, 19.1.

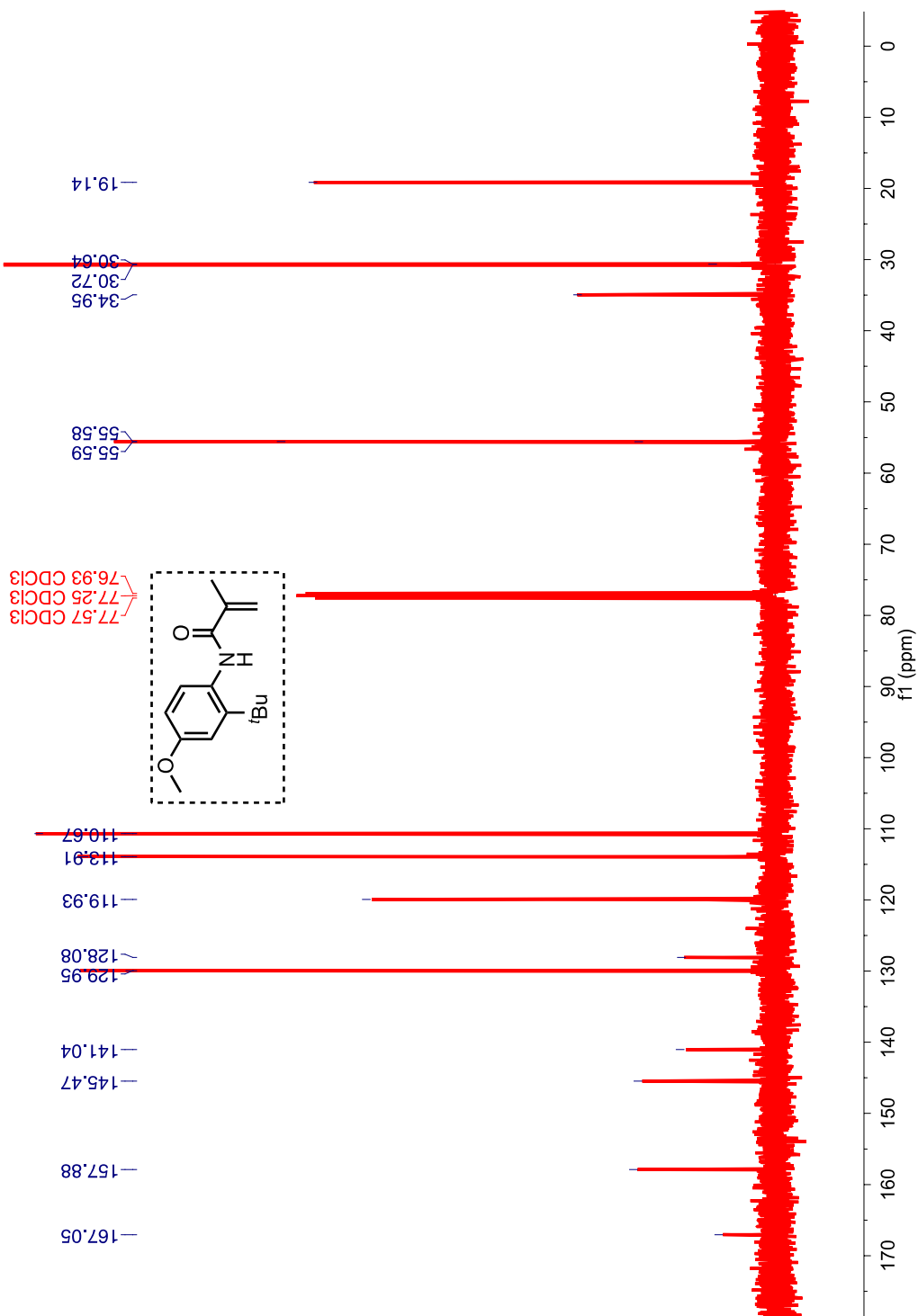


**Figure 2.30:**  $^{13}\text{C}$  NMR (100 MHz,  $\text{CDCl}_3$ ,  $\delta$  ppm) spectrum of secondary amide derivative **99c**.

### 2.11.7. Synthetic protocol for substituted atropisomeric amides **92a-d**

The same procedure was followed for the synthesis of atropisomeric amides **92a-d** as for secondary amide derivatives **99a-c** listed above for Scheme 2.12. The yields achieved were as follows,

**92a** = 70% yield (pale yellow solid)

**92b** = 60% yield (yellow liquid)

**92c** = 60 % yield (off white solid)

**92d** = 50 % yield (off white solid)

$^1\text{H}$  NMR (400 MHz,  $\text{CDCl}_3$ ,  $\delta$  ppm) 7.52-7.50 (m, 1H), 7.28 - 7.26 (m, 3H), 7.11 ? 7.02 (m, 1H), 6.93 (dd,  $J = 7.9, 1.6$  Hz, 1H), 5.78 (s, 1H), 5.10 ? 5.05 (m, 1H), 4.88 ? 4.86 (m, 1H), 4.66 (dt,  $J = 1.6, 0.8$  Hz, 1H), 3.33 (dd,  $J = 14.4, 0.9$  Hz, 1H), 2.33 ? 2.16 (m, 2H), 1.79 ? 1.75 (m, 3H), 1.38 (s, 9H), 0.99 (s, 3H), 0.84 (s, 3H).

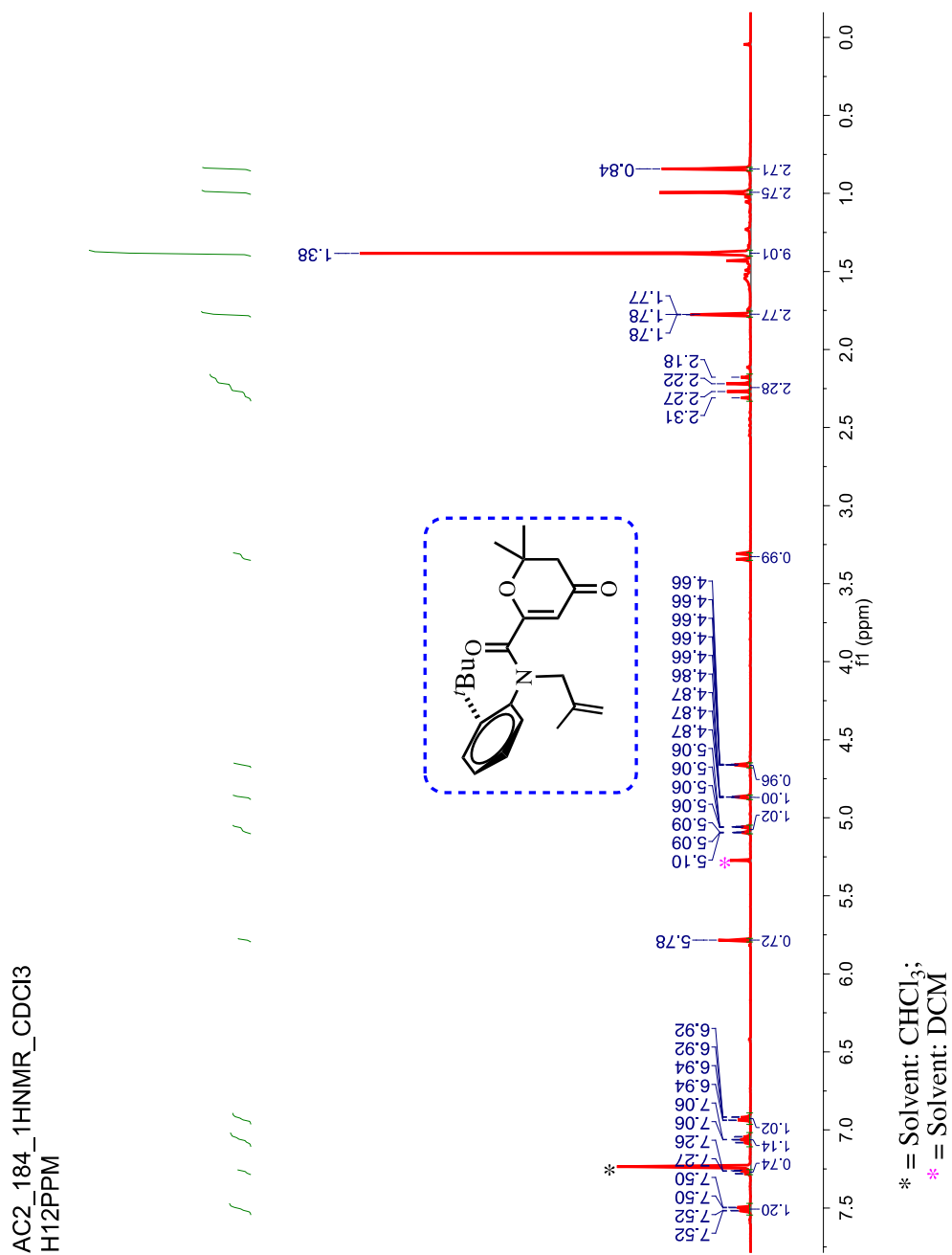


**Figure 2.31:**  $^1\text{H}$  NMR (400 MHz,  $\text{CDCl}_3$ ,  $\delta$  ppm) spectrum of atropisomeric amide derivative **92a**



$^{13}\text{C}$  NMR (100 MHz,  $\text{CDCl}_3$ ,  $\delta$  ppm) 192.7, 164.3, 163.2, 146.7, 139.6, 138.0, 132.3, 130.4, 128.8, 126.1, 115.4, 105.9, 82.7, 57.8, 47.5, 36.5, 32.7, 25.8, 24.9, 21.3.

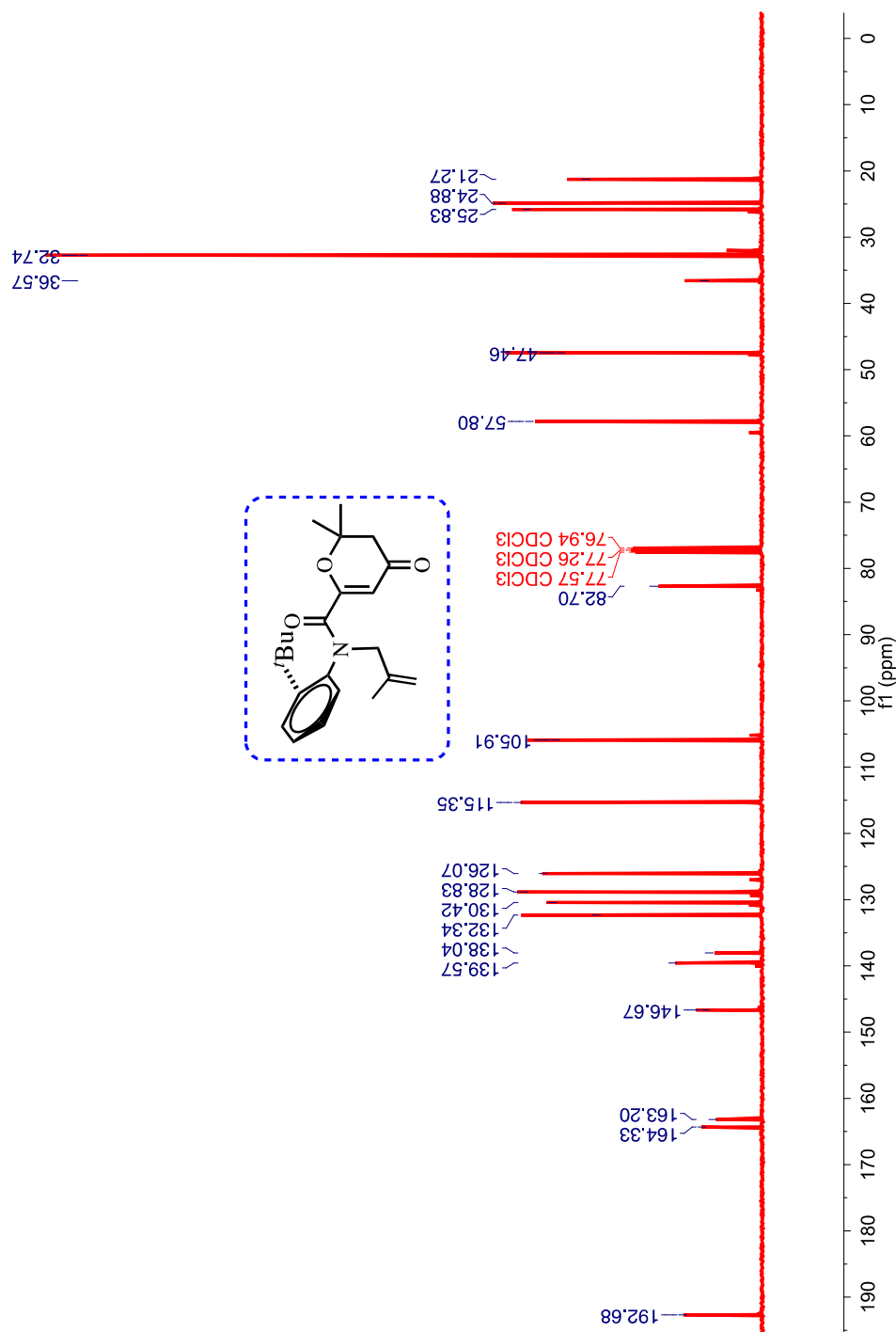


**Figure 2.32:**  $^{13}\text{C}$  NMR (100 MHz,  $\text{CDCl}_3$ ,  $\delta$  ppm) spectrum of atropisomeric amide derivative **92a**.

$^1\text{H}$  NMR (400 MHz,  $\text{CDCl}_3$ ,  $\delta$  ppm) 7.48 (dd,  $J = 8.1, 1.3$  Hz, 1H), 7.27 – 7.19 (m, 1H), 7.08 – 7.01 (m, 1H), 6.87 (dd,  $J = 7.8, 1.4$  Hz, 1H), 5.75 – 5.60 (m, 2H), 5.04 – 4.92 (m, 2H), 4.33 (ddd,  $J = 12.9, 10.0, 6.1$  Hz, 1H), 2.91 – 2.75 (m, 1H), 2.48 – 2.36 (m, 1H), 2.27 – 2.07 (m, 3H), 1.32 (d,  $J = 1.2$  Hz, 9H), 1.00 (s, 3H), 0.69 (s, 3H).

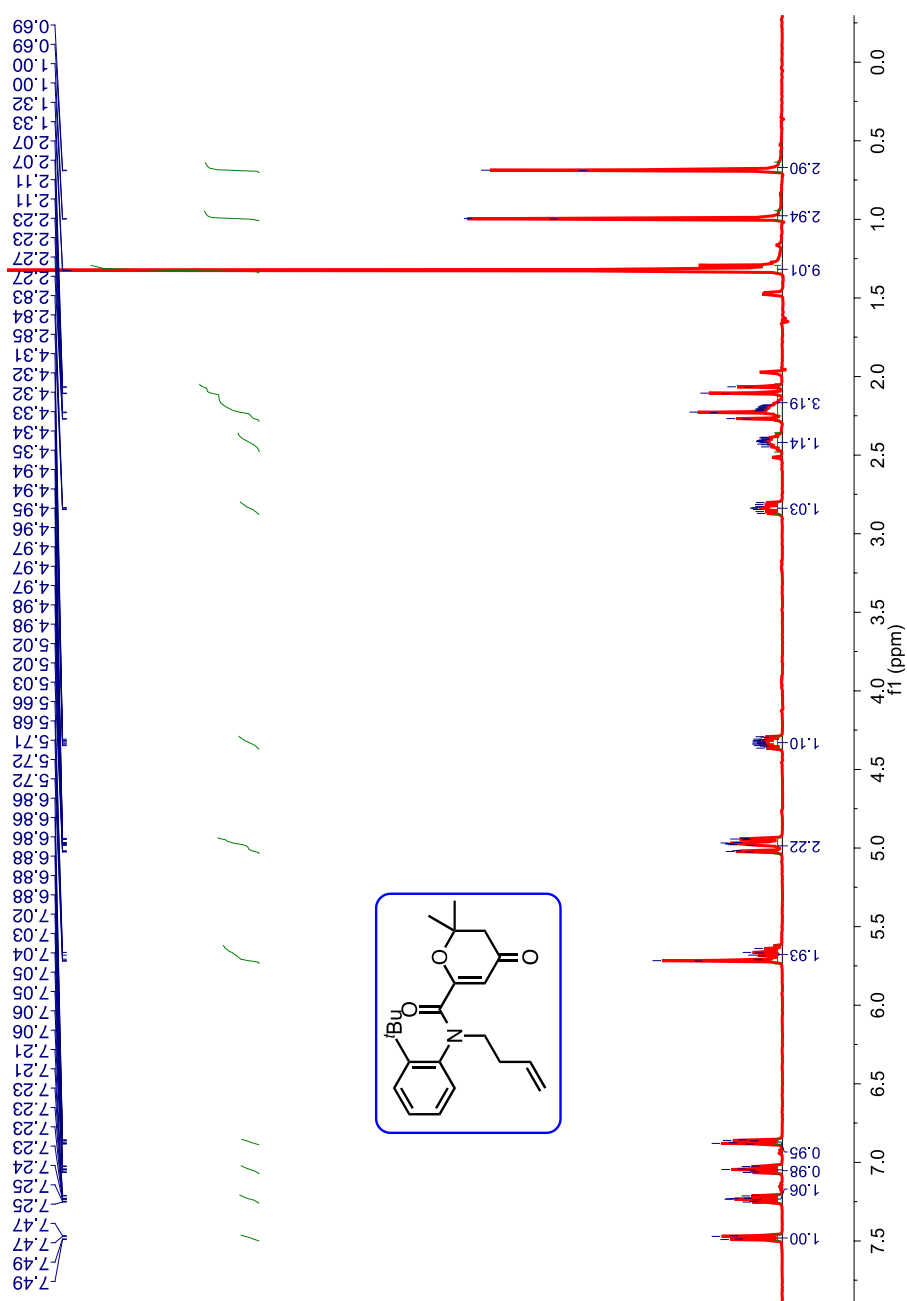


**Figure 2.33:** (400 MHz,  $\text{CDCl}_3$ ,  $\delta$  ppm) spectrum of atropisomeric amide derivative **92b**.

$^{13}\text{C}$  NMR (100 MHz,  $\text{CDCl}_3$ ,  $\delta$  ppm) 192.5, 164.1, 162.9, 146.8, 138.3, 134.93, 132.1, 130.6, 128.8, 126.3, 117.2, 105.9, 82.6, 51.6, 47.4, 36.5, 32.6, 30.9, 26.3, 24.3.

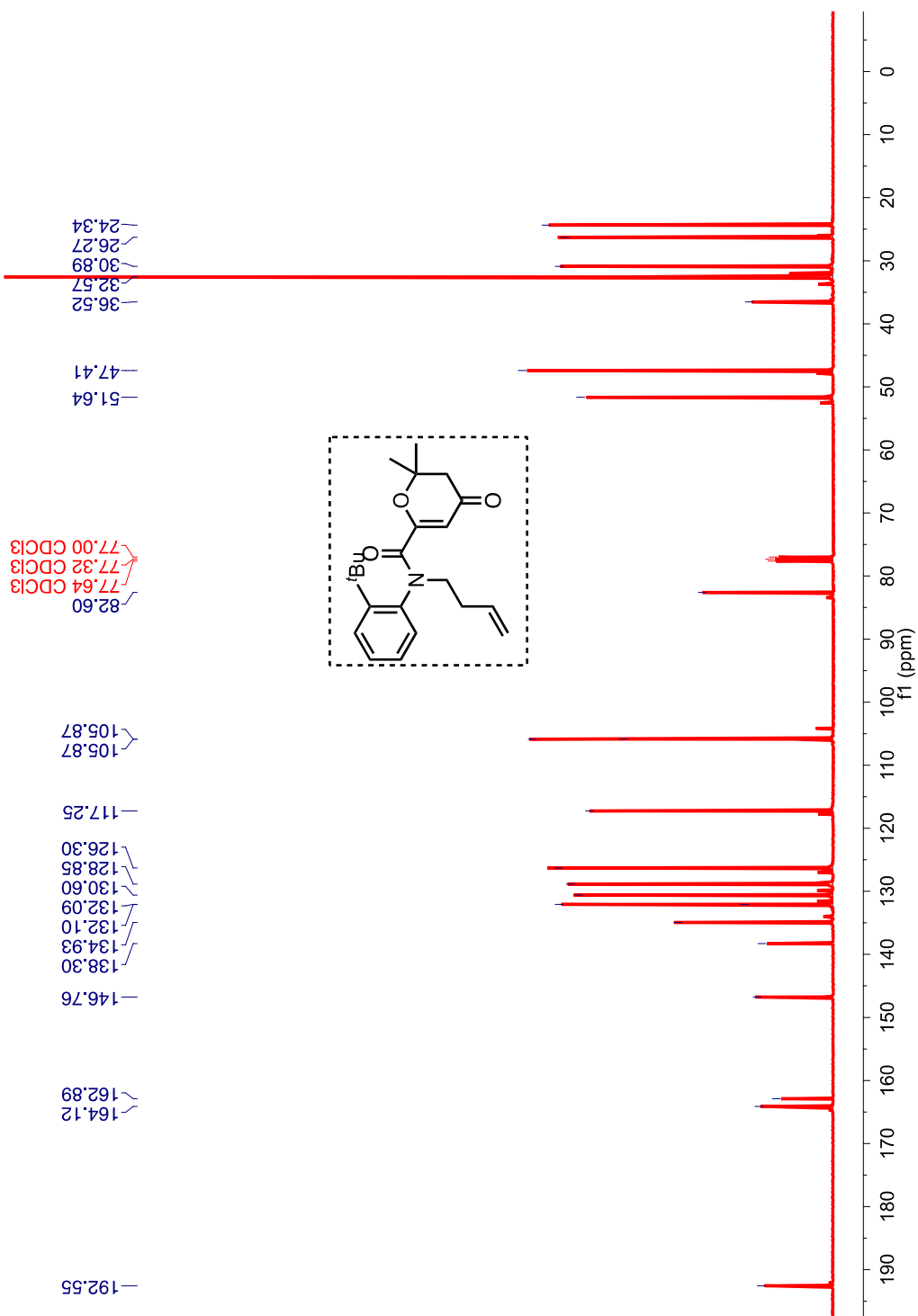


**Figure 2.34:**  $^{13}\text{C}$  NMR (100 MHz,  $\text{CDCl}_3$ ,  $\delta$  ppm) spectrum of atropisomeric amide derivative **92b**.

HRMS-ESI (m/z) ([M + H]):

Calculated : 356.2243

Observed : 356.2226

$|\Delta m|$  : 4.8 ppm

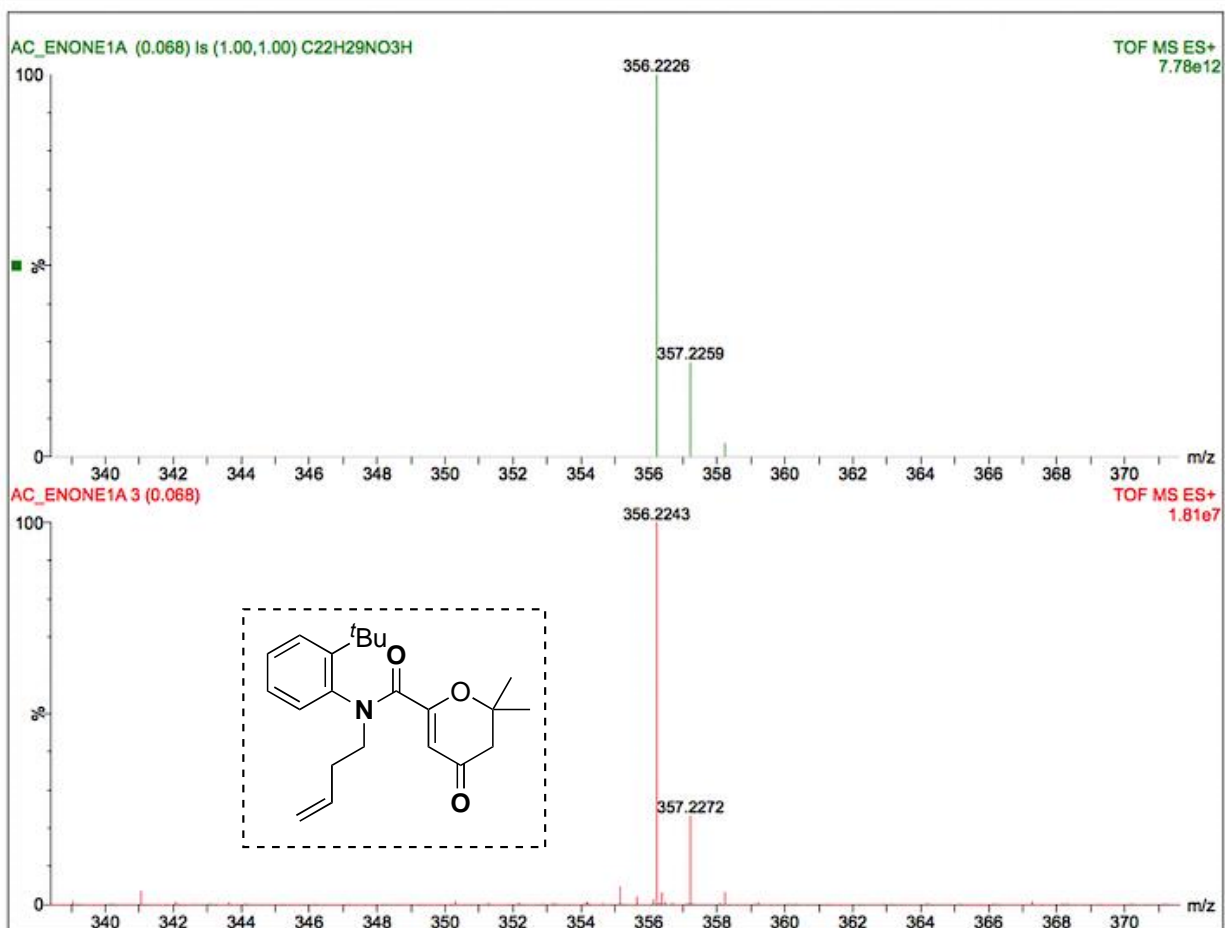
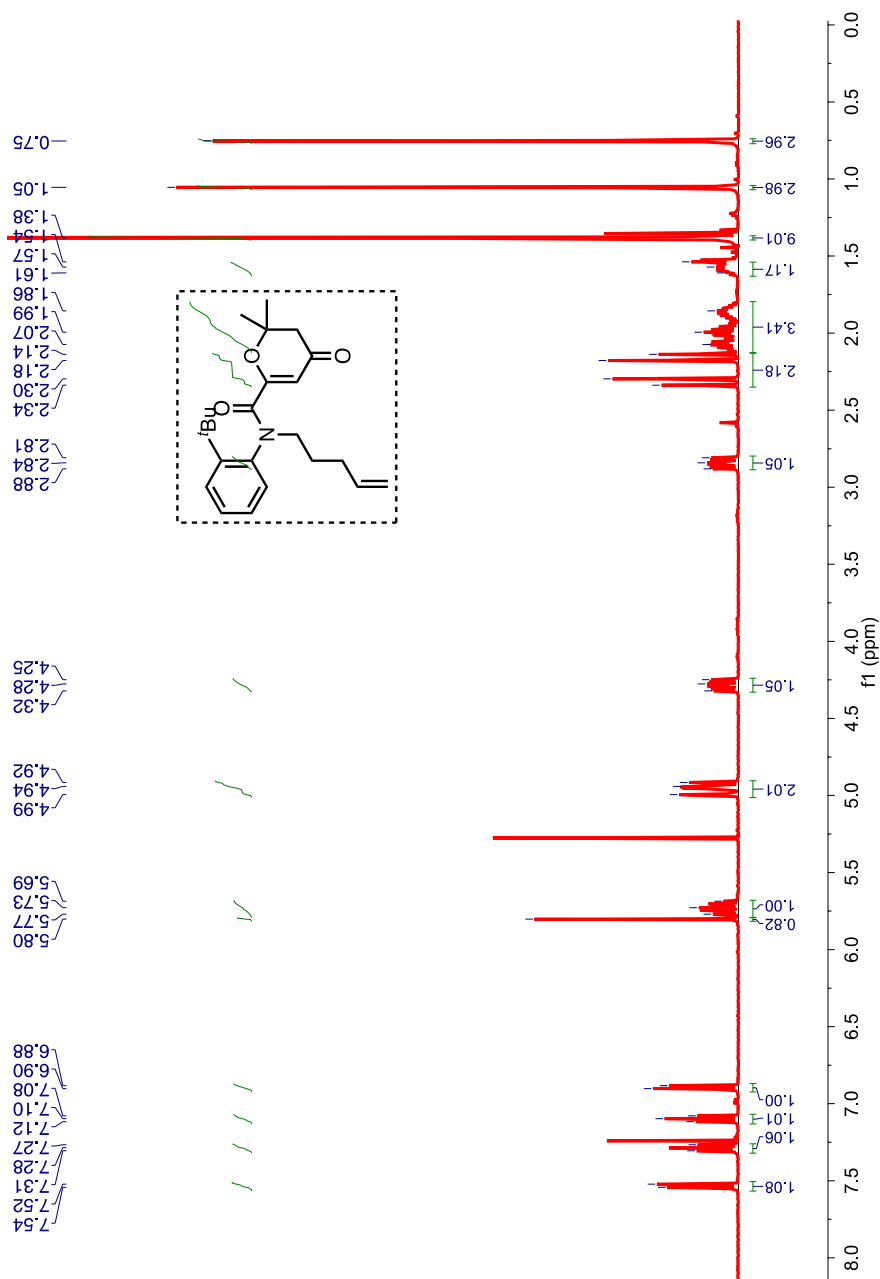


Figure 2.35: HRMS of atropisomeric amide derivative **92b**.

$^1\text{H}$  NMR (400 MHz,  $\text{CDCl}_3$ ,  $\delta$  ppm): 7.55 – 7.52 (m, 1H), 7.31 – 7.27 (m, 1H), 6.91 – 6.89 (m, 1H), 5.77 – 5.70 (m, 2H), 4.99 – 4.94 (m, 2 H), 4.32 – 4.25 (m, 1H), 2.88 – 2.81 (m, 1H), 2.34 – 2.14 (m, 2H), 2.07-1.86 (m, 4H) 1.61– 1.54 (m, 1H), 1.38 (s, 9H), 1.05 (s, 3H), 0.75 (s, 3H).



**Figure 2.36:**  $^1\text{H}$  NMR (400 MHz,  $\text{CDCl}_3$ ,  $\delta$  ppm) spectrum of atropisomeric amide derivative **92c**.

$^{13}\text{C}$  NMR (100 MHz,  $\text{CDCl}_3$ ,  $\delta$  ppm): 192.7, 164.2, 162.8, 146.7, 138.5, 137.6, 132.0, 130.6, 128.8, 126.3, 115.5, 105.9, 82.6, 52.2, 47.5, 36.6, 32.6, 31.3, 26.4, 25.4, 24.4.

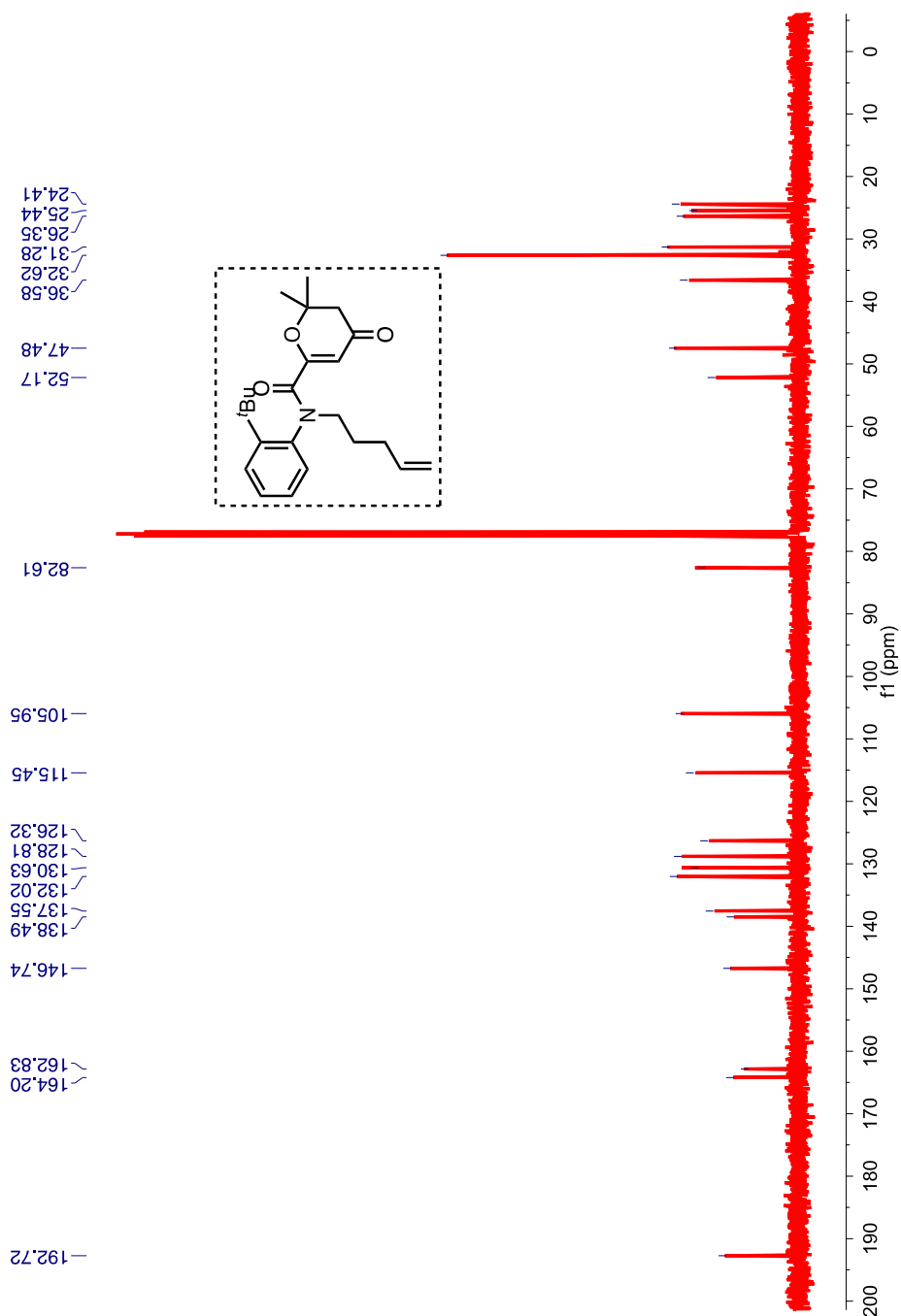


**Figure 2.37:**  $^{13}\text{C}$  NMR (100 MHz,  $\text{CDCl}_3$ ,  $\delta$  ppm) spectrum of atropisomeric-enone amide derivative **92c**.

HRMS-ESI (m/z) ([M + H]):

Calculated : 370.2385

Observed : 370.2382

$|\Delta m|$  : 0.8 ppm

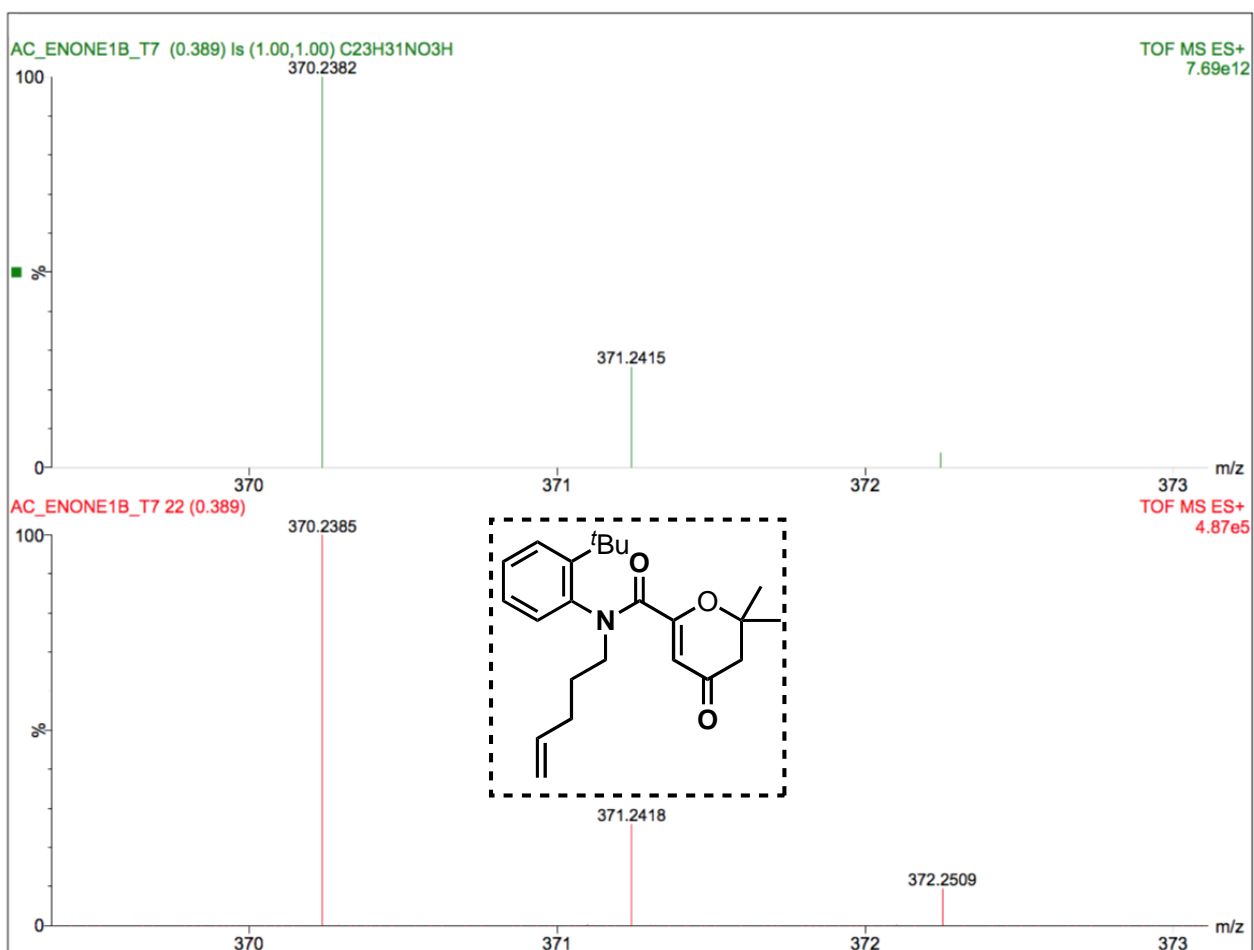


**Figure 2.38:** HRMS of atropisomeric-enone amide derivative **92c**.

HPLC analysis conditions for atropisomeric-enone amide **92c**.

HPLC analytical injections

Column : CHIRALPAK AD-H

Abs. detector wavelength : 254 nm and 270 nm

Mobile phase : Hexanes : Isopropyl alcohol (95 : 5)

Flow rate : 0.8 mL/min

Retention times : pkA ~16.89 min and pkB ~20.12 min

#### HPLC preparative conditions

Mobile phase : Hexanes : Isopropyl alcohol (95 : 5)

Flow rate : 2 mL/min

Retention times : pkA ~ 32.42 min and pkB ~38.10 min



$^1\text{H}$  NMR (400 MHz,  $\text{CDCl}_3$ ,  $\delta$  ppm): 7.03 – 7.02 (m, 1H), 6.83 – 6.80 (m, 1H), 6.63 – 6.61 (m, 1H), 5.78 – 5.68 (m, 2H), 4.99 – 4.91 (m, 2H), 4.29 – 4.22 (m, 1H), 3.77 (s, 3H), 2.84 – 2.77 (m, 1H), 2.35 – 2.15 (ABq,  $J = 16.4$  Hz, 2H), 2.10 – 2.05 (m), 1.99 – 1.88 (m, 1H), 1.83 – 1.79 (m, 1H), 1.63 – 1.61 (m, 1H), 1.36 (s, 9H), 1.10 (s, 3H), 0.82 (s, 3H).

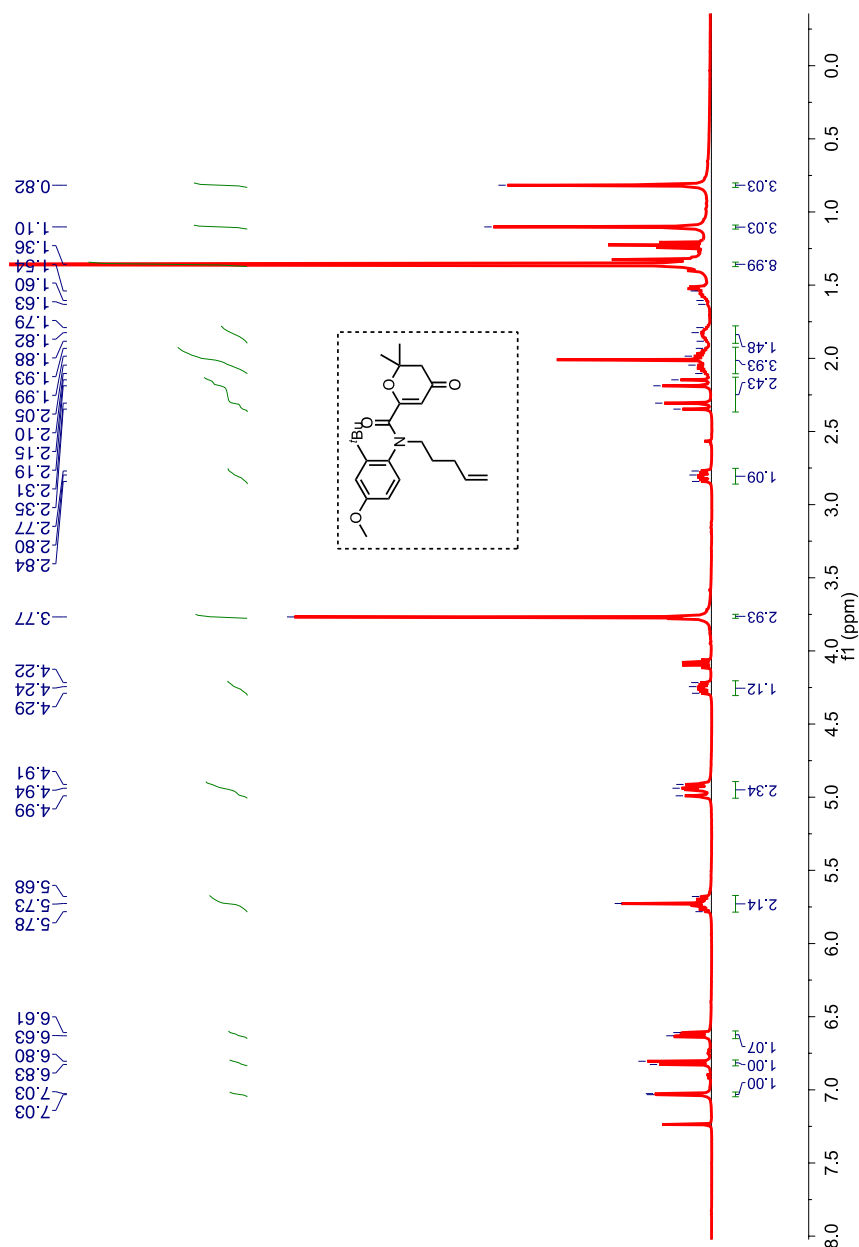


**Figure 2.39:**  $^1\text{H}$  NMR (400 MHz,  $\text{CDCl}_3$ ,  $\delta$  ppm) spectrum of atropisomeric-enone amide derivative **92d**.

$^{13}\text{C}$  NMR (100 MHz,  $\text{CDCl}_3$ ,  $\delta$  ppm): 192.7, 164.6, 163.2, 159.6, 148.3, 137.6, 133.1, 131.4, 116.6, 115.4, 110.6, 105.7, 82.6, 55.6, 47.5, 36.7, 32.5, 31.3, 26.4, 25.5, 24.6.

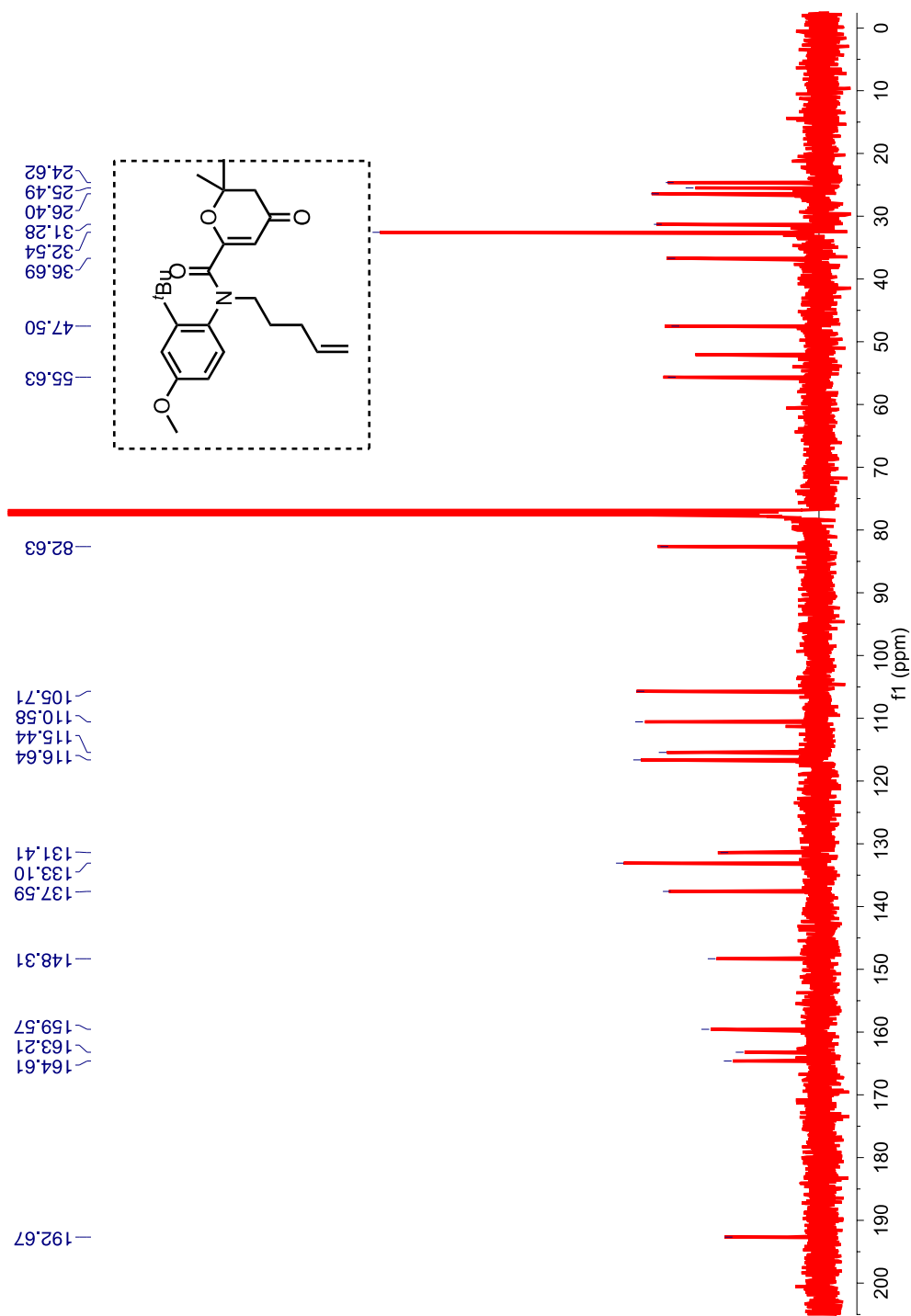


**Figure 2.40:**  $^{13}\text{C}$  NMR (100 MHz,  $\text{CDCl}_3$ ,  $\delta$  ppm) spectrum of atropisomeric-enone amide derivative **92d**.

HRMS-ESI (m/z) ([M + Na]):

Calculated : 422.2292

Observed : 422.2307

| $\Delta m$ | : 3.6 ppm

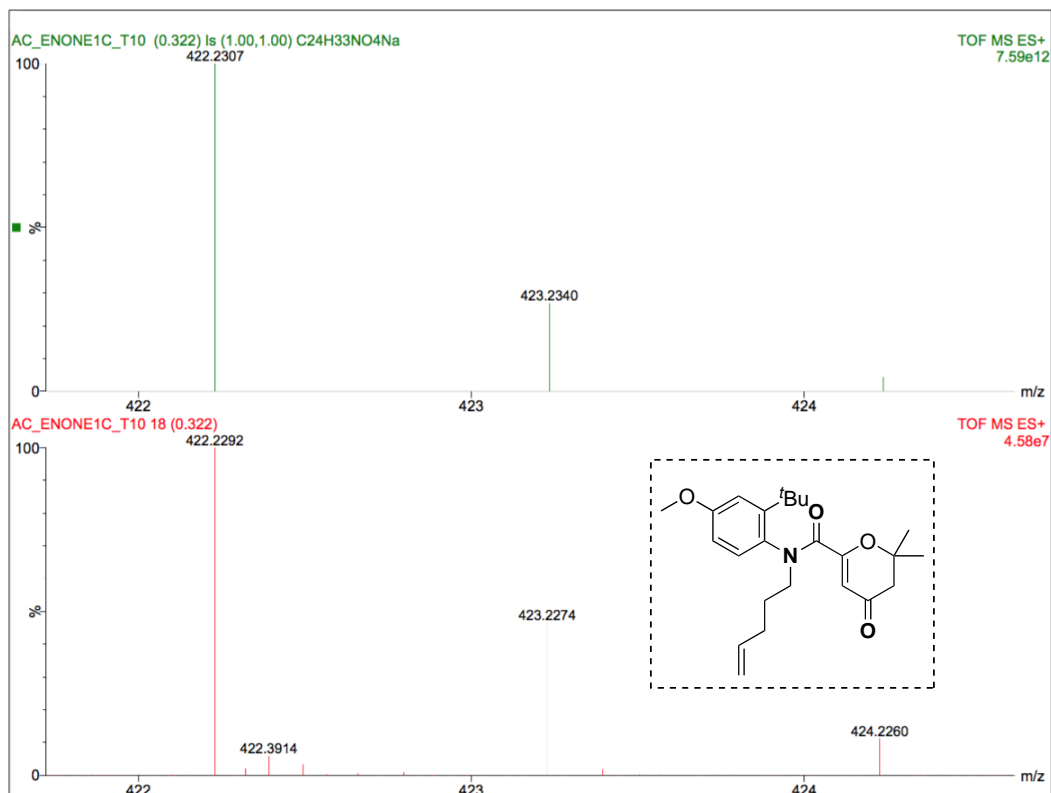


**Figure 2.41:** HRMS of atropisomeric-enone amide derivative **92d**.

HPLC analysis conditions for atropisomeric-enone amide derivative **92d**.

HPLC analytical injections

Column : (R,R) Whelk-01

Abs. detector wavelength : 254 nm and 270 nm

Mobile phase : Hexanes : Isopropyl alcohol (70 : 30)

Flow rate : 0.8 mL/min

Retention times : pkA ~45.87 min and pkB ~67.05 min

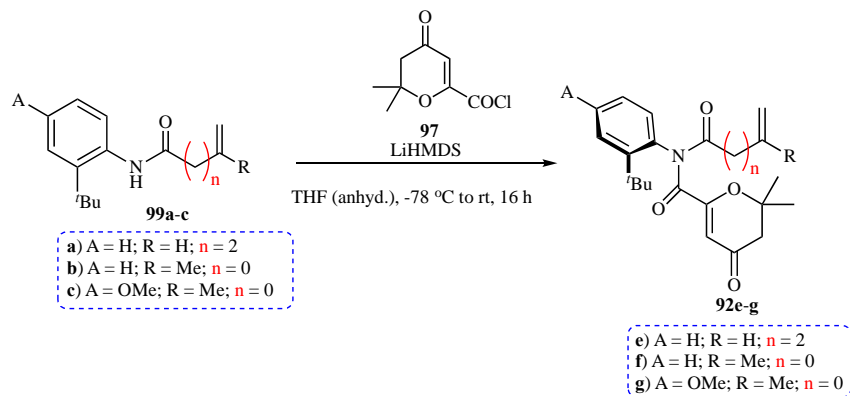
HPLC preparative conditions

Mobile phase : Hexanes : Isopropyl alcohol (70 : 30)

Flow rate : 2 mL/min

Retention times : pKA ~24.62 min and pKB ~33.08 min

### 2.11.8. Synthetic protocol for substituted atropisomeric-enone imides **92e-g**



#### Scheme 2.13: Synthesis of atropisomeric-enone imides **92e-g**.

Following a reported procedure<sup>75</sup>, to the aniline derivative **99a-c** (1.65 mmol, 1 equiv.) was taken in a dry round bottom flask and purged with N<sub>2</sub>, followed by the addition of dry THF (20 mL). The solution was cooled to -78 °C and LiHMDS (0.9 equiv.) was added dropwise. The solution was stirred at -78 °C for an hour before the slow addition of freshly prepared acid chloride (1.75 mmol, 1.05 equiv.). The reaction mixture was allowed to slowly rise to room temperature and stirred for 16 h. After 16 h the reaction mixture was quenched with H<sub>2</sub>O, washed with HCl, extracted with ethyl acetate and dried over Na<sub>2</sub>SO<sub>4</sub>, concentrated and purified using column chromatography. **92f** = 80% yield (white solid); **92g** = 80% yield (white solid).

$^1\text{H}$  NMR (400 MHz,  $\text{CDCl}_3$ ,  $\delta$  ppm) 7.58 - 7.56 (m, 1H), 7.40 - 7.36 (m, 1H), 7.28 - 7.24 (m, 1H), 6.95 - 6.92 (m, 1H), 5.76 (s, 1H), 5.74 - 5.65 (m, 1H), 5.15 - 4.93 (m, 2H), 2.57 - 2.47 (m, 2H), 2.32 (s, 3H), 1.42 (s, 3H), 1.38 (s, 4H), 1.33 (s, 9H).

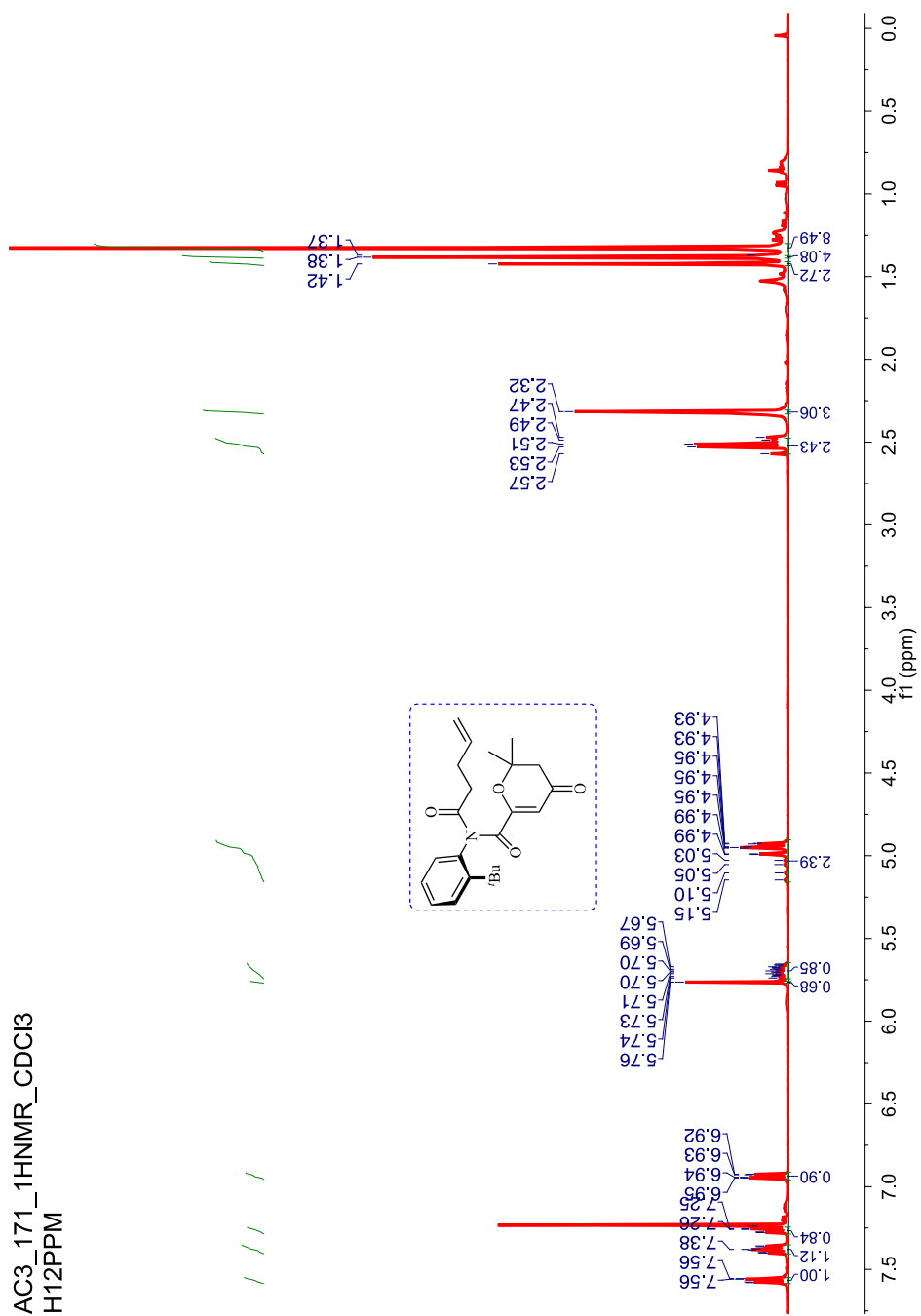


**Figure 2.42:**  $^1\text{H}$  NMR (400 MHz,  $\text{CDCl}_3$ ,  $\delta$  ppm) spectrum of atropisomeric-enone imide derivative **92e**.

$^1\text{H}$  NMR (400 MHz,  $\text{CDCl}_3$ ,  $\delta$  ppm) 7.55 – 7.52 (m, 1H), 7.33 – 7.29 (m, 1H), 7.23 – 7.17 (m, 1H), 6.89 – 6.86 (m, 1H), 6.02 (s, 1H), 5.6 (d,  $J = 14.9$  Hz, 2H), 2.4 (ABq,  $J = 16.6, 12.1$  Hz, 2H), 2.0 (s, 3H), 1.4 (s, 3H), 1.3 (s, 9H).

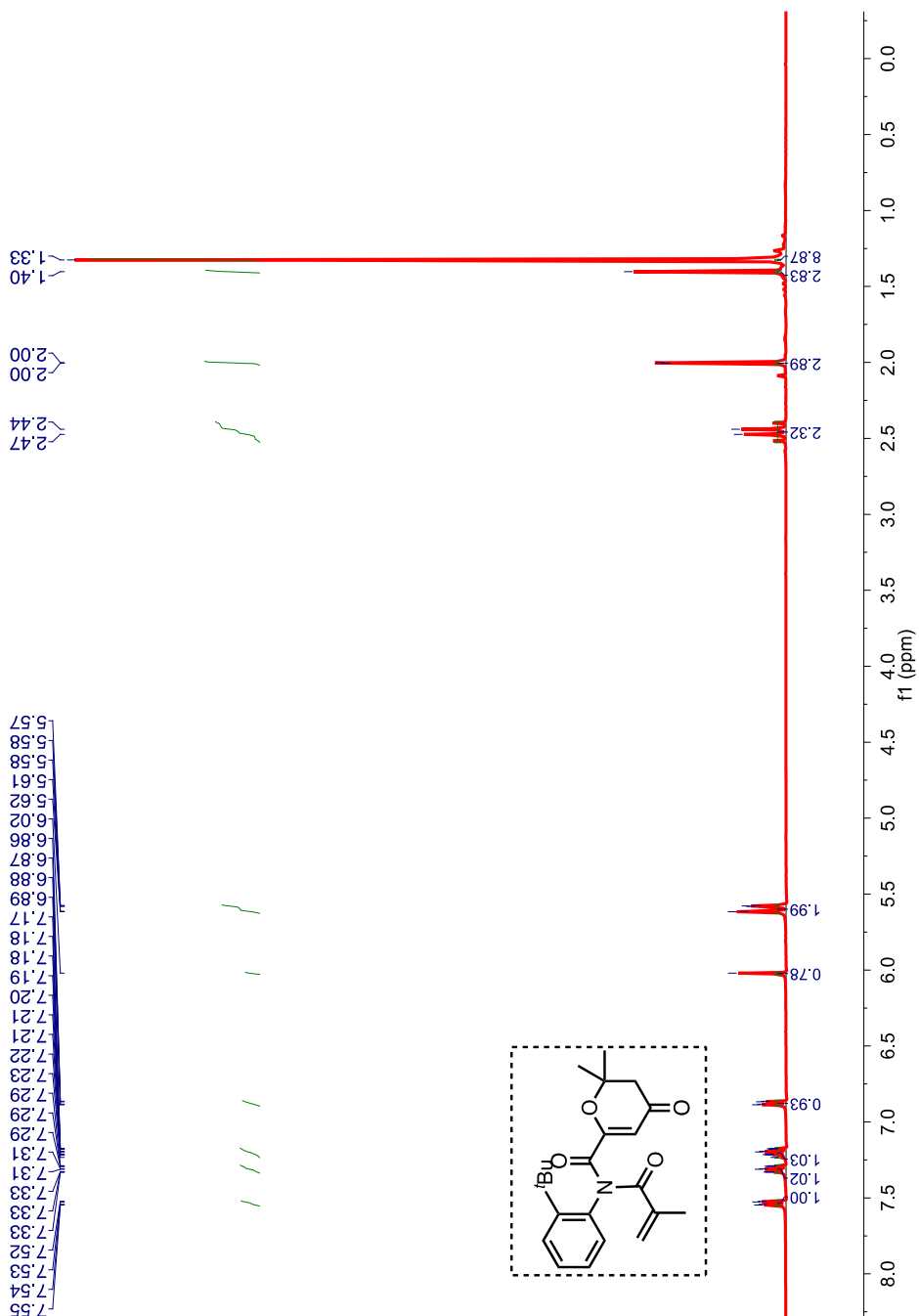


**Figure 2.43:**  $^1\text{H}$  NMR (400 MHz,  $\text{CDCl}_3$ ,  $\delta$  ppm) spectrum of atropisomeric-enone imide derivative **92f**.

$^{13}\text{C}$  NMR (100 MHz,  $\text{CDCl}_3$ ,  $\delta$  ppm) 192.6, 173.0, 167.5, 161.7, 147.8, 142.2, 136.0, 131.2, 129.7, 129.4, 127.4, 124.1, 106.8, 83.8, 47.9, 36.1, 32.0, 27.0, 24.9, 19.4.

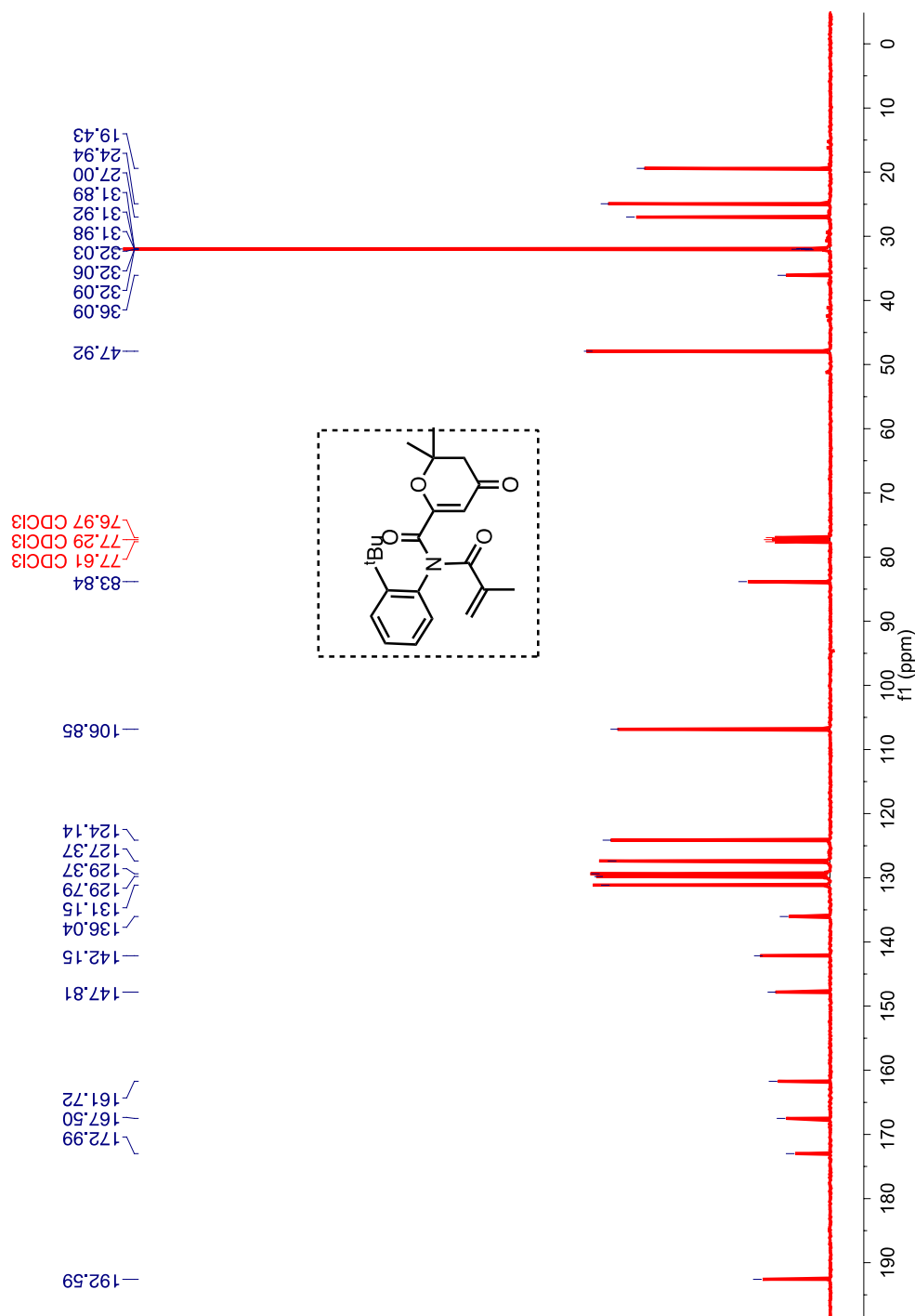


**Figure 2.44:**  $^{13}\text{C}$  NMR (100 MHz,  $\text{CDCl}_3$ ,  $\delta$  ppm) spectrum of atropisomeric-enone imide derivative **92f**.

HRMS-ESI (m/z) ([M + Na]):

Calculated : 392.1830

Observed : 392.1838

$|\Delta m|$  : 2.0 ppm

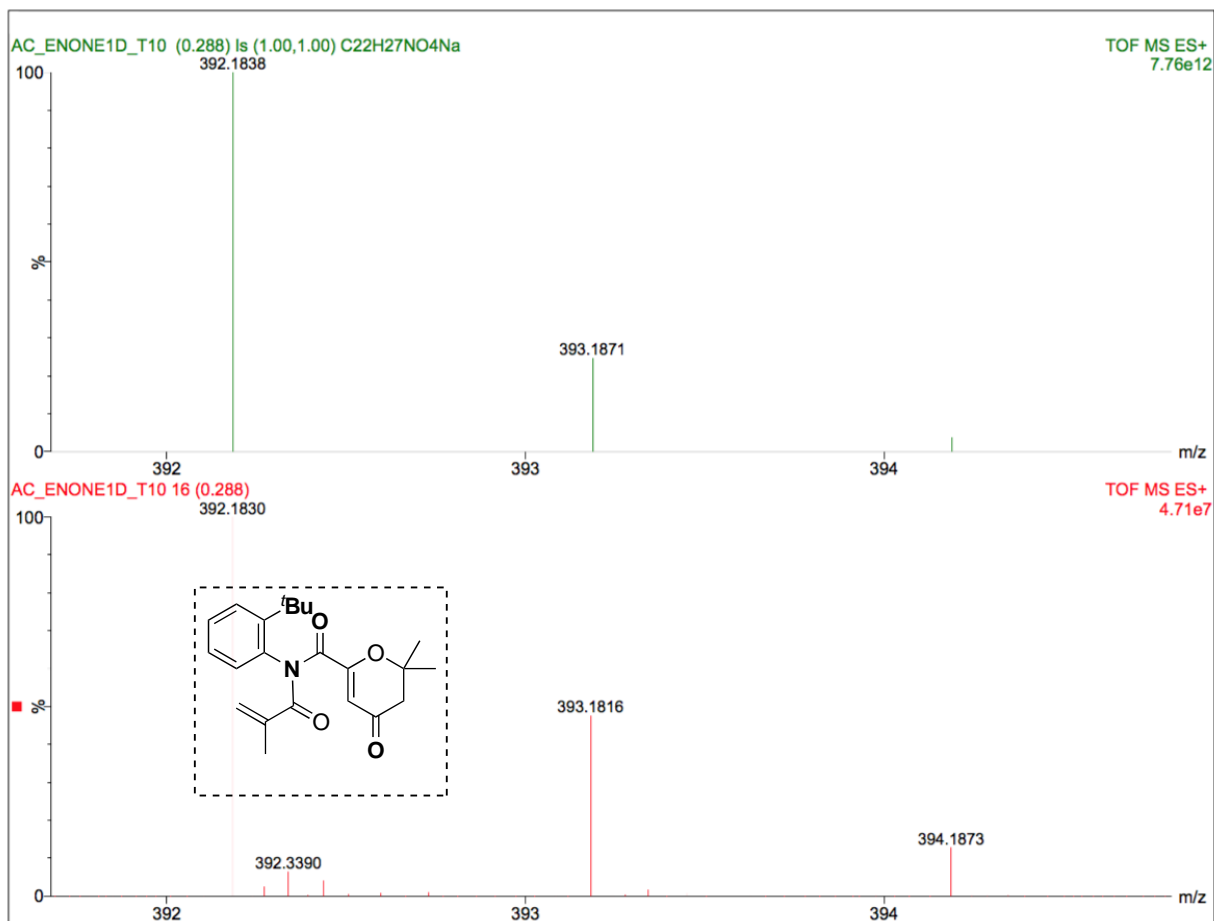


**Figure 2.45:** HRMS of atropisomeric-enone imide derivative **92f**.

HPLC conditions for atropisomeric-enone imide **92f**.

HPLC analytical injections:

Column : CHIRALPAK AD-H

Abs. detector wavelength: 254 nm and 270 nm

Mobile phase : Hexanes : Isopropyl alcohol (95 : 05)



Flow rate : 0.8 mL/min

Retention times : pkA ~17.6 min and pkB ~19.0 min

HPLC preparative conditions

Mobile phase : Hexanes : Isopropyl alcohol (95 : 05)

Flow rate : 3 mL/min

Retention times : pkA ~19.02 min and pkB ~19.97 min

$^1\text{H}$  NMR (400 MHz,  $\text{CDCl}_3$ ,  $\delta$  ppm) 7.07 - 7.06 (m, 1H), 6.83 – 6.81 (m, 1H), 6.76 – 6.73 (m, 1H), 6.02 (s, 1H), 5.57 (m, 2H), 3.79 (d,  $J = 0.6$  Hz, 3H), 2.54 - 2.42 (m, 2H), 2.00 (s, 3H), 1.44 (s, 3H), 1.36 (s, 3H), 1.32 (d,  $J = 0.6$  Hz, 9H).

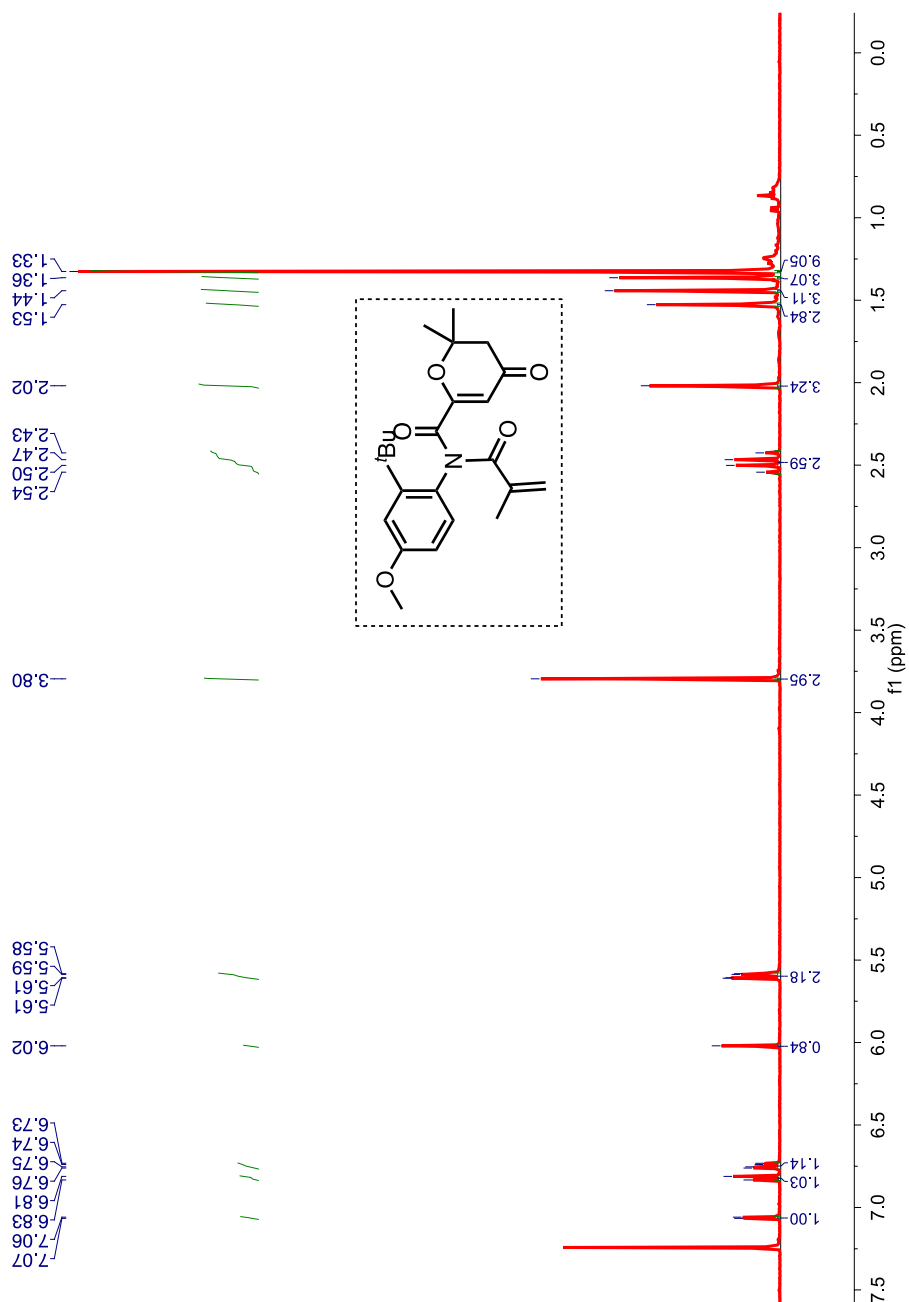


**Figure 2.46:**  $^1\text{H}$  NMR (400 MHz,  $\text{CDCl}_3$ ,  $\delta$  ppm) of atropisomeric-enone imide derivative **92g**.

$^{13}\text{C}$  NMR (100 MHz,  $\text{CDCl}_3$ ,  $\delta$  ppm) 192.6, 173.2, 167.8, 161.9, 159.8, 149.3, 142.2, 132.2, 128.8, 124.1, 116.0, 111.7, 106.7, 83.8, 55.5, 47.9, 36.1, 31.8, 27.1, 25.0, 19.5

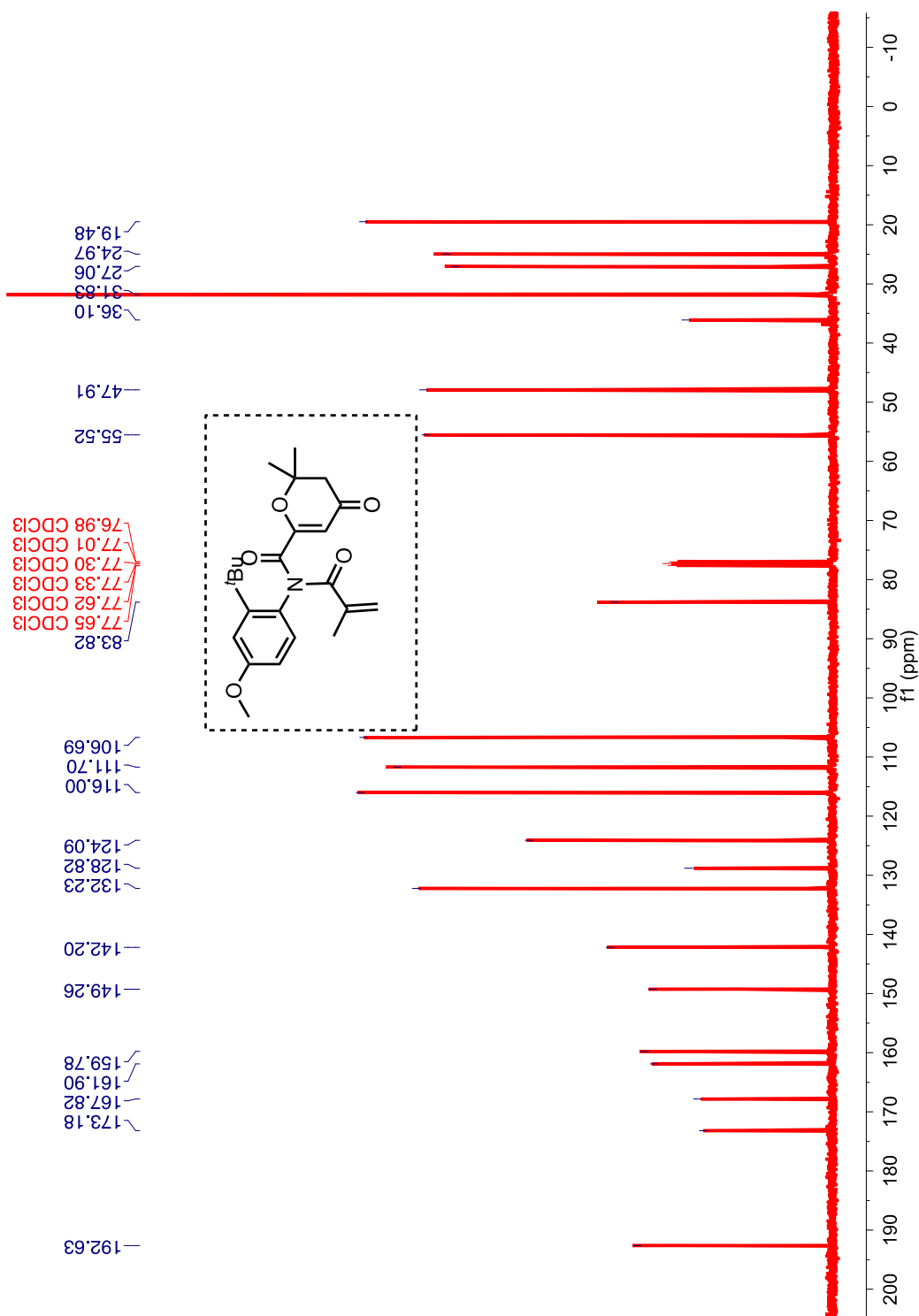


**Figure 2.47:**  $^{13}\text{C}$  NMR (100 MHz,  $\text{CDCl}_3$ ,  $\delta$  ppm) of atropisomeric-enone imide derivative **92g**.

HRMS-ESI (m/z) ([M + Na]):

Calculated : 422.1925

Observed : 422.1943

$|\Delta m|$  : 4.3 ppm

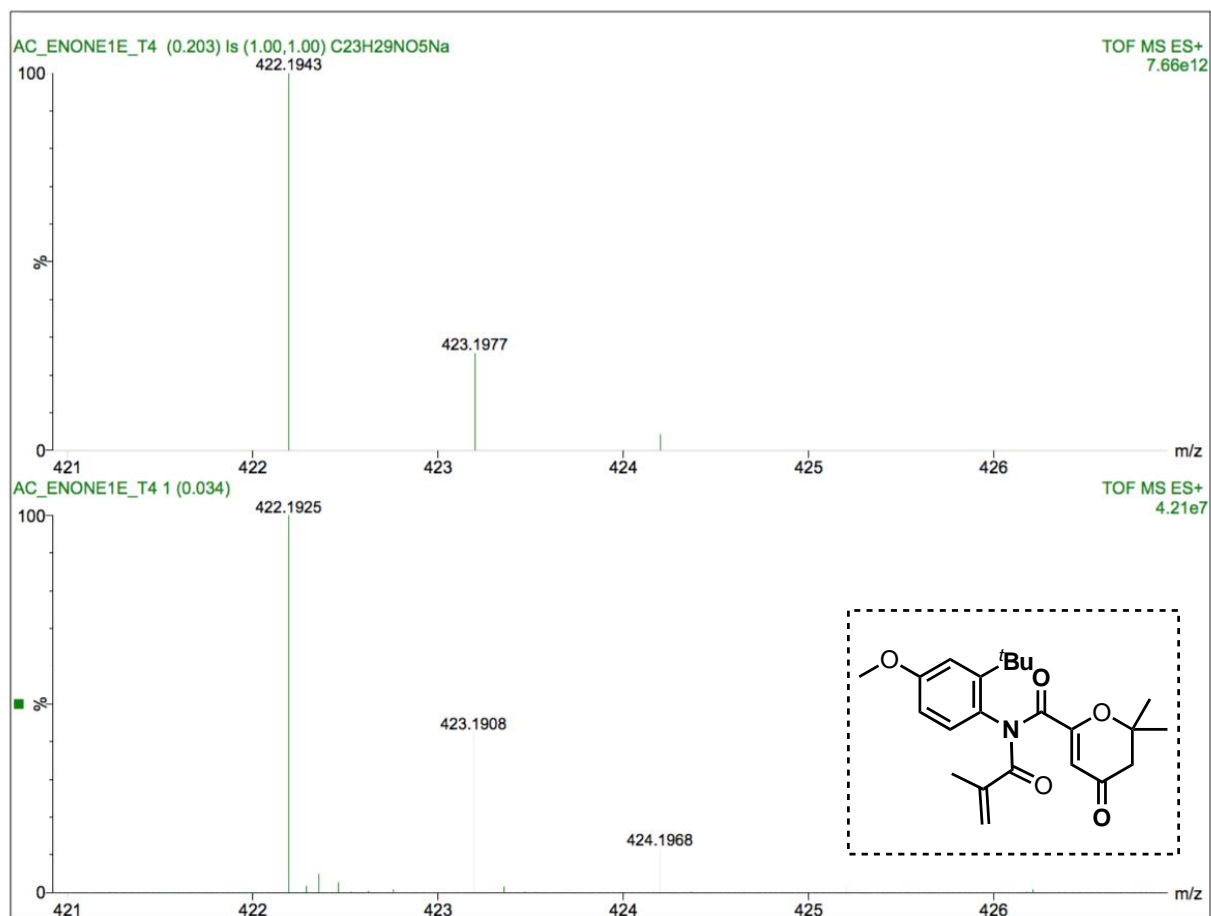


**Figure 2.48:** HRMS of atropisomeric-enone imide derivative **92g**.

HPLC conditions for atropisomeric enone-imide **92g**.

HPLC analytical injections:

Column : CHIRALPAK AD-H

Abs. detector wavelength : 254 nm and 270 nm

Mobile phase : Hexanes : Isopropyl alcohol (90 : 10)

Flow rate : 0.8 mL/min

Retention times : pkA ~13.4 min and pkB ~15.2 min

#### HPLC preparative conditions

Mobile phase : Hexanes : Isopropyl alcohol (90 : 10)

Flow rate : 3 mL/min

Retention times : pkA ~20.89 min and pkB ~23.40 min

## 2.12. General procedure for irradiation of atropisomeric-enones

### 2.12.1. Procedure for direct irradiation of atropisomeric-enones

In a Pyrex test-tube, respective atropisomeric-enone(s) **92a-g** (10mg in 10 mL) was dissolved in a given solvent and degassed with N<sub>2</sub> for 10 min. The solution was irradiated for the specified time interval in either a Rayonet reactor at ~350 nm, ~420 nm or using a 450 W medium pressure Hg lamp enclosed in a quartz jacket that was cooled with running water. When the reaction was complete, a stock solution of internal standard (triphenylmethane) was added and this solution was concentrated under reduced pressure to obtain the crude reaction mixture. <sup>1</sup>H NMR spectroscopy was recorded of the crude reaction mixture to determine the mass balance and percent yield. In some instances, isolated yields were also obtained.

### 2.12.2. Procedure for sensitized irradiation of atropisomeric-enones in the presence of TX-95

Atropisomeric-enones **92a-g** were dissolved in the appropriate solvent in a Pyrex test-tube (10mg in 10 mL); Thioxanthone (10 mol%) was dissolved in the same solvent and added to the atropisomeric-enone **92a-g** or a stock solution of TX-95 in the appropriate solvent was obtained and the necessary amount was added to a solution of **92a-g**. The reaction mixture was degassed with N<sub>2</sub> for ~10 min. The solution was irradiated for a specified time interval in a Rayonet reactor (~420 nm). After the reaction, a stock solution of internal standard (triphenylmethane) was added and this solution was concentrated under reduced pressure to obtain the crude reaction mixture. <sup>1</sup>H NMR spectroscopy was recorded of the crude reaction mixture to determine the mass balance and percent yield utilizing equation 2.10 (Eq. 2.10). In some instances, isolated yields were also obtained.

$$mol_a = mol_i \times \left(\frac{f_a}{f_i}\right) \times \frac{N_a}{N_i} \quad (\text{Eq. 2.10})$$

Where,

$mol_a$  = moles of the analyte

$mol_i$  = moles of the internal standard

$\int a$  = integration of the analyte from  $^1\text{H}$  NMR spectroscopy

$\int i$  = integration of the internal standard from  $^1\text{H}$  NMR spectroscopy

$N_a$  = number of nuclei giving rise to the chemical shift signal of interest of the analyte

$N_i$  = number of nuclei giving rise to the chemical shift signal of interest internal standard

1.1 Characterization of cyclized photoproduct 94a-f

### 2.12.3. $^1\text{H}$ and $^{13}\text{C}$ NMR of atropisomeric-enones

Sensitized irradiation of **94a** in  $\text{N}_2$  degassed acetonitrile for 14 hours afforded a complex mixture of photoproducts which composed of three fractions. Two fraction, based on  $^1\text{H}$  and  $^{13}\text{C}$  NMR analysis, mirrors that of **94f** and **94g** minor and major. The first two fractions make up ~90% of the product mixture. Figure 2.44 and 2.45,  $^1\text{H}$  and  $^{13}\text{C}$  NMR respectively, are tentatively assigned as the *cis,cis*-**94a** minor based upon analysis of similarly substituted **94f** and **94g**. Figures 2.46 and 2.47,  $^1\text{H}$  and  $^{13}\text{C}$  NMR respectively, are tentatively assigned as a mixture of isomers namely *cis,cis*-**94a** minor and major based upon analysis of similarly substituted **94f** and **94g**.

$^1\text{H}$  NMR (400 MHz,  $\text{CDCl}_3$ ,  $\delta$  ppm) 7.49-7.47 (m, 1H), 7.29 – 7.21 (m, 2H), 6.93 – 6.91 (m, 1H), 3.61 (d,  $J = 11.2$  Hz, 1H), 3.23 (d,  $J = 11.3$  Hz, 1H), 3.00 (d,  $J = 6.2$  Hz, 2H), 2.57 – 2.40 (m, 2H), 2.42 (dd,  $J = 9.9, 6.2$  Hz, 2H), 2.16 (d,  $J = 9.9$  Hz, 2H), 1.41 (s, 6H), 1.36 (s, 9H), 1.31 (s, 3H), 1.26 (s, 3H).

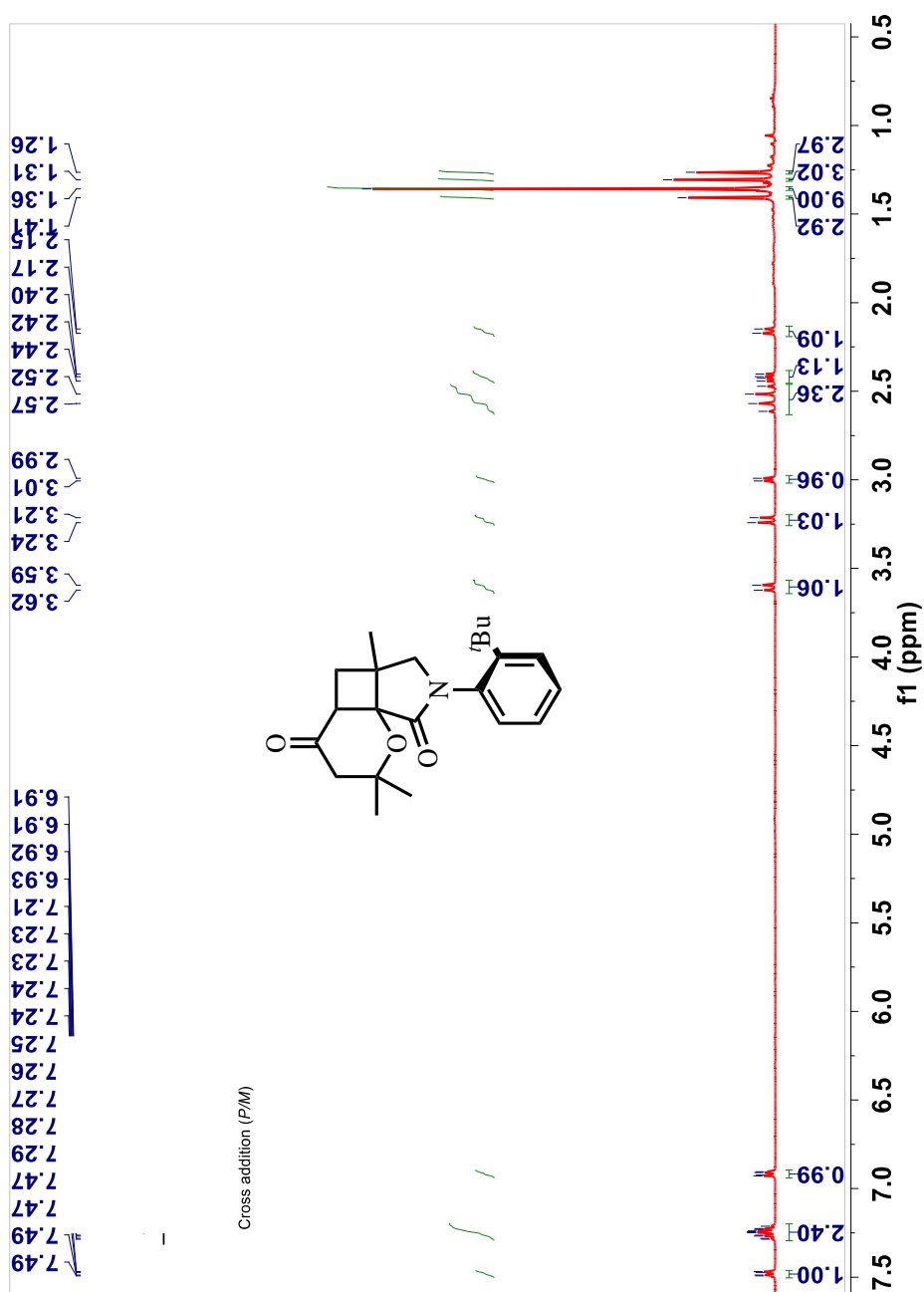


**Figure 2.49:**  $^1\text{H}$  NMR (400 MHz,  $\text{CDCl}_3$ ,  $\delta$  ppm) spectrum of *cis,cis*-94a minor.



$^{13}\text{C}$  NMR (100 MHz,  $\text{CDCl}_3$ ,  $\delta$  ppm) 173.2, 148.2, 139.4, 131.1, 129.0, 128.4, 128.0, 72.5, 64.0, 53.0, 52.1, 46.2, 37.0, 36.8, 36.1, 32.2, 30.3, 28.3, 19.9.

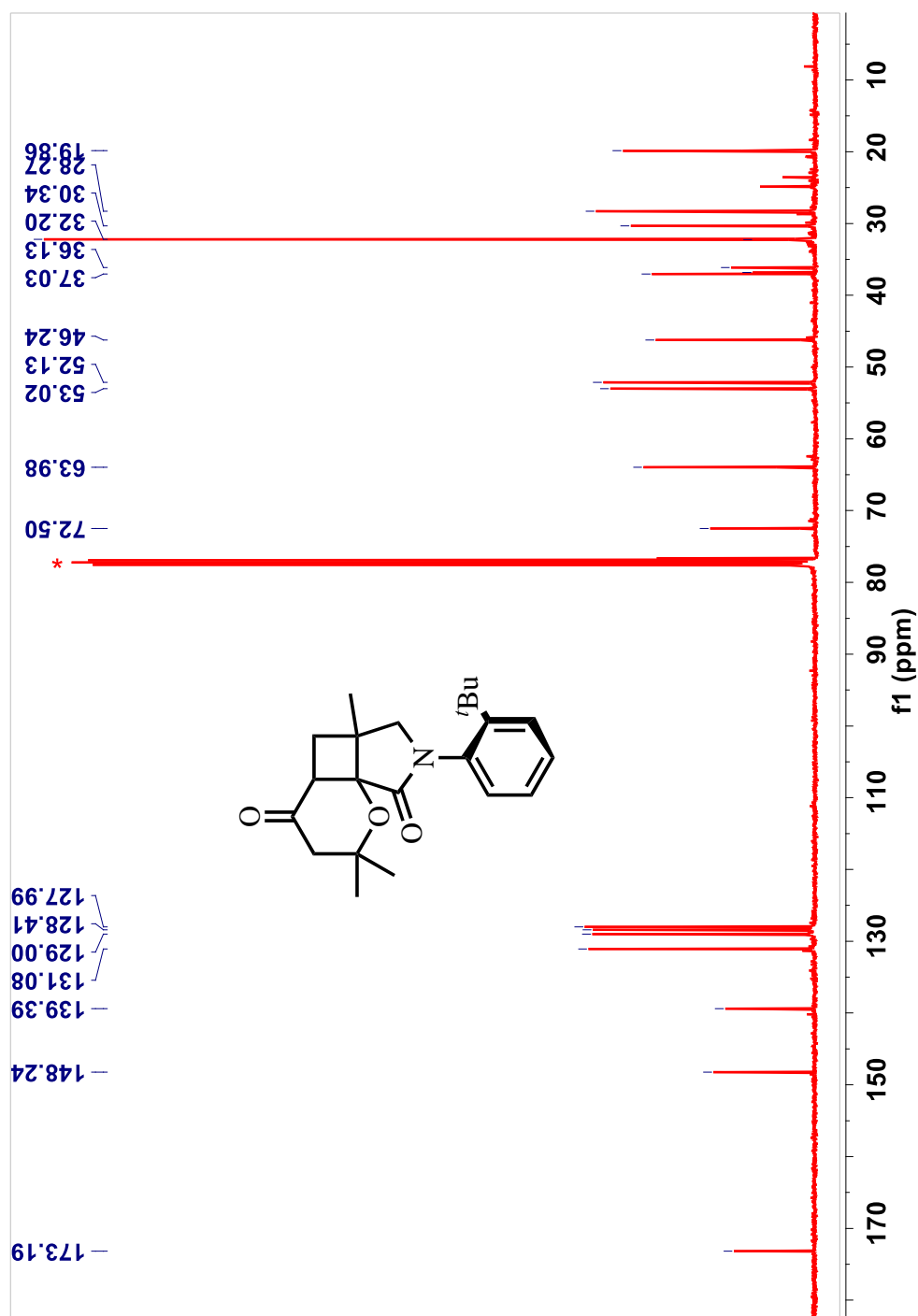


**Figure 2.50:**  $^{13}\text{C}$  NMR (100 MHz,  $\text{CDCl}_3$ ,  $\delta$  ppm) spectrum of *cis,cis*-94a minor.

$^1\text{H}$  NMR (400 MHz,  $\text{CDCl}_3$ ,  $\delta$  ppm) 7.5 (ddd,  $J = 14.0, 7.7, 1.8$  Hz, 3H), 7.3 – 7.2 (m, 4H), 7.06 (dd,  $J = 7.4, 1.8$  Hz, 2H), 6.9 (dd,  $J = 7.6, 1.6$  Hz, 1H), 3.67 (dd,  $J = 27.9, 10.5$  Hz, 3H), 3.42 (dd,  $J = 10.5, 3.5$  Hz, 3H), 3.17 (ddd,  $J = 15.6, 9.6, 5.6$  Hz, 3H), 2.6 – 2.51 (m, 6H), 2.24 – 2.20 (m, 2H), 2.2 – 2.07 (m, 2H), 1.5 (s, 5H), 1.5 (d,  $J = 7.3$  Hz, 8H), 1.4 (s, 5H), 1.4 (d,  $J = 1.2$  Hz, 24H), 1.4 (s, 4H), 1.2 (s, 6H), 1.2 (s, 3H).

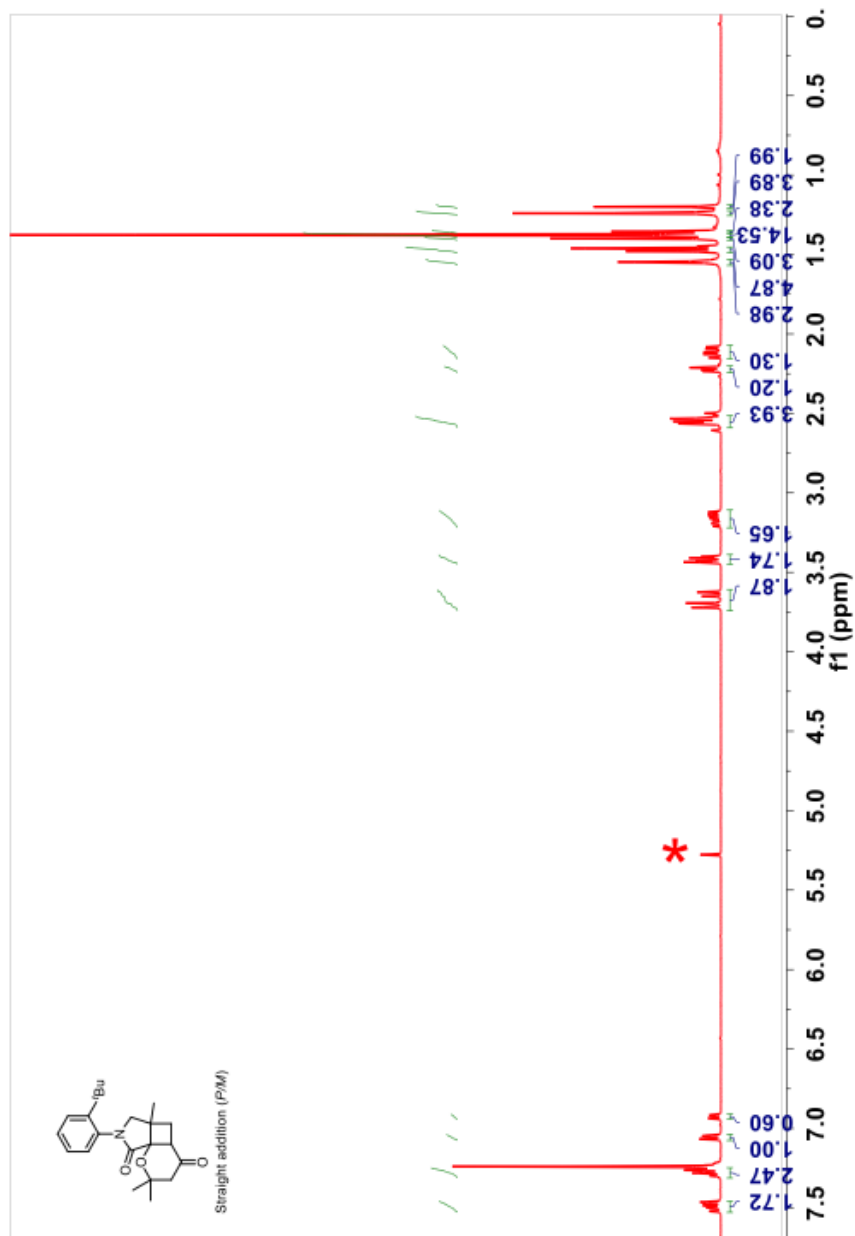


**Figure 2.51:**  $^1\text{H}$  NMR (400 MHz,  $\text{CDCl}_3$ ,  $\delta$  ppm) spectrum of *cis,cis*-94a mixture of isomers.

$^{13}\text{C}$  NMR (100 MHz,  $\text{CDCl}_3$ ,  $\delta$  ppm) 175.5, 148.7, 148.3, 138.6, 130.7, 129.9, 129.0, 128.7, 128.2, 127.9, 127.7, 63.9, 51.9, 51.7, 42.9, 42.2, 41.2, 40.6, 35.7, 34.1, 33.2, 32.0, 31.7, 30.8, 30.4, 30.0, 20.2, 19.3.

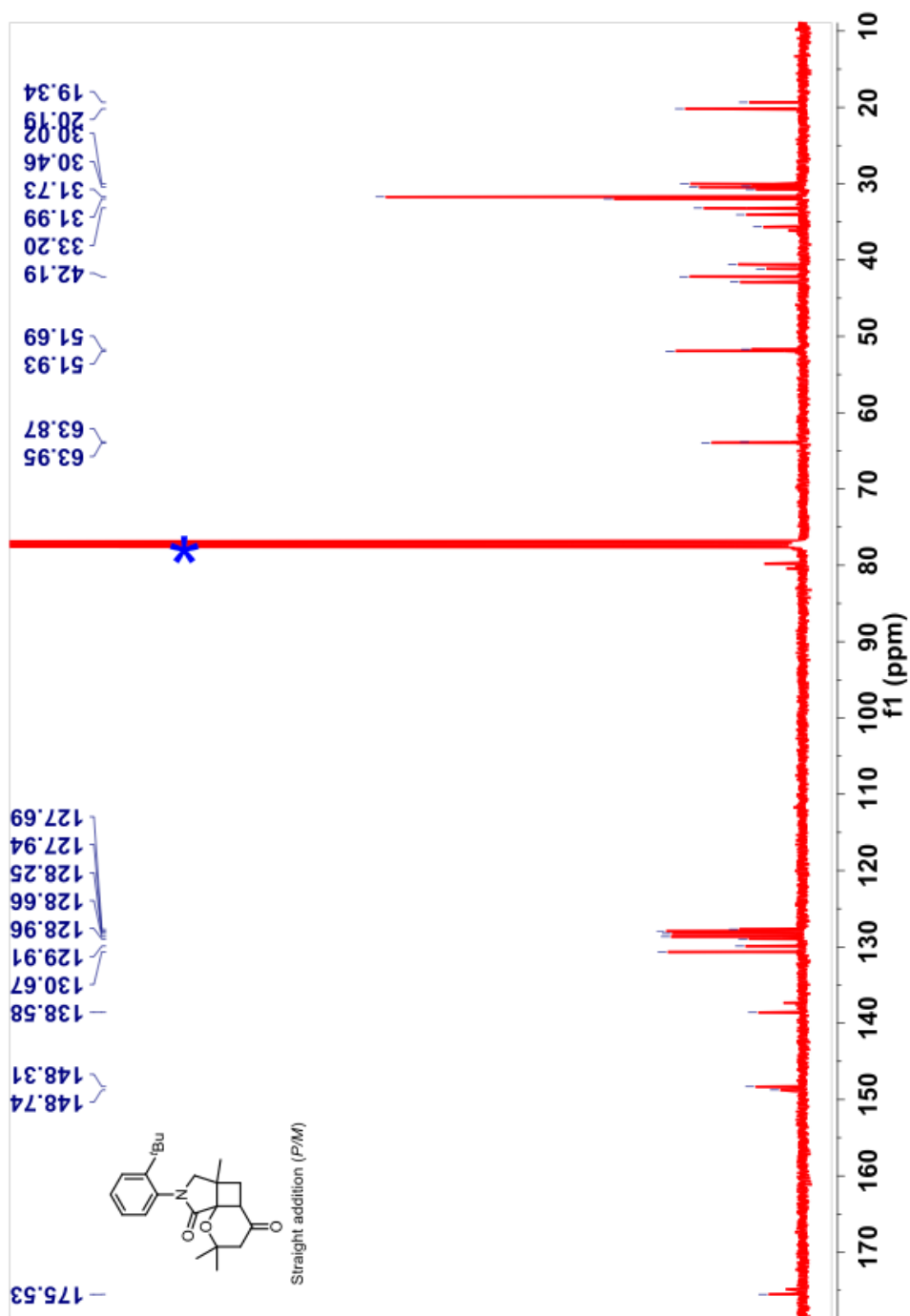


**Figure 2.52:**  $^{13}\text{C}$  NMR (100 MHz,  $\text{CDCl}_3$ ,  $\delta$  ppm) spectrum of *cis,cis*-94a mixture of isomers.

$^1\text{H}$  NMR (400 MHz,  $\text{CDCl}_3$ ,  $\delta$  ppm) 7.50 - 7.48 (m), 7.27 - 7.23 (m), 7.02 - 7.00 (m), 3.87 - 3.81 (m), 3.49 - 3.39 (m), 2.88 - 2.82 (m), 2.46 - 2.39 (m), 2.25 - 2.18 (m), 1.97 - 1.79 (m), 1.39 (s), 1.35 (s), 1.32 (s).

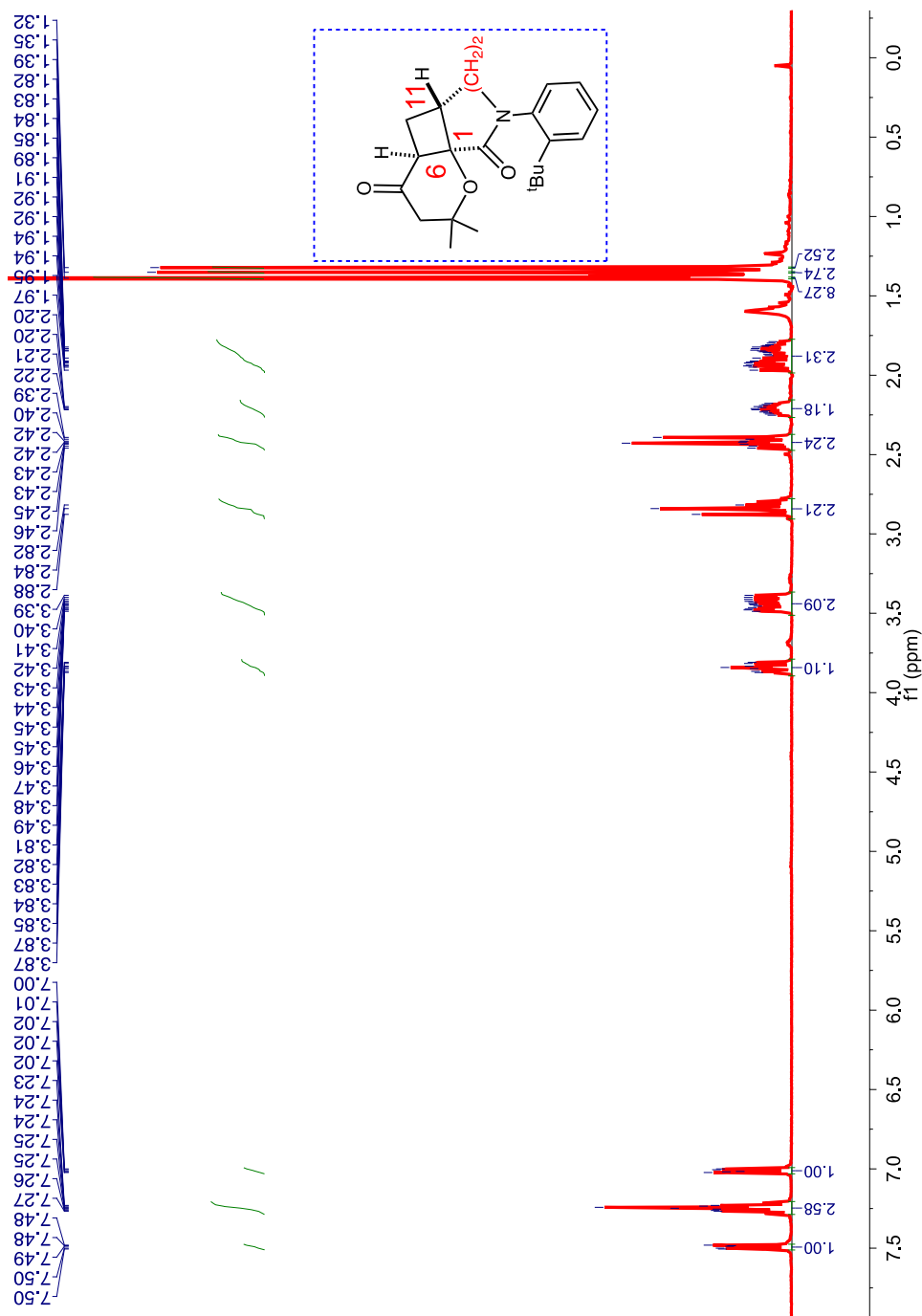


**Figure 2.53:**  $^1\text{H}$  NMR (400 MHz,  $\text{CDCl}_3$ ,  $\delta$  ppm) spectrum of *cis,cis*-94b.

$^{13}\text{C}$  NMR (100 MHz,  $\text{CDCl}_3$ ,  $\delta$  ppm) 170.9, 147.3, 142.6, 129.7, 128.6, 128.4, 127.9, 80.0, 78.8, 52.1, 51.5, 45.2, 42.8, 42.8, 35.8, 31.8, 30.6, 30.1, 29.9, 24.9.

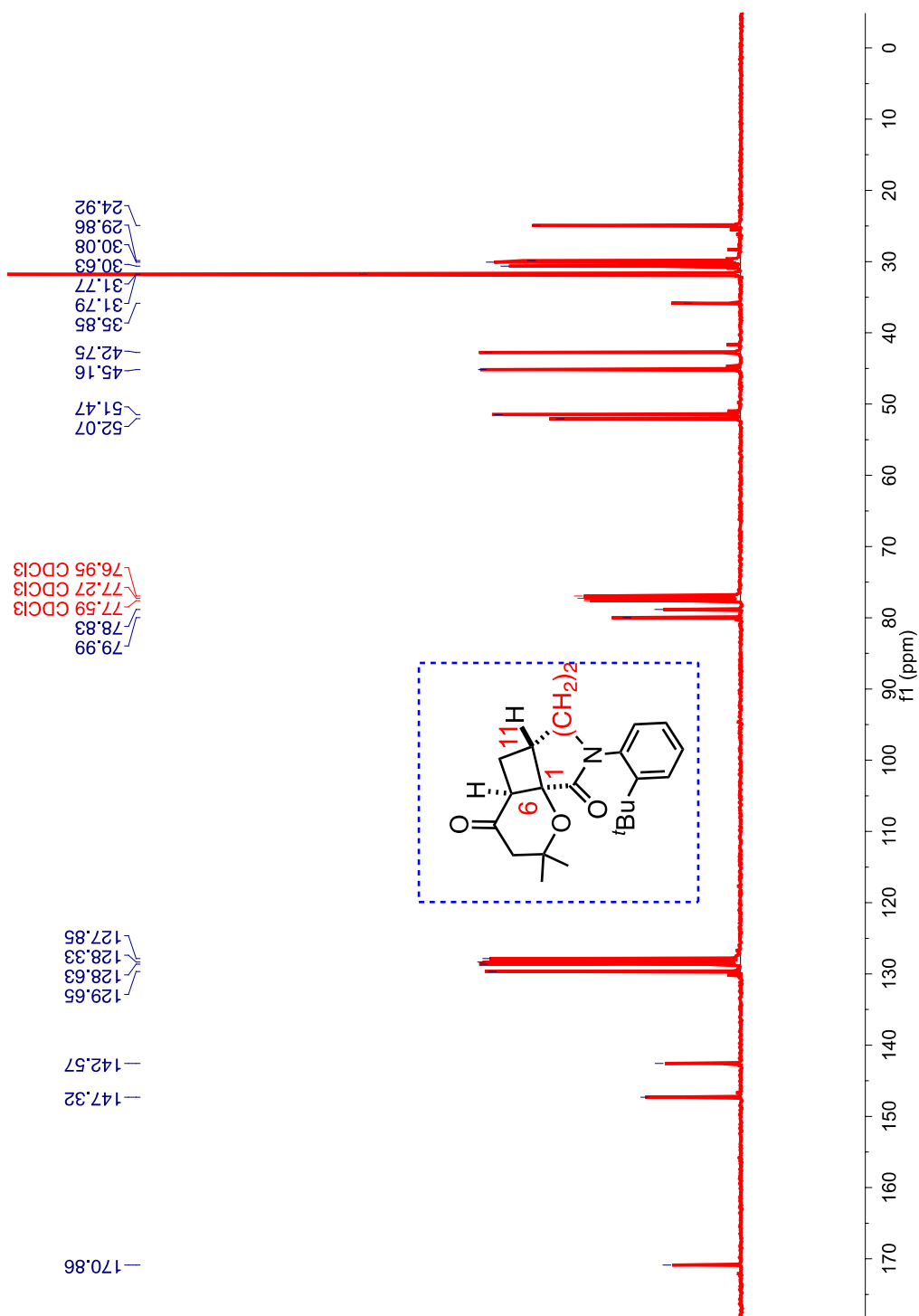


**Figure 2.54:**  $^{13}\text{C}$  NMR (100 MHz,  $\text{CDCl}_3$ ,  $\delta$  ppm) spectrum of *cis,cis*-94b mixture of isomers.

$^1\text{H}$  NMR (400 MHz,  $\text{CDCl}_3$ ,  $\delta$  ppm) 7.54 - 7.51 (m), 7.28 - 7.25 (m), 6.94 - 6.91 (m), 4.22 - 4.16 (m), 3.40 - 3.37 (m), 3.34 - 3.29 (m), 2.82 - 2.73 (m), 2.59 - 2.47 (m), 2.36 - 2.32 (m), 2.30 - 2.18 (m), 1.96 - 1.88 (m), 1.45 (s), 1.44 (s), 1.33 (s).

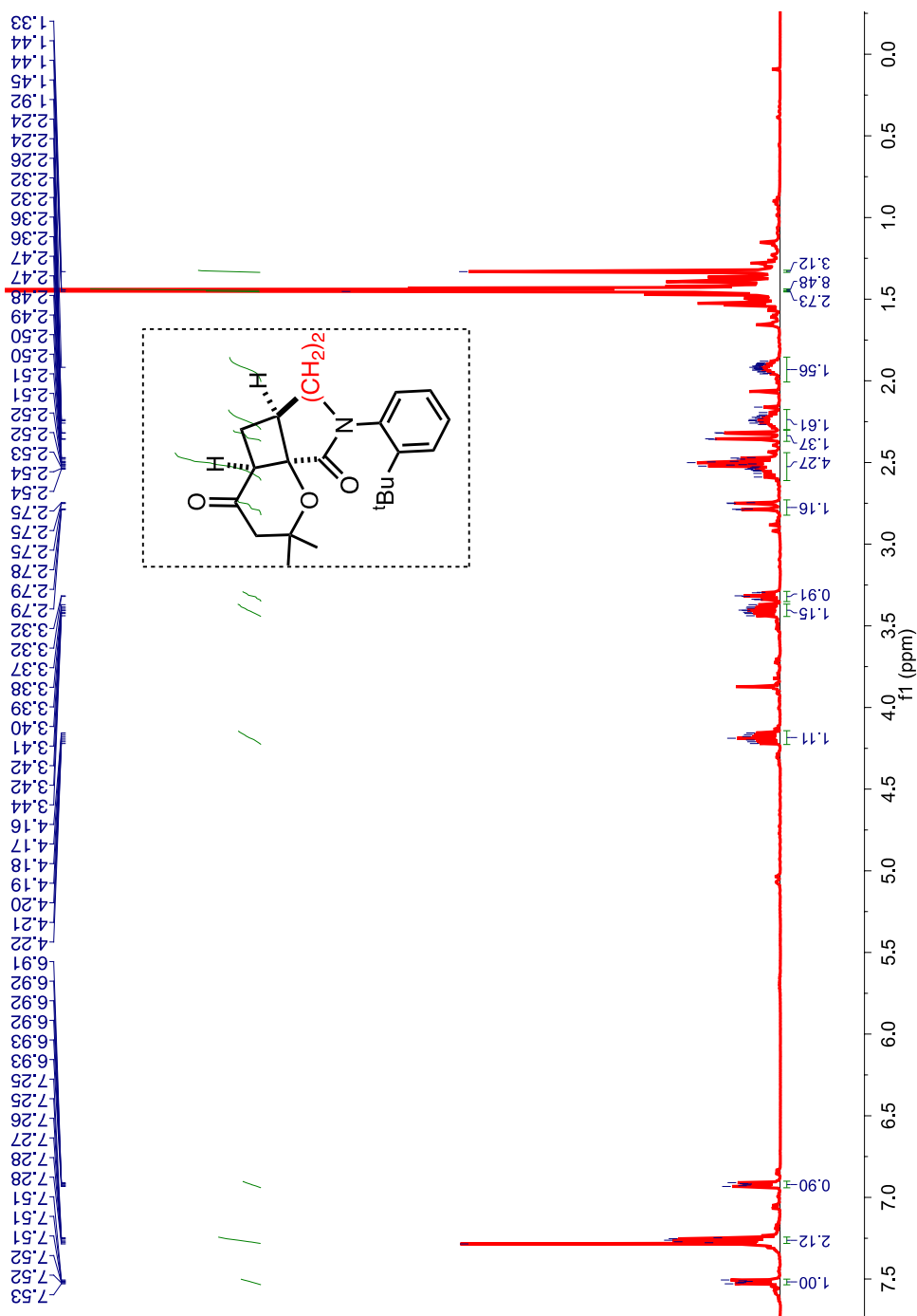


**Figure 2.55:**  $^1\text{H}$  NMR (400 MHz,  $\text{CDCl}_3$ ,  $\delta$  ppm) spectrum of *cis,trans*-94b.

$^{13}\text{C}$  NMR (100 MHz,  $\text{CDCl}_3$ ,  $\delta$  ppm): 206.5, 171.0, 147.6, 142.5, 130.2, 128.5, 127.8, 127.6, 78.5, 77.8, 77.2, 54.5, 49.6, 45.4, 39.4, 35.8, 31.8, 31.6, 30.5, 30.4, 27.0, 19.7

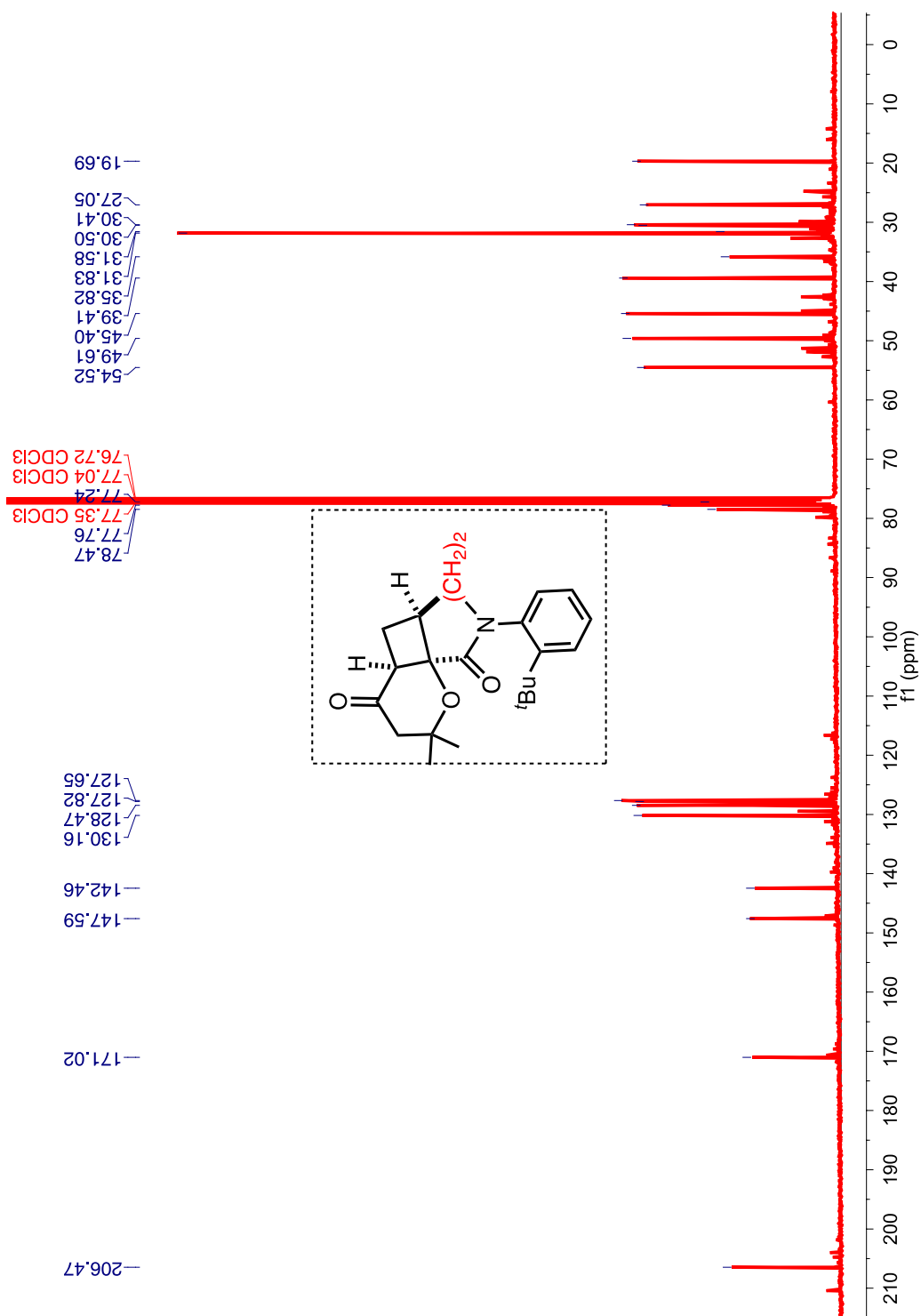


**Figure 2.56:**  $^{13}\text{C}$  NMR (100 MHz,  $\text{CDCl}_3$ ,  $\delta$  ppm) spectrum of *cis,trans*-94b

$^1\text{H}$  NMR (400 MHz,  $\text{CDCl}_3$ ,  $\delta$  ppm): 7.57 – 7.55 (m), 7.33 – 7.24 (m), 6.99 – 6.97 (m), 4.49 – 4.41 (m), 3.88 – 3.83 (m), 3.19 – 3.14 (m), 2.55 (s), 2.48 – 2.42 (m), 2.40 – 2.33 (m), 2.04 – 1.85 (m), 1.76 – 1.64 (m), 1.51 – 1.48 (m), 1.43 (s), 1.40 (s), 1.32 (s).

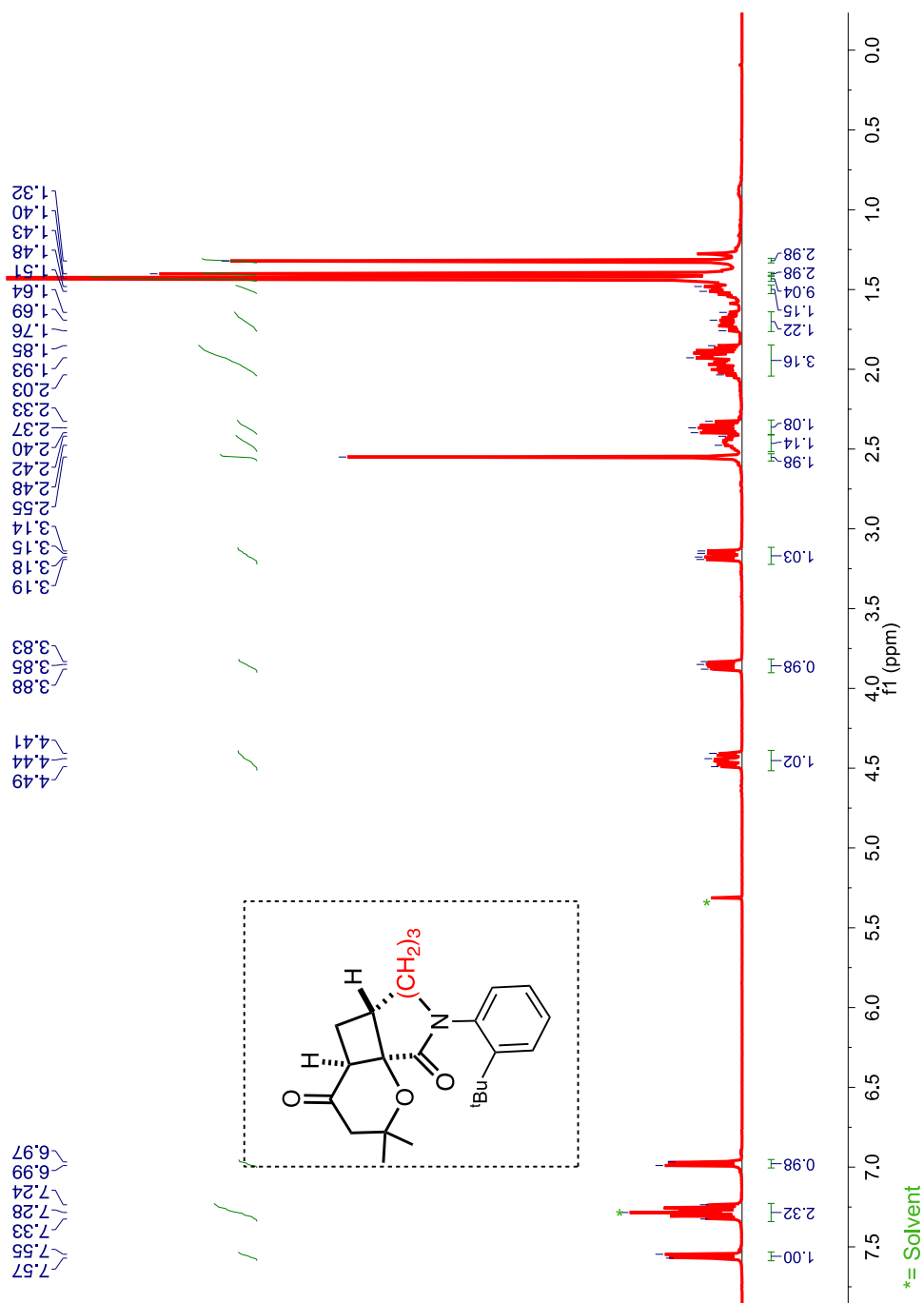


**Figure 2.57:**  $^1\text{H}$  NMR (400 MHz,  $\text{CDCl}_3$ ,  $\delta$  ppm) spectrum of *cis,cis*-94c.



$^{13}\text{C}$  NMR (100 MHz,  $\text{CDCl}_3$ ,  $\delta$  ppm): 210.1, 170.7, 146.8, 141.7, 130.4, 128.7, 127.9, 127.1, 82.5, 78.1, 51.5, 49.4, 42.6, 41.4, 35.9, 31.7, 29.9, 29.1, 27.7, 25.0, 22.9.

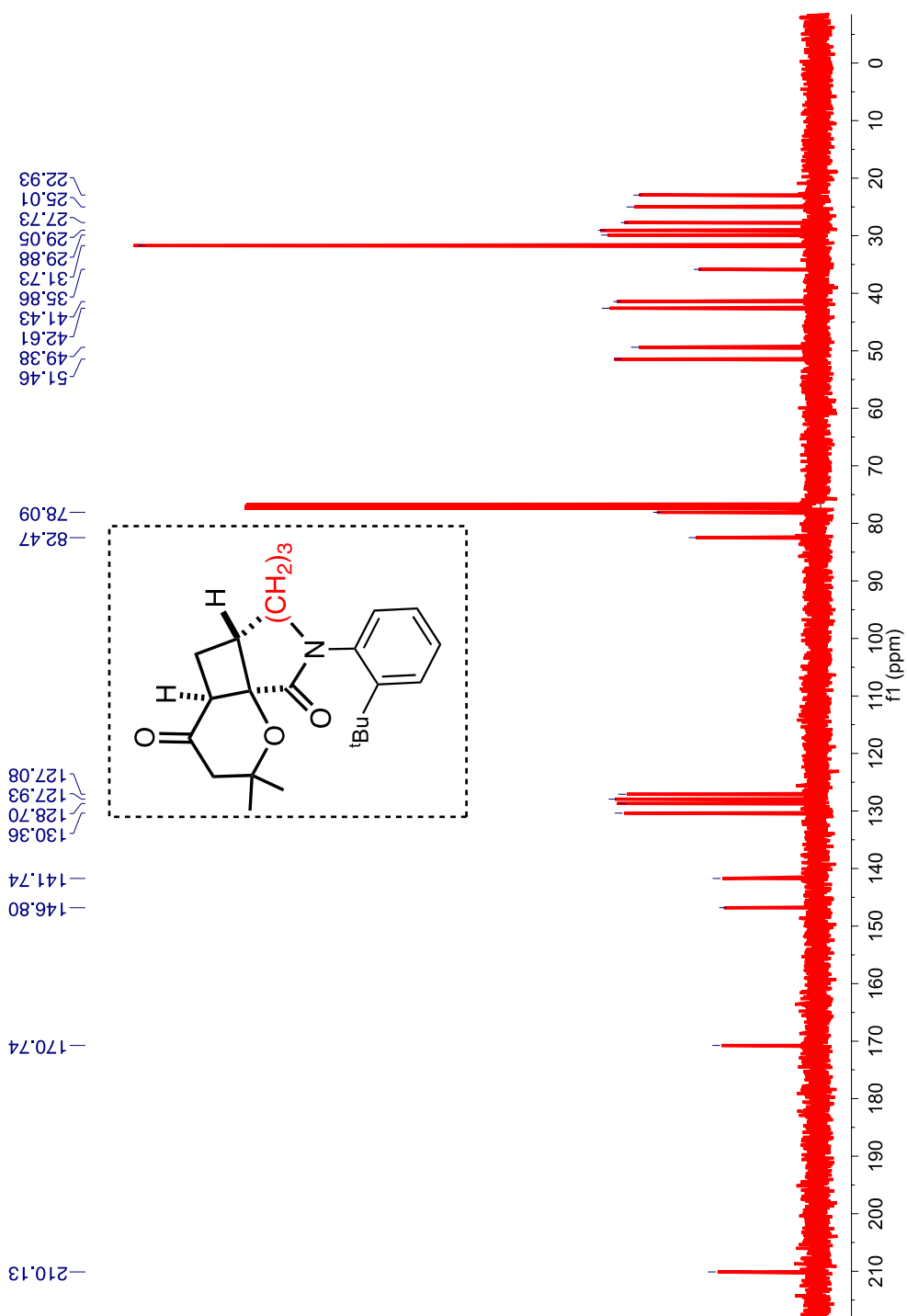


**Figure 2.58:**  $^{13}\text{C}$  NMR (100 MHz,  $\text{CDCl}_3$ ,  $\delta$  ppm) spectrum of *cis,cis*-94c

HPLC analysis conditions: photoproduct *cis-cis*-**94c**

HPLC analytical injections,

Column : CHIRALPAK AD-H

Abs. detector wavelength : 254 nm and 270 nm

Mobile phase : Hexanes : Isopropyl alcohol (95 : 05)

Flow rate : 0.8 mL/min

Retention times (min) : pKA ~22.89 min. and pKB ~26.58 min.

$^1\text{H}$  NMR (400 MHz,  $\text{CDCl}_3$ ,  $\delta$  ppm) 7.55 - 7.51 (m), 7.28 - 7.21 (m), 7.04 - 7.00 (m), 4.64 (m), 3.43 (m), 3.15 - 3.07 (m), 2.78 - 2.71 (m), 2.55 - 2.45 (m), 2.36 - 2.26 (m), 2.21 - 2.02 (m), 1.81 - 1.64 (m), 1.40 (s), 1.39 (s), 1.33 (s).

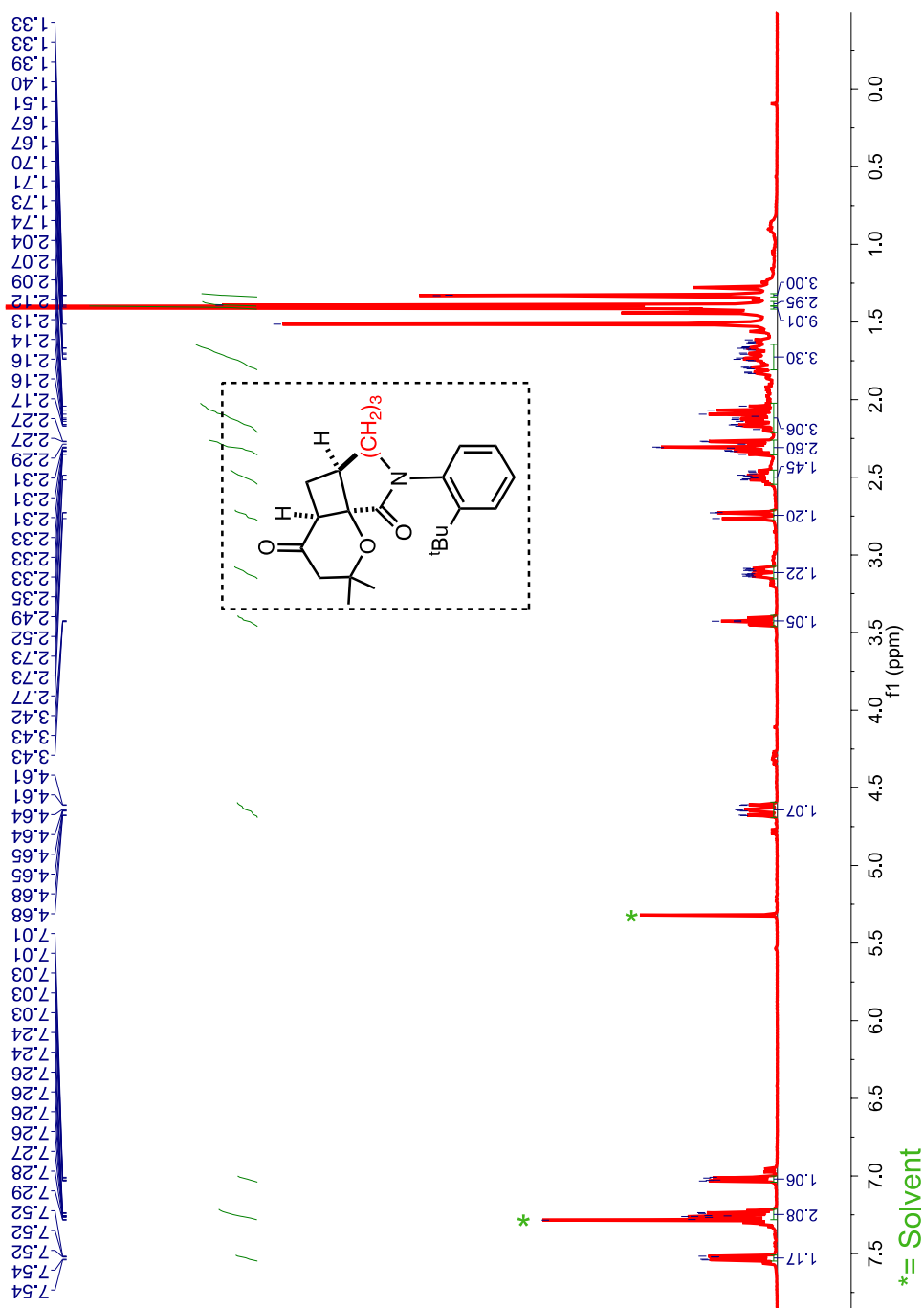


**Figure 2.59:**  $^1\text{H}$  NMR (400 MHz,  $\text{CDCl}_3$ ,  $\delta$  ppm) spectrum of *cis,trans*-94c

$^{13}\text{C}$  NMR (100 MHz,  $\text{CDCl}_3$ ,  $\delta$  ppm): 207.1, 174.0, 146.1, 143.7, 130.3, 128.6, 127.8, 127.2, 81.7, 77.6, 53.8, 49.2, 42.2, 41.2, 35.7, 31.7, 30.6, 28.4, 27.2, 26.4, 26.1.

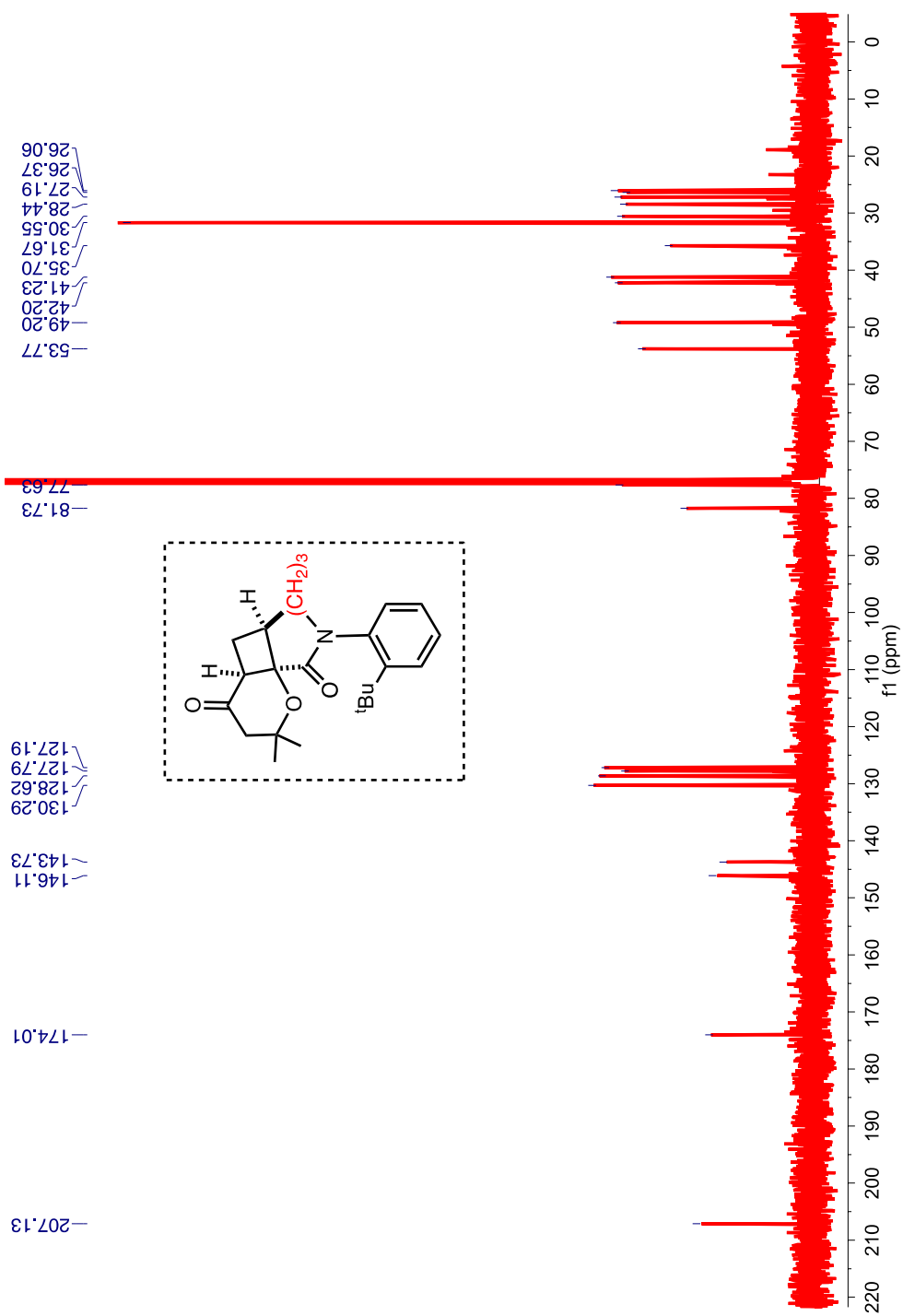


**Figure 2.60:**  $^{13}\text{C}$  NMR (100 MHz,  $\text{CDCl}_3$ ,  $\delta$  ppm) spectrum of *cis,trans*-94c.

$^1\text{H}$  NMR (400 MHz,  $\text{CDCl}_3$ ,  $\delta$  ppm): 7.09 – 7.08 (m), 6.92 – 6.90 (m, 1H), 6.79 – 6.77 (m), 4.47 – 4.39 (m), 3.88 – 3.85 (m), 3.83 (s), 3.17 – 3.12 (m), 2.55 (s), 2.49 – 2.33 (m), 2.04 – 1.84 (m), 1.73 – 1.46 (m), 1.42 (s), 1.40 (s), 1.32 (s).

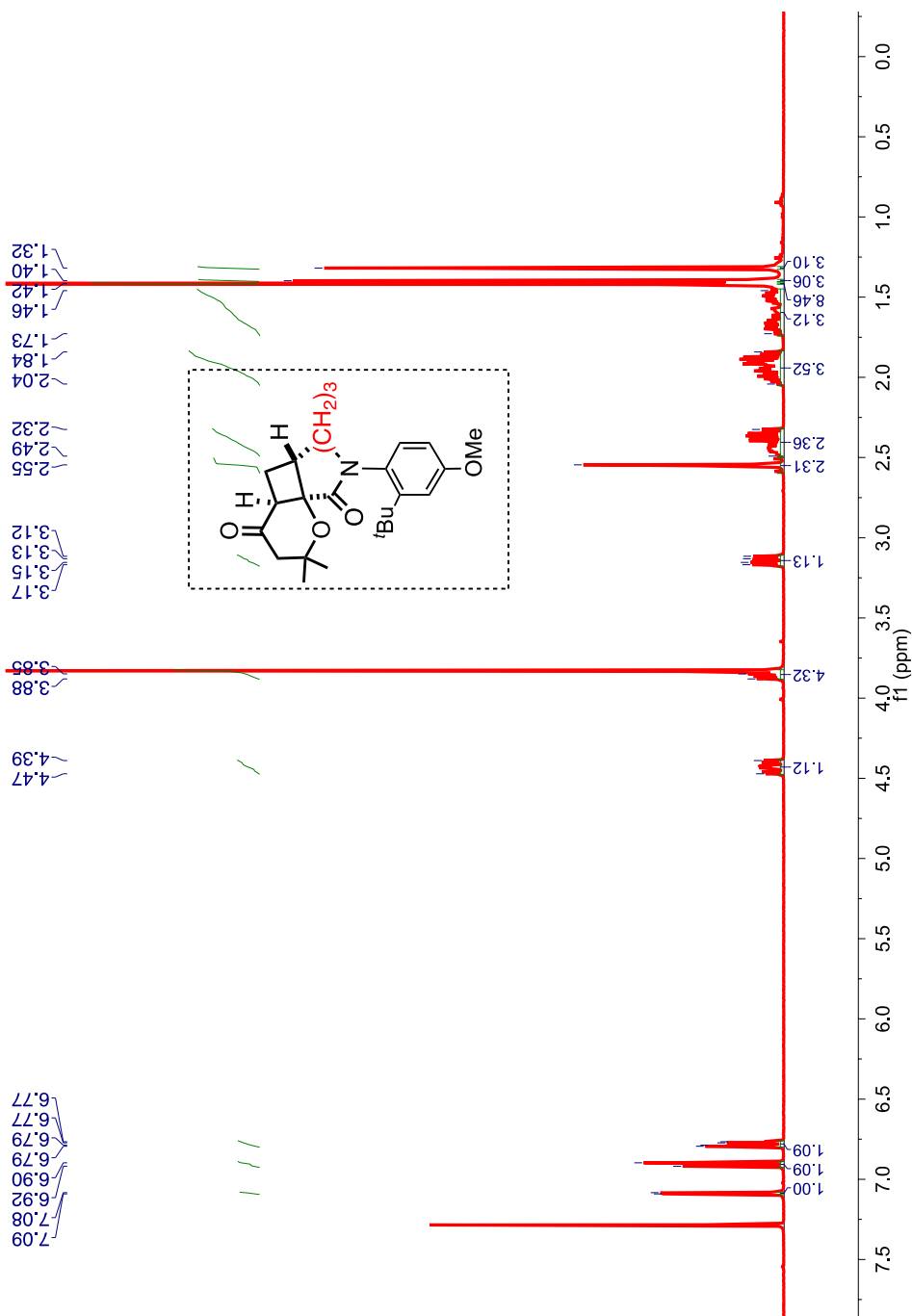


**Figure 2.61:**  $^1\text{H}$  NMR (400 MHz,  $\text{CDCl}_3$ ,  $\delta$  ppm) spectrum of *cis,cis*-94d.

$^{13}\text{C}$  NMR (100 MHz,  $\text{CDCl}_3$ ,  $\delta$  ppm): 210.2, 171.0, 158.6, 148.3, 134.8, 131.2, 115.2, 111.0, 82.5, 78.1, 55.3, 51.4, 49.6, 42.6, 41.5, 35.9, 31.6, 29.9, 29.1, 27.7, 25.0, 22.9.

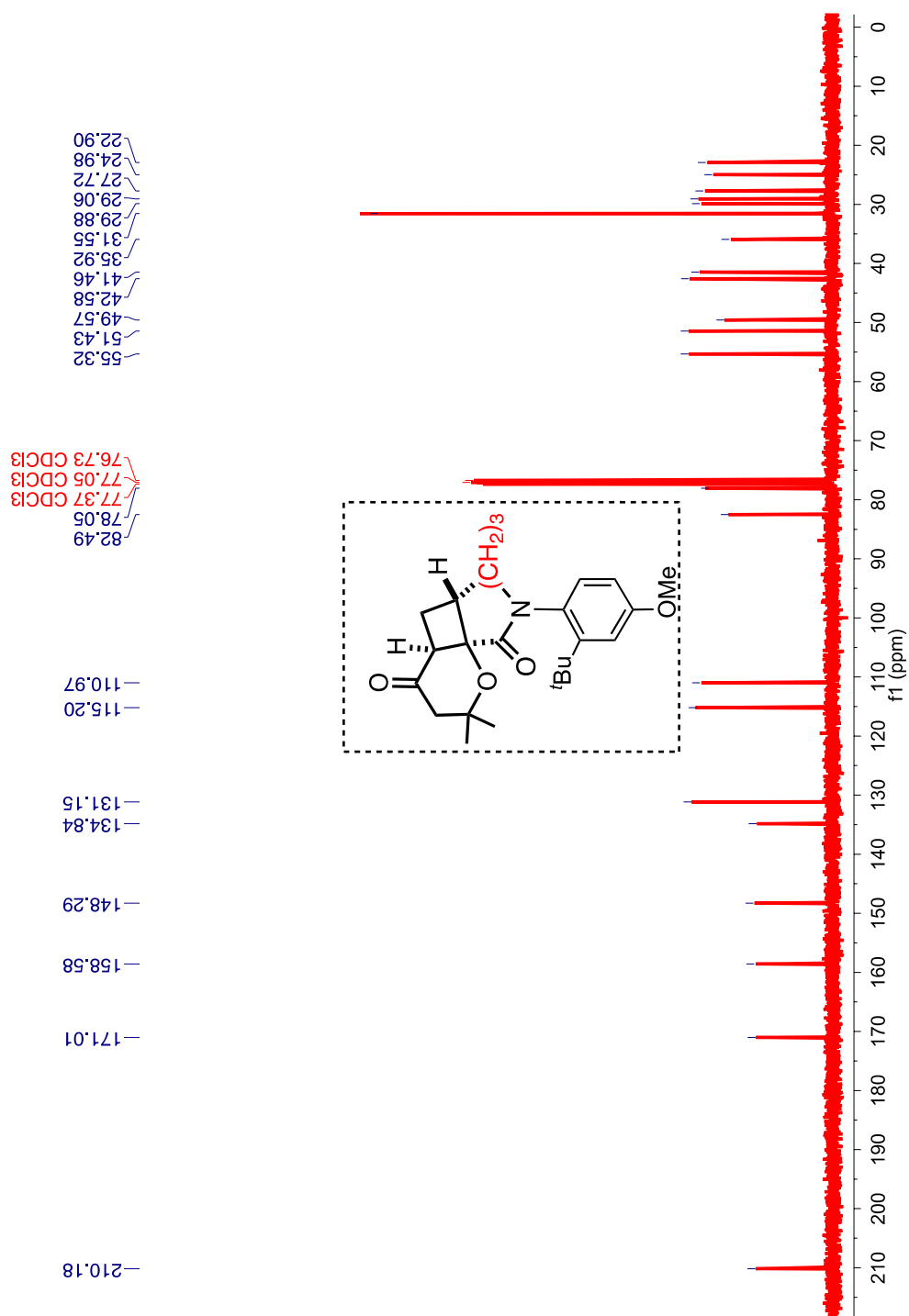


**Figure 2.62:**  $^{13}\text{C}$  NMR (100 MHz,  $\text{CDCl}_3$ ,  $\delta$  ppm) spectrum of *cis,cis*-94d.

HPLC analysis conditions for *cis,cis*-**94d**.

HPLC analytical injections,

Column : (R,R) Whelk-01

Abs. detector wavelength : 254 nm and 270 nm

Mobile phase : Hexanes : Isopropyl alcohol (70 : 30)

Flow rate : 0.8 mL/min

Retention times : pkA ~18.68 min and pkB ~33.63 min

$^1\text{H}$  NMR (400 MHz,  $\text{CDCl}_3$ ,  $\delta$  ppm): 7.06 – 7.05 (m, 1H), 6.96 – 6.94 (m, 1H), 6.77 – 6.75 (m, 1H), 4.66 – 4.60 (m, 1H), 3.82 (s, 3H), 3.45 – 3.40 (t, 1H), 3.12 – 3.07 (dd,  $J = 15.2, 5.2$  Hz, 1H), 2.75 – 2.72 (d,  $J = 15.2$  Hz, 1H), 2.51 – 2.43 (m, 1H), 2.35 – 2.27 (m, 2H), 2.19 – 2.03 (m, 2H), 1.84 – 1.64 (m, 3H), 1.51 (s, 3H), 1.39 (s, 9H), 1.32 (s, 3H).

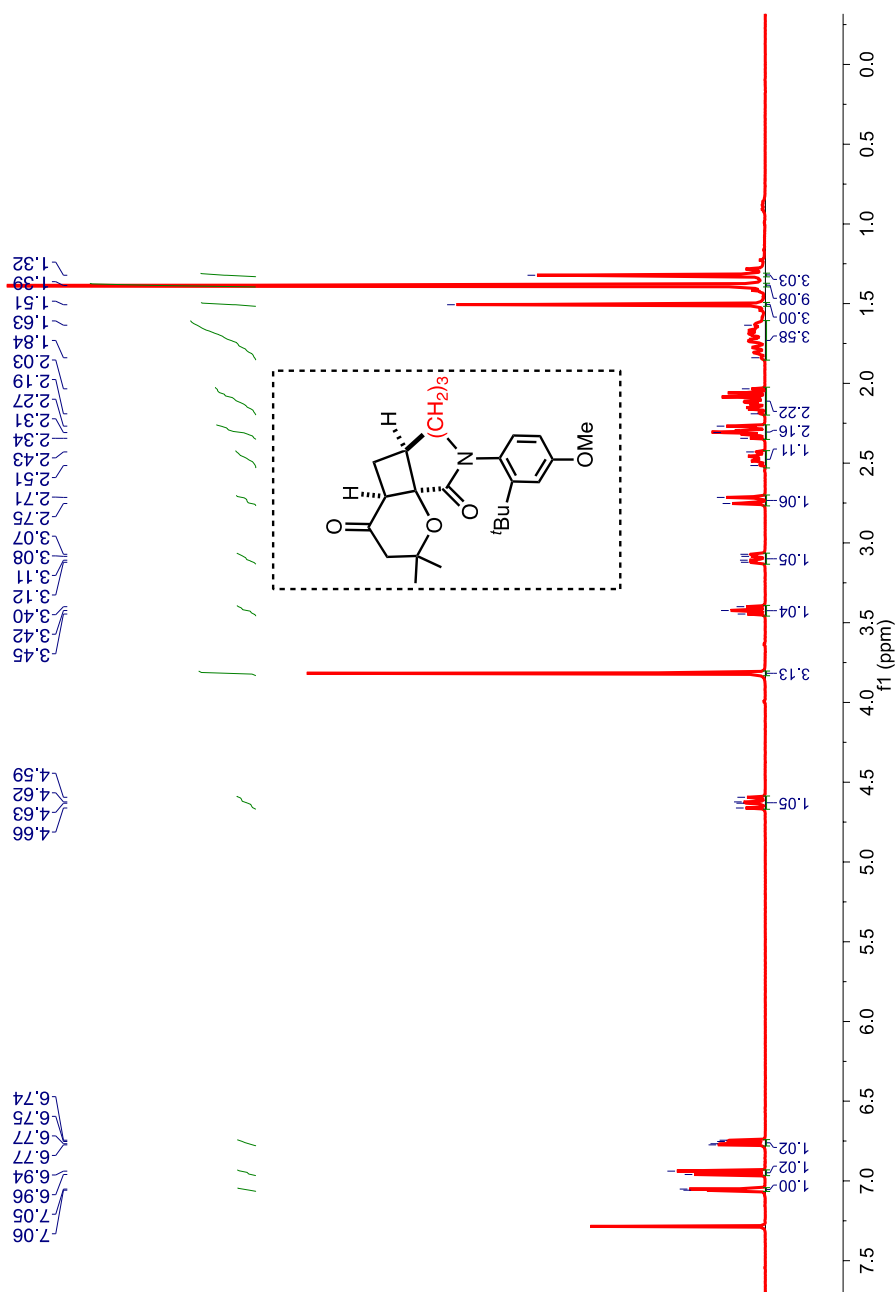


**Figure 2.63:**  $^1\text{H}$  NMR (400 MHz,  $\text{CDCl}_3$ ,  $\delta$  ppm) spectrum of *cis,trans*-94d.



$^{13}\text{C}$  NMR (100 MHz,  $\text{CDCl}_3$ ,  $\delta$  ppm): 207.1, 174.2, 158.5, 147.6, 136.9, 131.1, 115.1, 111.1, 81.8, 77.6, 55.3, 54.0, 49.2, 42.3, 41.3, 35.8, 31.5, 30.6, 28.5, 27.2, 26.4, 26.1.

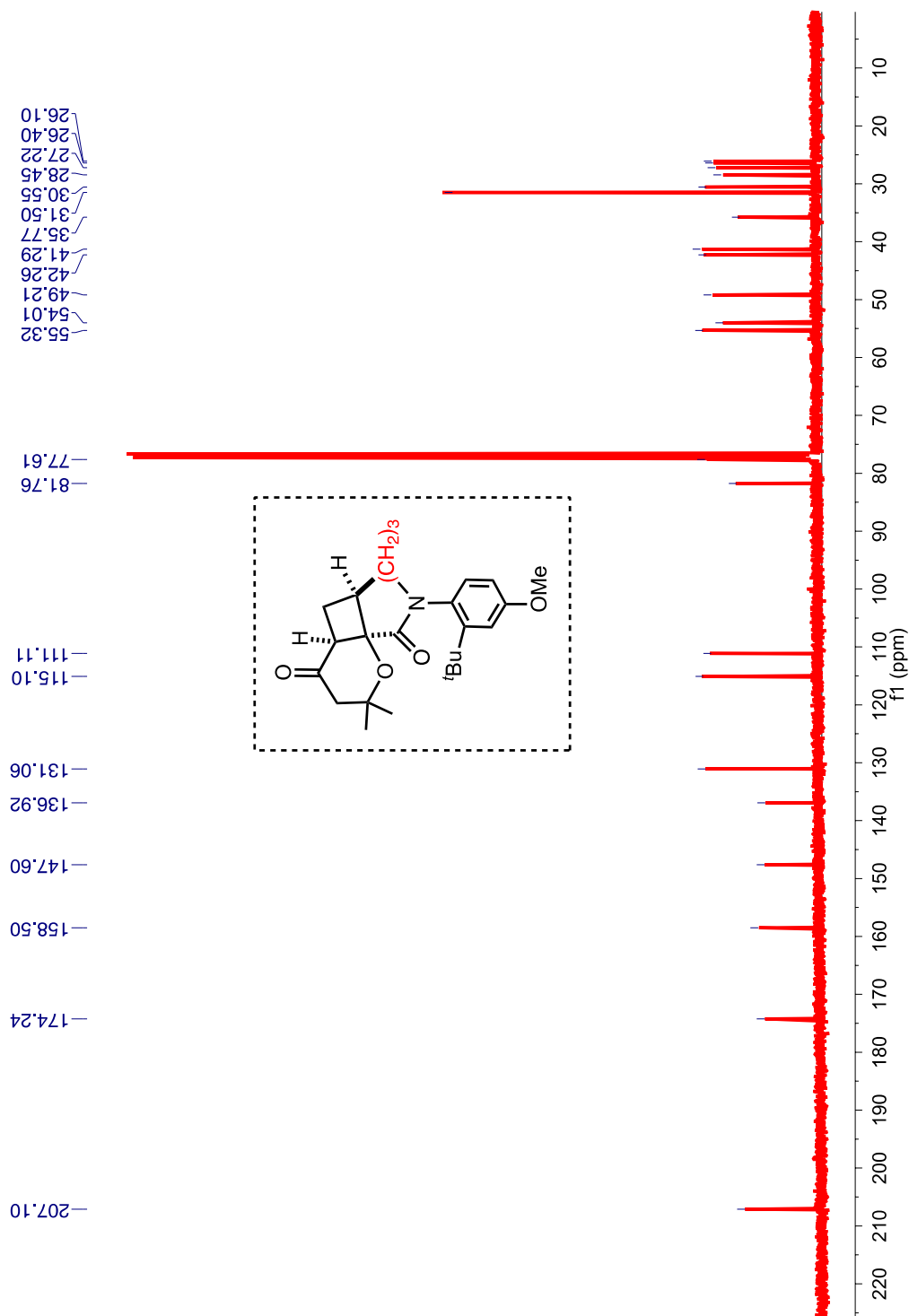


**Figure 2.64:**  $^{13}\text{C}$  NMR (100 MHz,  $\text{CDCl}_3$ ,  $\delta$  ppm) spectrum of *cis,trans*-94d.

HPLC analysis conditions for *cis,trans*-**94e**.

HPLC analytical injections,

Column : (R,R) Whelk-01

Abs. detector wavelength : 254 nm and 270 nm

Mobile phase : Hexanes : Isopropyl alcohol (70 : 30)

Flow rate : 0.8 mL/min

Retention times : pkA 25.00 min and pkB 35.08 min

$^1\text{H}$  NMR (400 MHz,  $\text{CDCl}_3$ ,  $\delta$  ppm) 7.58 - 7.56 (m, 1H), 7.40 - 7.36 (m, 1H), 7.30 - 7.26 (m, 1H), 6.81 - 6.78 (m, 1H), 3.17 - 3.15 (m, 1H), 2.67 - 2.56 (m, 3H), 2.29 - 2.24 (m, 1H), 1.47 (s, 3H), 1.42 (s, 3H), 1.39 (s, 3H), 1.28 (s, 9H).

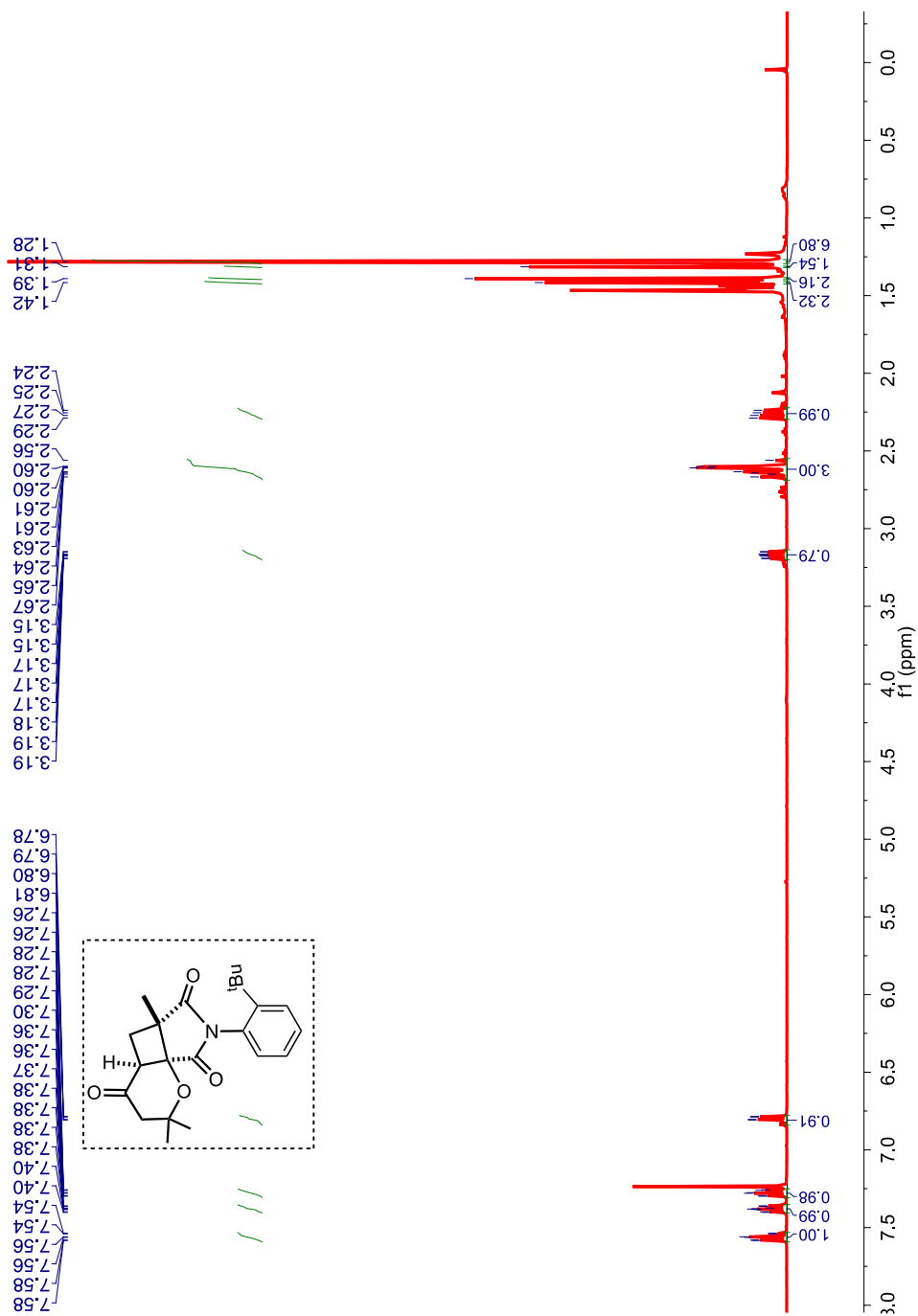


**Figure 2.65:**  $^1\text{H}$  NMR (400 MHz,  $\text{CDCl}_3$ ,  $\delta$  ppm) *cis,cis*-**94f** (mixture of  $N$ - $\text{C}_{\text{Aryl}}$  rotamers).

$^{13}\text{C}$  NMR (100 MHz,  $\text{CDCl}_3$ ,  $\delta$  ppm; mixture of  $N$ - $\text{C}_{\text{Aryl}}$  rotamers): 179.2, 176.9, 148.5, 131.5, 130.5, 130.1(d), 130.0, 129.2, 128.6, 127.8, 127.6, 79.4, 79.0, 51.4, 51.3, 47.2, 46.9, 41.1, 40.3, 36.0, 32.0, 31.9, 31.8, 31.4, 31.14, 30.3, 30.2, 29.9, 29.4, 29.2, 15.8, 15.3

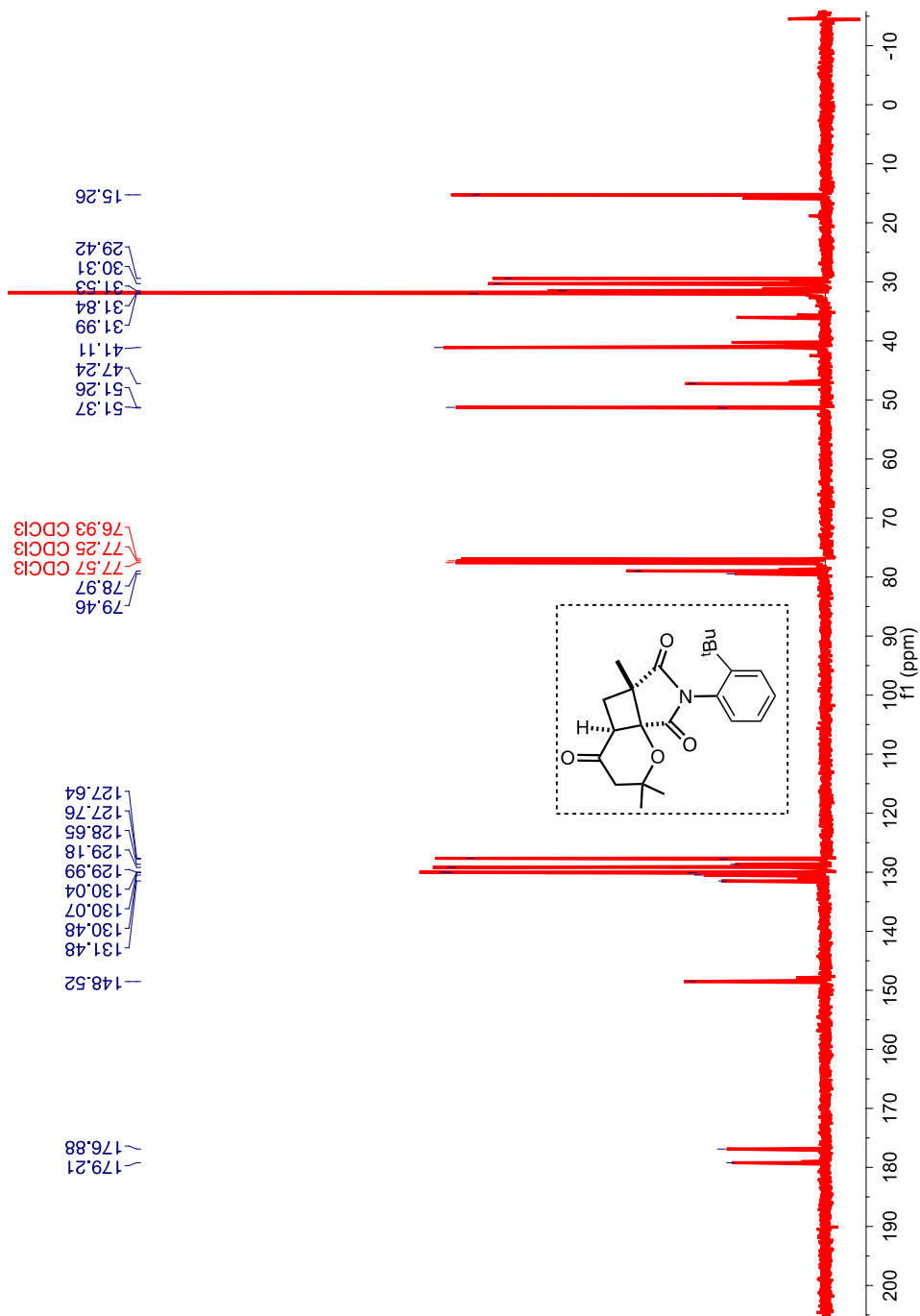


**Figure 2.66:**  $^{13}\text{C}$  NMR (100 MHz,  $\text{CDCl}_3$ ,  $\delta$  ppm) *cis,cis*-**94f** (mixture of  $N$ - $\text{C}_{\text{Aryl}}$  rotamers).

$^1\text{H}$  NMR (400 MHz,  $\text{CDCl}_3$ ,  $\delta$  ppm): 7.56 – 7.54 (m, 1H), 7.40 – 7.35 (m, 1H), 7.28 - 7.24 (m, 1H), 6.84 – 6.82 (m, 1H), 3.24 – 3.20 (m, 1H), 2.79 – 2.73 (m, 1H), 2.63 – 2.56 (m, 2H), 2.25 - 2.20 (m, 1H), 1.46 (s, 3H), 1.44 (s, 3H), 1.40 (s, 3H), 1.31 (s, 9H).

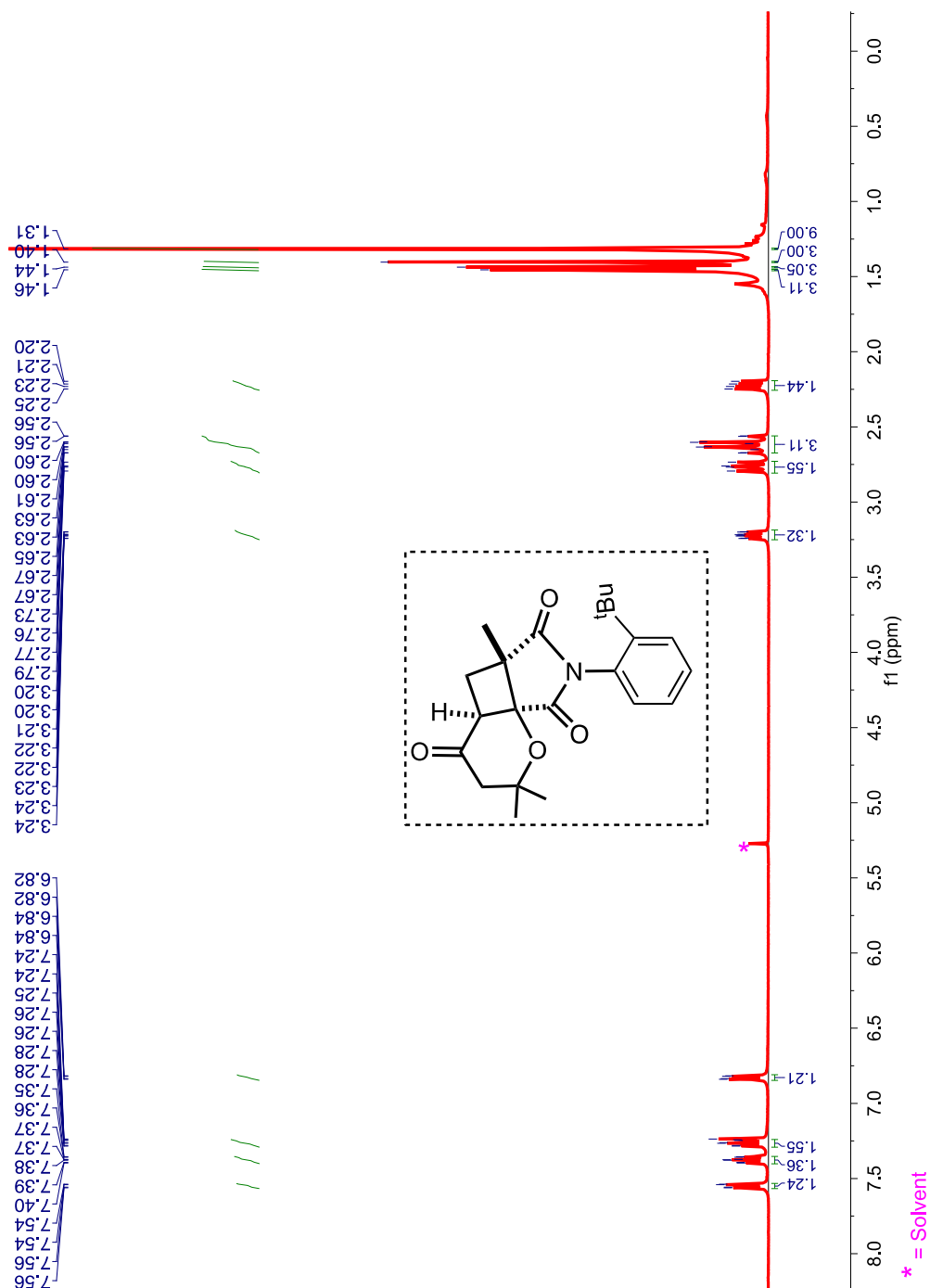


**Figure 2.67:**  $^1\text{H}$  NMR (400 MHz,  $\text{CDCl}_3$ ,  $\delta$  ppm) *cis,cis*-94f (minor  $N\text{-C}_{\text{Aryl}}$  rotamer).

$^{13}\text{C}$  NMR (100 MHz,  $\text{CDCl}_3$ ,  $\delta$  ppm): 177.1, 147.9, 131.5, 131.0, 131.1, 128.7, 127.8, 78.8, 78.7, 51.4, 46.9, 51.4, 46.9, 40.3, 35.6, 31.5, 31.2, 30.2, 29.2, 15.9

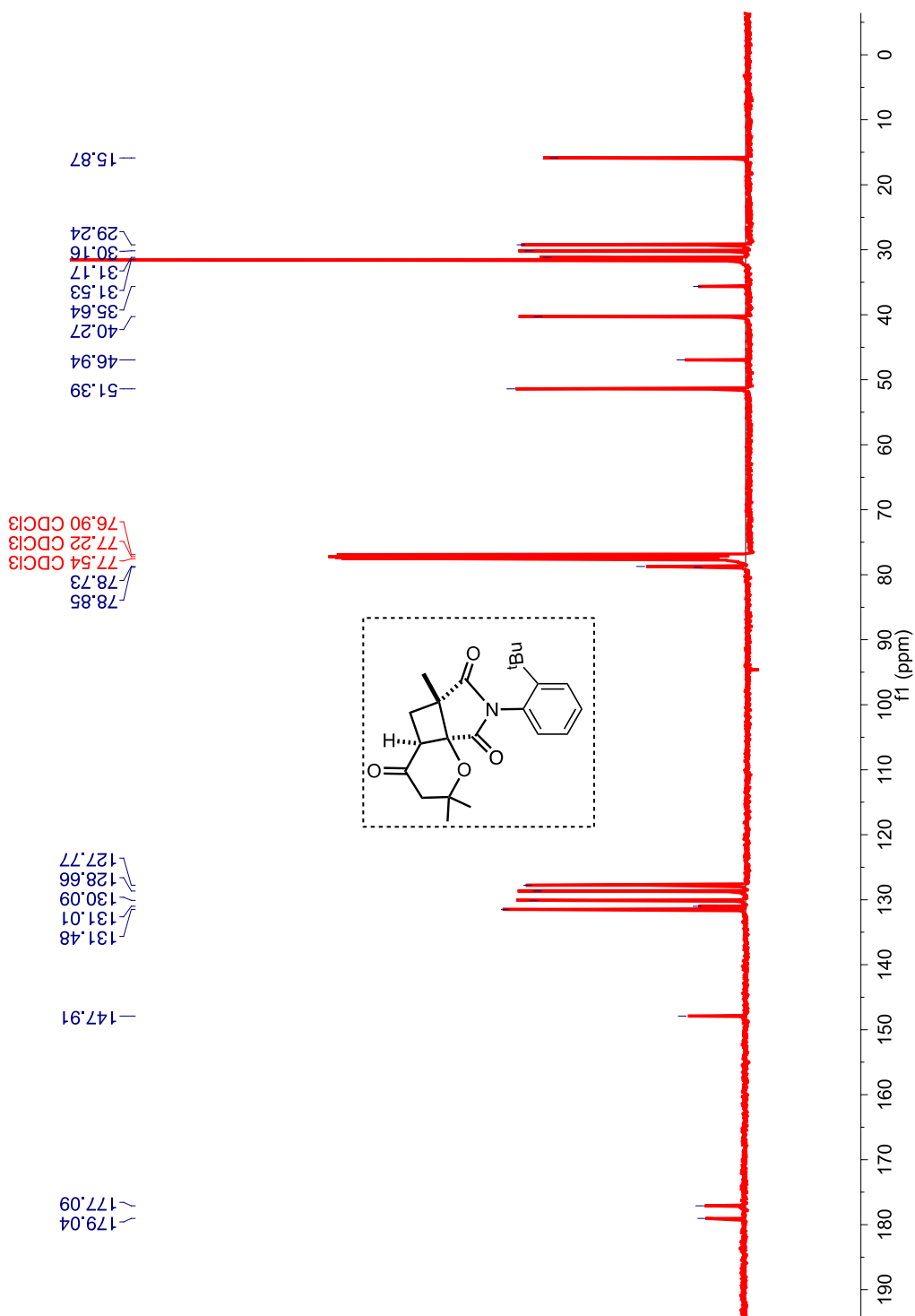


**Figure 2.68:**  $^{13}\text{C}$  NMR (100 MHz,  $\text{CDCl}_3$ ,  $\delta$  ppm) *cis,cis*-94f (minor  $N\text{-C}_{\text{Aryl}}$  rotamer).

$^1\text{H}$  NMR (400 MHz,  $\text{CDCl}_3$ ,  $\delta$  ppm): 7.13 – 7.12 (m, 1H), 6.85 – 6.82 (m, 1H), 6.78 – 7.76 (m, 1H), 3.84 (s, 3H), 3.22 – 3.17 (m, 1H), 2.69 - 2.63 (m, 3H), 2.29 (dd,  $J = 13.4, 6.7$  Hz, 1H), 1.50 (s, 3H), 1.45 (s, 3H), 1.42 (s, 3H), 1.30 (s, 9H).

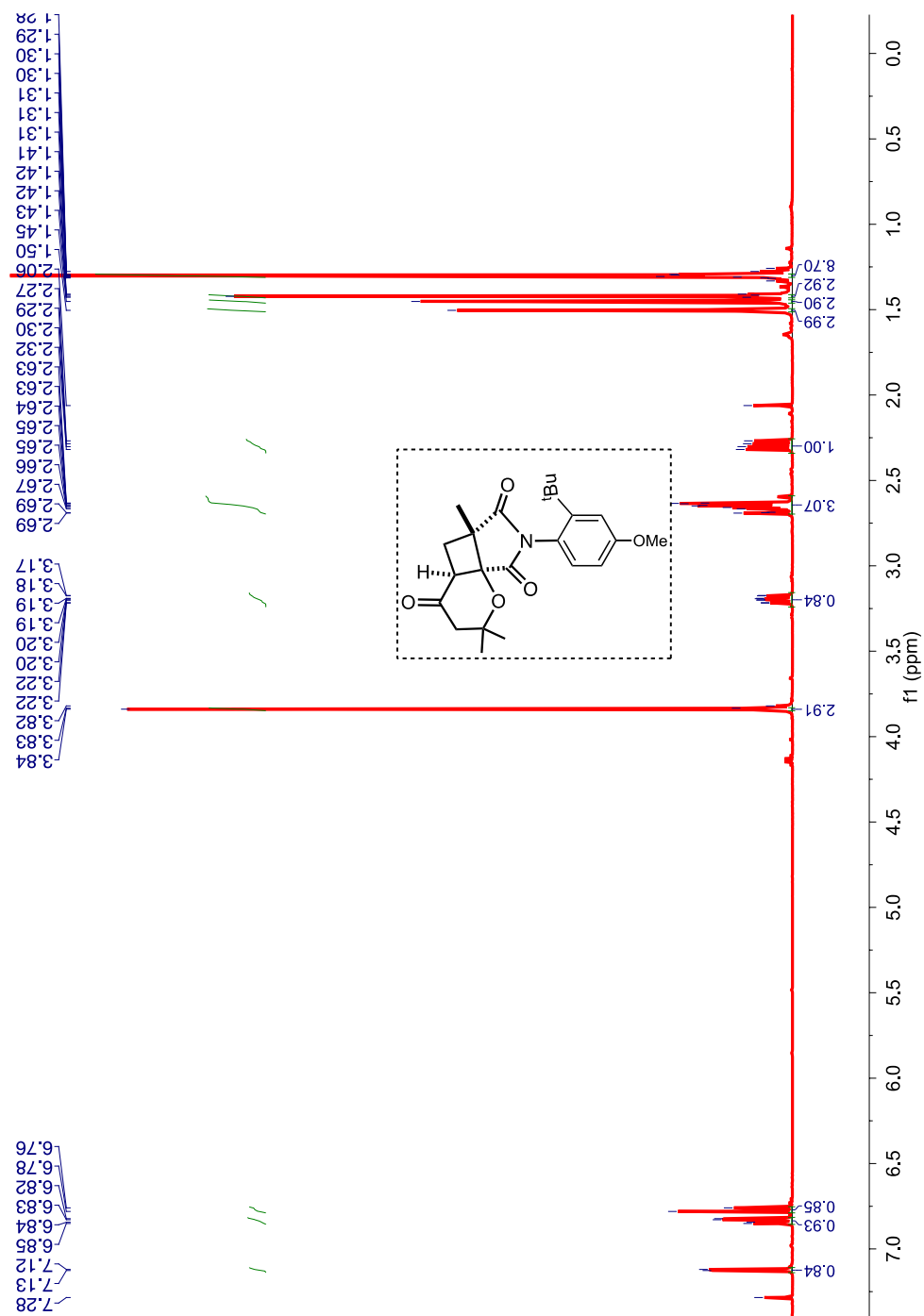


**Figure 2.69:**  $^1\text{H}$  NMR (400 MHz,  $\text{CDCl}_3$ ,  $\delta$  ppm) *cis,cis*-94g (major N-Caryl rotamers).

$^{13}\text{C}$  NMR (100 MHz,  $\text{CDCl}_3$ ,  $\delta$  ppm) 206.3, 179.4, 176.9, 160.2, 149.8, 130.9, 122.9, 115.5, 111.6, 79.2, 78.8, 55.4, 51.1, 46.9, 40.9, 35.8, 31.8, 31.5, 31.4, 30.1, 29.2, 15.1.

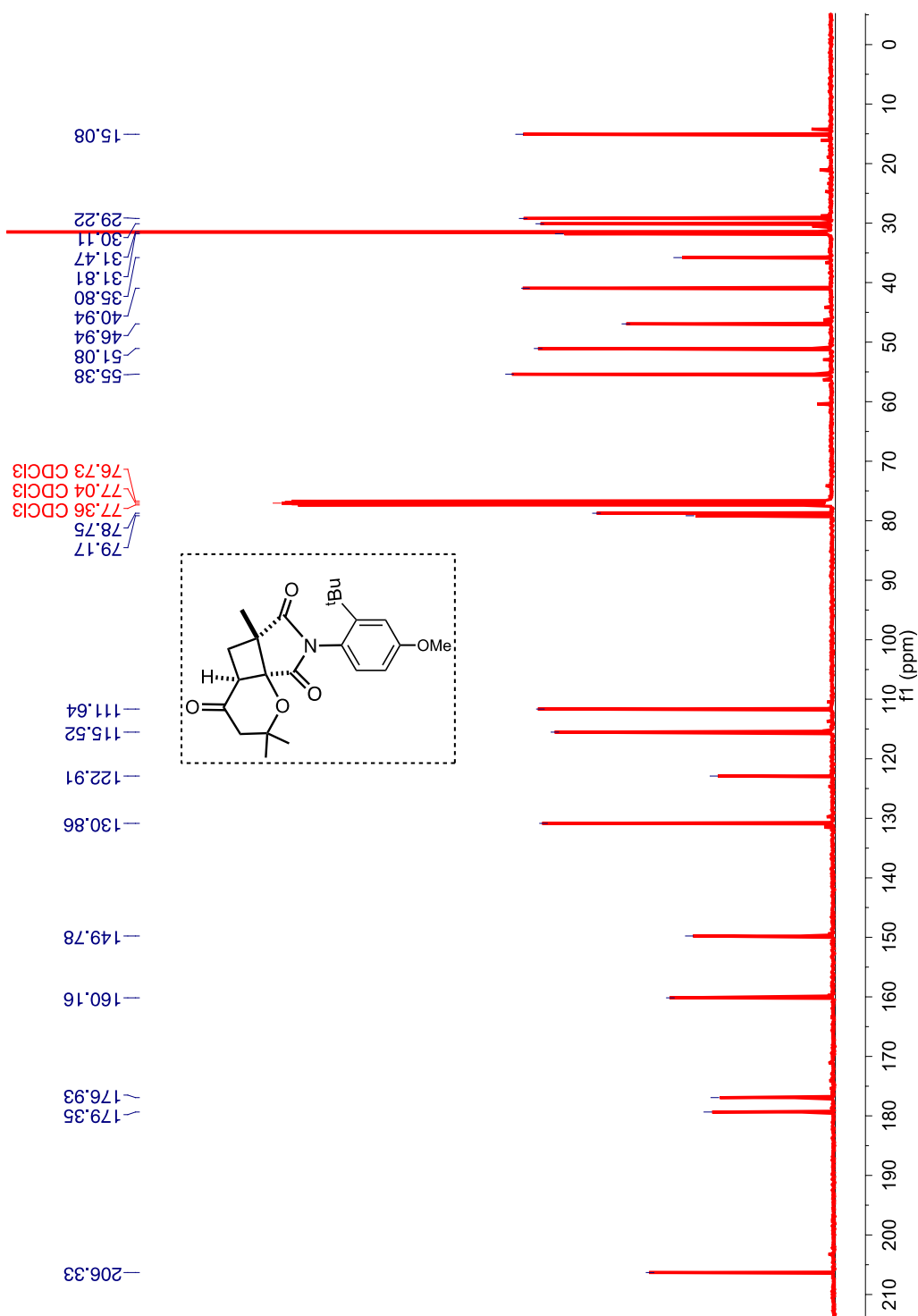


**Figure 2.70:**  $^{13}\text{C}$  NMR (100 MHz,  $\text{CDCl}_3$ ,  $\delta$  ppm) *cis,cis*-**94g** (major  $N\text{-C}_{\text{Aryl}}$  rotamers).



$^1\text{H}$  NMR (400 MHz,  $\text{CDCl}_3$ ,  $\delta$  ppm) 7.11- 7.10 (m, 1H), 6.84 – 6.79 (m, 2H), 3.84 (s, 3H), 3.27 – 3.23 (m, 1H), 2.80 (dd,  $J = 13.6, 10.5$  Hz, 1H), 2.73 - 2.60 (m, 3H), 2.26 (dd,  $J = 13.6, 6.8$  Hz, 1H), 1.57 (s, 2H), 1.50 (s, 3H), 1.48 (s, 3H), 1.44 (s, 3H), 1.34 (s, 9H).

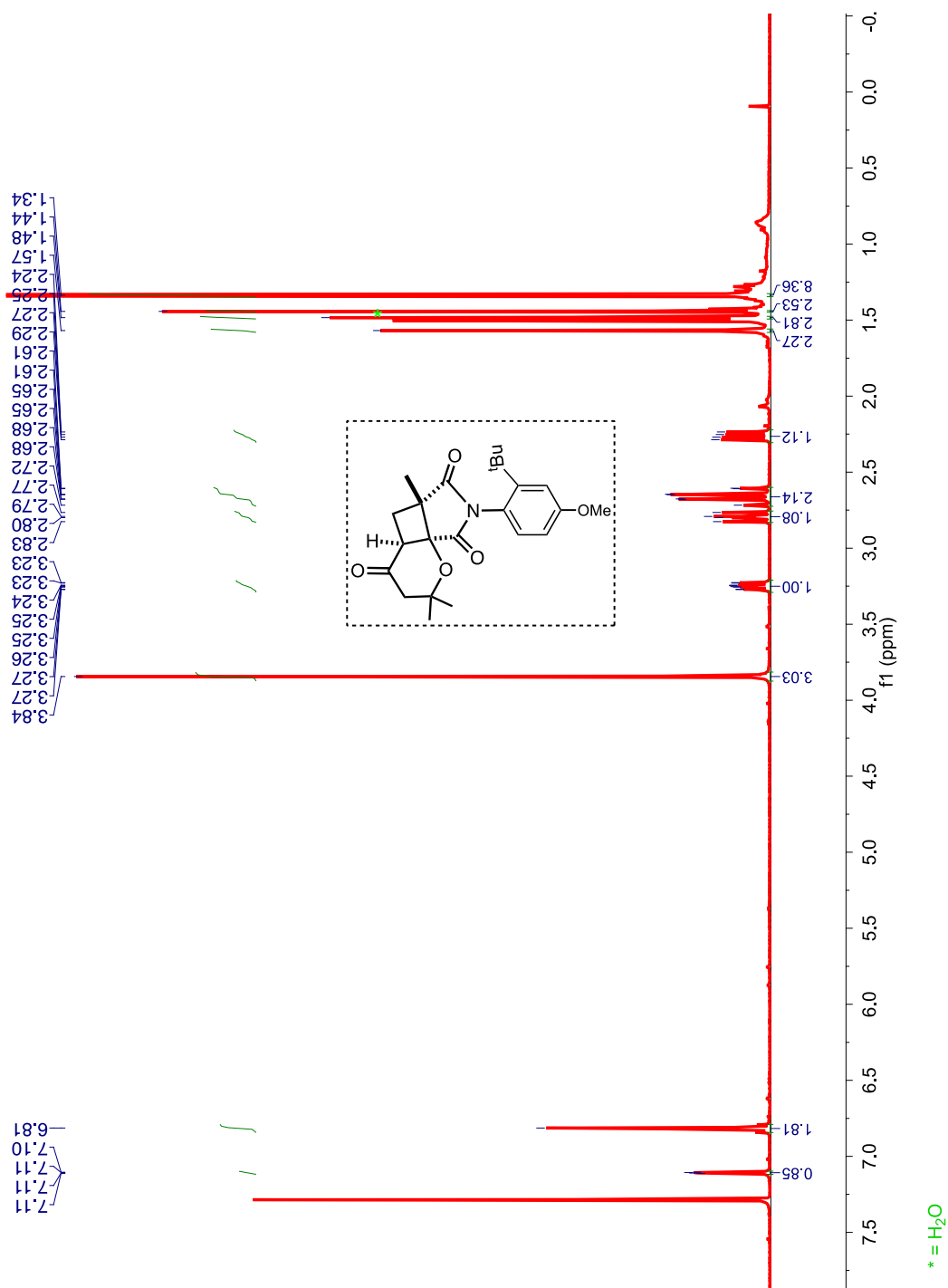


**Figure 2.71:**  $^1\text{H}$  NMR (400 MHz,  $\text{CDCl}_3$ ,  $\delta$  ppm) (minor  $N\text{-C}_{\text{Aryl}}$  rotamer).

$^{13}\text{C}$  NMR (100 MHz,  $\text{CDCl}_3$ ,  $\delta$  ppm; minor  $N\text{-C}_{\text{Aryl}}$  rotamer): 206.2, 179.1, 177.2, 160.2, 149.2, 132.3, 123.3, 115.2, 111.5, 100.0, 78.6, 78.5, 77.2, 55.4, 51.2, 46.6, 40.1, 35.4, 31.2, 31.0, 30.0, 29.1, 15.7.

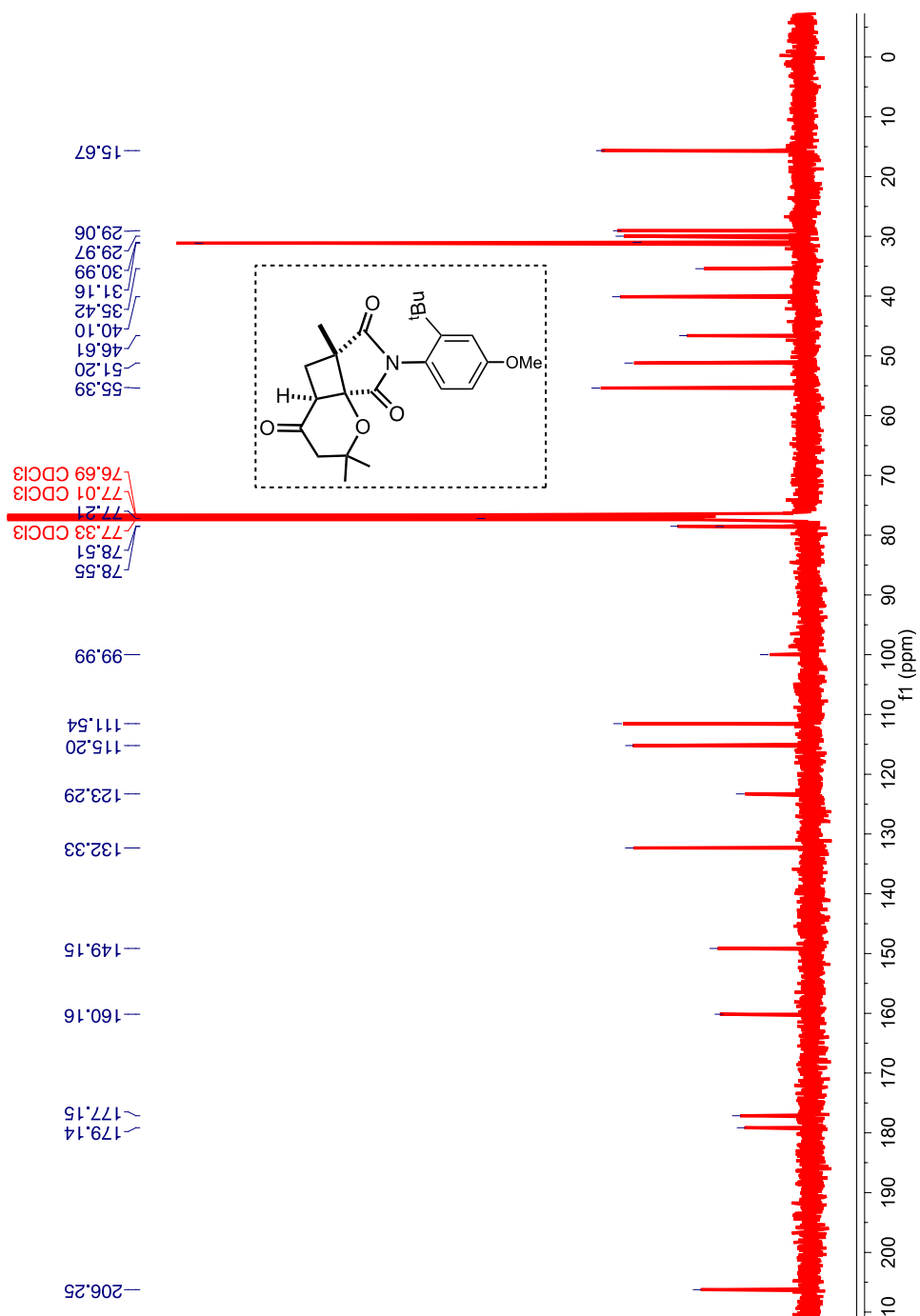


**Figure 2.72:**  $^{13}\text{C}$  NMR (100 MHz,  $\text{CDCl}_3$ ,  $\delta$  ppm) spectrum of minor  $N\text{-C}_{\text{Aryl}}$  rotamer.

#### 2.12.4. X-Ray crystal structure data for atropisomeric enone photoproducts

**Table 2.5:** X-ray crystal data for atropisomeric enones.

	<i>cis,cis-94b</i>	<i>cis,trans-94b</i>	<i>cis,cis-94c</i>	<i>cis,cis-94d</i>
Formula	C <sub>22</sub> H <sub>29</sub> NO <sub>3</sub>	C <sub>22</sub> H <sub>29</sub> NO <sub>3</sub>	C <sub>23</sub> H <sub>31</sub> NO <sub>3</sub>	C <sub>24</sub> H <sub>33</sub> NO <sub>4</sub>
FW	355.46	355.46	369.49	399.51
Cryst. Size_max [mm]	0.327	0.25	0.25	0.187
Cryst. Size_mid [mm]	0.276	0.166	0.12	0.164
Cryst. Size_main[mm]	0.077	0.07	0.05	0.056
Cryst. system	Orthorhombic	monoclinic	Orthorhombic	monoclinic
Space Group, Z	Pccn	C2/c	P2 <sub>1</sub> 2 <sub>1</sub> 2 <sub>1</sub>	P2 <sub>1</sub> /c
a [Å]	16.2407(5)	32.5617(9)	6.2306(2)	20.7554(7)
b [Å]	18.9857(6)	12.2539(3)	15.6867(5)	6.2296(2)
c [Å]	12.4646(4)	19.7547(5)	41.3174(13)	17.0708(6)
α [°]	90	90	90	90
β [°]	90	98.588(2)	90	101.719(2)
γ [°]	90	90	90	90
V [Å <sup>3</sup> ]	3843.3(2)	7793.9(4)	4038.3(2)	2161.21(13)
ρ <sub>calc</sub> [g/cm <sup>3</sup> ]	1.229	1.212	1.215	1.228
μ [mm <sup>-1</sup> ]	0.641	0.633	0.629	0.66
Radiation Type	Cu	Cu	Cu	Cu
(F000)	1536	3072	1600	864
No of refl. (≥ 2σ)	18521	24883	16255	21165
No of indep. Refl.	3387	6620	6440	3832
No of refl. (≥ 2σ)	3053	5395	4112	3076
Resolution [Å]	0.84	0.84	0.84	0.84
R <sub>1</sub> /wR <sub>2</sub> (≥ 2σ) <sup>a</sup> [%]	R <sub>1</sub> = 3.51, wR <sub>2</sub> = 8.85	R <sub>1</sub> = 4.72, wR <sub>2</sub> = 11.3	R <sub>1</sub> = 2.65, wR <sub>2</sub> = 6.56	R <sub>1</sub> = 4.32, wR <sub>2</sub> = 10.58
R <sub>1</sub> /wR <sub>2</sub> (all data) <sup>a</sup> [%]	R <sub>1</sub> = 3.94, wR <sub>2</sub> = 9.20	R <sub>1</sub> = 6.01, wR <sub>2</sub> = 12.06	R <sub>1</sub> = 2.76, wR <sub>2</sub> = 6.63	R <sub>1</sub> = 5.58, wR <sub>2</sub> = 11.35

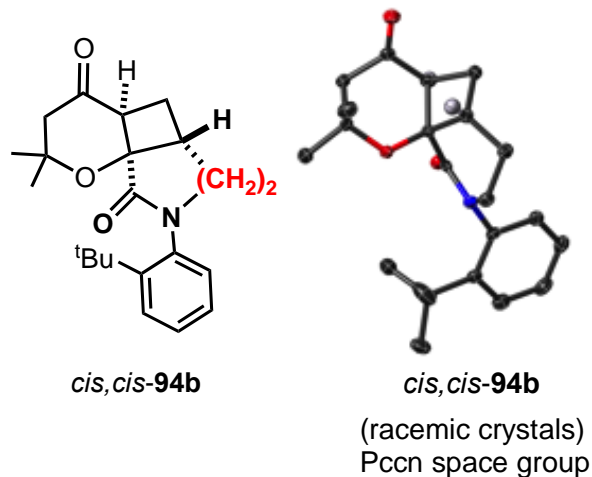


**Figure 2.73:** Photoproduct *cis,cis-94b* (crystallized from: hexanes/chloroform).

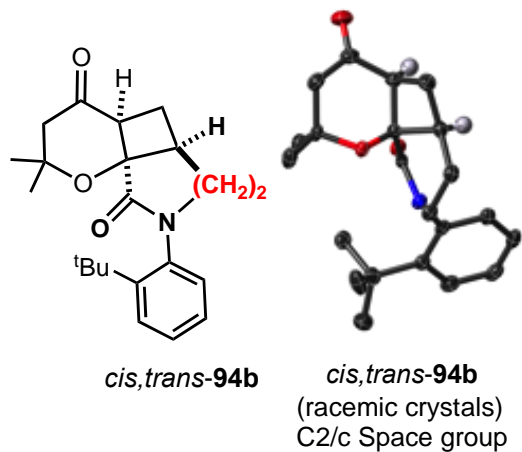


**Figure 2.74:** Photoproduct *cis,trans-94b* (crystallized from: hexanes/chloroform).

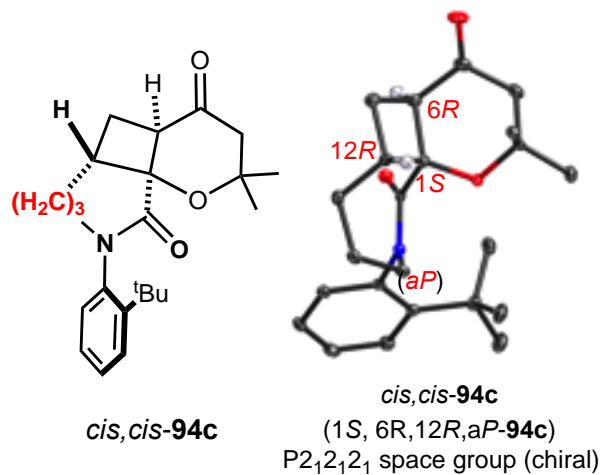


**Figure 2.75:** Photoproduct (*1S*, *6R*, *12R*, *aP*)-*cis,cis-94c* (crystallized from: hexanes/chloroform).

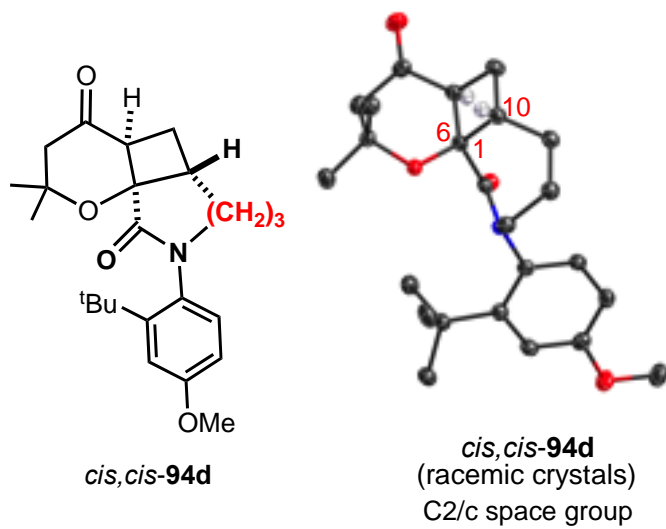


**Figure 2.76:** Photoproduct *cis,cis-94d* (crystallized from: hexanes/chloroform).

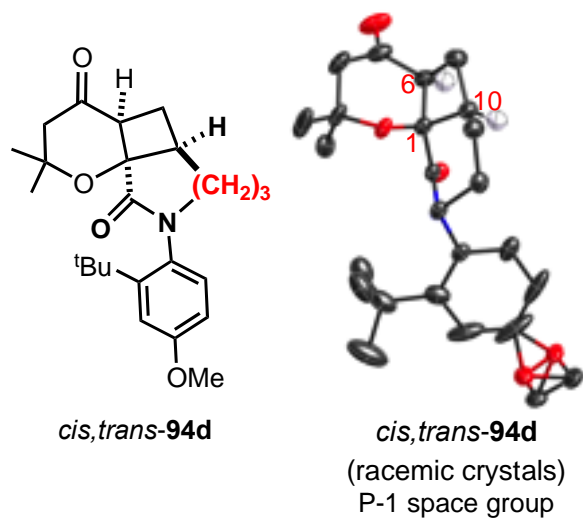


**Figure 2.77:** Photoproduct *cis,trans-94d* (crystallized from: hexanes/chloroform).

**Table 2.6** : X-ray crystal data for atropisomeric enones continued.

	<i>cis,trans-94d</i>	<i>cis,cis-94f</i> (major rotamer)	<i>cis,cis-94f</i> (minor rotamer)	<i>cis,cis-94f</i> (major rotamer)
Formula	C <sub>24</sub> H <sub>33</sub> NO <sub>4</sub>	C <sub>22</sub> H <sub>27</sub> NO <sub>4</sub>	C <sub>22</sub> H <sub>27</sub> NO <sub>4</sub>	C <sub>23</sub> H <sub>29</sub> NO <sub>5</sub>
FW	399.51	369.44	369.44	399.47
Cryst. Size_max [mm]	0.219	0.3	0.29	0.225
Cryst. Size_mid [mm]	0.207	0.185	0.22	0.13
Cryst. Size_main[mm]	0.131	0.1	0.18	0.085
Cryst. system	triclinic	monoclinic	orthorhombic	orthorhombic
Space Group, Z	P-1	P2 <sub>1</sub> /c	P2 <sub>1</sub> 2 <sub>1</sub> 2 <sub>1</sub>	P2 <sub>1</sub> 2 <sub>1</sub> 2 <sub>1</sub>
a [Å]	11.7956(4)	14.8270(14)	7.9328(3)	8.0354(6)
b [Å]	12.4371(4)	10.2711(9)	14.3352(5)	13.7812(10)
c [Å]	16.1837(5)	14.4324(13)	16.9365(7)	18.9887(14)
α [Å]	101.858(2)	90	90	90
β [Å]	99.6140(10)	115.034(4)	90	90
γ [Å]	105.0390(10)	90	90	90
V [Å <sup>3</sup> ]	2182.12(12)	1991.4(3)	1925.99(13)	2102.8(3)
ρ <sub>calc</sub> [g/cm <sup>3</sup> ]	1.216	1.232	1.274	1.262
μ [mm <sup>-1</sup> ]	0.654	0.68	0.703	0.719
Radiation Type	Cu	Cu	Cu	Cu
(F000)	864	792	792	856
No of refl. (≥ 2σ)	27433	8770	3295	12152
No of indep. Refl.	7541	3321	3295	3521
No of refl. (≥ 2σ)	6486	2778	3245	2140
Resolution [Å]	0.84	0.84	0.84	0.84
R <sub>1</sub> /wR <sub>2</sub> (≥ 2σ) <sup>a</sup> [%]	R <sub>1</sub> = 4.23, wR <sub>2</sub> = 9.84	R <sub>1</sub> = 5.13, wR <sub>2</sub> = 15.91	R <sub>1</sub> = 2.61, wR <sub>2</sub> = 6.60	R <sub>1</sub> = 2.82, wR <sub>2</sub> = 7.08
R <sub>1</sub> /wR <sub>2</sub> (all data) <sup>a</sup> [%]	R <sub>1</sub> = 4.98, wR <sub>2</sub> = 10.33	R <sub>1</sub> = 6.71, wR <sub>2</sub> = 18.27	R <sub>1</sub> = 2.66, wR <sub>2</sub> = 6.63	R <sub>1</sub> = 2.87, wR <sub>2</sub> = 7.12

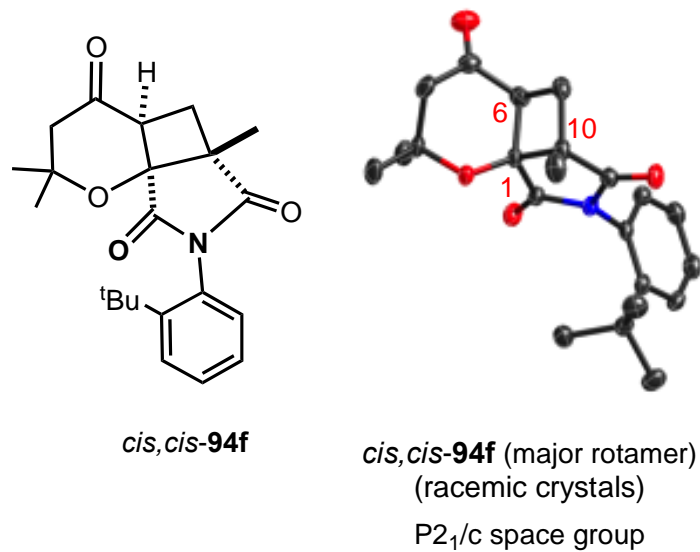


**Figure 2.78:** Photoproduct *cis,cis-94f* (major rotamer) (crystallized from: hexanes/chloroform).

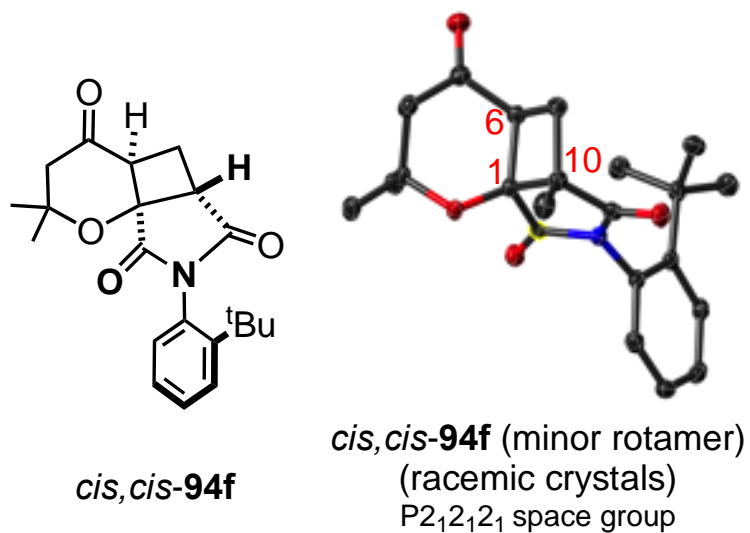


**Figure 2.79:** Photoproduct *cis,cis-94f* (minor rotamer) (crystallized from: hexanes/chloroform).

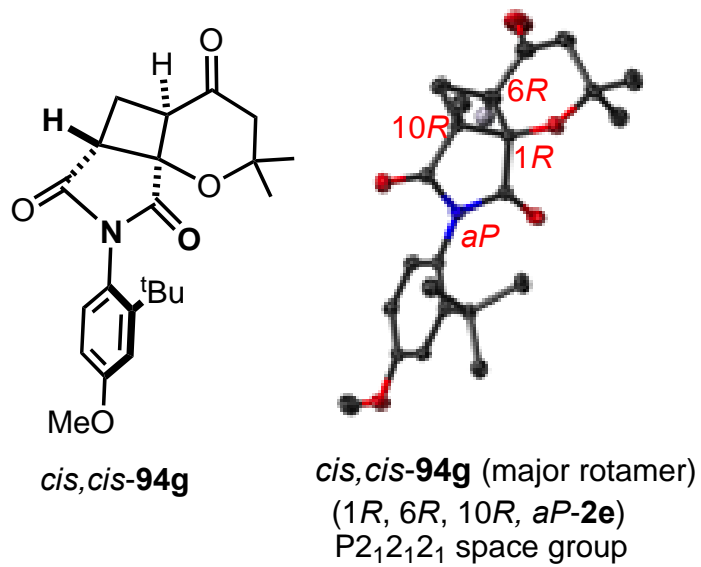


**Figure 2.80:** Photoproduct *cis,cis*-94g (major rotamer) (crystallized from: hexanes/chloroform).



### 2.13. References

1. Crimmins, M. T. Synthetic applications of intramolecular enone-olefin photocycloadditions. *Chem. Rev.* **1988**, 88, 1453-1473.
2. Albini, A.; Fagnoni, M. 1908: Giacomo Ciamician and the Concept of Green Chemistry. *ChemSusChem* **2008**, 1, 63 - 66.
3. Albini, A.; Dichiarante, V. The 'belle époque' of photochemistry. *Photochemical & Photobiological Sciences* **2009**, 8, 248-254.
4. Crimmins, M. T. Synthetic applications of intramolecular enone-olefin photocycloadditions. *Chemical Reviews* **1988**, 88, 1453-1473.
5. Büchi, G.; Goldman, I. M. Photochemical Reactions. VII.1 The Intramolecular Cyclization of Carvone to Carvonecamphor. *Journal of the American Chemical Society* **1957**, 79, 4741 - 4748.
6. Liu, R. S. H.; Hammond, G. S. Photosensitized internal addition of dienes to olefins. *Journal of the American Chemical Society* **1967**, 89, 4936-4944.
7. Tamura, Y.; Ishibashi, H.; Hirai, M.; Kita, Y.; Ikeda, M. Photochemical syntheses of 2-aza- and 2-oxabicyclo 2.1.1 hexane ring systems. *Journal of Organic Chemistry* **1975**, 40, 2702 - 2710.
8. Turro, N. J.; Schuster, G. Photochemical Reactions as a Tool in Organic Syntheses. *Science* **1975**, 187, 303.
9. Turro, N. J.; Ramamurthy, V.; Scaiano, J. C.: *Modern Molecular Photochemistry of Organic Molecules*, 2010.
10. Oppolzer, W. The Intramolecular [2 + 2] Photoaddition/Cyclobutane-Fragmentation Sequence in Organic Synthesis. *Acc. Chem. Res.* **1982**, 15, 135-141.

11. Namyslo, D. E. The Application of Cyclobutane Derivatives in Organic Synthesis. *Chemical Reviews* **2003**, *103*, 1485 - 1538.
12. Iriondo-Alberdi, J.; Greaney, M. F. Photocycloaddition in Natural Product Synthesis. *European Journal of Organic Chemistry* **2007**, *2007*, 4801 - 4815.
13. Dembitsky, V. M. Bioactive cyclobutane-containing alkaloids. *Journal of Natural Medicines* **2007** *62*, 1-33.
14. Bach, T.; Hehn, J. P. - Photochemical Reactions as Key Steps in Natural Product Synthesis. *Angewandte Chemie International Edition* **2011**, *50*, 1000 - 1045.
15. Wroblewski, M. L.; Reichard, G. A.; Paliwal, S.; Shah, S.; Tsui, H.-C.; Duffy, R. A.; Lachowicz, J. E.; Morgan, C. A.; Varty, G. B.; Shih, N.-Y. Cyclobutane Derivatives as Potent NK1 Selective Antagonists. *Bioorganic & Medicinal Chemistry Letters* **2006**, *16*, 3859 - 3863.
16. Secci, F.; Frongia, A.; Piras, P. P. Stereocontrolled Synthesis and Functionalization of Cyclobutanes and Cyclobutanones. *Molecules* **2013**, *18*, 15541 - 15572.
17. Fan, Y.-Y.; Gao, X.-H.; Yue, J.-M. Attractive Natural Products with Strained Cyclopropane and/or Cyclobutane Ring Systems. *Science China Chemistry* **2016**, *59*, 1126-1141.
18. Throup, A.; Patterson, L. H.; Sheldrake, H. M. Y. Intramolecular thermal stepwise 2 + 2 cycloadditions: Investigation of a Stereoselective Synthesis of N.2.0 -bicyclic lactones. *Organic & Biomolecular Chemistry* **2016**, *14*, 9554-9559.
19. Tateyama, S.; Masuo, S.; Suvannasara, P.; Oka, Y.; Miyazato, A.; Yasaki, K.; Teerawatananond, T.; Muangsin, N.; Zhou, S.; Kawasaki, Y.; Zhu, L.; Zhou, Z.; Takaya,

- N.; Kaneko, T. Ultrastrong, Transparent Polytruxillamides Derived from Microbial Photodimers. *Macromolecules* **2016**.
20. Gutekunst, W. R.; Baran, P. S. Applications of C–H Functionalization Logic to Cyclobutane Synthesis. *Journal of Organic Chemistry* **2014**, *79*, 2430-2452.
21. Duan, G.-J.; Ling, J.-B.; Wang, W.-P.; Luo, Y.-C.; Xu, P.-F. Y. Organocatalytic Formal [2+2] Cycloaddition initiated by Vinylogous Friedel-Crafts Alkylation: Enantioselective Synthesis of Substituted Cyclobutane Derivatives. *Chemical Communications* **2013**, *49*, 4625-4627.
22. Nagib, D. A.; MacMillan, D. W. C. Trifluoromethylation of Arenes and Heteroarenes by Means of Photoredox Catalysis. *Nature* **2011**, *480*, 224-228.
23. Nicewicz, D. A.; MacMillan, D. W. C. Merging Photoredox Catalysis with Organocatalysis: The Direct Asymmetric Alkylation of Aldehydes. *Science* **2008**, *322*, 77-80.
24. Prier, C. K.; Rankic, D. A.; Macmillan, D. W. C. Visible Light Photoredox Catalysis with Transition Metal Complexes: Applications in Organic Synthesis. *Chemical Reviews* **2013**, *113*, 5322 - 5363.
25. Svoboda, J.; Konig, B. Templated Photochemistry: Toward Catalysts Enhancing The Efficiency and Selectivity of Photoreactions in Homogeneous Solutions. *Chemical Reviews* **2006**, *106*, 5413 - 5430.
26. *Photoprocesses of Organic Molecules included in Zeolites*; Ramamurthy, V., Ed.; Wiley-VCH: New York, 1991, pp 429-493.

27. Vallavoju, N.; Sivaguru, J. Supramolecular photocatalysis: Combining Confinement and Non-Covalent Interactions to Control Light Initiated Reactions. *Chem. Soc. Rev.* **2014**, *43*, 4084-4101.
28. Pemberton, B. C.; Raghunathan, R.; Volla, S.; Sivaguru, J. From Containers to Catalysts: Supramolecular Catalysis within Cucurbiturils. *Chem. Eur. J.* **2012**, *18*, 12178-12190.
29. Kranz, D. P.; Griesbeck, A. G.; Alle, R.; Perez-Ruiz, R.; Neudörfl, J. M.; Meerholz, K.; Schmalz, H.-G. Molecular Oxygen as a Redox Catalyst in Intramolecular Photocycloadditions of Coumarins. *Angew. Chem. Int. Ed.* **2012**, *51*, 6000-6004.
30. Bergonzini, G.; Schindler, C. S.; Wallentin, C.-J.; Jacobsen, E. N.; Stephenson, C. R. J. Photoredox Activation and Anion Binding Catalysis in The Dual Catalytic Enantioselective Synthesis of [small beta]-amino esters. *Chem. Sci.* **2014**, *5*, 112-116.
31. Condie, A. G.; González-Gómez, J. C.; Stephenson, C. R. J. Visible-Light Photoredox Catalysis: Aza-Henry Reactions via C-H Functionalization. *J. Am. Chem. Soc.* **2010**, *132*, 1464-1465.
32. Narayanam, J. M. R.; Stephenson, C. R. J. Visible Light Photoredox Catalysis: Applications in Organic Synthesis. *Chem. Soc. Rev.* **2011**, *40*, 102-113.
33. Nicewicz, D. A.; MacMillan, D. W. C. Merging Photoredox Catalysis with Organocatalysis: The Direct Asymmetric Alkylation of Aldehydes. *Science* **2008**, *322*, 77-80.
34. Tucker, J. W.; Zhang, Y.; Jamison, T. F.; Stephenson, C. R. J. Visible-light photoredox catalysis in flow. *Angew. Chem. Int. Ed.* **2012**, *51*, 4144-4147.
35. Curran, D. P.; DeMello, N. C. Origins of Regioselectivity in Radical Reactions of Axially Twisted Anilides. *Chem. Commun.* **1993**, 1314-1317.

36. Curran, D. P.; Qi, H.; Geib, S. J.; DeMello, N. C. Atroposelective Thermal Reactions of Axially Twisted Amides and Imides. *J. Am. Chem. Soc.* **1994**, *116*, 3131-3132.
37. Thayumanavan, S.; Beak, P.; Curran, D. P. Asymmetric Deprotonation of *N,N*-Dihexyl-1-naphthamides to Provide Atropisomers of *N,N*-dihexyl-2-alkyl-1-naphthamides. *Tetrahedron Lett.* **1996**, *37*, 2899-2902.
38. Curran, D. P.; Geib, S.; DeMello, N., Rotational Features of Carbon-nitrogen bonds in *N*-aryl maleimides. Atroposelective Reactions of *O*-tert-butylphenylmaleimides. *Tetrahedron* **1999**, *55*, 5681-5704.
39. Clayden, J. Non-Biaryl Atropisomers: New Classes of Chiral Reagents, Auxiliaries, and Ligands *Angew. Chem. Int. Ed.* **1997**, *36*, 949-951.
40. Clayden, J. Stereocontrol with Rotationally Restricted Amides. *Synlett* **1998**, 810-816.
41. Clayden, J.: Non-Biaryl Atropisomers: New Classes of Chiral Reagents, Auxiliaries and Ligands In *Organic Synthesis Highlights IV*; Wiley-VCH Verlag GmbH, 2000; pp 48-52.
42. Clayden, J. Atropisomers and Near-atropisomers: Achieving Stereoselectivity by Exploiting The Conformational Preferences of Aromatic Amides. *Chemical Communications* **2004**, 127-135.
43. Clayden, J.; Lai, L. W.; Helliwell, M. Dynamic Resolution of Atropisomeric Amides Using Proline-Derived Imidazolines and Ephedrine Derived Oxazolidines. *Tetrahedron* **2004**, *60*, 4399-4412.
44. Kumarasamy, E.; Raghunathan, R.; Sibi, M. P.; Sivaguru, J. Nonbiaryl and Heterobiaryl Atropisomers: Molecular Templates with Promise for Atroposelective Chemical Transformations. *Chem. Rev.* **2015**, *115*, 11239-11300.

45. Ayitou, A. J.-L.; Sivaguru, J. Light-Induced Transfer of Molecular Chirality in Solution: Enantiospecific Photocyclization of Molecularly Chiral Acrylanilides. *J. Am. Chem. Soc.* **2009**, *131*, 5036-5037.
46. Ayitou, A. J.-L.; Vallavoju, N.; Ugrinov, A.; Sivaguru, J. Enantiospecific  $6\pi$ -Photocyclization of Atropisomeric  $\alpha$ -substituted Acrylanilides in the Solid-state: Role of Crystalline Confinement on Enantiospecificity. *Photochem. Photobiol. Sci.* **2011**, *2011*, 1380-1383.
47. Ayitou, A. J.-L.; Sivaguru, J. Reactive Spin State Dependent Enantiospecific Photocyclization of Axially Chiral  $\alpha$ -substituted Acrylanilides. *Chem. Commun.* **2011**, *47*, 2568-2570.
48. Ayitou, A. J.-L.; Clay, A.; Kumarasamy, E.; Jockusch, S.; Sivaguru, J. Enantiospecific photochemical  $6\pi$ -ring closure of  $\alpha$ -substituted Atropisomeric Acrylanilides - Role of Alkali metal ions. *Photochem. Photobiol. Sci.* **2014**, *13*, 141-144.
49. Ayitou, A. J.-L.; Jesuraj, J. L.; Barooah, N.; Ugrinov, A.; Sivaguru, J. Enantiospecific Photochemical Norrish/Yang Type II Reaction of Nonbiaryl Atropchiral  $\alpha$ -Oxoamides in Solution, Axial to Point Chirality Transfer. *J. Am. Chem. Soc.* **2009**, *131*, 11314-11315.
50. Jesuraj, J. L.; Sivaguru, J. Photochemical Type II Reaction of Atropchiral Benzoylformamides to Point Chiral Oxazolidin-4-ones. Axial chiral Memory Leading to Enantiomeric Resolution of Photoproducts. *Chem. Commun.* **2010**, *46*, 4791-4793.
51. Kumarasamy, E.; Jesuraj, J. L.; Omlid, J. N.; Ugrinov, A.; Sivaguru, J. Light-Induced Enantiospecific  $4\pi$  Ring Closure of Axially Chiral 2-Pyridones: Enthalpic and Entropic Effects Promoted by H-Bonding. *J. Am. Chem. Soc.* **2011**, *133*, 17106-17109.

52. Raghunathan, R.; Kumarasamy, E.; Iyer, A.; Ugrinov, A.; Sivaguru, J. Intramolecular Paterno-Buchi Reaction of Atropisomeric  $\alpha$ -oxoamides in Solution and in The Solid-state. *Chem. Commun.* **2013**, *49*, 8713-8715.
53. Kumarasamy, E.; Sivaguru, J. Light Induced Stereospecific Intramolecular [2+2]-Cycloaddition of Atropisomeric 3,4-dihydro-2-pyridones. *Chem. Commun.* **2013**, *49*, 4346-4348.
54. Iyer, A.; Jockusch, S.; Sivaguru, J. Dictating Photoreactivity through Restricted Bond Rotations: Cross-Photoaddition of Atropisomeric Acrylimide Derivatives Under UV/Visible-Light Irradiation. *J. Phys. Chem. A* **2014**, *43*, 1816 - 1825
55. Kumarasamy, E.; Raghunathan, R.; Jockusch, S.; Ugrinov, A.; Sivaguru, J. Tailoring Atropisomeric Maleimides for Stereospecific [2 + 2] Photocycloaddition—Photochemical and Photophysical Investigations Leading to Visible-Light Photocatalysis. *Journal of American Chemical. Society* **2014**, *136*, 8729-8737.
56. Kärkäs, M. D.; Porco, J. A. J.; Stephenson, C. R. J. Photochemical Approaches to Complex Chemotypes: Applications in Natural Product Synthesis. *Chemical Reviews* **2016**, *116*, 9683 - 9747.
57. Turro, N. J.; Ramamurthy, V.; Scaiano, J. C.: *Modern Molecular Photochemistry of Organic Molecules*; University Science Books: Sausalito, CA, 2010. pp. 801-845.
58. Schuster, D. I.; Lem, G.; Kaprinidis, N. A. New Insights into an Old Mechanism: [2 +2] Photocycloaddition of Enones to Alkenes. *Chemical Reviews* **1993**, *93*, 3-22.
59. De Mayo, P. Photochemical syntheses. 37. Enone Photoannulation. *Accounts of Chemical Research* **1971**, *4*, 41-47.

60. Fort, D. A.; Woltering, T. J.; Nettekoven, M.; Knust, H.; Bach, T. Synthesis of Fluorinated Tricyclic Scaffolds by Intramolecular [2+2] Photocycloaddition Reactions. *Angewandte Chemie International Edition* **2012**, *51*, 10169-10172.
61. Meyer, C.; Piva, O.; Pete, J.-P. [2+2] Photocycloadditions and Photorearrangements of 2-Alkenylcarboxamido-2-cycloalken-1-ones. *Tetrahedron* **2000**, *56*, 4479-4489.
62. Sylvie Le, B.; Jean-Pierre, P.; Olivier, P. Intramolecular [2+2] Photocycloaddition of Oxoesters and Oxoamides. *Tetrahedron Letters* **1993**, *34*, 635-638.
63. Wolf, C.: *Dynamic Stereochemistry of Chiral Compounds. Principles and Applications*; RSC publishing: Cambridge, UK., 2008.
64. Trapp, O.: Interconversion of Stereochemically Labile Enantiomers (Enantiomerization). *Topics in Current Chemistry*; Springer Berlin Heidelberg, 2013; pp 1-39.
65. Betson, M. S.; Clayden, J.; Helliwell, M.; Johnson, P.; Lai, L. W.; Pink, J. H.; Stimson, C. C.; Vassiliou, N.; Westlund, N.; Yasin, S. A.; Youssef, L. H. Conformational Preference in Aromatic Amides Bearing Chiral Ortho Substituents: Its Origin and Application to Relayed Stereocontrol. *Organic & Biomolecular Chemistry* **2006**, *4*, 424-443.
66. Clayden, J.; Lai, L. W. (-)-Ephedrine as an Auxiliary For The Asymmetric Synthesis of Atropisomeric Amides by Dynamic Resolution Under Thermodynamic Control. *Tetrahedron Letters* **2001**, *42*, 3163-3166.
67. Satzger, H.; Schmidt, B.; Root, C.; Zinth, W.; Fierz, B.; Krieger, F.; Kiefhaber, T.; Gilch, P. Ultrafast Quenching of the Xanthone Triplet by Energy Transfer: New Insight into the Intersystem Crossing Kinetics. *The Journal of Physical Chemistry. A.* **2004**, *108*, 10072-10079.

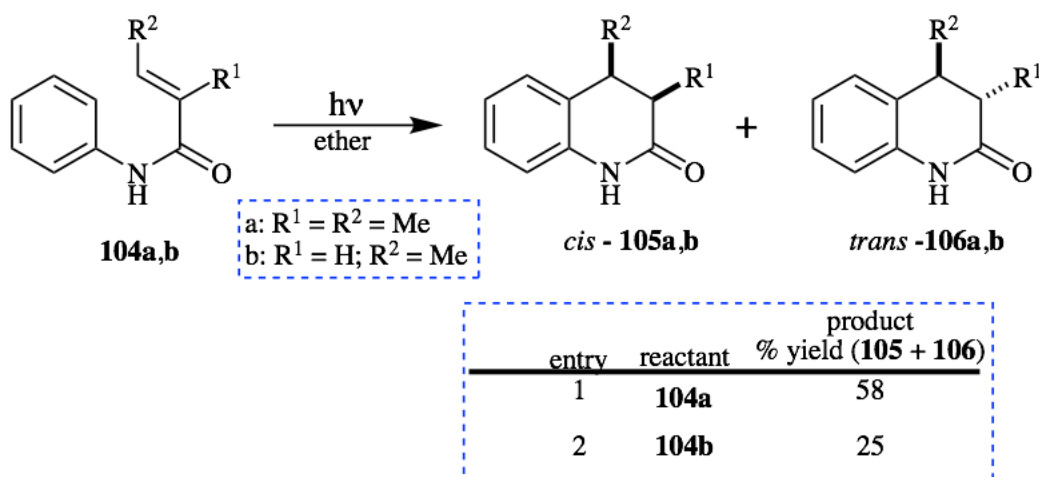


68. Vallavoju, N.; Selvakumar, S.; Jockusch, S.; Sibi, M. P.; Sivaguru, J. Enantioselective Organo-Photocatalysis Mediated by Atropisomeric Thiourea Derivatives. *Angewandte Chemie International Edition* **2014**, *53*, 5604-5608.
69. Vallavoju, N.; Selvakumar, S.; Jockusch, S.; Prabhakaran, M. T.; Sibi, M. P.; Sivaguru, J. Evaluating Thiourea Architecture for Intramolecular [2+2] Photocycloaddition of 4-Alkenylcoumarins. *Advances of Synthesis and Catalysis* **2014**, *356*, 2763-2768.
70. Vallavoju, N.; Selvakumar, S.; Pemberton, B. C.; Jockusch, S.; Sibi, M. P.; Sivaguru, J. Organophotocatalysis: Insights into the Mechanistic Aspects of Thiourea-Mediated Intermolecular [2+2] Photocycloadditions. *Angewandte Chemie International Edition* **2016**, *55*, 5446 - 5451.
71. Neumann, J. J.; Rakshit, S.; Dröge, T.; Glorius, F. Palladium-Catalyzed Amidation of Unactivated C(sp<sup>3</sup>) H Bonds: from Anilines to Indolines. *Angewandte Chemie International Edition* **2009**, *48*, 6892-6895.
72. Brecker, L.; Pogorevc, M.; Griengl, H.; Steiner, W.; Kappe, T.; W. Ribbons, D. Synthesis of 2,4-diketoacids and Their Aqueous Solution Structures. *New Journal of Chemistry* **1999**, *23*, 437-446.
73. Kumarasamy, E.; Raghunathan, R.; Jockusch, S.; Ugrinov, A.; Sivaguru, J. Tailoring Atropisomeric Maleimides for Stereospecific [2 + 2] Photocycloaddition—Photochemical and Photophysical Investigations Leading to Visible-Light Photocatalysis. *Journal of American Chemical Society* **2014**, *136*, 8729-8737.
74. Amougay, A. C.; Pete, J.-P.; Piva, O. Intramolecular [2+2] photocycloaddition of N-alkenoyl - enaminones. *Tetrahedron Letters* **1992**, *33*, 7347-7350.

### 3. INVESTIGATING $6\pi$ -PHOTOCYCLIZATION OF ATROPISOMERIC ACRYLANILIDES

#### 3.1. Introduction: $6\pi$ -photocyclization of acrylanilides

In 1967 Chapman and Cleveland detailed the first photochemical electrocyclic ring closure of  $\alpha,\beta$ -unsaturated acrylanilides to the cyclized dihydroquinolinone type product (Scheme 3.1).<sup>1,2</sup> Ogata and co-workers later investigated various substituted acrylanilides. Their investigations unveiled the sensitivity of  $6\pi$ -photocyclization to solvents and the differing reactivity of the excited states of acrylanilides. Additionally, Ogata and co-workers were able to afford the desired dihydroquinolinone photocyclized product, employing a sensitizer (e.g. acetophenone or benzophenone).<sup>3</sup> Photophysical investigations unveiled phosphorescence quenching of the employed sensitizer. Phosphorescence quenching of the triplet sensitizer allowed for the acrylanilide to access the triplet excited state. This indicated that  $6\pi$ -photocyclization of acrylanilides can be achieved via the triplet excited state. Subsequent, photophysical investigations revealed respectable quantum yields of photocyclization (0.26). Altering the experimental conditions photocyclization of acrylanilides could occur from either  $S_1$  or  $T_1$  excited state efficiently.



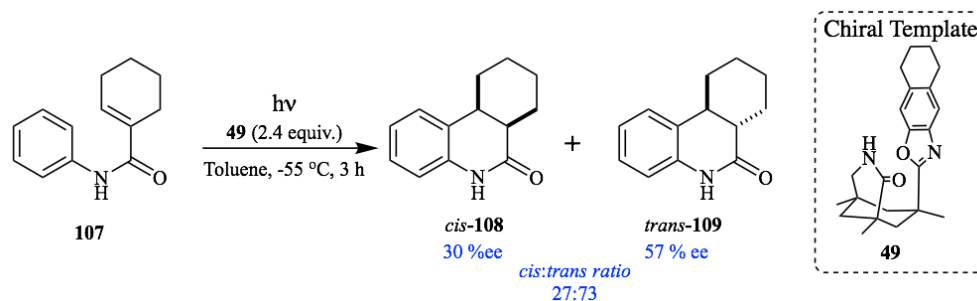
**Scheme 3.1:**  $6\pi$ -photocyclization of acrylanilides.

By way of mechanism  $6\pi$ -photocyclization follows Woodward and Hoffman rules of pericyclic reactions. Thus the aforementioned photocyclization reaction from the singlet excited state occurs via con-rotatory ring closure. Subsequent investigations hypothesized a zwitterionic intermediate along the reaction pathway eventually followed by either an H-transfer or [1,5]-H shift depending on the specific reaction conditions.<sup>3-7</sup>

**3.2. Asymmetric photochemistry of acrylanilides in solution**

As mentioned in Section 1.6.5 Ninomiya and coworkers employed chiral template **44** in the photocyclization of enamides **41**. The chiral ditoluoyltartaric acid template **44** attained respectable selectivity up to 42 % *ee*. (Scheme 1.11a). Further advancing the methodology employing templates for asymmetric synthesis Bach and coworkers utilized chiral template **49** for the  $6\pi$ -photocyclization of acrylanilide **107** achieving selectivity up to 57 % *ee* (Scheme 3.2).<sup>6, 8</sup> Moderate selectivity, low temperature and superstoichiometric amounts of chiral template **49** were major drawbacks of employing chiral template **49**. Focusing on the reactivity of the substrate Sivaguru and coworkers developed a methodology wherein built in molecular

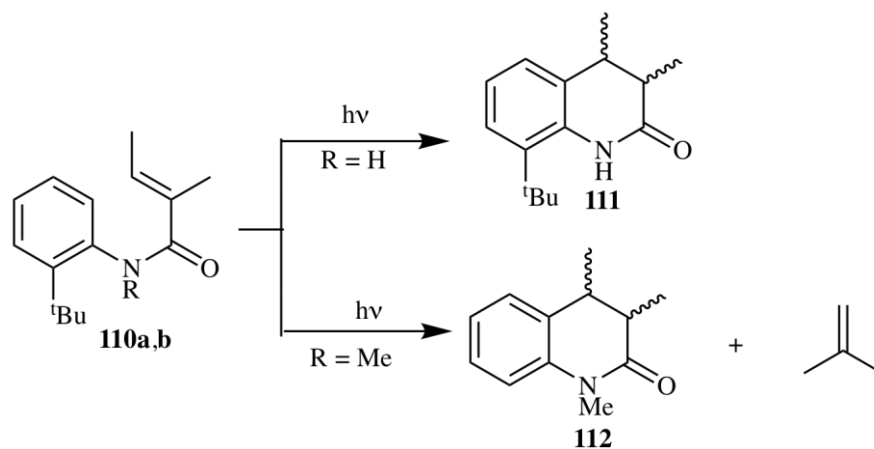
restriction of the substrate dictated the photochemical reactivity and thus controlled selectivity (Scheme 1.15a).



**Scheme 3.2:** Asymmetric synthesis of acrylanilide using chiral template **49**.

### 3.3. Photochemical investigations of $\alpha,\beta$ -unsaturated atropisomeric acrylanilides

Sivaguru and coworkers outlined a detailed investigation of atropisomeric acrylanilides in which *ortho*-substituted acrylanilide **110** featuring *N*-substitution dictated the regiochemistry of the photocyclized dihydroquinolinone type product.<sup>9</sup> The *N*-Me substituted **110b** cyclized at the *ortho*-position bearing the *tert*-butyl group eliminating isobutene as a byproduct (Scheme 3.3).<sup>9</sup> Conversely, **110a** afforded the cyclized product where cyclization occurred at the unsubstituted *ortho*-position yielding **111**.<sup>10</sup> Additional investigations highlighted that  $\alpha,\beta$ -substitution dictated enantioselectivity during direct irradiation of optically pure atropisomeric acrylanilide(s) affording the desired cyclized product from the singlet excited state leading to high enantioselectivity (Scheme 1.15b). Indeed, the molecular chirality/axial chirality, afforded great control over the photocyclization of  $\alpha,\beta$ -substituted acrylanilides.<sup>11, 12</sup>



**Scheme 3.3:** Regioselectivity in  $6\pi$ -photocyclization of  $\alpha,\beta$ -substituted atropisomeric acrylanilide.

### 3.4. Photochemical investigations of $\alpha$ -substituted atropisomeric acrylanilides

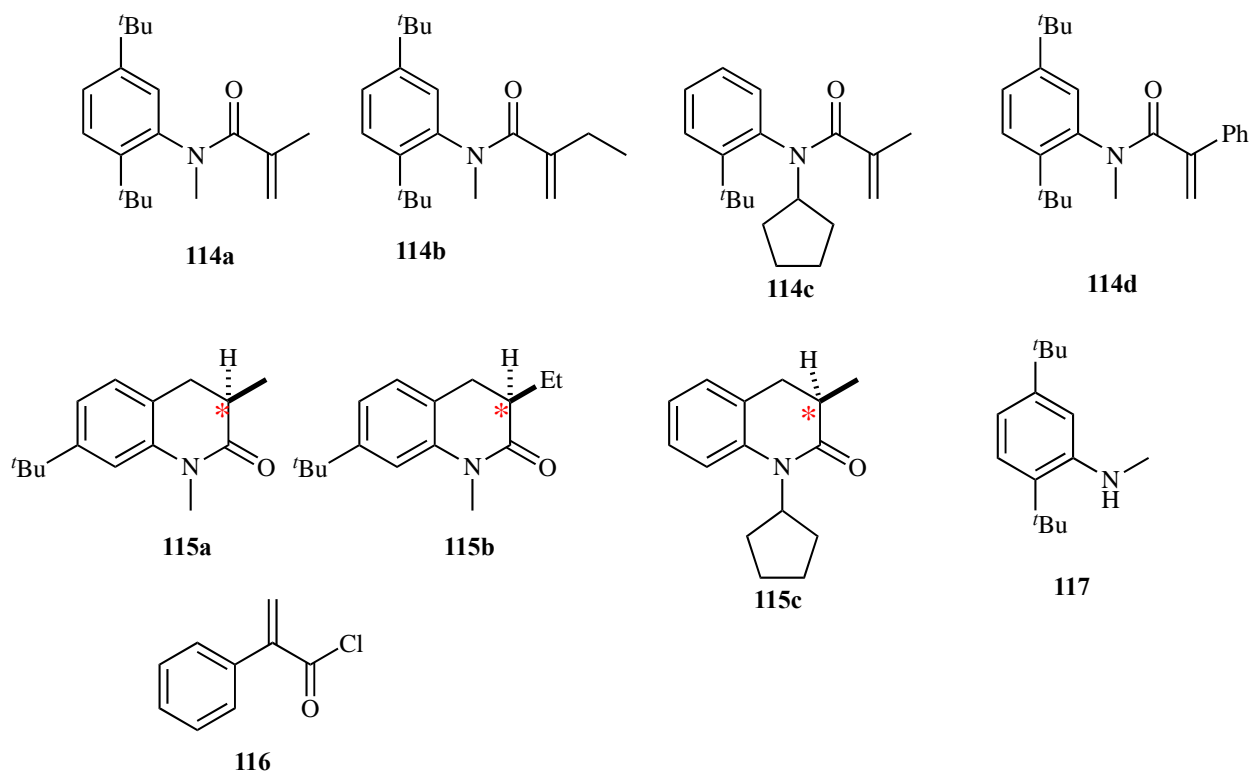
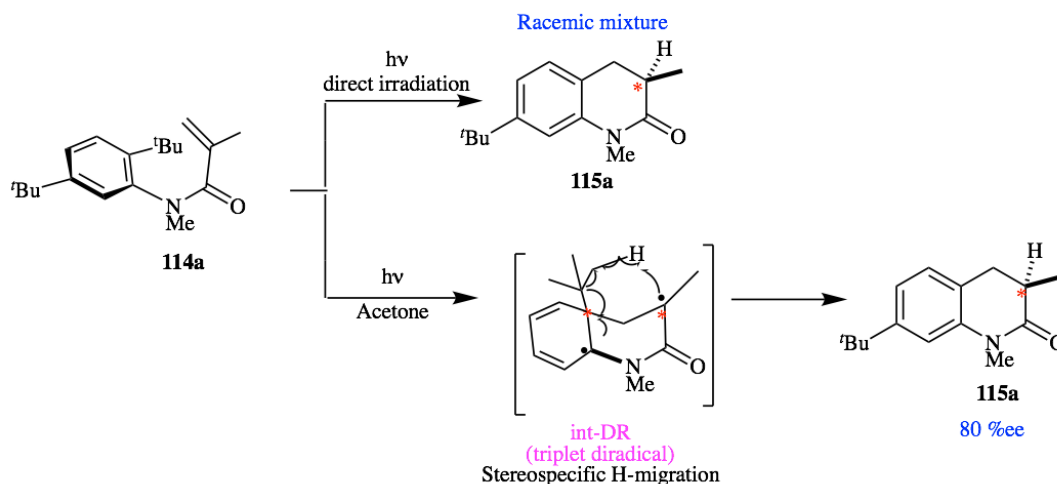


**Chart 3.1:** Structures of  $\alpha$ -substituted atropisomeric acrylanilides, their corresponding photoproducts and the precursors/reactants employed.

Sivaguru and coworkers displayed that high selectivity was obtainable with regards to direct irradiation of optically pure  $\alpha,\beta$ -substituted acrylanilides. Mechanistic investigations

brought to light that the substitution at the  $\beta$ -carbon was essential for chirality transfer. Direct irradiation of optically pure  $\alpha$ -substituted atropisomeric acrylanilides afforded a racemic mixture of the cyclized product(s). Conversely, triplet sensitized irradiation of optically pure  $\alpha$ -substituted atropisomeric acrylanilides in acetone, where acetone was both the solvent and sensitizer, afforded the cyclized product in moderate to high enantiomeric excess (%ee). Sensitized irradiation of  $\alpha$ -substituted atropisomeric acrylanilides allowed for population of the triplet  $\pi\pi^*$  ( $T_1 \pi\pi^*$ ) excited state. This triplet excitation is expected to involve a diradicaloid intermediate which mediates stereospecific intramolecular hydrogen shift affording the observed selectivity.



**Scheme 3.4:** Acetone sensitized photochemical reaction of  $\alpha$ -substituted atropisomeric acrylanilides.

### 3.5. Role of alkali metal ions during photochemical investigations of $\alpha$ -substituted atropisomeric acrylanilides

As shown above, sensitized irradiation of optically pure  $\alpha$ -substituted acrylanilide can be employed to attain the desired photocyclized product in high enantiomeric excess (>90%).

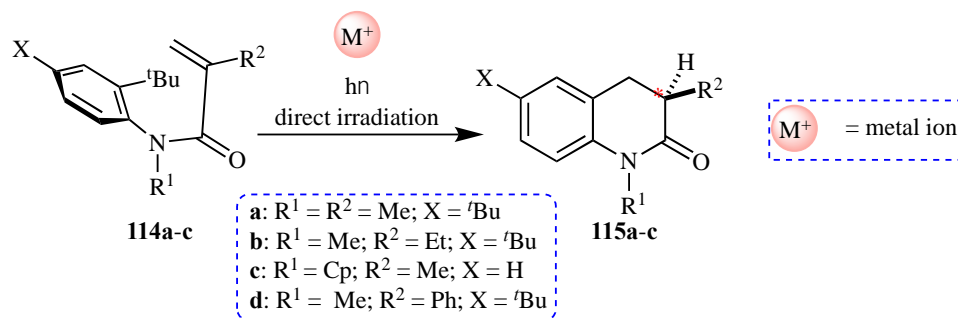
However, in the case of direct irradiation of optically pure  $\alpha$ -substituted acrylanilide the afforded

photocyclized product mixture is racemic. In this regard investigations were aimed at achieving high selectivity in the photocyclized product upon direct irradiation of optically pure  $\alpha$ -substituted atropisomeric acrylanilides.

Metal ions are crucial for numerous life sustaining processes. Intermolecular interactions between metal ions and some molecular guest range from cation- $\pi$  interactions<sup>13, 14</sup> to cation-lone pair (from a heteroatom) interactions,<sup>15, 16</sup> which can be exploited to alter molecular properties. Exploiting non-bonding interactions between metal ions and chemical compounds chemist have been able to develop systems for molecular recognition and modulate chemical reactivities.<sup>17</sup> In light induced processes, metal ions have been used extensively for altering the photophysics of organometallic compounds, and alter the excited state photoreactivity of organic molecules both in solution and within confined environments.<sup>18-25</sup>

We have evaluated the influence of alkali metal ions on the stereochemical course of the light induced conrotatory  $6\pi$ -photocyclization of optically pure  $\alpha$ -substituted atropisomeric acrylanilides. Our studies indicate that alkali metal ions alter the excited state chemistry of atropisomeric acrylanilides leading to enhanced enantioselectivity in the photoproduct.

### 3.5.1. Photochemical investigation of $\alpha$ -substituted atropisomeric acrylanilides in the presence of alkali metals



**Scheme 3.5:**  $6\pi$ -Photocyclization of  $\alpha$ -substituted acrylanilides **114a-c** in the presence metal ions.

Atropisomeric  $\alpha$ -substituted acrylanilide **114a-d** were synthesized by literature-reported procedures. In preparation for photoreactions, optically pure isomers of **114a-d** were dissolved either in trifluoroethanol (TFE) or TFE saturated with various alkali metal ions (CsF, KF, and NaF). Before dissolution in TFE the alkali metal ion additives were flame dried then allowed to stir overnight to aid in dissolution. After approximately 12 hours the colloidal suspension was passed through a microfilter. Irradiation of the samples was performed in a Pyrex test tube using a 450 W medium pressure Hg lamp. The 3,4-dihydro-2-quinolin-2-one **115** (Scheme 3.5) was observed as the photoproduct and characterized by <sup>1</sup>H NMR spectroscopy, polarimetry and HRMS.<sup>9, 26, 27</sup> The *ee* values of **115a-c** were ascertained by HPLC analysis of the reaction mixture on a chiral stationary phase.



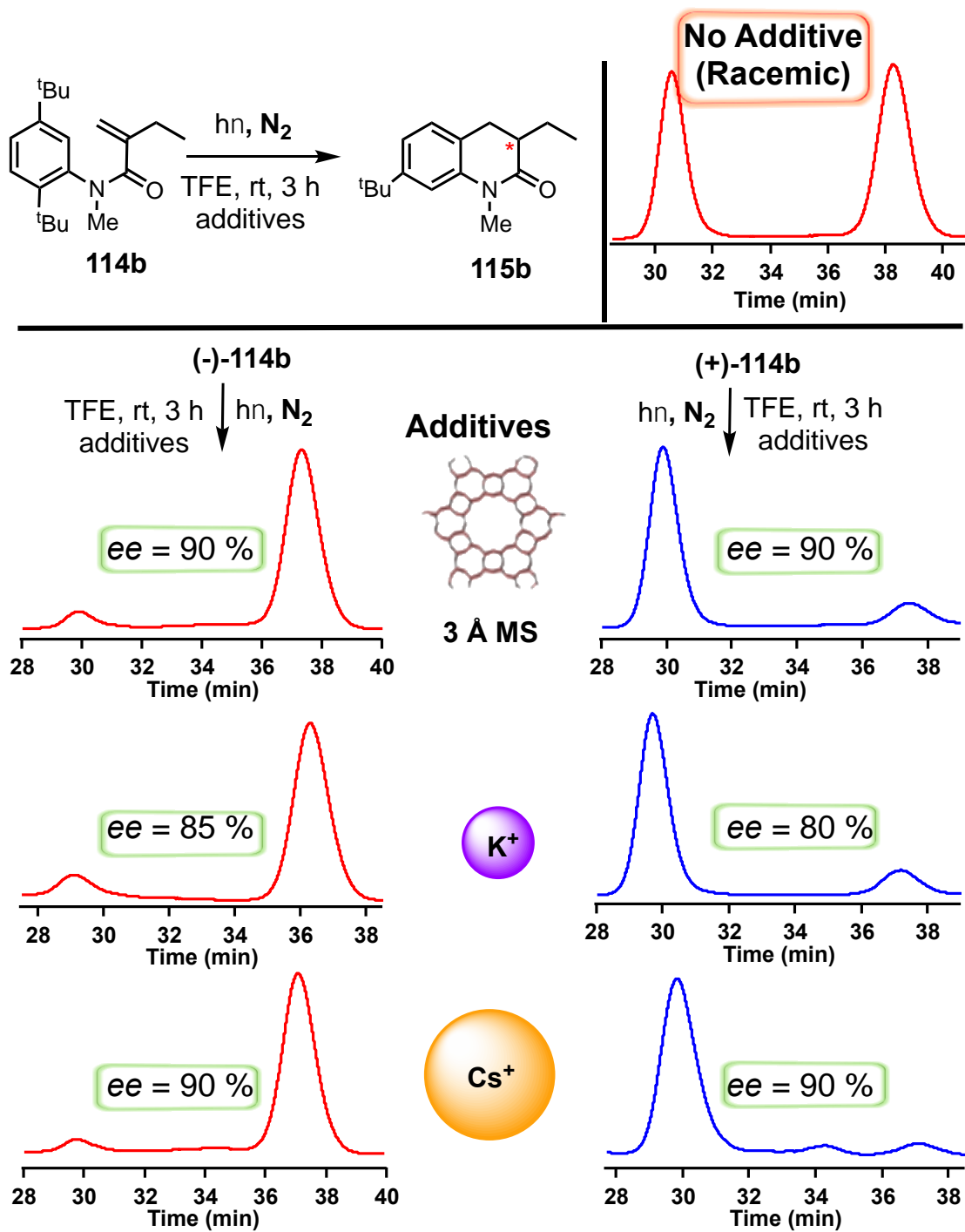


**Figure 3.1:** Atropselectivity in  $6\pi$ -photocyclization of  $\alpha$ -substituted acrylanilide **114b** in the presence of various additives.<sup>28</sup>

**Table 3.1:** Enantioselective 6 $\pi$ -photocyclization of atropisomeric acrylanilides in the presence of alkali metal ions.<sup>a,b</sup>

entry	cmpd	% ee values in the presence and absence of additives below <sup>c</sup>						
		No additives	CsF	KF	KF/ 3 Å MS	NaF	NaF / 3 Å MS	3 Å MS
1	(-)- <b>114a</b>	Racemic	90(B)	90(B)	88(B)	---	90(B)	88(B)
2	(+)- <b>114a</b>	Racemic	87(A)	90(A)	85(A)	---	90(A)	85(A)
3	(-)- <b>114b</b>	Racemic	90(B)	85(B)	85(B)	---	95(B)	90(B)
4	(+)- <b>114b</b>	Racemic	90(A)	80(A)	80(A)	---	89(A)	90(A)
5	(+)- <b>114c</b> ( <b>P</b> ) <sup>b</sup>	Racemic	(+)-90 (R)	(+)-77 (R)	-	(-)-16 (S)	(+)-80 (R)	(+)-70 (R)
6	(-)- <b>114c</b> ( <b>M</b> ) <sup>b</sup>	Racemic	(-) 85 (S)	(-)-77 (S)	-	(+)-16 (R)	(-)-80 (S)	(-)-70 (S)

<sup>a</sup>CP= cyclopentyl; EtOH = Ethanol; TFE = trifluoroethanol. <sup>b</sup>(+) and (-) represent the signs of the cotton effect at 285 nm in methylcyclohexane (MCH) for compounds **114a** and **114b**, and in methanol for compound **114c**. Irradiation was carried out for 3 h in trifluoroethanol (TFE) at ambient temperature. The additives such as alkali metal salts and molecular sieves (3 Å MS) were flame dried and dissolved in TFE overnight and passed through a microfilter and then added to the sample prior to irradiation. The reported values are the average of a minimum of 3 runs with  $\pm 8\%$  error. <sup>c</sup>For compound **114c**, absolute configuration taken from ref. 10. <sup>d</sup>From ref. 10. <sup>e</sup>A and B refer to the first and second peaks that elute from the HPLC chiral stationary phase separation for a given pair of enantiomers. For photoproduct **115c**, the absolute configuration and optical rotation values were compared to the established literature values reported previously (10). The optical rotation value for **115c** is in CHCl<sub>3</sub>. The conversion in all samples was kept between 10 and 30% to ascertain the true ee values in the presence of cations as the photoproduct can also bind competitively to alkali metal ions.

Direct irradiation of optically pure **114a-c** in TFE gave racemic mixture of the photoproduct **115a-c** (Table 3.1). Conversely, in regards to direct irradiation of optically pure **114a-c** in TFE saturated with alkali metal cations, high selectivity (ee values) in the cyclized photoproduct was obtained. For example, irradiation of (-)-**114a** in the presence of KF resulted in 90% ee with **115a** enantiomer as the major photoproduct (Table 3.1, entry 1). Changing the cation to CsF had no bearing with respect to product selectivity in the case of cyclized product **115a**. Conversely, upon changing the cation from CsF to KF resulted in a slight decrease in ee value, viz. 77% ee, favoring the (*R*)-4c photoproduct in the case of irradiation of (+)-**114c** (Table 31, entry 5). To our dismay, in the case of NaF, (*S*)-**115c** photoproduct was observed albeit with an ee value of 16%. Thus, use of NaF afforded the opposite antipode with respect to the other

cations employed. Due to the high charge density of small alkali metal ions like Na<sup>+</sup> it is possible that moisture is still present despite flame drying the alkali cation. It is possible that the presence of moisture interfered with the reaction, diminishing selectivity. In order to remove moisture, we carried out the reaction in the presence of 3 Å molecular sieves (3 Å MS). Irradiation of (*P*)-**114c** in the presence of NaF and 3 Å MS resulted in 80% ee. More importantly (*R*)-**115c** enantiomer was enhanced, i.e., the same stereoisomer that was obtained in the presence of CsF and KF. As a control, irradiation of (*P*)-**114c** in the presence of only 3 Å MS was investigated, in order to determine whether or not the 3 Å MS played a role in the obtained selectivity. Irradiation of (*P*)-**114c** in 3 Å MS exposed TFE resulted in 80% ee in the (*R*)-**115c** photoproduct. Undoubtedly the metal ions have altered the photochemistry which lead to increased selectivity in the 6π-photocyclization of α-substituted acrylanilide(s) **114a-c** under direct irradiation.

The influence of mol% was also investigated (Table 3.2). We were interested in knowing if substoichiometric amounts of heavy alkali cation could possibly afford high selectivity in the cyclized product. Optically pure **114b** was dissolved in a solution with quantitative amount of CsF dissolved in TFE. The photochemical reaction proceeded exactly as outlined above. Unfortunately, investigations unveiled that excess CsF was necessary to obtain high selectivity (> 500 mol%). It must be that increased amounts of CsF allows for increased interaction between Cs cation and acrylanilide **114** resulting in increased selectivity. Increased Cs cation diminishes the background reaction wherein the acrylanilide reacts without the influence of Cs<sup>+</sup> which erodes selectivity.

**Table 3.2:** Enantioselective  $6\pi$ -photocyclization of **114b** in the presence of varying CsF mol%.<sup>a-d</sup>

entry	cmpd	mol% CsF	<b>115b</b> (% ee)
1	(-)- <b>114b</b>	10	15
2	(-)- <b>114b</b>	50	50
3	(-)- <b>114b</b>	100	54
4	(-)- <b>114b</b>	500	69

<sup>a</sup>CP = cyclopentyl; EtOH = Ethanol; TFE = trifluoroethanol. <sup>b</sup>(+) and (-) represent the signs of the cotton effect at 285 nm in methylcyclohexane (MCH). Irradiation was carried out for 3 h in trifluoroethanol (TFE) at ambient temperature. The additives such CsF was flame dried and dissolved in TFE overnight and passed through a microfilter and then added to the sample prior to irradiation. The reported values are the average of a minimum of 3 runs with  $\pm 5\%$  error. <sup>c</sup>The conversion in all samples was kept between 10 and 30% to ascertain the true *ee* values in the presence of cations as the photoproduct can also bind competitively to alkali metal ions.

### 3.5.2. Photophysical investigations of $\alpha$ -substituted atropisomeric acrylanilides **114a** and **114d**

Photophysical investigations commenced with obtaining absorbance spectra of various  $\alpha$ -substituted atropisomeric acrylanilides. Following the absorbance spectra, the emission (fluorescence) properties were also investigated.

### 3.5.3. UV/Vis spectra of **114a** and **114d**

To commence photophysical investigations absorbance spectra were recorded in ethanol (EtOH) and acetonitrile (MeCN).

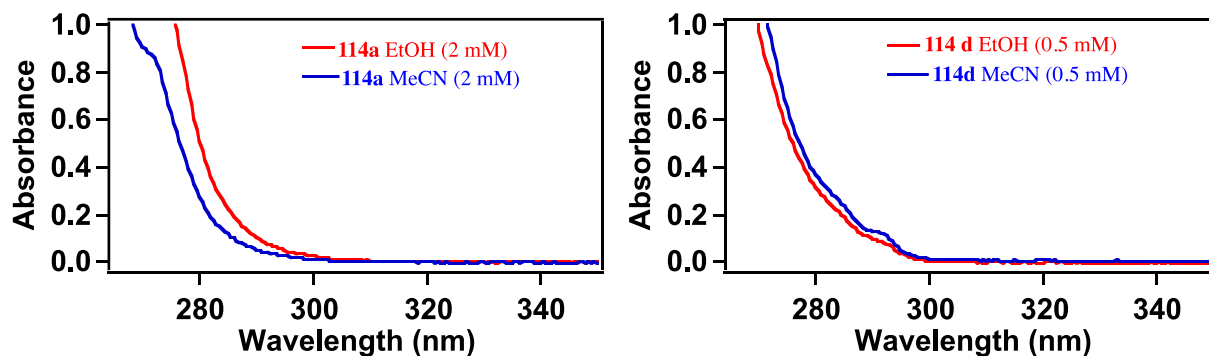


**Figure 3.2:** UV-Vis spectra of **3a** (left) and **3d** (right) in ethanol and acetonitrile respectively.

### 3.5.4. Emission spectra of 114a and 114d

In an attempt to understand the influence of alkali metal cations on the excited state reactivity of atropisomeric acrylanilides, steady state emission and fluorescence lifetime measurements were recorded at room temperature and 77 K, in the presence and absence of alkali metal ions. The acrylanilides **114a** and **114d** were representative examples. Inspection of Figures 3.3 and 3.4 reveals that acrylanilides **114a** and **114d** are weakly fluorescent at room temperature in ethanol. In the case of **114a**, the fluorescence intensity is significantly enhanced at 77 K in ethanol glass (Figure 3.3). This displays that the singlet excited state is readily deactivated at room temperature, which is reflected in the photochemical reactivity eventually leading to racemic photoproducts. At 77 K enhancement of fluorescence intensity is noticed. Due to the rigid ethanol matrix at 77 K, the photoreaction cannot proceed efficiently resulting in the observed fluorescence intensity.

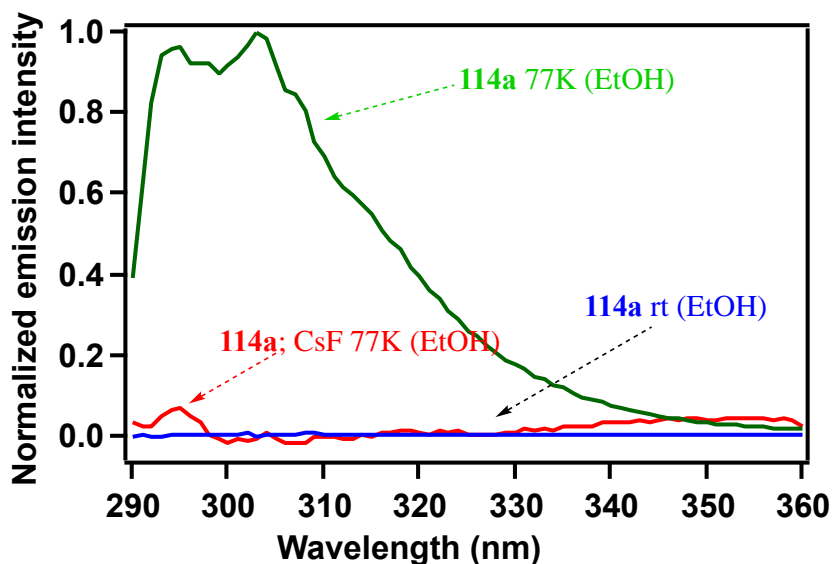


**Figure 3.3:** Fluorescence spectra of **114a** in ethanol at 77K (— green), at rt (— blue) and in presence of CsF at 77 K (— red). [**114a**] = 2mM.

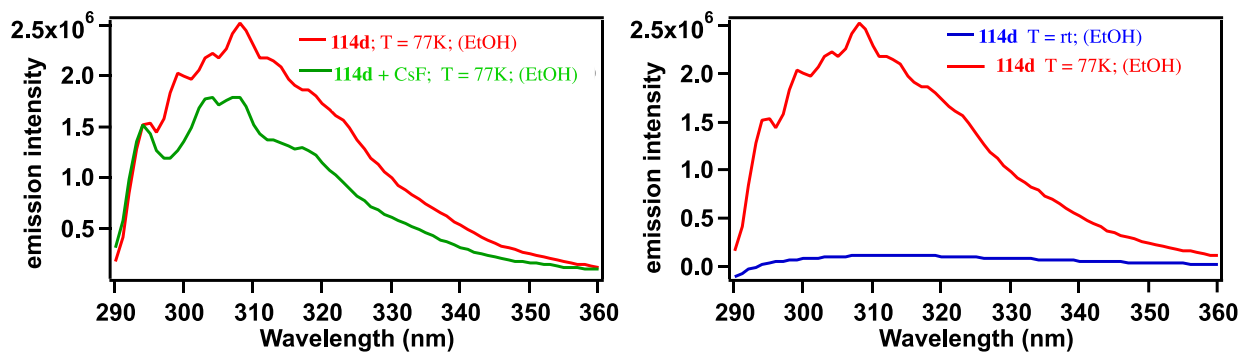


**Figure 3.4:** Left: Luminescence of **114d** in ethanol glass (—red) and **114d** in presence of CsF in ethanol (—green) at 77K. Right: Fluorescence of **3d** in ethanol at 77K (—red) and at RT (—blue). [**114d**] = 0.5 mM).

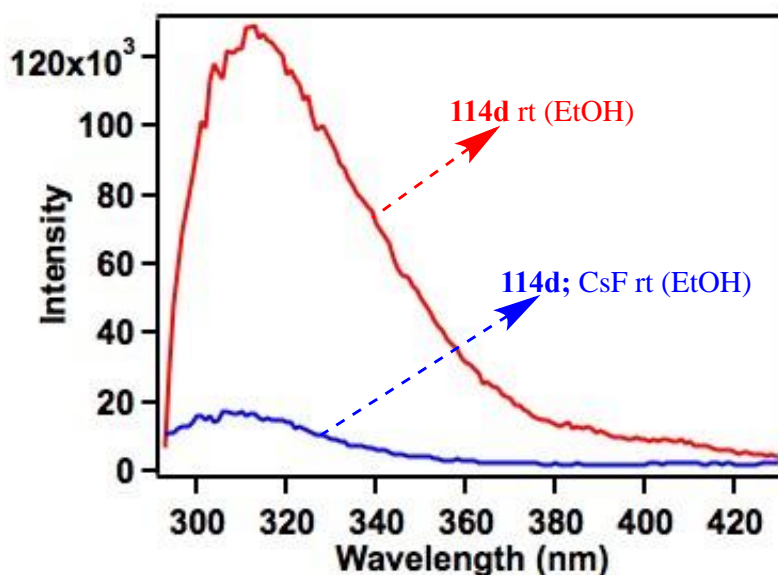


**Figure 3.5:** Fluorescence spectra of **114d** in ethanol, at rt (—blue) and in presence of CsF at rt (—red). [**114d**] = 0.5m

The fluorescence lifetime at 77 K was recorded with lifetimes of **114a** and **114d** of similar duration  $\sim 9 \pm 4$  ns. The fluorescence decay was multiexponential likely caused by the two N-CO rotamers that exist in solution.<sup>27-30</sup> Matrix inhomogeneity is commonly observed at 77 K and is another likely cause of the multiexponential fluorescence decay. Only very weak fluorescence was observed in the presence of Cs<sup>+</sup> both at room temperature and at 77 K. An

efficient deactivation pathway of the excited singlet state of **114a,d** is likely the cause of the drastic decrease in fluorescence intensity in the presence of  $\text{Cs}^+$ . We believe that in the presence of heavy alkali metal cations, like  $\text{Cs}^+$ , spin-orbit coupling between **114** and  $\text{Cs}^+$  occurred which enhanced intersystem crossing (ISC) from the singlet excited-state to the triplet excited-state of **114**.<sup>31</sup> This manifests itself in the triplet reactivity of atropisomeric acrylanilides **115** in the presence of heavy alkali metal cations leading to high enantioselectivity in the photocyclized product **115**.

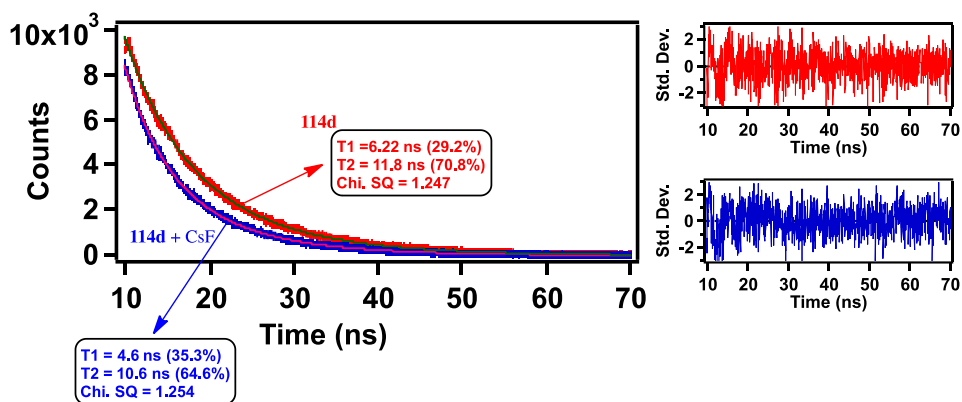


**Figure 3.6:** Left: Fluorescence lifetime of **3d** in ethanol (—red), **3d** in presence of  $\text{CsF}$  in ethanol (—blue) at 77K. Right: Standard deviation of fit for **3d** in ethanol (—red, top) and **3d** in presence of  $\text{CsF}$  in ethanol (—blue, bottom) ( $[\mathbf{114d}] = 0.5 \text{ mM}$ ).

### 3.5.5. Mechanistic rationale $6\pi$ -photocyclization $\alpha$ -substituted atropisomeric acrylanilides

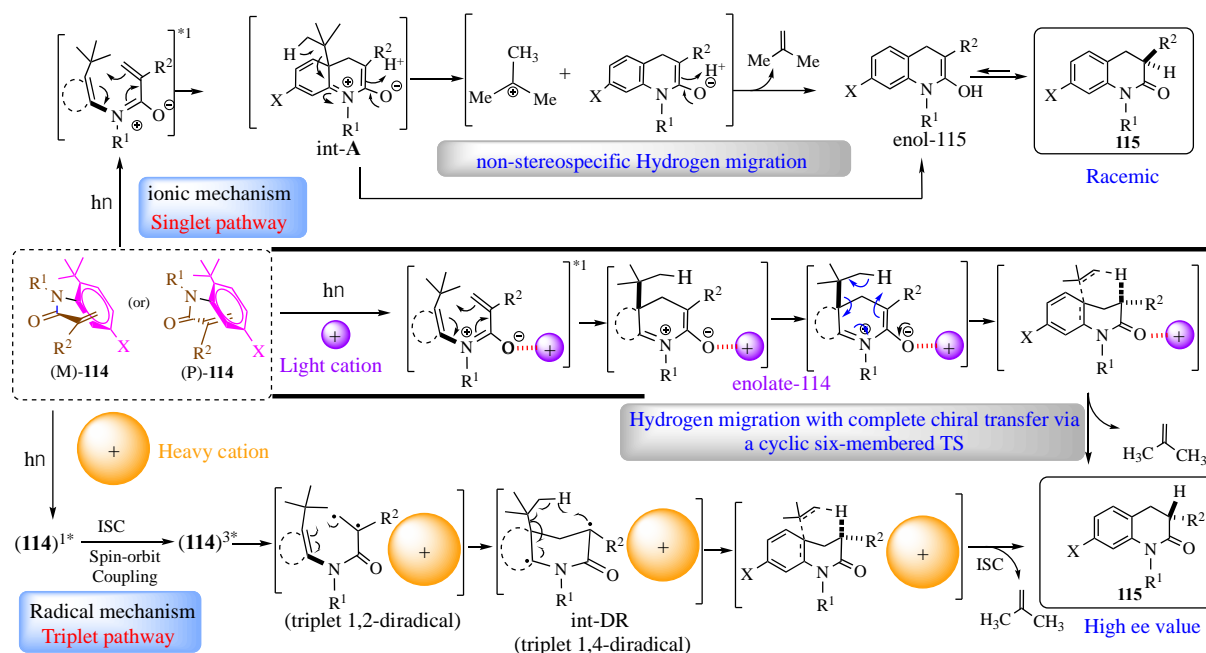
We previously proposed that ‘con’ rotatory  $6\pi$ -photocyclization of *o-tert*-butylacrylanilides with *N*-alkyl substitution led to a zwitterionic intermediate “int-A” (Scheme 3.6, top). Depending on the solvent and the availability of a proton source the zwitterionic intermediate “int-A” undergoes H-migration followed by re-aromatization leading to cyclized photoproduct **115**, with the elimination of the *o-tert*-butyl substituent. Direct irradiation leads to racemic mixture of cyclized photoproduct which likely occurred due to the reactivity from the singlet excited state of atropisomeric acrylanilide **114** in solution. It is also likely that a non-stereospecific H-migration from the zwitterionic intermediate occurred through “enol-**114**” which tautomerizes to the 3,4-dihydro-2-quinolin-2-one **115**. Previously we postulated a radical type mechanism for triplet sensitized  $6\pi$ -photocyclization of atropisomeric acrylanilides, leading to high selectivity in the cyclized photoproduct.<sup>32</sup>

In the presence of alkali metal cations we believe that the photochemical reactivity is likely influenced by Lewis acidity and spin-orbit coupling of the cations.<sup>31</sup> In the presence of heavy metal ions, we believe that it is likely that the photocyclization occurs via the triplet excited-state of **114** through a radical mechanism (Scheme 3.6). This presumption is based on the  $\pi\pi^*$  excited state of **114**. Since the singlet–triplet gap of a  $\pi\pi^*$  excited state is large, it is likely that the presence of heavy metal ions aids in facilitating intersystem crossing which leads to the triplet  $\pi\pi^*$  [ $T_1(\pi\pi^*)$ ] excited state. Based on the photochemical reactivity paradigm, conrotatory  $6\pi$ -photocyclization from the  $T_1(\pi\pi^*)$  excited state leads to a triplet diradical intermediate “int-DR” (Scheme 3.6, bottom). This diradical subsequently abstracts a hydrogen atom from the *ortho-tert*-butyl substituent leading to the cyclized photoproduct **115**. The high enantiomeric excess achieved (Table 3.1) upon photocyclization forming **115** indicates a stereospecific



hydrogen abstraction via a cyclic six membered transition state (Scheme 3.6, bottom) from the triplet diradical intermediate (int-DR).

The observed selectivity in the photoproduct in the presence of both molecular sieves and light alkali cations must be addressed. At present we do not have a clear understanding of the influence of light cations and molecular sieves. Lack of clear understanding leaves us to merely speculate on how light cations and molecular sieves aid in the observed selectivity. We believe that enolate **114** could efficiently interact with the cations of high charge density. An interaction of sufficient magnitude between cations of high charge density could facilitate the stereospecific H-migration (Scheme 3.6, middle). Our results also indicated that moisture may be significant in effecting the selectivity of the photochemical reaction. The effect of moisture is likely subdued in the presence of molecular sieves, but the exchangeable alkali metal present on the surface of the 3 Å molecular sieves influences the reactivity of the substrates leading to the observed selectivity. It is also worth mentioning that 3 Å molecular sieves have exchangeable heavy alkali metal cations that could potentially interact with the reactants influencing the reactivity and selectivity. Taking into account the selectivity and the photophysical investigations it is clear that in the presence of heavy alkali metal cations, there is significant involvement of the triplet excited-state of **114** that influences the selectivity in the cyclized photoproduct.



**Scheme 3.6:** Mechanistic rationale for atropselective  $6\pi$ -photocyclization of  $\alpha$ -substituted acrylanilides **114a-c** in the presence of alkali metal ions.

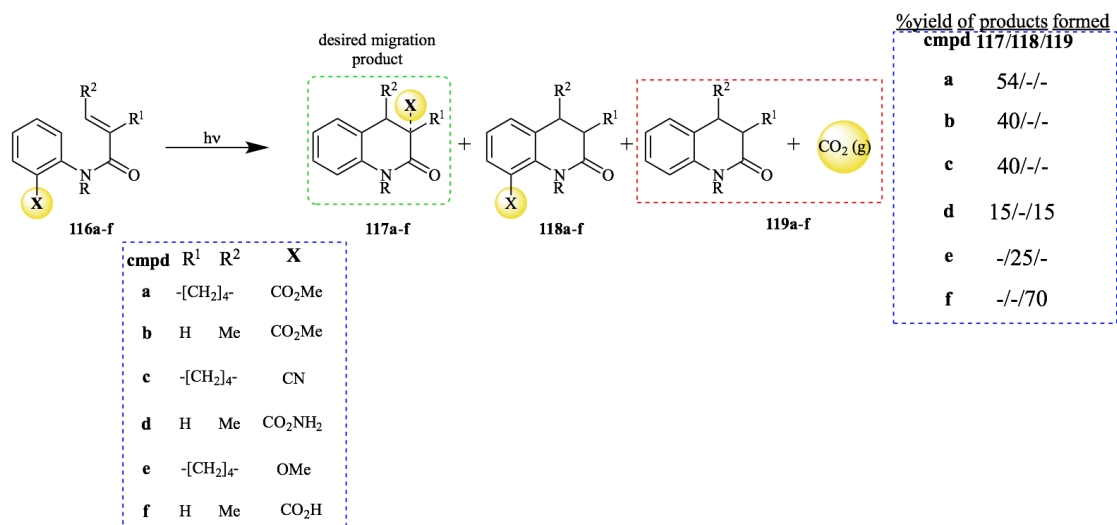
### 3.5.6. Summary and outlook of $6\pi$ -photocyclization $\alpha$ -substituted atropisomeric acrylanilides

Our results point to a subtle change in the reactive environment by the addition of alkali metal ions altering the excited state chemistry during  $6\pi$ -ring closure of atropisomeric acrylanilides **114a-c**. Altering the chemical reactivity by manipulating the interactions of metal ions in solutions presents opportunities to develop catalysts that can influence reactivity and selectivity.

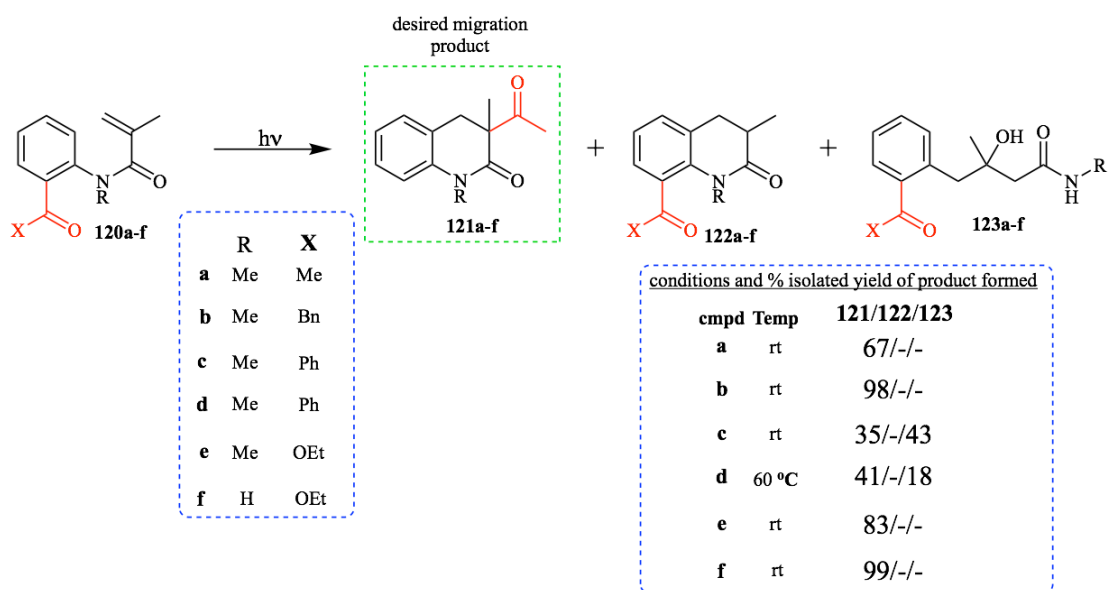
### 3.6. 6 $\pi$ -photocyclization of various acyl *ortho*-substituted acrylanilides

#### 3.6.1. Background of acyl substituted acrylanilides

The unexpected cyclization at the *ortho*-position bearing the *tert*-butyl substitution of  $\alpha,\beta$ -unsaturated acrylanilide **110b** and **114a-c** warranted further investigation. The ability to eliminate and/or cause migration of a substituent piqued our interest as such a transformation can be synthetically useful for various functional group manipulations. In 1980 Ninomiya and coworkers investigated variously *ortho*-substituted acrylanilides.<sup>33</sup> Amongst the acrylanilides investigated, methyl-ester, nitrile and carbamoyl substituent all underwent 6 $\pi$ -photocyclization affording the dihydroquinolinone type product (Scheme 3.7). By way of mechanism, Ninomiya and coworkers hypothesized that upon irradiation acrylanilide **116** underwent ring closure followed by thermal [1,5] migration of the *ortho*-substituent to afford the acyl migrated photocyclized product. Nishio and coworkers investigated similar substituted acrylanilides obtaining the expected 6 $\pi$ -photocyclized product in most cases. However, in the case of **120f** *ortho*-benzoyl derivative the obtained product afforded a rearranged product **123f**.<sup>34</sup> This is a prime example of the difference in reactivity that can arise due to the accessed excited state and reactant conformation. Heating the reaction to 60 °C Nishio and coworkers were able to reduce the formation of the rearrangement product but not achieve the exclusive formation of the cyclized product **121f**. This displays that heating as an external stimulus was not sufficient to obtain control over excited state reactivity.



**Scheme 3.7:** Photocyclization of *ortho*-acyl substituted acrylanilides.

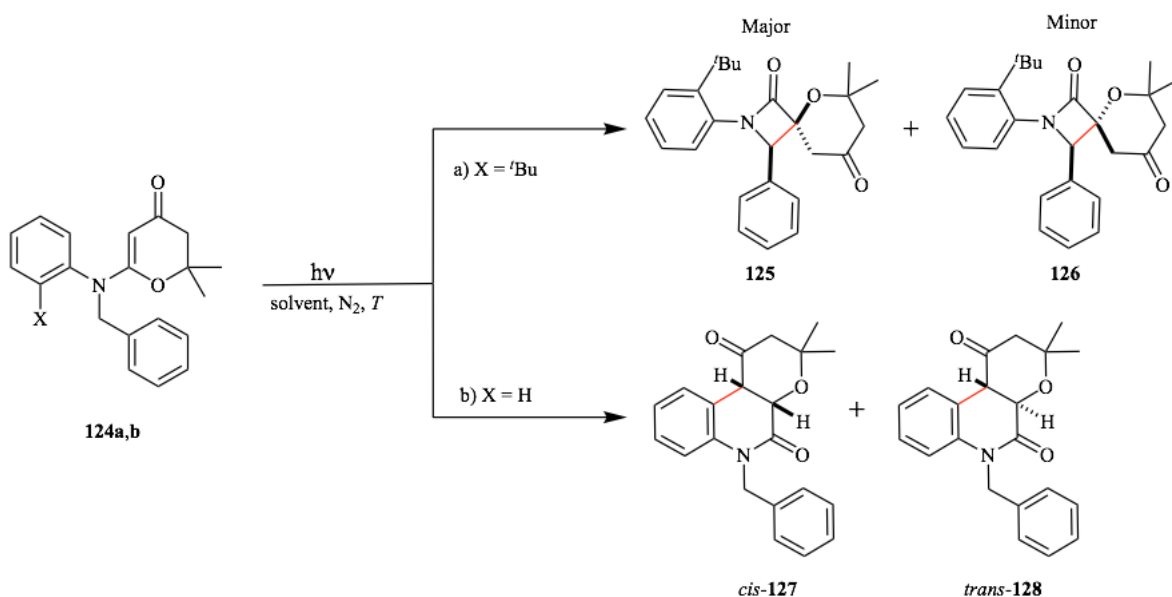


**Scheme 3.8:** Differing photoreactivity of acyl substituted acrylanilides.

Atropisomers have been highlighted due to their ability to control excited state reactivity.

As mentioned above, Sivaguru and coworkers have displayed that photocyclization of *N*-Me substituted atropisomeric acrylanilide **110b** cyclized at the *ortho* position bearing the *tert*-butyl substitution. Thus the restricted *N*-C<sub>aryl</sub> bond, atropisomer, dictated the regiochemistry. Further investigation upon photoreactivity of atropisomeric chromophores carried out by Sivaguru and

coworkers, unveiled that the achiral enone carboxamides **124b** underwent  $6\pi$ -photocyclization upon irradiation.<sup>35</sup> In contrast, upon irradiation atropisomeric **124a** underwent Norrish Yang reaction forming the spirocyclic  $\beta$ -lactams **125** and **126**, displaying that ability of atropisomer to control the excited state reactivity.



**Scheme 3.9:** Differing reactivity of enone-carboxamides axial chiral vs. achiral reactivity.

Acyl substituted acrylanilides, a familiar system, provides us a motif wherein we can utilize atropisomers to alter the excited state properties. Our aim is to probe the mechanistic pathway involved in the *ortho*-substituent migration and probe the excited state characteristics, namely triplet vs singlet while in route to synthesizing uniquely substituted 2,4-dihydroquinolinone type product(s). We hope to shift the wavelength of absorbance into the visible region and utilize visible light to mediate the classical  $6\pi$ -photocyclization. As acyl groups are electron withdrawing groups and is expected to red shift the wavelength of absorbance. We aim to achieve excited state control and afford a single product in high selectivity, yet again highlighting the great utility of atropselective photoreactions.

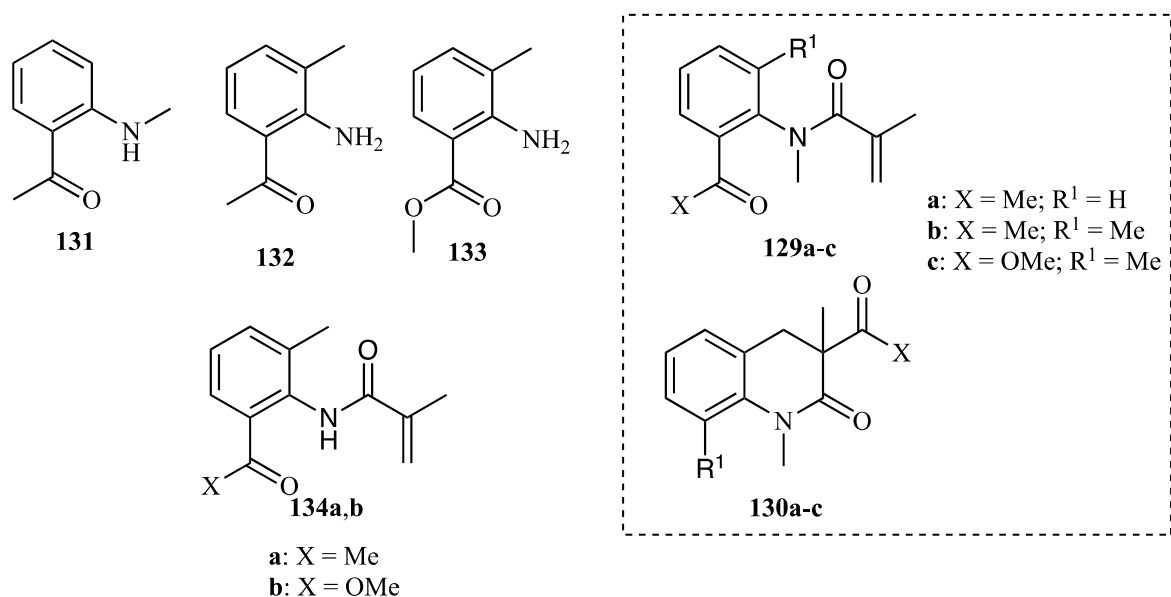
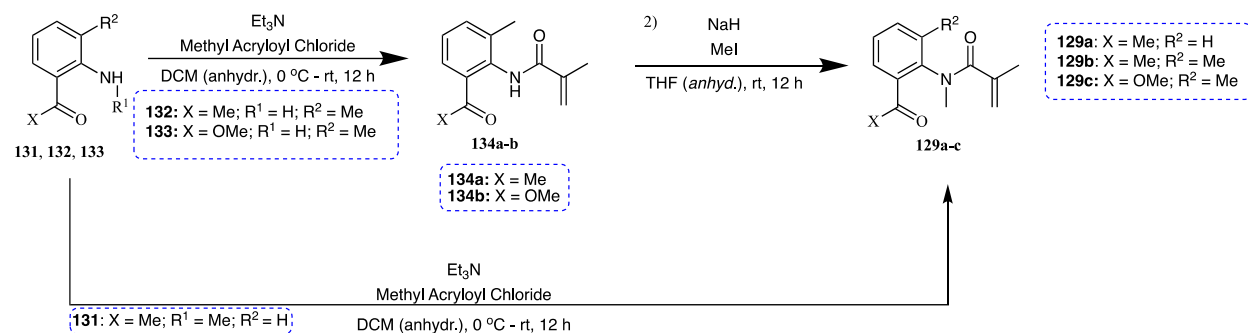


**Chart 3.2:** Structures of acyl substituted acrylanilides, their corresponding photoproducts and precursors/reactants employed in the study.

### 3.7. Photochemistry of atropisomeric acrylanilides



**Scheme 3.10:** Synthesis of acyl substituted acrylanilides.

Acyl substituted acrylanilides were synthesized in a few simple steps (Scheme 3.10). In efforts to optimize the reaction conditions of acyl substituted acrylanilides, irradiation of acrylanilide **129a** was carried out under both direct and sensitized irradiation (Table 3.3 and 3.4). Thioxanthone was utilized as the triplet sensitizer. After the completion of the photoreaction, the reaction mixture was concentrated and the photoproduct(s) purified by column chromatography and characterized by <sup>1</sup>H and <sup>13</sup>C NMR spectroscopy and single crystal XRD.

**Table 3.3:** 6 $\pi$ -photocyclization of acyl substituted acrylanilide **129a** under direct and sensitized irradiation conditions.

entry	Irradiation conditions	%mb	%yield
1	Direct irr., BB 3 h	54	52
2	Direct irr., RR, 350 nm, 5.25 h	66	66
3	Direct irr. RR, ~420 nm 24 h	86	70
4	Direct irr., purple LED 16 h	54	46
5	Tx (10 mol%)/RR ~420 nm 11 h	86	85
6	Tx (10 mol%) purple LED 9 h	88	88

Reaction conditions: [**129a**]  $\approx$  4 mM; MeCN used as solvent under N<sub>2</sub>. Mass balance (mb) and yields determined by <sup>1</sup>H NMR spectroscopy using Ph<sub>3</sub>CH as internal standard.

The conversion, yield and mass balance were calculated by <sup>1</sup>H NMR spectroscopy using triphenylmethane as an internal standard. Under all employed conditions of irradiation, acrylanilide **129a** afforded the desired cyclized product. Decreased yields were noticed under direct irradiation employing purple LED where the wavelength of irradiation centered at 400  $\pm$  5 nm (Table 3.3 entry 4). Acrylanilide **129a** underwent photocyclization cleanly in the presence of Tx as the sensitizer under irradiation of both purple LED and ~420 nm Rayonet Reactor. Additionally, reaction times were reduced when thioxanthone (Tx) was employed as the triplet sensitizer (Table 3.3, entry 5, 6) indicating that the reaction is favorable when accessing the triplet excited state of the acyl substituted acrylanilide. The role of solvent was next investigated. Inspection of Table 3.4 brings to light that irrespective of the solvent the photoreaction of **129a** behaved similar upon irradiation of either ~420 nm (RR) or purple LED in the presence of Tx as sensitizer. Acetone proved to be a sufficient solvent for the reaction affording yields similar to MeCN. Reduced yields were afforded in non-polar solvents (Table 3.4 entries 2,5 and 8).

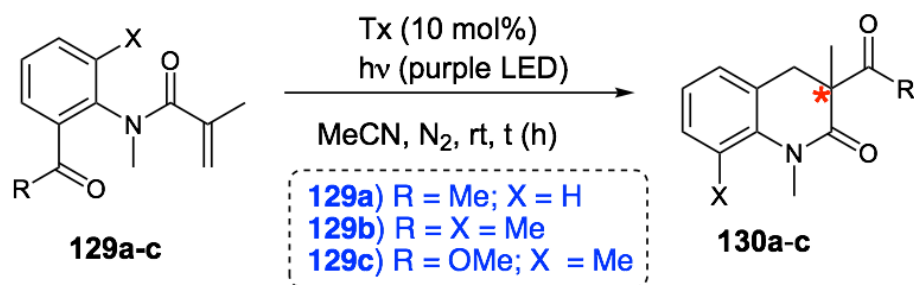
Reduced yields were also afforded in solvents where H-abstraction from the solvent was possible (Table 3.4, entries 3,4 and 9). As Tx was employed as the sensitizer it is possible that the reduced yield is due to Tx undergoing H-abstraction from the solvent followed by some secondary reaction with the substrate **129a** leading to the decomposition of **129a**. At current our investigation cannot rule out such a process.

**Table 3.4:** Optimization of solvent during visible light irradiation of acrylanilide **129a**.

Tx (10 mol%)/RR ~420 nm 11 h			
Entry	solvent	%mb	% yield
1	MeCN	86	85
2	Toluene	35	30
3	CHCl <sub>3</sub>	31	31
4	Methanol	35	35
5	Methylcyclohexanes	18	18
Tx (10 mol%) purple LED 9 h			
7	MeCN	88	88
8	Toluene	35	35
9	DCM	68	59
10	Acetone	89	88
Reaction conditions: [ <b>129a</b> ] ≈ 4 mM; MeCN used as solvent under N <sub>2</sub> . Mass balance (mb) and yields determined by <sup>1</sup> H NMR spectroscopy using Ph <sub>3</sub> CH as internal standard.			

After determining the optimal reaction conditions irradiation of **129a-c** utilizing visible light was investigated. It was displayed that atropisomeric acyl substituted acrylanilide **129b** afforded the cyclized product in moderate yields. Under visible light irradiation ester derivative **129c** did not afford the desired product. In contrast, direct irradiation (broad band light source  $\lambda \geq 290$  nm) of **129c** afforded the desired cyclized product in high isolated yields (Table 3.5, entry 3).





**Scheme 3.11:** Visible light mediated acyl migration of acyl *ortho*-substituted acrylanilides.

**Table 3.5:** Visible light mediated acyl migration of acyl *ortho*-substituted acrylanilides.

entry	cmpd.	t (h)	mb (%) <sup>b</sup>	% yield <sup>b</sup>
1	<b>129a</b>	7	88	88 (67) <sup>c</sup>
2	<b>129b</b>	24	72	60 (52) <sup>c</sup>
3	<b>129c</b>	12	~100	0 (88) <sup>d</sup>

Reaction conditions: [**129a-c**]  $\approx$  4 mM; Reactions performed under N<sub>2</sub> atmosphere in MeCN, under purple LED irradiation. Data is an average of three trials with error  $\pm$ 5% <sup>b</sup>Mass balance (mb) and yields determined by <sup>1</sup>H NMR spectroscopy with Ph<sub>3</sub>CH as internal standard. <sup>c</sup>Isolated yields of desired product. <sup>d</sup>Data represents isolated yield from reaction performed under broad band (BB) direct irradiation (using medium pressure mercury lamp).

Lastly, attempts were made to separate acrylanilides **129b-c** on a chiral stationary phase using preparative HPLC. Unfortunately, base to base separation of the atropisomeric **129b** was not possible on the chiral phases employed. Conversely, acrylanilide **129c** was separable on a chiral stationary phase. However, racemization occurred immediately after HPLC separation. Further investigations must be done in order to determine whether or not the acyl migration occurs in a stereospecific fashion as well as if the migration can be influenced or controlled by atropisomers.

### 3.8. Summary and outlook of acyl substituted acrylanilides

Under direct and sensitized irradiation acrylanilides **129a-b** underwent visible light mediated  $6\pi$ -photocyclization. Thus the triplet excited state of acrylanilide **129a,b** afforded the product favorably. Separation of the atropisomeric acrylanilides **129b** and **129c** were unsuccessful as **129b** was inseparable utilizing the employed chiral stationary phases. In the case of **129c** where racemization occurred quickly it must be that the  $N$ -C<sub>Aryl</sub> barrier to rotation was too low to warrant stable atropisomers at room temperature. By way of mechanism, it is suspected that the mechanism of acyl migration mirrors that of Scheme 3.6 bottom the only difference being that the acyl group migrates instead of the hydrogen depicted. Further investigations must be done in order to give validity to these suspicions and to determine the role of atropisomers in the photoreaction.

### 3.9. Experimental section

#### 3.9.1. General methods

All commercially obtained reagents/solvents were used as received; chemicals were purchased from Alfa Aesar<sup>®</sup>, Sigma-Aldrich<sup>®</sup>, Acros organics<sup>®</sup>, TCI America<sup>®</sup>, Mallinckrodt<sup>®</sup>, and Oakwood<sup>®</sup> Products, and were used as received without further purification. Spectrophotometric grade solvents (ethanol and methylcyclohexane) were purchased from Sigma-Aldrich<sup>®</sup> and used without further purification for emission measurements. Unless stated otherwise, reactions were conducted in oven-dried glassware under nitrogen atmosphere. <sup>1</sup>H NMR and <sup>13</sup>C NMR spectra were recorded on Varian 400 MHz (100 MHz for <sup>13</sup>C) and on 500 MHz (125 MHz for <sup>13</sup>C) spectrometers. Data from the <sup>1</sup>H NMR spectroscopy are reported as chemical shift ( $\delta$  ppm) with the corresponding integration values. Coupling constants ( $J$ ) are reported in hertz (Hz). Standard abbreviations indicating multiplicity were used as follows: s

(singlet), b (broad), d (doublet), t (triplet), q (quartet), m (multiplet) and virt (virtual). Data for  $^{13}\text{C}$  NMR spectra are reported in terms of chemical shift ( $\delta$  ppm). In many instances it was not possible to obtain the signal for the carbonyl carbon where ever possible we have reported all the signals. High-resolution mass spectrum data in Electrospray Ionization mode were recorded on a Bruker – Daltronics<sup>®</sup> BioToF mass spectrometer in positive (ESI+) ion mode. HPLC analyses were performed on Waters<sup>®</sup> HPLC equipped with 2525 pump or on Dionex<sup>®</sup> Ultimate 3000 HPLC. Waters<sup>®</sup> 2767 sample manager was used for automated sample injection on Waters<sup>®</sup> HPLC or Ultimate 3000 sample injector was used for injection on Dionex<sup>®</sup> HPLC. All HPLC injections on Waters<sup>®</sup> HPLC were monitored using a Waters<sup>®</sup> 2487 dual wavelength absorbance detector at 254 and 270 nm or on Dionex<sup>®</sup>. HPLC were monitored using a diode array detector (DAD3000125). Analytical and semi-preparative injections were performed on chiral stationary phase using various columns as indicated below.

Regis<sup>®</sup> PIRKLE COVALENT (*R,R*) WHELK–01

- a) 25 cm x 4.6 mm column for analytical injections.
- b) 25 cm x 10 mm column for semi-preparative injections.

CHIRAPAK<sup>®</sup> AD-H

- a) 0.46 cm x 25 cm column for analytical injections.
- b) 10 mm x 25 cm column for semi-preparative injections.

Masslynx software version 4.1 was used to monitor/analyze the HPLC injections on Waters<sup>®</sup> and to process HPLC traces. Chromeleon 7 software was used to monitor and process HPLC injections on Dionex<sup>®</sup> HPLC. Igor Pro<sup>®</sup> Software version 6.0 was used to process the HPLC graphics. When necessary, the compounds were purified by combiflash equipped with dual wavelength UV-Vis absorbance detector (Teledyne ISCO) using hexanes: ethyl acetate as

the mobile phase and Redisep® cartridge filled with silica (Teledyne ISCO) as stationary phase. In some cases, compounds were purified by column chromatography on silica gel (Sorbent Technologies®, silica gel standard grade: porosity 60 Å, particle size: 230 x 400 mesh, surface area: 500 – 600 m<sup>2</sup>/g, bulk density: 0.4 g/mL, pH range: 6.5 – 7.5). Unless indicated, the Retardation Factor (*R<sub>f</sub>*) values were recorded using a 5-50% hexanes:ethyl acetate as mobile phase and on Sorbent Technologies®, silica Gel TLC plates (200 mm thickness w/UV254).

### 3.9.2. General methods for photophysical investigations

Spectrophotometric solvents (Sigma-Aldrich®) were used when necessary unless or otherwise mentioned. UV quality fluorimeter cells (with range until 190 nm) were purchased from Luzchem®. Absorbance measurements were performed using a Cary 300 UV-Vis spectrophotometer.

### 3.9.3. UV/Vis spectra of acyl substituted acrylanilides

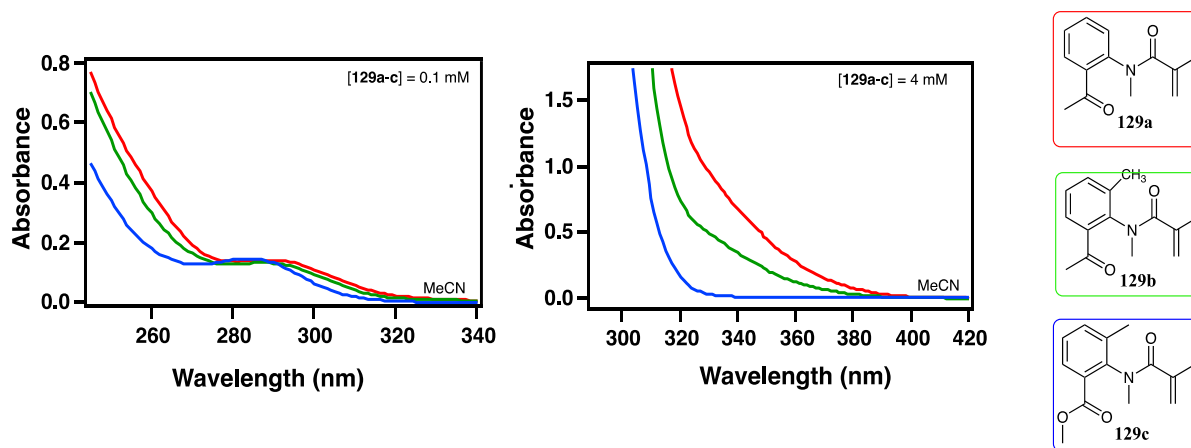


**Figure 3.7:** Absorbance spectra of acrylanilides **129a-c** recorded in MeCN. [129a-c] = 0.1 mM and 4 mM respectively.

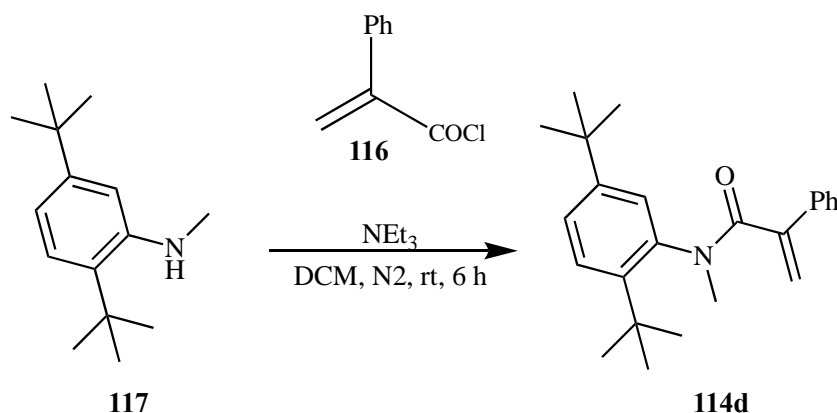
### 3.10. General procedure for the synthesis of $\alpha$ -substituted atropisomeric acrylanilides

The synthesis and characterization of  $\alpha$ -substituted acrylanilides **114a-c** and its photoproducts **115a-c** were previously reported by our group.<sup>9, 24, 25</sup>

### 3.10.1. Synthetic protocol for acid chloride **116**

To a solution of atopic acid (1.1 g, 7.33 mmol, 1.0 equiv) in DCM (10 mL) at room temperature two drops of DMF (catalytic amount) was added. Followed by the addition of oxalyl chloride (2.5 equiv). It was noticed that the solution slowly effervesced after addition of oxalyl chloride. The mixture was allowed to stir for 1 h then the solvent and excess oxalyl chloride was removed under reduced pressure while the temperature was maintained at 25 °C. The vacuum was released under N<sub>2</sub> and the residue was taken up in DCM and directly taken to next step without further analysis or purification.

### 3.10.2. Synthetic protocol for $\alpha$ -substituted atropisomeric acrylanilides **114d**



#### Scheme 3.12: Synthesis of atropisomeric acrylanilide **114d**

An oven dried flask was evacuated, charged with *N*-Methyl aniline derivative **117** (1.0 g, 1.0 equiv) and purged with nitrogen atmosphere. The aniline derivative **117** was dissolved in dry DCM (15 mL) followed by the addition of triethylamine (2.0 equiv) at 0 °C. Also under N<sub>2</sub> atmosphere acyl chloride **116** (1.1 equiv) was added. The resulting solution was slowly allowed to warm to room temperature over 6 h. After 6 h the reaction was quenched with water, stirred and the layers were separated. The organic layer was washed with DI water (2 X 15 mL), dried over *anhy.* Na<sub>2</sub>SO<sub>4</sub>, filtered and the solvent was removed under reduced pressure to yield crude

product. The crude product was purified by combiflash using hexanes:ethyl acetate mixture. The yield for **114d** was ~90%.

$^1\text{H-NMR}$  (400 MHz,  $\text{CDCl}_3$ ,  $\delta$  ppm) mixture of rotamers major:minor = 3:2: 7.58-7.55 (m, 2H, minor), 7.44-7.27 (m, 5H, major+minor), 7.21-7.11 (m, 6H, major+minor), 6.93 (d,  $J = 2$  Hz, 1H, minor), 6.45 (d,  $J = 1.6$  Hz, 1H, major), 5.76 (s, 1H, minor), 5.47 (s, 1H, minor), 5.34 (s, 1H, major), 5.32 (s, 1H, major), 5.28-5.27 (m, 1H, minor), 3.28 (s, 3H, major), 3.11 (s, 2H, minor), 1.39 (s, 6H, minor), 1.297-1.29 (m, 15H, major+minor) and 0.96 (s, 9H, major).

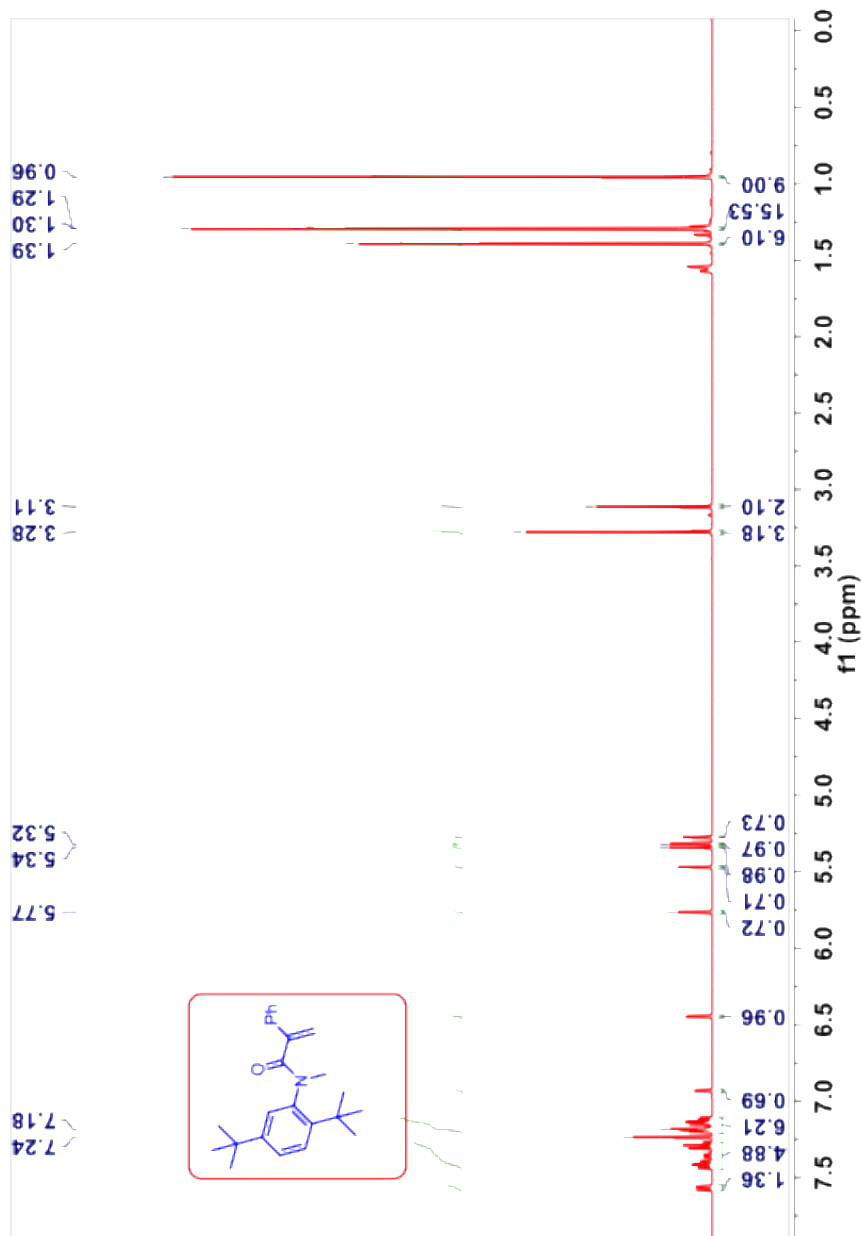


**Figure 3.8:**  $^1\text{H-NMR}$  (400 MHz,  $\text{CDCl}_3$ ,  $\delta$  ppm) spectrum of atropisomeric acrylanilide **114d**.

$^{13}\text{C}$ -NMR (100 MHz,  $\text{CDCl}_3$ ,  $\delta$  ppm) mixture of rotamers major:minor = 3:2: 171.5, 170.6, 150.7, 149.3, 146.8, 146.3, 143.9, 142.8, 141.5, 139.5, 137.96, 135.94, 130.0, 129.1, 128.8, 128.63, 128.56, 128.2, 128.1, 126.4, 126.2, 126.1, 125.7, 125.4, 117.3, 114.0, 42.2, 39.9, 35.97, 35.5, 34.4, 33.9, 32.4, 31.8, 31.4 and 30.9.

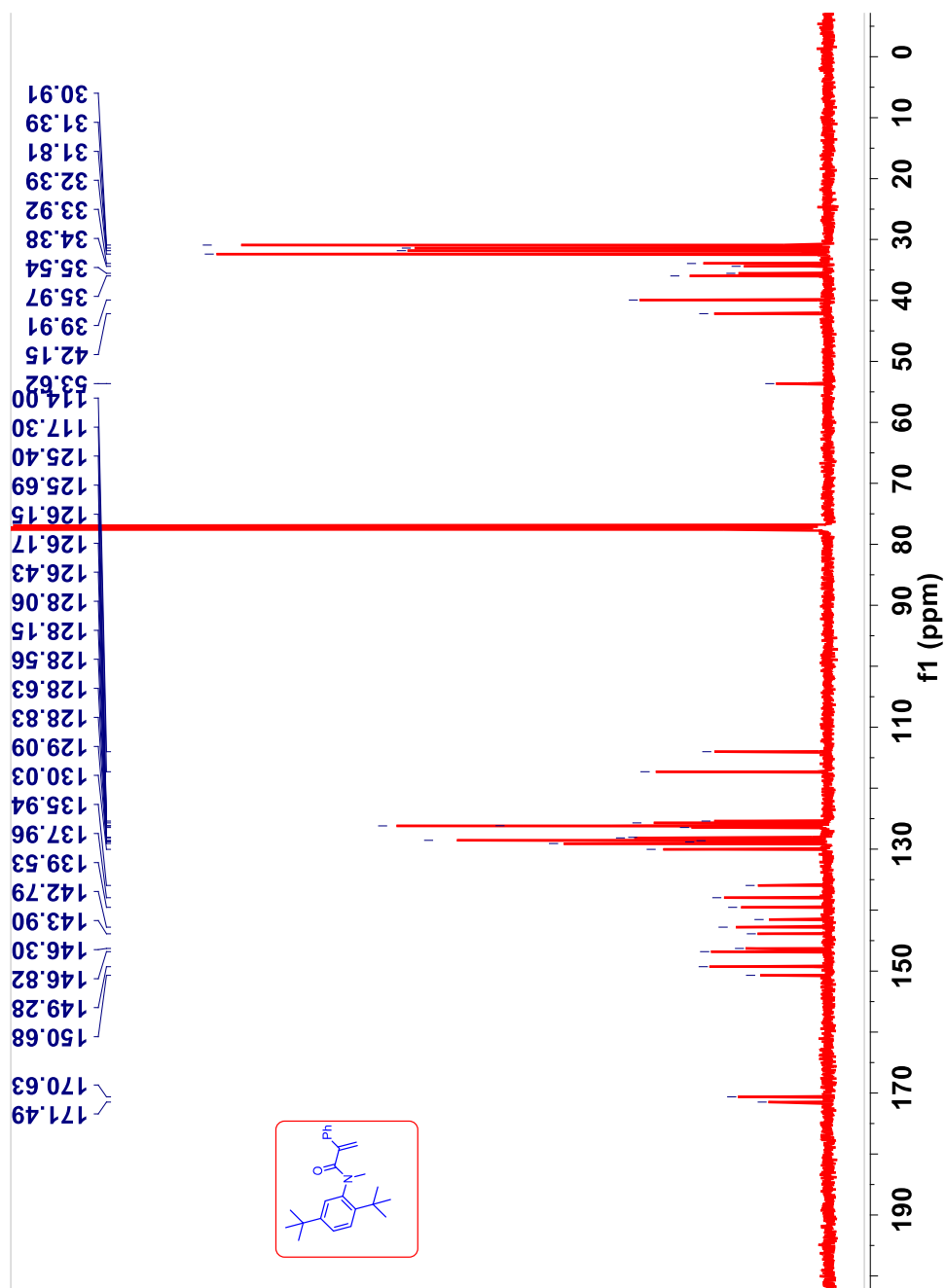


**Figure 3.9:**  $^{13}\text{C}$ -NMR (100 MHz,  $\text{CDCl}_3$ ,  $\delta$  ppm) spectrum of atropisomeric acrylanilide **114d**.



HRMS-ESI (m/z) ([M<sup>+</sup> Na]<sup>+</sup>):

Calculated : 350.2478

Observed : 350.2483

$\Delta m$  : 1.4 ppm

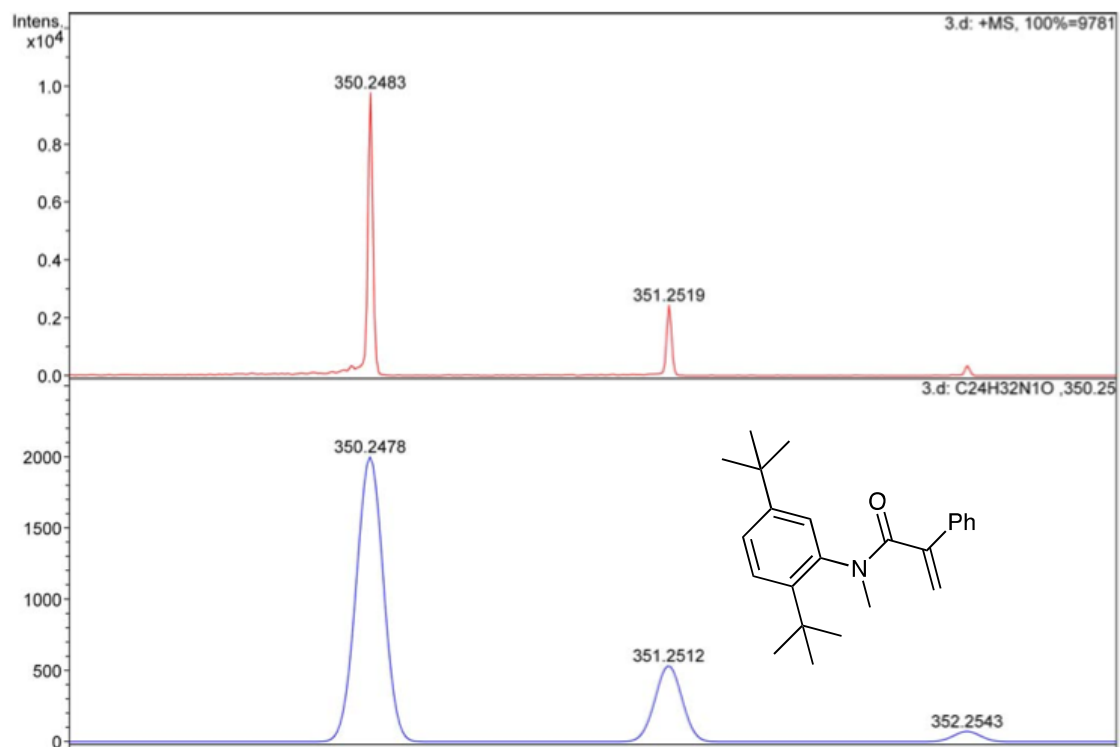
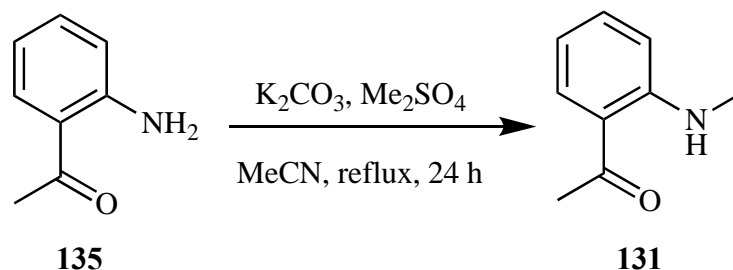


**Figure 3.10:** HRMS of atropisomeric acryanilide **114d**.

### 3.11. General procedure for the synthesis and characterization of acyl substituted acrylanilides 129a-d and their precursors

#### 3.11.1. Synthetic protocol for primary amine 133



#### Scheme 3.13: Synthesis of primary amine 131.

To a solution of 2-aminoacetophenone **135** ( 1 g, 7.4 mmol, 1.0 equiv.) in MeCN (40 mL) at room temperature K<sub>2</sub>CO<sub>3</sub> (2.2 equiv.) was added followed by the dropwise addition of dimethyl sulphate (1.5 equiv.). The reaction mixture was placed under N<sub>2</sub> atmosphere and set to reflux for 24 h. After 24 h the solvent was removed via rotary evaporation, followed by addition of H<sub>2</sub>O:EtOAc (1:1) (ethyl acetate) mixture, stirred and the layers were separated. The aqueous layer was extracted with EtOAc (3x30 mL), and the organic layers were combined. The organic layer was washed with NaHCO<sub>3</sub>, distilled water and dried over *anhyd.* Na<sub>2</sub>SO<sub>4</sub>, filtered and the solvent was removed under reduced pressure to yield the crude product. The crude product was purified by CombiFlash using hexanes:ethyl acetate mixture. Purification afforded the product **133** in approximately 60 % yield as a yellow crystalline solid.

$^1\text{H}$  NMR (400 MHz,  $\text{CDCl}_3$ ,  $\delta$  ppm)  $\delta$  8.75 (bs, 1H), 7.73-7.71 (m, 1H), 7.39 – 7.33 (m, 1H), 6.68-6.66 (m, 1H), 6.59 – 6.54 (m, 1H), 2.89 (s, 3H), 2.55 (s, 3H).

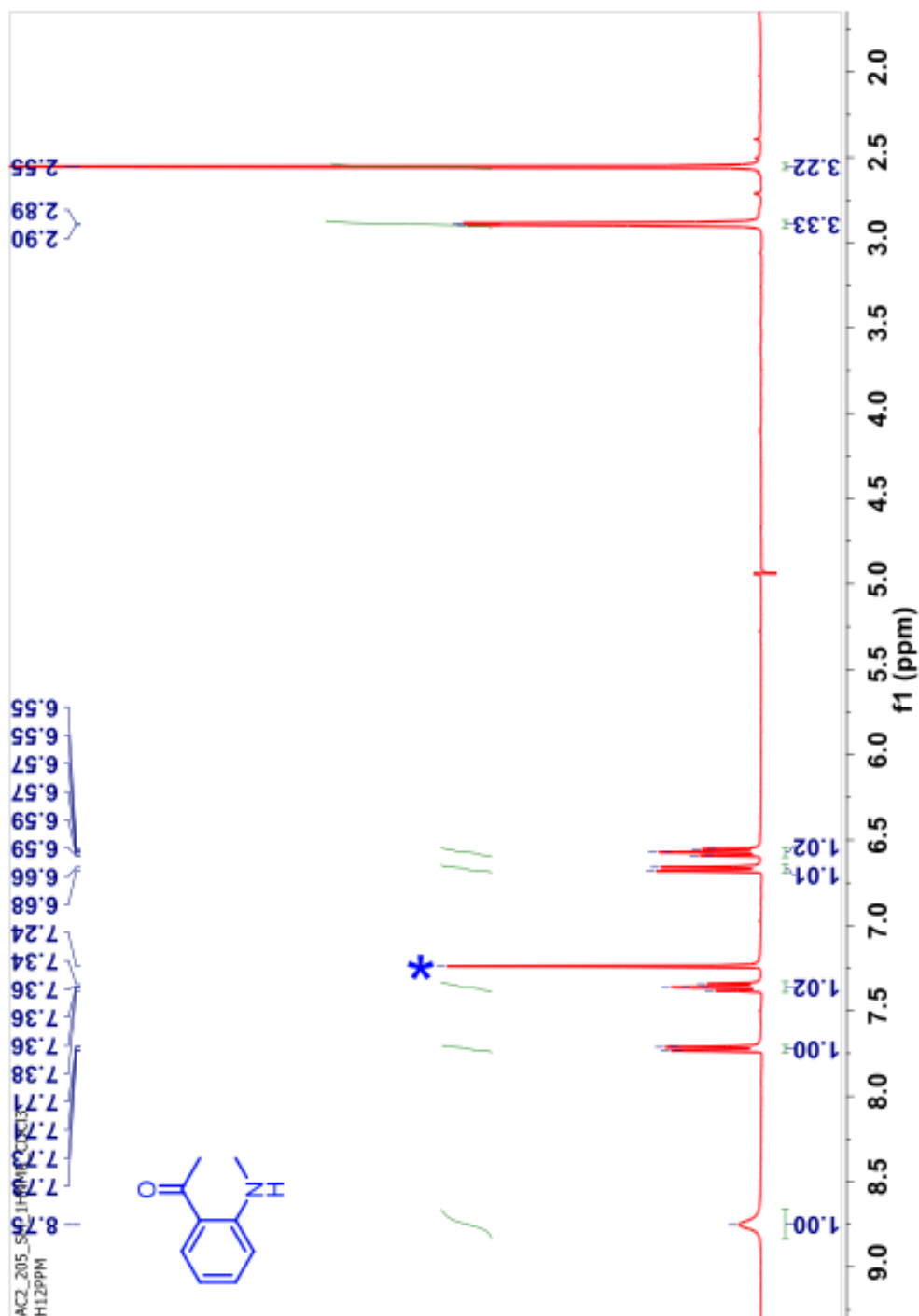


**Figure 3.11:**  $^1\text{H}$  NMR (400 MHz,  $\text{CDCl}_3$ ,  $\delta$  ppm) spectrum of primary amine **131**.

$^{13}\text{C}$  NMR (100 MHz,  $\text{CDCl}_3$ ,  $\delta$  ppm) 200.9, 152.1, 135.2, 132.8, 117.8, 114.0, 111.3, 30.0, 29.4,

28.0

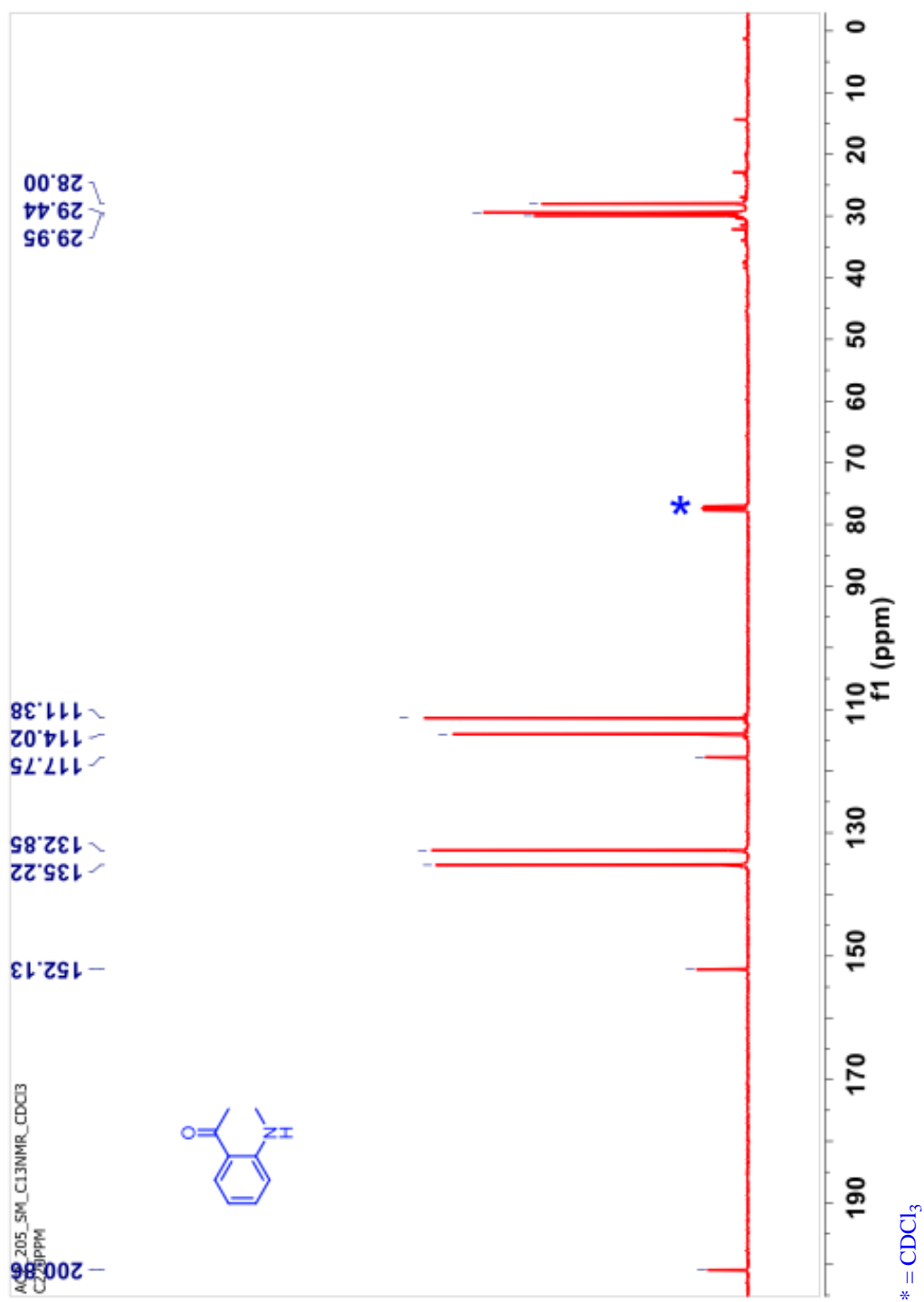
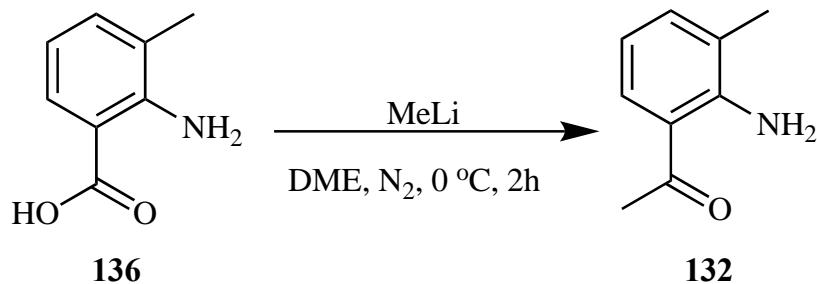


**Figure 3.12:**  $^{13}\text{C}$  NMR (100 MHz,  $\text{CDCl}_3$ ,  $\delta$  ppm) spectrum of primary amine **131**.

### 3.11.2. Synthetic protocol for primary amide 132



#### Scheme 3.14: Synthesis of primary amide 132.

The amine, 2-amino-3-methylbenzoic acid **136** (6.62 mmol, 1 eq.) was added to a round bottom flask and stir bar combination then dissolved in 24 mL of dimethoxy ethane (DME). Then methyl lithium solution in diethoxy methane (23.15 mmol, 3.50 eq.) was added to the solution of **135** dropwise all while the solution stirred at 0°C under nitrogen gas. The reaction was allowed to stir at 0°C for two hours. The reaction was stopped after two hours and allowed to war to room temperature then the reaction was quenched with 30 mL of NH<sub>4</sub>Cl solution. Extraction was done with DCM, and then the solution was dried over Na<sub>2</sub>SO<sub>4</sub> then concentrated. The mixture was then purified utilizing column chromatography done via combiflash: silica gel (40 g); solvent system (8 % EtOAc: Hexane); flow rate (21 mL/min). The product was afforded in 58% yield as a yellow solid.

$^1\text{H}$  NMR (400 MHz,  $\text{CDCl}_3$ ,  $\delta$  ppm) 7.61-7.59 (m, 1H), 7.16-7.17 (m, 1H), 6.58-6.55(m, 1H), 6.35(bs, 1H), 2.56 (s, 3H), 2.13 (s, 3H).

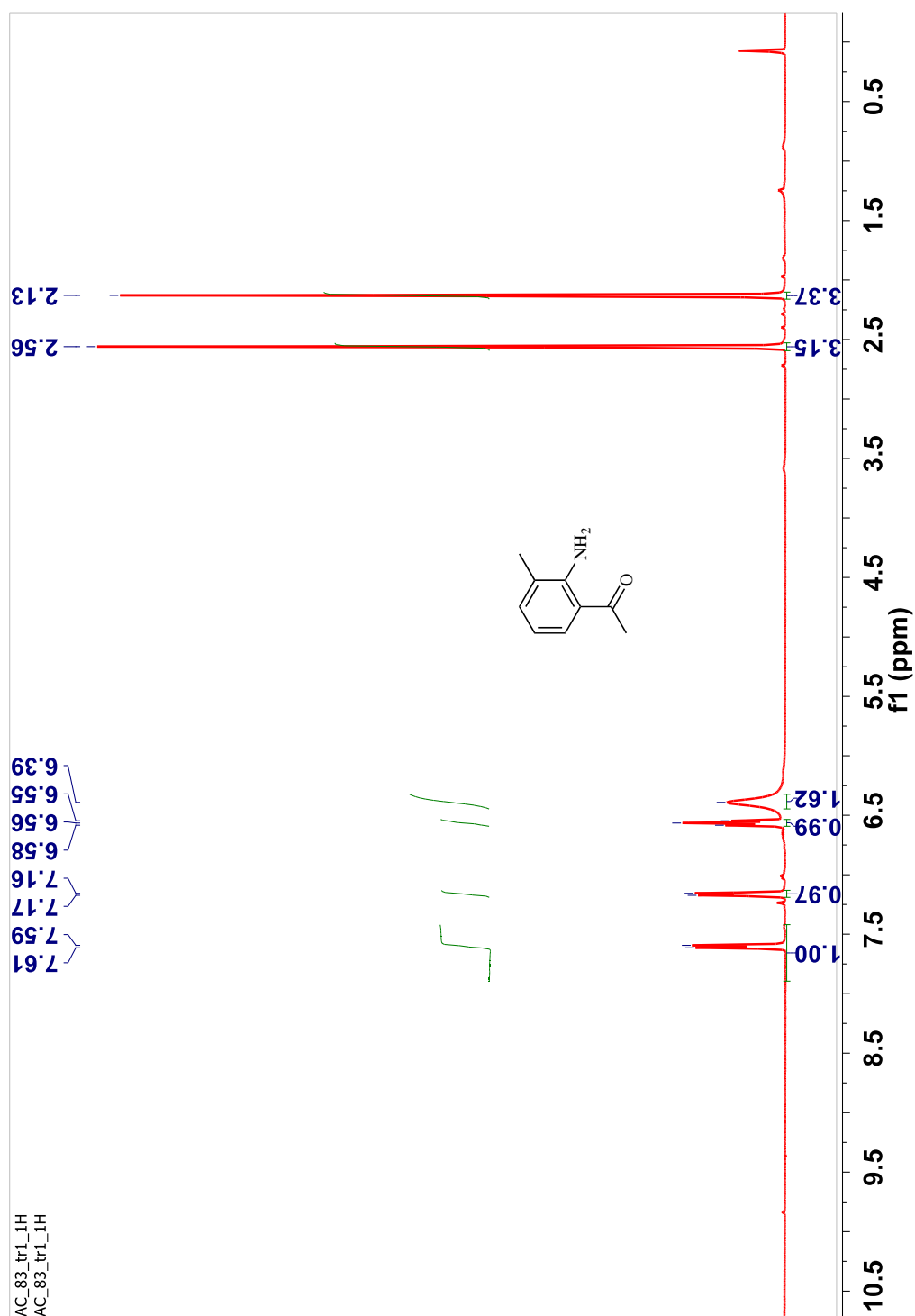


**Figure 3.13:**  $^1\text{H}$  NMR (400 MHz,  $\text{CDCl}_3$ ,  $\delta$  ppm) spectrum of amine **132**.

$^{13}\text{C}$  NMR (100 MHz,  $\text{CDCl}_3$ ,  $\delta$  ppm) 201.2, 149.0, 135.3, 130.3, 117.8, 115.2, 115.2, 28.3, 17.4

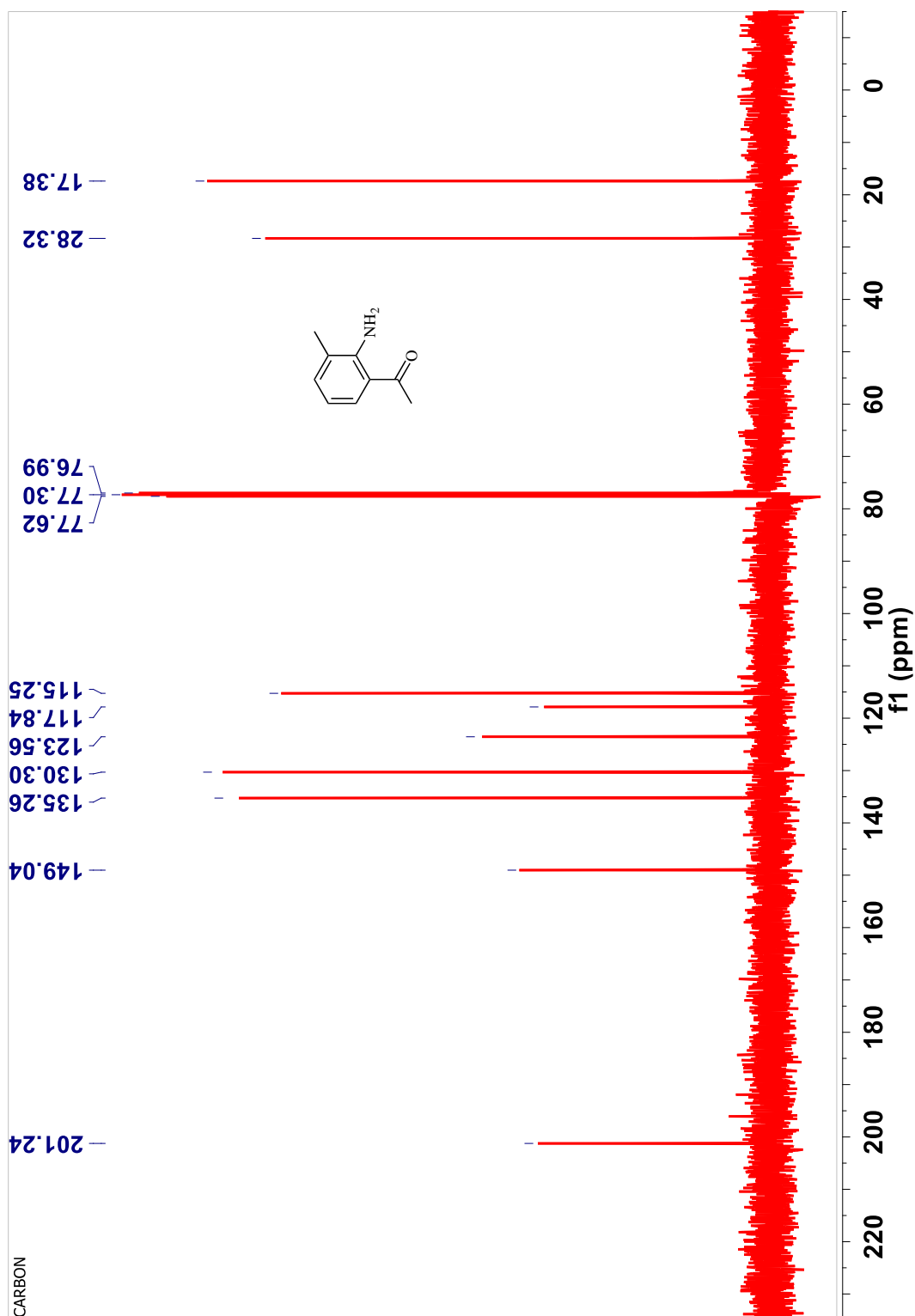
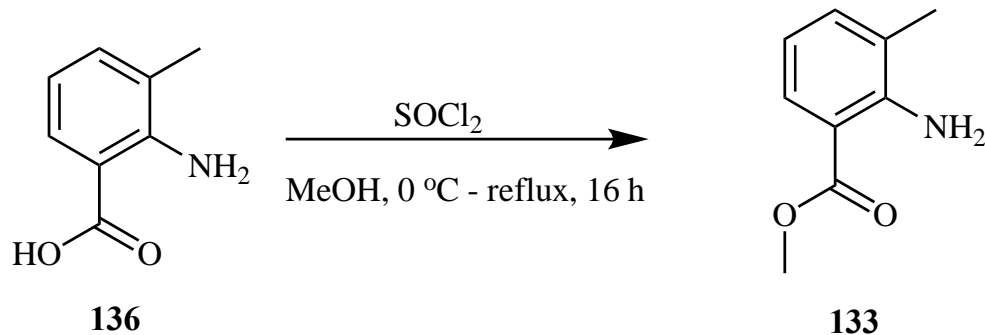


**Figure 3.14:**  $^{13}\text{C}$  NMR (100 MHz,  $\text{CDCl}_3$ ,  $\delta$  ppm) spectrum of amine 132.

### 3.11.3. Synthetic protocol for primary ester substituted amine 133a



#### **Scheme 3.15:** Synthesis of *ortho*-ester substituted primary amine **133**.

To a stirred solution of 2-amino-3-methylbenzoic acid (2.0 g, 14.59 mmol) in MeOH (70 ml.) at 0°C was added SOCl<sub>2</sub> (7 g, 140 mmol) dropwise. The mixture was heated to reflux overnight. Then the reaction mixture was concentrated under reduced pressure. DCM and saturated aqueous NaHCO<sub>3</sub> were added and the aqueous phase extracted with DCM. The combined organic layers were washed with brine, dried over sodium sulfate and concentrated to afford Methyl 3-methyl 2-aminobenzoate (80% yield).



$^1\text{H}$  NMR (400 MHz,  $\text{CDCl}_3$ ,  $\delta$  ppm) 7.76-7.74 (m, 1H), 7.17-7.16 (m, 1H), 6.58- 6.54 (m, 1H), 5.79 (bs, 2H), 3.84 (s, 3H), 2.15 (s, 3H).

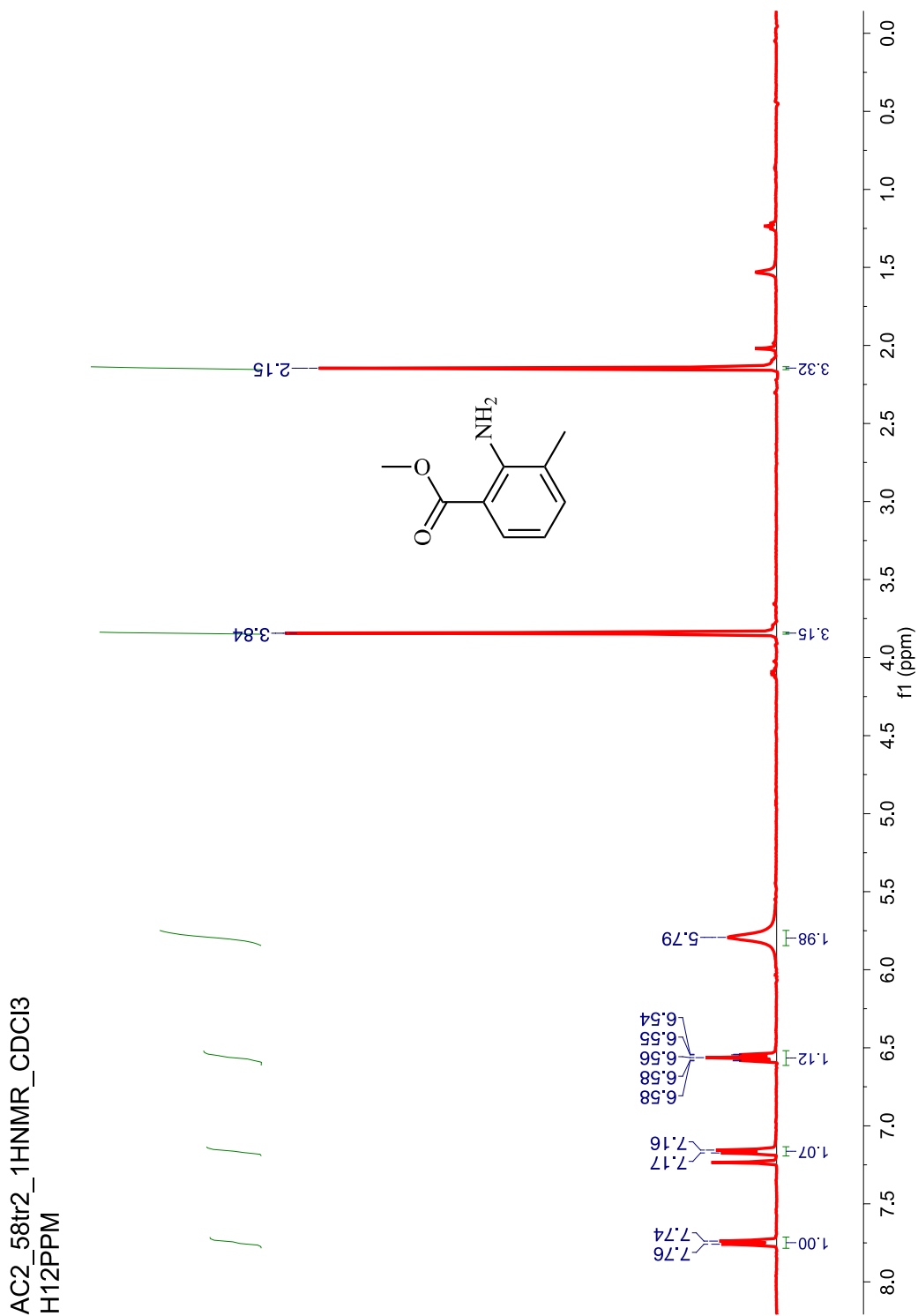


**Figure 3.15:**  $^1\text{H}$  NMR (400 MHz,  $\text{CDCl}_3$ ,  $\delta$  ppm) spectrum of ester substituted amine **133**.

#### **3.11.4. Synthetic protocol for acyl substituted acrylanilide **129a** and secondary amides **132a-c****

In order to synthesize acyl substituted acrylanilide **129a** and the secondary amides **134a,b** the same procedure for as outlined in Section 3.10.2.

$^1\text{H}$  NMR (400 MHz,  $\text{CDCl}_3$ ,  $\delta$  ppm) 83% yield-Mixture of rotamers: 7.65-7.62 (m, 2H, major + minor), 7.47-7.42 (m, 2H, major + minor), 7.31-7.29 (m, 2H, major + minor), 7.17-7.15 (m, 2H, major + minor), 5.21-5.17 (m, 1H, minor), 4.90 (s, 1H, major), 4.81 (s, 1H, major), 3.3- 3.22 (s, 4H, major + minor), 2.45 (s, 4H, major + minor), 1.94 (s, 1H, minor), 1.60 (s, 3H, major).

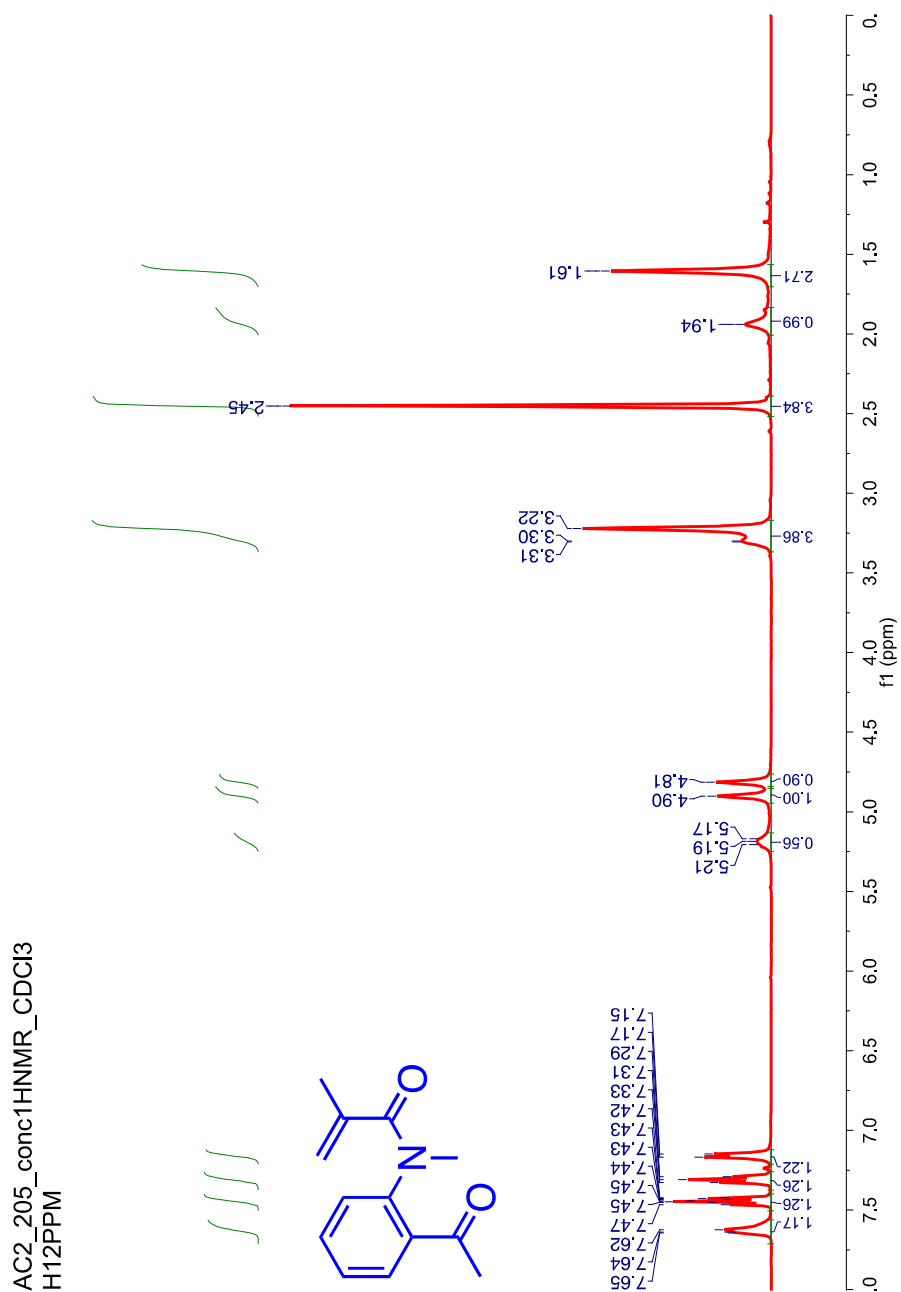


**Figure 3.16:**  $^1\text{H}$  NMR (400 MHz,  $\text{CDCl}_3$ ,  $\delta$  ppm) Mixture of rotamers of acrylanilide **129a**.

$^{13}\text{C}$  NMR (100 MHz,  $\text{CDCl}_3$ ,  $\delta$  ppm) Mixture of rotamers-199.0, 171.3, 143.0, 140.5, 135.9, 132.9, 130.2, 129.6, 127.9, 120.0, 38.0, 29.3, 20.2.

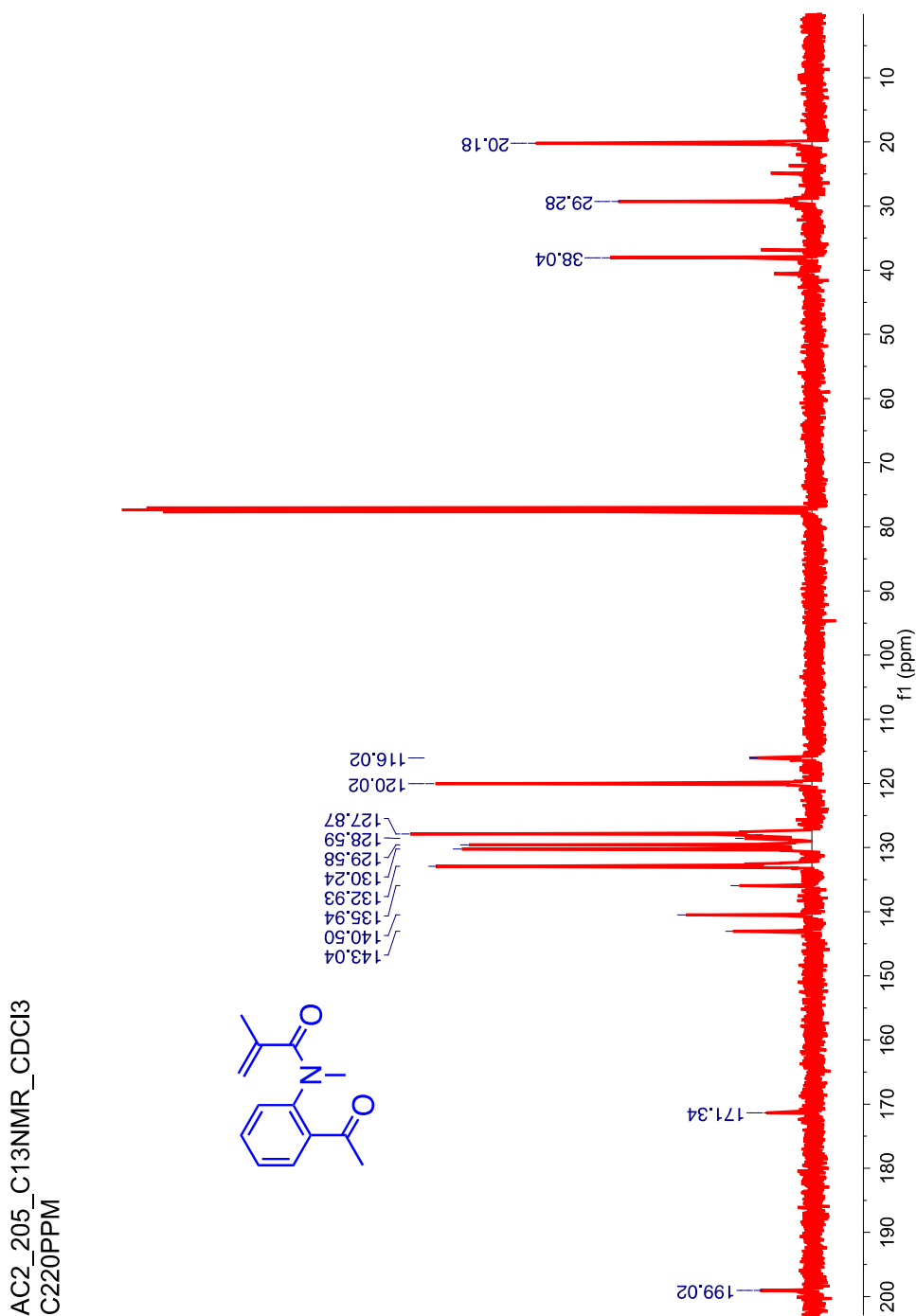


**Figure 3.17:**  $^{13}\text{C}$  NMR (100 MHz,  $\text{CDCl}_3$ ,  $\delta$  ppm) Mixture of rotamers- spectrum of acrylanilide **129a**.

$^1\text{H}$  NMR (400 MHz,  $\text{CDCl}_3$ ,  $\delta$  ppm) 10.10 (s, 1H), 7.66-7.64-7.79 (m, 1H), 7.43-7.41 (m, 1H), 7.19-7.17 (m, 1H), 6.00 (s, 1H), 5.98-5.97 (s, 1H), 5.50-5.49 (m, 1H), 2.60 (s, 3H), 2.25 (s, 3H), 2.08 (s, 3H).

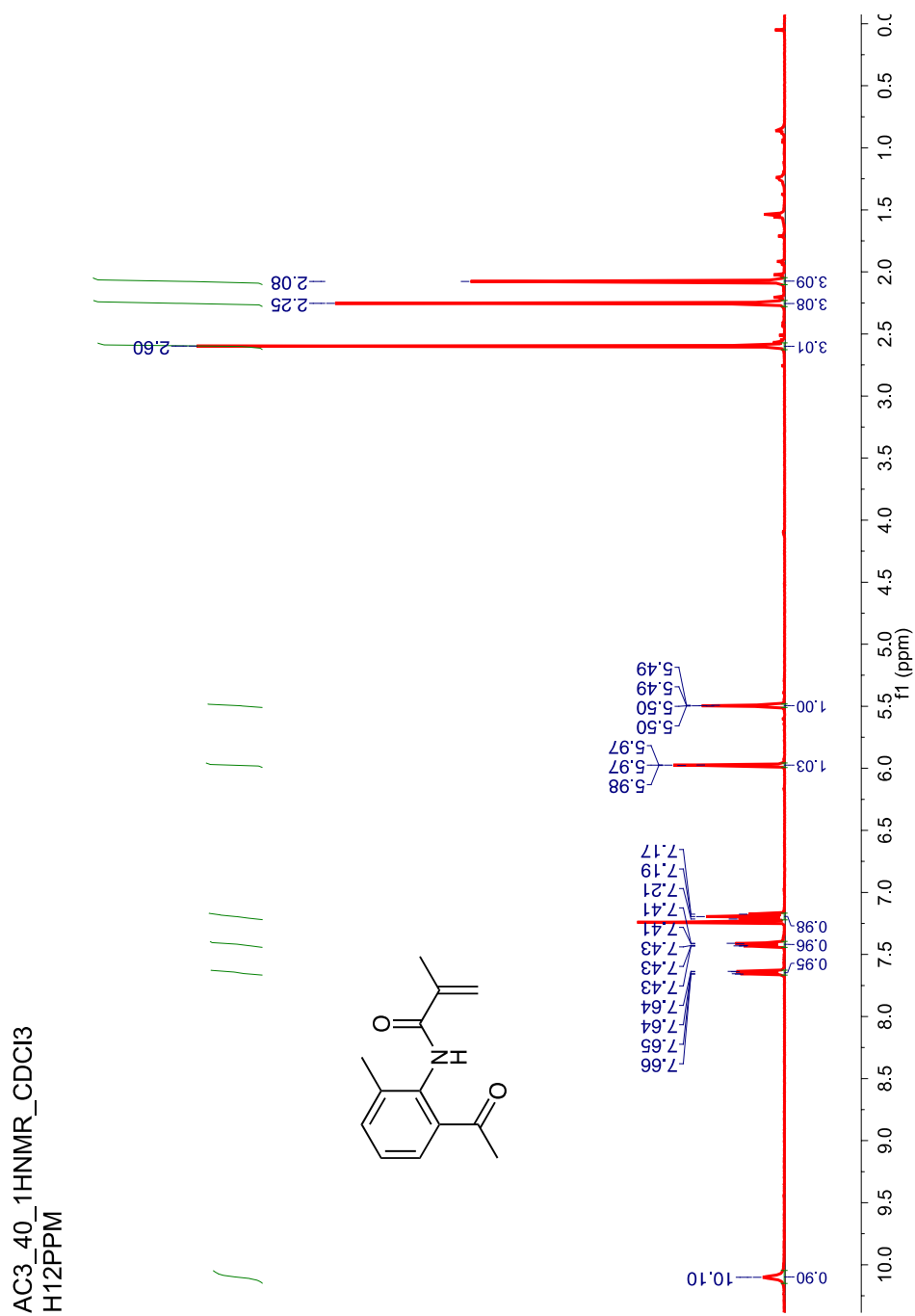


**Figure 3.18:**  $^1\text{H}$  NMR (400 MHz,  $\text{CDCl}_3$ ,  $\delta$  ppm) spectrum of secondary amide **134a**.

$^{13}\text{C}$  NMR (100 MHz  $\text{CDCl}_3$ ,  $\delta$  ppm) 202.5, 166.6, 140.2, 136.2, 136.17, 135.9, 130.6, 128.1, 125.3, 121.4, 29.0, 19.5, 18.8

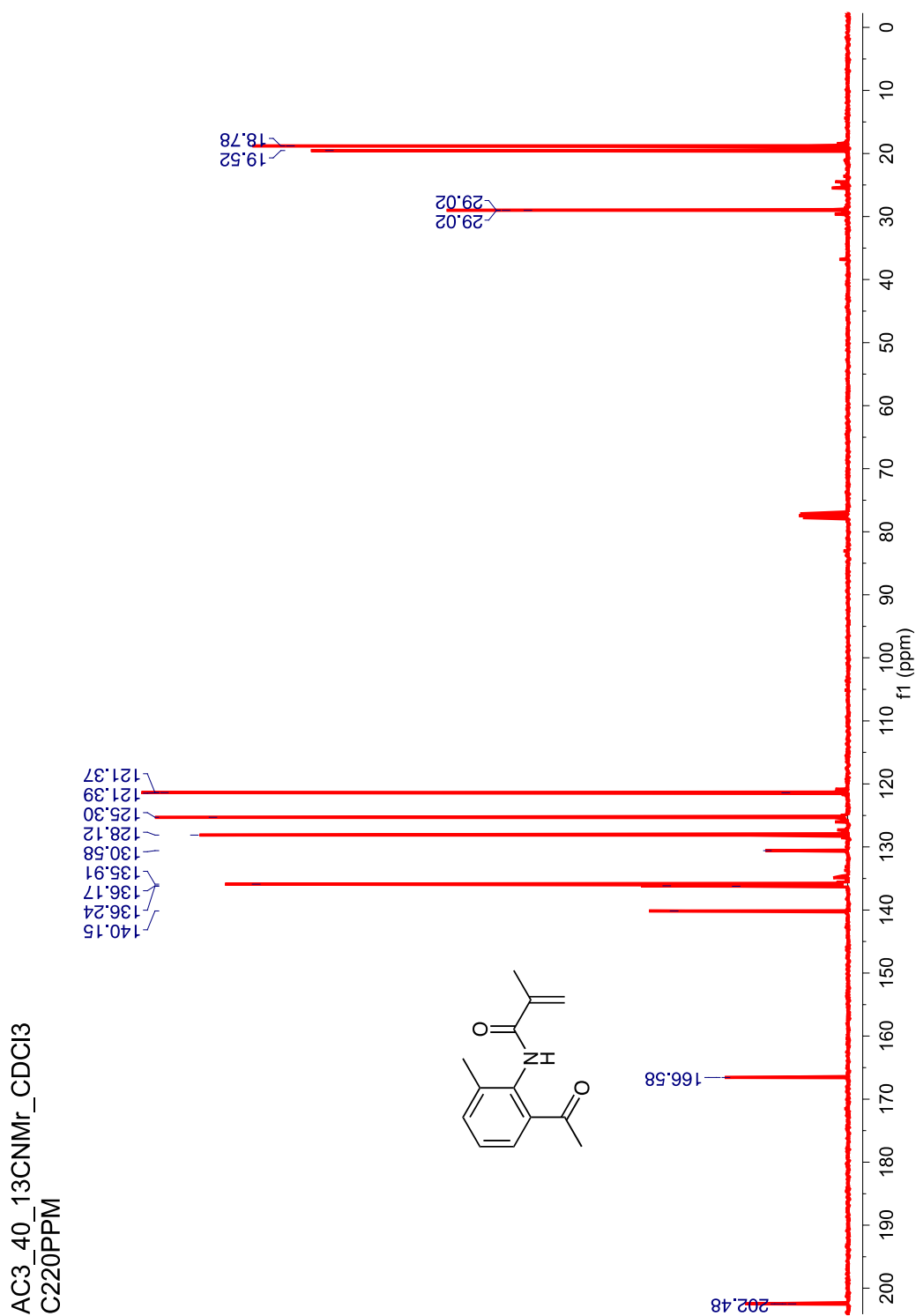


**Figure 3.19:**  $^{13}\text{C}$  NMR (100 MHz,  $\text{CDCl}_3$ ,  $\delta$  ppm) spectrum of secondary amide **134a**

$^1\text{H}$  NMR (400 MHz,  $\text{CDCl}_3$ ,  $\delta$  ppm) 9.68 (bs, 1H), 7.80-7.78 (m, 1H), 7.43-7.41 (m, 1H), 7.18-7.14 (m, 1H), 5.99-5.98 (m, 1H), 5.50 (m, 1H), 3.87 (s, 3H), 2.26 (s, 3H), 2.08 (s, 3H).

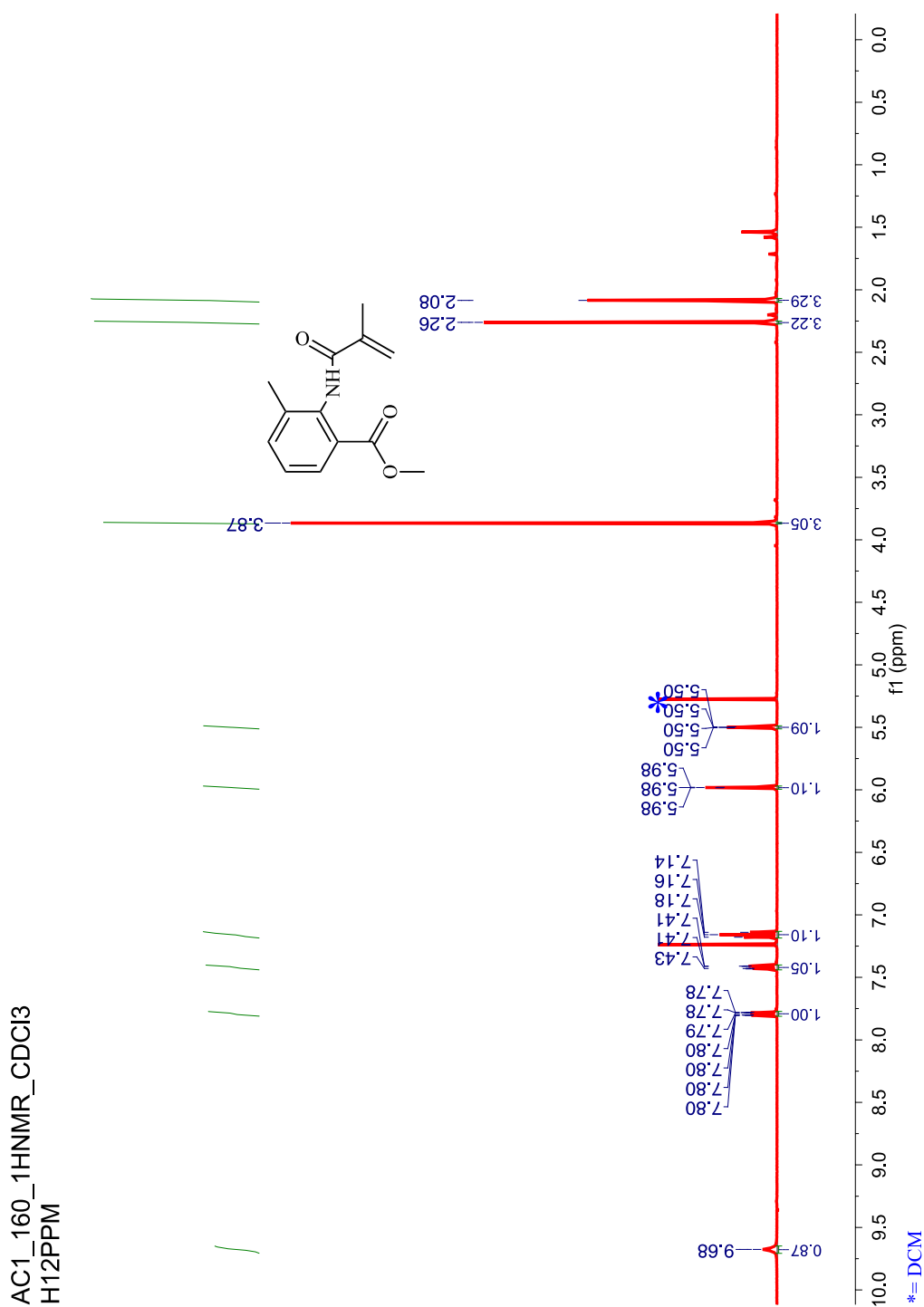


**Figure 3.20:**  $^1\text{H}$  NMR (400 MHz,  $\text{CDCl}_3$ ,  $\delta$  ppm) spectrum of secondary amide **134b**.

$^{13}\text{C}$  NMR (100 MHz  $\text{CDCl}_3$ ,  $\delta$  ppm) 168.2, 166.3, 140.1, 137.4, 135.8, 128.3, 127.5, 125.3, 122.9, 121.2, 52.3, 19.4, 18.7

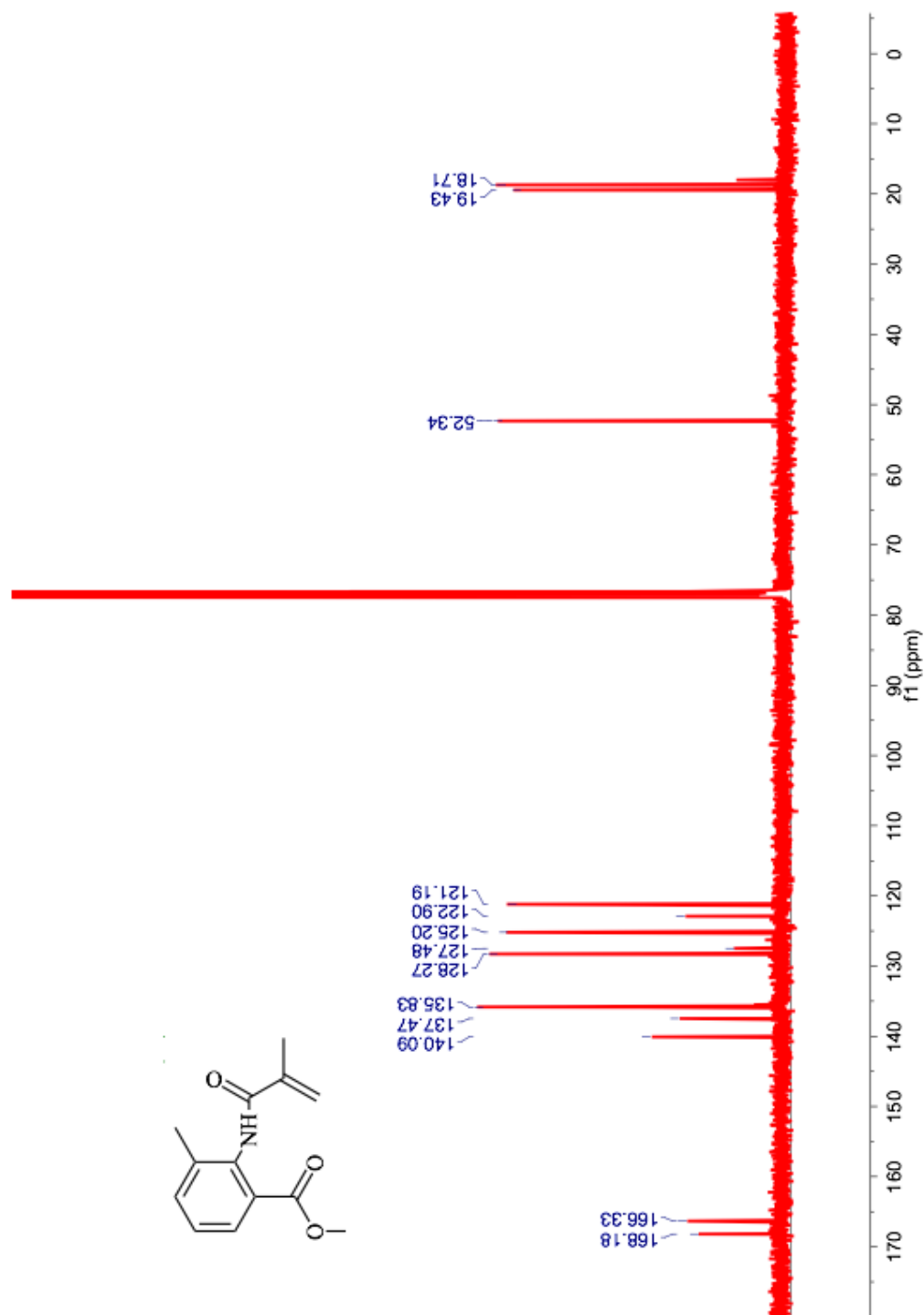


**Figure 3.21:**  $^{13}\text{C}$  NMR (100 MHz,  $\text{CDCl}_3$ ,  $\delta$  ppm) spectrum of secondary amide **134b**



### 3.11.5. Synthetic protocol for *ortho*-acyl substituted acrylanilides **129b,c**

NaH (1.5 equiv.) was added to a stir bar flask combination evacuated in flask purged with N<sub>2</sub> followed by dissolution in THF and cooled to 0 °C. The amide derivative was evacuated in a separate flask and separately purged with N<sub>2</sub> **134b,c** (1 equiv.) dissolved in THF and cooled to 0 °C. The amide solution was added to the NaH solution dropwise. After the solution was allowed to stir for approximately five minutes MeI was added dropwise. The reaction was allowed to slowly rise to room temperature and stir overnight. After approximately 16 h the reaction was again cooled to 0 °C and quenched by the dropwise addition of distilled water, extracted with EtOAc (3x30 mL), the organic layers were separated and combined. The organic layers were washed with brine, dried with Na<sub>2</sub>SO<sub>4</sub>, concentrated in vacuo and purified to give the desired product **129b** as a yellow solid (60% yield) and **129c** as a white crystalline solid (70% yield).

$^1\text{H}$  NMR (400 MHz,  $\text{CDCl}_3$ ,  $\delta$  ppm) Mixture of rotamers-7.50-7.49 (m, 2H), 7.40-7.38 (m, 2H), 7.37-7.27 (m, 2H), 5.27-5.26 (m, 1H), 5.23- 5.22 (m, 1H), 4.92 (s, 1H), 4.78-4.79 (m, 1H), 3.23 (s, 2H), 3.20 (s, 2H), 2.50 (s, 2H), 2.47 (s, 3H), 2.29 (s, 3H), 2.24 (s, 2H), 2.02-2.01 (m, 2H), 1.61-1.60 (m, 3H).

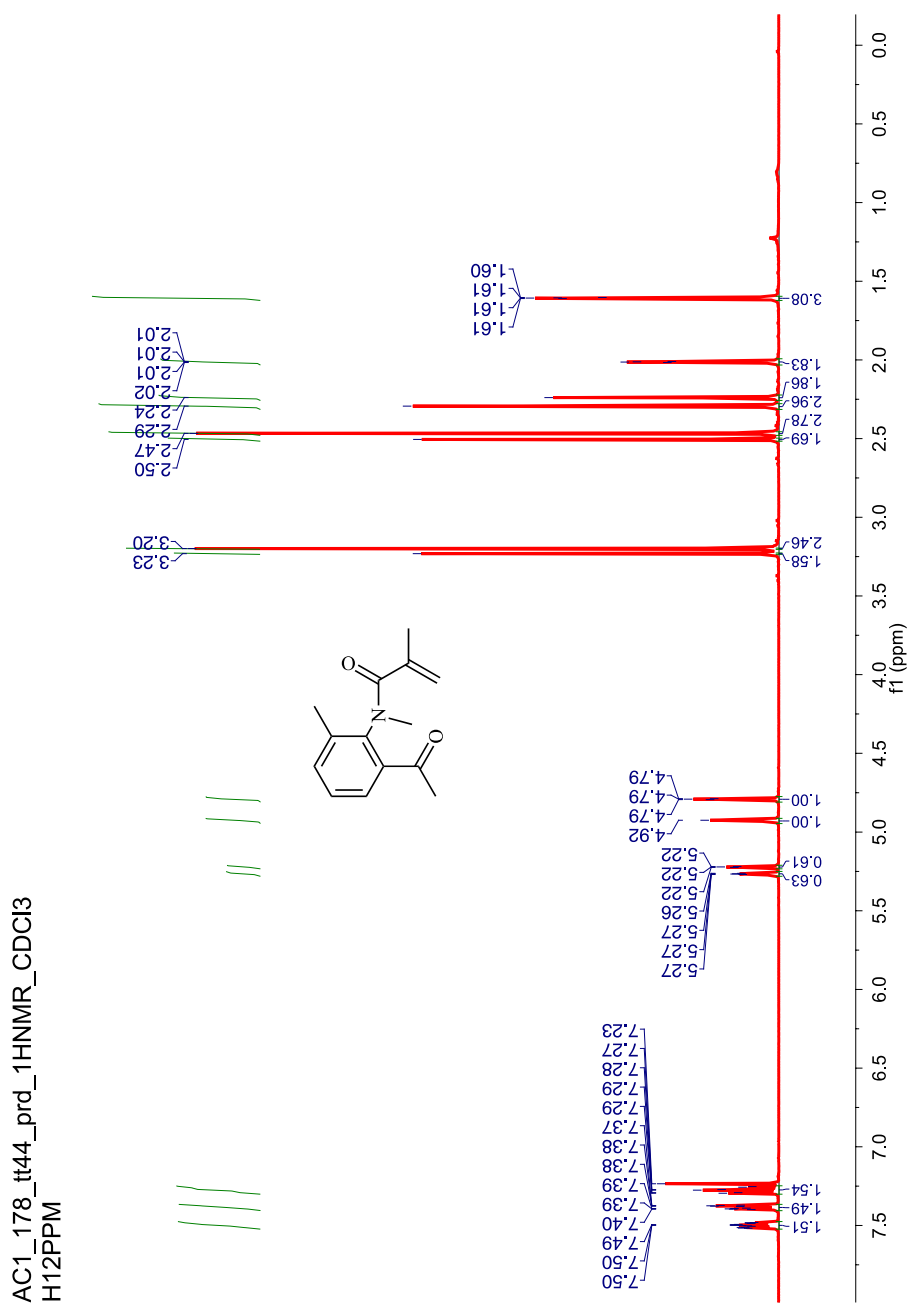


**Figure 3.22:**  $^1\text{H}$  NMR (400 MHz,  $\text{CDCl}_3$ ,  $\delta$  ppm) spectrum of acrylanilide **129b**.

$^{13}\text{C}$  NMR (100 MHz  $\text{CDCl}_3$ ,  $\delta$  ppm) Mixture of rotamers: 200.5, 199.2, 172.1, 170.9, 140.9, 140.6, 140.3, 138.9, 137.3, 137.2, 136.9, 136.6, 134.8, 134.3, 127.7, 127.7, 127.5, 126.9, 119.1, 115.8, 39.2, 36.9, 29.4, 29.3, 19.9, 19.7, 17.8, 17.2

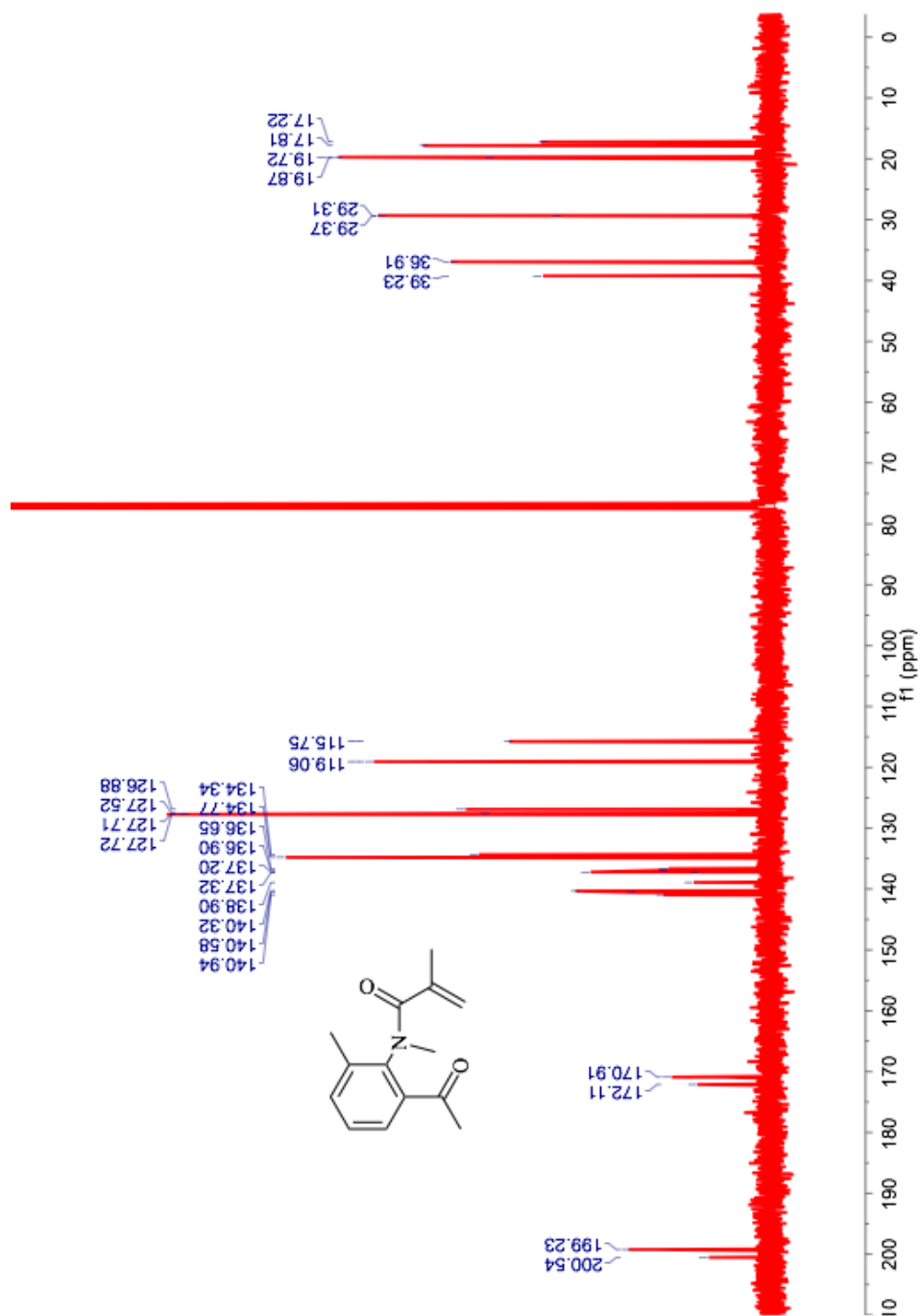


**Figure 3.23:**  $^{13}\text{C}$  NMR (100 MHz,  $\text{CDCl}_3$ ,  $\delta$  ppm) spectrum of acrylanilide **129b**.

$^1\text{H}$  NMR (400 MHz,  $\text{CDCl}_3$ ,  $\delta$  ppm) Mixture of rotamers- 7.84-7.82 (m, 1H), 7.75-7.72 (m, 1H), 7.45-7.39 (m, 1H), 7.28-7.24 (m, 1H), 5.29-5.27 (m, 1H), 4.91-4.90 (m, 1H), 4.79-4.78 (m, 1H), 3.84 (s, 3H), 3.83 (s, 1H), 3.24 (s, 1H), 3.19 (s, 3H), 2.31 (s, 3H), 2.25 (s, 1H), 2.05 (s, 1H), 1.62 (s, 3H).

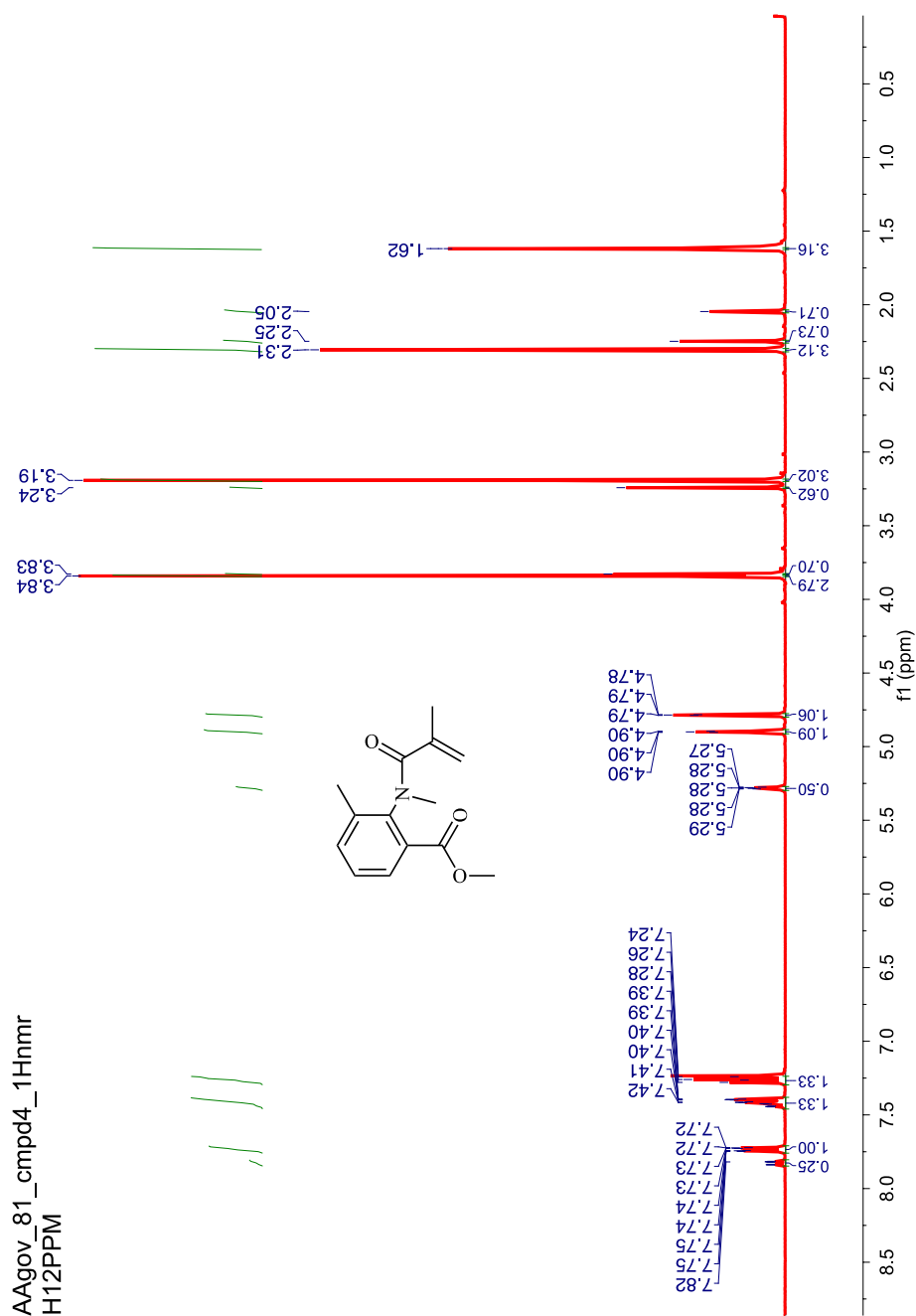


**Figure 3.24:**  $^1\text{H}$  NMR (400 MHz,  $\text{CDCl}_3$ ,  $\delta$  ppm) spectrum of acrylanilide **129c**.

### 3.12. General procedure for irradiation of $\alpha$ -substituted atropisomeric acrylanilides **114a-c**

A stock solution of 2,2,2-trifluoroethanol saturated with the corresponding additive was prepared an evening prior to the respective photoreaction. The additive was flame dried while simultaneously being evacuated under high vacuum. Then the additives were purged and sealed with a septum under N<sub>2</sub>. The additives were then dissolved in 2,2,2-trifluoroethanol. The resulting solution was passed through a microfilter and used to dissolve optically pure atropisomeric acrylanilides **114a-c**. Quite often a turbid solution resulted which was filtered through a microfilter a second time. The resulting solution was then irradiated at 25 °C for 3 h in Pyrex test tube with a 450 W medium pressure mercury lamp placed inside a water cooled quartz well under constant flow of nitrogen. After irradiation, the solvent was evaporated under reduced pressure, dissolved in a polar organic solvent then again filtered all before the enantiomeric excess was determined by HPLC on a chiral stationary phase.

### 3.13. General procedure for irradiation of acyl *ortho*-substituted acrylanilides **129a-c**

#### 3.13.1. Procedure for direct irradiation of acrylanilides **129a-c**

In a Pyrex test-tube, acyl *ortho*-substituted acrylanilide(s) **129a-c** (10mg in 10 mL) was dissolved in a given solvent and degassed with N<sub>2</sub> for 10 min. The solution was irradiated for the specified time interval in either a Rayonet reactor at ~420 nm, using a 450 W medium pressure Hg lamp enclosed in a quartz jacket that was cooled with running water or purple led strips light source. When the reaction was complete, a stock solution of internal standard (triphenylmethane) was added and this solution was concentrated under reduced pressure to obtain the crude reaction mixture. <sup>1</sup>H NMR spectroscopy was recorded of the crude reaction mixture to determine the mass balance and percent yield. In some instances, isolated yields were also obtained.

### 3.13.2. Procedure for sensitized irradiation of acyl *ortho*-substituted acrylanilides **129a-c**

Acrylanilides **129a-c** were dissolved in the appropriate solvent in a Pyrex test-tube (10mg in 10 mL); Thioxanthone (10 mol%) was dissolved in the same solvent and added to the acrylanilides **129a-c** or a stock solution of thioxanthone in the appropriate solvent was obtained and the necessary amount was added to a solution of acrylanilides **129a-c**. The reaction mixture was degassed with N<sub>2</sub> for ~10 min. The solution was irradiated for a specified time interval in a Rayonet reactor (~420 nm). After the reaction, a stock solution of internal standard (triphenylmethane) was added and this solution was concentrated under reduced pressure to obtain the crude reaction mixture. <sup>1</sup>H NMR spectroscopy was recorded of the crude reaction mixture to determine the mass balance and percent yield utilizing equation 2.10 (Eq. 2.10). In some instances, isolated yields were also obtained.

### 3.14. Characterization of cyclized photoproduct(s) **130a-c**

$^1\text{H}$  NMR (400 MHz,  $\text{CDCl}_3$ ,  $\delta$  ppm) 7.24-7.14 (m, 2H), 7.01-6.93 (m, 2H), 3.39 (s, 3H), 3.33 (d,  $J = 15.5$  Hz, 1H), 2.75 (d,  $J = 15.5$  Hz, 1H), 2.10 (s, 3H), 1.39 (s, 3H).

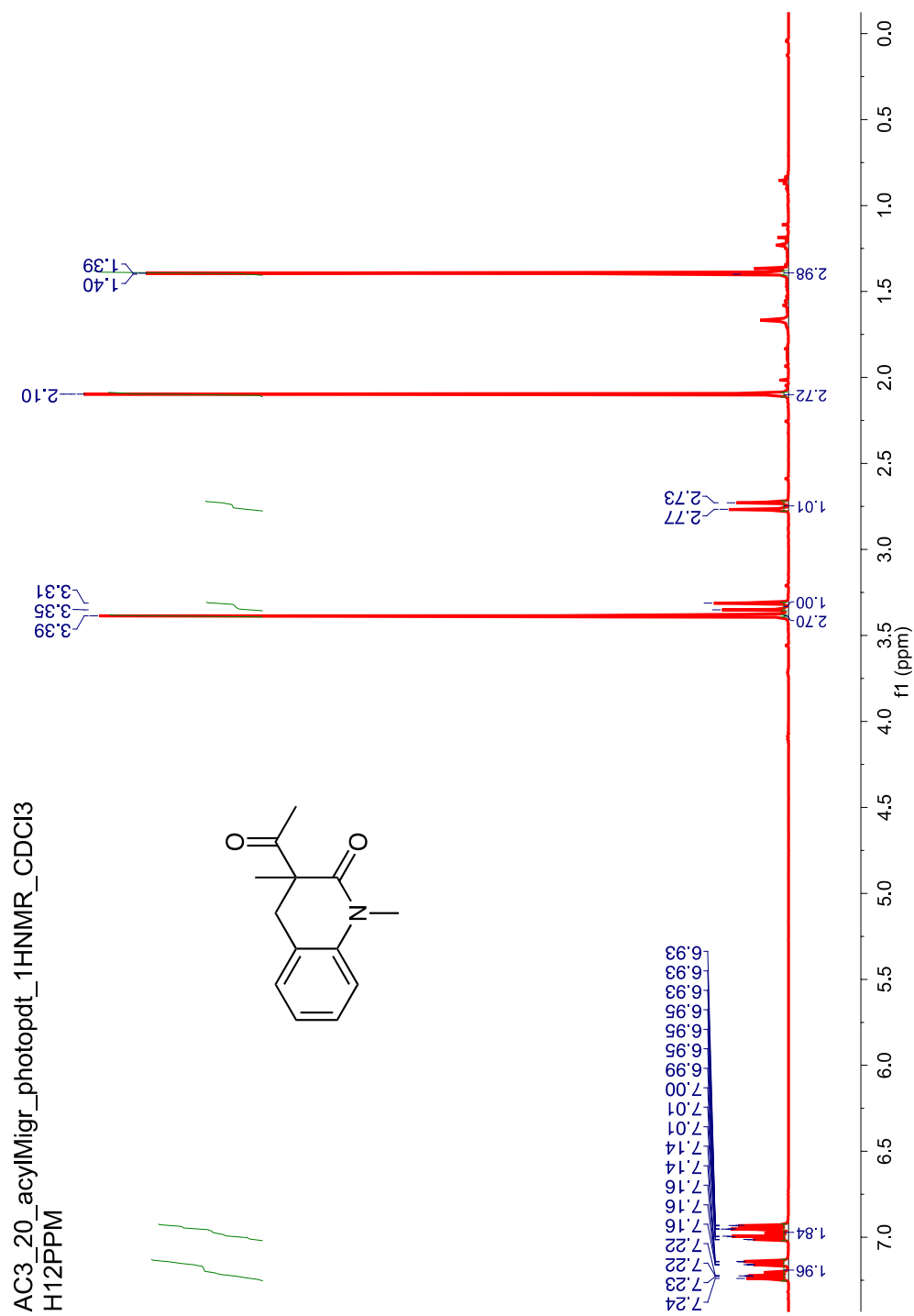


**Figure 3.25:**  $^1\text{H}$  NMR (400 MHz,  $\text{CDCl}_3$ ,  $\delta$  ppm) spectrum of acyl migration photoproduct **130a**.

$^{13}\text{C}$  NMR (100 MHz,  $\text{CDCl}_3$ ,  $\delta$  ppm) 170.9, 139.6, 128.4, 127.9, 124.4, 123.5, 114.8, 55.4, 35.5, 30.4, 26.2, 20.6.

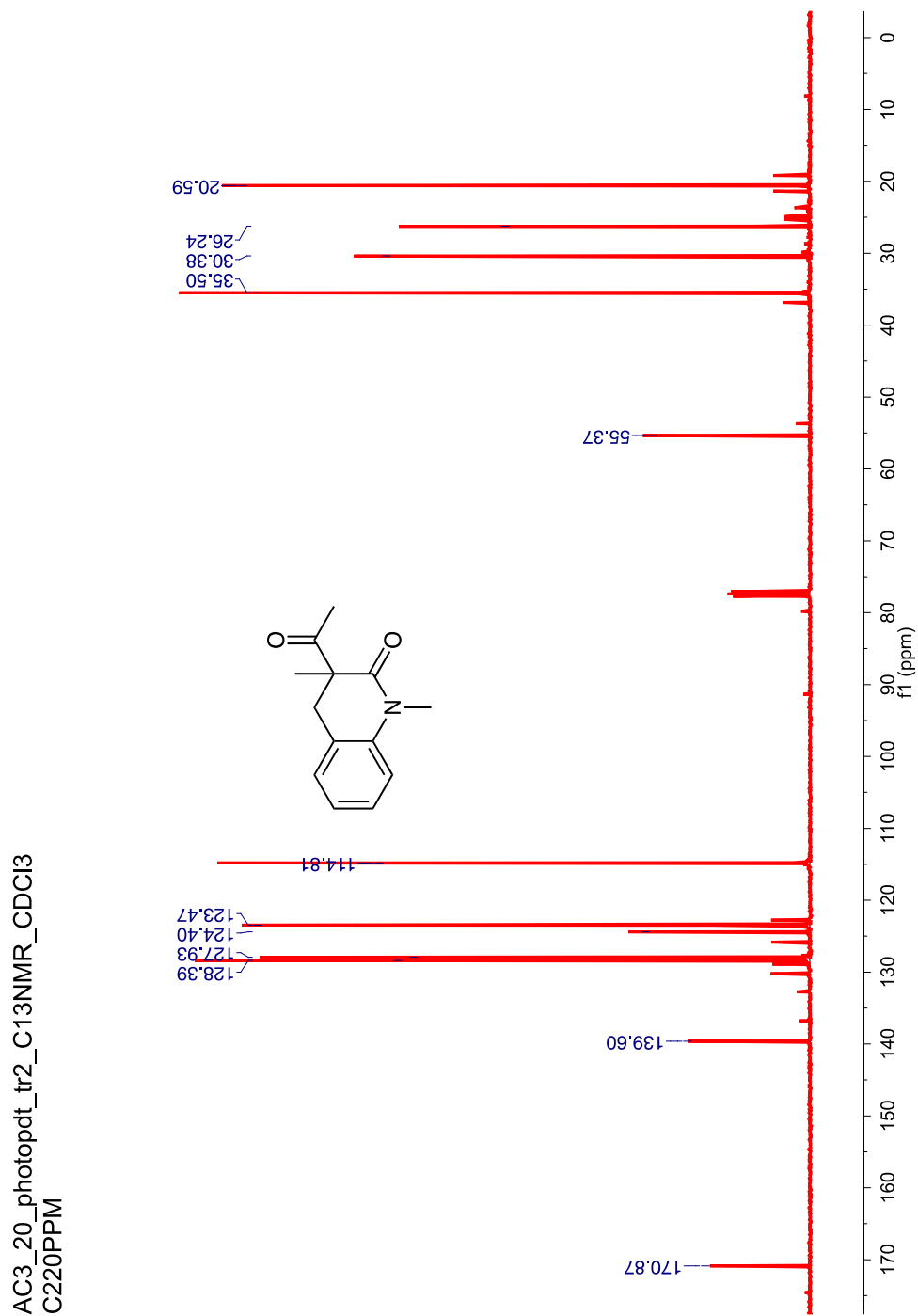


**Figure 3.26:**  $^{13}\text{C}$  NMR (100 MHz,  $\text{CDCl}_3$ ,  $\delta$  ppm) spectrum of acyl migration photoproduct 130a.



$^1\text{H}$  NMR (400 MHz,  $\text{CDCl}_3$ ,  $\delta$  ppm) mixture of rotamers 7.05-6.93 (m, 4H), 3.36 (s, 3H), 3.17 (d,  $J = 15.4$  Hz, 1H), 2.76 (d,  $J = 15.4$  Hz, 1H), 2.70 (s, 1H), 2.59 (s, 1H), 2.31 (s, 3H), 2.14 (s, 1H), 2.01 (s, 3H), 1.83 (s, 1H), 1.61 (s, 1H), 1.38 (s, 3H).

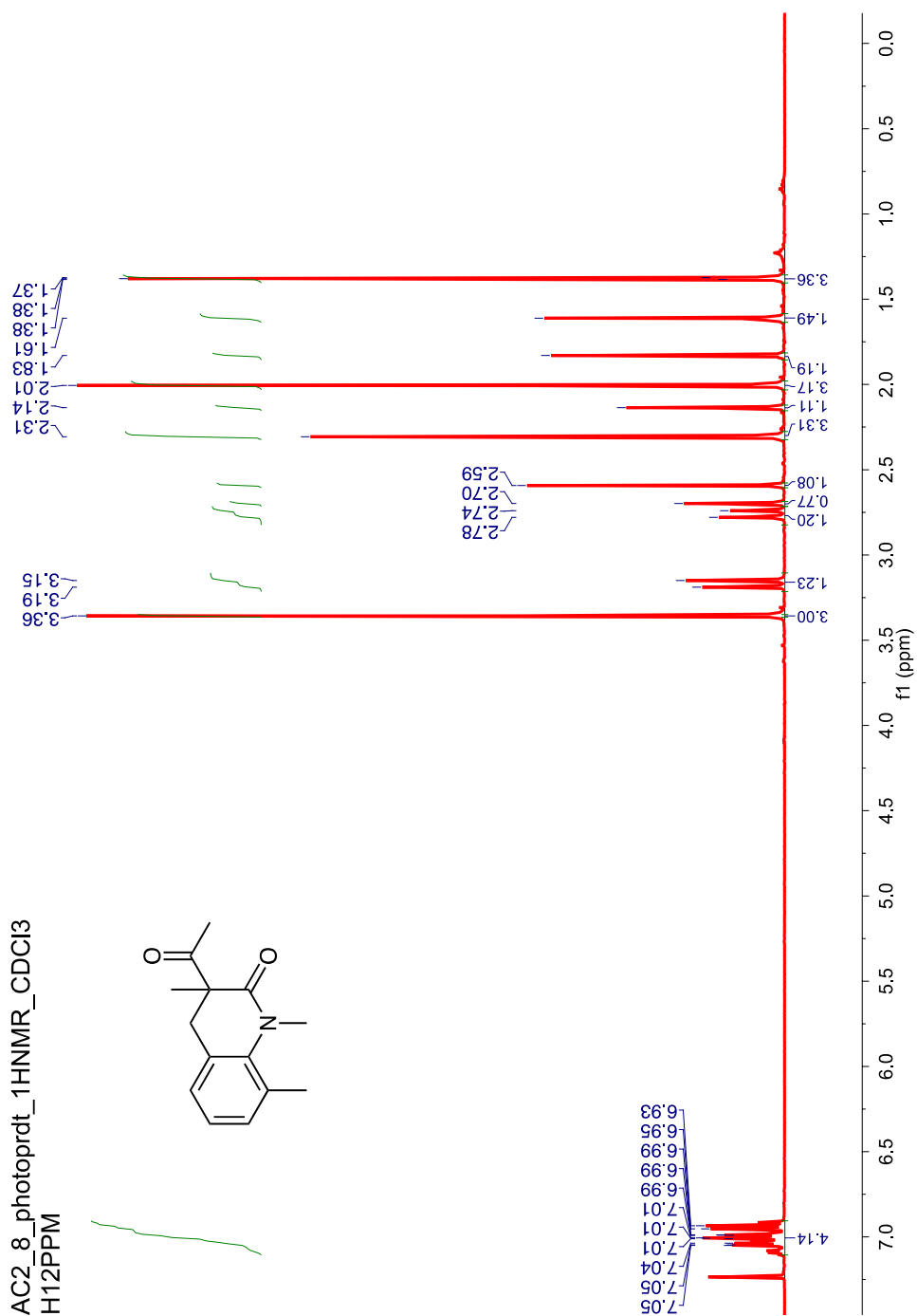


**Figure 3.27:**  $^1\text{H}$  NMR (400 MHz,  $\text{CDCl}_3$ ,  $\delta$  ppm) spectrum of acyl migration photoproduct 130b.

$^{13}\text{C}$  NMR (100 MHz,  $\text{CDCl}_3$ ,  $\delta$  ppm) Mixture of rotamers: 206.1, 174.6, 173.1, 140.0, 137.8, 136.1, 131.5, 130.9, 130.2, 128.6, 127.5, 125.7, 125.2, 124.5, 120.3, 91.2, 79.4, 56.2, 36.5, 36.2, 34.0, 29.7, 26.1, 25.1, 21.4, 20.8, 20.4, 19.3, 18.6

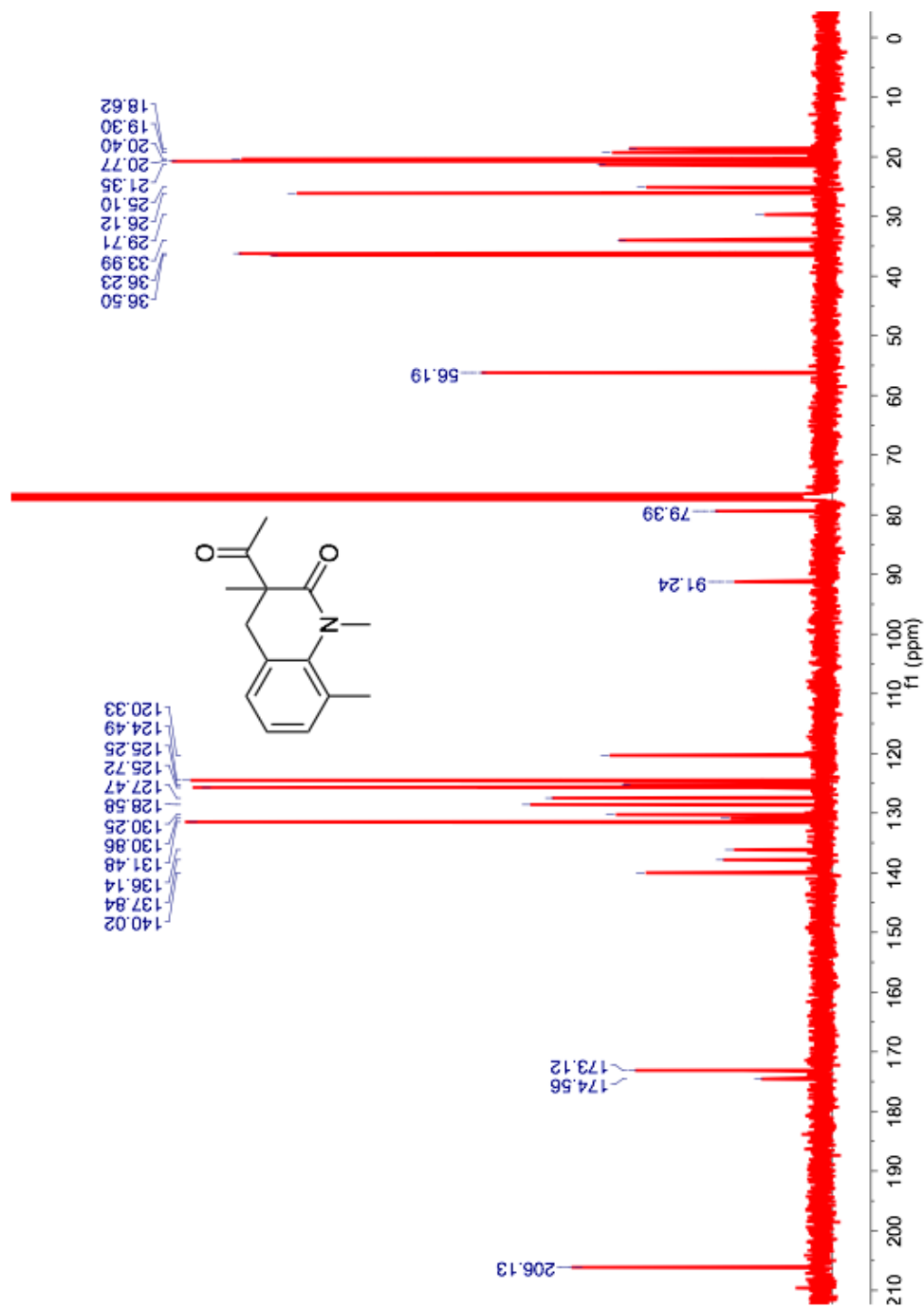


**Figure 3.28:**  $^{13}\text{C}$  NMR (100 MHz,  $\text{CDCl}_3$ ,  $\delta$  ppm) spectrum of **130b**.

$^1\text{H}$  NMR (400 MHz,  $\text{CDCl}_3$ ,  $\delta$  ppm) 7.05-6.92 (m, 3H), 3.48 (s, 3H), 3.35 (s, 3H), 3.19 (d,  $J = 15.3$  Hz, 1H), 2.80 (d,  $J = 15.3$  Hz, 1H), 2.32 (s, 3H), 1.47 (s, 3H).

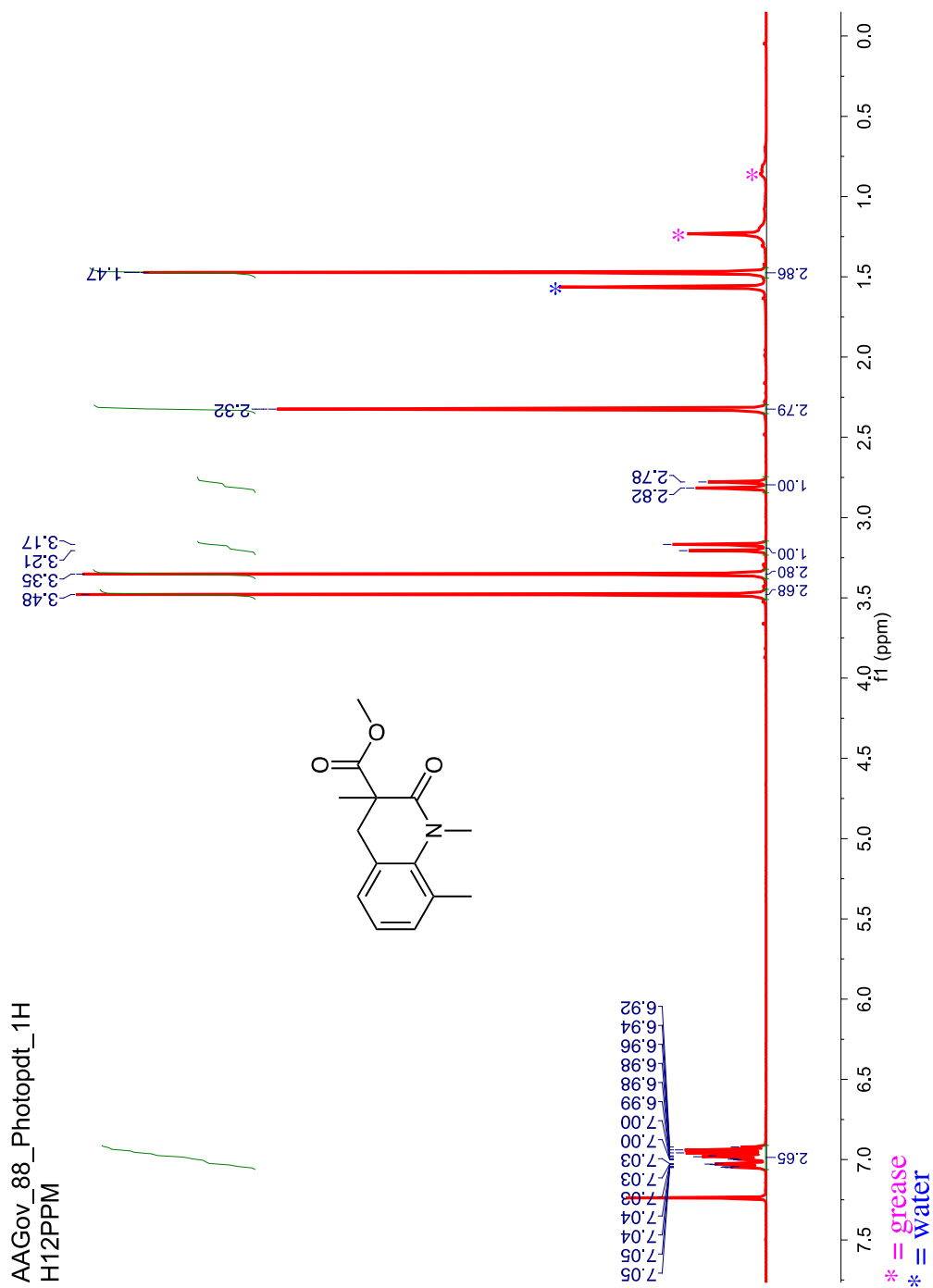


**Figure 3.29:**  $^1\text{H}$  NMR (400 MHz,  $\text{CDCl}_3$ ,  $\delta$  ppm) spectrum of acyl migration photoproduct **130c**.

$^{13}\text{C}$  NMR (100 MHz,  $\text{CDCl}_3$ ,  $\delta$  ppm) 172.6, 171.8, 140.3, 131.5, 128.1, 127.5, 125.6, 124.3, 52.4, 50.5, 37.5, 36.4, 29.7, 20.7, 20.6

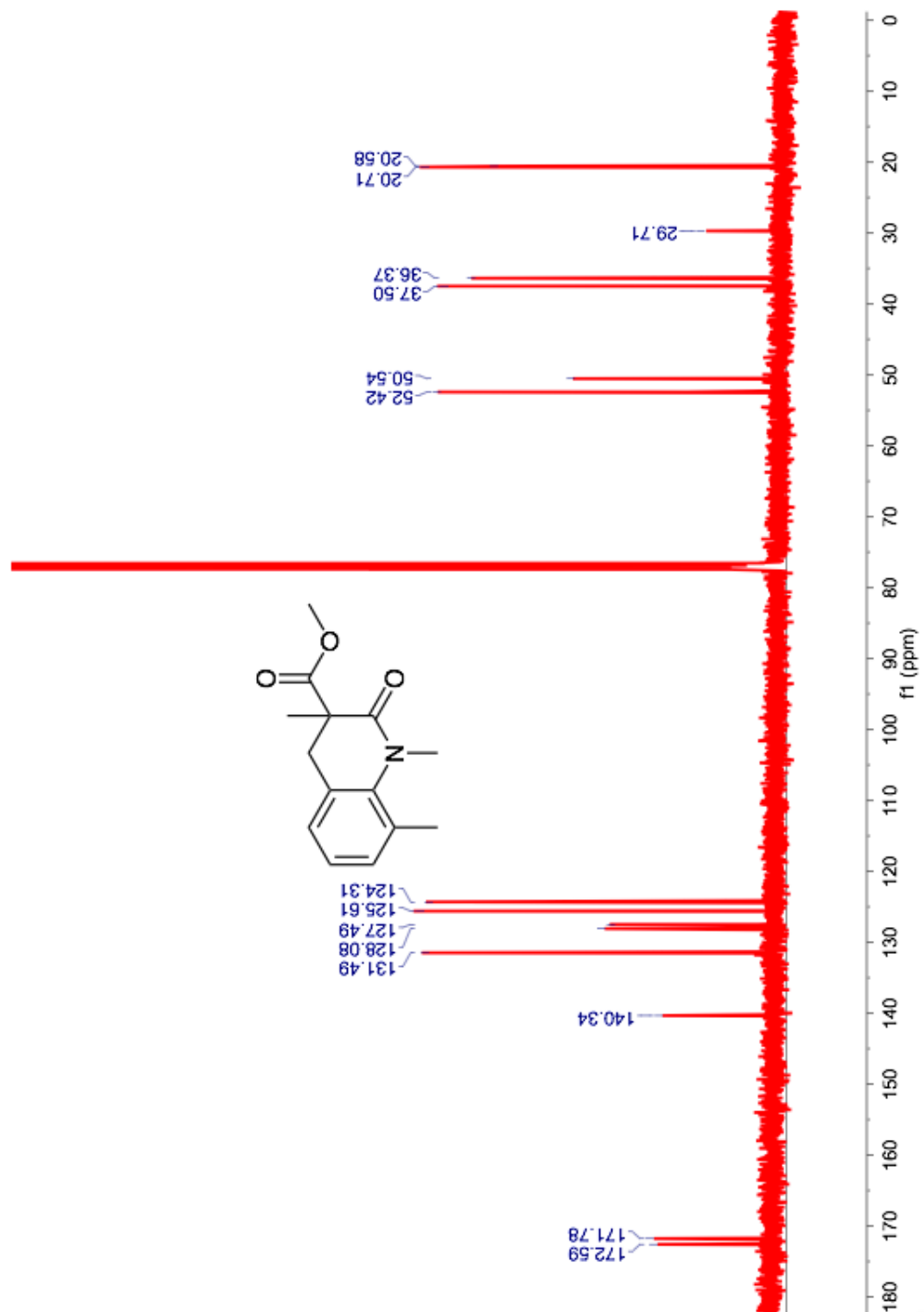


**Figure 3.30**  $^{13}\text{C}$  NMR (100 MHz,  $\text{CDCl}_3$ ,  $\delta$  ppm) spectrum of **130c**.

### 3.14.1. X-ray crystal structure data for acyl migration product 130b

**Table 3.6:** Crystal structure data for acyl migration product **130b**.

Compound	<b>130b</b>
Formula	C <sub>14</sub> H <sub>17</sub> NO <sub>2</sub>
FW	231.28
Cryst. Size_max [mm]	0.275
Cryst. Size_mid [mm]	0.138
Cryst. Size_main [mm]	0.03
Cryst. system	monoclinic
Space Group, Z	P2 <sub>1</sub> /c
a [Å]	12.7182 (4)
b [Å]	7.1694 (3)
c [Å]	13.6389 (5)
a [Å]	90
b [Å]	101.773 (2)
g [Å]	90
V [Å <sup>3</sup> ]	1217.46 (8)
ρ <sub>calc</sub> [g/cm <sup>3</sup> ]	1.262
m [mm <sup>-1</sup> ]	0.674
Radiation Type	Cu
(F000)	496
No of refl. (≥2s)	15011
No of indep. Refl.	2151
No of refl. (≥ 2s)	1745
Resolution [Å]	0.84
R <sub>1</sub> /WR <sub>2</sub> (≥2s) <sup>a</sup>	R <sub>1</sub> = 0.0462, wR <sub>2</sub> = 0.1263
R <sub>1</sub> /wR <sub>2</sub> (all data) <sup>a</sup> [%]	R <sub>1</sub> = 0.0569, wR <sub>2</sub> = 0.1337

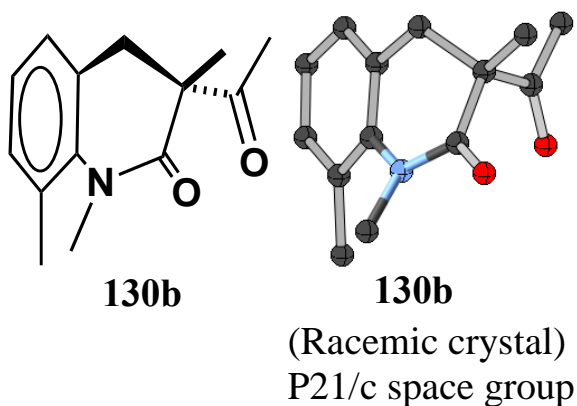


**Figure 3.31:** Photoproduct **130b** (crystallized from: hexanes/chloroform).

### 3.15. HPLC separation and analysis conditions for $\alpha$ -substituted atropisomeric acrylanilides

#### 114a-c and photoproducts 114a-c

*Note:* For **114a** and **114b** (-) and (+) are assigned based on the sign of CD spectra at 285 nm in methylenecyclohexane, for **114c** (-) and (+) are assigned based on the sign of CD spectra at 250 nm in MeOH. Peak-A (pkA) and Peak-B (pkB) refers to the elution order for a given pair of enantiomers on a chiral stationary phase.

HPLC separation and analysis conditions for 114a

HPLC separation conditions for **114a**

Column: (R,R) WHELK-O1; Abs. detector: 254 nm and 270 nm

Mobile phase: Hexanes:IPA= 98:2; Flow rate: 3 mL/min

Retention time (min): (-)-**114a** ~49.55 and (+)-**114a** ~51.22

HPLC analysis conditions for **114a**

Column: (R,R) WHELK-O1; Abs. detector: 254 nm and 270 nm

Mobile phase: Hexanes:IPA= 98:2; Flow rate: 1 mL/min

Retention time (min): (-)-**114a** ~47.50 and (+)-**114a** ~53.82

HPLC separation and analysis conditions for 114b

HPLC separation conditions

Column: (R,R) WHELK-O1; Abs. detector: 254 nm and 270 nm

Mobile phase: Hexanes:IPA= 98:2; Flow rate: 4 mL/min

Retention time (min): (-)-**114b** ~30.72 and (+)-**114b** ~40.52

HPLC analysis conditions

Column: (R,R) WHELK-O1; Abs. detector: 254 nm and 270 nm

Mobile phase: Hexanes:IPA= 98:2; Flow rate: 1 mL/min

Retention time (min): (-)-**114b** ~36.85 and (+)-**114b** ~45.57

HPLC separation and analysis conditions for 114c

HPLC separation conditions

Column: AD-H; Abs. detector: 254 nm and 270 nm

Mobile phase: Hexanes:IPA= 98:2; Flow rate: 3 mL/min

Retention time (min): (+)-**114c** ~13.42 and (-)-**114c** ~18.73

HPLC analysis conditions

Column: (R,R) WHELK-O1; Abs. detector: 254 nm and 270 nm

Mobile phase: Hexanes:IPA= 98:2; Flow rate: 1 mL/min

Retention time (min): (+)-**3c**: ~47.62 and (-)-**3c**: ~67.7

HPLC separation and analysis conditions for 115a

HPLC analysis conditions

Column: (R,R) WHELK-O1; Abs. detector: 254 nm and 270 nm

Mobile phase: Hexanes:IPA= 98:2; Flow rate: 1 mL/min

Retention time (min): (pkA)-**115b**: ~ 33.55 and (pkB)-**115b**: ~ 35.36

HPLC analysis conditions

Column: (R,R) WHELK-O1; Abs. detector: 254 nm and 270 nm

Mobile phase: Hexanes:IPA= 98:2; Flow rate: 1 mL/min

Retention time (min): (pk A)-**115b**: ~29.50 and (pkB)-**115b**: ~37.85

HPLC analysis conditions

Column: (R,R) WHELK-O1; Abs. detector: 254 nm and 270 nm

Mobile phase: Hexanes:IPA= 98:2; Flow rate: 1 mL/min

Retention time (min): (pkA)-**115c**: ~14.80 and (pkB)-**115c**: ~ 20.00



### 3.16. References

1. Chapman, O. L.; Adams, W. R., Photochemical transformations. XXII. Photoisomerization of Substituted Acrylic Acids and Acrylamides to .beta.-lactones and .beta.-lactams. *Journal of the American Chemical Society* **1968**, *90* (9), 2333-2342.
2. Cleveland, P. G.; Chapman, O. L. Y., Non-oxidative Photocyclization of Alkyl-substituted Acrylic Acid Anilides to Dihydrocarbostyrils. *Chemical Communications (London)* **1967**, *0* (20), 1064-1065.
3. Ogata, Y.; Takagi, K.; Ishino, I., Photocyclization of Acrylanilides. *The Journal of Organic Chemistry* **1971**, *36* (25), 3975-3939.
4. Turro, N. J.; Ramamurthy, V.; Scaiano, J. C., *Modern Molecular Photochemistry of Organic Molecules*. 2010; p 1084.
5. Lenz, G. R., Enamide photochemistry. Stereochemistry of Photocyclization of 1-ethylidene and 1-benzylidene 2-benzoyltetrahydroisoquinolines. *Journal of Organic Chemistry* **1976**, *41* (12), 2201-2207.
6. Bach, T.; Grosch, B.; Strassner, T.; Herdtweck, E., Enantioselective  $6\pi$ -Photocyclization Reaction of an Acrylanilide Mediated by a Chiral Host. Interplay Between Enantioselective Ring Closure and Enantioselective Protonation. *Journal of Organic Chemistry* **2003**, *68* (3), 1107-1116.
7. Ninomiya, I.; Yamauchi, S.; Kiguchi, T.; Shinohara, A.; Naito, T. Y., Photocyclisation of Enamides. Part V. Photocyclisation of Small  $\alpha$  small  $\beta$  -unsaturated Anilides. *Journal of the Chemical Society, Perkin Transactions 1* **1974**, *0* (0), 1747-1751.
8. Inoue, Y., Asymmetric Photochemical Reactions in Solution. *Chemical Reviews* **1992**, *92* (5), 741 - 770.

9. Ayitou, A. J.-L.; Ugrinov, A.; Sivaguru, J. Y., 6pi-Photocyclization of *O*-tert-butylacrylanilides. *N*-substitution Dictates The Regiochemistry of Cyclization. *Photochemical & Photobiological Sciences* **2009**, *8* (6), 751-754.
10. Ayitou, A. J.-L.; Sivaguru, J., Light-Induced Transfer of Molecular Chirality in Solution: Enantiospecific Photocyclization of Molecularly Chiral Acrylanilides. *The Journal of American Chemical Society* **2009**, *131* (14), 5036-5037.
11. Clay, A.; Kumarasamy, E.; Ayitou, A. J. L.; Sivaguru, J., Photochemistry of Atropisomers: Non-biaryl Atropisomers for Stereospecific Phototransformations. *Chemistry Letters* **2014**, *43* (12), 1816-1825.
12. Kumarasamy, E.; Ayitou, A. J. L.; Vallavoju, N.; Raghunathan, R.; Iyer, A.; Clay, A.; Kandappa, S. K.; Sivaguru, J., Tale of Twisted Molecules. Atropselective Photoreactions: Taming Light Induced Asymmetric Transformations through Non-biaryl Atropisomers. *Accounts of Chemical Research* **2016**, *49* (12), 2713-2724.
13. Dunbar, R. C., Complexation of Na<sup>+</sup> and K<sup>+</sup> to Aromatic Amino Acids: A Density Functional Computational Study of Cation- $\pi$  Interactions. *The Journal of Physical Chemistry A* **2000**, *104* (34), 8067-8074.
14. Ma, J. C.; Dougherty, D. A., The Cation- $\pi$  Interaction. *Chemical Reviews* **1997**, *97* (5), 1303-1324.
15. Raber, D. J.; Raber, N. K.; Chandrasekhar, J.; Schleyer, P. v. R., Geometries and Energies of Complexes Between Formaldehyde and First-and Second-row Cations. A Theoretical Study. *Inorganic Chemistry* **1984**, *23* (24), 4076-4080.
16. Hoyau, S.; Ohanessian, G., Interaction of Alkali Metal Cations (Li<sup>+</sup>-Cs<sup>+</sup>) with Glycine in The Gas Phase: A Theoretical Study. *Chem.-Eur. J.* **1998**, *4* (8), 1561-1569.

17. Sreenath, K.; Allen, J. R.; Davidson, M. W.; Zhu, L. Y., A FRET Based Indicator For Imaging Mitochondrial Zinc Ions. *Chemical Communications* **2011**, 47 (42), 11730-1132.
18. Jockusch, S.; Sivaguru, J.; Turro, N. J.; Ramamurthy, V., Direct Measurement of The Singlet Oxygen Lifetime in Zeolites by Near-IR Phosphorescence. *Photochemical & Photobiological Sciences* **2005**, 4 (5), 403-405.
19. Ramamurthy, V.; Casper, J. V.; Corbin, D. R.; Schlyer, B. D.; Maki, A. H., Triplet-state Photophysics of Naphthalene and  $\alpha$ ,  $\omega$ -diphenylpolyenes Included in Heavy Cation Exchanged Zeolites. *The Journal of Physical Chemistry* **1990**, 94 (9), 3391-3393.
20. Ramamurthy, V., *Photoprocesses of Organic Molecules included in Zeolites*. Wiley-VCH: New York, 1991; p 429-493.
21. Ramamurthy, V.; Caspar, J. V.; Kuo, E. W.; Corbin, D. R.; Eaton, D. F., Heavy-atom-Induced Phosphorescence of Aromatics and Olefins Included Within zeolites. *Journal of The American Chemical Society* **1992**, 114 (10), 3882-3892.
22. Sivaguru, J.; Sunoj, R. B.; Wada, T.; Origane, Y.; Inoue, Y.; Ramamurthy, V., Enhanced Diastereoselectivity via Confinement: Diastereoselective Photoisomerization of 2,3-Diphenylcyclopropane-1-carboxylic Acid Derivatives Within Zeolites. *Journal of Organic Chemistry* **2004**, 69, 6533-6547.
23. Lewis, F. D.; Barancyk, S. V., Lewis Acid Catalysis of Photochemical Reactions. Photodimerization and Cross-cycloaddition of Coumarin. *Journal of The American Chemical Society* **1989**, 105 (23), 8653-8661.
24. Ayitou, A. J.-L.; Sivaguru, J., Light-Induced Transfer of Molecular Chirality in Solution: Enantiospecific Photocyclization of Molecularly Chiral Acrylanilides. *Journal of the American Chemical Society* **2009**, 131 (14), 5036-5037.

25. Ayitou, A. J.-L.; Vallavoju, N.; Ugrinov, A.; Sivaguru, J., Enantiospecific  $6\pi$ -Photocyclization of atropisomeric  $\alpha$ -substituted acrylanilides in the solid-state: role of crystalline confinement on enantiospecificity. *Photochemical & Photobiological Sciences* **2011**, *2011* (10), 1380-1383.
26. Ayitou, A. J.-L.; Clay, A.; Kumarasamy, E.; Jockusch, S.; Sivaguru, J., Enantiospecific Photochemical  $6\pi$ -ring closure of  $\alpha$ -substituted Atropisomeric Acrylanilides - Role of Alkali Metal Ions. *Photochemical & Photobiological Sciences* **2014**, *13* (2), 141-144.
27. Ates, A.; Curran, D. P., Synthesis of Enantioenriched Axially Chiral Anilides from Atropisomerically Enriched Tartarate Ortho-Anilides. *Journal of the American Chemical Society* **2001**, *123* (21), 5130-5131.
28. Curran, D. P.; Hale, G. R.; Geib, S. J.; Balog, A.; Cass, Q. B. I.; Degani, A. L. G.; Hernandez, M. Z.; Freitas, L. C. G., Rotational Features of Carbon-Nitrogen Bonds in Axially Chiral *O*-tert-butyl Anilides and Related Molecules. Potential Substrates for The 'Prochiral Auxiliary' Approach to Asymmetric Synthesis. *Tetrahedron: Asymmetry* **1997**, *8* (23), 3955-3975.
29. Clayden, J., Atropisomers and Near Atropisomers: Achieving Stereoselectivity by Exploiting The Conformational Preferences of Aromatic Amides. *Chemical Communications* **2004**, (2), 127-135.
30. Degenhardt, C. F.; Lavin, J. M.; Smith, M. D.; Shimizu, K. D., Conformationally Imprinted Receptors: Atropisomers With "Write", "Save", and "Erase" Recognition Properties. *Organic Letters* **2005**, *7* (19), 4079-4081.
31. Montalti, M.; Credi, A.; Prodi, L.; Gandolfi, M. T., Handbook of Photochemistry. 3rd ed.; CRC press: Boca Raton, Fl., 2006; pp 617-623.

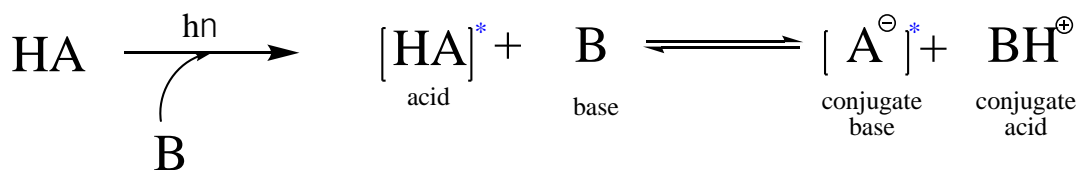
32. Ayitou, A. J.-L.; Jesuraj, J.; Barooah, N.; Ugrinov, A.; Sivaguru, J., Enantiospecific Photochemical Norrish/Yang Type II Reaction of Non-biaryl Atropchiral  $\alpha$ -Oxoamides In Solution – Axial to Point Chirality Transfer. *Journal of the American Chemical Society* **2009**, *131* (32), 11314–11315.
33. Ninomiya, I.; Kiguchi, T.; Yamauchi, S.; Naito, T. Y., Photocyclisation of enamides. Part 14. Substituent effects in the photocyclisation of N- small alpha , small beta-unsaturated acylanilides. *Journal of the Chemical Society, Perkin Transactions 1* **1980**, *0* (0), 197-202.
34. Nishio, T.; Tabata, M.; Koyama, H.; Sakamoto, M., Photochemistry of N-(2-Acylphenyl)-2-methylprop-2-enamides: Competition between Photocyclization and Long-Range Hydrogen Abstraction. *Helvetica Chimica Acta* **2005**, *88* (1), 78-86.
35. Vallavoju, N.; Sreenithya, A.; Ayitou, A. J. L.; Jockusch, S.; Sunoj, R. B.; Sivaguru, J., Photoreactions with a Twist: Atropisomerism-Driven Divergent Reactivity of Enones with UV and Visible Light. *Chemical European Journal* **2016**, *22* (32), 11339-11348.

## 4. EVALUATING EXCITED STATE ACIDITY OF BIOBASED PHOTOACIDS

### 4.1. Introduction

Acid base interactions are ever-present and central to interactions in chemical and biological systems.<sup>1-3</sup> Thus, the ability to govern these interactions by use of non-invasive external stimuli has been proven to be beneficial. Photoacids allow for control utilizing light as an external stimulus. Photoacids are compounds, often hydroxy substituted aromatics, that have an excited state acidity greater than its ground state acidity. Irradiation of an appropriately substituted chromophore affords proton dissociation in the excited state.<sup>4-9</sup> Credi and coworkers utilized a merocyanine based metastable photoacid to regulate the threading and dethreading of a pseudorotaxane molecular machine.<sup>10</sup> Huppert and coworkers investigated the ability of substituted hydroxypyrene photoacids' to transfer a proton to biopolymers chitin and cellulose highlighting the importance that excited state proton transfer (ESPT) processes may play in biological systems.<sup>11</sup>

Photoacidity is synonymous with the term excited state proton transfer. The excited state acidity arises due to proton dissociation (or transfer) to a solvent molecule or available base upon excitation. As photoacidity is a proton transfer processes the acidity thereof follows Brönsted acidity. Thus photoacids are Brönsted acids (Scheme 4.1), where HA can then be substituted as HA\* due to the absorbance of a photon.



**Scheme 4.1:** Brönsted acid base equilibrium of photoacid.

Förster explained the unusually large Stokes shift in the fluorescence of several aromatic dyes which included the naphthols.<sup>12</sup> He indicated that the observed Stokes shift was a

consequence of proton-transfer which resulted in the formation of the excited conjugate base (anion).<sup>7-9</sup> Realizing the relationship of the conjugate acid and conjugate base and the observable optical properties, Förster recognized that a thermodynamic cycle could estimate the change in acidity upon excitation. The Förster cycle is a thermodynamic cycle, it connects the optical properties of the photoacid and conjugate photobase with the thermodynamic properties of the excited-state proton transfer process. Practically speaking, the Förster cycle gives a rough estimation of the photoacidity without unveiling any information regarding the molecular process(s) involved. Time resolved measurements provide a more direct method of determining photoacidity. However, limitations such as instrumentation and emission quantum yields most often hinder such measurements.

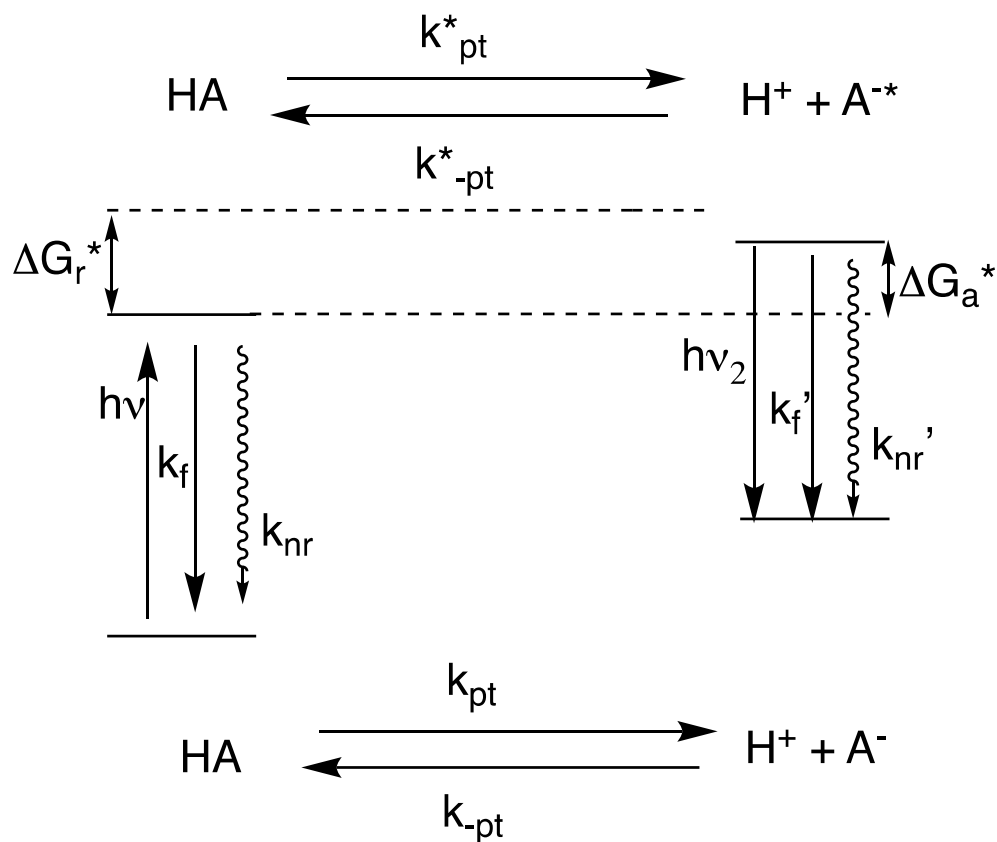


**Figure 4.1:** Depiction of thermodynamic cycle (Förster Cycle) for proton transfer and decay processes in reversible photoacids.<sup>7</sup>

$$pK_a^* = pK_a + (E_{A^-} - E_{HA})/2.3RT.^1 \quad (4.1)$$

Where,

$pK_a^*$  = excited state  $pK_a$

$E_{A^-}$  = Energy corresponding to 0,0 transition of  $S_0$  to  $S_1$  of conjugate base

$E_{HA}$  = Energy corresponding to 0,0 transition of  $S_0$  to  $S_1$  of conjugate acid

R = Ideal gas constant (8.31 J/(Kmol))

T = Temperature in Kelvin (K)

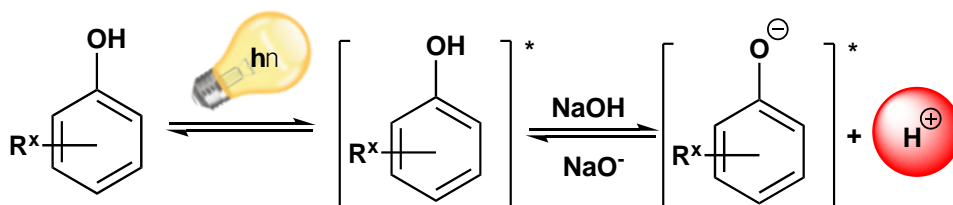
The Förster cycle finds great utility since it allows for the estimation of the excited-state acidity of photoacids employing readily obtainable optical measurements establishing the correlation between ground-state acidity and excited-state acidity allowing for the treatment of both in a similar fashion from a thermodynamic point of view.<sup>7-9</sup> It is worth mentioning that the Förster cycle alone does not validate or prove photoacidity.

## 4.2. Biobased vanillin derived photoacids

Since the turn of the century conscious efforts have been made towards eco-friendly scientific advancements which includes petro-chemical free innovations. Developing molecules and materials from sustainable renewable sources is becoming an increasing aspiration for scientists of varying disciplines. Lignin is found in wood type plants consisting of a highly polymerized matrix. Lignin is actually the main component in wood. Lignin is the second most abundant biopolymer in the world.<sup>13-15</sup> Various industries including the paper industry has lignin as a byproduct by way of aromatic small molecule derivatives.<sup>16</sup> Finding utility for these small molecule derivatives aids in the march towards sustainability and has the potential to unearth interesting chemistry. These efforts are intimately tied to sustainability, reducing reliance on fossil fuels as well as utilizing biobased feed stocks. Vanillin and its analogs, biobased feedstocks obtainable from lignin, afforded us a scaffold with unique substitution pattern.



Vanillins include an hydroxy arene ripe for investigation which is in line with green chemistry efforts, to forge high utility molecules from green sustainable sources. As substitution and functionality can alter the extent and/or efficacy of photoacidity we were interested in evaluating the feasibility of vanillin derivatives as photoacids.



**Scheme 4.2:** Photoacidity of phenols

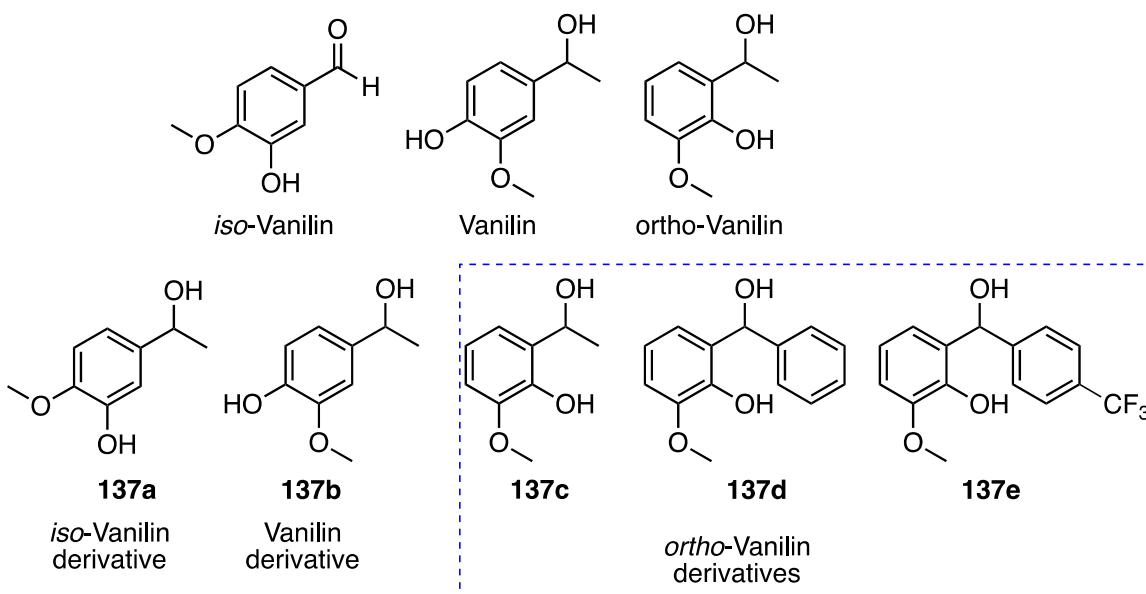
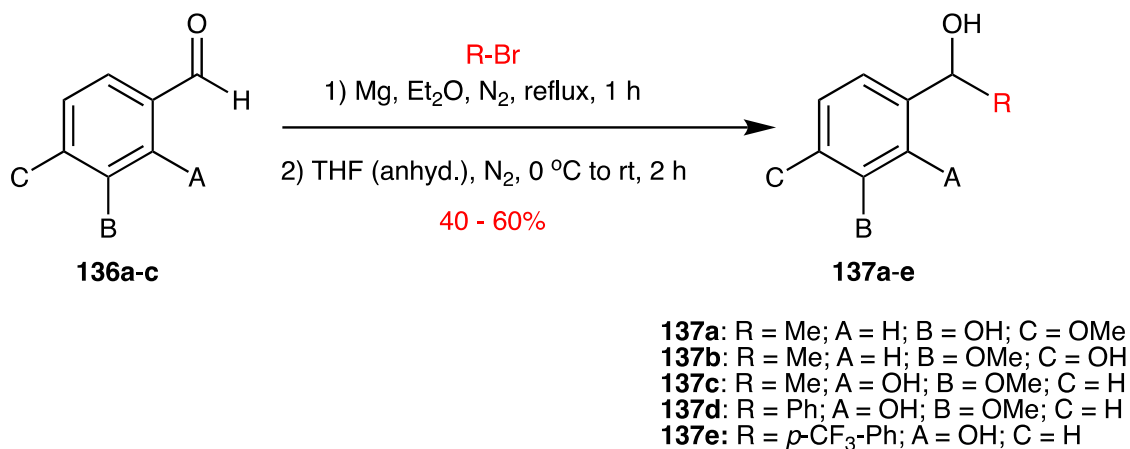


**Chart 4.1:** Vanillin analogs and derivatives.

### 4.3. Photoacidity of vanillin derivatives



**Scheme 4.3:** Synthesis of biobased photoacids

Vanillin and its derivatives feature a phenol substitution, a necessity with respect to reversible photoacids. The vanillin scaffold allowed us an opportunity to evaluate its excited state acidity. However, due to the presence of a carbonyl group the lowest excited state chemistry in these systems is likely  $n\pi^*$  in nature. In contrast, photoacidity is most predominant in phenolic systems with  $\pi\pi^*$  lowest excited states. This necessitated a simple structural modification. Employing Grignard reaction (Scheme 4.3) enabled us to vary the functionality in a systematic fashion which allowed us to investigate the photoacidity of vanillin derivatives 137a-e. The extent and/or existence of excited state proton transfer, photoacidity, was evaluated in terms of  $pK_a^*$  (photoacidity constant). The  $pK_a^*$  was determined from UV/Vis spectra in aqueous solution at varying pH. HCl and NaOH, as acid and base respectively, were used to adjust the pH. Figure 4.2 displays the pH dependent absorbance spectra of 137a (0.05 mM) and the resulting  $\alpha$ -plot. Upon addition of HCl (increased acidity) there was marginal change in the absorbance with absorbance maxima ( $\lambda_{\text{max}}$ ) at 278 nm. Decrease in absorbance between 267 - 279 nm with a simultaneous increase in absorbance between 279 - 315 nm, featuring two new relative maxima at 242 nm and 293 nm were observed upon addition of base (NaOH). In the

basic aqueous solution, the relative maxima of 137a differed in both wavelength and intensity with respect to that in acid aqueous solution. Inspection of the pH dependent absorbance spectra displayed four new isobestic points (224, 231, 267, and 279 nm). The appearance of the four isobestic points, indicates a smooth transition from one species to another namely conjugate acid to conjugate base, from acidic solution to basic solution respectively. This behavior is similar to phenol derivatives reported in literature.<sup>7, 17</sup>

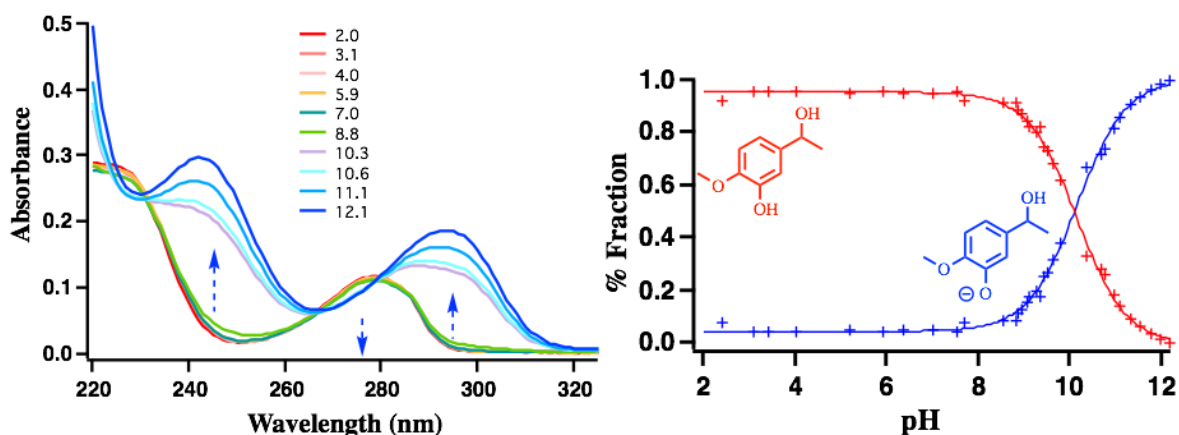


**Figure 4.2:** Left: Absorbance of 137a at various pH in aqueous solution. [137a] = 0.05 mM. Right:  $\alpha$ -plot of 137a in acidic (HCl) and basic (NaOH) aqueous solution. [137a] = 0.05 mM;

From the pH dependent absorbance spectrum an  $\alpha$ -plot was constructed. Figure 4.2 right displays the  $\alpha$ -plot depicting the pH dependent mol% of conjugate acid and conjugate base in aqueous solution. The  $\alpha$ -plot ranges between pH 2-12 with only one intersection indicating a well behaved system. Upon inspection of the  $\alpha$ -plot it can be seen that below pH = 8 the equilibrium is shifted towards that of the conjugate acid. Not until above pH = 8 was the rise of the conjugate base noticed. Intersection of the conjugate acid and conjugate base yields the ground state pKa. The pK<sub>a</sub> of 137a was pK<sub>a</sub> = 10.1. Similarly, the ground state acidity of vanillin derivatives 137b-137e were determined (Table 1).

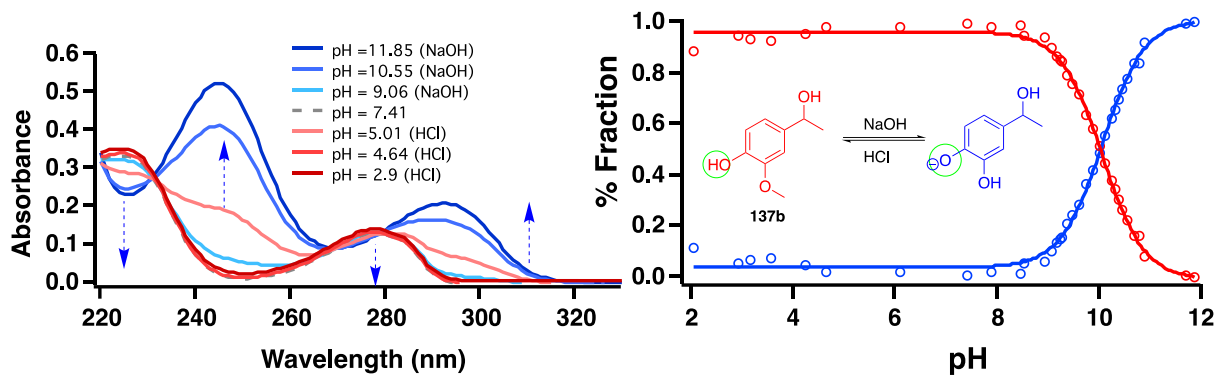


**Figure 4.3:** Left: pH dependence of conjugate acid vs conjugate base in aqueous solution and Right:  $\alpha$ -plot of **137b**; [**137b**] = 0.05 mM.

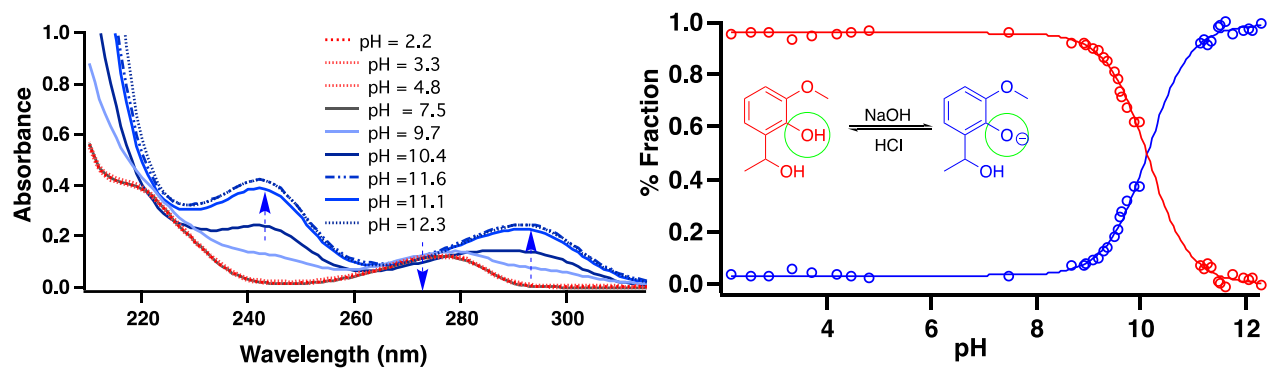


**Figure 4.4:** Left: pH dependence of conjugate acid vs conjugate base in aqueous solution and Right:  $\alpha$ -plot of **137c**. [**137c**] = 0.05 mM;

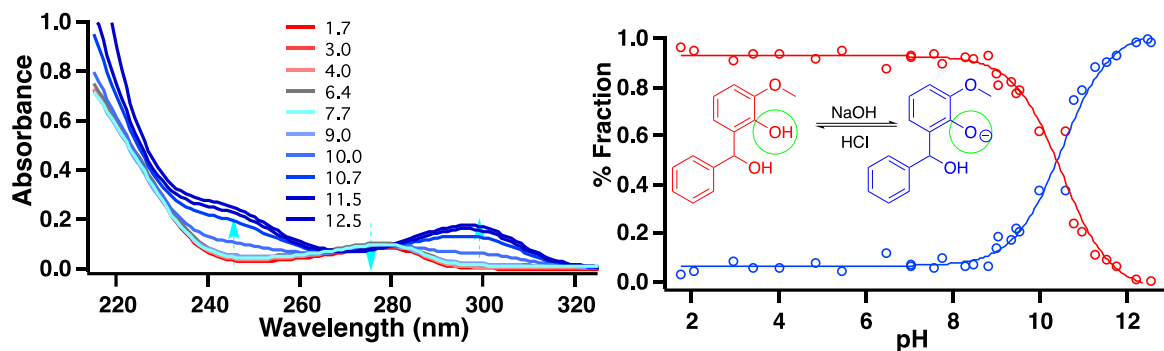


**Figure 4.5:** Left: pH dependence of conjugate acid vs conjugate base in aqueous solution and Right:  $\alpha$ -plot of **137d**. [**137d**] = 0.05 mM;

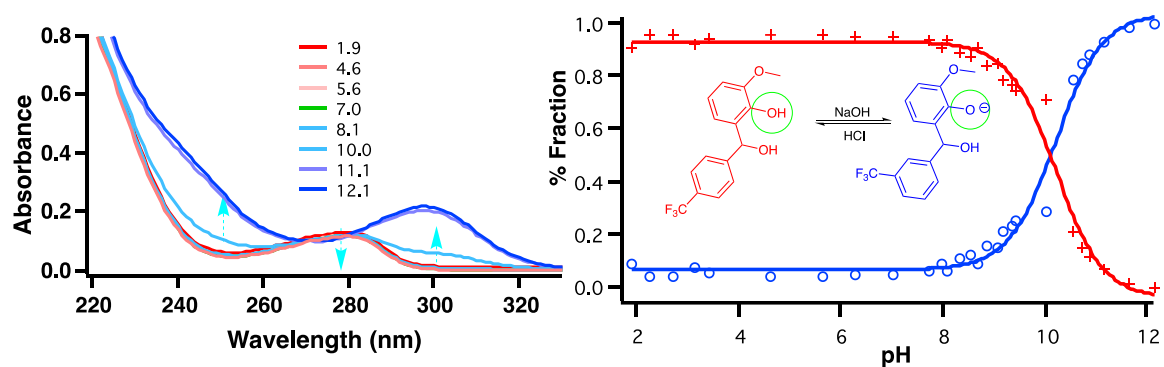


**Figure 4.6:** Left: pH dependence of conjugate acid vs conjugate base in aqueous solution and Right:  $\alpha$ -plot of **137e**. [**137e**] = 0.05 mM;

In route to determining the photoacidity, the fluorescence spectra of 137a were recorded in acidic and basic aqueous solutions (Figure 4.7). Inspection of Figure 4.7 shows that the fluorescence decreased upon changing the pH from acidic to basic. At pH 10.4 only 2% fluorescence was observable compared to pH 2.7, which further decreased at higher pH. Evidenced by the overlap of absorbance and corresponding excitation spectra ( $\lambda_{\text{emission}} = 320$  nm) the respective emission spectra ( $\lambda_{\text{exc}} = 265$  nm) was determined to result from emission of conjugate acid in acidic pH up to pH 11 (Figure 4.6). At pH 12 the emission of the conjugate acid was completely quenched. After adjusting the OD at  $\lambda_{\text{exc}}$  (OD = 0.2) weak emission of the conjugate base was observed (Figure 4.6 left inset). This was evidenced by overlap of

absorbance spectra and excitation emission spectra of the conjugate base in basic solution (Figure 4.6 bottom right).

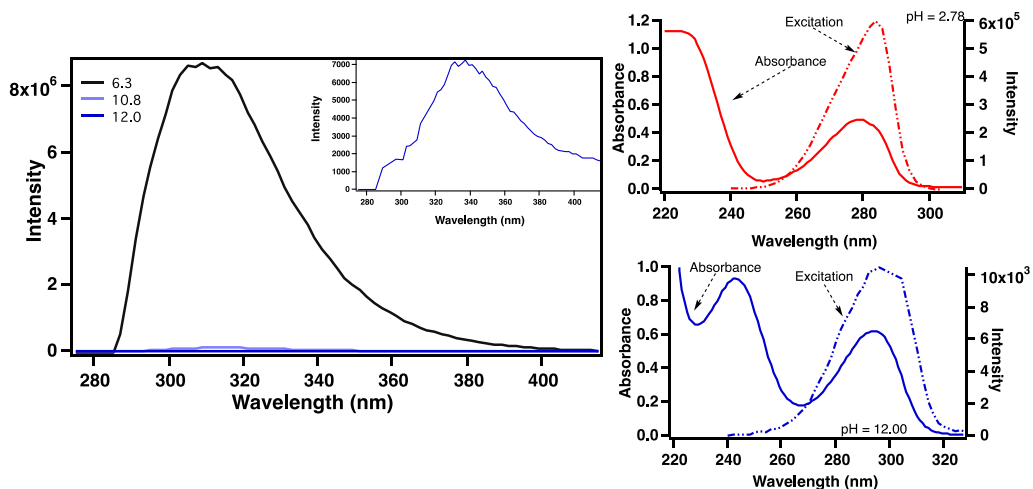


**Figure 4.7:** Top left - pH dependent fluorescence spectra of **137a**  $\lambda_{exc} = 265$  nm; OD @  $\lambda_{exc} \approx 0.2$ ; Top right: excitation spectra recorded in acidic aqueous solution.  $\lambda_{em} = 309$  nm,  $\lambda_{exc} = 240 - 304$  nm; Bottom right: excitation spectra recorded in basic aqueous solution.  $\lambda_{em} = 335$  nm,  $\lambda_{exc} = 240 - 330$  nm; HCl and NaOH used to adjust pH in acidic and basic aqueous solutions respectively.

In the cases of 137b,c the emission was observable under acidic conditions, while there was no observable emission under similar basic conditions (Figures 4.9-4.10). Due to the lack of emission, we were restricted to employing the absorbance maxima of the acid ( $E_{HA}$ ) and the conjugate base ( $E_A$ ) in the Förster cycle (Eq 4.1)<sup>8</sup> to estimate the excited state acidity ( $pK_a^*$ ) (Table 4.1).<sup>2</sup>

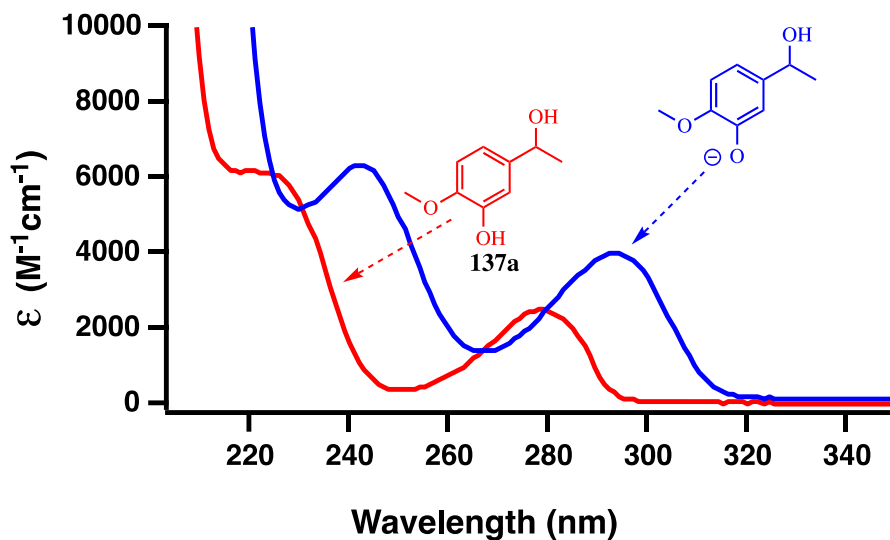


**Figure 4.8:** Molar extinction coefficient of **137a** (red) and conjugate base (blue) recorded in aqueous solution.  $[137a] = 0.05 \text{ mM}$ ; HCl and NaOH used respectively to adjust pH.

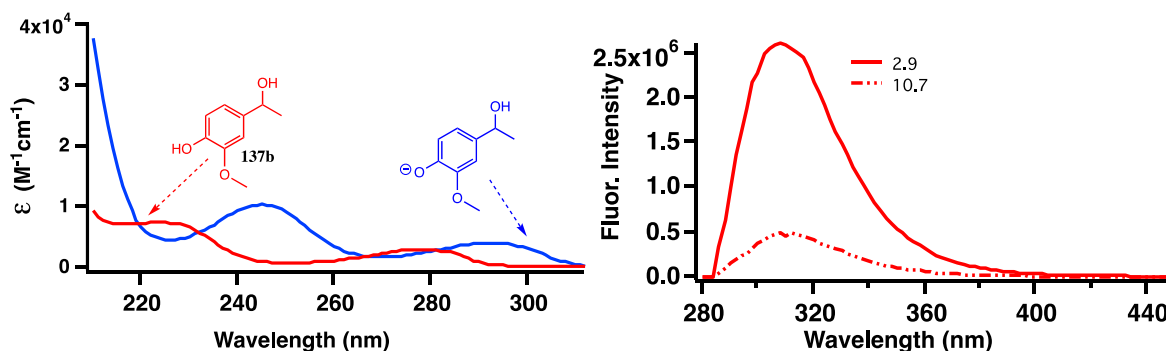


**Figure 4.9:** Molar extinction coefficient of **137b** (red) and conjugate base (blue) recorded in aqueous solution.  $[137b] = 0.05 \text{ mM}$ ; HCl and NaOH used respectively to adjust pH. Right: Fluorescence of **137b** at pH = 2.9 and decreased fluorescence at pH = 10.7 in aqueous solution.  $OD@ \lambda_{exc} \approx 0.2$ . HCl and NaOH used respectively to balance pH.  $\lambda_{exc} = 269 \text{ nm}$ . No fluorescence was observed upon adding more NaOH.

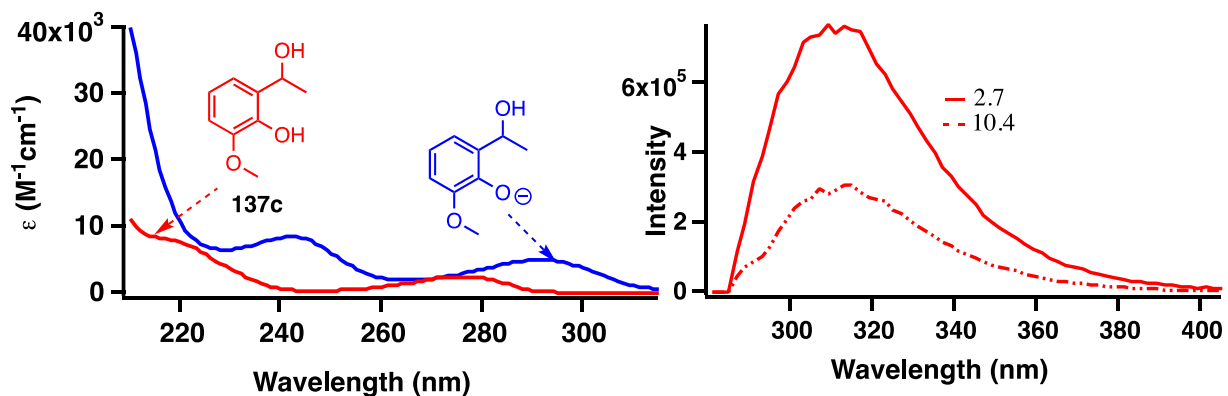


**Figure 4.10:** Left: Molar extinction coefficient of 137c (red) and conjugate base (blue) recorded in aqueous solution.  $[137c] = 0.05$  mM HCl and NaOH used respectively to adjust pH. Right: Fluorescence of 137c at pH = 2.7 and decreasing fluorescence at pH = 10.4. HCl and NaOH used respectively to adjust pH.  $\lambda_{exc} = 268$  nm. No fluorescence was observed upon adding more NaOH.

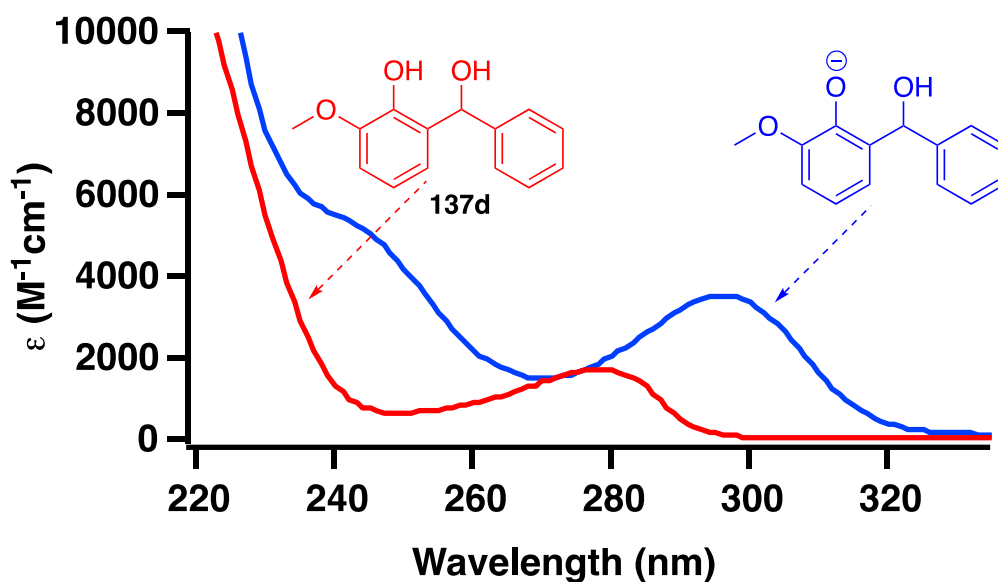


**Figure 4.11:** Molar extinction coefficient of conjugate acid (red) and conjugate base (blue) of **137d** recorded in aqueous solution.  $[137d] = 0.05$  mM. HCl and NaOH used respectively to adjust pH. No observable emission from either the conjugate acid nor conjugate base under similarly employed conditions as derivatives **137a-c**.



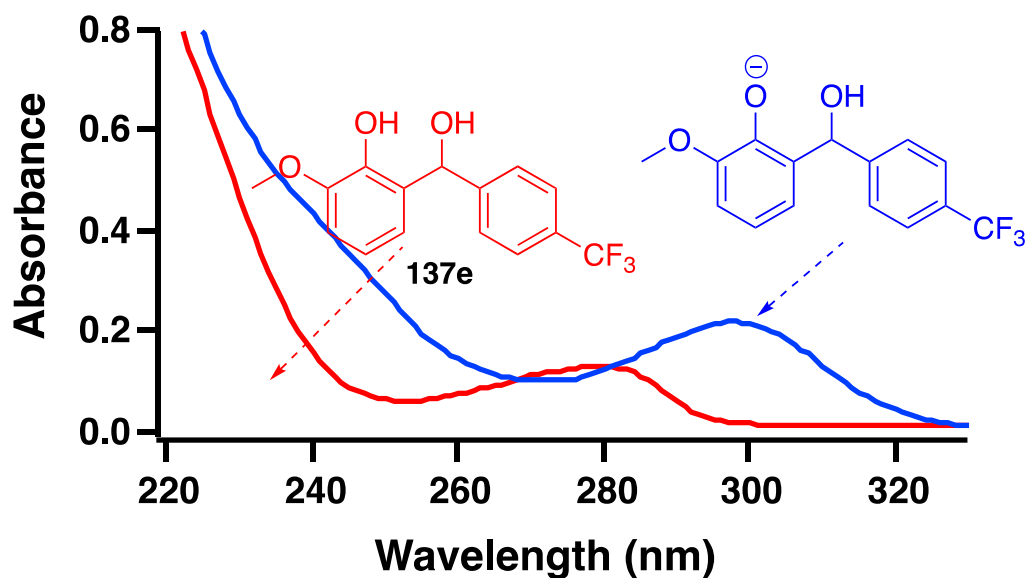


**Figure 4.12:** Absorbance spectrum of conjugate acid (red) and conjugate base (blue) of **137e** recorded in aqueous solution. [**137e**] = 0.05 mM. HCl and NaOH used respectively to adjust pH. No observable emission from either the conjugate acid nor conjugate base under similarly employed conditions as derivatives **137a-d**.

**Table 4.1:** Ground and excited state acidity of vanillin derivatives **137a-e**<sup>a</sup>

entry	cmpd	pK <sub>a</sub>	$\lambda_{\max}$ (nm) <sup>b</sup> at acidic conditions	$\lambda_{\max}$ (nm) <sup>b</sup> at basic conditions	pK <sub>a</sub> <sup>*b</sup>	$\Delta$ pK <sub>a</sub>
1	<b>137a</b>	10.1	278	293	6.2	3.8
2	<b>137b</b>	10.0	278	292	6.4	3.6
3	<b>137c</b>	10.0	276	292	5.8	4.2
4	<b>137d</b>	10.3	278	296	5.7	4.3
5	<b>137e</b>	10.1	279	298	5.3	4.8

<sup>a</sup>**137a-d** = 0.5 mM. HCl and NaOH were utilized to balance the acidity. <sup>b</sup>Data reported from  $\lambda_{\max}$  of absorbance spectra recorded in pH adjusted aqueous solution utilizing the Förster equation.

There are inherent limitations in employing the Förster cycle especially with respect to utilizing only absorbance maxima for estimations.<sup>8</sup> However, by looking at the process from a thermodynamic perspective the Förster cycle does provide a simple and readily employable method to evaluate the photo-acidity. Thus Förster cycle provides a simple and effective way to

estimate the changes in acidity of a compound upon interaction with light. Inspection of Table 4.1 displays that the acidity of vanillin derivatives **137a-e** increases (by 4 pK<sub>a</sub> units) upon excitation with light. In other words, the acidity of the vanillin derivatives was greater in the excited state than in the ground state, thus photoacidity was observed. We also noticed that the *ortho*-vanillin derivatives (**137c-e**) were comparatively more acidic than the *iso*-vanillin and parent vanillin compounds. Additionally, vanillin derivative bearing the CF<sub>3</sub> (electron withdrawing group) functionality in the para-position of the distal ring afforded the greatest acidity in the excited state. Substitution of the distal aromatic ring proved to alter the excited state acidity more so than the ground state acidity (Table 4.1, entry 5). It is likely that both inductive and mesomeric effects aid to stabilize the anion upon deprotonation in the excited state.<sup>7,9</sup> Our investigation unveiled that the vanillin derived photoacids are actually less acidic in the excited state compared to mono-substituted phenol derivatives whose excited state acidity (pK<sub>a</sub><sup>\*</sup>) is near 3.<sup>17,18</sup> Examining the structure of vanillin derived photoacids indicates that the methoxy and alkyl substituents contribute to positive mesomeric effect leading to the decreased stability of the phenoxide. This in turn exhibits the diminished acidity of vanillin derivatives that is noticed when compared to mono-substituted phenols.

#### 4.4. Summary and outlook

Vanillin derivatives were subjected to Grignard reaction in order to synthesize operable photoacids. Vanillin derived photoacids were synthesized and their photoacidity was evaluated. The emission intensity decreased in the presence of strong base. The excited state acidity of vanillin derivatives is greater than that of their ground state. The *ortho*-vanillin derivatives **137d-e** were more acidic in the excited state than the corresponding *iso*-vanillin and vanillin derivatives. The positive mesomeric effect of the substituents in the naturally occurring vanillin

chromophore play a crucial role in the extent of the excited state acidity. We are currently evaluating the role of different substituents to modulate the acidity of these compounds in materials.

## 4.5. Experimental section

### 4.5.1. General methods

All commercially obtained reagents/solvents were used as received; chemicals were purchased from Alfa Aesar<sup>®</sup>, Sigma-Aldrich<sup>®</sup>, Acros organics<sup>®</sup>, TCI America<sup>®</sup>, Mallinckrodt<sup>®</sup>, and Oakwood<sup>®</sup> Products, and were used as received without further purification. Nanopure water was obtained. Unless stated otherwise, reactions were conducted in oven-dried glassware under nitrogen atmosphere. <sup>1</sup>H-NMR and <sup>13</sup>C-NMR spectra were recorded on Bruker 400 MHz (100 MHz for <sup>13</sup>C) and on 500 MHz (125 MHz for <sup>13</sup>C) spectrometers. Data from the <sup>1</sup>H-NMR spectroscopy are reported as chemical shift ( $\delta$  ppm) with the corresponding integration values. Coupling constants ( $J$ ) are reported in hertz (Hz). Standard abbreviations indicating multiplicity were used as follows: s (singlet), b (broad), d (doublet), t (triplet), q (quartet), m (multiplet) and virt (virtual). Data for <sup>13</sup>C NMR spectra are reported in terms of chemical shift ( $\delta$  ppm). High-resolution mass spectrum data in Electrospray Ionization mode were recorded on a Bruker – Daltronics<sup>®</sup> BioToF mass spectrometer in positive (ESI+) ion mode.

UV-Vis spectra were recorded on Carey 300 UV-Vis spectrometer using UV quality fluorimeter cells (with range until 190 nm) purchased from Luzchem. When necessary, the compounds were purified by combiflash equipped with dual wavelength UV-Vis absorbance detector (Teledyne ISCO) using hexanes:ethyl acetate as the mobile phase and Redisep<sup>®</sup> cartridge filled with silica (Teledyne ISCO) as stationary phase. In some cases, compounds were purified by column chromatography on silica gel (Sorbent Technologies<sup>®</sup>, silica gel standard

grade: porosity 60 Å, particle size: 230 x 400 mesh, surface area: 500 – 600 m<sup>2</sup>/g, bulk density: 0.4 g/mL, pH range: 6.5 – 7.5).

#### **4.5.2. Photophysical methods**

Spectrophotometric solvents (Sigma-Aldrich<sup>®</sup>) were used whenever necessary unless or otherwise mentioned. UV quality fluorimeter cells (with range until 190 nm) were purchased from Luzchem<sup>®</sup>. Emission spectra were recorded on a Horiba Scientific<sup>®</sup> Fluorolog 3 spectrometer (FL3-22) equipped with double-grating monochromators, dual lamp housing containing a 450-watt CW xenon lamp and a UV xenon flash lamp (FL-1040), Fluorohub/MCA/MCS electronics and R928 PMT detector. Emission and excitation spectra were corrected in all the cases for source intensity (lamp and grating) and emission spectral response.

### **4.6. General procedure for synthesis of vanillin derived photoacids 137a-e**

#### **4.6.1. Synthetic procedure for the synthesis of vanillin derived photoacids 137a-e**

A clean oven dried round bottom flask equipped with stir bar, and vanillin analog namely vanillin, *iso*-vanillin or *ortho*-vanillin (1 equiv), was evacuated and purged with N<sub>2</sub> followed by dissolution in tetrahydrofuran (THF). The mixture was cooled to 0 °C followed by dropwise addition of the corresponding Grignard reagent (3 equiv.) (methyl magnesium bromide in diethyl ether or phenyl magnesium derivative in diethyl ether). The reaction mixture was allowed to slowly rise to room temperature and stir for 12 hours. After approximately 12 hours the reaction was cooled to 0 °C and quenched with sat'd. NH<sub>4</sub>Cl<sub>(aq)</sub> (10 mL). The organic and aqueous layers were separated. The organic phase was washed with 2 N HCl, distilled water, extracted with ethyl acetate (EtOAc) (3 x30 mL). The organic layers were combined then washed with NaHCO<sub>3</sub> (10 mL), H<sub>2</sub>O, and brine then H<sub>2</sub>O, followed by drying over NaSO<sub>4</sub> (anhyd.) then concentrated

in vacuo. The crude reaction mixture was purified over silica gel with 20/80 EtOAc/Hex as eluent. The products were obtained as viscous clear liquids (30 – 65% yield).

$^1\text{H}$  NMR (500 MHz,  $\delta$  ppm,  $\text{CDCl}_3$ ) 6.92 (d,  $J = 2.0$  Hz, 1H), 6.85 (d,  $J = 8.2$  Hz, 1H), 6.76 (dd,  $J = 8.2, 2.0$  Hz, 1H), 5.64 (s, 1H), 4.18 (q,  $J = 6.5$  Hz, 1H), 3.93 (s, 3H), 1.36 (d,  $J = 6.5$  Hz, 3H).

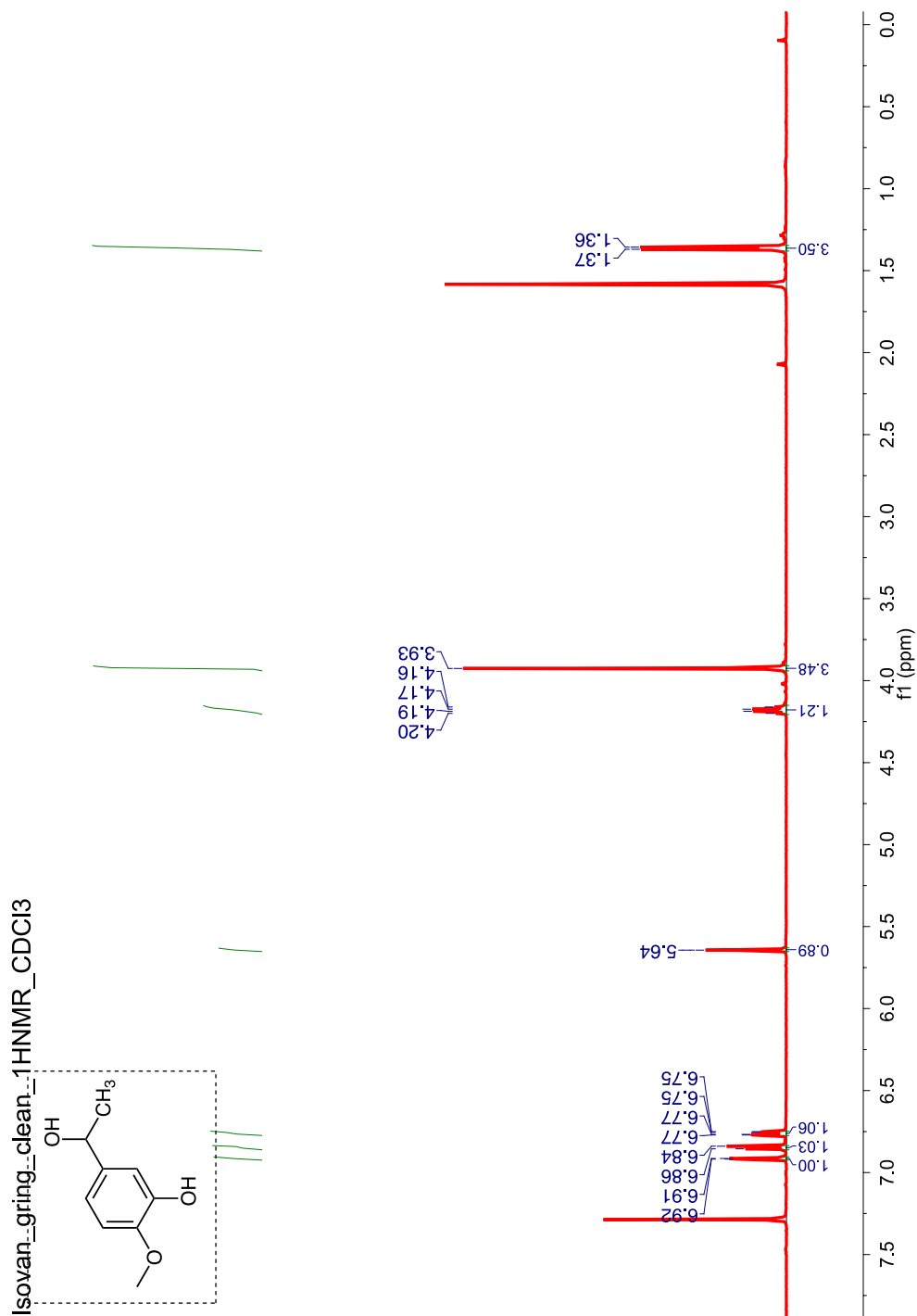


**Figure 4.13:**  $^1\text{H}$  NMR (500 MHz,  $\delta$  ppm,  $\text{CDCl}_3$ ) spectrum of vanillin derivative **137a**.

$^{13}\text{C}$  NMR (125 MHz,  $\delta$  ppm, Chloroform-*d*) 146.0, 137.6, 118.3, 112.8, 110.8, 74.25, 56.2, 24.8.

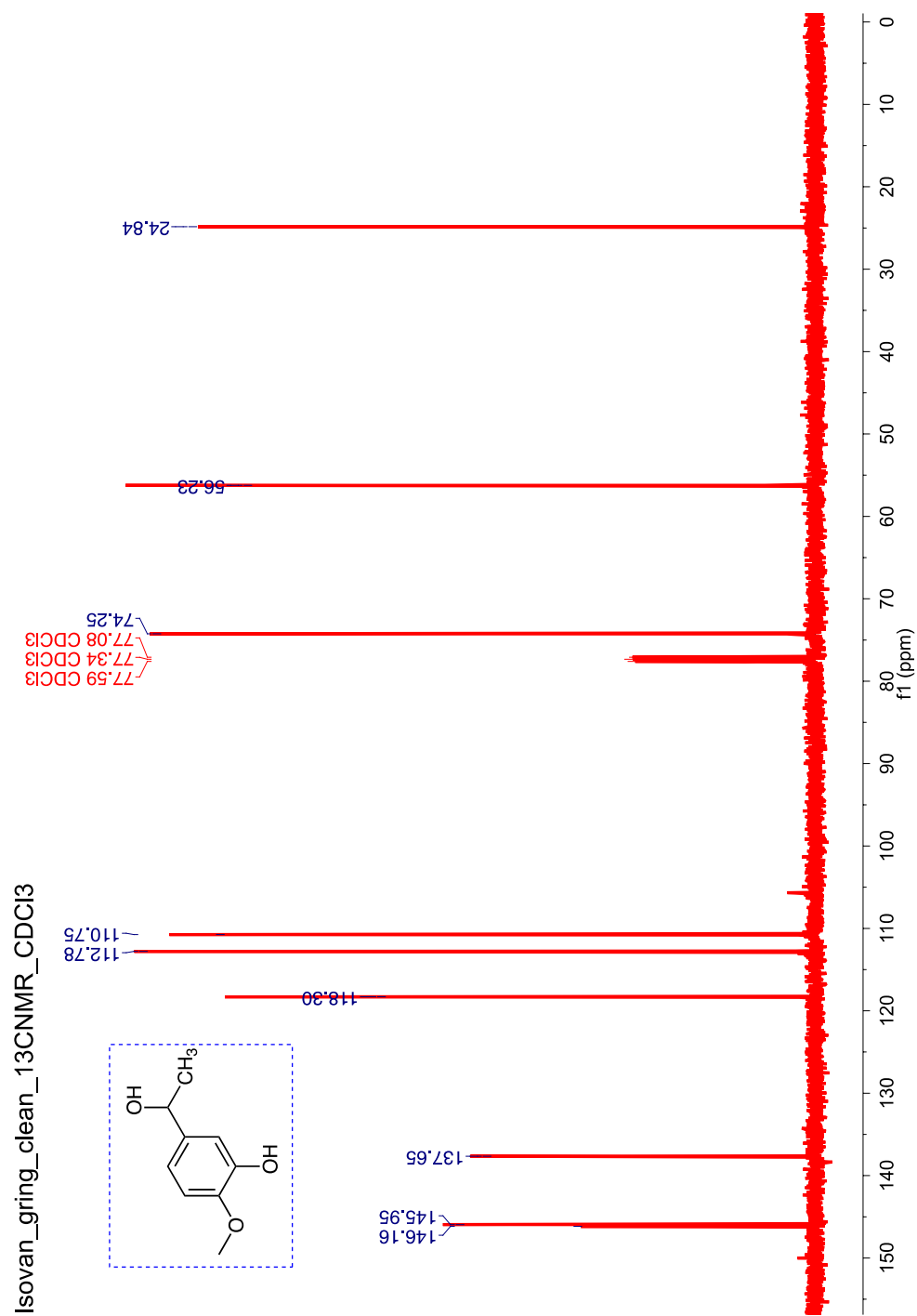


**Figure 4.14:**  $^{13}\text{C}$  NMR (125 MHz,  $\delta$  ppm,  $\text{CDCl}_3$ ) spectrum of vanillin derivative **137a**.

HRMS-ESI (m/z) ([M+Na]):

Calculated : 191.0684

Observed : 191.0685

$|\Delta m|$  : 0.52 ppm

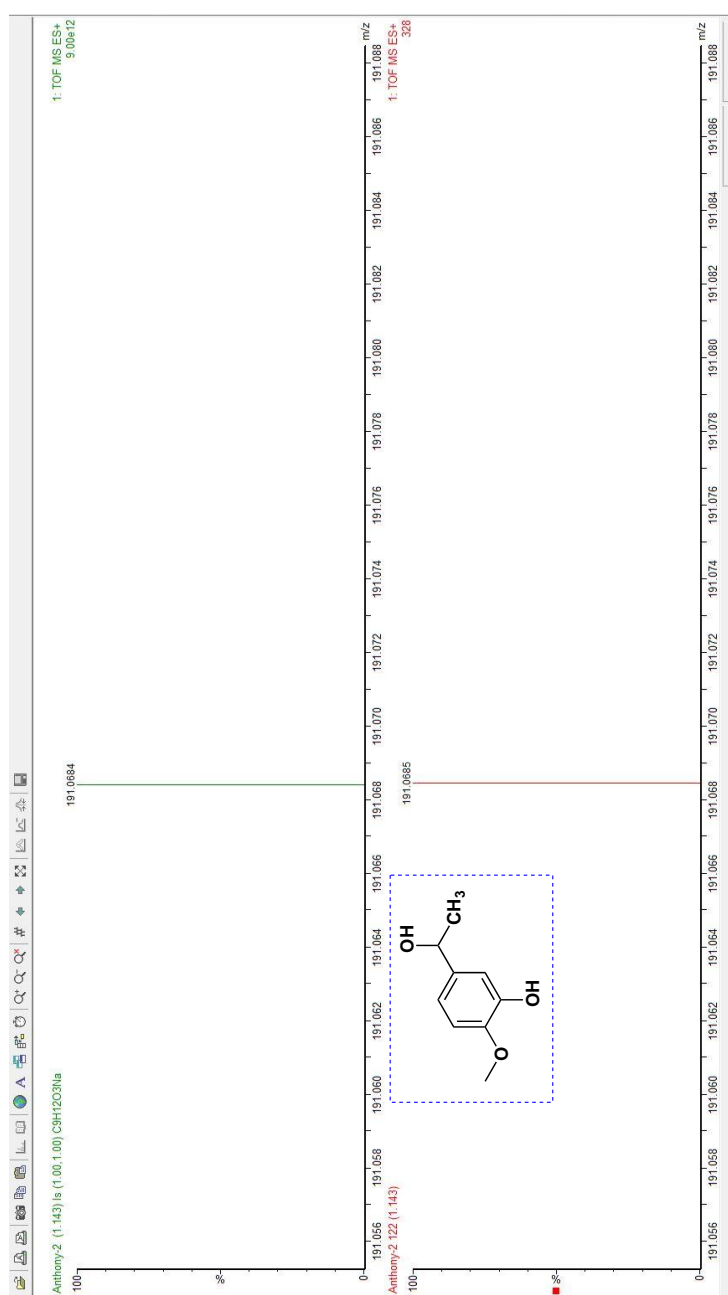
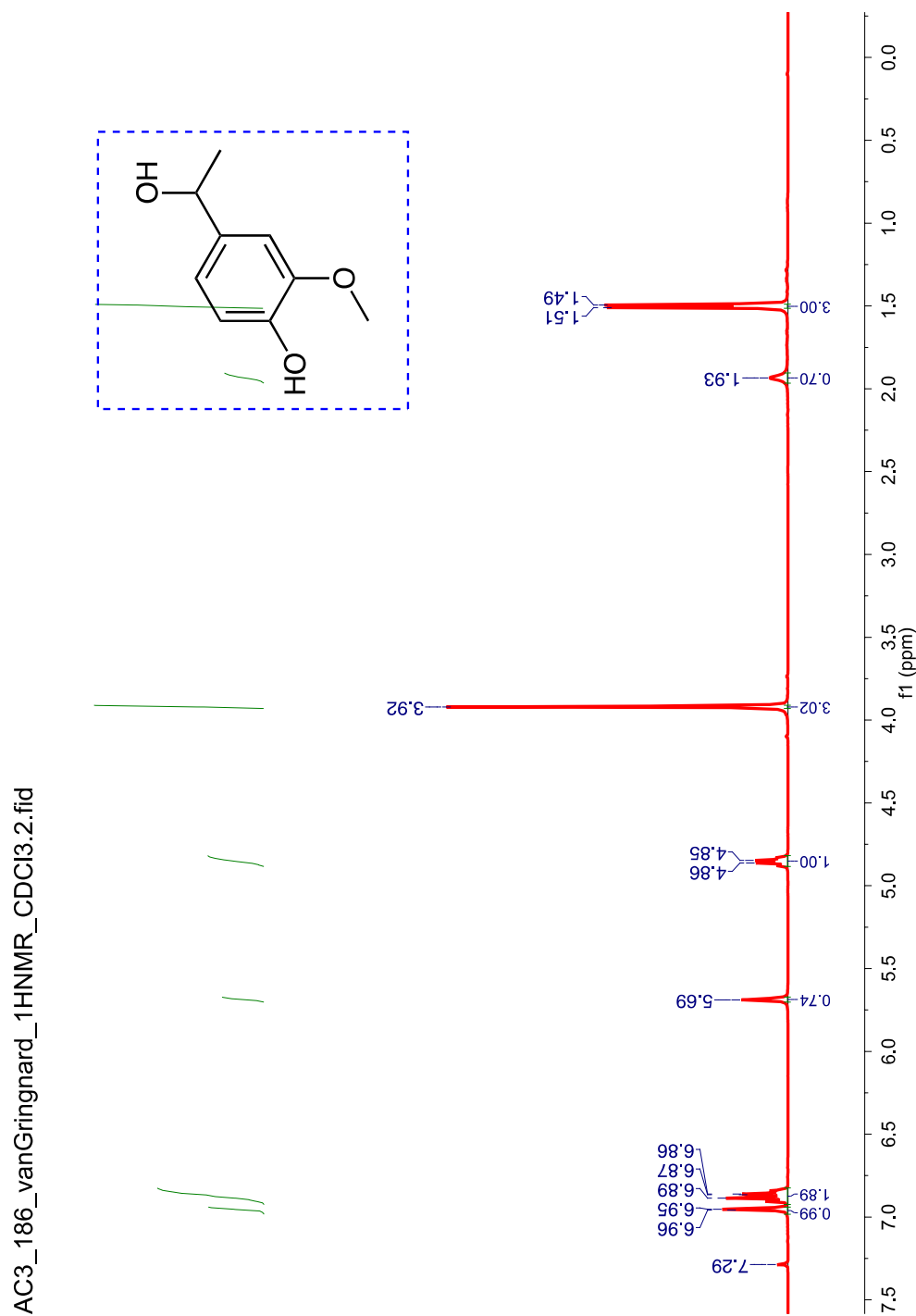


Figure 4.15: HRMS of vanillin derivative **137a**.



$^1\text{H}$  NMR (400 MHz,  $\delta$ ppm,  $\text{CDCl}_3$ ) 6.96-6.86 (d,  $J = 1.9$  Hz, 1H), 6.92 - 6.82 (m, 2H), 5.69 (s, 1H), 4.85 (d,  $J = 6.4$  Hz, 1H), 3.92 (s, 3H), 1.93 (s, 1H), 1.50 (d,  $J = 6.3$  Hz, 3H).



**Figure 4.16:**  $^1\text{H}$  NMR (400 MHz,  $\delta$ ppm,  $\text{CDCl}_3$ ) spectrum of vanillin derivative **137b**.

$^{13}\text{C}$  NMR (125 MHz,  $\delta$ ppm,  $\text{CDCl}_3$ ) 146.9, 145.2, 138.2, 118.5, 114.5, 108.4, 70.5, 56.1, 25.3.

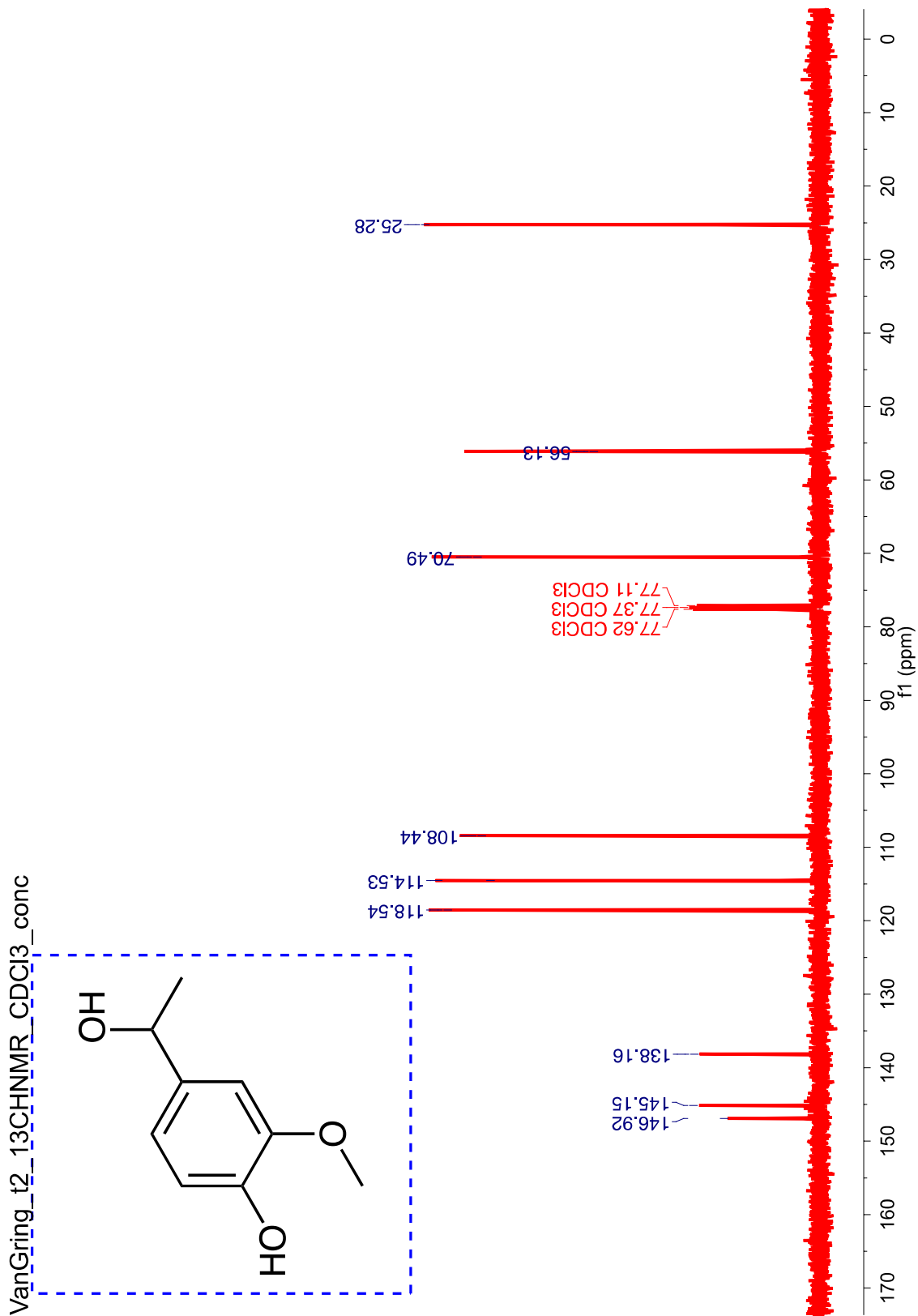


**Figure 4.17:**  $^{13}\text{C}$  NMR (125 MHz,  $\delta$  ppm,  $\text{CDCl}_3$ ) spectrum of vanillin derivative **137b**.

HRMS-ESI (m/z) ([M+Na]):

Calculated : 191.0684

Observed : 191.0684

| $\Delta m$ | : 0 ppm

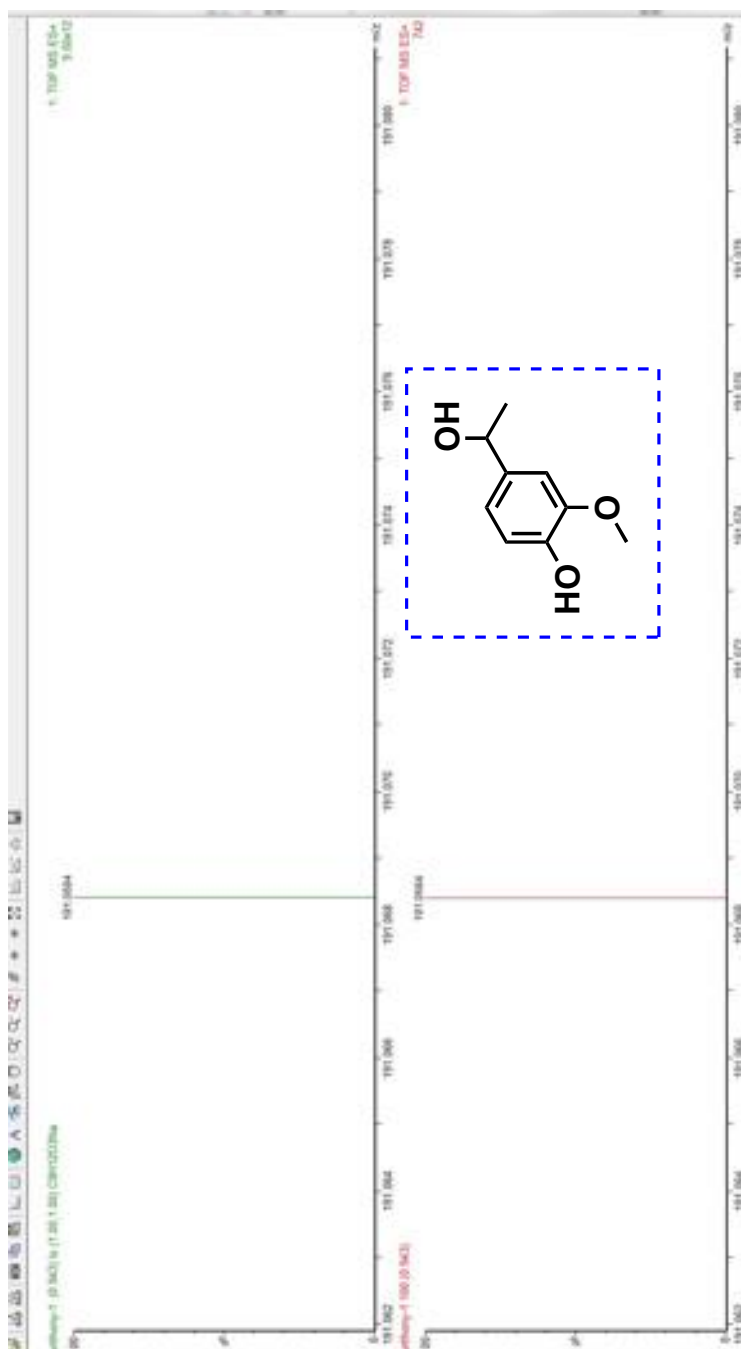


**Figure 4.18:** HRMS of vanillin derivative **137b**.

$^1\text{H}$  NMR (500 MHz,  $\delta$  ppm,  $\text{CDCl}_3$ ) 7.05 - 6.54 (m, 4H), 5.11 (dd,  $J = 6.6, 4.4$  Hz, 1H), 3.87 (s, 3H), 3.36 (d,  $J = 4.4$  Hz, 1H), 1.54 (d,  $J = 6.6$  Hz, 3H).

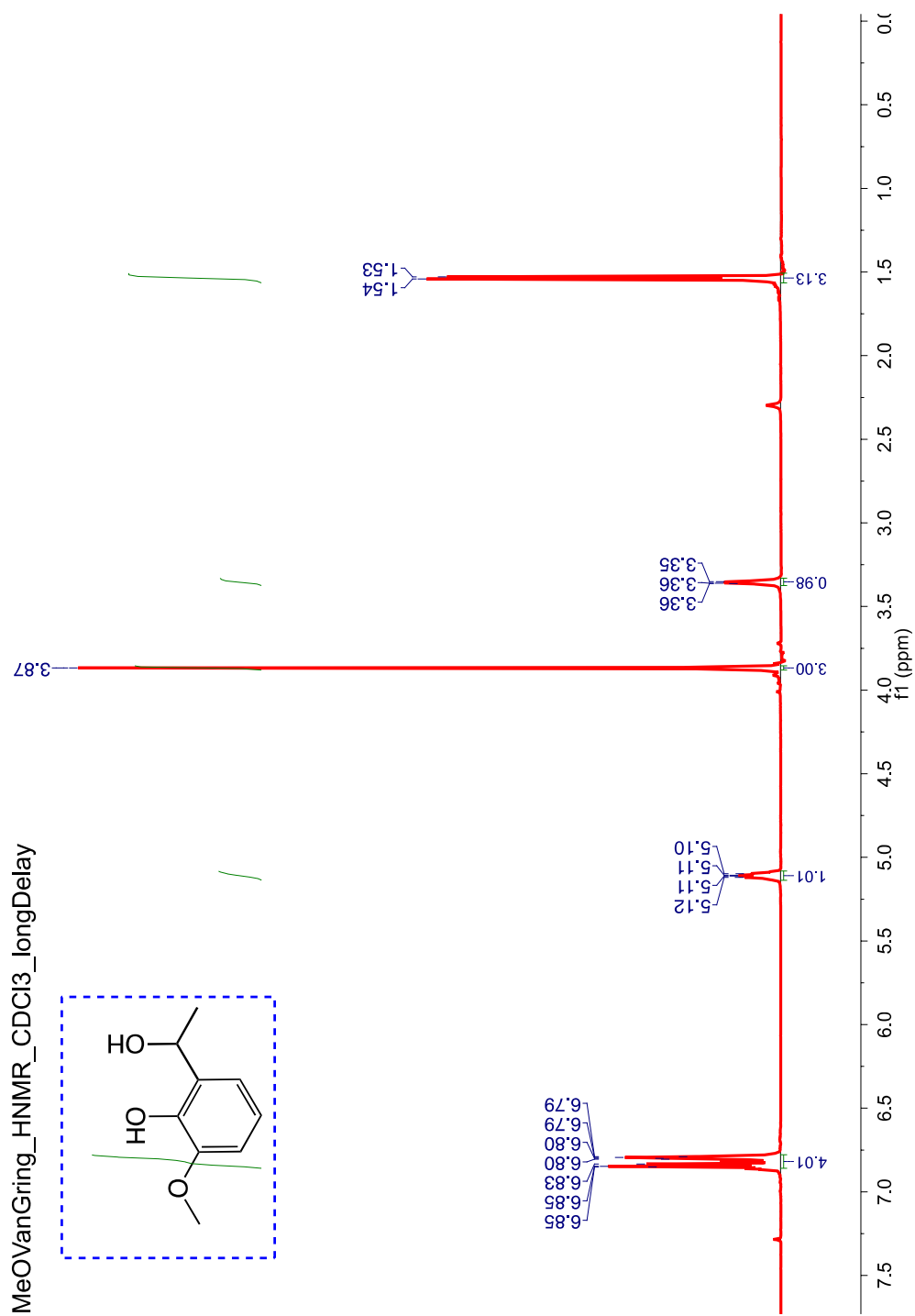


**Figure 4.19:**  $^1\text{H}$  NMR (500 MHz,  $\delta$  ppm,  $\text{CDCl}_3$ ) spectrum of vanillin derivative **137c**.

$^{13}\text{C}$  NMR (125 MHz,  $\delta$ ppm,  $\text{CDCl}_3$ ) 147.1, 143.4, 130.9, 119.9, 118.6, 110.2, 67.9, 56.3, 23.3.

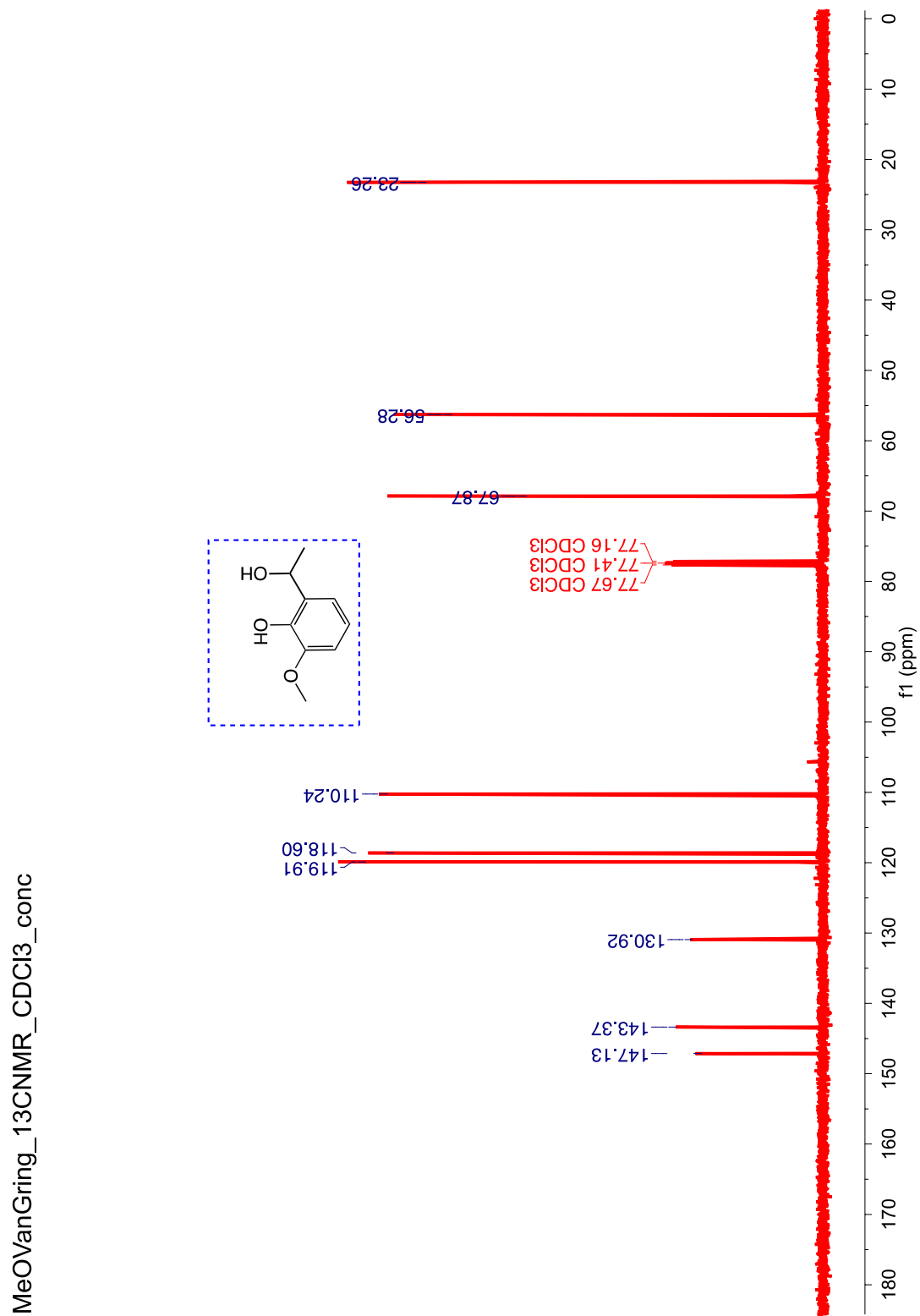


**Figure 4.20:**  $^{13}\text{C}$  NMR (125 MHz,  $\delta$ ppm,  $\text{CDCl}_3$ ) spectrum of vanillin derivative **137c**.

HRMS-ESI (m/z) ([M + Na]):

Calculated : 191.0684

Observed : 191.0675

$|\Delta m|$  : 4.71 ppm

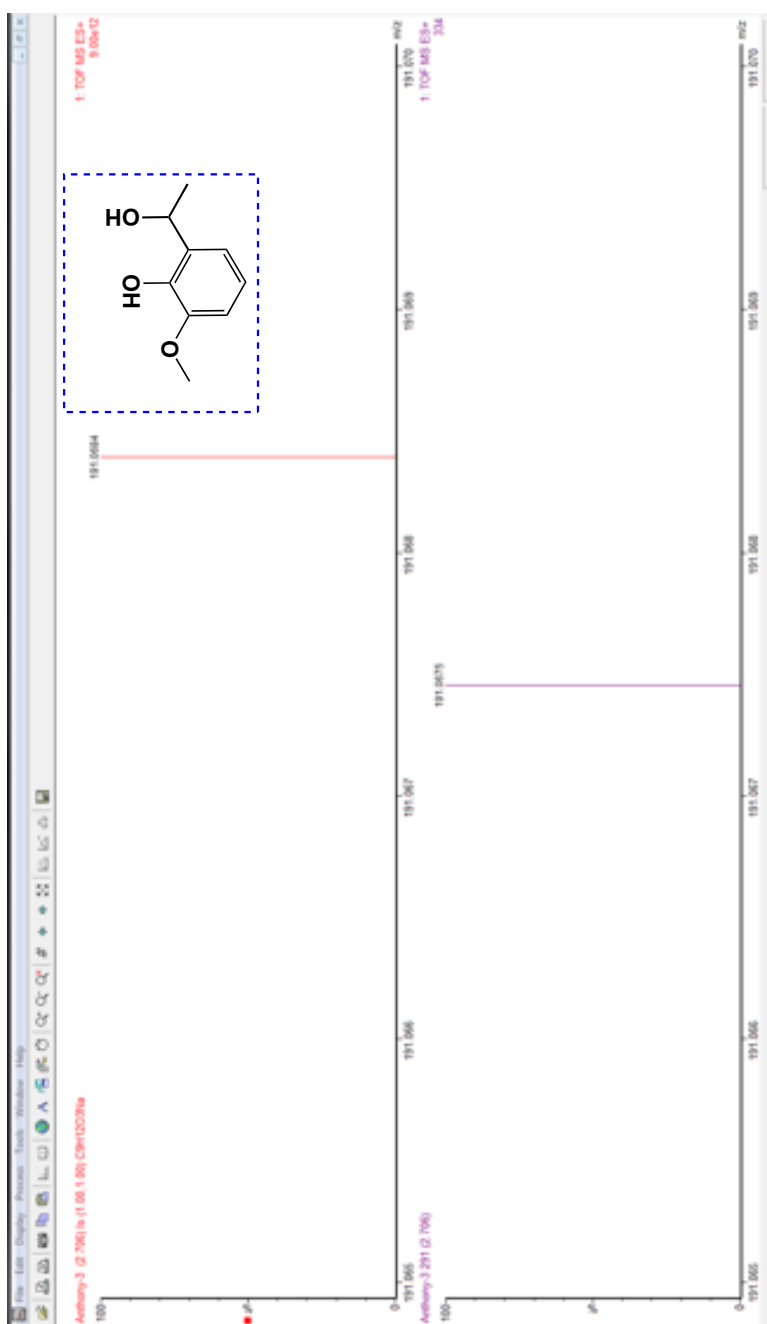
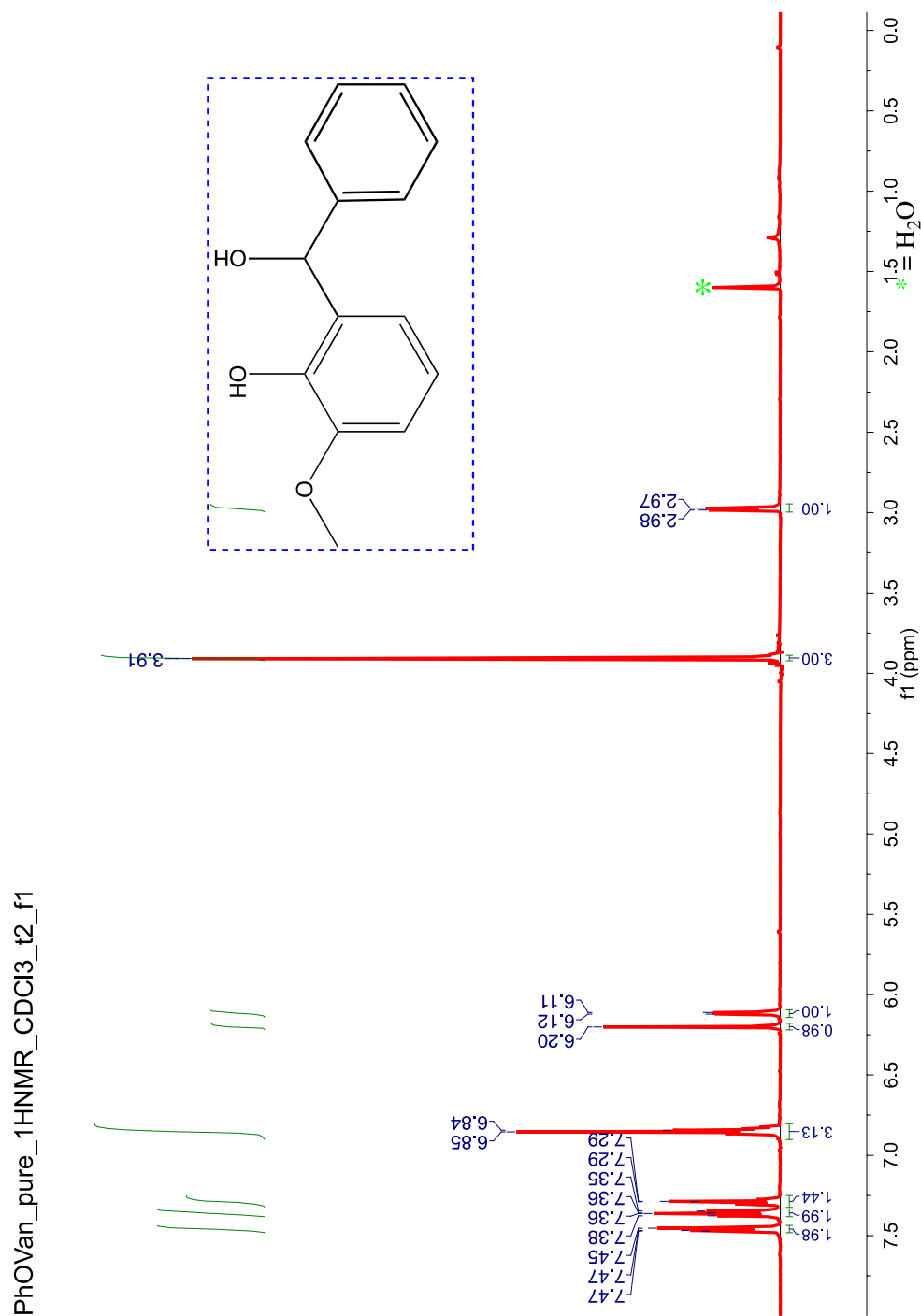


Figure 4.21: HRMS of vanillin derivative **137c**.

$^1\text{H}$  NMR (500 MHz,  $\delta$ ppm,  $\text{CDCl}_3$ ) 7.48 -7.44 (m, 2H), 7.36 (t,  $J = 7.6$  Hz, 2H), 7.29 (d,  $J = 1.2$  Hz, 1H), 6.85 (d,  $J = 5.3$  Hz, 3H), 6.20 (s, 1H), 6.12 (d,  $J = 5.1$  Hz, 1H), 3.91 (s, 3H), 2.98 (d,  $J = 5.2$  Hz, 1H).



**Figure 4.22:**  $^1\text{H}$  NMR (500 MHz,  $\delta$ ppm,  $\text{CDCl}_3$ ) spectrum of vanillin derivative **137d**.

$^{13}\text{C}$  NMR (125 MHz,  $\delta$ ppm,  $\text{CDCl}_3$ ) 147.0, 143.4, 143.2, 129.4, 128.5, 127.6, 126.8, 120.1, 120.0, 110.4, 77.6, 77.3, 77.1, 73.0, 56.3.

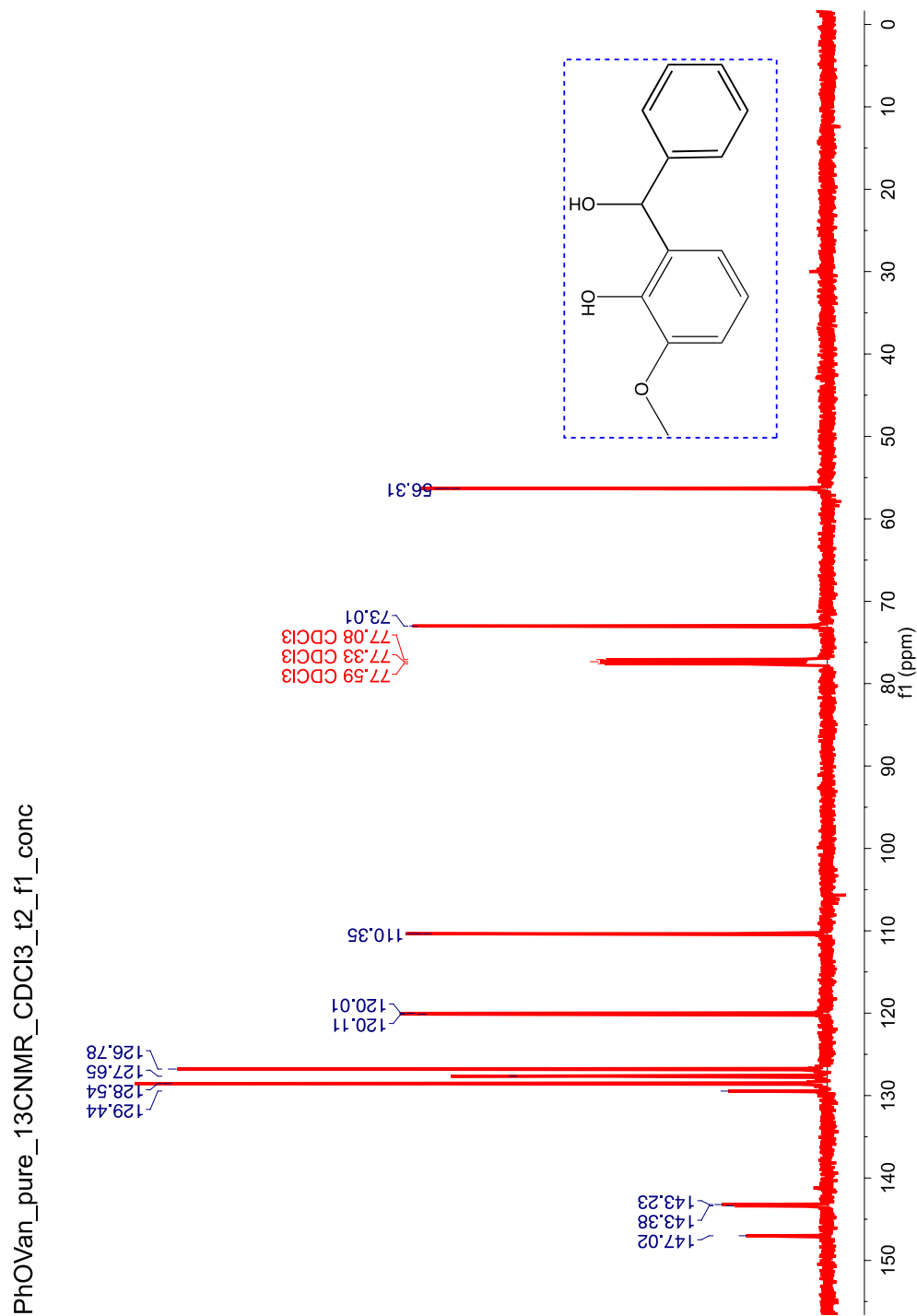


**Figure 4.23:**  $^{13}\text{C}$  NMR (125 MHz,  $\delta$ ppm,  $\text{CDCl}_3$ ) spectrum of vanillin derivative **137d**.

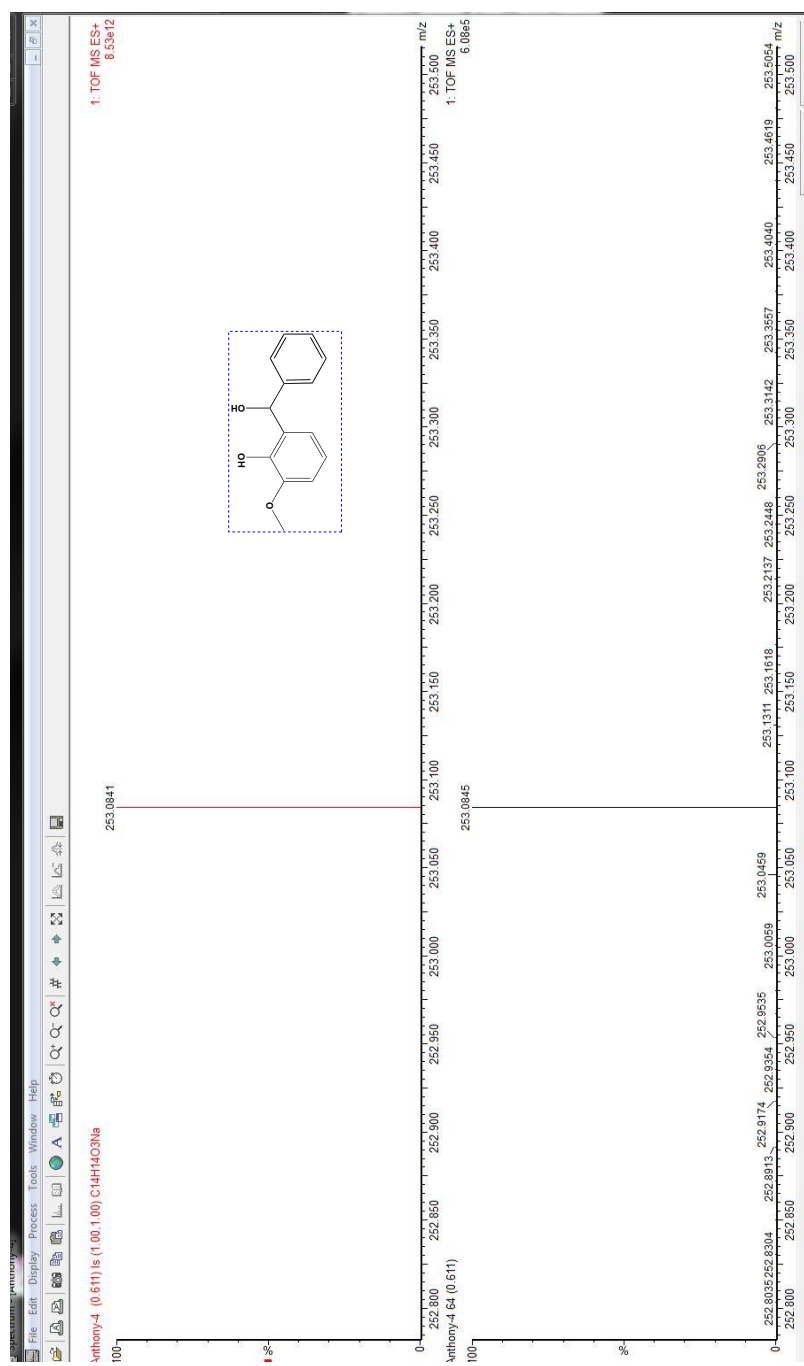


HRMS-ESI (m/z) ([M + Na]):

Calculated : 253.0841

Observed : 253.0845

$|\Delta m|$  : 1.58 ppm



$^1\text{H}$  NMR (400 MHz,  $\delta$ ppm,  $\text{CDCl}_3$ ) 7.53-7.52 (m, 4H), 6.80-6.81 (m, 3H), 6.17-6.08 (m, 2H), 3.84 (s, 3H), 3.34 (s, 1H).

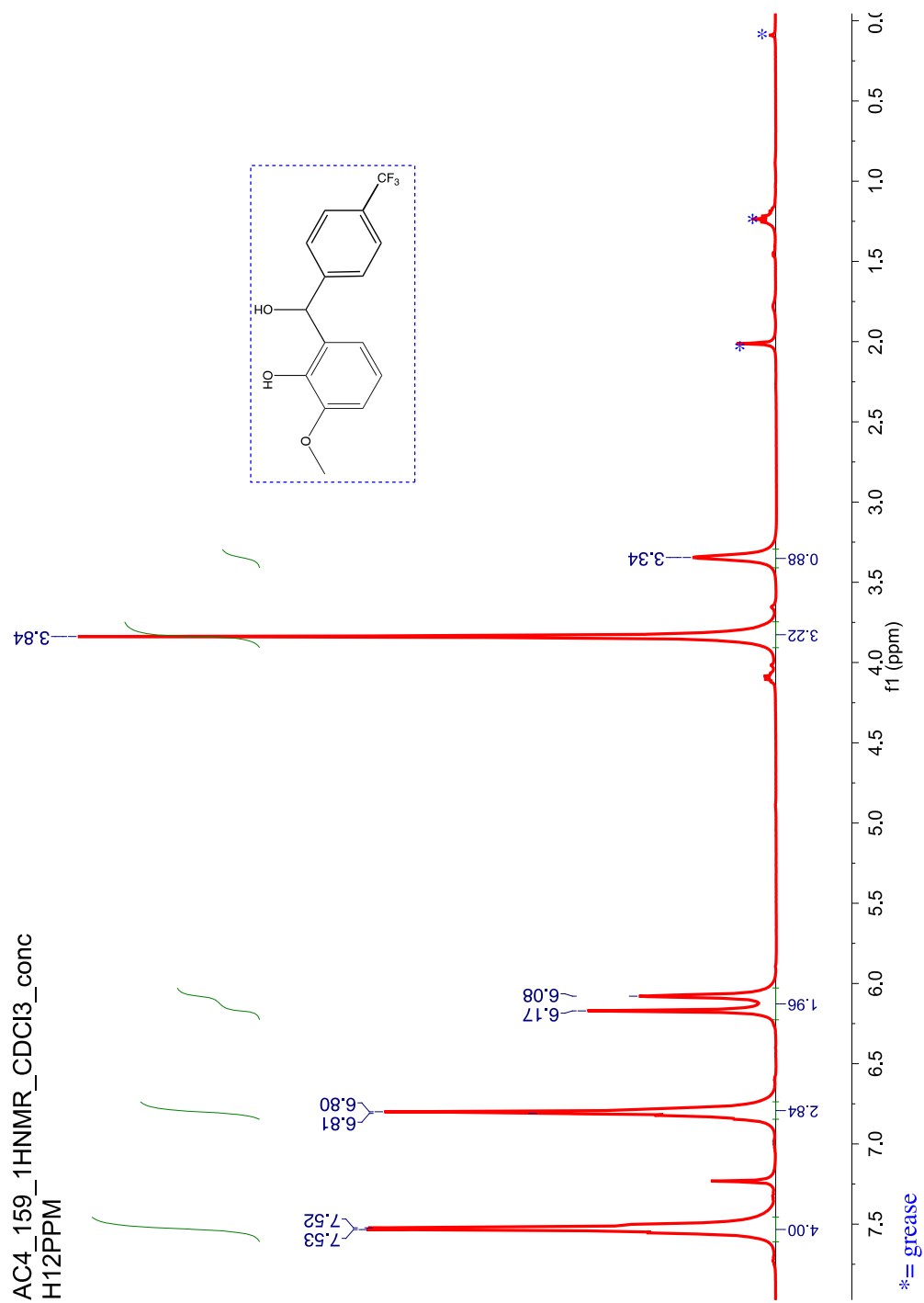


**Figure 4.25:**  $^1\text{H}$  NMR (400 MHz,  $\delta$ ppm,  $\text{CDCl}_3$ ) spectrum of vanillin derivative **137e**.

$^{13}\text{C}$  NMR (100 MHz,  $\delta$ ppm  $\text{CDCl}_3$ ) 147.3, 146.9, 143.1, 128.9, 126.8, 125.4, 125.3, 120.3, 119.8, 110.5, 71.9, 56.2.

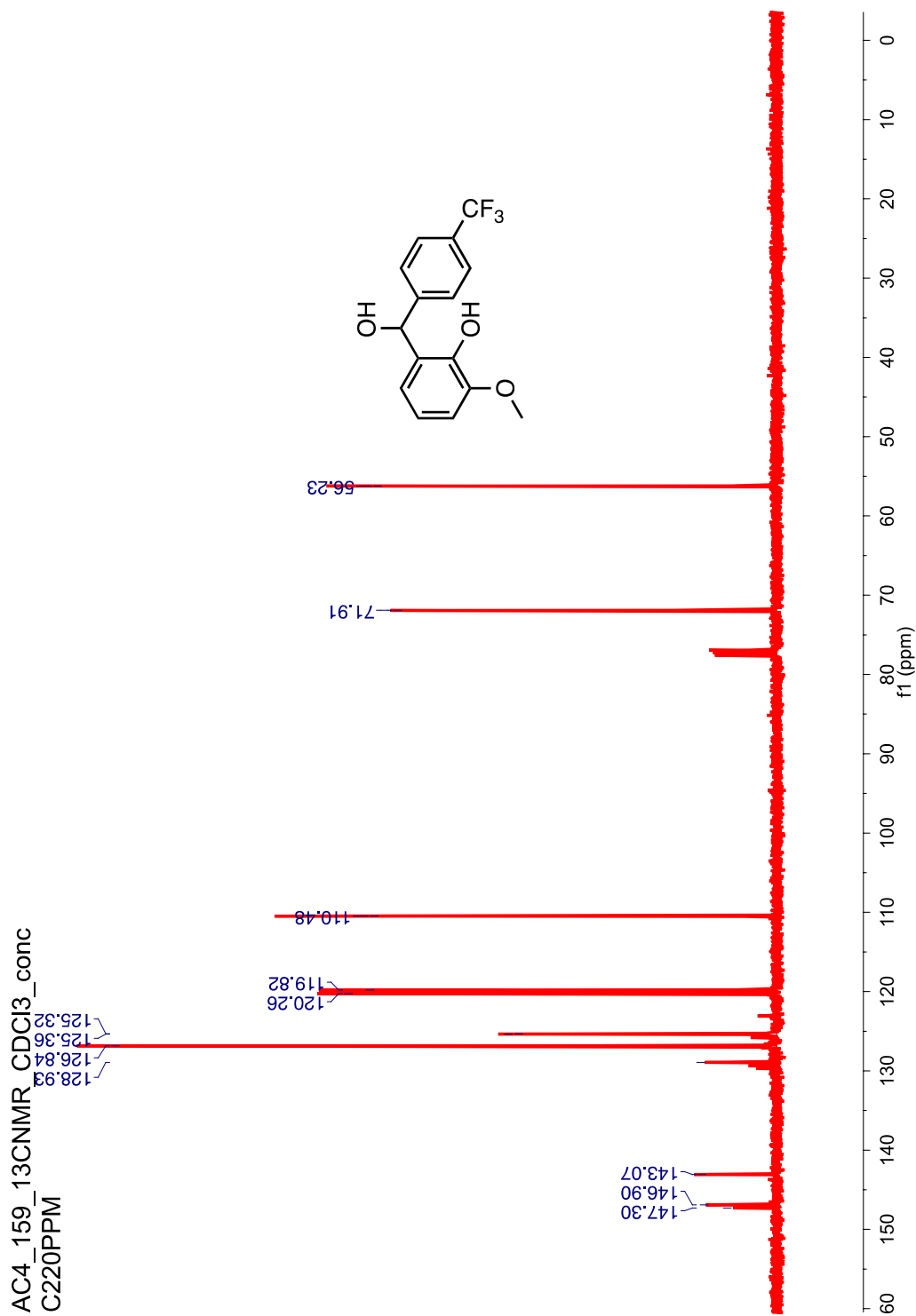


**Figure 4.26:**  $^{13}\text{C}$  NMR (100 MHz,  $\delta$ ppm  $\text{CDCl}_3$ ) spectrum of vanillin derivative **137e**.

HRMS-ESI (m/z) ([M + Na]):

Calculated : 321.0714

Observed : 321.0719

$|\Delta m|$  : 1.56 ppm

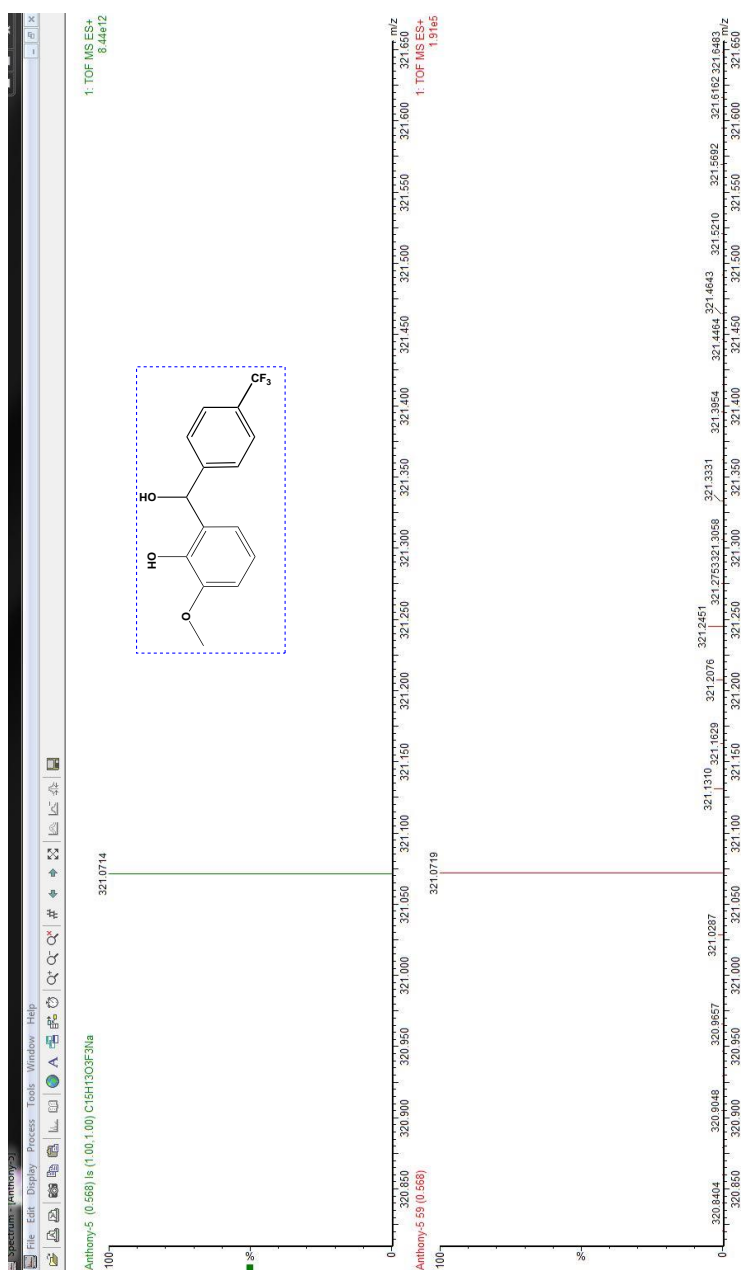


Figure 4.27: HRMS of vanillin derivative **137e**.

#### 4.7. References

1. Eigen, M., Proton Transfer, Acid-Base Catalysis, and Enzymatic Hydrolysis. Part I: ELEMENTARY PROCESSES. *Angewandte Chemie International Edition in English* **1964**, 3 (1), 1-19.
2. Bell, R. P., *The proton in chemistry*. 2nd ed.; Cornell University Press: Ithaca, N.Y., **1973**; p 310 p.
3. Liao, Y., Design and Applications of Metastable-State Photoacids. *Accounts of Chemical Research* **2017**, 50 (8), 1956-1964.
4. Förster, T., Dissoziation Angeregter Moleküle. *Z. Elektrolytische* **1950**, 54 (1), 42-46.
5. Beens, H.; Grellmann, K. H.; Gurr, M.; Weller, A. H. Y., Effect of Solvent and Temperature on Proton Transfer Reactions of Excited Molecules. *Discussions of the Faraday Society* **1965**, (39), 183- 193.
6. Weller, A., Protolytische Reaktionen des Angeregten Acridins. *Zeitschrift für Elektrochemie, Berichte der Bunsengesellschaft Für Physikalische Chemie* **1958**, 61 (8), 956 - 961.
7. Pines, E., UV-Visible spectra and photoacidity of Phenols, Naphthols and Pyrenols. . In *The chemistry of phenols*, Rappoport, Z., Ed. Wiley: Chichester, England ; Hoboken, NJ, **2003**.
8. Pines, E., The Kinetic Isotope Effect in The Photo-Dissociation Reaction of Excited-State Acids in Aqueous Solution. In *Isotope effects in Chemistry and Biology*, Kohen, A.; Limbach, H.-H., Eds. Taylor & Francis: Boca Raton, **2006**; pp 451-464.

9. Pines, D.; Pines, D., Solvent Assisted Photoacidity. In *Hydrogen-Transfer Reactions*, Hynes, T.; Klinman, J. P.; Limbach, H.-H.; Schowen, R. L., Eds. Wiley Imprint: Weinheim, Germany, **2007**.
10. Silvi, S.; Arduini, A.; Pochini, A.; Secchi, A.; Tomasulo, M.; Raymo, F. M.; Baroncini, M.; Credi, A., A Simple Molecular Machine Operated by Photoinduced Proton Transfer. *Journal of the American Chemical Society* **2007**, *129* (44), 13378-13379.
11. Simkovitch, R.; Huppert, D., Excited-State Proton Transfer of Weak Photoacids Adsorbed on Biomaterials: 8-hydroxy-1,3,6-pyrenetrisulfonate on Chitin and Cellulose. *J. Phys. Chem. A* **2015**, *119* (10), 1973-1982.
12. Förster, T., *Naturwissenschaften* **1949**, *36*, 186.
13. Upton, B. M.; Kasko, A. M., Strategies for the Conversion of Lignin to High-Value Polymeric Materials: Review and Perspective. *Chemical Reviews* **2016**, *116* (4), 2275-2306.
14. Kai, D.; Tan, M. J.; Chee, P. L.; Chua, Y. K.; Yap, Y. L.; Loh, X. J. Y., Towards Lignin Based Functional Materials in a Sustainable World. *Green Chemistry* **2016**, *18* (5), 1175.
15. Stewart, D., Lignin as a Base Material for Materials Applications: Chemistry, Application and Economics. *7th Forum of the International Lignin Institute* **2008**, *27* (2), 202 - 207.
16. Van den Bosch, S.; Schutyser, W.; Vanholme, R.; Driessen, T.; Koelewijn, S. F.; Renders, T.; De Meester, B.; Huijgen, W. J. J.; Dehaen, W.; Courtin, C. M.; Lagrain, B.; Boerjan, W.; Sels, B. F. Y., Reductive Lignocellulose Fractionation into Soluble Lignin Derived Phenolic Monomers and Dimers and Processable Carbohydrate Pulps. *Energy & Environmental Science* **2015** *8*(6), 1748-1763.

17. Bartok, W.; Lucchesi, P. J.; Snider, N. S., Protolytic Dissociation of Electronically Excited Organic Acids. *Journal of the American Chemical Society* **1962**, *84* (10), 1842 - 1844.
18. Bartok, W.; Hartman, R. B.; Lucchesi, P. J., Substituent Effects on the Protolytic Dissociation of Electronically Excited Phenols\*. *Photochemistry and Photobiology* **1965**, *4* (3), 499 - 504.

## 5. VANILLIN DERIVED PHOTOINITIATORS

### 5.1. Introduction

Smart materials have gained notoriety over the past decade for their inherent physical properties and varying utility in numerous facets of industry as well as fundamental investigations. Smart materials also referred to stimuli responsive polymers are polymers which exhibit a modification of their physical and/or chemical properties when submitted to a chemical or physical stimuli such as pH, redox, temperature ionic strength (e.g. polarity) or light, to simply list a few.<sup>1-3</sup> Utilizing light as a stimuli has proven advantageous due to the spatial and temporal control, the reduction in byproducts and/or usage of excess reagents and the ability to fine tune the system.<sup>4</sup> By choosing the correct wavelength of irradiation it is possible to exclusively excite one particular chromophore over another, making it possible to have a multi-responsive, multicomponent light responsive system. Smart materials have displayed time release of drug molecules, swelling and shrinking of hydrogels, and coloration and discoloration for materials applications to simply list a few.<sup>5-7</sup>

Surface modified photoresponsive polymers have also been displayed to tune various properties upon irradiation of light.<sup>8</sup> Chen and coworkers cross linked azo-benzene chromophores and polycaprolactone achieving photoresponsive nanofibers capable of controlled surface wettability.<sup>9</sup> Kondo and coworkers displayed the ability of anthracene side groups in a acrylate polymer to cause deformation of the polymer upon irradiation due to reversible photodimerization of the anthracene side groups.<sup>10</sup>

Thus photopolymerization has proven to be a viable method of synthesizing various polymers including smart materials. As our expertise is in light initiated processes we were interested in the development of photoresponsive materials. In order for a material to respond to



light irradiation, it is necessary that the material contains an appropriate chromophore or light responsive molecule. In this regard we have focused our attention on biobased photoinitiators as they play a key role in the photopolymerization process.

## 5.2. Biobased vanillin derived photoacids

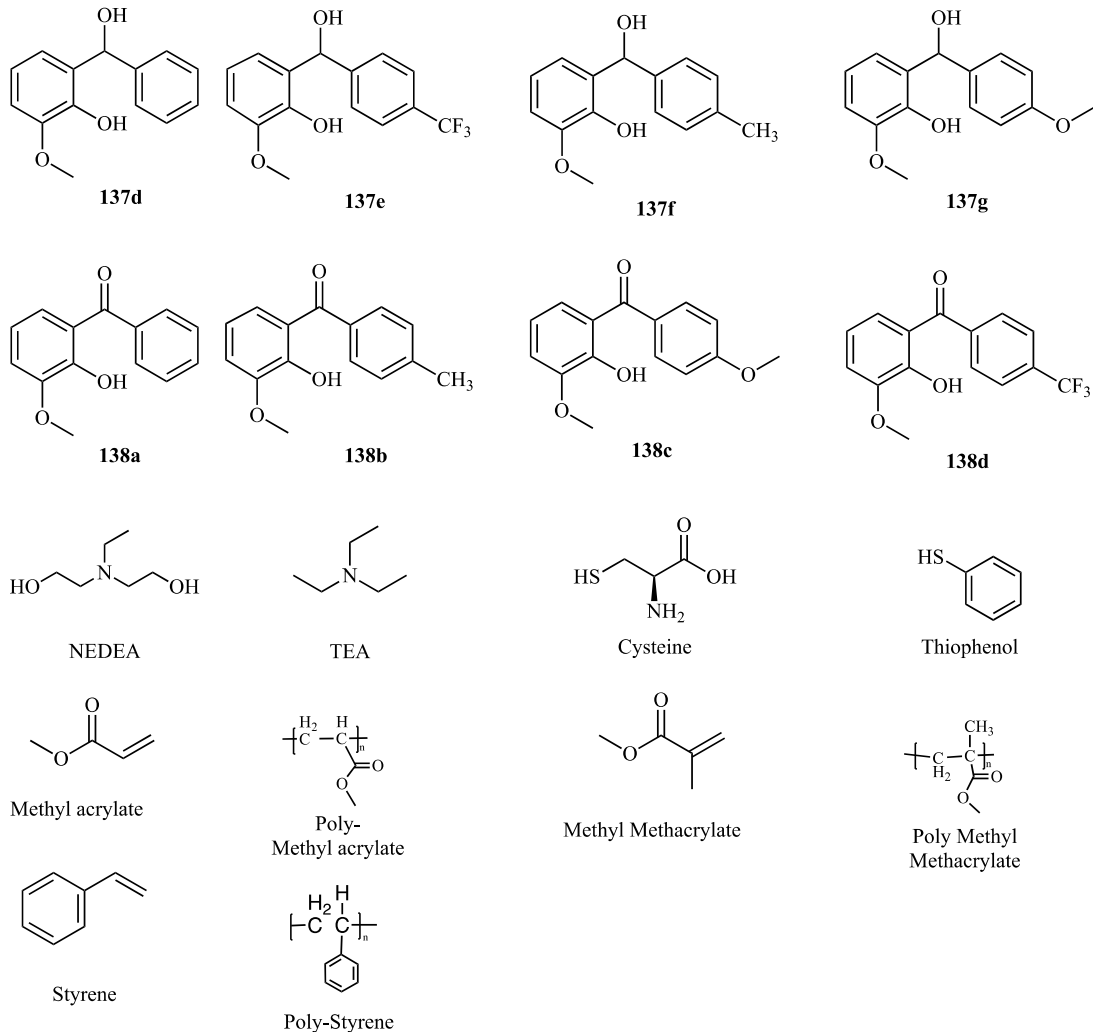
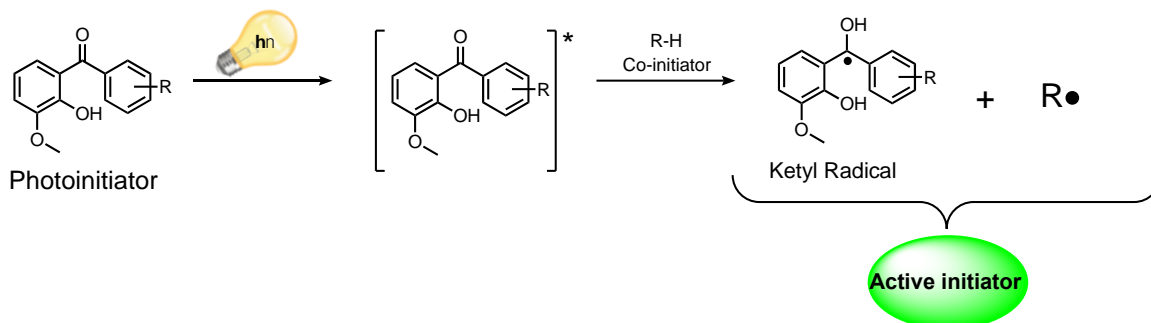


**Chart 5.1:** Vanillin photoinitiators, precursors and reagents utilized to investigate photoinitiators.

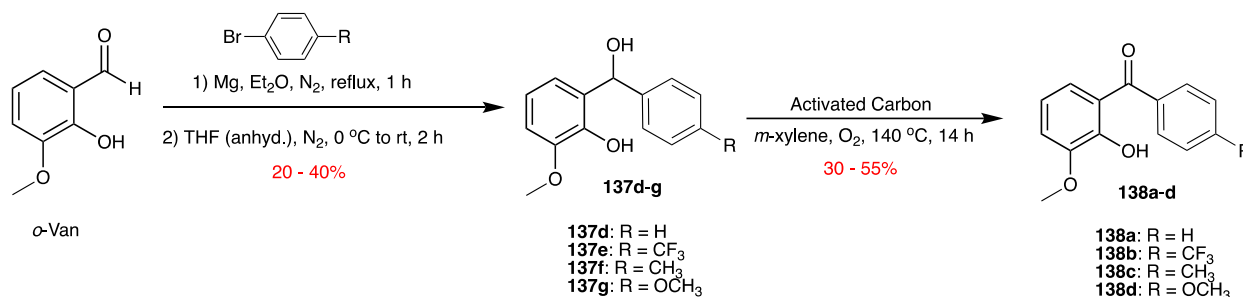
The predominance of photoinitiated polymerization in various industrial processes i.e. lithography, photocuring and device fabrication, accentuates the relevance of photoinitiators. Spatial control, temporal control and the ability to initiate polymerization processes at ambient conditions are highlights of light mediated polymerization.<sup>11</sup> There exists a number of industrially employed photoinitiators, e.g. benzoin ethers, acyl phosphines thioxanones, and benzophenones to simply name a few. The latter, benzophenone (BP), is a well-established photoinitiator for UV curing of various monomers in the presence of numerous co-initiators/H-

donors most commonly amines.<sup>12-15</sup> Over the past six decades the photophysical properties of benzophenone has been well documented and exploited for various photochemical processes.<sup>11, 16-18</sup> Additionally, various surface enhanced smart materials have been synthesized with the aid of benzophenone. The mechanistic pathway involved for photochemical polymerization of benzophenone and other Type II photoinitiators is hydrogen abstraction wherein an available hydrogen is abstracted from a suitable donor (co-initiator), forming a ketyl radical of the photoinitiator and radical of the co-initiator.<sup>15, 19</sup> Photochemical polymerization via Type II photoinitiators goes via step growth polymerization. The radical of the co-initiator is most commonly the radical which initiates polymerization. Thus co-initiator choice is vital to the polymerization process. Additionally, ground state interactions as well as excited state interactions govern the efficiency of the hydrogen abstraction and thus can determine the efficiency of the photochemical process. Usage of benzophenone as a photoinitiator limits utility to the UV region of the electromagnetic spectrum. UV light is hazardous, often less efficient due to energy wastage as heat dissipation and suffers from low depth penetration with respect to utility in photopolymerization in films and/or solid state irradiation. A shift into the visible region of the spectrum would decrease energy output, increase depth of penetration allowing for thicker films and more efficient solid state irradiation and device fabrication, making the process more green. Additionally, benzophenone is derived from petroleum feedstocks a non-renewable source. Due to the electronics of the two aromatic rings selective and differential substitution of benzophenone is challenging. Charging towards sustainability herein we developed visible light harvesting photoinitiators from biobased starting materials, namely vanillin. Usage of vanillin affords multiple functional group handles for later substitution, absorbance in the visible region of the spectrum and the ability to differentially substitute both aromatic rings. Variable

substitution allows for tuning of ground state electronic properties, excited state properties, light harvesting wavelength allowing for the ability to fine tune photopolymerization.



### Scheme 5.1: Biobased Type II photoinitiators.



### Scheme 5.2: synthesis of vanillin derived photoinitiators.

#### 5.3. Vanillin derived photoinitiators

Vanillin derived photoinitiators were synthesized from *ortho*-vanillin in two simple steps according to Scheme 5.2. Usage of Grignard reagent of varying substitution was employed followed by benzylic oxidation in the presence of activated carbon in xylene as solvent heated at reflux under oxygen atmosphere. The structures of photoinitiators were confirmed by <sup>1</sup>H NMR, <sup>13</sup>C NMR spectroscopy. The method of synthesis allowed for differential substitution allowing for systematic investigation, aimed at physical organic study of the photophysical properties. Absorbance spectra of the newly synthesized vanillin derived photoinitiators **138a-d** displayed a bathochromic shift in absorbance with respect to structurally similar benzophenone (BP) (Figure 5.1). Additionally, varying substitution on the para-position of the nucleophilic aromatic ring

merely altered absorbance, hyper vs hypochromic effect, and had little bearing on the structure of the absorbance profile.

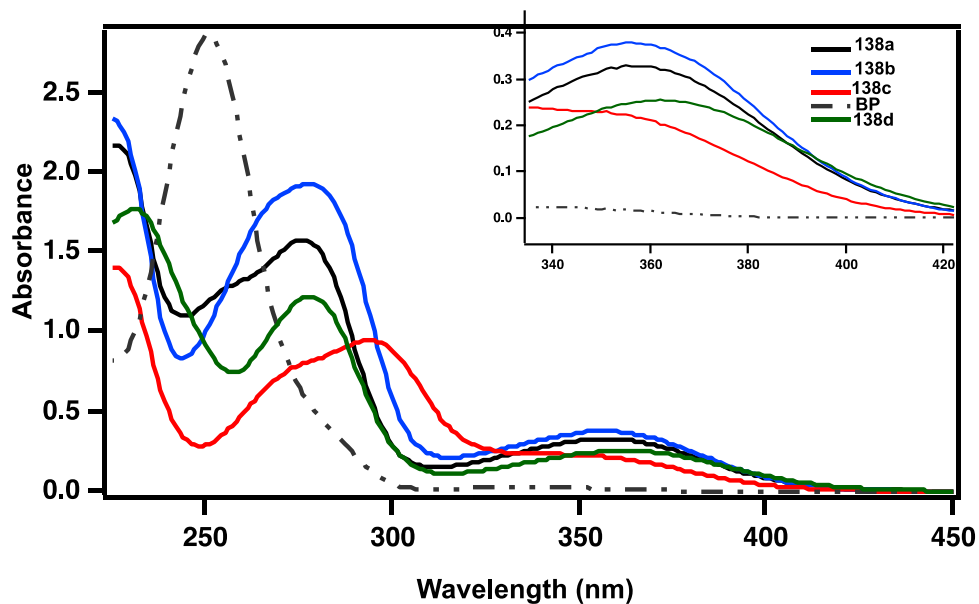


**Figure 5.1:** Absorbance spectra of vanillin derived photoinitiators.  $[138a-d] = 0.15mM$

In order to test the efficacy of photopolymerization under low energy irradiation, visible light, photopolymerization commenced utilizing purple LED (pLED,) with spectral distribution centered at 400nm (400 nm + 5 nm). As polymerization of methyl acrylate to poly methyl acrylate is well established in the literature, methyl acrylate was employed as the monomer for optimization of reaction conditions and co-initiator in combination with newly synthesized photoinitiator **138a** (Table 5.1). Photoinitiator and co-initiator were taken in a solution of the monomer which was purged with  $N_2$  before 1 h of irradiation under purple LED illumination. Polymer formation was determined based on precipitation which was noticed upon dissolving the reaction mixture in MeOH. Additionally,  $^1H$  NMR spectroscopy displayed broad  $CH_2$  peaks also indicating polymerization had occurred. The precipitate was washed with MeOH, dried in vacuo and analyzed by GPC analysis. Table 5.1 displays co-initiator trials and optimization of photopolymerization reaction. Inspection of Table 5.1 displays that polymer was afforded only in

the presence of thiophenol as H-donor/co-initiator (Table 5.1, entry 7). To our surprise no appreciable polymer was formed utilizing commonly employed amine co-initiators (Table 5.1, entries 3 and 4). Under the same reaction conditions, in absence of co-initiator polymer formation was not noticed. In contrast, increasing the photoinitiator concentration from 4 mM ( $4 \times 10^{-4}$  mol%) to 0.4 M (0.4 mol%) afforded polymer with better control over PDI and increased molecular weights with respect to similarly employed reaction conditions (Table 5.1 entry 2 vs entry 7). Polydispersity index (PDI) or  $M_w/M_n$  for radical chain polymerization is expected to be circa 2 for a well behaved system. However, early termination due to excess radical species can cause deviation from the expected value of 2 for PDI.<sup>20</sup> In contrast, combination of two propagating chains can give rise to more uniformity and thus decrease the PDI which can approach 1.5. It is likely that in the case of **138a** when employed as both the initiator and co-initiator (Table 5, entry 2) the propensity and/or combination of kinetic chains is greater than when thiophenol is used as co-initiator.

**Table 5.1:** Optimization of photopolymerization of PI **138a**: Co-initiator trials.<sup>a,b</sup>

entry	PI	CI	Solvent	t/h	M <sub>w</sub> (g/mol) <sup>b</sup>	M <sub>n</sub> (g/mol) <sup>b</sup>	PDI <sup>b</sup>
1	<b>138a</b>	-	MeCN	4	- <sup>c</sup>	-	- <sup>c</sup>
2 <sup>d</sup>	<b>138a</b>	-	MeCN	1	76,560	60,278	1.3
3	<b>138a</b>	nedeaa	CHCl <sub>3</sub>	4	- <sup>c</sup>	-	- <sup>c</sup>
4	<b>138a</b>	tea	CHCl <sub>3</sub>	4	- <sup>c</sup>	-	- <sup>c</sup>
5	<b>138a</b>	cysteine	MeCN	4	- <sup>c</sup>	-	- <sup>c</sup>
6	<b>138a</b>	tps	MeCN	1	- <sup>c</sup>	-	- <sup>c</sup>
7	<b>138a</b>	thiophenol	CHCl <sub>3</sub>	4	157,848	64,933	2.4
8	<b>138a</b>	thiophenol	MeCN	1	50,206	25,614	2.0

<sup>a</sup>purple LED employed for irradiation spectral distribution centered at 400±5 nm; 4x10<sup>-4</sup> mol% of photo-initiator (PI) and co-initiator (CI) were used unless other wise stated. Polymer formation was indicated by precipitation from MeOH. <sup>b</sup>Molecular weights (M<sub>w</sub>, M<sub>n</sub>) and PDI were determined by GPC analysis. <sup>c</sup>No polymer noticed after dissolution in Methanol. <sup>d</sup>[138a] = 0.4 mol %; NEDEA= n-ethyl diethanolamine; TEA = trimethylamine; TPS = triphenylsillane.

After establishing the optimized reaction conditions, photopolymerization employing photoinitiators **138b-d** were investigated. Additionally, for comparison benzophenone was also employed for photopolymerization utilizing methyl acrylate as the monomer. Since benzophenone does not efficiently absorb light at 400 nm, 350 nm irradiation in a Rayonet Reactor was employed. Photoinitiator **138a** was irradiated in a similar fashion as BP at 350 nm (Table 5.2, entry 2). Table 5.2 displays the photopolymerization of methyl acrylate (MA) with various photoinitiators. Inspection of 5.2 displays that **138a** was similarly reactive towards photopolymerization of MA under the same reaction conditions affording similar PDI molecular weights. Shifting the wavelength of irradiation to 400 nm, photopolymerization employing **138a** under pLED irradiation afforded similar PDI and molecular weight as the higher energy 350 nm irradiation. This indicated that the reactivity of **138a** was maintained even at longer, lower energy wavelengths. Further inspection of Table 5.2 displays that photoinitiators with electron donating groups afforded polymers of the highest molecular weight and greatest conversion

(Table 5.2 entries 4 and 5). Photoinitiator **138c** garnished with para-methoxy substituent on the distal aromatic ring afforded the greatest extent of conversion (Table 5.2, entry 5) Table 5.2 displays that all photoinitiators are effective in the photopolymerization of methyl acrylate to poly methyl acrylate affording appreciable polymer upon irradiation employing purple LED illumination under N<sub>2</sub> atmosphere for 1 hour.

**Table 5.2:** Photopolymerization of MA and thiophenol as co-initiator with various PIs.

entry	PI	$\lambda$ (nm) <sup>c,d</sup>	M <sub>w</sub> (g/mol) <sup>b</sup>	M <sub>n</sub> (g/mol) <sup>b</sup>	PDI <sup>b</sup>	%conv. <sup>e</sup>
1	BP	350	96,227	41,104	2.3	Not recorded
2	<b>138a</b>	350	50,206	25,614	2.0	Not recorded
3	<b>138a</b>	400	50,108	31,600	1.6	11
4	<b>138b</b>	400	2,996,397 87,755	2,814,774 61,797	1.1 1.4	16
5	<b>138c</b>	400	2,818,155 87,907	2,483,992 61,481	1.1 1.4	24
6	<b>138d</b>	400	91,585	70,204	2.0	4

<sup>a</sup>4x10<sup>-4</sup> mol% of photo-initiator (PI) and co-initiator (CI) were used unless other wised stated. <sup>1</sup>H NMR spectroscopy was used to display polymer formation. All reactions were an average of a minimum of two trials. <sup>b</sup>Molecular weights (M<sub>w</sub>, M<sub>n</sub>) and PDI were determined by GPC analysis. <sup>c</sup>purple LED employed for irradiation spectral distribution centered at 400±5 nm <sup>d</sup>Rayonet Reactor equipped with 14x16 watt light bulbs was employed for 350 nm irradiation. <sup>e</sup> %Conv. Determined by gravimetric analysis where %Conv. = mass of monomer (starting reaction) / (mass of polymer after reaction).

It is well documented in the literature that methyl acrylate can also undergo thermal polymerization in the absence of photopolymer, indicating the ease of polymerization of methyl acrylate.<sup>21</sup> The more sterically hindered methyl methacrylate monomer is more stable to thermal polymerization and is therefore more difficult to polymerize due to the added steric hindrance. In order to determine the influence of steric hindrance on the photopolymerization methyl methacrylate (MMA) was utilized as a monomer unit and polymerized in the presence of



photoinitiators **138a-d** (Table 5.3). Table 5.3 displays the photopolymerization utilizing methyl methacrylate as the monomer (MMA) under purple LED illumination. Inspection of Table 5.3 displays that PIs **138a-d** were employable as initiators to afford poly methyl methacrylate. Under atmospheric conditions PI **138a** afforded polymer with respectable molecular weights and respectable control over PDI albeit longer reaction times were necessary to obtain appreciable polymer. It can be seen that in all cases where MMA was employed as the monomer decreased photopolymerization conversions were noticed (Table 5.3). Photoinitiator **138d** afforded the least amount of polymer with only a mere 1% conversion. Further inspection of Table 5.3 unveils that lower control over PDI was afforded employing EDG PIs' **138b-c**, where PDI was circa 3.6.

**Table 5.3:** Photopolymerization of MMA with various PIs.<sup>a,b</sup>

entry	PI	Time (h)	M <sub>w</sub> (g/mol)	M <sub>n</sub> (g/mol)	PDI	%conv. <sup>c</sup>
1	<b>138a</b>	3 <sup>c</sup>	68,326 <sup>d</sup>	40,175 <sup>d</sup>	1.7 <sup>d</sup>	4 <sup>e</sup>
2	<b>138b</b>	1	200,225	56,699	3.5	12
3	<b>138c</b>	1	221,650	59,145	3.7	9
4	<b>138d</b>	1	70,292	35,098	2.0	1

<sup>a</sup>All reactions were done under inert atmosphere (N<sub>2</sub>) unless otherwise stated; MeCN was used to insure PIs were fully dissolved. Thiophenol was used as the coinitiator. Purple LED employed for irradiation; 4x10<sup>-3</sup> mol% of PI and CI was used. <sup>b</sup>Molecular weights (M<sub>w</sub>) and PDI were determined by GPC analysis. <sup>c</sup>%Conv. determined by gravimetric analysis where %Conv. = mass of monomer (starting reaction) / (mass of polymer after reaction). <sup>d</sup>Irradiation occurred under ambient conditions. <sup>e</sup>Determined from separate experiment where N<sub>2</sub> atmosphere was utilized and only 1 h of pLED irradiation was employed.

Further investigation of the newly synthesized PI commenced with employing styrene as the monomer. Literature reports indicate that photopolymerization of styrene monomer towards polystyrene is sluggish, likely due to electronics.<sup>22-24</sup> In efforts to determine the efficacy of photopolymerization of electronically encumbered monomer styrene, photopolymerization of styrene as the monomer was investigated. Employing the optimized conditions, N<sub>2</sub> atmosphere, thiophenol as the coinitiator and pLED as the light source, photopolymerization with styrene was investigated. Table 5.4 displays the results of photopolymerization of styrene. As expected, irrespective of the PI employed conversions of styrene to polystyrene were extremely low after one hour of irradiation (Table 5.4). Increasing the time of irradiation to nine hours only increased the conversion above 1%. Photoinitiators **138a-c** afforded polymer of similar molecular weight with similar control over PDI indicating similar reactivity with the styrene monomer. Employing PI **138d** afforded low molecular weight polymer with low control over PDI (Table 5.4, entry 2).

**Table 5.4:** Photopolymerization of Styrene with various PIs.<sup>a,b</sup>

entry	PI	M <sub>w</sub> (g/mol)	M <sub>n</sub> (g/mol)	PDI	%conv <sup>c</sup>
1	<b>138a</b>	59,701	36,847	1.5	0.6
2	<b>138b</b>	69,157	42,147	1.6	0.4
3	<b>138c</b>	63,698	38,744	1.6	4x10 <sup>-3</sup>
4	<b>138d</b>	9,353	2,111	4.4	<<0.1

<sup>a</sup>All reactions were done under inert atmosphere (N<sub>2</sub>) unless otherwise stated; MeCN was used to insure PIs were fully dissolved. Thiophenol was used as the co-initiator. Purple LED employed for irradiation; 4x10<sup>-3</sup> mol% of PI and CI was used. <sup>b</sup>Molecular weights (M<sub>w</sub>) and PDI were determined by GPC analysis. <sup>c</sup>%Conv. determined by gravimetric analysis where %Conv. = mass of monomer (starting reaction) / (mass of polymer after reaction), data is a result of minimum two trials.

#### 5.4. Photophysical investigation of PIs 138a-d

Photophysical investigations were conducted in efforts to ascertain a fundamental understanding of the reactive excited states and their involvement in photopolymerization. A hypsochromic shift can be seen from the absorbance spectra recorded in polar solvent ethanol and comparatively non-polar CHCl<sub>3</sub>, indicating a  $\pi\pi^*$  lowest singlet excited state character in the case of **138a**. Additionally, plotting together the absorbance and phosphorescence spectra displays overlap indicating a small singlet triplet gap (Figure 5.4).

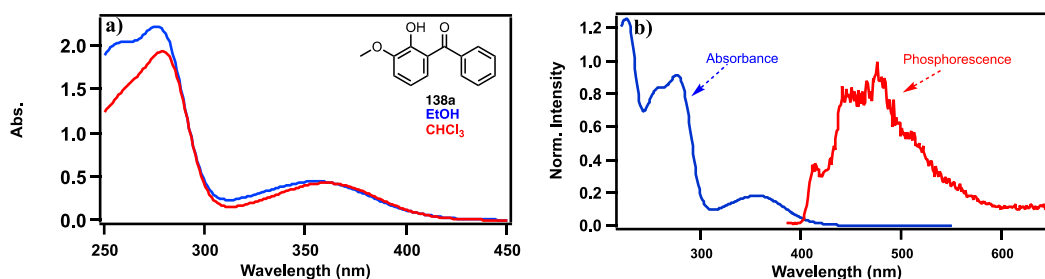


**Figure 5.2:** a) Absorbance spectra of **138a** recorded in various solvents [**138a**] = 0.15 mM; b) absorbance (blue) and phosphorescence (red) at 77 K in EtOH.  $\lambda_{\text{exc}}$  385 nm, OD. @  $\lambda_{\text{exc}}$  = 0.35,  $\lambda_{\text{em}}$  400 nm to 750 nm.

In efforts to compare the low temperature luminescence between the PIs **138a-d** steady state and time resolved luminescence spectra were recorded in ethanol glass at 77 K. It can be seen from Figure 5.3 and 5.4 that the emission spectra of **138a-d** are all similar in structure. From the similarity in the structure of the low temperature luminescence and phosphorescence spectra it can be implied that low temperature luminescence contains a large extent of phosphorescence. Thus low temperature luminescence in a rigid matrix (ethanol glass) occurs mainly from the triplet excited state. Seen by Figure 5.3 the vanillin derived photoinitiator garnishing *para*-methyl-substitution yields the most intense luminescence intensity (Figure 5.3). Additionally, transient absorbance investigations were conducted of **138a-d** utilizing 355 nm NdYag light source recorded in MeCN as solvent. After various attempts no transient species was observed for any of the newly synthesized photoinitiators. Benzophenone quite readily affords minimally a transient signal for the ketyl radical centered at 540 nm (recorded in MCH as solvent).<sup>25</sup> It is possible that the phenolic hydrogen is readily abstracted at room temperature quenching the excited state (Scheme 5.3). However, this conjecture necessitates further photophysical investigation.

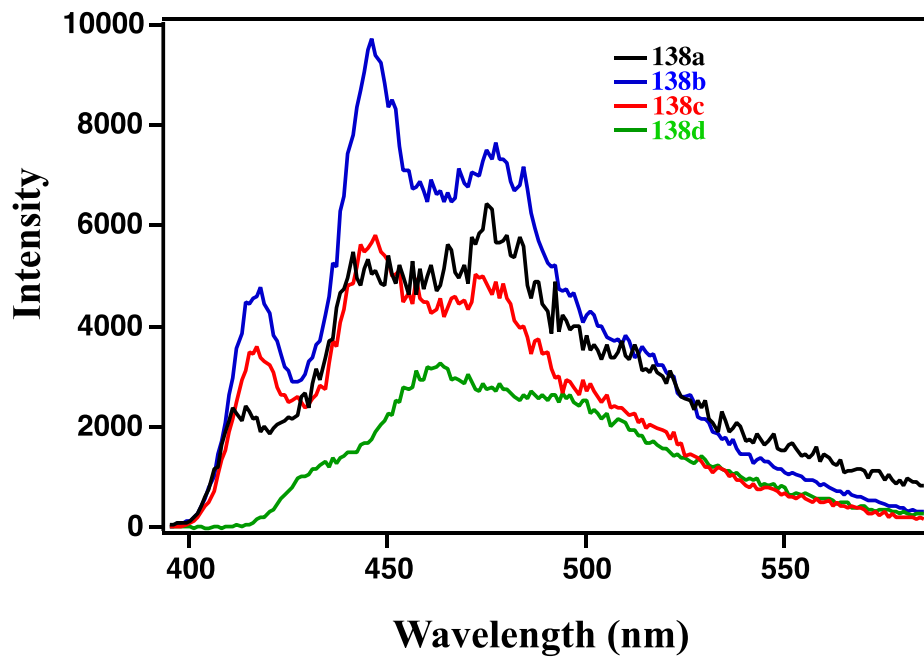
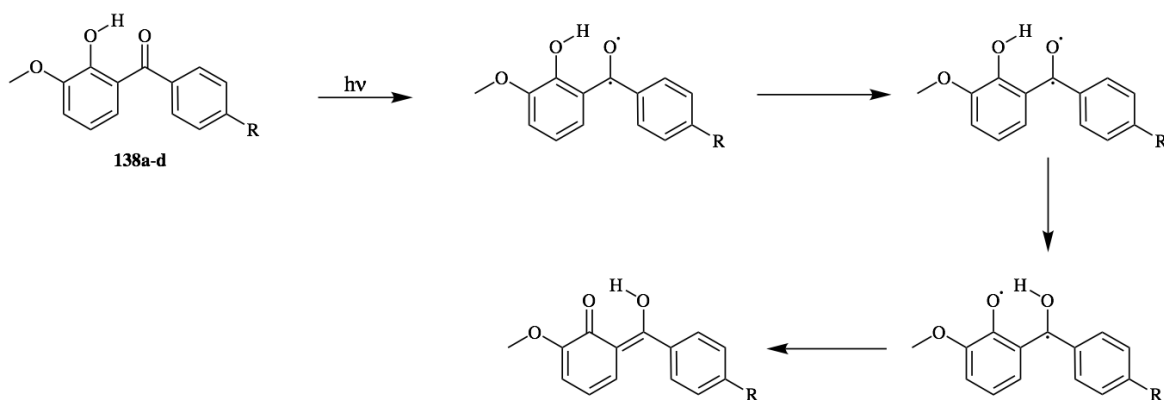


**Figure 5.3:** Phosphorescence of PIs **138a-d** recorded at 77 K in EtOH glass,  $\lambda_{exc}$  385 nm,  $\lambda_{em}$  400 nm to 750 nm.



**Scheme 5.3:** Possible excited state reactivity of photoinitiators **138a-d**.

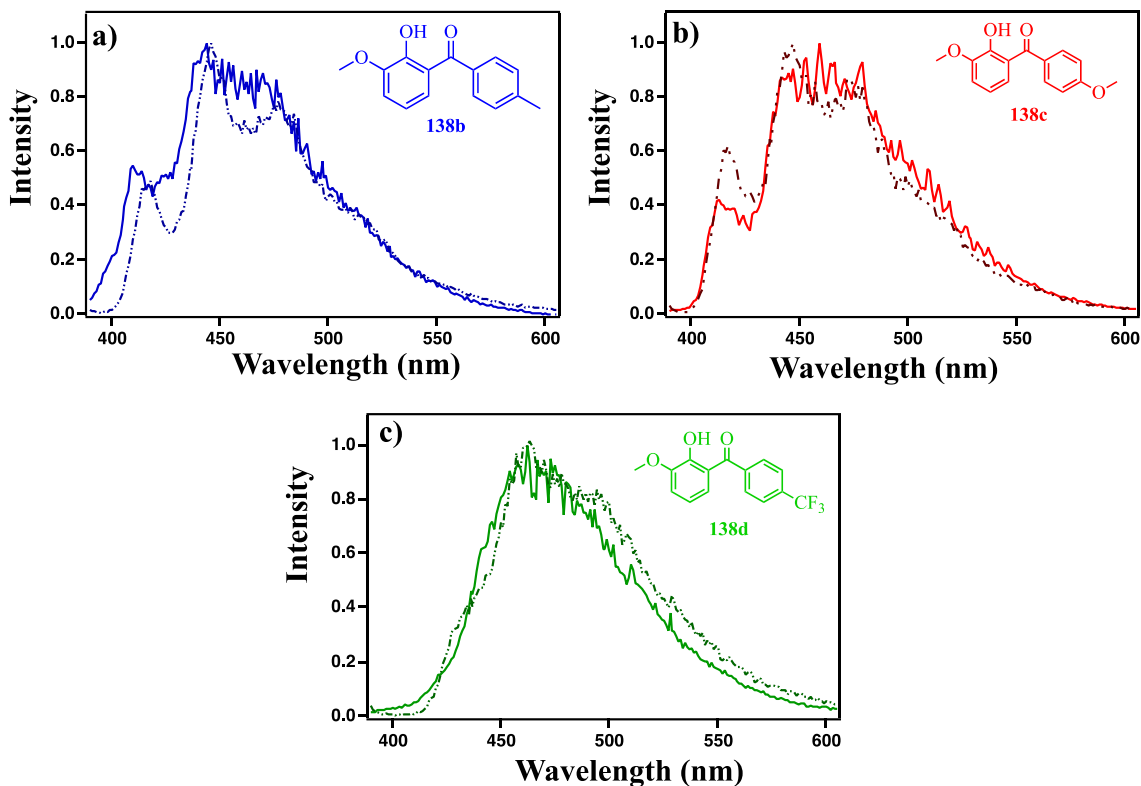


**Figure 5.4:** Low temperature luminescence (solid lines) and phosphorescence (dotted lines) recorded at 77 K in EtOH glass,  $\lambda_{exc}$  385 nm,  $\lambda_{em}$  400 nm to 750 nm of PIs **138b-d** respectively.

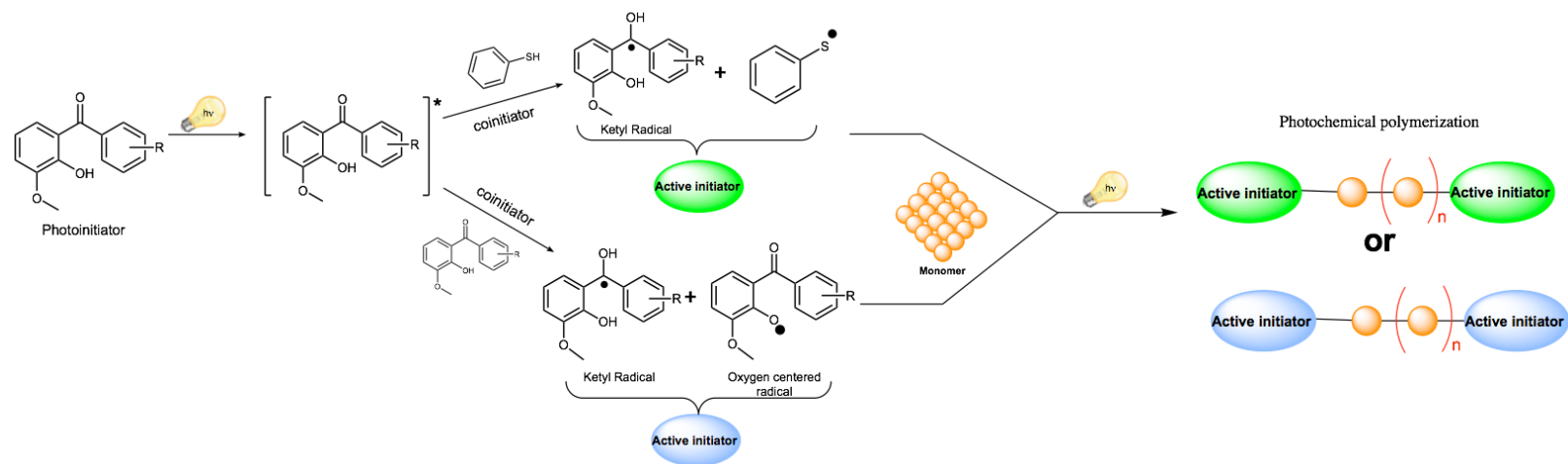
From the phosphorescence emission spectra, the triplet energy was obtained. Table 5.5 displays the  $\lambda_{max}$ , the triplet energy and the phosphorescence lifetimes of newly synthesized biobased photoinitiators. Inspection of Table 5.5 displays the bathochromic shift in PIs **138a-d**. Additional inspection of Table 5.5 displays that the triplet energies of **138a-c** are similar to that of benzophenone. Thus the substitution on the distal aromatic ring which caused the bathochromic shifting of the absorbance spectra of PIs **138a-c** did not cause a subsequent shift in the triplet energy. Thus it can be implied that the substitution effected the singlet energy to a greater extent than the triplet excited state of PIs **138a-c**. Conversely, the triplet energy of **138d** was lower than that of the other PIs indicating that the electron withdrawing group ( $CF_3$ ) likely stabilized the triplet excited state. Phosphorescence lifetimes were recorded at 77 K in ethanol rigid glass of benzophenone, **138a** and **138b**. Phosphorescence lifetimes of PIs **138a,b** were on

the same time scale as that of benzophenone. Based on the preliminary photophysical investigations conducted it can be inferred that the triplet excited state is likely  $n\pi^*$  in character much like benzophenone and that excitation of **138a-d** populates the singlet excited state which intersystem crosses to the triplet excited state. It is the triplet excited state that undergoes hydrogen abstraction forming the active initiator pair primed for photopolymerization with an appropriate monomer.

**Table 5.5:** Photophysical parameters of **138a-d** and BP.

entry	cmpd	$\lambda_{\max}^a$ (nm)	$\lambda_{\text{onset}}^a$ (nm)	$E_{T,b,c}$ (kcal/mol)	$\tau_T$ (msec)
1	BP	340	~375	69.6	5.4
2	<b>138a</b>	355	~415	69.6	3±0.4
3	<b>138b</b>	355	~415	69.1	4±0.1
4	<b>138c</b>	351	~415	68.9	---
5	<b>138d</b>	362	~420	66.8	---

<sup>a</sup>Taken from absorbance spectra recorded in ethanol. <sup>b</sup>Recorded at 77 K in ethanol glass.  $\lambda_{\text{exc}}$  385 nm; OD @  $\lambda_{\text{exc}} \leq 0.3$ . <sup>c</sup>Taken from left most peak of phosphorescence spectra.



**Scheme 5.4:** Photopolymerization utilizing PIs 138a-



## 5.5. Summary and outlook

Photochemical and photophysical investigations have unfolded that **138a-d** can be utilized to polymerize MA, MMA and styrene monomers to their corresponding polymers. The absorbance profile, low temperature luminescence and phosphorescence spectra were provided. Triplet energies of **138a-c** were determined to be similar to that of BP. The electron withdrawing group (CF<sub>3</sub>) of **138d** caused a decrease in the triplet energy of **138d** with respect to similarly para-substituted **138a-c**. Phosphorescence lifetimes of **138a** and **138b** were similar to that of BP. All in all, photophysical data namely phosphorescence lifetimes, triplet energy and structured emission indicate a similarity to benzophenone. However, the photoreactivity of **138a-d** differs from that of benzophenone in the fact that photopolymerization with the aid of commonly employed amines as coinitiators afforded no appreciable polymerization when utilizing **138a-d**. Additionally, the transient absorbance of **138a-d** displayed no signal of the expected ketyl radical.

Further Photophysical investigations must be conducted to answer key questions such as quantum yield of triplet formation and why the ketyl radical is not observed as a reactive species in transient absorption. Utilizing increased concentration of PI **138a**, photochemical investigations unveiled that photopolymerization could occur in the absence of coinitiator. The mechanism of this photopolymerization needs to be further investigated. It is possible that the phenolic hydrogen could undergo H-abstraction leading to oxygen centered radical which along with the ketyl radical becomes the plausible active initiator feasibly initiating the polymerization process (Scheme 5.4 bottom). Thus investigations regarding active initiator and mechanism of photopolymerization must be conducted. What radical is attached to the newly formed polymer

and is the oxygen centered radical formed throughout the polymerization processes are questions that need to be addressed.

The photopolymerization of vanillin derived photoinitiators opens avenues to visible light polymerization and other visible light mediated processes. As benzophenone has been utilized to synthesize and operate smart materials in the UV region photoinitiators **138a-d** allows for the synthesis and operation of similarly and differentially functionalized materials under more ecofriendly conditions, visible light irradiation, unlocking the possibility of exciting new materials.

## **5.6. Experimental section**

### **5.6.1. General methods**

All commercially obtained reagents/solvents were used as received; chemicals were purchased from Alfa Aesar<sup>®</sup>, Sigma-Aldrich<sup>®</sup>, Acros organics<sup>®</sup>, TCI America<sup>®</sup>, Mallinckrodt<sup>®</sup>, and Oakwood<sup>®</sup> Products, and were used as received without further purification. Nano pure water was obtained. Unless stated otherwise, reactions were conducted in oven-dried glassware under nitrogen atmosphere. <sup>1</sup>H-NMR and <sup>13</sup>C-NMR spectra were recorded on Bruker 400 MHz (100 MHz for <sup>13</sup>C) and on 500 MHz (125 MHz for <sup>13</sup>C) spectrometers. Data from the <sup>1</sup>H-NMR spectroscopy are reported as chemical shift ( $\delta$  ppm) with the corresponding integration values. Coupling constants ( $J$ ) are reported in hertz (Hz). Standard abbreviations indicating multiplicity were used as follows: s (singlet), b (broad), d (doublet), t (triplet), q (quartet), m (multiplet) and virt (virtual). Data for <sup>13</sup>C NMR spectra are reported in terms of chemical shift ( $\delta$  ppm). High-resolution mass spectrum data in Electrospray Ionization mode were recorded on a Bruker – Daltonics<sup>®</sup> BioToF mass spectrometer in positive (ESI+) ion mode.

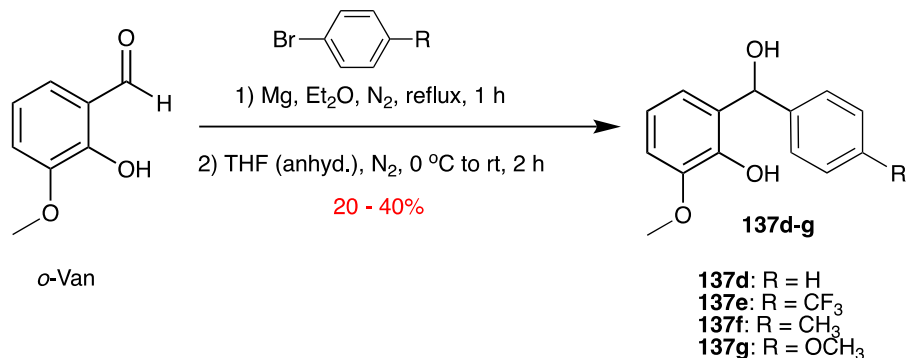
UV-Vis spectra were recorded on Carey 300 UV-Vis spectrometer using UV quality fluorimeter cells (with range until 190 nm) purchased from Luzchem. When necessary, the compounds were purified by combiflash equipped with dual wavelength UV-Vis absorbance detector (Teledyne ISCO) using hexanes:ethyl acetate as the mobile phase and Redisep<sup>®</sup> cartridge filled with silica (Teledyne ISCO) as stationary phase. In some cases, compounds were purified by column chromatography on silica gel (Sorbent Technologies<sup>®</sup>, silica gel standard grade: porosity 60 Å, particle size: 230 x 400 mesh, surface area: 500 – 600 m<sup>2</sup>/g, bulk density: 0.4 g/mL, pH range: 6.5 – 7.5).

### **5.6.2. Photophysical methods**

Spectrophotometric solvents (Sigma-Aldrich<sup>®</sup>) were used whenever necessary unless or otherwise mentioned. UV quality fluorimeter cells (with range until 190 nm) were purchased from Luzchem<sup>®</sup>. Emission spectra were recorded on a Horiba Scientific<sup>®</sup> Fluorolog 3 spectrometer (FL3-22) equipped with double-grating monochromators, dual lamp housing containing a 450-watt CW xenon lamp and a UV xenon flash lamp (FL-1040), Fluorohub/MCA/MCS electronics and R928 PMT detector. Emission and excitation spectra were corrected in all the cases for source intensity (lamp and grating) and emission spectral response.

## 5.7. General procedure for synthesis of vanillin derived photoinitiators

### 5.7.1. Synthetic protocol for secondary alcohol 137a-e



**Scheme 5.3:** Synthesis for secondary alcohol 137a-e.

A clean oven dried round bottom flask equipped with stir bar, and vanillin analog namely vanillin, *iso*-vanillin or *ortho*-vanillin (1 equiv), was evacuated and purged with N<sub>2</sub> followed by dissolution in tetrahydrofuran (THF). The mixture was cooled to 0 °C followed by dropwise addition of the corresponding Grignard reagent (3 equiv.) (methyl magnesium bromide in diethyl ether or phenyl magnesium derivative in diethyl ether). The reaction mixture was allowed to slowly rise to room temperature and stir for 12 hours. After approximately 12 hours the reaction was cooled to 0 °C and quenched with sat'd. NH<sub>4</sub>Cl<sub>(aq)</sub> (10 mL). The organic and aqueous layers were separated. The organic phase was washed with 2 N HCl, distilled water, extracted with ethyl acetate (EtOAc) (3 x30 mL). The organic layers were combined then washed with NaHCO<sub>3</sub> (10 mL), H<sub>2</sub>O, and brine then H<sub>2</sub>O, followed by drying over NaSO<sub>4</sub> (anhyd.) then concentrated in vacuo. The crude reaction mixture was purified over silica gel with 20/80 EtOAc/Hex as eluent. The products were obtained as viscous clear liquids (30 – 65% yield).

Note: Compounds **137d** and **137e** were characterized in Chapter 4.

$^1\text{H}$  NMR (500 MHz,  $\delta$  ppm,  $\text{CDCl}_3$ ) 7.44 -7.35 (m, 2H), 7.22-7.20 (m, 2H), 6.90- 6.84 (m, 3H), 6.08 (s, 1H), 5.88 (d, 1H), 3.88 (s, 3H), 3.54f(m, 1H), 2.41 (s, 3H).

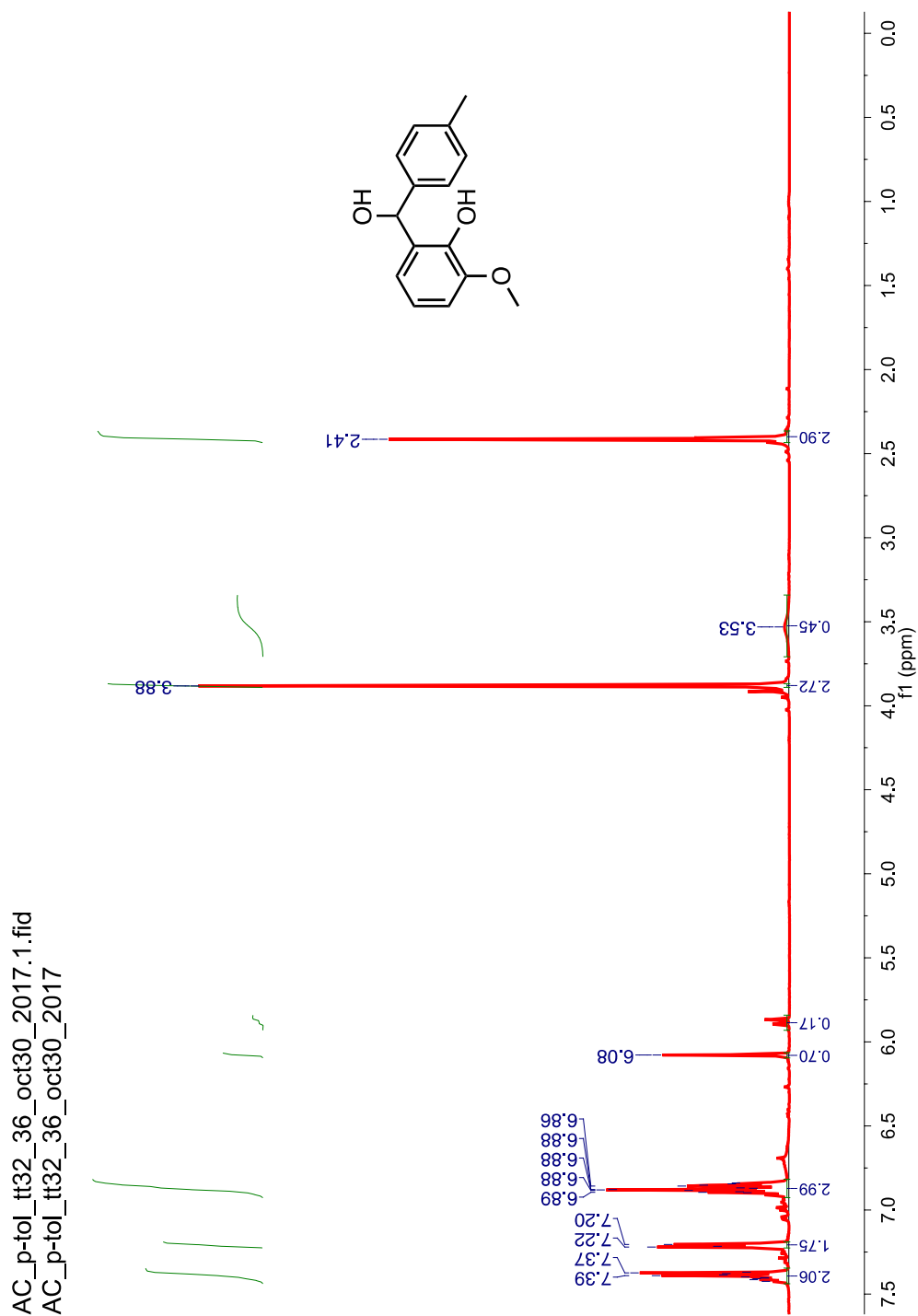


**Figure 5.5:**  $^1\text{H}$  NMR (500 MHz,  $\delta$  ppm,  $\text{CDCl}_3$ ) spectrum of secondary alcohol **137f**.

$^{13}\text{C}$  NMR (125 MHz,  $\text{CDCl}_3$ ,  $\delta$  ppm) 147.0, 143.3, 140.1, 137.1, 129.3, 129.1, 127.5, 126.6, 119.9, 119.7, 110.1, 73.00, 56.1, 21.2.

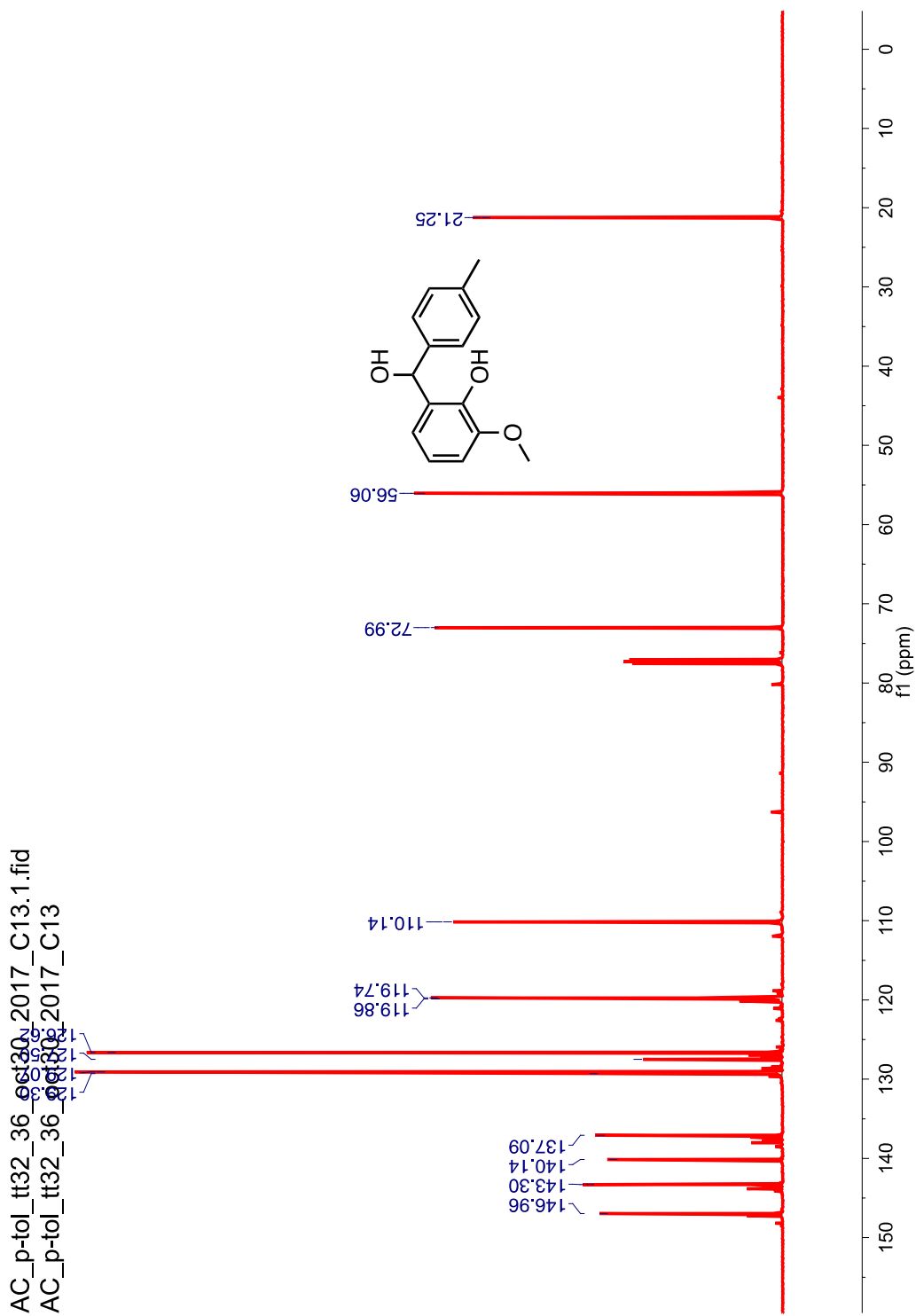


**Figure 5.6:**  $^{13}\text{C}$  NMR (125 MHz,  $\text{CDCl}_3$ ,  $\delta$  ppm) spectrum of secondary alcohol **137f**.

$^1\text{H}$  NMR (500 MHz,  $\text{CDCl}_3$ ,  $\delta$  ppm) 7.37-7.34 (m, 2H), 6.96-6.91 (m, 1H), 6.89- 6.81 (m, 5H), 6.77 (s, 1H), 5.77 (d,  $J = 7.7$  Hz, 1H), 3.88 (s, 3H), 3.81 (s, 3H).

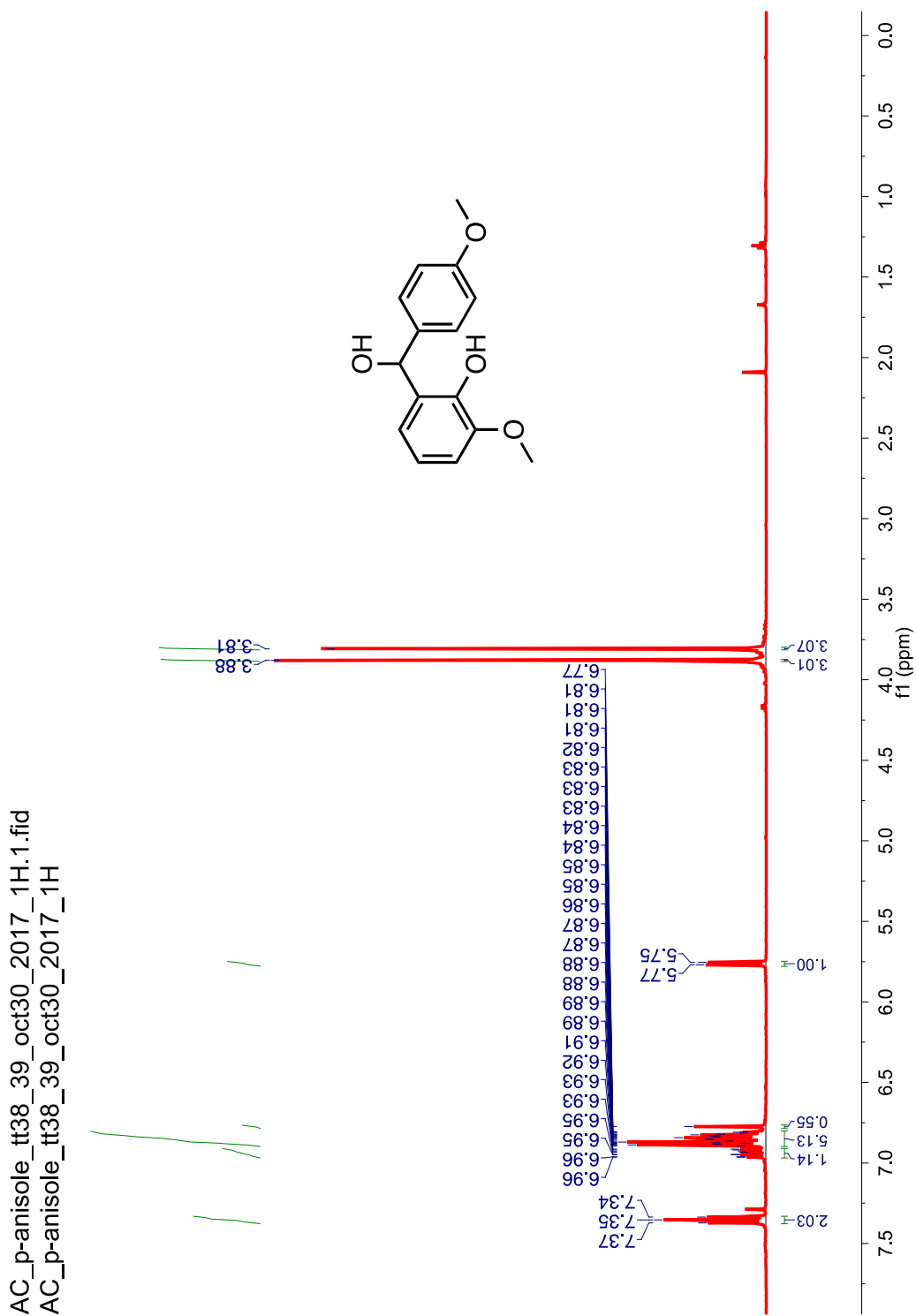


**Figure 5.7:**  $^1\text{H}$  NMR (500 MHz,  $\text{CDCl}_3$ ,  $\delta$  ppm) spectrum of secondary alcohol **137g**.

$^{13}\text{C}$  NMR (125 MHz,  $\text{CDCl}_3$ ,  $\delta$  ppm) 159.1, 159.06, 147.2, 147.1, 143.7, 143.6, 133.0, 132.7, 128.9, 128.8, 127.3, 126.8, 120.0, 119.9, 119.6, 113.8, 113.7, 110.1, 110.0, 77.0, 76.8, 55.9, 55.2.

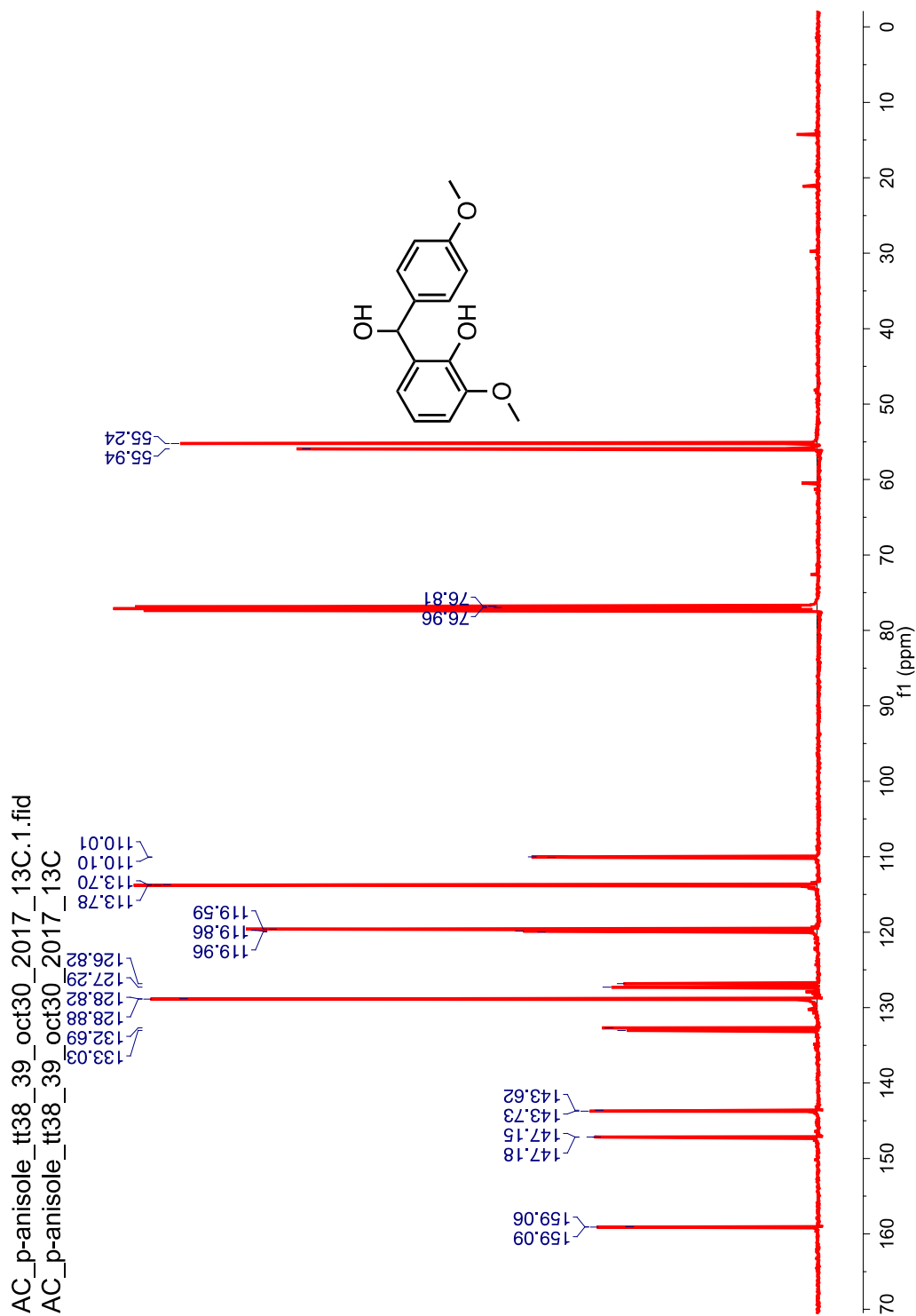
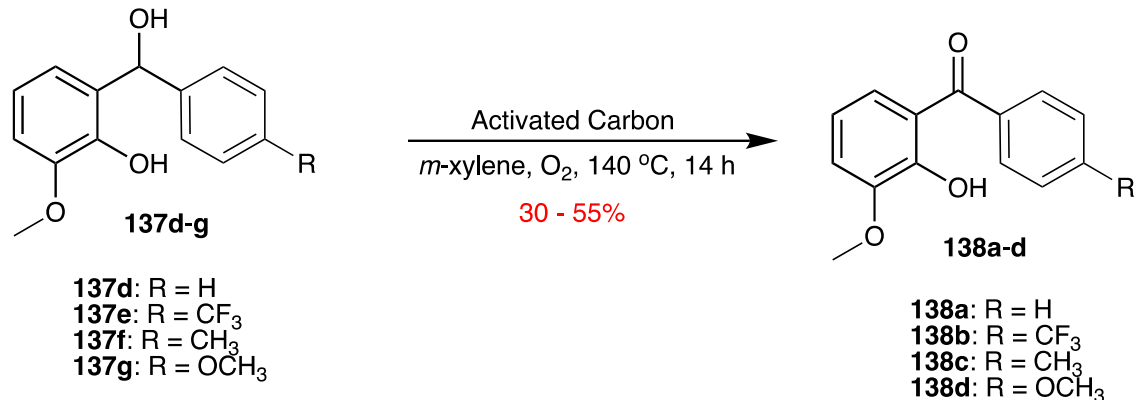


**Figure 5.8:**  $^{13}\text{C}$  NMR (125 MHz,  $\text{CDCl}_3$ ,  $\delta$  ppm) spectrum of secondary alcohol **137g**.



### 5.7.2. Synthetic protocol for vanillin derived photoinitiators



**Scheme 5.4:** Synthesis of vanillin derived photoinitiator.

To a solution of the benzylic alcohol **137d-g** (0.88 mmol, 1 equiv.) *meta*-xylene was added, purged with O<sub>2</sub> then heated to 140 °C, and allowed to stir for fourteen hours. After fourteen hours the reaction was allowed to cool to room temperature and filtered through celite. The filter-cake was washed with acetone and ethyl acetate. The combined organic solvents were evaporated in vacuo then purified via column chromatography. The products were afforded as yellow liquids except in the case of **138d** a yellow solid was afforded.



$^{13}\text{C}$  NMR (100 MHz,  $\text{CDCl}_3$ ,  $\delta$  ppm) 201.8, 153.4, 149.0, 137.9, 132.0, 129.2, 128.3, 124.8, 119.3, 118.0, 117.1, 56.3.

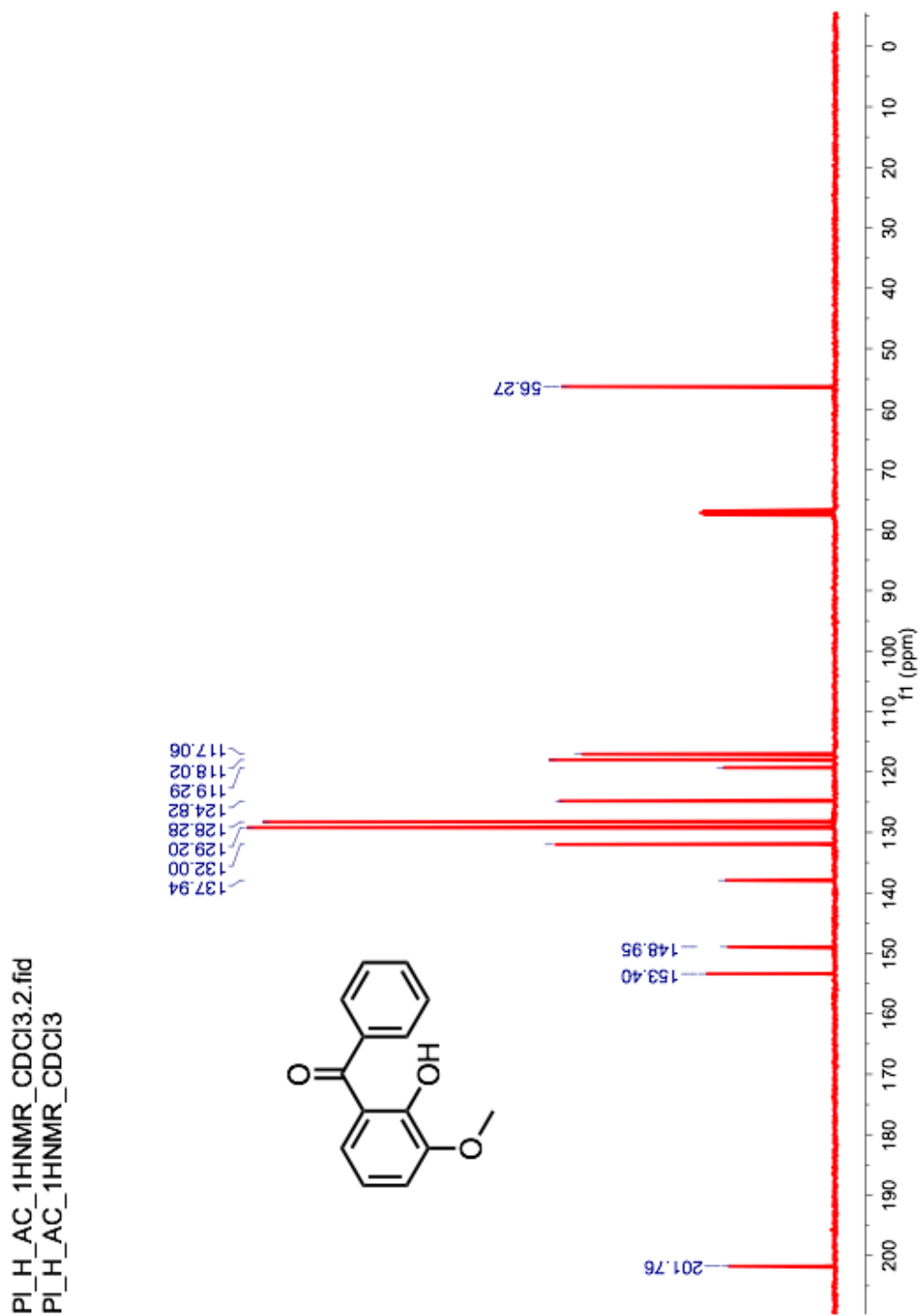


**Figure 5.10:**  $^{13}\text{C}$  NMR (100 MHz,  $\text{CDCl}_3$ ,  $\delta$  ppm) spectrum of photoinitiator **138a**.

$^1\text{H}$  NMR (400 MHz,  $\text{CDCl}_3$ ,  $\delta$  ppm) 12.26 (s, 1H), 7.63 – 7.61 (m, 2H), 7.32 – 7.30(m, 1H), 7.23 – 7.22 (m, 1H), 7.11 - 7.09 (m, 1H), 6.85 - 6.82 (m, 1H), 3.95 (s, 3H), 2.46 (s, 3H).

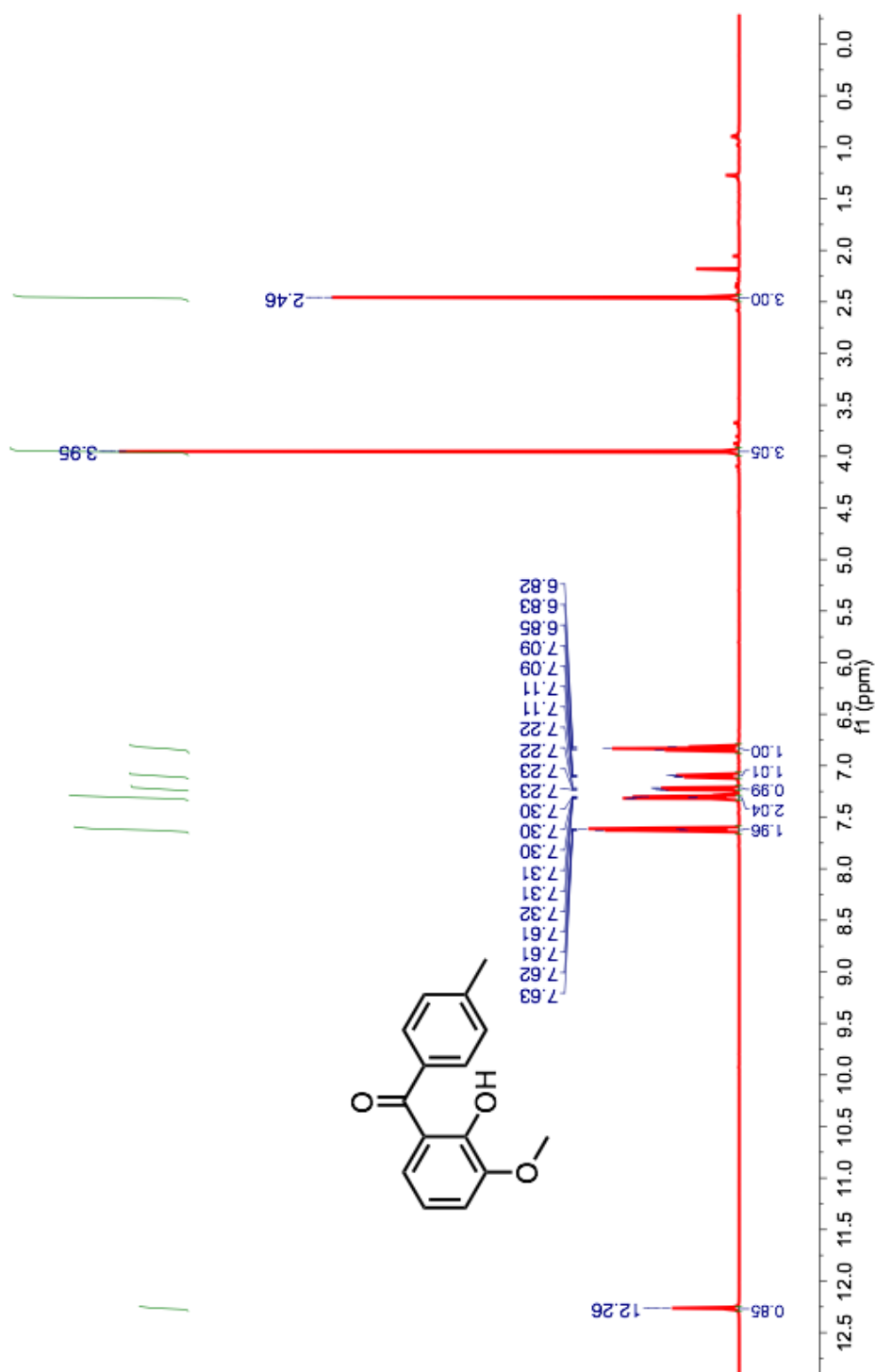


**Figure 5.11:**  $^1\text{H}$  NMR (400 MHz,  $\text{CDCl}_3$ ,  $\delta$  ppm) spectrum of photoinitiator **138b**.

$^{13}\text{C}$  NMR (100 MHz,  $\text{CDCl}_3$ ,  $\delta$  ppm) 201.5, 153.2, 148.9, 142.9 135.2, 129.5, 129.0, 124.8, 119.4, 117.9, 116.8, 56.2, 21.6.

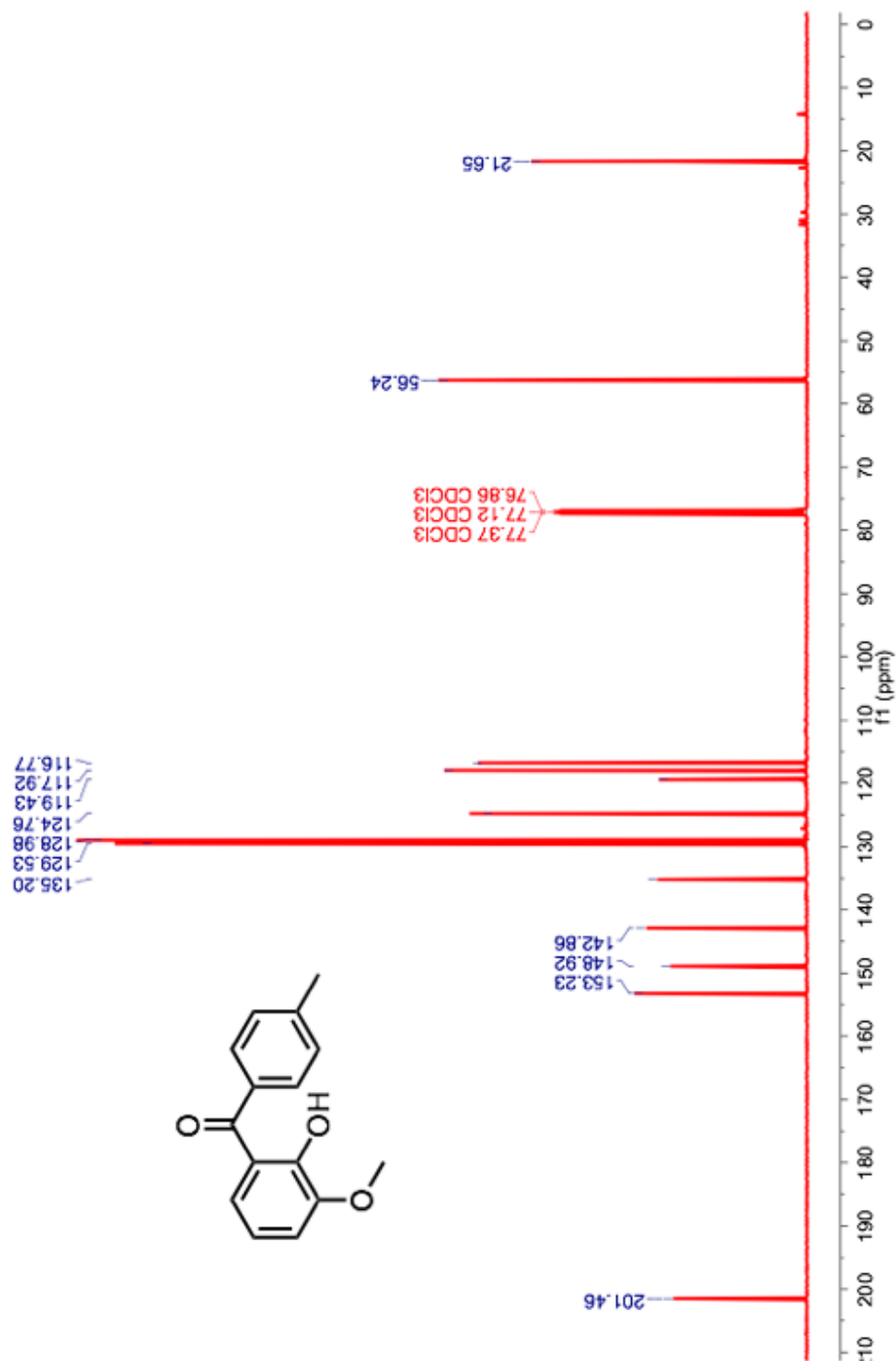


**Figure 5.12:**  $^{13}\text{C}$  NMR (100 MHz,  $\text{CDCl}_3$ ,  $\delta$  ppm) spectrum of photoinitiator **138b**.

$^1\text{H}$  NMR (400 MHz,  $\text{CDCl}_3$ ,  $\delta$  ppm) 12.11 (s, 1H), 7.76 - 7.74 (m, 2H), 7.26 - 7.24 (m, 1H), 7.12 - 7.09 (m, 1H), 7.02 - 7.00 (m, 2H), 6.87 - 6.83 (m, 1H), 3.96 (s, 3H), 3.92 (s, 3H).

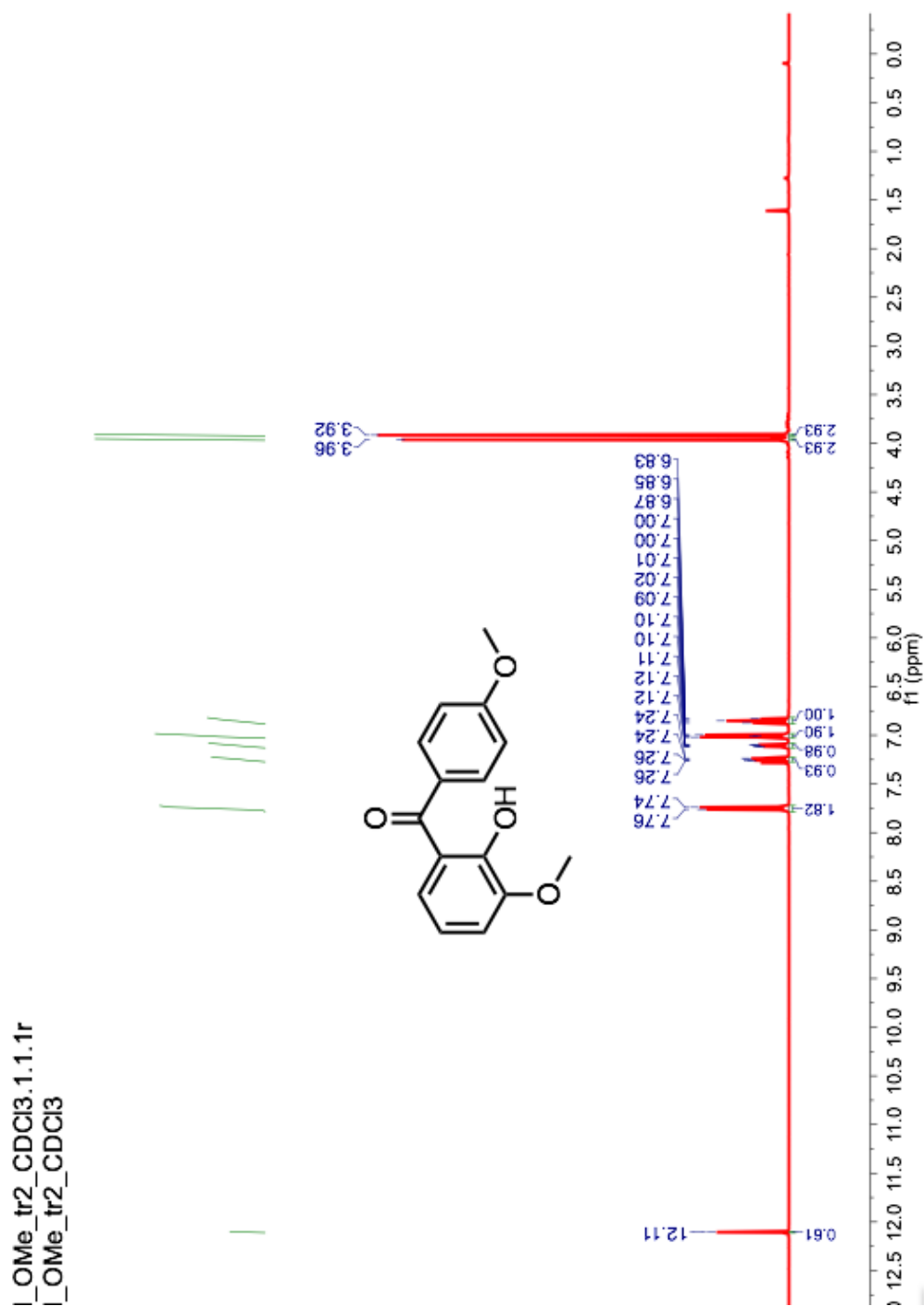


**Figure 5.13:**  $^1\text{H}$  NMR (400 MHz,  $\text{CDCl}_3$ ,  $\delta$  ppm) spectrum of photoinitiator **138c**.

$^{13}\text{C}$  NMR (100 MHz,  $\text{CDCl}_3$ ,  $\delta$  ppm) 200.1, 163.0, 153.0, 149.0, 131.9, 130.4, 124.5, 119.7, 117.8, 116.6, 113.6, 56.3, 55.5.

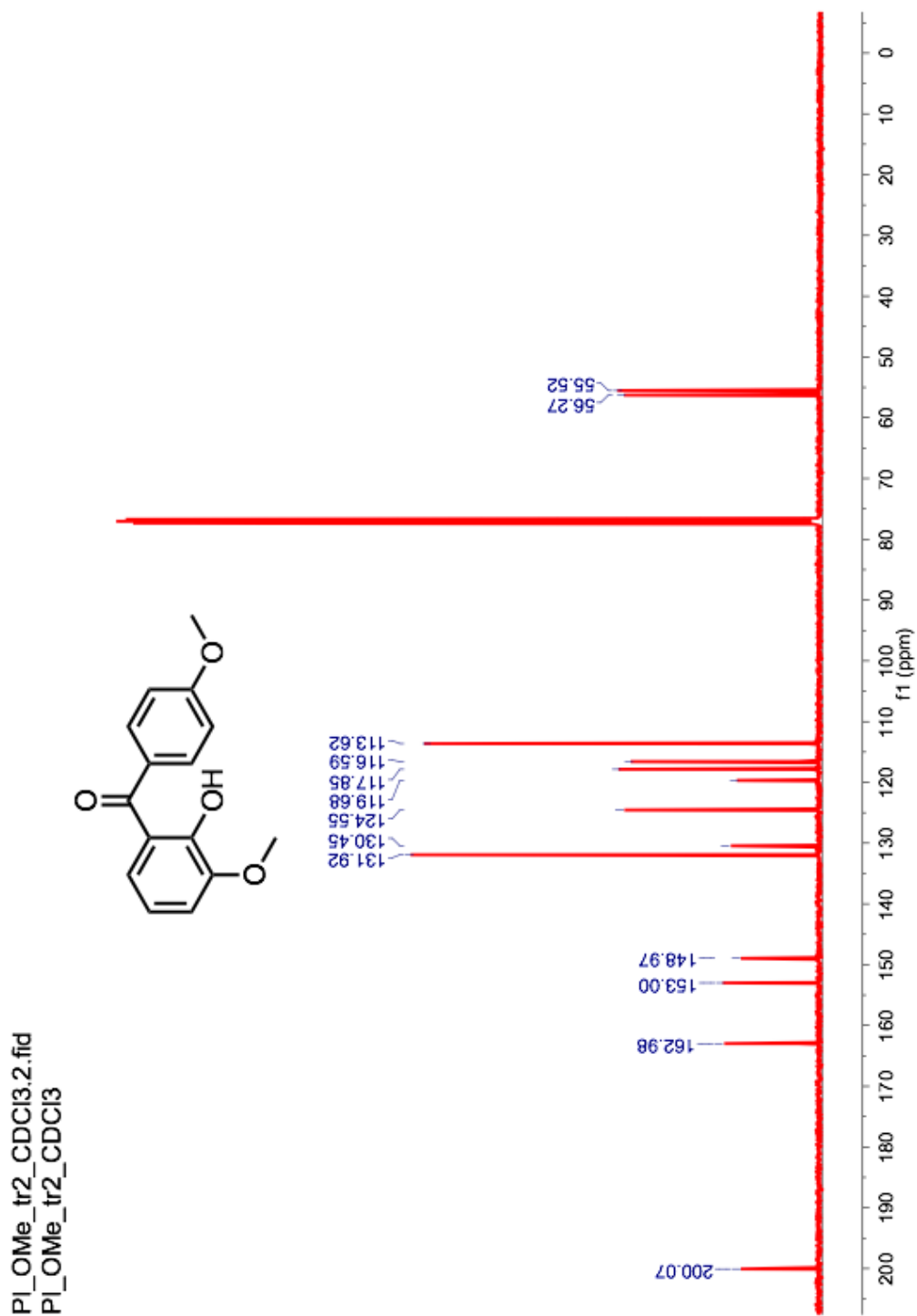


**Figure 5.14:**  $^{13}\text{C}$  NMR (100 MHz,  $\text{CDCl}_3$ ,  $\delta$  ppm) spectrum of photoinitiator **138c**.

$^1\text{H}$  NMR (400 MHz,  $\text{CDCl}_3$ ,  $\delta$  ppm) 12.03 (s, 1H), 7.81 (d,  $J = 1.1$  Hz, 3H), 7.16 - 7.11 (m, 2H), 6.89 - 6.85 (m, 1H), 3.98 (s, 3H).

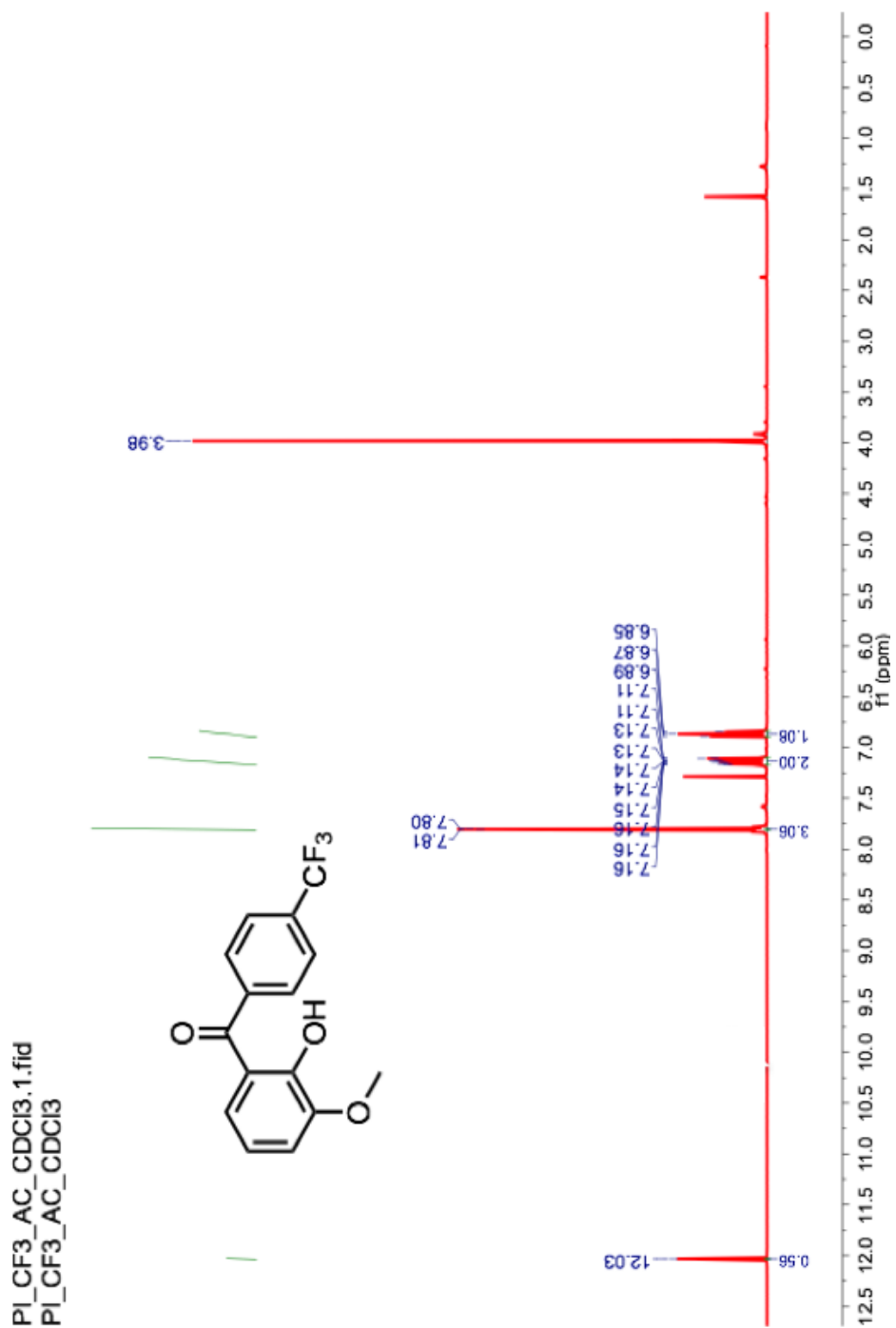


**Figure 5.15:**  $^1\text{H}$  NMR (400 MHz,  $\text{CDCl}_3$ ,  $\delta$  ppm) spectrum of photoinitiator **138d**.



$^{13}\text{C}$  NMR (100 MHz,  $\text{CDCl}_3$ ,  $\delta$  ppm) 200.5, 153.5, 149.1, 141.0, 133.3(q,  $J = 32.8$  Hz), 129.3, 125.3 (q,  $J = 3.7$  Hz), 118.9, 118.4, 117.5, 56.2.

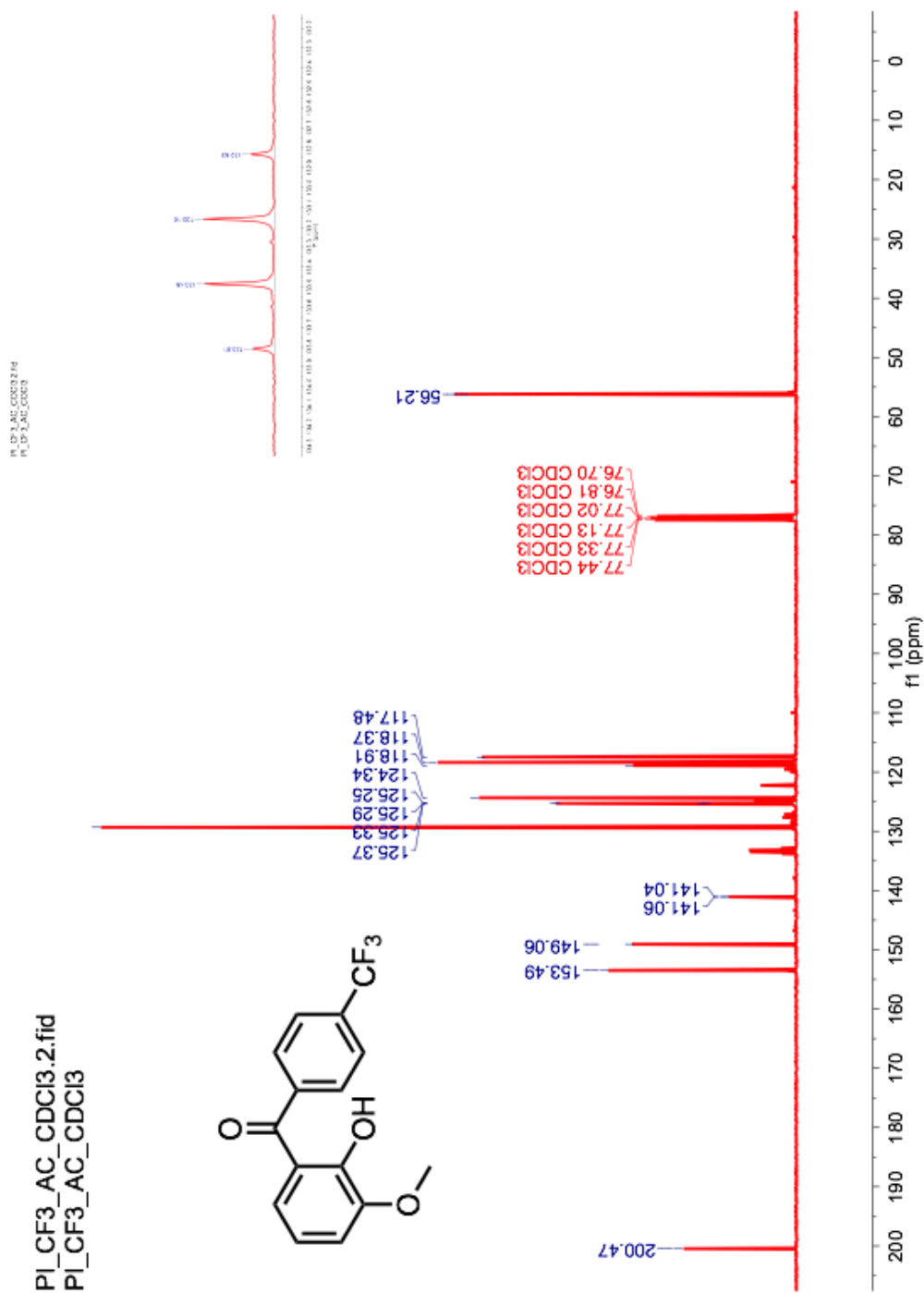


**Figure 5.16:**  $^{13}\text{C}$  NMR (100 MHz,  $\text{CDCl}_3$ ,  $\delta$  ppm) spectrum of photoinitiator **138d**.

$^{19}\text{F}$  NMR (375 MHz,  $\text{CDCl}_3$ ,  $\delta$  ppm) 63.03 .

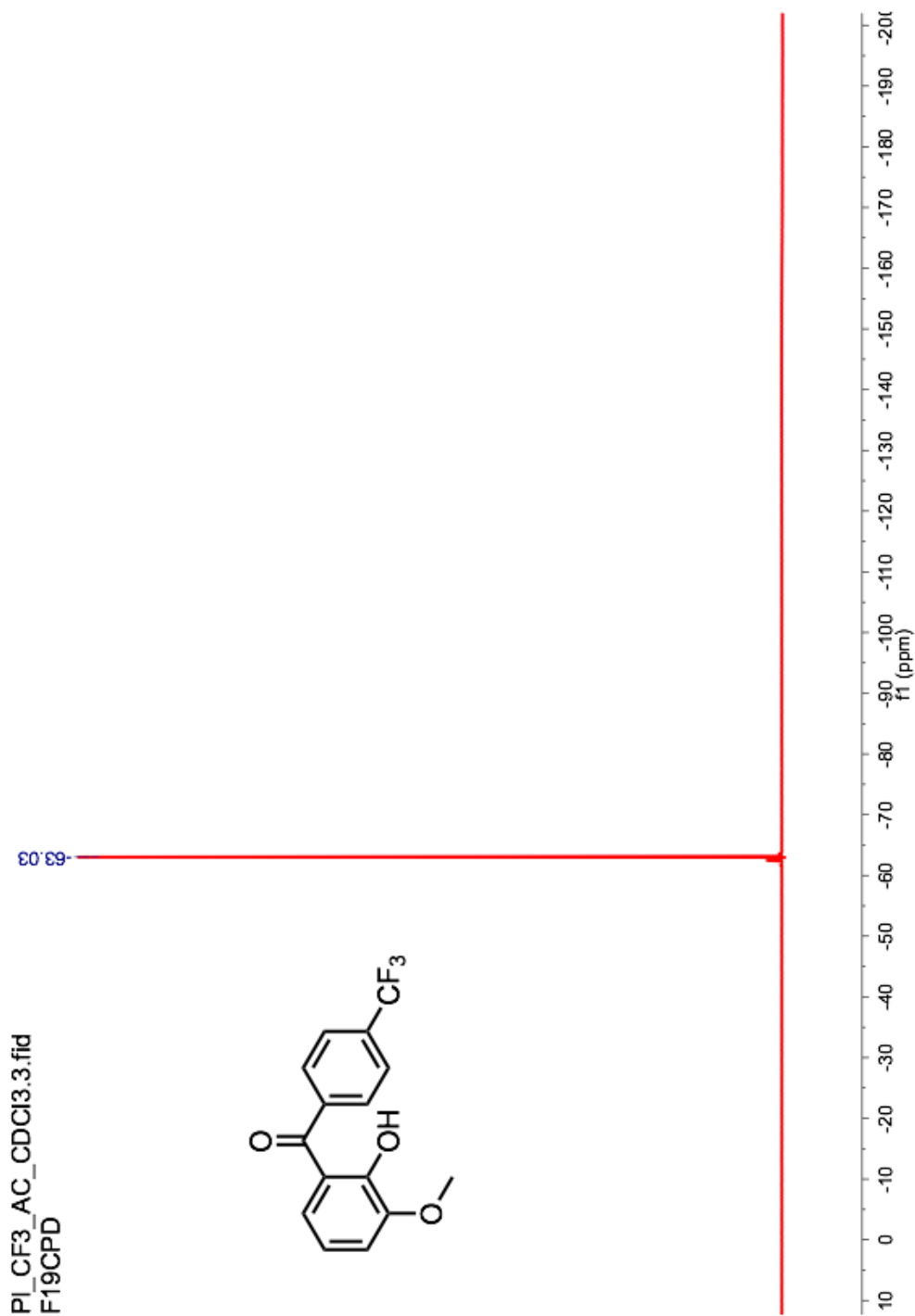
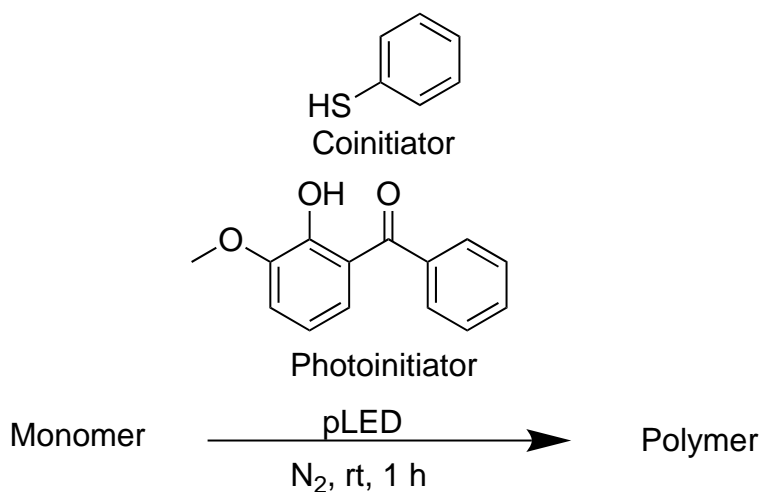


**Figure 5.17:**  $^{13}\text{C}$  NMR (375 MHz,  $\text{CDCl}_3$ ,  $\delta$  ppm) spectrum of photoinitiator **138d**.

## 5.8. Procedures for photochemical investigations

### 5.8.1. Synthetic protocol for photopolymerization of MA, MMA and styrene monomers



**Scheme 5.5:** Synthesis for photopolymerization of MA, MMA and styrene monomers.

Photoinitiator (0.008 mmol in MeCN), coinitiator (0.008 mmol in MeCN) and acrylate monomer (2 mL  $\simeq$  21 mmol ) were added to a vial equipped with a septum. The reaction mixture was then degassed with N<sub>2</sub> for approximately 3 minutes. The reaction mixture was then irradiated with purple LED (pLED) ( $\lambda_{\text{em}} = 395 - 405 \text{ nm}$ ) for one hour. After irradiation the reaction mixture was diluted in MeOH wherein the polymer precipitated as a white solid. The solvent was then removed under reduced pressure. The reaction mixture was washed with methanol. The mixture was weighed. The washing and drying was repeated until constant mass was achieved. The mass of the polymer was recorded. Then the polymer was analyzed by GPC analysis.

## 5.9. References

1. Bertrand, O.; Gohy, J.-F. Y., Photoresponsive polymers: Synthesis and Applications. *Polym. Chem.* **2017**, *8* (1), 52.
2. Hu, J.; Meng, H.; Li, G.; Ibekwe, S. I., A Review of stimuli-responsive Polymers for Smart Textile Applications. *Smart Mater. Struct.* **2012**, *21* (5), 1-23.
3. Wang, D.; Green, M. D.; Chen, K.; Daengngam, C.; Kotsuchibashi, Y., Stimuli Responsive Polymers: Design, Synthesis, Characterization, and Applications. *Int. J. Poly. Sci.* **2016**, *2016*, 1-2.
4. Guardado-Alvarez, T. M.; Russell, M. M.; Zink, J. I. Y., Nanovalve Activation by Surface Attached Photoacids. *Chem. Comm.* **2014**, *50* (61), 8388 - 8390.
5. Dongen, S. F. M.; de Hong, H.-P. M.; Peters, R. J. R. W.; Nallani, M.; Nolte, R. J. M.; van Hest, J. C. M., Biohybrid Polymer Capsules. *Chem. Rev.* **2009**, *109* (11), 6212-6274.
6. Wei, M.; Gao, Y.; Li, X.; Serpe, M. J. Y., Stimuli-responsive Polymers and Their Applications. *Polym. Chem.* **2017**, *8* (1), 127-143.
7. Esser-Kahn, A. P.; Odom, S. A.; Sottos, N. R.; White, S. R.; Moore, J. S., Triggered Release from Polymer Capsules. *Macromolecules* **2011**, *44* (14), 5539-5553.
8. Wagner, N.; Theato, P., Light Induced Wettability Changes on Polymer Surfaces. *Polymer* **2014**, *55* (16), 3436-3453.
9. Chen, M.; Besenbacher, F., Light-Driven Wettability Changes on a Photoresponsive Electrospun Mat. *ACS Nano* **2011**, *5* (2), 1549-1555.
10. Kondo, M.; Matsuda, T.; Fukae, R.; Kawatsuki, N., Photoinduced Deformation of Polymer Fibers with Anthracene Side Groups. *Chem. Lett.* **2010**, *39* (3), 234-235.

11. Chatani, S.; Kloxin, C. J.; Bowman, C. N. Y., The Power of Light in Polymer Science: Photochemical Processes to Manipulate Polymer Formation, Structure and Properties. *Polym. Chem.* **2014**, *5* (7), 2187-2201.
12. Hou, G.; Shi, S.; Liu, S.; Nie, J., Synthesis and Evaluation of 4-benzophenone Methoxyl Methacrylate As a Polymerizable Photoinitiator. *Polymer Journal* **2008**, *40* (3), 228-332.
13. Sun, F.; Zhang, N.; Nie, J.; Du, H. Y., Control of Concentration Gradient and Initiating Gradient Photopolymerization of Polysiloxane Benzophenone Photoinitiator. *J. Mater. Chem.* **2011**, *21* (43), 17290-17296.
14. Neckers, D. C.; Abu-Abdoun, I. I., p,p'-Bis((triphenylphosphonio)methyl)benzophenone Salts as Photoinitiators of Free Radical and Cationic Polymerization. *Macromolecules* **1984**, *17* (12), 2468-2473.
15. Sandner, M. R.; Osborn, C. L.; Trecker, D. J., Benzophenone/triethylamine-Photoinitiated Polymerization of Methyl Acrylate. *J. Polym. Sci. A-1 Polym. Chem.* **1972**, *10* (11), 3173-3181.
16. Kumasaka, R.; Kikuchi, A.; Yagi, M., Photoexcited States of UV Absorbers, Benzophenone Derivatives. *Photochem. Photobiol.* **2014**, *90* (4), 727-733.
17. Colman, P.; Dunne, A.; Quinn, M. F. Y., Flash Photolysis Studies of Benzophenone in Ethanol. *J. Chem. Soc., Faraday Trans. 1* **1976**, *72* (0), 2605-2609.
18. Flamigni, L.; Barigelletti, F.; Bortolus, P., Photophysical Study on a New Class of Benzophenone Containing Photoinitiators of Polymerization: Properties of poly(4-acryloxybenzophenone) and a Model Compound. *Eur. Polym. J.* **1983**, *20* (2), 171-175.
19. Turro, N. J.; Ramamurthy, V.; Scaiano, J. C., *Modern Molecular Photochemistry of Organic Molecules*. 2010; p 1084.

20. Odian, G., *Principles of Polymerization*. 2nd ed.; John Wiley and Sons: Staten Island, New York, 1981; p 731.
21. Srinivasan, S.; Kalfas, G.; Petkovska, V. I.; Bruni, C.; Grady, M. C.; Soroush, M., Experimental Study of The Spontaneous Thermal Homopolymerization of Methyl and *N*-butyl Acrylate. *J. Appl. Polym. Sci.* **2010**, *118* (4), 1898-1909.
22. Taylor, H. S.; Vernon, A. A., The Photo-Polymerization of Styrene and Vinyl Acetate. *J. Am. Chem. Soc.* **1931**, *53* (7), 2527-2536.
23. Chen, H. B.; Chang, T. C.; Chiu, Y. S.; Ho, S. Y., Photopolymerization of Styrene, p-chlorostyrene, Methyl Methacrylate, and Butyl Methacrylate with Polymethylphenylsilane as Photoinitiator. *J. Polym. Sci. A Polym. Chem.* **1996**, *34* (4), 679-685.
24. Krüger, K.; Tauer, K.; Yagci, Y.; Moszner, N., Photoinitiated Bulk and Emulsion Polymerization of Styrene – Evidence for Photo-Controlled Radical Polymerization. *Macromolecules* **2011**, *44* (24), 9539-9549.
25. Sakamoto, M.; Cai, X.; Hara, M.; Tojo, S.; Fujitsuka, M.; Majima, T., Transient Absorption Spectra and Lifetimes of Benzophenone Ketyl Radicals in the Excited State. *J. Phys. Chem. A* **2004**, *108* (40), 8147-8150.